Cytochrome Oxidase in Neuronal Metabolism and Alzheimer's Disease

Edited by
F. Gonzalez-Lima

Cytochrome Oxidase in Neuronal Metabolism and Alzheimer's Disease

Cytochrome Oxidase in Neuronal Metabolism and Alzheimer's Disease

Edited by

F. Gonzalez-Lima

The University of Texas at Austin
Austin, Texas

Springer Science+Business Media, LLC

Library of Congress Cataloging-in-Publication Data

Cytochrome oxidase in neuronal metabolism and Alzheimer's disease /
edited by F. Gonzalez-Lima.
p. cm.
"Proceedings of an international symposium on cytochrome oxidase in neuronal metabolism and Alzheimer's disease, held October 28, 1997 in New Orleans, Louisiana"--T.p. verso.
Includes bibliographical references and index.
ISBN 978-1-4757-9938-5 ISBN 978-1-4757-9936-1 (eBook)
DOI 10.1007/978-1-4757-9936-1
1. Alzheimer's disease--Pathophysiology--Congresses.
2. Cytochrome oxidase--Pathophysiology--Congresses. 3. Brain--Histochemistry--Congresses. 4. Neurons--Congresses. 5. Brain--Metabolism--Congresses. I. Gonzalez-Lima, Francisco, 1955-
[DNLM: 1. Cytochrome-c Oxidase--physiology congresses.
2. Neurons--metabolism congresses. 3. Alzheimer Disease--metabolism congresses. 4. Neurochemistry--methods congresses. QU 140C995 1998]
RC523.C98 1998
616.8'3107--dc21
DNLM/DLC
for Library of Congress 98-34611
CIP

Proceedings of an international symposium on Cytochrome Oxidase in Neuronal Metabolism and Alzheimer's Disease, held October 28, 1997, in New Orleans, Louisiana

ISBN 978-1-4757-9938-5

Originally published by Plenum Press, New York in 1998
Softcover reprint of the hardcover 1st edition 1998

http://www.plenum.com

10 9 8 7 6 5 4 3 2 1

In honor of
Dr. Margaret T. T. Wong-Riley,
on the occasion of the twentieth
anniversary of the introduction of her
cytochrome oxidase histochemical method

PREFACE

This book is based on an international symposium titled "Cytochrome oxidase in energy metabolism and Alzheimer's disease," held as a satellite to the 27th meeting of the Society for Neuroscience, New Orleans, 1997. The symposium was dedicated in honor of Dr. Margaret T. T. Wong-Riley because, in our opinion, the cytochrome oxidase histochemical method introduced by Dr. Wong-Riley in 1979 was the most significant breakthrough to map energy metabolism in the entire brain since the 2-deoxyglucose method introduced by Dr. Louis Sokoloff and colleagues in 1977. Both of these metabolic mapping techniques have made monumental contributions to brain research by allowing an integral view of brain activity. They have also developed into various specialized techniques, including applications to the human brain. One of these new applications, which is described in detail in this book, is the quantitative cytochrome oxidase cytochemical method used to study Alzheimer's disease.

The objective of this book is to describe the role of cytochrome oxidase in neuronal metabolism and Alzheimer's disease. Whether genetic or environmental, the pathogenesis of Alzheimer's disease involves a cascade of multiple intracellular events, eventually resulting in failure of oxidative energy metabolism. Could impairment of cytochrome oxidase in energy metabolism initiate the degenerative process? Cytochrome oxidase function and dysfunction are discussed in relationship to neuronal energy metabolism, neurodegeneration, and Alzheimer's disease.

The book is made up of 10 chapters, divided into three major parts. Part I introduces neuronal metabolism and cytochrome oxidase function. Part II covers Alzheimer's disease and cytochrome oxidase dysfunction. Part III is an appendix atlas of cytochrome oxidase histochemistry of the rat brain.

Part I leads off with the contribution of Wong-Riley and colleagues (Wong-Riley, Nie, Hevner, and Liu) on cytochrome oxidase in energy metabolism and neuronal function. This chapter sets the stage for the book by providing a comprehensive overview of the involvement of cytochrome oxidase in cellular energy metabolism and neuronal activity. The essential role of this mitochondrial enzyme in neuronal function and its bigenomic regulation are discussed. A second major chapter is contributed by Gonzalez-Lima and Cada, who explain the theory and methods of quantitative histochemistry of cytochrome oxidase. This chapter also discusses the differential vulnerability of brain regions to cytochrome oxidase inhibition, which provides the basis for chapters in Part II dealing with cytochrome oxidase dysfunction. The other three chapters in Part I provide specific examples of the applications of cytochrome oxidase histochemistry to map neuroanatomical

patterns (Hevner), brain functions related to learning and memory (Poremba, Jones, and Gonzalez-Lima), and the neural basis of behavior in genetic animal models (Papa, Sadile, Sergeant, Shumake, and Gonzalez-Lima).

Part II starts with a chapter by Gonzalez-Lima, Valla, and Jorandby that postulates how cytochrome oxidase inhibition may lead to dementia in sporadic Alzheimer's disease. This chapter integrates the literature into a coherent picture of how a cytochrome oxidase systemic deficiency may compromise energy metabolism and lead to neurodegeneration in Alzheimer's disease. Methods for assessing cytochrome oxidase activity in individual neurons are discussed in relationship to the selective vulnerability of larger projection neurons in Alzheimer's brains. New findings are presented that suggest that peripheral tissue biopsy may be used as an early diagnostic test in patients suspected of sporadic Alzheimer's disease.

Cytochrome oxidase gene expression in Alzheimer's disease is discussed in a chapter by Chandrasekaran, Hatanpää, Liu, and Rapoport. They review and critique the evidence for a genetic impairment of cytochrome oxidase in Alzheimer's disease. The molecular biology of cytochrome oxidase is discussed in relationship to the vulnerability of selective regions in Alzheimer's brains. The last two chapters in Part II discuss animal models of chronic cytochrome oxidase inhibition and their usefulness in Alzheimer's research. Pharmacological cytochrome oxidase inhibition as a model of Alzheimer's disease is discussed by Bennett and Rose. They review behavioral and physiological characteristics of rats infused chronically with sodium azide, a selective inhibitor of cytochrome oxidase. The effects on learning and memory tasks and the advantages and limitations of this model are discussed. A surgical model of chronic brain hypoperfusion that produces failure of oxidative energy metabolism is discussed by Abdollahian, Cada, Gonzalez-Lima, and de la Torre. They explain the link between oxidative energy metabolism and neuronal degeneration. The cascade of metabolic events leading to cellular histopathology is discussed with examples from animal models of aging and chronic ischemia. It is proposed that cytochrome oxidase may serve as a useful marker for predicting potential neurodegeneration.

This book is timely given the recent studies indicating that mitochondrial electron transport dysfunction is involved in various neurodegenerative diseases, including Parkinson's disease, Huntington's disease and Alzheimer's disease. Although much attention has been devoted to Alzheimer's disease, relatively little has been devoted to the role of energy metabolism in this disease. This is the first book on cytochrome oxidase that explores the clinical significance of this enzyme in Alzheimer's disease.

The cooperation of all the contributors made possible a successful symposium and fast publication of this book. I am grateful to all of them for their generous and enlightening contributions.

F. Gonzalez-Lima

CONTENTS

Part I: Neuronal Metabolism and Cytochrome Oxidase Function

1. Brain Cytochrome Oxidase: Functional Significance and Bigenomic Regulation in the CNS 1
   Margaret T. T. Wong-Riley, Feng Nie, Robert F. Hevner, and Suyan Liu

2. Quantitative Histochemistry of Cytochrome Oxidase Activity: Theory, Methods, and Regional Brain Vulnerability 55
   F. Gonzalez-Lima and A. Cada

3. Cytochrome Oxidase and Neuroanatomical Patterns: What Is the Connection? . . 91
   Robert F. Hevner

4. Functional Mapping of Learning-Related Metabolic Activity with Quantitative Cytochrome Oxidase Histochemistry 109
   Amy Poremba, Dirk Jones, and F. Gonzalez-Lima

5. Functional Imaging Probes to Study the Neural Bases of Behavior in Genetic Animal Models of ADHD: A Comparative Analysis of Short and Long-Term Markers of Neuronal Activity 145
   Michele Papa, Adolfo G. Sadile, Joseph A. Sergeant, Jason Shumake, and F. Gonzalez-Lima

Part II: Alzheimer's Disease and Cytochrome Oxidase Dysfunction

6. Cytochrome Oxidase Inhibition in Alzheimer's Disease 171
   F. Gonzalez-Lima, J. Valla, and L. Jorandby

7. Molecular Mechanisms of Impaired Mitochondrial Gene Expression in Alzheimer's Disease 203
   Krish Chandrasekaran, Kimmo Hatanpää, Li-Ing Liu, and Stanley I. Rapoport

8. Behavioral, Electrophysiological, and Biochemical Consequences of Chronic Cytochrome Oxidase Inhibition in Rats 217
   M. C. Bennett and G. M. Rose

9. Cytochrome Oxidase: A Predictive Marker of Neurodegeneration 233
N. P. Abdollahian, A. Cada, F. Gonzalez-Lima, and J. C. de la Torre

Part III: Appendix

10. Cytochrome Oxidase Atlas of Rat Brain 263
F. Gonzalez-Lima and A. Cada

Contributors 281

Index 283

1

BRAIN CYTOCHROME OXIDASE

Functional Significance and Bigenomic Regulation in the CNS

Margaret T. T. Wong-Riley,* Feng Nie, Robert F. Hevner,† and Suyan Liu

Department of Cellular Biology and Anatomy
Medical College of Wisconsin
Milwaukee, Wisconsin 53226

ABSTRACT

Cytochrome oxidase is a ubiquitous housekeeping enzyme that holds one of the important keys to life. As a major oxidative enzyme and an energy-generating enzyme, cytochrome oxidase serves as a reliable indicator of neurons' oxidative capacity and energy metabolism. The tight coupling between energy metabolism and neuronal activity further enables cytochrome oxidase to serve as a sensitive metabolic marker for neuronal functional activity, which includes firing rates of neurons and slow depolarizing potentials occurring primarily in dendrites. In the past two decades, much has been learned about the heterogeneous distribution of cytochrome oxidase in neurons at the regional, laminar, cellular and subcellular levels. The local activity of cytochrome oxidase is correlated with the physiological activity of each area, cell, or subcellular compartment. Regions of high cytochrome oxidase activity are dominated by excitatory, glutamatergic synapses. Changes in the physiological activity of neurons can induce parallel changes in the activity of cytochrome oxidase in developing and adult systems. Cytochrome oxidase activity is controlled mainly by regulation of protein amount, which is regulated transcriptionally. Being bigenomically encoded, cytochrome oxidase is under complex interactive regulation of both mitochondrial and nuclear gene expression. Cytochrome oxidase subunit complementary DNAs were isolated from a murine complementary DNA library, cloned and sequenced. Transcripts from the two genomes have distinct subcellular as well as compartmental distributions suggestive of different regulatory mechanisms. Antibodies generated

* Send correspondence to: Margaret Wong-Riley, Ph.D., Department of Cellular Biology and Anatomy, Medical College of Wisconsin, Milwaukee, Wisconsin 53226. Tel: (414) 456–8467; Fax: (414) 456-6517; e-mail: MWR@MCW.edu.

† Present address: Department of Psychiatry, University of California, San Francisco, San Francisco, California 94143-0984.

Cytochrome Oxidase in Neuronal Metabolism and Alzheimer's Disease,
edited by Gonzalez-Lima, Plenum Press, New York, 1998.

against subunit proteins from the two genomes also showed differential distributions among neuronal compartments. Nuclear-encoded subunits are translated exclusively in the cell bodies and are delivered intramitochondrially to distal processes. A precursor pool exists in dendrites, where further processing of nuclear-encoded subunits and holoenzyme assembly are presumably governed by local energy demands. Under normal and functionally altered states, cytochrome oxidase activity is linked more closely to transcripts and subunit proteins derived from mitochondrial than from nuclear sources. This indicates that local cytochrome oxidase activity in neurons is controlled mainly by regulation of the mitochondrial genes that encode the catalytic subunits of the enzyme.

1. INTRODUCTION

1.1. Cytochrome c Oxidase as a Neuronal Metabolic Marker

Cytochrome c oxidase (CO; cytochrome aa_3, ferrocytochrome C: oxygen oxidoreductase, EC 1.9.3.1) is the terminal enzyme or complex IV of the electron transport chain, catalyzing the oxidation of cytochrome c and the reduction of molecular oxygen (Fig. 1), yielding ATP via the coupled processes of electron transport and oxidative phosphorylation (Hatefi, 1985; Capaldi et al., 1987). Cytochrome oxidase has a long evolutionary history, being present in the cell membrane of some prokaryotes. It is an integral protein of the inner mitochondrial membrane in almost all eukaryotes (with red blood cells as one of the exceptions). This enzyme is vital to neurons, which depend almost solely on oxidative metabolism for their energy supply. Without the terminal enzyme, oxidative metabolism cannot be carried to completion, energy generation is severely compromised, and the survival of neurons is gravely jeopardized. This close relationship enables cytochrome oxidase to be an ideal indicator of the neuron's oxidative capacity and its energy metabolism.

1.2. Cytochrome c Oxidase as a Sensitive Indicator of Neuronal Functional Activity

As one of the key energy-generating enzymes, then, cytochrome oxidase offers a window through which we can gain insight into neuronal energy metabolism. Energy metabo-

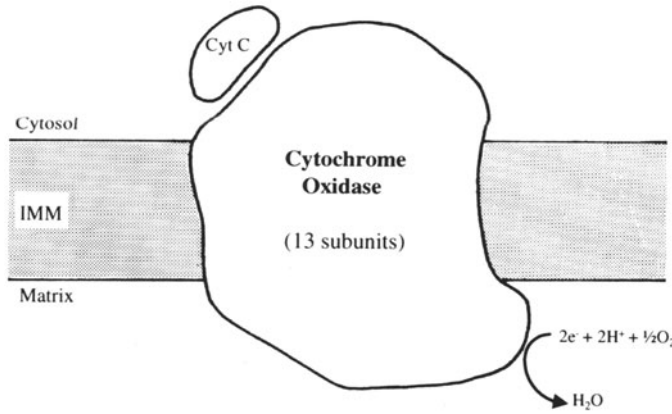

Figure 1. Model of cytochrome oxidase as an integral protein of the inner mitochondrial membrane (IMM). Cytochrome oxidase catalyzes the transfer of electrons from its substrate, cytochrome c (Cyt C) to oxygen to form water.

lism, in turn, reflects energy demands imposed by the workings of neurons. Of the three major types of work: synthesis of neurotransmitters and other molecules, fast axoplasmic transport, and active ion transport, the last process consumes by far the bulk of the energy (Sokoloff, 1974; Bachelard, 1975; Lowry, 1975). With increased neuronal activity, at least two major events occur: one consumes energy to restore the resting membrane potential for reactivation, and this is done primarily by ATPases, such as Na^+K^+ATPase. The other generates energy via increased blood flow and glucose utilization, leading to increased cellular respiration and ATP synthesis, mainly within the mitochondria, and cytochrome oxidase is an integral part of this process (Wong-Riley, 1989) (Fig. 2). These two major, interdependent events form the basis for cytochrome oxidase to be a reliable metabolic marker for neuronal activity. Thus, neuronal activity and energy metabolism are tightly coupled, and under normal conditions, it is neural activity that controls energy expenditure and not vice versa (Krnjevic, 1975; Lowry, 1975). However, under pathological conditions, when energy metabolism becomes defective, neuronal activity will be adversely affected.

Cytochrome oxidase has proven to be a sensitive and reliable marker of neuronal activity. It has also revealed a number of neuronal properties that were elusive in the past. In this chapter, we shall review some of the studies that highlight the relationship between cytochrome oxidase, energy metabolism, and neuronal activity. Furthermore, we shall probe the mechanism of its regulation in neurons, particularly with regard to its dual regulation by mitochondrial and nuclear genes.

2. METHODS

2.1. Biochemical Assay of Cytochrome Oxidase Activity

2.1.1. Preparation of Rat Brain Tissue Homogenates. Rats were deeply anesthetized with phiobupabarbital (100 mg/kg, i.p.) and decapitated. Barbiturates such as phiobupabarbital do not affect CO activity (Cohen, 1973). The brains were immediately removed, and either weighed and homogenized whole, or dissected into regions, which were then weighed and homogenized separately. The brain regions were kept frozen on dry ice covered with aluminum foil until they could be weighed and homogenized.

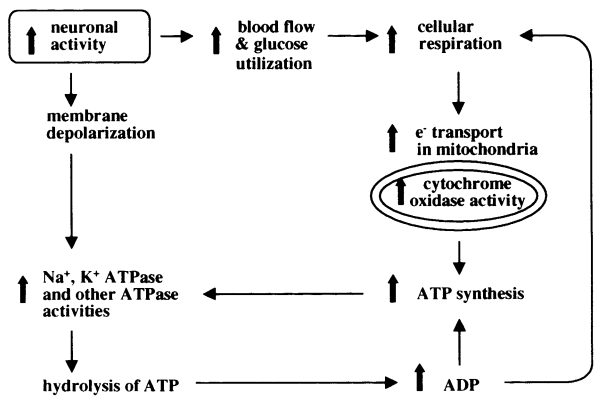

Figure 2. Schematic diagram of the relationship between neuronal activity and energy metabolism. Energy consumed by active ion transport is generated mainly by oxidative metabolism, of which cytochrome oxidase is an integral part. These processes are tightly coupled. (Modified from Wong-Riley, 1989).

2.1.2. Biochemical Assay. The brain samples were homogenized, solubilized, and assayed for CO activity using a spectrophotometric assay (Errede et al., 1978; Wharton and Tzagoloff, 1967), modified as described previously (Hevner et al., 1993). Briefly, each brain or region was homogenized with isolation buffer (0.32 M sucrose, 1 mM dipotassium EDTA, 10 mM Tris, pH 7.4) to prepare a 20% homogenate, which was subsequently kept on ice. A motor-driven Teflon-glass (Potter-Elvehjem type) homogenizer was used for whole brain, while hand-held 1.5 ml polypropylene microfuge tubes and matched polypropylene pestles (Kimble) were used for homogenizing brain regions. Aliquots of the 20% homogenates were solubilized with deoxycholate (dCh), diluted with additional isolation buffer, and assayed for CO activity within 30 minutes of solubilization. We found the following combinations to be optimal for various regions of the rat brain: gray matter (0.25% homogenate and 0.5% dCh), white matter (1.0% homogenate and 1.0% dCh), and retina (0.5% homogenate and 0.75% dCh) (Hevner et al., 1993). Assays were done in triplicate at 30°C using a dual-beam spectrophotometer at 550 nm. The assay is linear with time (over the 1 min assay period), and with added cytochrome aa_3 or brain tissue. Enzyme activity was expressed as units (U), where 1 unit (U) of enzyme activity was defined as 1 μmol cytochrome c oxidized/min. Homogenates (20% or dCh-solubilized) were frozen after CO assay and stored at –20°C until needed for protein determination, done by the BCA method (Pierce) using bovine serum albumin (BSA) as the standard.

2.2. Cytochrome Oxidase Histochemistry

2.2.1. Animal Tissue Preparation. All experiments were carried out in accordance with the National Institute of Health guide for the care and use of Laboratory animals (NIH Publications No. 80-23, revised 1978). All efforts were made to prevent animal suffering, to reduce the number of animals used, and to utilize alternatives to *in vivo* techniques, when available.

Adult animals of both sexes (BALB/c mice or Swiss Webster mice, Sprague-Dawley rats, and *Macaca mulatta* or *Macaca fascicularis* monkeys) were deeply anesthetized with an intraperitoneal injection of sodium pentobarbital (35 mg/kg body weight for mice and rats; 55 mg/kg for monkeys) or of chloral hydrate (0.4 mg/g body weight for rats) (Wong-Riley and Carroll, 1984b; Hevner et al., 1995; Nie and Wong-Riley, 1996c). They were perfused intracardially with an initial warm (37°C) 0.1 M phosphate buffered saline (PBS) followed by cold (4°C) fixative. We have tried a number of fixatives with comparable results: 4% paraformaldehyde, 4% paraformaldehyde and 0.1% to 0.5% glutaraldehyde, or 2.5% paraformaldehyde and 1.5% glutaraldehyde, all in 0.1 M sodium phosphate buffer, pH 7.4, in 4% sucrose. In general, glutaraldehyde was excluded for immunohistochemistry but included for electron microscopy. After 1 hr of postfixation in the same fixative, brain tissues were cryoprotected in 10%, 20%, and 30% sucrose in 0.1 M phosphate buffer. They were frozen-sectioned at 15–30 μm thickness.

We have also studied brains of bats, cats, ferrets, tree shrews, squirrel monkeys and human (Wong-Riley, 1979; Carroll and Wong-Riley, 1984; Kageyama and Wong-Riley, 1982, 1984; Wong-Riley and Norton, 1988; Wong-Riley et al., 1993) as well as neural crest cells in culture (Liu et al., 1990). The details of those protocols can be found in the respective references.

2.2.2. Light Microscopic Histochemistry. Our original protocol (Wong-Riley, 1979) is still being used in our laboratory. The concentrations of diaminobenzidine and cytochrome c, as well as the time of incubation, were varied according to species, age, and

brain regions. In general, primate tissue required a higher concentration of diaminobenzidine (0.05–0.06% (w/v) in 0.1 M sodium phosphate buffer and 4% sucrose for primate; 0.05% (w/v) for rodent) and cytochrome c (0.05% (w/v) for primate; 0.02–0.03% (w/v) for rodent). Sections from control and experimental preparations were incubated at the same time in the same incubation medium, with constant agitation at 37°C. Rodent tissue required less incubation time (~1–2 hr) than that of primate (~4–6 hr). The sections were then rinsed in 3 changes of the same buffer, and mounted with filtered tap water.

We prefer not to use any heavy metals such as cobalt or nickel in the incubation medium for enhancement purposes. They tend to cause structural disruption undesirable for electron microscopy, and the heavy deposit of reaction product tend to obliterate heterogeneous enzyme distribution among brain regions. We found a #47 Wratten blue filter to be sufficient for contrast enhancement.

2.2.3. Electron Microscopic Cytochemistry. The protocol for EM study is again as described before (Wong-Riley, 1979). Briefly, the fixative used was 2.5% paraformaldehyde and 1.5% glutaraldehyde in 0.1 M phosphate buffer with 4% sucrose, pH 7.4. Brain blocks were postfixed in the same fixative for 1 hr followed by three washes in the same buffer. They were sectioned with a Vibratome at 60 μm thickness, and were processed for CO cytochemistry. After incubation, regions of interest were dissected with a blade or trepanated with a modified hypodermic needle (23 or 25 gauge) under the dissecting microscope. They then underwent osmication in 0.5% osmium tetroxide for 1 hr at room temperature (RT), were dehydrated in an alcoholic series, and were embedded in Epon or Durcupan resin.

2.3. Antibody Generation against Cytochrome Oxidase Subunit Polypeptides

Previously, we have generated polyclonal antibodies against brain cytochrome oxidase holoenzyme (Hevner and Wong-Riley, 1989). In immunoblots, these antibodies reacted strongly with subunit IV and much less so with subunits II and I. For subunit-specific antibodies, we used synthetic peptides as antigens. Based on the peptide sequence program of GCG Database, short-chain amino acid sequences of CO subunits were chosen for their high antigenicity index and synthesized on a MilliGen 9050 peptide synthesizer using the solid phase method. The sequences used for CO IV precursor protein, CO III and CO Vb subunit polypeptides were reported previously (Liu and Wong-Riley, 1994; Nie and Wong-Riley, 1996c). The synthetic peptides were coupled to the carrier protein keyhole limpet hemocyanin (KLH) with a glutaraldehyde link, and were used as antigens for the generation of polyclonal antibodies. IgG purification, enzyme-linked immunosorbent assay (ELISA), gel electrophoresis, immunoblotting, and appropriate controls were performed for each set of antibodies as described before (Hevner and Wong-Riley, 1989; Liu and Wong-Riley, 1994; Nie and Wong-Riley, 1996c).

2.4. Cytochrome Oxidase Immunohistochemistry

2.4.1. Light Microscopic Immunohistochemistry. Protocols were as described previously (Hevner and Wong-Riley, 1989). Free-floating sections were blocked for 12 hr at 4°C in phosphate buffered saline-nonfat dry milk mixture (PBS-NFDM) containing 1% Triton X-100 and 5% (v/v) normal goat serum (NGS). After rinsing in PBS, sections were incubated in primary antibodies diluted in PBS-NFDM with 1% Triton X-100 and 5%

NGS for 4 hr at RT, then for 24 hr at 4°C. The concentrations of various primary antibodies were as follows: (a) anti-CO holoenzyme (anti-CO) at 1: 5,000; (b) anti-CO subunit III (anti-CO III) at 1:2000; (c) anti-CO subunit Vb (anti-CO Vb) at 1:2000; and (d) anti-CO subunit IV precursor protein (anti-pCOIV) at 1:2,000–10,000. The sections were rinsed, then incubated with secondary antibodies (Bio-Rad blotting grade goat anti-rabbit conjugated to horseradish peroxidase (GaR-HRP)) at 1:100 in PBS-NFDM with 5% NGS for 12 hr at 4°C. The sections were again rinsed in 0.1 M PBS, pH 7.0, then incubated in the same buffer with 0.05% (w/v) 3,3′diaminobenzidine-4HCl (DAB) and 0.004% (w/v) H_2O_2 for 5–10 min at RT. The DAB-reacted sections were rinsed with PBS, then mounted and coverslipped by standard procedures. Immunohistochemical controls (pre-immune sera, IgGs preadsorbed with the corresponding antigen, or no primary antibodies) were run with all tissues and processed identically with other sections.

2.4.2. Cytochrome Oxidase Postembedding Immuno-Electron Microscopy. Protocols were as described previously (Liu and Wong-Riley, 1994; modified in Nie and Wong-Riley, 1996c). Ultrathin sections of Durcupan-embedded brain tissue were cut and placed on nickel mesh grids. They were treated with 4% aqueous solution of sodium metaperiodate for 40 min and rinsed three times in distilled water. They were then placed in Tris (10 mM) phosphate (10 mM) buffered isotonic saline (TPBS), pH 7.6, containing 0.1% Triton X-100 and 1% NGS for 30 min. Grids were then transferred to drops containing the affinity-purified primary antibodies (anti-pCOIV IgG at 1:100–200; anti-CO III IgG at 1:100, or anti-CO Vb IgG at 1:100) in the same TPBS buffer for 6 hr or more at RT. Sections were then rinsed three times in TPBS and incubated in the secondary antibodies (goat anti-rabbit IgG conjugated to 10 nm colloidal gold; Amersham) diluted 1:15 in TPBS, pH 8.2, for 2 hr at RT. They were rinsed again in TPBS and distilled water, and were stained with alcoholic uranyl acetate and lead citrate. To evaluate the specificity of these antibodies, sections were processed in the same way as described above, except that the primary antibodies were preadsorbed with their corresponding subunit synthetic peptide-glutaraldehyde-KLH conjugate, or replaced with preimmune sera.

2.5. Combined Cytochrome Oxidase Histochemistry and Immunohistochemistry

2.5.1. Double Labeling of Cytochrome Oxidase: Histochemistry and Immunohistochemistry on the Same Section. Frozen sections were reacted for CO histochemistry followed by CO immunohistochemistry by means of the immunogold silver staining (IGSS) technique (modified from Luo et al., 1989; Zhang and Wong-Riley, 1996). The C.O.-reacted sections were first blocked in 10% normal goat serum (NGS) in phosphate buffered saline, pH 7.6 (PBS) overnight at 4°C. Anti-CO IgG was diluted in 5% NGS to 1:100,000 and applied to sections for 4 hr at room temperature and overnight at 4°C. After incubation with immunogold (goat anti-rabbit IgG, 10 nm gold conjugate, 1:100 in PBS) for 4 hr at room temperature, signals were detected with IntenSE M (Amersham, Arlington Heights, IL) for 18–21 min in the dark. Between steps, sections were rinsed in PBS three times. Prior to, and after, IntenSE M the sections were rinsed with filtered tap water.

2.5.2. Double Labeling of Cytochrome Oxidase and Other Neurochemicals at the Light Microscopic Level. The protocol was the same as the above, except that the primary antibodies were different (e.g., GABA), and their concentrations were determined empirically (Luo et al., 1989; Zhang and Wong-Riley, 1996).

2.5.3. Double Labeling of Cytochrome Oxidase and Other Neurochemicals at the EM Level. For double labeling of cytochrome oxidase and other neurochemicals, such as GABA and glutamate, Vibratome sections were first reacted for cytochrome oxidase histochemistry and core samples were taken with a modified #25 gauge hypodermic needle. They were postfixed for 1 hr in 1% osmium tetroxide in 0.1 M phosphate buffer, pH 7.35, at 4°C, rinsed in the same buffer, dehydrated, embedded in Durcupan ACM (Fluka), and cured for 72 hr at 56°C. Ultrathin sections were cut from the superficial 5μm where cytochrome oxidase reaction product was clearly visible, and were processed for post-embedding immuno-EM as described above in section 2.4.2. Primary antibodies against GABA were kindly provided by Dr. P. Somoghy, and were used at a concentration of 1:1,000. Anti-glutamate antisera (Arnel Co.) were used at a 1:4,000 dilution. The level of CO reactivity was assessed by the extent to which the inner membrane of mitochondria was covered by reaction product: greater than 50% was considered as darkly-reactive, less than 50% but still detectable was considered as moderately-reactive, while those with undetectable levels of reaction product were classified as lightly-reactive (Wong-Riley et al., 1989a).

2.6. Experimental Paradigms

For monocular enucleation, the right eyes of adult rats or mice were removed by surgical excision under anesthesia (chloral hydrate 0.4 mg/g body weight), and the animals survived from 1 to 18 days.

For monocular tetrodotoxin (TTX) injections, 19 μg of TTX dissolved in 10 μl of sterile distilled water was injected into the left eyes of adult monkeys under acepromazine (0.8 mg/kg) and Ketamine (40 mg/kg) anesthesia (Wong-Riley and Carroll, 1984b; Hevner and Wong-Riley, 1990). This dosage blocks action potentials without blocking axoplasmic transport in retinal ganglion cells (Wong-Riley and Riley, 1983), and the effect was entirely reversible (Wong-Riley, 1989; Wong-Riley et al., 1989a). The action of TTX was confirmed by an absence of the pupillary light reflex, which did not return for at least four days after a single injection. Injections were done twice a week, and animals survived for varying periods of time.

2.7. Optical Densitometry

A Zeiss Zonax MPM 03 photometer system was used. Lighting conditions were held constant between sections and cell types. The background was subtracted by setting zero over a blank area in each slide. For cellular measurements, optical density readings (arbitrary units) were taken from perikarya in different sections of each animal. The mean optical densities of each cell type in individual animals were then averaged across animals (Wong-Riley and Kageyama, 1986; Hevner et al., 1995).

2.8. Brain Cytochrome Oxidase Subunit cDNAs: Isolation and Characterization

The following protocols were based on our recently published report (Wong-Riley et al., 1997a).

2.8.1. Isolation of CO Subunits III and VIa. Oligonucleotides were synthesized as primers for isolating CO subunits III (mitochondrial) and VIa (nuclear) from a mouse brain cDNA library. Synthesis was done by the Protein/Nucleic Acid Shared Facility of the Medi-

cal College of Wisconsin. Each set of primers corresponded close to or at the 5′ and 3′ ends of known rodent CO III (mouse L cell; Bibb et al., 1981) and CO VIa genes (rat liver; Schlerf et al., 1988), respectively. Primers 1 and 2 for CO III were: 5′-ACTCATGCATAT-CACATAGTTA-3′ and 5′-AATGGAGACGTATAGGAAAAG-3′, corresponding to nucleotides #13–34 at the 5′ end and nucleotides #748–768 at the 3′ end, respectively. Those for CO VIa were: 5′-CGAGTGGCGCCCACGG-3′ and 5′-ATCTTCATAGCCAGTCGGAA-3′, corresponding to nucleotides #2–17 at the 5′ end and nucleotides #233–252 at the 3′ end, respectively. All primers were designed to have a Tm of 58°C. Synthesized primers were desalted and used in a polymerase chain reaction (PCR) to isolate and amplify CO III and VIa genes from a murine brain cDNA library (Stratagene, La Jolla, CA). PCRs were done with a hot start and 30 cycles of denaturation (94°C), anneal (53°C) and elongation (72°C). Amplified PCR products were run on a 1.5% low-melting agarose gel, stained with ethidium bromide, determined to be of the correct sizes, excised from the gels, transferred onto DEAE-cellulose membrane, eluted with high-salt (1 M NaCl) elution buffer, extracted with phenol-chloroform and precipitated with ethanol (Sambrook et al., 1989).

2.8.2. Subcloning and Sequencing. The isolated CO III and VIa cDNAs were blunt-end treated with Klenow fragment of E. coli DNA polymerase I and subcloned into the EcoRV position within the multiple cloning site (MCS) of plasmid vector pBluescript II KS(+) (Stratagene), which contained phage T3 and T7 promoters flanking the MCS. Some PCR products were subcloned directly into the EcoRI site of plasmid pCR™II (TA cloning kit, Invitrogen, San Diego, CA) which contained phage SP6 and T7 promoters. Both plasmids have the lacZ gene for blue/white color selection and the Ampicillin resistance gene. The plasmids with inserts were amplified in white colonies of transformed DH5a cells or OneShot competent cells (Invitrogen) and purified on a Qiagen plasmid column, according to the manufacturer's instructions (Qiagen, Chatsworth, CA). Purified plasmids were then subjected to restriction enzyme digest (EcoRV for pBluescript II KS(+) and EcoRI for pCR™II plasmid inserts, respectively) for confirmation that inserted DNAs were of the correct sizes. Insert DNAs were then sequenced by the dideoxy sequencing method of Sanger et al. (1977) using the Sequenase version 2.0 reaction, according to the manufacturer's instructions (US Biochemical, Cleveland, OH).

2.8.3. Riboprobe Synthesis. Purified plasmids of CO III and VIa were linearized by restriction enzyme digestion (Sambrook et al., 1989). Antisense and sense riboprobes were generated by *in vitro* transcription using sets of restriction enzymes and RNA polymerases (Hind III and T7 for CO III antisense, and EcoRI and T3 for CO III sense for inserts cloned in pBluescript II KS(+); BamHI and T7 for CO VIa antisense, and EcoRV and Sp6 for CO VIa sense for inserts cloned in plasmid pCR™II). Riboprobes were labeled with a-^{35}S-thioUTP (uridine 5′-[a-^{35}S-thio]triphosphate; 1250 Ci/mmol from Amersham) as described previously for light microscopic *in situ* hybridization (Hevner and Wong-Riley, 1991) or with Digoxigenin-11-UTP (Boehringer-Mannheim, Indianapolis, IN) according to the manufacturer's instructions. Digoxigenin-labeled antisense and sense riboprobes were analyzed for size in a 1.2% denaturing agarose gel with formaldehyde, transferred to positively-charged nylon membrane (Qiabrane Plus, Qiagen), and detected with Lumi-Phos 530 chemiluminescence according to the manufacturer's instructions (Genius System, Boehringer Mannheim).

2.8.4. Northern (RNA) Hybridization. Total RNA was purified from brains of mice by extraction with guanidine isothiocyanate followed by cesium chloride gradient

(Ausubel et al., 1994). RNA yield was ~0.6 mg/gm brain. Formaldehyde agarose gel electrophoresis was used to separate RNA by size (Ausubel et al., 1994) and RNAs were transferred by capillary action to positively-charged nylon membrane. Prehybridization, hybridization, wash, and chemiluminescent detection with Lumi-Phos 530 were done according to manufacturer's protocols (Genius System, Boehringer Mannheim). Digoxigenin-labeled antisense probes for mouse CO III and VIa were used at a concentration of 50 ng/ml hybridization solution for both, and hybridizations were done overnight at 50°C for CO III and 65°C for CO VIa. Detection was carried out with anti-Digoxigenin Fab fragments conjugated to alkaline phosphatase, followed by Lumi-Phos 530 reaction with conjugates, and exposure of reacted blots to Kodak XAR-5 film.

2.8.5. Animal Preparation. For light microscopic *in situ* hybridization, the animals were deeply anesthetized with chloral hydrate (0.6 mg/g body weight), decapitated, and the brains were immediately removed and frozen on dry ice. For EM *in situ* hybridization, the animals were anesthetized and perfused with an initial 0.1 M sodium phosphate buffered saline (PBS) flush (pH 7.35) followed by a mixture of 4% paraformaldehyde and 0.1% glutaraldehyde in 0.1M sodium phosphate buffer (pH 7.35) and 4% sucrose at 4°C. The brains were postfixed in 4% paraformaldehyde in phosphate buffer for 2 hr at 4°C, rinsed in PBS, then in 0.1M phosphate buffer with 15% sucrose overnight at 4°C. Vibratome sections were cut and processed as indicated below.

2.8.6. Light Microscopic in Situ Hybridization. Frozen 10 μm sections of mouse brains were cut on a cryostat, thaw mounted on slides coated with gelatin (300 Bloom, Sigma, St. Louis, MO)/chromium potassium sulfate, and frozen at −80°C until the day of use. Solutions for *in situ* hybridization were treated with 0.1% diethylpyrocarbonate (DEPC) to destroy RNAse activity and autoclaved (Sambrook et al., 1989). Protocols for *in situ* hybridization of cryostat sections were as described previously (Hevner and Wong-Riley, 1991) using single-stranded riboprobes labeled to a specific activity of ~3×10^8 dpm/μg with a-^{35}S-thioUTP (1250 Ci/mmol; Amersham). Antisense riboprobes were used to hybridize with CO III and CO VIa mRNAs, respectively, and sense riboprobes for each of the two CO subunits were used as controls for nonspecific binding.

2.8.7. Electron Microscopic in Situ Hybridization. Digoxigenin-labeled RNA probes were applied to Vibratome sections. The protocols were modifications of the manufacturer's instructions (Boehringer-Mannheim) and of Trembleau et al.'s procedures (Trembleau et al., 1994). Briefly, 40–60 μm sections were cut with a Vibratome and incubated for 1 hr at 37°C in a prehybridization solution consisting of 4x SSC, 1x Denhardt's solution, and 10 μg/ml wheat germ tRNA. They were immersed overnight at 37°C in the hybridization solution consisting of 50% formamide, 600 mM NaCl, 80 mM Tris-HCl, pH 7.5, 0.1% sodium pyrophosphate, 4 mM EDTA, 10 μg/ml wheat germ tRNA, and 10 nM of nonradioactive probes. The sections were then washed in 2x SSC followed by 0.1x SSC at 37°C and immersed in PBS. Digoxigenin-labeled probes were detected by means of immunohistochemical reaction consisting of an overnight incubation at 4°C in sheep anti-Digoxigenin antibody (Boehringer-Mannheim) diluted (1:1,000) in PBS-BSA. After washing in PBS, the sections were incubated with a biotinylated anti-sheep antibody (Vector, Burlingame, CA) (1:200 in PBS-BSA) for 2 hr at RT followed by an incubation in avidin-biotin-peroxidase complex (ABC, Vector) diluted in PBS, according to the manufacturer's instructions, for 2 hr at RT. Sections were rinsed in PBS and reacted in 0.025% DAB and 0.006% hydrogen peroxide in 50 mM Tris buffer, pH 7.6. The reaction was monitored un-

der a light microscope and was arrested by transfer into PBS. They were then osmicated and processed for EM (Wong-Riley et al., 1997a). Sections serial to those processed for *in situ* hybridization were reacted histochemically for CO activity by our published method (Wong-Riley 1979) modified for cryostat sections (Hevner and Wong-Riley, 1991).

3. METABOLIC MAP OF CYTOCHROME OXIDASE IN THE RAT BRAIN

3.1. Biochemical Assays of the Rat Brain

We have optimized a spectrophotometric method (Errede et al., 1978; Wharton and Tzagoloff, 1967) for determining the full activity of cytochrome oxidase in rat brain tissue homogenates (Hevner et al., 1993). Whole brain CO activity was determined to be 158 ± 5 U/g tissue, and specific CO activity in the whole brain was 1760 ± 100 mU/mg protein. Based on the data of Brown et al. (1991), who reported that the adult Sprague-Dawley rat brain contains 5.5 nmol cytochrome aa_3/g tissue, and our value of 158 ± 5 U/g tissue, we calculated a molecular activity or turnover number of the rat brain CO to be 479 s^{-1}. This value is in the upper range of maximal turnover numbers reported previously (Smith and Camerino, 1963; Vanneste et al., 1974; Rosevear et al., 1980; Vik and Capaldi, 1980), indicating that the full activity of CO was detected.

Compared to the whole brain, most regions of gray matter had about the same content of CO activity, and surprisingly little variation was seen among regions such as the cerebellar cortex, caudate nucleus, and thalamus. Likewise, none of the white matter regions differed significantly from one another in their CO activity. The CO activity content (by wet weight) was generally about 10- to 12-fold higher in gray matter than in white matter (Fig. 3A), while the specific activity of the enzyme was about 8- to 10-fold higher in gray than in white matter (Fig. 3B). The greater difference for CO activity content is related to the fact that white matter had a lower protein content than did gray matter. Statistically significant differences were found on all pair-wise comparisons between gray and white matter regions, for both CO activity content and CO specific activity ($P < 0.001$ for each comparison, one factor ANOVA with least significant difference test). However, CO levels differed little or not at all among major brain regions of the same type (i.e. gray or white matter) when relatively large brain regions (e.g. entire thalamus, hippocampus, etc.) were sampled biochemically.

3.2. Cytochrome Oxidase Histochemical Patterns

In contrast to the relatively homogeneous data obtained biochemically from gray matter regions, histochemically reacted sections show a distinctly heterogeneous pattern among and within all brain regions examined. Figure 4 is a representative horizontal section of the rat brain reacted histochemically for CO (Hevner et al., 1995). It is clear that (a) gray matter has higher CO activity than does white matter; (b) the intensity of staining in gray matter areas vary markedly among different structures; (c) CO reactivity in gray matter is not correlated with the density of neuronal cell bodies; for example, granule cells of the dentate gyrus have low levels of CO; and (d) the neuropil is not consistently high in CO.

3.3. Cytochrome Oxidase Densitometry

Optical densitometry provides a semi-quantitative analysis of relative CO activity in histochemically reacted sections (Kageyama and Wong-Riley, 1985; Mjaatvedt and Wong-

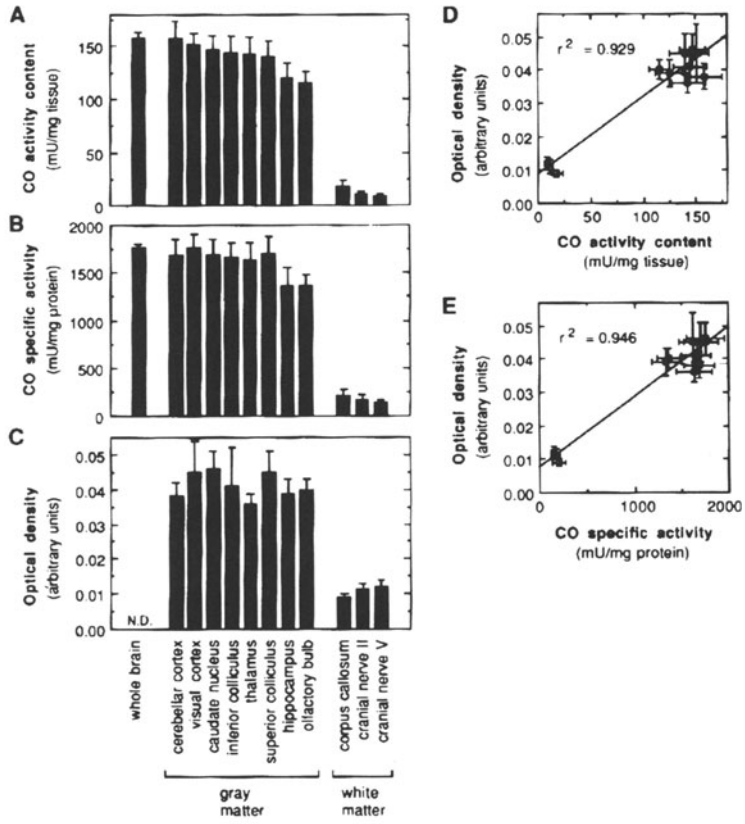

Figure 3. Cytochrome oxidase activity in the whole rat brain and in various gray matter and white matter areas. CO activity content (by tissue wet weight) (**A**) and CO specific activity (**B**) were determined by biochemical assays of tissue homogenates. Optical density measurements were done on CO histochemically reacted sections from the same areas (**C**). In comparing these approaches (**D** and **E**), it is clear that CO activity was well correlated with histochemical staining intensity. All data shown as mean ± SEM. N.D., not determined. (Taken from Hevner et al., 1995).

Riley, 1986; Wong-Riley and Norton, 1988; Gonzalez-Lima and Garrosa, 1991; Nobrega et al., 1993). When it was done on large brain regions (using a large diameter aperture of 625 μm), the values were found to be similar to those from biochemical assays (Hevner et al., 1995). Gray matter regions stained darker than did white matter regions in all cases ($P < 0.001$ for all pairwise gray-white comparisons), but within groups of gray or white matter regions, no significant differences of staining intensity were found (Fig. 3C). Linear regression analysis showed that CO staining intensity was highly correlated with both the CO activity content (by wet weight) (Fig. 3D; $r^2 = 0.929$) and the CO specific activity (Fig. 3E; $r^2 = 0.946$) in regions of gray and white matter.

When individual neurons were analyzed densitometrically by means of a small diameter aperture (2 μm), staining intensities were found to vary widely, spanning almost a two-fold range of optical density values (Hevner et al., 1995). Among the different types examined, neurons of the mesencephalic trigeminal nucleus had the highest optical density. That value was significantly greater than in any other neuron type examined ($P < 0.05$ for all pairwise comparisons, one-factor ANOVA with least significant difference test), and was 78% higher than in dentate granule cells (the lightest stained cell type examined).

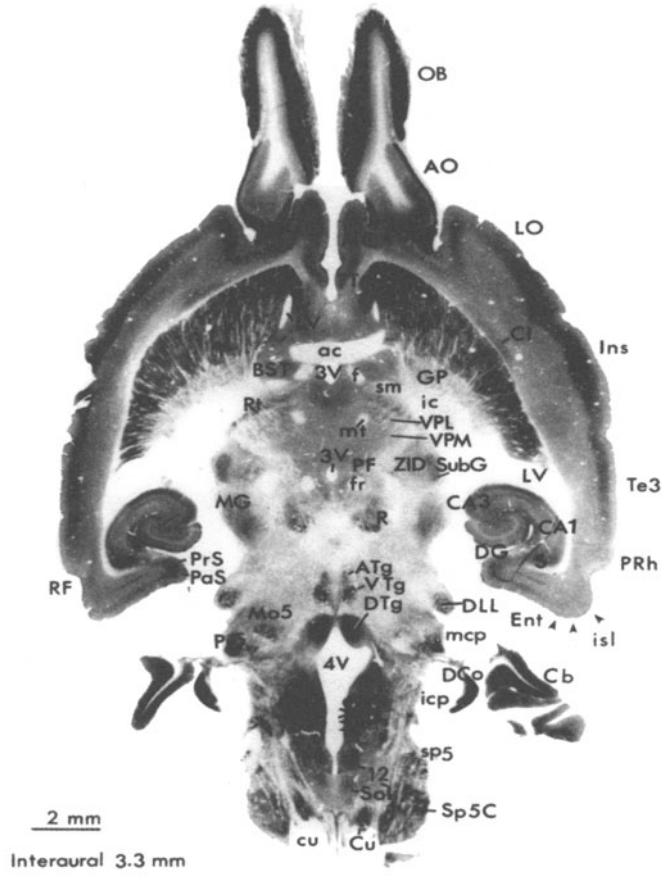

Figure 4. Cytochrome oxidase histochemically-reacted horizontal section through the whole rat brain. Note the heterogeneous pattern of enzyme distribution in various parts of the brain. (Taken from Hevner et al., 1995: see reference for keys to abbreviations).

Even within the same brain region, closely related neuron types had significantly different optical density values. CA3 pyramids of the hippocampus, for example, was significantly more reactive than CA1 pyramids ($P < 0.05$) (Hevner et al., 1995). This was consistent with our earlier data based on EM cytochemistry of the hippocampus (Kageyama and Wong-Riley, 1982).

3.4. Comparison with 2-deoxyglucose

The observed patterns of CO activity were mostly similar to the reported patterns of 2-deoxyglucose (2-DG) uptake in conscious, "resting" animals (Sokoloff et al., 1977; Schwartz and Sharp, 1978), though some differences were found. For example, whereas 2-DG uptake was about three-fold higher in gray matter than in white matter (Sokoloff et al., 1977), cytochrome oxidase activity was about 8- to 12-fold higher. This and other discrepancies probably reflect basic differences between these two methods (DiRocco et al., 1989). Compared to 2-DG, CO is more specific for oxidative rather than glycolytic metabolism, and more reflective of overall neuronal functional activity occurring over longer time periods lasting hours to weeks, rather than minutes. The anatomical resolution of

cytochrome oxidase histochemistry is also finer than that of 2-DG, extending to the electron microscopic level.

4. ULTRASTRUCTURAL LOCALIZATION OF CYTOCHROME OXIDASE

4.1. Mitochondria Constitute a Heterogeneous Population Even within a Single Neuron

What is the subcellular basis for variations in energy metabolism among neurons and even among compartments of a single neuron? The answer lies in the organelle of oxidative energy metabolism, the mitochondrion. Extensive quantitative analysis at the electron microscopic level indicates that mitochondria differ in size, shape, and cytochrome oxidase content among neurons and among compartments of a single neuron (Kageyama and Wong-Riley, 1982; Carroll and Wong-Riley, 1984; Wong-Riley and Carroll, 1984a; Kageyama and Wong-Riley, 1985; Mjaatvedt and Wong-Riley, 1988; Wong-Riley et al., 1989a,b; Wong-Riley et al., 1994; Nie and Wong-Riley, 1996c). Mitochondria exhibit varying degrees of CO reactivity that falls on a continuum, but they can be subdivided into three major categories: darkly reactive ones have more than 50% of their inner mitochondrial membrane occupied by detectable reaction product; lightly reactive ones have little or no detectable amount of reaction product; and moderately reactive ones are in between (Fig. 5A-C). Dendrites of almost all cells contain mitochondria that are darkly and moderately reactive for CO; while

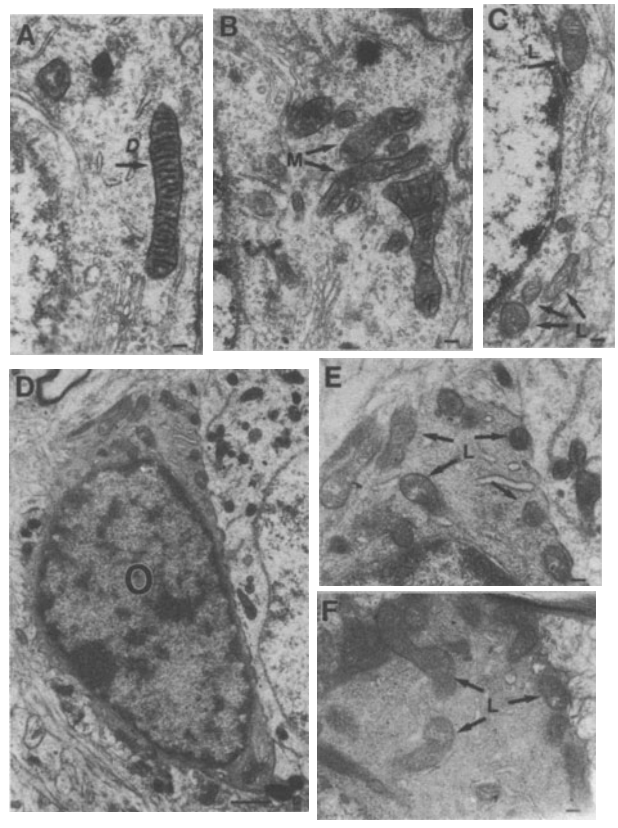

Figure 5. Examples of perikaryal mitochondria that are (**A**) darkly-reactive (D and arrow), (**B**) moderately-reactive (M and arrows), and (**C**) lightly-reactive (L and arrows) for cytochrome oxidase (see section 2.5 in the text for classifications). (**D**) The perineuronal oligodendrocyte (O) has electron dense cytoplasm but only lightly-reactive mitochondria, while the neuron on its right has electron lucent cytoplasm but much more CO-reactive mitochondria. (**E**) An enlargement of the upper portion of D, showing lightly-reactive mitochondria (L and arrows). (**F**) Lightly-reactive mitochondria in another oligodendrocyte. Scale bars in A-C and E-F: 0.1 μm. Scale bar in D: 1 μm. (Taken from Wong-Riley et al., 1994).

cell bodies and axon trunks, in general, have relatively small mitochondria that are only lightly reactive for CO. There is a positive relationship between the mean size of mitochondria and their level of CO, and the mean size of darkly reactive mitochondria in axon trunks can be significantly smaller than those in dendrites (Fig. 6C; see also Wong-Riley et al., 1989b). This indicates that mitochondria in one neuronal compartment may not intermix extensively with those in other compartments, suggesting that these distinct subpopulations may sense and respond to local energy demands.

4.2. Neuron versus Glia

While neurons are known to be highly dependent on oxidative metabolism for their energy supply, glial cells may be more reliant on anaerobic glycolysis. While there is a relatively low concentration of glycogen in the brain, it resides mainly in astrocytes (Siegel et al., 1989), and glycogen phosphorylase is also distributed primarily in astrocytes (Ignacio et al., 1990; Pfeiffer et al., 1990). At the electron microscopic level, both oligodendrocytes and astrocytes have relatively little cytoplasm and a sparse number of mitochondria, most of which are only lightly reactive for cytochrome oxidase (Wong-Riley et

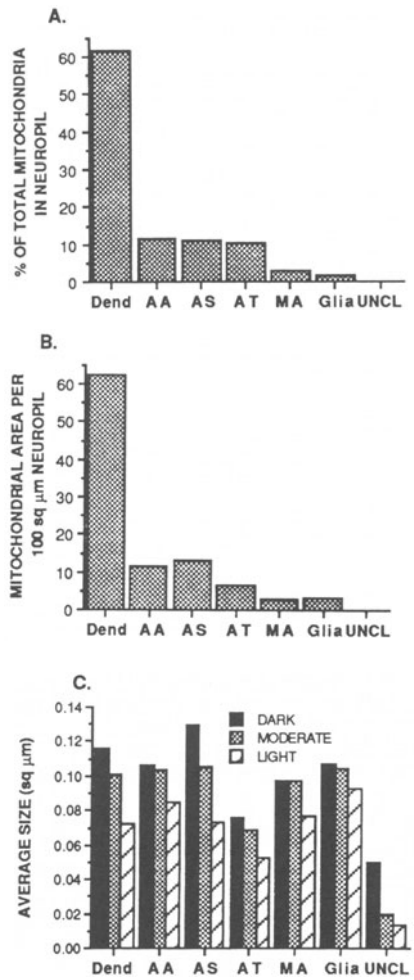

Figure 6. Quantitative analysis of mitochondria in the neuropil of the primate visual cortex. (**A**) Percentage distribution of mitochondria in various profiles of the neuropil. (**B**) Areal density of mitochondria in various profile per unit area of the neuropil. 60% of mitochondria by count and area reside in dendrites (Dend). (**C**) Comparisons of the mean size of dark, moderate, and lightly reactive mitochondria in various neuropil profiles. A positive relationship exists between the mean size and reactivity of mitochondria, but the mean sizes differ among the profile types. AA, axon terminals making asymmetric (presumed excitatory) synapses; AS, axon terminals making symmetric (presumed inhibitory) synapses; AT, axon trunk; MA, myelinated axons; UNCL, unclassified profiles. (Taken from Wong-Riley et al., 1989b).

al., 1994) (Fig. 5D-F). In the neuropil of macaque cortical puffs, only 2% of the mitochondria reside in glia, as compared to about 60% in dendrites (Wong-Riley et al., 1989b) (Fig. 6A,B). The majority of glial processes contain few, if any, mitochondria, and most of them are only lightly reactive for cytochrome oxidase. The glial limitans and a few reactive astrocytes are more darkly reactive for cytochrome oxidase, but their mitochondrial content is relatively low compared to neurons. Thus, cytochrome oxidase is an indicator of primarily *neuronal* energy metabolism. Markers of glucose uptake, such as 2-deoxyglucose (Sokoloff et al., 1977), potentially label both neurons and glia because glucose is metabolized via either the oxidative or the glycolytic pathway. Significantly, under conditions in which neurons die, glial cells survive and may even proliferate to produce gliosis.

5. SPIKING ACTIVITY VERSUS SLOW POSTSYNAPTIC DEPOLARIZING ACTIVITY: DENDRITES ARE THE MAIN CONSUMERS OF ENERGY

Neuronal activity has often been regarded as synonymous with spiking activity, whether spontaneous or evoked. Indeed, high oxidative demand in neurons has been positively correlated with a high level of maintained or synaptically evoked activity (Schwartz et al., 1979; Mata et al., 1980; Mawe and Gershon, 1986). How well does spiking activity correlate with cytochrome oxidase levels? This issue was recently examined in the primate visual cortex (DeYoe et al., 1995). In layer 4C, which receives potent thalamic input, the background multiunit spike rate is the highest among the layers, and cytochrome oxidase staining is also the most intense. However, this relationship does not hold in layer 4B where the densely myelinated axonal plexus gives rise to high spiking rates, but cytochrome oxidase activity is relatively low. The same is true for the white matter in general.

How do we reconcile such discrepancies? The answer becomes clearer when we consider the fact that spiking activity utilizes only 0.3 to 3.0% of the energy consumption of the cortex (Creutzfeldt, 1975). Spiking activity is the consummate output of the neuron or neuronal population, but the true business end of a neuron is its vast dendritic tree, which is the major receptive site of synaptic input. Local, slow depolarizing activities in dendrites impart a high energy cost for membrane repolarization. Such depolarizing activities may not yield action potentials and may not invade the cell bodies. Neurons meet these demands by providing a rich supply of mitochondria with high cytochrome oxidase activity mainly in dendrites rather than throughout the cell (Wong-Riley et al., 1989b). Thus, dendrites are the major energy consumers of the brain. The high energy demand of layer 4C is not incurred by action potentials, but by numerous postsynaptic depolarizing events which result from high presynaptic spiking activity. Layer 4B, on the other hand, contains few synapses, and energy demand is low there despite intense spiking activity (DeYoe et al., 1995). The negative relationship between action potentials and energy metabolism is exemplified in the white matter, which has uniformly low levels of cytochrome oxidase, glucose uptake, and blood flow (Wong-Riley, 1979; Sokoloff, 1981, Darriet et al., 1986; Hevner et al., 1995).

6. WHICH FACTOR HAS THE GREATEST INFLUENCE ON ENERGY METABOLISM IN NEURONAL CELL BODIES?

The striking difference in oxidative capacity between dendrites and axon trunks indicates that energy metabolism in neurons is controlled at a very local subcellular level.

What are the major factors that influence energy metabolism in neuronal cell bodies? Studies in the last decade have shed some light on this issue. First, the size of the cell body is a poor predictor of CO levels in the cell body. Large Purkinje cells in the cerebellum consistently exhibit low levels of enzyme; while large relay neurons in the lateral geniculate nucleus have high levels (Kageyama and Wong-Riley, 1985; Mjaatvedt and Wong-Riley, 1988). Likewise, small neurons in the spinal ventral horn often have intense enzyme staining; while those in the visual cortex usually contain low levels of enzyme (Wong-Riley and Kageyama, 1986; Wong-Riley et al., 1989a). Second, the type of neurotransmitter contained in a neuron is also a poor predictor of oxidative capacity. GABA-immunoreactive neurons in the lateral geniculate nucleus have low levels of oxidative enzymes; whereas those in the perigeniculate nucleus have high levels (Luo et al., 1989). Third, a major factor that is positively correlated with perikaryal enzyme level is the type of synapses the cell body receives. Neurons whose somata are contacted by excitatory synapses have distinctly greater CO activity than those that receive exclusively inhibitory synapses. During postnatal development, cerebellar Purkinje cells transiently express somatic spines to receive incoming excitatory climbing fiber input. This is when their cell bodies exhibit the highest level of cytochrome oxidase. When the climbing fibers move away to synapse with the newly-elaborated dendritic tree, the somatic spines retract, leaving the cell bodies with exclusively inhibitory basket cell input. The level of cytochrome oxidase drops, even though the neurons continue to enlarge in size. CO levels remain low throughout adult life (Mjaatvedt and Wong-Riley, 1988). Removal of climbing fiber input at birth severely reduces cytochrome oxidase levels in Purkinje cell bodies (Mjaatvedt and Wong-Riley, 1991). Energy metabolism in the cell bodies of developing neurons, then, is governed primarily by the proportion of excitatory and inhibitory synapses that they receive. This relationship persists into adulthood (see Section 8 below).

7. METABOLIC INHOMOGENEITY AMONG COMPARTMENTS OF SINGLE NEURONS

Ultrastructural analyses of a number of brain regions in which cell bodies are clearly separated from their dendrites and axons (such as the cerebellum and the hippocampus) have consistently shown that subcellular compartments of neurons often have distinctly different levels of cytochrome oxidase. Whereas dendrites of almost all cells are rich in CO, cell bodies can have low, moderate, or high levels of CO. Axon trunks, especially if they are myelinated, usually are CO-poor; whereas axon terminals can have varying levels of CO (Fig. 7). These findings testify to the remarkable ability of neurons to regulate their energy metabolism at exquisitely discrete local levels.

8. CYTOCHROME OXIDASE-RICH ZONES ARE DOMINATED BY EXCITATORY SYNAPSES: GABA VERSUS GLUTAMATE

What is the neurochemical basis for the metabolic inhomogeneity among neurons and among brain regions? Since depolarizing activities consume more energy for membrane repolarization than hyperpolarizing activities, one might expect CO-rich zones to receive more excitatory synapses than CO-poor ones. To explore this issue, we chose the monkey visual cortex, where a clear metabolic map has been established (reviewed in

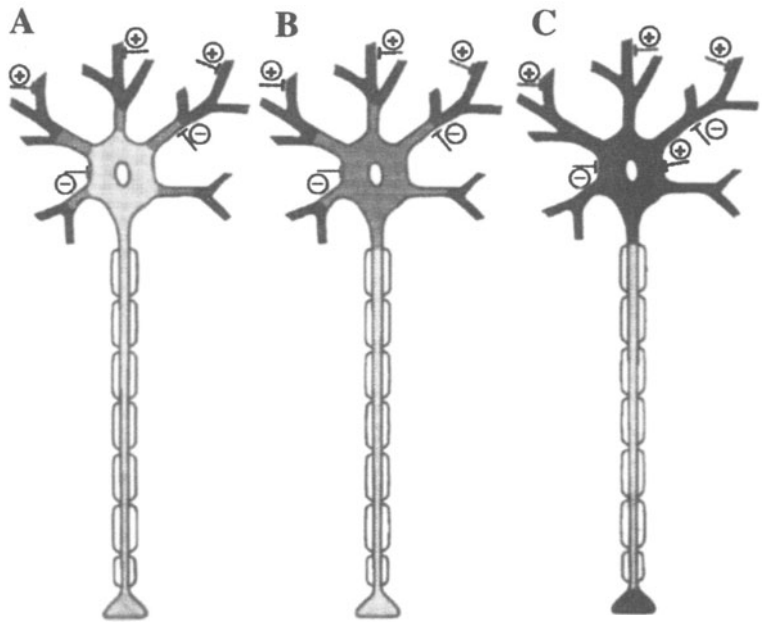

Figure 7. Schematic diagrams of the heterogeneous distribution of cytochrome oxidase within single neurons. The density of shading represents the relative levels of CO activity. The cell bodies may have (**A**) low, (**B**) moderate, or (**C**) high levels of enzyme in relation to their spontaneous activity and their synaptic inputs (+ is excitatory and − is inhibitory). The dendrites, especially the more distal ones, receive the bulk of excitatory inputs and have intense enzyme activity. Axon trunks often have low levels, while axon terminals may have high (C) or lower levels (A and B) of CO. (Taken from Wong-Riley, 1989).

Wong-Riley, 1994), and where cytochrome oxidase-rich zones exhibit a higher level of maintained neuronal activity (Livingstone and Hubel, 1984; DeYoe et al., 1995) and Na^+K^+ATPase activity (Hevner et al., 1992) relative to CO-poor ones. The question asked was whether there was a differential distribution of two major neurotransmitters in metabolically distinct zones and neurons. Glutamate is the most prevalent excitatory neurotransmitter in the brain (Fonnum, 1984; Hicks et al., 1987); while GABA is the major inhibitory neurotransmitter (Krnjevic and Schwartz, 1966; Krnjevic, 1984). By combining CO cytochemistry with GABA or glutamate immuno-electron microscopy on the *same* ultrathin sections, we analyzed the relationship between levels of CO and GABA or glutamate, respectively (Nie and Wong-Riley, 1995, 1996a,b). The results indicate that (a) the majority of neurons received exclusively GABA-IR synapses on their cell somata, and even though they were themselves Glu-IR, they exhibited low levels of CO (Fig. 8A, B). On the other hand, (b) the only type of neurons that received both Glu-IR and GABA-IR axo-somatic synapses (type C; GABA-IR) had three times as many mitochondria darkly reactive for CO than Glu-rich neurons (Figs. 8C,D and 9). (c) GABA-IR neurons in CO-rich puffs received a significantly higher ratio of Glu-IR to GABA-IR axosomatic synapses and contained about twice as many darkly CO-reactive mitochondria than those in CO-poor interpuffs. (d) There were significantly more glutamate-immunoreactive (Glu-IR) synapses and a higher ratio of Glu- to GABA-IR synapses in CO-rich puffs than in CO-poor interpuffs (Table 1). Finally, (e) Glu-IR axon terminals in puffs contained approximately three times more darkly CO-reactive mitochondria than those in interpuffs, suggesting that the former may be more tonically active. Dominance

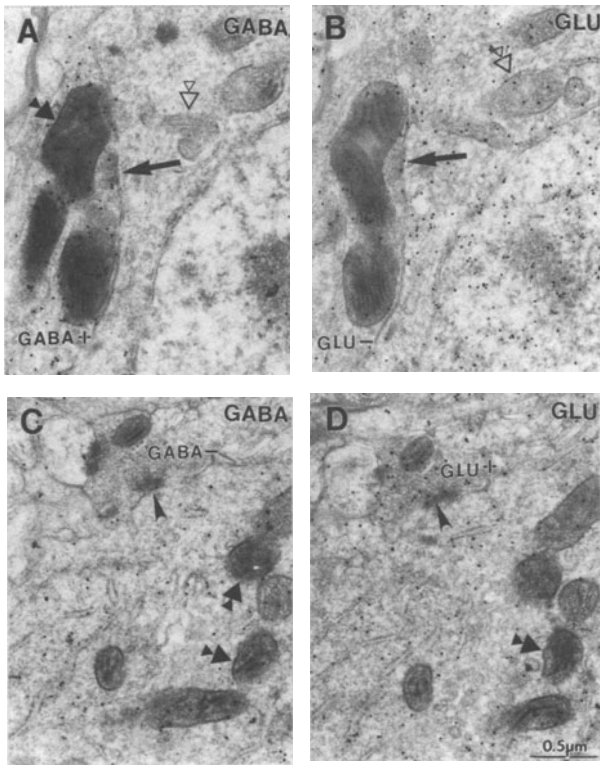

Figure 8. Double labeling of cytochrome oxidase and GABA or glutamate in the same EM section. Combined CO cytochemistry and postembedding GABA (A and C) or glutamate (B and D) immunocytochemistry were used. In the serial pair of sections (**A** and **B**), the neuron is contacted (at the arrow) by a GABA-immunoreactive terminal (A) with darkly reactive mitochondria (double solid arrows in A). The neuron itself is immunoreactive for glutamate (B), but has lightly reactive mitochondria (double open arrows). In another serial pair of sections (**C** and **D**), the neuron is contacted (at the arrowhead) by glutamate-immunoreactive terminal (D). The neuron itself is GABA-immunoreactive (C) and has darkly reactive mitochondria (double solid arrows).

by glutamatergic synaptic input is characteristic of both neurons and neuropil in the monkey visual cortex that are rich in CO. This relationship is consistent with a greater energy demand for membrane repolarization subsequent to depolarization than to hyperpolarization (Ruscak and Whittam, 1967; Lowry, 1975; Erecinska and Silver, 1989; Wong-Riley, 1989, 1994). Thus, the proportion of excitatory versus inhibitory synapses received is far more critical to the neuron's energy metabolism than the type of neurotransmitter it liberates. It is also pertinent that CO-rich neurons are more susceptible to functional insults than CO-poor ones (Wong-Riley et al., 1989a; Nie and Wong-Riley, 1996b; see also section 9.2.2. below).

The positive correlation between cytochrome oxidase levels and the prevalence of excitatory glutamatergic synapses suggests that receptors and other neurochemicals triggered by these synapses would bear a relationship with CO activity as well. As a first step in probing this relationship, we studied the distribution of *N*-methyl-D-aspartate receptor subunit 1 (NMDAR1) and nitric oxide synthase (NOS) in relationship to cytochrome oxidase in the rat brain and the macaque visual system (Zhang and Wong-Riley, 1996; Wong-Riley et al., 1998a,b). NMDA receptor is one of the major glutamate receptors strongly implicated in activity-dependent synaptic plasticity (Fagg, 1985; Collingridge and Singer, 1990; Nakanishi, 1992; Malenka and Nicoll, 1993), and NOS is the synthesizing enzyme of nitric oxide, NO, which is an inter- and intra-cellular messenger mediating a wide range of functions. NO is closely associated with and activated by NMDA receptors (Garthwaite, 1991; Dawson and Snyder, 1994). We found that brain areas and neurons with high cytochrome oxidase activity often had elevated levels of NMDAR1 and NOS, suggesting that a functional link may exist between NMDA receptor activation, NOS induction, and

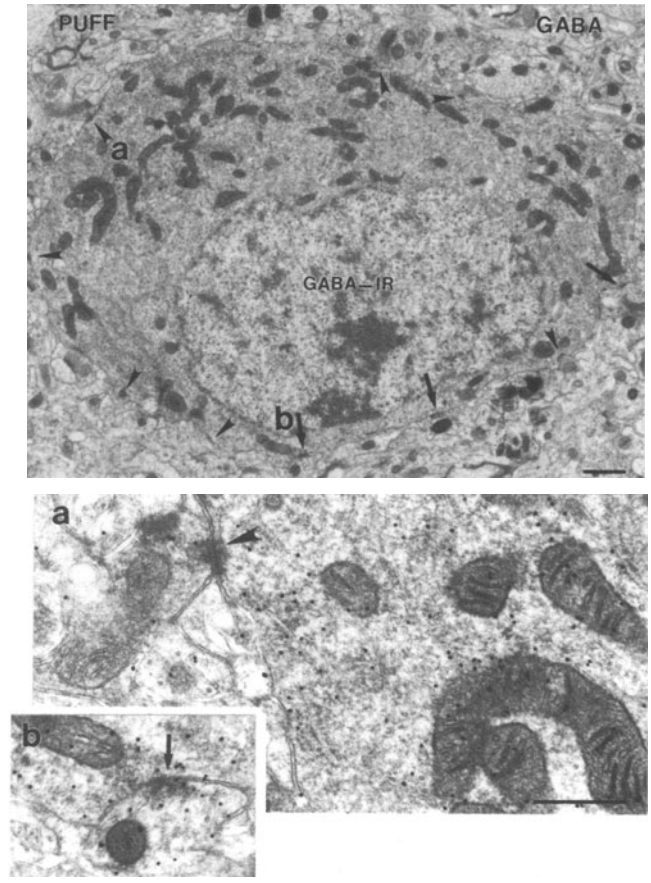

Figure 9. A neuron in the macaque visual cortex (cytochrome oxidase-rich puff) doubly labeled for CO and GABA. This cell receives 7 asymmetric synapses (presumed excitatory; one of which is enlarged in **a**) and 3 GABA-immunoreactive symmetric synapses (arrows, one of which is enlarged in **b**) in this plane of section. The cell itself is GABA-immunoreactive and has darkly-reactive mitochondria (enlarged in a). Scale bars: 1 μm. (Modified from Nie and Wong-Riley, 1995).

increased oxidative metabolism for ATP generation. With blockage of retinal impulse activities by TTX, these neuro-proteins were all down-regulated in deprived retinal ganglion cells and cortical ocular dominance columns, substantiating the activity-dependent nature of their regulation (Wong-Riley et al., 1998a,b). However, the levels of these neuro-proteins varied extensively among neurons, and no consistent relationships can be established across brain regions and neuronal subtypes.

Table 1. Comparisons of Glu-IR, GABA-IR, and non-Glu-IR/non-GABA-IR synapses in the neuropil of puffs and interpuffs[a]

Synapses per 100 μm² neuropil	Puffs		Interpuffs		Statistical comparisons
	AA[b]	AS[c]	AA	AS	
Glu-IR	24.27 ± 1.32	—	15.13 ± 0.84	—	$P < 0.001$
GABA-IR	—	10.11 ± 0.72	—	8.32 ± 0.51	$P < 0.05$
Non-Glu-IR	4.62 ± 0.25	—	2.72 ± 0.16	—	$P < 0.001$
Non-GABA-IR	—	0.40 ± 0.02	—	0.33 ± 0.14	$P < 0.05$
Ratio of Glu-/GABA-IR	2.41 ± 0.11		1.81 ± 0.08		$P < 0.01$

[a]Total count of synapses: 4,732 from puffs and 3,184 from interpuffs.
[b]Synapses from asymmetric axon terminals.
[c]Synapses from symmetric axon terminals.

9. REGULATION OF CYTOCHROME OXIDASE IN NEURONS

Despite substantial progress made in studies of brain energy metabolism, little is known of the mechanisms regulating cytochrome oxidase in neurons. Does neural functional activity signal changes in molecular activity of the enzyme or its amount? Is regulation exerted at the translational or transcriptional level? As a bigenomic enzyme, cytochrome oxidase can also serve as a useful model for the study of interactions between the nuclear and the mitochondrial genomes. This issue is particularly relevant in neurons because their extensive processes produce separation of the two genomes by great distances. How do distal dendrites and axon terminals regulate their local energy demand? Are the two genomes coordinately or disproportionately regulated in neurons? Answers to these and other questions are important for understanding the functional link between neuronal activity and energy metabolism. They are also pertinent to the appreciation of how defective energy metabolic regulation leads to neurological and muscular diseases (Morgan-Hughes, 1986; Wallace, 1992).

Two mechanisms may be involved in the regulation of CO levels in neurons: short term and long term regulation (Erecinska and Silver, 1989; Hevner and Wong-Riley, 1990). Short term regulation could involve allosteric alterations in response to local changes in the ADP/ATP ratio, pH values, and other metabolites (Erecinska and Silver, 1989). Excitatory depolarizing activity consumes energy and leads to a local increase in ADP/ATP ratio. Increased ADP could signal mitochondria to cluster in regions of high ATP demand (Bereiter-Hahn and Voth, 1983). ADP could also induce conformational changes in the enzyme and affect its kinetics (Reimann et al., 1988). Long term regulation of CO activity, on the other hand, could occur at the transcriptional and/or translational levels by affecting the number of functional enzyme molecules (Hevner and Wong-Riley, 1990, 1993). Chronic electrical stimulation of skeletal muscles in rats, for example, results in an increased expression of mRNAs for CO subunits and an elevated level of CO activity (Williams et al., 1987; Hood, 1990).

9.1. Physiological Activity of the Enzyme Reflects Its Relative Amount

Biochemical mechanisms that link functional activity and energy metabolic capacity cause CO activity levels to vary locally within neural tissue. How does CO activity relate to its amount? Two types of regulatory mechanisms can be considered under physiological conditions. If CO activity is regulated by its turnover number (molecular activity), then the amount should stay constant when variations in activity occur. On the other hand, if the activity is governed by the relative amount, then CO protein content should co-vary with the activity in different regions or cells of the brain. Many metabolic enzymes are known to be regulated at the level of amount (Schimke and Doyle, 1970), while others are known to be regulated at the level of turnover number, by mechanisms such as covalent modification (Cohen, 1980a,b).

We conducted studies to distinguish whether the amount or turnover number of CO is primarily regulated in neural tissue (Hevner and Wong-Riley, 1989; 1990). To determine the relative distribution of CO amount, antibodies against purified calf brain CO were generated and used to label CO immunohistochemically in brain tissue sections. The CO immunohistochemical pattern in each region was then compared with the CO histochemical activity pattern. Several brain regions known to have unique and characteristic patterns of CO activity were examined (e.g., hippocampus, olfactory bulb, somatosensory (barrel) cortex, cerebellum, and the primate visual cortex). In each region tested, the CO immuno-

histochemical pattern closely matched the CO histochemical pattern (Fig. 10A, B were from the monkey striate cortex). At the single cell level, a positive relationship between the relative activity of CO (shown by histochemistry) and its relative amount (indicated by the intensity of immunogold silver staining of anti-CO antibodies) in the same cell was also found (Luo et al., 1989) (Fig. 10C). Thus, under physiological conditions the heterogeneous distribution of CO molecules could account for the histochemical pattern of CO activity without postulating a major role for regulation of CO turnover number.

9.2. Regulation of Cytochrome Oxidase Protein Levels by Neuronal Functional Activity

How is CO regulated in mature neurons whose functions are perturbed? Will changes in CO activity induced by altered neural functional activity reflect changes mainly in its molecular activity or its protein content?

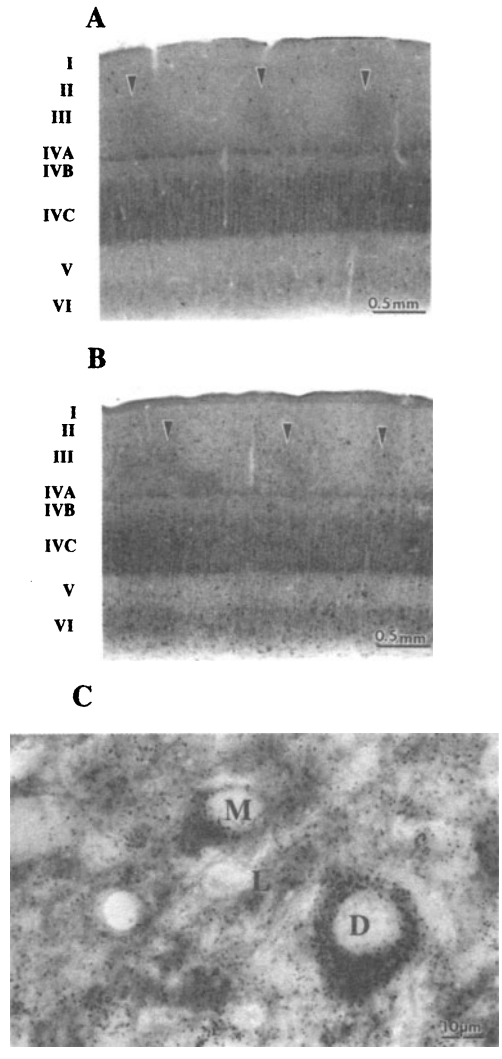

Figure 10. Cytochrome oxidase activity reflects its amount. Adjacent sections (A and B) cut perpendicular to the surface of the visual cortex from a normal macaque monkey. The layers are numbered on the left. The patterns shown by CO histochemistry (**A**) and CO immunohistochemistry (**B**) are highly comparable, and supragranular puffs (arrowheads) are in exact alignment. (**C**) A section cut from a normal cat lateral geniculate nucleus and reacted for CO histochemistry followed by CO immunogold silver staining. Note that the intensity of histochemical reaction closely matches the density of immunogold silver particles for darkly-reactive (D), moderately-reactive (M) and lightly-reactive (L) neurons. (A and B, modified from Hevner and Wong-Riley, 1990; C, modified from Luo et al., 1989).

To investigate this issue further, we injected macaque monkeys monocularly with TTX for 3–4 weeks and examined their visual system by both CO histochemistry and CO immunohistochemistry. Treatment with TTX blocks retinal impulse activity and causes CO activity to decline in laminae of the lateral geniculate nucleus (LGN) and columns of the primary visual (striate) cortex specific to the treated eye (Wong-Riley and Carroll, 1984b). CO protein levels were decreased in the same regions showing reduced CO activity (Hevner and Wong-Riley, 1990) (Fig. 11). These results suggest that CO activity is regulated mainly at the level of the local amount rather than the turnover number of the enzyme and imply that the rates of CO synthesis and/or degradation are regulated by neural functional activity.

The amount-regulated model is further supported by our ultrastructural studies which showed that the fraction of tissue volume occupied by mitochondria decreases in visual cortical puffs specific to injected-eye columns following monocular TTX treatment (Wong-Riley et al., 1989a,b). Similar correlations between changes in oxidative enzyme activities and mitochondrial volume fraction have been observed in skeletal muscle following contractile stimulation (Schwerzmann et al., 1989).

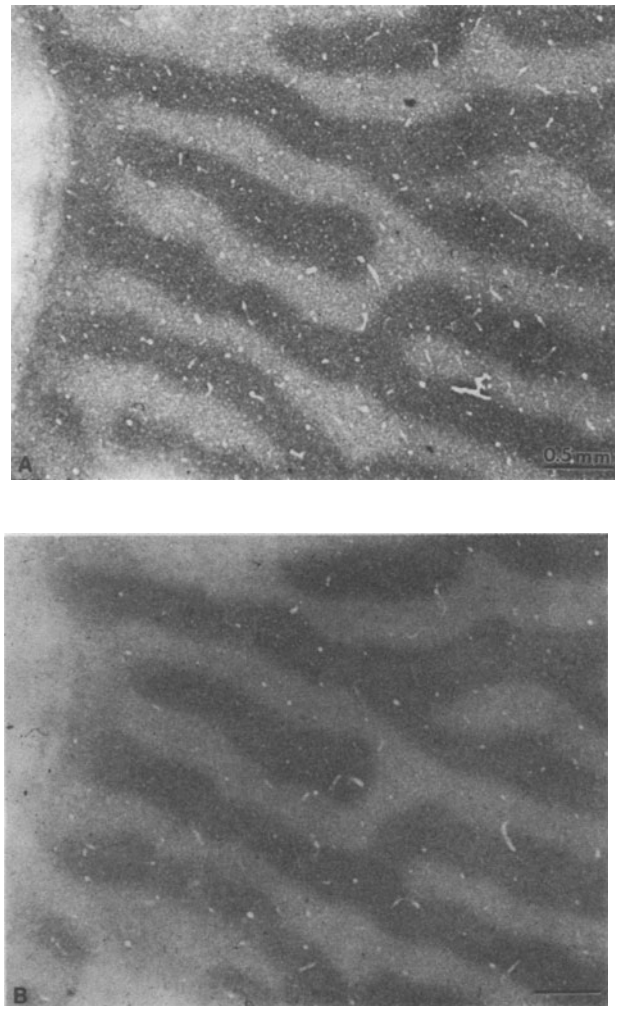

Figure 11. Adjacent sections cut tangential to the surface of the visual cortex from a macaque monkey monocularly treated with TTX for 4 weeks. Identical dark and light ocular dominance stripes are visible in layer IVC by CO histochemistry (**A**) and by CO immunohistochemistry (**B**). Scale bars: 0.5 mm. (Modified from Hevner and Wong-Riley, 1990).

9.2.1. Metabolic Plasticity in Mature Neurons. The exquisite sensitivity of cytochrome oxidase to changing functional demands has led to an appreciation of mature neurons as a dynamic rather than a static entity. With functional perturbations, adult neurons respond by adjusting their levels of cytochrome oxidase and, hence, their energy production. In the last decade, mature neurons have been shown to respond to a variety of functional insults, such as different forms of visual deprivation (reviewed in Wong-Riley, 1994), functional silencing in one ear (Wong-Riley et al., 1978, 1981), auditory learning (reviewed in Gonzalez-Lima, 1992), cochlea removal (Hyde and Durham, 1990), somatosensory deprivation (Wong-Riley and Welt, 1980; Land and Simons, 1985; Yip et al., 1987; Warren et al., 1989), dentate gyrus deafferentation (Borowsky and Collins, 1989), ischemia (Dimlich et al., 1990), and hypoxia (La Manna et al., 1996). Up-regulation of CO has also been demonstrated under conditions of increased neuronal activity, either by chemical or electrical means (Wong-Riley et al., 1981; Mawe and Gershon, 1986).

Figure 12 illustrates the effect of monocular impulse blockade on CO activity in the adult primate visual cortex. In layer IVC, where enzyme level is normally uniformly high (Fig. 12A), TTX induced a down-regulation of CO in deprived ocular dominance columns (Fig. 12F). Likewise, TTX caused alternating rows of deprived supragranular puffs to become paler and smaller in size (compare Fig. 12B with 12G). Changes in layer IVC were detectable 14 hours after a single intravitreal injection of TTX (Fig. 12C). Earlier time periods have not yet been investigated. These histochemical changes were preceded by a dramatic reduction in background multiunit spike rates in deprived layer IVC or supragranular zones (to an average of about 50% of pre-TTX levels) recordable approximately 1 hr after TTX (DeYoe et al., 1995) (Fig. 12D). Thus, the adjustment of CO levels is in response to altered neuronal activity. Moreover, the response is fully reversible because the treatment condition does not involve denervation and degeneration (Wong-Riley et al., 1989a; Wong-Riley, 1989, 1994) (Fig. 12E). These findings underscore the critical role of neuronal activity in regulating cytochrome oxidase levels in the brain.

9.2.2. Metabolically Most Active Neurons Are Most Vulnerable to Functional Deprivation. Do all mature neurons respond alike to the same functional insult? In a quantitative analysis of the visual cortex in adult monkeys monocularly treated with tetrodotoxin (TTX), it was found that the majority of neurons which normally had low levels of cytochrome oxidase were not significantly affected by the afferent impulse blockade (Wong-Riley et al., 1989a). Neurons that were moderately reactive for cytochrome oxidase before the treatment exhibited a reduction of their enzyme activity, but they retained their normal mean size. However, neurons that previously had high levels of cytochrome oxidase suffered a significant reduction in both enzyme levels as well as in cell size. Thus, the metabolically most active neurons appear to be most vulnerable to functional insults, even in the adult.

9.3. Regulation at the Subunit Protein Level: Mitochondrial- and Nuclear-Encoded Subunit Proteins

Cytochrome oxidase in mammalian cells comprises 13 subunits, the first three of which are mitochondrial-encoded, and the rest are nuclear-encoded (Kadenbach et al., 1983; Azzi and Muller, 1990; Capaldi, 1990). The biosynthesis of CO holoenzyme requires the coordinated expression of both genomes to yield complexes with subunits in 1:1 stoichiometry (Kadenbach et al., 1983; Poyton et al., 1988; Azzi and Müller, 1990; Capaldi, 1990). This basic cellular problem is compounded in neurons, which have distinct energy requirements and unique cellular architecture. Neurons are highly reliant on mito-

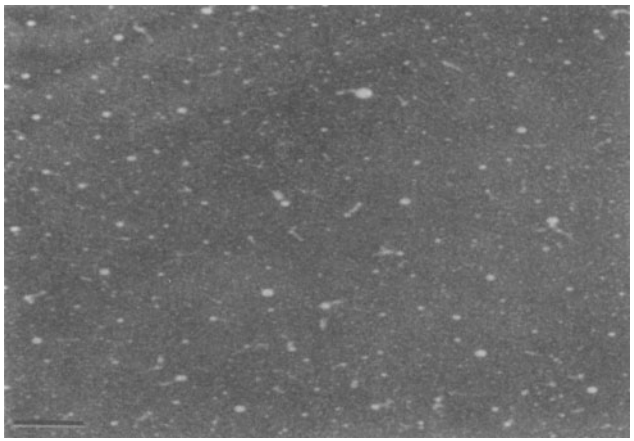
A

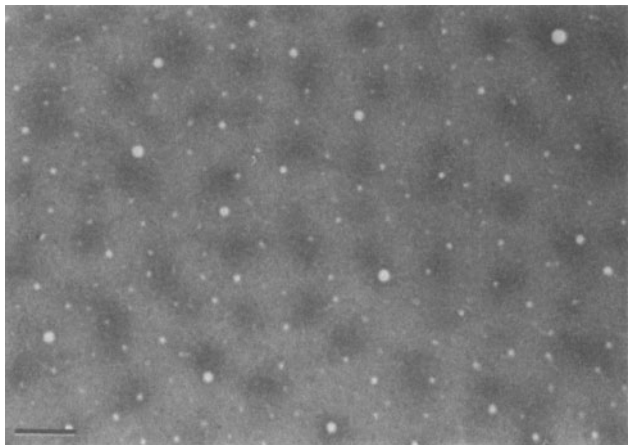
B

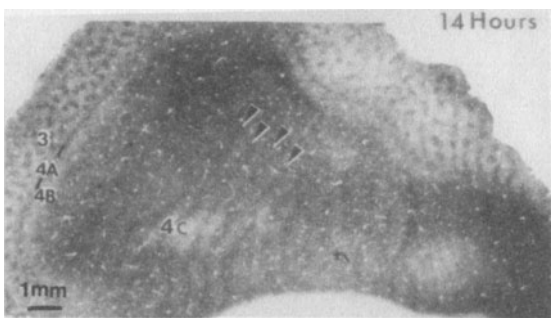
C
14 Hours
3
4A
4B
4C
1mm

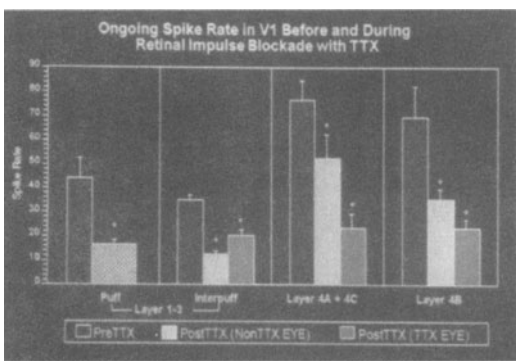
D
Ongoing Spike Rate in V1 Before and During
Retinal Impulse Blockade with TTX
Spike Rate
Puff
Interpuff
Layer 1-3
Layer 4A + 4C
Layer 4B
PreTTX
PostTTX (NonTTX EYE)
PostTTX (TTX EYE)

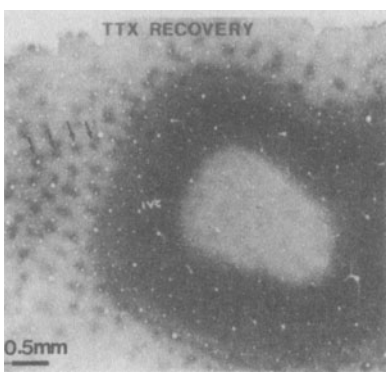
E
TTX RECOVERY
0.5mm

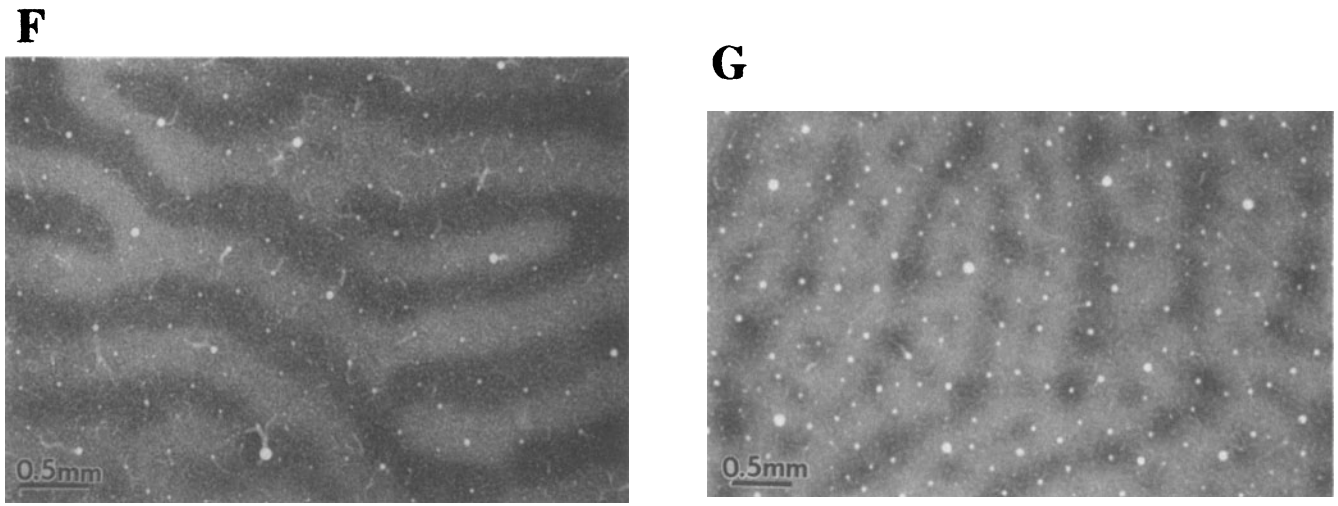

Figure 12. Metabolic plasticity in the adult primate visual cortex. Frozen sections (A, B, C, E, F and G) were cut tangential to the surface of macaque visual cortex and reacted for CO histochemistry. Staining patterns in normal layer IVC (**A**) and supragranular puffs (**B**) were altered by 4 weeks of monocular TTX (**F** and **G**, respectively). The ocular dominance banding pattern in layer IVC was detectable in the visual cortex 14 hr after a single intravitreal injection of TTX (**C**). The histochemical pattern was preceded by a suppression of maintained spiking activity recordable from the visual cortex (**D**). With sufficient recovery period from TTX, the process was reversible, and layer IVC recovered its homogeneous reactivity for CO (**E**). (C and E, modified from Wing-Riley, 1994; D, modified from DeYoe et al., 1995). Scale bars for A, B, E, F, G: 0.5 mm; for C: 1 mm.

chondrial respiration (Erecinska and Silver, 1989), and are severely affected by disruption of the oxidative pathway, as occurs in the mitochondrial genetic diseases (Harding, 1991). Proper mitochondrial functioning is thus of crucial importance to neurons. However, nuclear-mitochondrial coordination is complicated in neurons because most mitochondria reside far from the cell body, in axons and dendrites. In neurons, the nucleus must interact with mitochondria in distinct axonal and dendritic processes that are often thousands of microns or more away. It is not known if CO subunit proteins from the two genomes are proportionately distributed among various neuronal compartments, and if their levels are correlated with the local level of CO activity. Verification of this issue requires quantitative EM analysis in CO immuno-reacted tissue.

We undertook a study to examine the subcellular distributions of mitochondrial- and nuclear-encoded CO subunit proteins in normal neurons to determine if their distribution bears any relationship with local CO activity and to compare the time course and degree of their changes after the removal of sensory input (Nie and Wong-Riley, 1996c). Two antibodies, one against CO subunit III (mitochondrial-encoded) and one against CO Vb (nuclear-encoded), were generated (Fig. 13) to differentiate between CO subunit proteins from the two genomes at the subcellular level. They were used to label CO subunits by postembedding immunogold technique at the EM level. The rodent cerebellum was chosen as a model because its ultrastructural features and subcellular distribution of CO activity (shown cytochemically) have been well characterized (Palay and Chan-Palay, 1974; Mjaatvedt and Wong-Riley, 1988). Subcellular distributions of immunoreactivity for the two subunits in the cerebellum were quantitatively analyzed, and their local levels were compared to local CO activity defined by CO cytochemistry. In order to study the regulation of the two CO subunits, we used the mouse superior colliculus as a model, and quantitatively compared changes in the relative amount of each CO subunit proteins as well as in the relative level of CO activity one to seven days after monocular enucleation.

Our results indicate that mitochondrial- and nuclear-encoded CO subunit proteins in neurons differed in their compartmental distribution, correlation with CO activity, and regulation by neuronal activity (Nie and Wong-Riley, 1996c). At the light microscopic level, immunoreactivity for CO III (mitochondrial-encoded) in the cerebellum was more

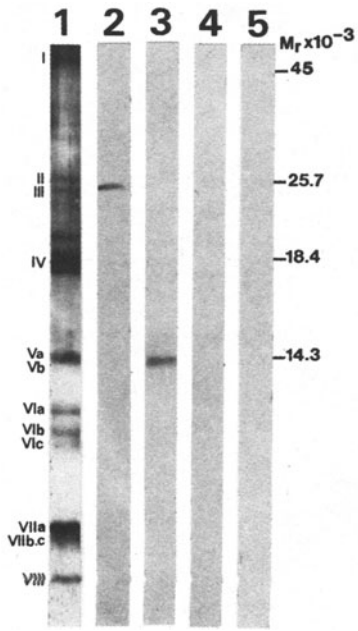

Figure 13. Immunoblot analysis of anti-CO III and anti-CO Vb antibodies. CO purified from bovine brains (5.0 μg) was separated into its 13 subunits by sodium dodecylsulfate-polyacrylamide gel electrophoresis (SDS-PAGE) shown in lane 1. For lanes 2–5, crude mouse brain tissue was homogenized in 10% SDS, and an equivalent amount (50 μg/lane) was loaded in each lane. Lanes from the same gel were either stained with silver to show CO subunits (lane **1**) or transferred to nitrocellulose and immunoblotted with anti-CO III (lane **2**), anti-CO Vb (lane **3**), or preimmune sera (lane **4** for CO III and lane **5** for CO Vb). The positions for molecular weight markers are shown at the right. Note that anti-CO III and anti-CO Vb reacted only with their respective CO subunits. (Taken from Nie and Wong-Riley, 1996c).

intense in neuronal processes than in cell bodies (Fig. 14a), a pattern similar to that of CO activity (Fig. 14c). On the other hand, immunoreactivity for CO Vb (nuclear-encoded) was uniformly distributed in cell bodies and neuronal processes of this region (Fig. 14b), consistent with previous reports (Hevner and Wong-Riley, 1989; Isashiki et al., 1991). At the EM level, both antibodies were localized almost exclusively to mitochondria (Fig. 15), and quantitative analysis confirmed a different distribution for the two subunit proteins (Table 2). Whereas CO Vb immunogold particles were homogeneously distributed over all neuronal compartments, significantly more CO III immunogold particles were found in mitochondria of dendrites and axon terminals than of neuronal cell bodies. The distribution of CO III subunit proteins, then, is higher in functionally more active compartments (Woodward et al., 1971; Palay and Chan-Palay, 1974; Creutzfeldt, 1975), where CO activity is also more intense. Thus, the local level of mitochondrial-encoded subunit proteins (but not of nuclear-encoded ones) is positively correlated with the local level of synaptic activity.

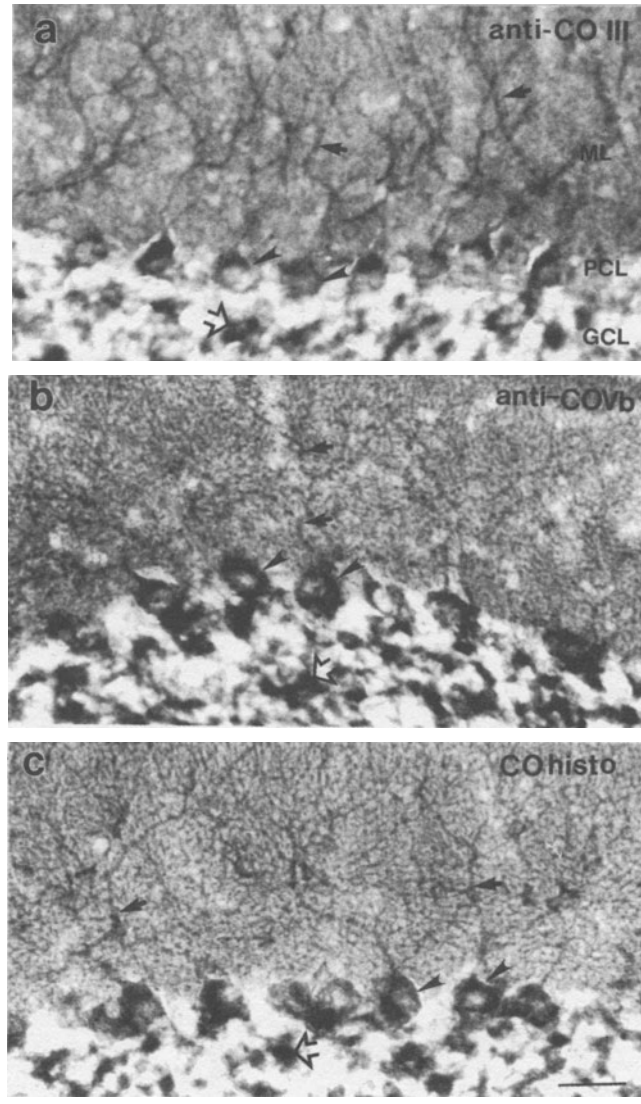

Figure 14. Serial frozen parasagittal section of the mouse cerebellum were reacted for anti-CO III (**a**), anti-CO Vb (**b**), and CO histochemistry (**c**), respectively. The dendrites in the molecular layer (ML) were intensely stained by all three methods, although anti-CO Vb showed the least distinct morphology. Purkinje cell bodies (arrowheads) in its layer (PCL) were densely immunostained by anti-CO Vb, but only the basket cell terminals surrounding the Purkinje cells (and not the cells themselves) were intensely labeled by CO III and CO histochemistry. In the granule cell layer (GCL), all three procedures showed intensely stained patchy profiles (open arrows) presumed to be mossy fiber terminals. Scale bar: 0.03 mm. (Taken from Nie and Wong-Riley, 1996c).

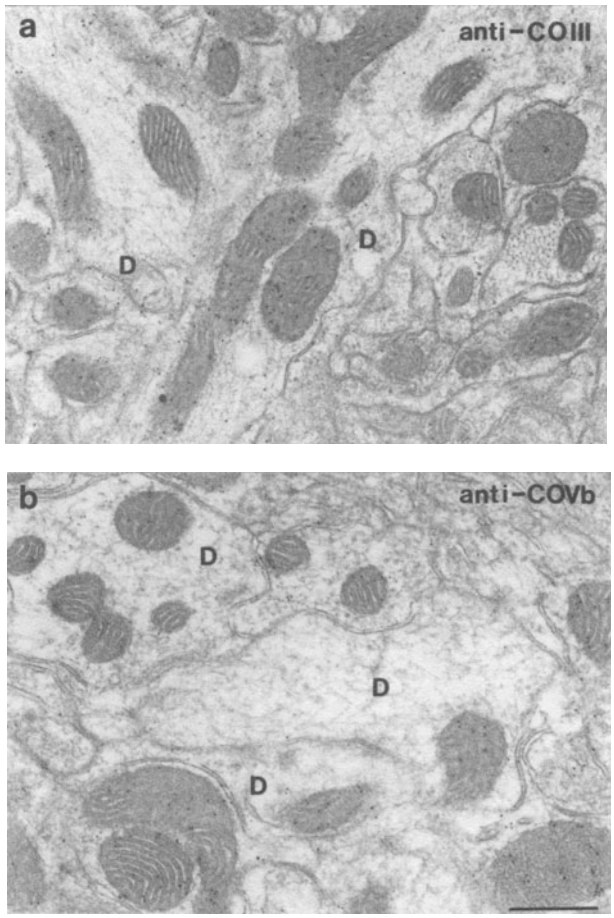

Figure 15. Electron micrographs of the mouse cerebellar molecular layer, showing the subcellular distribution of immunoreactivity for CO III (**a**) and CO Vb (**b**). Immunogold particles for both antibodies were found in significantly higher numbers within mitochondria than in extra-mitochondrial cytoplasm ($P < 0.0001$). Note the density of immunogold particles is much higher in mitochondria of dendrites (D) than in surrounding profiles for CO III. In contrast, the distribution of gold particles for CO Vb is relatively homogeneous in dendrites and other profiles. Scale bar: 0.5 μm. (Taken from Nie and Wong-Riley, 1996c).

Table 2. Comparisons of gold particles over mitochondria in five types of neuronal profiles in the cerebellum[1]

Mitochondrial localization	Mean gold particles per μm^2 ± SEM	Measured area (μm^2)	Statistical comparisons			
CO III						
Dendrites (D)	92.34 ± 4.61	87.76	D			
Mossy fibers (MF)	74.68 ± 3.15	112.34	*	MF		
Basket terminals (BT)	70.92 ± 4.07	76.58	*	—	BT	
Purkinje cells (PC)	32.40 ± 0.18	123.08	***	***	***	PC
Granule cells	28.94 ± 0.17	38.17	***	***	***	—
CO Vb						
Dendrites	69.50 ± 3.47	91.26	D			
Mossy fibers	73.38 ± 4.66	123.57	—	MF		
Basket terminals	71.36 ± 5.81	69.24	—	—	BT	
Purkinje cells	76.48 ± 6.21	11.35	—	—	—	PC
Granule cells	75.06 ± 4.29	41.61	—	—	—	—

[1](*): $P < 0.05$, (***): $P < 0.001$, (—): NS.

Do different mechanisms exist for regulating the local expression and/or redistribution of CO subunit proteins from the two genomes? Our present findings support the following hypothesis: Sufficient amounts of nuclear-encoded CO subunit proteins can be delivered intramitochondrially to individual neuronal compartments for both immediate and delayed assembly of CO holoenzyme, while the local capacity for CO assembly depends mainly on the local amount of mitochondrial-encoded subunit proteins whose distribution is closely regulated by the local energy demand. Based on this hypothesis, mitochondria in regions of higher energy consumption (e.g. dendrites and synaptic axon terminals) contain more mitochondrial-encoded subunit proteins. This permits rapid assembly of holoenzyme molecules and thus elevated levels of CO activity. It seems unlikely that CO holoenzymes are assembled mainly in cell bodies because both mitochondrial-encoded subunit proteins and CO activity are low in many neuronal somata. However, the mechanisms involved in each step of subunit protein processing and assembly in neurons are unresolved.

The above hypothesis is further supported by our findings that CO activity and CO III proteins (mitochondrial-encoded), but not CO Vb proteins (nuclear-derived), are proportionately regulated by neuronal activity. Both CO III proteins and CO activity were reduced in parallel after the removal of afferent input, and their levels were changed earlier and to a greater degree than nuclear-encoded proteins (CO Vb) (Fig. 16). These data suggest that the expression of mitochondrial-encoded subunit proteins is more tightly regulated by neuronal activity than nuclear-encoded ones. Parallel changes in CO activity and CO III level also imply that the amount of mitochondrial-derived subunit proteins may play a dominant role in controlling the level of CO holoenzyme and its activity during periods of adjustment, because these components constitute the catalytic core of this enzyme (Azzi and Muller, 1990;

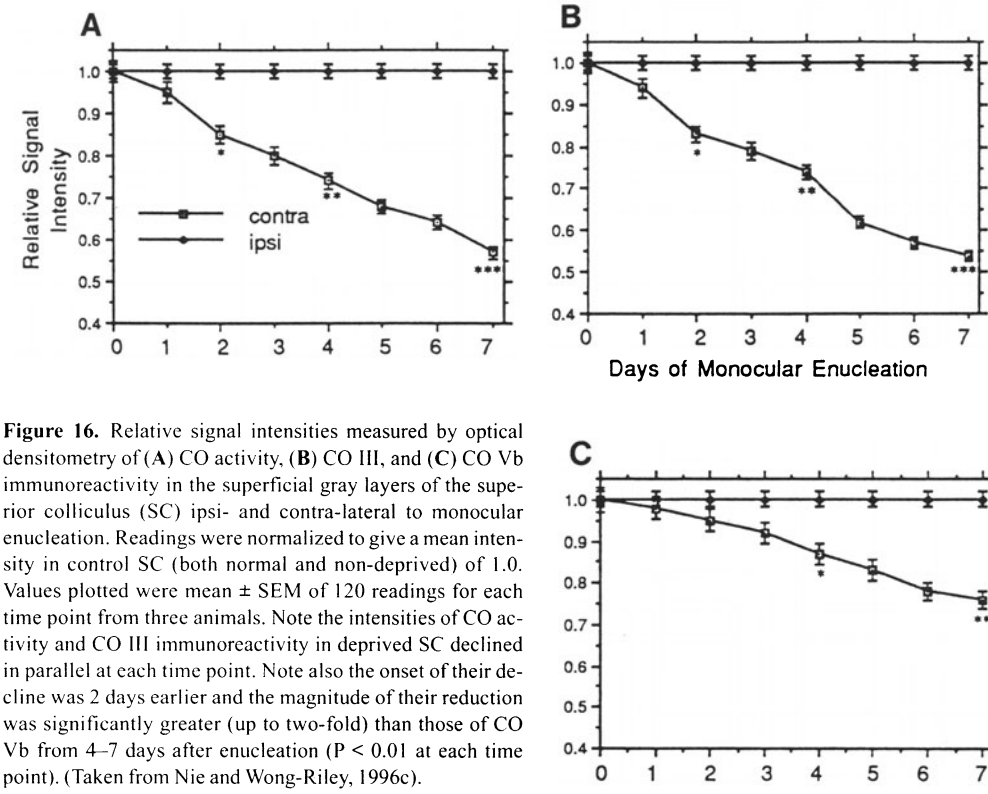

Figure 16. Relative signal intensities measured by optical densitometry of (**A**) CO activity, (**B**) CO III, and (**C**) CO Vb immunoreactivity in the superficial gray layers of the superior colliculus (SC) ipsi- and contra-lateral to monocular enucleation. Readings were normalized to give a mean intensity in control SC (both normal and non-deprived) of 1.0. Values plotted were mean ± SEM of 120 readings for each time point from three animals. Note the intensities of CO activity and CO III immunoreactivity in deprived SC declined in parallel at each time point. Note also the onset of their decline was 2 days earlier and the magnitude of their reduction was significantly greater (up to two-fold) than those of CO Vb from 4–7 days after enucleation ($P < 0.01$ at each time point). (Taken from Nie and Wong-Riley, 1996c).

Capaldi, 1990). In muscle, chronic stimulation induced increases in CO activity that were dependent on mitochondrial protein synthesis (Williams and Harlan, 1987).

9.4. How Do Nuclear-Encoded Cytochrome Oxidase Subunit Proteins Reach Dendrites?

Mitochondria are ubiquitous organelles found in all cytoplasmic compartments of neurons, and their numerous proteins constitute about 10–20% of intracellular proteins. However, the mitochondrial genome encodes only a small fraction of proteins necessary for electron transport and oxidative phosphorylation. The vast majority of proteins found in mitochondria are specified by nuclear genes and are imported into mitochondria (Maccecchini et al., 1979; Kaput et al., 1982; Viebrock, et al., 1982). In neurons, mitochondrial genomes in dendrites and axons can be far away from the nuclear genes. To regulate functions in distal processes, neurons need efficient ways to deliver nuclear-derived precursor proteins to mitochondria in these regions. The mechanism underlying transportation and distribution of these proteins to dendrites and axon terminals is poorly understood.

Nuclear-encoded mitochondrial proteins are synthesized on cytoplasmic polysomes as large precursor proteins with cleavable N-terminal presequences. These presequences function as mitochondrial targeting signals and are proteolytically removed upon import (Maccecchini et al., 1979; Kaput et al., 1982; Viebrock et al., 1982; Attardi and Schatz, 1988). Are the precursor proteins transported to dendrites and axons before or after incorporation into the mitochondrial compartment? If the transportation is mediated by mitochondria, can the precursor proteins be detected in neurons *in vivo*? Their reported half lives are only seconds to minutes in yeast and in rat hepatocytes (Mori et al., 1981; Reid et al., 1982).

To address these questions, we used CO subunit IV specified by nuclear-genes as a model system to study the distribution of precursor proteins in the rat brain (Liu and Wong-Riley, 1994). Our previously generated antibodies against CO holoenzyme recognize primarily subunit IV mature protein (Hevner and Wong-Riley, 1989) and can be used for comparison. In order to label precursor proteins at the exclusion of the mature form, we generated polyclonal antibodies against synthetic presequence specific only to the precursor form of rat brain CO subunit IV (pCOIV; Goto et al., 1989). Although all presequences of nuclear-encoded mitochondrial proteins share the same characteristics (such as a richness in basic and hydroxylated amino acids), there is no sequence consensus among them (Hartl et al., 1989). The specificity of antibodies to pCOIV was tested by Western blots (Fig. 17) and ELISA. Anti-pCOIV antibodies were applied to rat brain sections for immunohistochemical localizations at light and EM levels. The pattern of pCOIV distribution was also compared with that of the mature form of CO subunit IV (Hevner and Wong-Riley, 1989) and with that of CO activity demonstrated histochemically (Wong-Riley, 1979). To determine if precursor proteins are regulated by neuronal functional activity, monocular enucleation was performed on rats to prevent retinal impulses from reaching visual centers in the brain. Possible changes in the level of pCOIV were examined in a major retinal-recipient center, the superior colliculus.

9.4.1. CO Precursor Proteins Are Found Primarily in the Mitochondrial Compartment. Immunoreactivity against pCOIV was detectable in the mammalian brain *in vivo*. Moreover, pCOIV was located not only in cell bodies but unexpectedly also in distal dendrites and axon terminals (Fig. 18), suggesting that the precursor form of CO IV can be transported to distal processes of neurons and reside there for relatively long periods before it is degraded by mitochondrial matrical proteases. The physical distance between den-

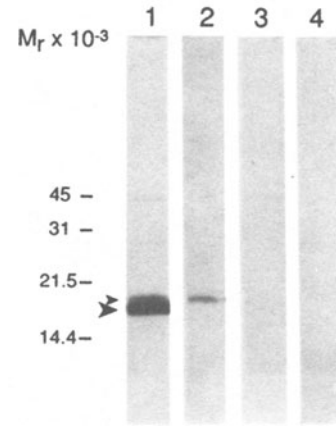

Figure 17. Crude rat brain homogenates were subjected to SDS-PAGE (100 μg protein/lane) and immunoblotted with anti-CO IV precursor protein antibodies (anti-pCOIV) or anti-CO holoenzyme antibodies that recognized primarily the mature form of CO IV (anti-CO IV). The immunoreactive bands were visualized by ECL Western blot reagents. Lane **1**, anti-CO IV reacts with precursors of CO IV (upper small arrowhead; M_r of 19.1 kDa) as well as mature CO IV (lower arrowhead; M_r of 17.5 kDa). Lane **2**, anti-pCOIV reacts with pCOIV but not with the mature form of CO IV. Lane **3**, purified IgG preadsorbed with synthetic presequence polypeptides. Lane **4**, no primary antibodies. (Taken from Liu and Wong-Riley, 1994).

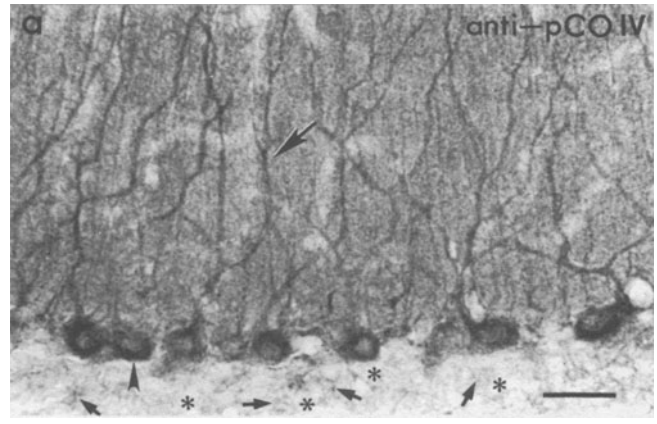

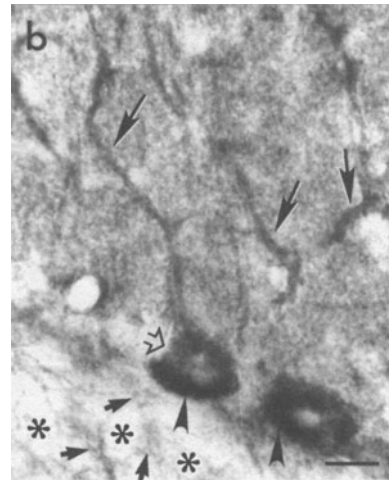

Figure 18. Immunohistochemical localization of anti-pCOIV antibodies in the rat cerebellum. (**a**) Purkinje cell bodies and their dendrites (arrow) were labeled. (**b**) At a higher magnification, Purkinje cell bodies were found to be only moderately immunoreactive, while presumed basket cell terminals close to the cell bodies (arrowheads) were intensely labeled. Granule cell bodies (*) had light immunostaining, while neighboring mossy fiber terminals (small arrows) were moderately immunoreactive. Scale bars: a, 0.2 mm; b, 0.06 mm. (Taken from Liu and Wong-Riley, 1994).

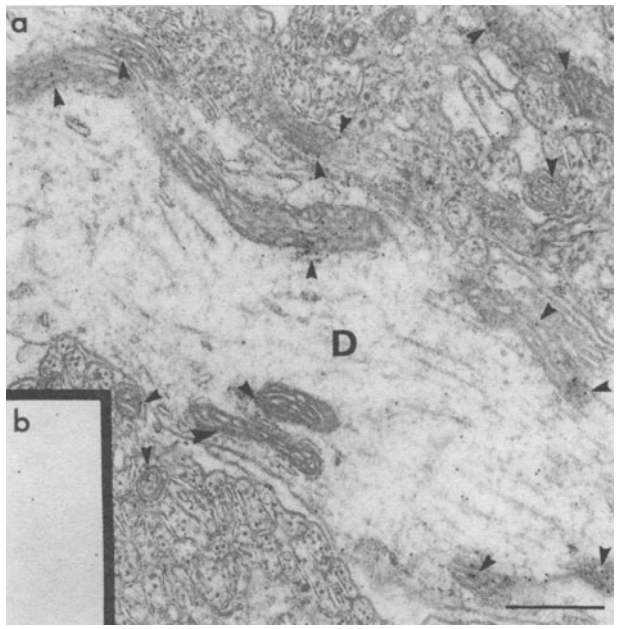

Figure 19. Immuno-EM localization of pCOIV in the molecular layer of the rat cerebellum. (**a**) The majority of immunogold particles were found in mitochondria (arrowheads) of Purkinje cell dendrites (D) and very few gold particles were seen in dendritic cytoplasm outside of mitochondria. (**b**) Blank regions of Durcupan resin showed very low counts of immunogold particles. Scale bar: 1 μm. (Taken from Liu and Wong-Riley, 1994).

Table 3. Density of gold labeling in mitochondria and extramitochondrial cytoplasm of neurons

Cell compartment	Area (μm^2)	# Gold particles/ $\mu m^2 \pm SE$	Significance of comparisons[a]
Neuronal processes			
a. Mitochondria (357)[b]	42.45	58.33 ± 6.26	
1. Dendrites (141)	10.63	60.13 ± 4.80	
2. Basket terminals (119)	14.25	68.28 ± 3.57	
3. Mossy fiber terminals (97)	17.57	37.80 ± 6.40	
b. Extramito. cytoplasm	182.1	4.76 ± 0.45	
a vs. b			$\rho < 0.0001$
Cell bodies (Purkinje)			
c. Mitochondria (214)	15.92	39.30 ± 6.55	
d. Extramito. cytoplasm	93.71	6.55 ± 0.59	
c vs. d			$\rho < 0.0001$
Control[c]			
e. Mitochondria (142)	10.74	6.38 ± 0.85	
f. Extramito. cytoplasm	72.31	4.92 ± 0.81	
e vs f			NS
b vs f			NS
d vs f			NS
b vs d			$\rho < 0.05$
a_1 vs c			$\rho < 0.05$
a_2 vs c			$\rho < 0.05$
a_3 vs c			NS

[a]Differences in the density of immunogold particles over mitochondria and over extramitochondrial cytoplasm were evaluated using one-way ANOVA.
[b]Number of mitochondria analyzed is in parentheses.
[c]Control samples were treated with anti-pCOIV antibodies preadsorbed with synthetic presequence peptide of COIV.

dritic/axonal mitochondria and the nucleus requires the existence of an efficient transport system to bring newly synthesized mitochondrial proteins from the soma to their distant targets. At the EM level, pCOIV immunogold particles were located mainly in mitochondria and much less so in non-mitochondrial cytoplasm of cell bodies, and almost exclusively in mitochondria of dendrites and axon terminals (Fig. 19 and Table 3). This indicates that the bulk of newly synthesized nuclear-encoded precursor proteins is incorporated without delay into mitochondria of neuronal cell bodies and transported to dendrites and axons within the mitochondrial compartment. These results are consistent with previous reports that newly synthesized, nuclear-derived mitochondrial polypeptides are rapidly imported into mitochondria, perhaps within 30 sec to 2 min in the somatic cytoplasm (Mori et al., 1981; Reid et al., 1982). When import was blocked experimentally in cultures of chicken embryo fibroblasts, precursor proteins were degraded within 5 min in the cytosol (Jaussi et al., 1982). Our data also imply that soon after the precursor proteins are imported into perikaryal mitochondria, mitochondria are transported away from the somata. Evidence for this is that pCOIV is present at a low level in many cell bodies, such as dentate granule cells and cerebellar Purkinje and granule cells. However, pCOIV is rich in dendrites of almost all neurons examined and is present in some axonal terminals, such as basket and mossy fiber terminals in the rat cerebellum (Liu and Wong-Riley, 1994).

9.4.2. CO Precursor Proteins Are Delivered to Neuronal Processes via the Mitochondrial Compartment. Our data further indicate that precursor proteins can be delivered intramitochondrially over a great distance, even to distal dendrites. Mitochondrial movement in neuronal processes involves fast and slow transport along microtubules in a stop-and-go (saltatory) fashion (Jeffrey et al., 1972; Lorenz and Willard, 1978). It would be more efficient for neurons to deliver nuclear-derived mitochondrial proteins to dendritic and axonal destinations via mitochondrial compartments, as our data indicate, rather than via the dendritic cytosol. First, the rate of mitochondrial transport is much faster than that of bulk cytosolic flow (Jeffrey et al., 1972; Lorenz and Willard, 1978; Vale et al., 1985). This would allow proteins to be distributed rapidly to their final destinations. Second, it has been reported that mitochondrial transport in axons *in vitro* is regulated by both a recruitment between stationary and moving states and direct regulation of anterograde motors (Morris and Hollenbeck, 1993). Different rates of mitochondrial transport provide the opportunity for mitochondria to be shuttled to discrete neuronal compartments at varying rates regulated by local metabolic demands. Indeed, CO activity and CO proteins are both distributed heterogeneously in neurons, and their patterns of distribution correlate with local energy demands (Hevner and Wong-Riley, 1989; Wong-Riley, 1989). However, we cannot rule out the possibility that: (a) A small amount of the precursors may simply diffuse in the extramitochondrial compartment of dendrites and remain undetectable by our approach; and (b) CO IV mRNA might be present in a low amount in distal dendrites, where it is translated to precursor proteins. Our findings of anti-pCOIV in axon terminals, which lack mRNA and ribosomes, further strengthen the posttranslational means of delivery to neuronal processes.

9.4.3. Nuclear-Encoded CO Subunit Proteins Can Form a Precursor Pool in Dendrites and Axon Terminals. The presence of a clearly detectable amount of pCOIV indicates that, at least in neurons, a pool of nuclear-encoded precursor proteins exists in dendritic and axon terminal mitochondria. Is the accumulation of pCOIV attributable to an overproduction and/or slow maturation of CO subunit IV in neurons? It has been reported that an excess amount (exceeding mitochondrial requirement) of nuclear-encoded mitochondrial precursor proteins are imported into mitochondria under normal or abnormal conditions

(Hundt et al., 1980; Forsburg and Guarente, 1989; Mita et al., 1989). First, nuclear-derived CO subunits could accumulate in mitochondria in the absence of holoenzyme assembly in yeast (Forsburg and Guarente, 1989). Second, free CO subunit IV in mitochondria could be detected even when mitochondrial-derived subunits are depleted in human muscles with mitochondrial DNA mutation (Mita et al., 1989). Third, CO is assembled in the absence of cytoplasmic protein synthesis for 5 hours in isolated hepatocytes (Hundt et al., 1980), indicating that biosynthesis of CO involves large pools of the cytoplasmic precursor. Thus, it is quite likely that pCOIV is overproduced by neurons, and excess pCOIV is imported into mitochondria and contributes to the precursor pool. The precise half life of pCOIV cannot be determined by our study; instead, an estimate of minimal half life for pCOIV is assessed based on the lengths of neuronal dendrites and the rate of mitochondrial transport in mammalian axons. There is evidence for both slow (1–4 mm/day) and fast (50 mm/day) movements of mitochondria in normal mammalian axons (Jeffrey et al., 1972; Lorenz and Willard, 1978). The essential features of dendritic transport are quite similar to those in axons (Grafstein and Forman, 1980). By slow movement, pCOIV could have a half life of at least 2.6 hours (the length of Purkinje cell dendrites is about 220 μm, and the velocity of mitochondrial transport is averaged to 2 mm/day). In contrast, by fast transport, mitochondria might have a half life of a few minutes (220 μm; 50 mm/day). In sum, it is most likely that the half life of pCOIV can vary within the same neuron depending on its energy demand, and pCOIV can have a half life of a few minutes to 2.6 hours or more. This indicates that the processing of pCOIV in the mammalian brain tissue *in vivo* is considerably slower than precursor proteins found in yeast or in mammalian liver cells (having a half life of 30 sec to 2 min) described by a number of investigators (Reid et al., 1982; Mori et al., 1981). Thus, the slow maturation rate of nuclear-encoded mitochondrial proteins could be one of the mechanisms for preserving a large intramitochondrial precursor pool in neurons.

9.4.4. Regulation by Neuronal Activity. Just as local energy demands control the distributions of CO activity and CO subunit proteins (Hevner and Wong-Riley, 1989; 1990; Wong-Riley, 1989; Nie and Wong-Riley, 1996c), monocular enucleation led to a down-regulation of CO IV precursor proteins in the contralateral superior colliculus (Fig. 20). The decline of pCOIV in 15 days post deafferentation was proportional to that of the mature form of CO subunit IV and CO activity (Liu and Wong-Riley, 1994). This suggests that the mitochondrial CO precursor pool can be regulated by metabolic demands imposed by neuronal functional activity, and changes in CO proteins depend more on altering protein synthesis than on protein degradation.

9.5. Regulation of Mitochondrial and Nuclear Gene Expression for Cytochrome Oxidase Subunits in Neurons

How are mitochondrial and nuclear gene expression coordinated to yield respiratory complexes containing subunits from both genomes in fixed stoichiometries? The sizable separation between the nuclear genes in the cell body and the mitochondrial genes in neuronal processes that could be millimeters or even centimeters away poses a distinct problem for neurons. Moreover, neurons are heterogeneous in their metabolic needs, and neuronal compartments differ in their CO content, even in the same neuron (Kageyama and Wong-Riley, 1982; Hevner and Wong-Riley, 1989). Is nuclear-encoded subunit mRNA selectively transported to physiologically active compartments that need more CO? Are mitochondrial-encoded mRNAs expressed in direct proportion to mitochondrial DNA

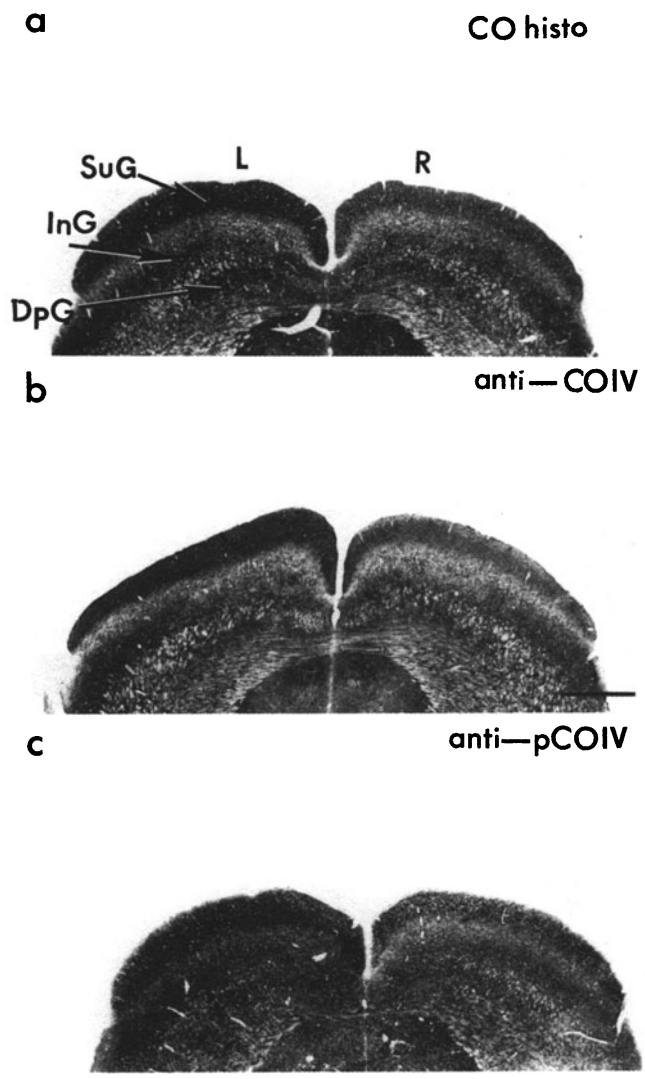

Figure 20. Effect of left monocular enucleation on the distribution of cytochrome oxidase in the rat superior colliculus. Note the level of CO activity shown histochemically (**a**), and the intensity of CO IV (**b**) and pCOIV immunoreactivity (**c**) were all reduced in the right superior colliculus (R). Superficial gray (Sup), intermediate gray (InG), and deep gray (DpG) layers were affected to varying degrees. Scale bar: 0.5 mm. (Taken from Liu and Wong-Riley, 1994).

(mtDNA) content? How are the distribution of mtDNA and CO subunit mRNAs related to each other and to CO activity and protein amount? Are the levels of mtDNA and of CO subunit mRNAs regulated by functional activity in neurons?

9.5.1. Expression of Mitochondrial and Nuclear Genes for CO Subunits: In Situ Hybridization at the Light Microscopic Level. To address the above questions, riboprobes from CO subunits I (mitochondrial encoded), IV and VIII (nuclear encoded) cDNAs were generated (Fig. 21) and applied to brain sections from normal monkeys and from monkeys monocularly treated with TTX (Hevner and Wong-Riley, 1991; 1993). In all regions examined at the light microscopic level, the local content of mtDNA was similar, though not identical, to the activity and amount of CO. Mitochondrial DNA was distributed throughout neurons but more highly concentrated in neuronal compartments of higher CO activity, namely dendrites. Expression of CO I mRNA was not proportional to mtDNA abundance or CO activity and protein. Instead, it was highest in cell bodies, lower in den-

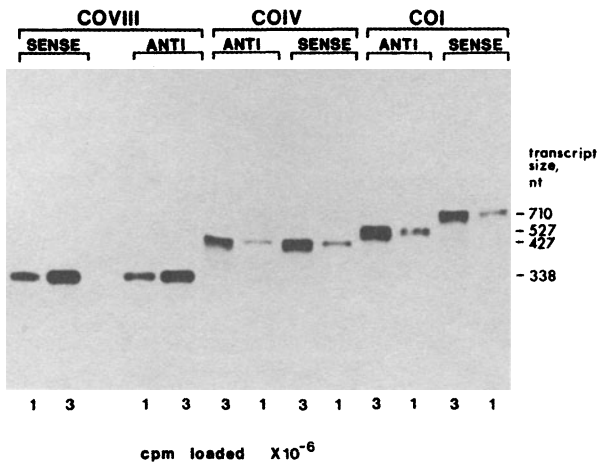

Figure 21. ^{35}S-labeled riboprobes for CO I, CO IV, and CO VIII were analyzed by denaturing gel electrophoresis and film autoradiography. Each riboprobe appeared as a major band of the size expected for full-length transcripts. CO I riboprobes were transcribed from *Pst*I-cut template DNA, causing the sense and antisense transcripts to differ in size. nt, nucleotides; cpm, counts per minute. (Taken from Hevner and Wong-Riley, 1991).

dritic regions, and undetectable in axon terminal areas. CO IV and CO VIII mRNAs were detected virtually exclusively in perikarya (Fig. 22). These findings suggest that the mitochondrial- and nuclear-encoded CO subunits are translated to some extent in different subneuronal compartments. The nuclear encoded subunits are probably translated mainly in neuronal cell bodies and allocated to other compartments posttranslationally. Holoenzyme assembly and distribution are also accomplished post-translationally. In general, however, nuclear-encoded CO mRNA levels in the cell body are probably determined by the overall CO needs of the whole neuron, including dendrites and axons. In contrast, mtDNA and CO I mRNA are distributed intraneuronally to sites of high local oxidative metabolism. Thus, levels of these markers in the cell body more likely reflect local, rather than overall, neuronal demands.

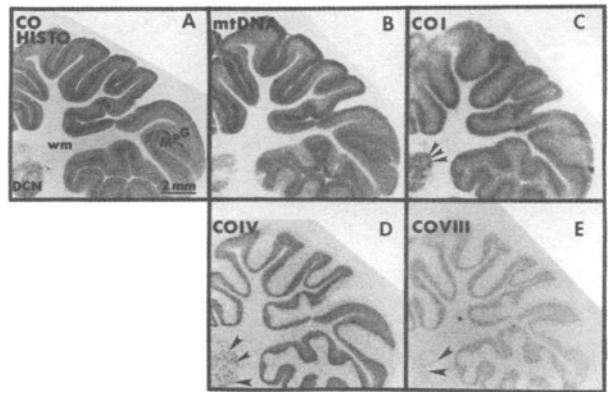

Figure 22. CO activity, mtDNA, and CO subunit mRNA in the normal macaque cerebellum. CO histochemical activity (**A**) was high in the cerebellar cortex and deep cerebellar nuclei (DCN), and low in white matter (WM). The molecular layer (M) was more darkly reactive than the granule cell layer (G). mtDNA (**B**) strongly resembled CO in its distribution. CO I mRNA (**C**) was highest in the granule and Purkinje (P) cell layers and in neurons of the DCN (arrowheads), but was detectable in the molecular layer and in neuropil of the DCN. CO IV (**D**) and CO VIII (**E**) mRNA were detected only in cell bodies of cerebellar cortex and DCN (arrowheads). B–E show film autoradiograms. (Taken from Hevner and Wong-Riley, 1991).

9.5.2. Regulation of CO Subunit Gene Expression by Neuronal Activity

9.5.2.1. Disproportionate Regulation of Mitochondrial and Nuclear mRNA Expression.

To determine if neuronal activity differentially regulates CO subunit expression from the two genomes, adult monkeys were subjected to 3 days and 7 days of monocular TTX treatment, and levels of mitochondrial- and nuclear-encoded CO subunit mRNAs were noted in lateral geniculate neurons and in the visual cortex (Hevner and Wong-Riley, 1993). Levels of mRNA were also compared with those of CO activity, CO protein and mtDNA. Results indicate parallel changes in all five markers in specific LGN layers: layers 1, 4 and 6 contralateral and layers 2, 3 and 5 ipsilateral to TTX-treated eye (Fig. 23).

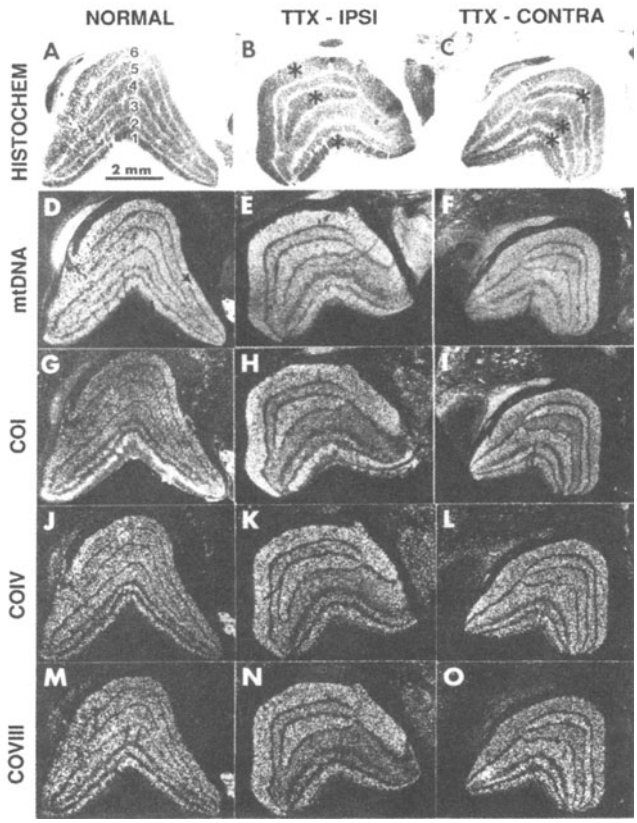

Figure 23. Effect of 1 week of monocular TTX on CO activity, mtDNA, and CO subunit mRNA levels in the adult macaque lateral geniculate nucleus (LGN). A–C, CO activity (histochemistry). In the normal LGN (**A**), enzyme activity was about the same in each layer (numbered), except that layer 1 showed the highest level. In TTX-treated animal, enzyme activity was reduced in layers 2, 3, and 5 of the ipsilateral LGN (**B**), and in layers 1, 4, and 6 of the contralateral LGN (**C**). These changes were more prominent in the ipsilateral than in the contralateral LGN. *Asterisks* indicate normal enzyme activity in layers receiving input from the untreated eye. D–F, mtDNA. All six layers had similar mtDNA levels in the normal LGN (**D**). TTX induced mtDNA to decrease in deprived layers of the ipsilateral (**E**) and contralateral (**F**) LGN. Ipsilateral changes were greater than contralateral ones. G–I, CO I mRNA. In the normal LGN (**G**), CO I mRNA levels were highest in layer 1, but were about equal in other layers. TTX treatment caused a reduction of CO I mRNA in deprived LGN layers ipsilaterally (**H**) and contralaterally (**I**). J–L, CO IV mRNA. Layers of the normal LGN (**J**) contained about equal levels of CO IV mRNA. TTX induced a greater change in ipsilateral (**K**) than in contralateral (**L**) LGN. M–O, CO VIII mRNA. This transcript was also evenly distributed in layers of normal LGN (**M**), but decreased in deprived layers of the ipsilateral (**N**) and contralateral (**O**) LGN after TTX. (Taken from Hevner and Wong-Riley, 1993).

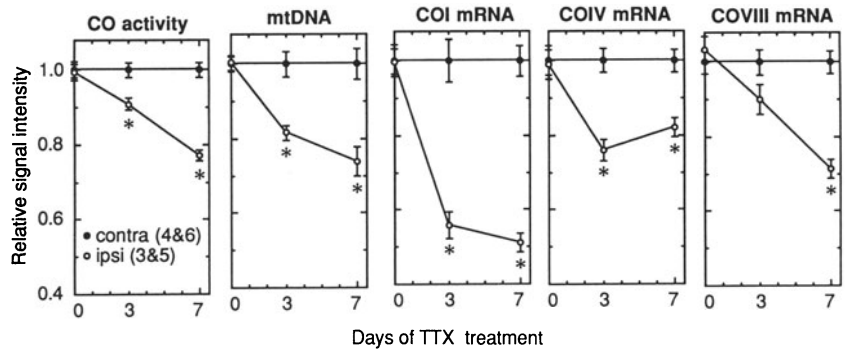

Figure 24. Quantitative analysis of the effect of monocular TTX on CO activity, mtDNA, and CO subunit mRNAs in LGN neurons. Individual neurons in the parvicellular layers (3–6) of the ipsilateral LGN from normal and 3–7 d monocular TTX-treated monkeys were analyzed for CO activity (histochemistry) by densitometry, and for mtDNA and CO subunit mRNAs by computer-assisted grain counting. For each marker, 22 neurons were analyzed in each layer. Neurons were grouped according to innervation from the contralateral, untreated eye (layers 4 and 6), or from the ipsilateral, treated eye (layers 3 and 5). Measurements were normalized to give a mean relative signal in the contralateral input group of 1.0. The graphs show that monocular TTX induced significant decreases of each marker in neurons receiving input from the TTX-treated eye. The mitochondrial- (CO I) and nuclear-encoded (CO IV, CO VIII) mRNAs did not fall by the same amount. Rather, CO I mRNA fell 1.5- to 4-fold more than CO IV or CO VIII mRNA, depending on the treatment period. Values shown are mean ± SEM of 44 measurements. Significant differences (Student's *t* test, two-tailed) between ipsilateral and contralateral input groups are indicated by an *asterisk* (each indicated difference was significant to $P < 0.001$). (Taken from Hevner and Wong-Riley, 1993).

Quantitative analysis by computer-assisted grain counting of mRNA and mtDNA labels, and by optical densitometry of CO activity further indicated that, whereas there were proportionate decreases in CO activity and CO protein in LGN neurons, there were disproportionate decreases in CO I, CO IV, and CO VIII mRNA levels. After 7 days of TTX, CO I mRNA fell by 49 ± 3% (mean ± SEM) in LGN neurons, while CO IV and CO VIII mRNAs fell by only 18 ± 3% and 29 ± 3%, respectively. In comparison, CO activity decreased by 23 ± 2%, and mtDNA by 26 ± 4% (Fig. 24).

Qualitative observations in striate cortex also indicated that CO I mRNA changed more than CO IV mRNA, CO VIII mRNA, mtDNA, or CO activity in deprived ocular dominance columns (Fig. 25). Furthermore, the width of affected columns was narrower for CO IV mRNA and CO VIII mRNA than for CO activity. This indicates that the regulation of nuclear-encoded mRNAs was blunted near column borders. It is possible that border-zone neurons continued to receive significant functional and metabolic activation via dendrites that extended into adjacent columns (see Katz et al., 1989) even during TTX treatment, and the effects of TTX on their CO IV and CO VIII mRNA levels were thereby attenuated. In contrast, the zones of decreased mtDNA and CO I mRNA were about the same width as histochemically defined columns. This suggests that mtDNA and CO I mRNA are regulated locally with high spatial resolution in subcellular compartments, whereas CO IV and CO VIII mRNAs are regulated globally in accordance with the integrated metabolic activity of the whole neuron.

Thus, our results demonstrate that CO activity in neurons is regulated through complex changes in both mitochondrial and nuclear gene expression. They suggest that the local distribution of CO within neurons, and acute regulatory changes in CO activity occurring over periods of days, are controlled mainly by regulation of the mitochondrial genes that encode the catalytic subunits of the enzyme.

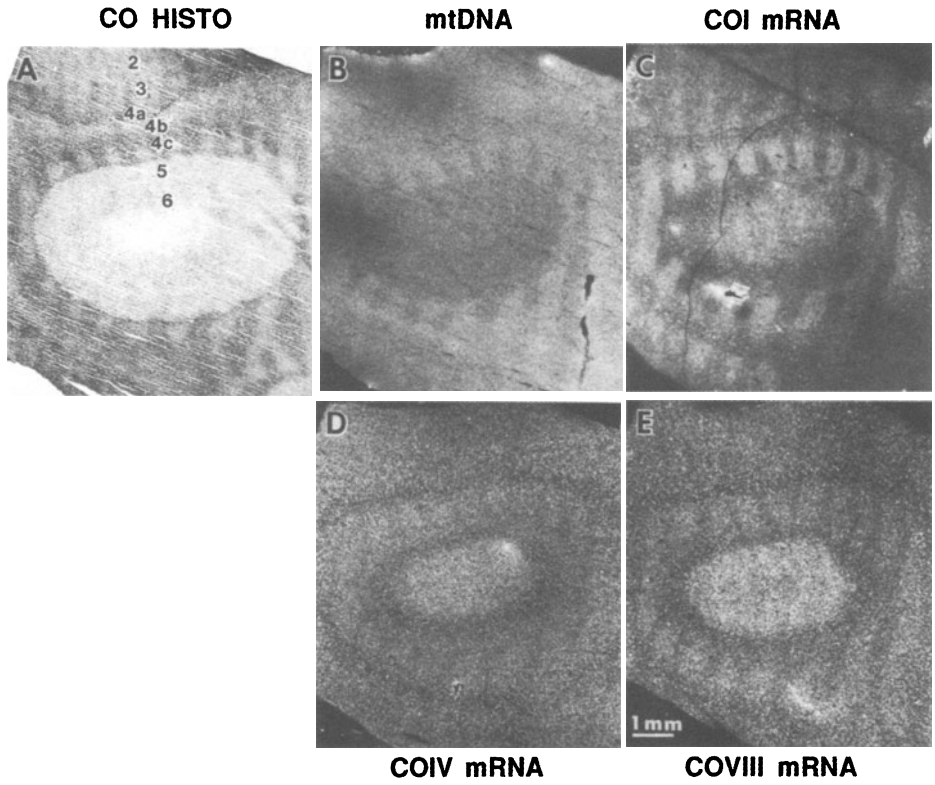

Figure 25. Effect of 1 week of monocular TTX on CO activity, mtDNA, and CO subunit mRNA levels in the adult macaque visual cortex (tangential sections). (**A**) CO activity (histochemistry): Ocular dominance banding was evident in layers 2–3, 4a, 4c, 5 and 6. Note that the columns of dark CO staining (photographed with bright field) correspond to the columns of bright *in situ* hybridization signal (photographed with dark field) in B–E. (**B**) mtDNA: Changes were clearly evident in layer 4c, and appeared faintly in layers 2–3. The width of decreased mtDNA columns appeared about the same as for CO activity. (**C**) CO I mRNA: Changes were similar to those of mtDNA and CO activity. (**D**) CO IV mRNA: Ocular dominance banding was also clear in layer 4c, but the width of affected columns was narrower than for CO activity. (**E**) CO VIII mRNA: changes were comparable to those of CO IV mRNA, with deprived columns in layer 4c being narrower than those with reduced CO activity (Taken from Hevner and Wong-Riley, 1993).

9.5.2.2. Mitochondrial mRNA and mtDNA Copy Number. Mitochondrial mRNA expression may be controlled by mtDNA copy number. The mechanisms controlling mtDNA replication and turnover are not well understood, but our data indicate that mtDNA levels were regulated by neuronal activity. This implies that mtDNA is not a static repository of genetic information but an active molecule responsive to metabolic demands and susceptible to regulation. This is consistent with reports that mtDNA undergoes robust synthesis and turnover (half-life, ~30 d) in rat brain (Gross et al., 1969; Woodford and Blanks, 1989). The mtDNA copy number is also regulated in muscle by contractile activity (Williams, 1986; Williams et al., 1986). TTX-induced changes in mtDNA copy number, however, did not account for the full magnitude of changes in CO I (mitochondrial) mRNA expression. CO I mRNA declined by almost 50% after 7 days of TTX, while mtDNA declined by only ~25%. This two-fold difference implies that not only the gene copy number, but also the rates of CO I mRNA transcription and/or turnover were regulated. In muscle, levels of mtDNA and cytochrome b mRNA (mitochondrial) increased proportion-

ately after contractile stimulation, implying that increases in mitochondrial mRNA were secondary to elevated mtDNA levels (Williams, 1986; Williams et al., 1986). This inconsistency between our results and those from muscle suggests that there may be tissue-specific differences in mitochondrial regulatory mechanisms.

9.5.2.3. Regulation of Nuclear mRNAs. Are the nuclear-encoded mRNAs for mitochondrial polypeptides regulated proportionately? Our results show some disproportion between CO IV and CO VIII mRNA regulation in LGN neurons. In liver, different nuclear-encoded mRNAs are regulated disproportionately in response to thyroid hormone treatment (Virbasius and Scarpulla, 1990). The ratio of cytochrome c mRNA to CO IV mRNA (both nuclear encoded) also differs among rat tissues (Virbasius and Scarpulla, 1990). The promoter regions of nuclear respiratory genes, including CO subunit genes, contain different regulatory elements (Suske et al., 1988; Virbasius and Scarpulla, 1990; Yamada et al., 1990; Basu and Avadhani, 1991). In agreement with these other data, our results suggest that levels of the nuclear-encoded mRNAs for mitochondrial polypeptides are regulated independently.

In summary, our analysis showed that various CO subunit mRNAs were regulated disproportionately. The greatest changes were detected in CO I mRNA, a mitochondrial transcript. Less dramatic changes were detected in the nuclear-encoded mRNAs (CO IV and CO VIII) and mtDNA. CO activity and CO protein decreased proportionately. These findings suggest that, over periods of days to weeks, CO activity is regulated by complex genetic mechanisms involving differential regulation of CO subunit mRNAs and mtDNA. CO activity was linked more closely to CO I mRNA than to CO IV or CO VIII mRNA. This close relationship suggests that mitochondrial mRNA regulation, similar to mitochondrial subunit protein regulation (see section 9.3. above), plays a major role in controlling local CO activity in neurons. This is not surprising, given that the catalytic centers of the enzyme reside in the mitochondrial-encoded subunits (Azzi and Muller, 1990; Capaldi, 1990).

10. BRAIN CYTOCHROME OXIDASE SUBUNIT GENES AND GENE EXPRESSION

10.1. Isolation of CO Subunit Genes from Murine Brain cDNA Library

Our data thus far point to a differential distribution of subunit mRNAs and a disproportionate regulation of transcripts from the two genomes. The genes from which these studies were based were derived from non-neuronal sources (Hevner and Wong-Riley, 1991; 1993), and the possibility remains that the findings were not specific to the brain. To definitively rule out this possibility, we isolated two CO subunits from murine brain cDNA library. They were cloned and sequenced, and riboprobes were obtained and applied to brain tissue sections at both the light and electron microscopic levels (Wong-Riley et al., 1997a). We chose subunit III (mitochondrial) because of our study on its subunit proteins (Nie and Wong-Riley, 1996c). Subunit VIa (nuclear) was chosen because it is known to have tissue-specific isoforms in other species: the ubiquitous liver isoform and the heart/muscle isoform (Kadenbach and Merle, 1981; Kadenbach et al., 1982; Lomax and Grossman, 1989), and we wished to determine its degree of homology with either form. Subunit VIa also has known binding sites for ATP, which effectively affects the kinetics of this enzyme (Taanman et al., 1994).

Results indicated that the isolated cDNAs (Fig. 26A,B) and riboprobes (Fig. 26C,D) were of the expected sizes for the two subunits, respectively. Brain CO subunit III (mitochondrial) shared 100% identity with that of murine L cells (Bibb et al., 1981). Our brain subunit VIa shared 93% homology with that of the rat liver (Schlerf et al., 1988) and 100% identity with murine liver isoform (reported after our study was completed; Grossman et al., 1995) which is only 62% identical to that of the rat heart isoform. *In situ* hybridization with riboprobes revealed mRNA labeling that was similar, though not identical, to that of cytochrome oxidase histochemistry. Monocular enucleation in adult mice induced a significant down-regulation of both subunit messages in the contralateral lateral geniculate nucleus. However, the decrease in subunit III mRNAs surpassed that of subunit VIa at all time periods examined, suggesting that mitochondrial gene expression is more tightly regulated by neuronal activity than that of nuclear ones. These findings are consistent with our previous reports (Hevner and Wong-Riley, 1991, 1993).

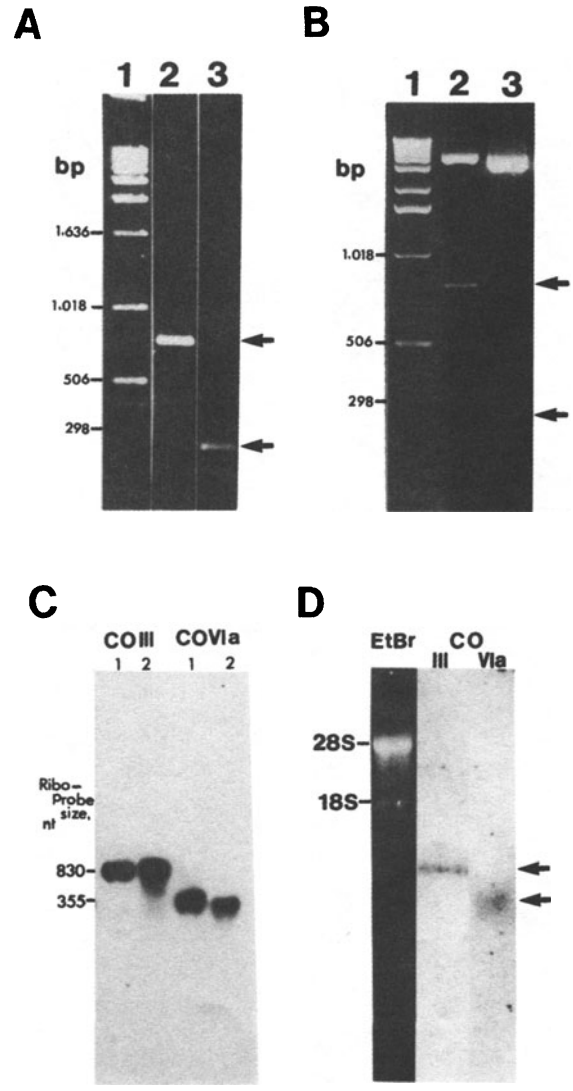

Figure 26. (**A**) Agarose gel electrophoresis of CO III (lane 2) and CO VIa (lane 3) isolated and amplified by PCR from a mouse brain cDNA library. Lane 1 contains 1 kb ladder, with base pair sizes indicated on the left. Arrows show a single band each that is of the expected size for CO III (756 base pairs) and CO VIa (251 base pairs), respectively. (**B**) Subsequent to cloning and purification, the cDNAs released from their respective plasmids by restriction digest were also of the expected sizes (arrows show CO III in lane 2 and CO VIa in lane 3; lane 1 contains 1 kb ladder). (**C**) Digoxigenin-11-UTP-labeled CO III and CO VIa riboprobe size analysis by denaturing gel electrophoresis and detection by chemiluminescence with Lumi-Phos 530. Each antisense (lanes 1) and sense (lanes 2) riboprobe appeared as a major band of the correct size (indicated by nucleotide numbers on the left) for full-length transcript of our CO III and CO VIa cDNAs, respectively. Each transcript encompassed portions of transcribed vectors as well. (**D**) In Northern blots, total RNA was prepared from murine brain, run on formaldehyde agarose gel, and transferred to positively-charged nylon membrane. Hybridization was done with Digoxigenin-labeled antisense transcripts for CO III and CO VIa and detection was by chemiluminescence with Lumi-Phos 530. Each transcript hybridized specifically to a single band of RNA at the appropriate size position expected for murine CO III and CO VIa transcripts, respectively (arrows). The positions for ethidium bromide (EtBr)-labeled 28S and 18S ribosomal RNAs are indicated on the left. (Modified from Wong-Riley et al., 1997a).

10.2. Subcellular Localization of CO III and CO VIa mRNAs

In situ hybridization at the electron microscopic level revealed a difference in the subcellular localization of CO subunits derived from the two genomes (Wong-Riley et al., 1997a). CO III mRNAs were localized exclusively to the mitochondrial compartment in both cell bodies and processes (Fig. 27). CO VIa mRNAs, on the other hand, were found only in the extramitochondrial compartment of somatic cytoplasm, primarily associated with the cytoplasmic side of the rough endoplasmic reticulum and highlighting the outer membrane of the nuclear envelope (Fig. 28).

When we traced dendrites of Purkinje cells from the somata to the molecular layer, we found CO III-labeled mitochondria from the proximal to the most distal portions of these dendrites (Fig. 27). The intensity of labeling, however, was highest in the cell bodies and decreased distally in the dendrites. Labeled mitochondria were also present in some axon terminals, but the prevalence of CO III mRNA was distinctly lower in the neuropil than in neuronal cell bodies.

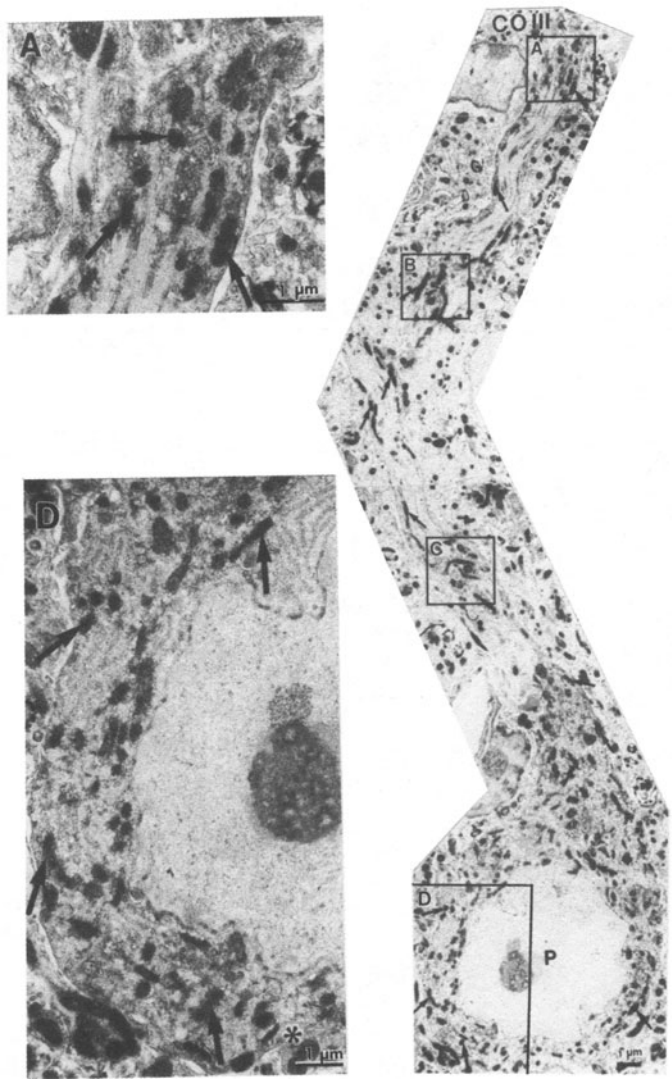

Figure 27. Ultrathin section of mouse cerebellum processed for EM *in situ* hybridization with CO III antisense riboprobes labeled with Digoxigenin-11-UTP. CO III mRNAs were localized exclusively within the mitochondrial compartment (arrows) of Purkinje cell body (P). An enlargement of a portion of the cell body (D) is seen to the lower left. When traced to its dendrites in the molecular layer (low magnification montage on the right), CO III mRNA-labeled mitochondria (arrows) were found throughout the entire length of these dendrites (one of which (A) is shown at a higher magnification on the upper left). Labeled mitochondria were also present in some axon terminals, but the prevalence of CO III mRNA was distinctly lower in the neuropil than in neuronal cell bodies. (Modified from Wong-Riley et al., 1997a).

In contrast to CO III, the labeling of nuclear-encoded CO VIa message ended abruptly at the commencement of the Purkinje cells' (and other cells') basal dendrites. Despite careful tracing from proximal to distal portions of dendrites, we did not detect any labeling of rough endoplasmic reticulum or other organelles for CO VIa mRNA within dendrites of the molecular layer (Fig. 28). Not surprisingly, labeling was also absent in axons and terminals, where rough endoplasmic reticulum and ribosomes are not known to be present. The lack of signal for CO VIa message in the neuropil was a very consistent finding.

Our results indicate that the unique properties of neurons impose special requirements for subunits of a single mitochondrial enzyme with dual genomic origins. At sites of high energy demands (such as postsynaptic dendrites and some axon terminals), mitochondrial-encoded cytochrome oxidase subunits can be locally transcribed and translated, and they provide the framework for the subsequent importation and incorporation of nuclear-encoded subunits, which are strictly synthesized in the cell bodies. Dynamic local energy needs are met when subunits from the two genomic sources are assembled to form functional holoenzymes.

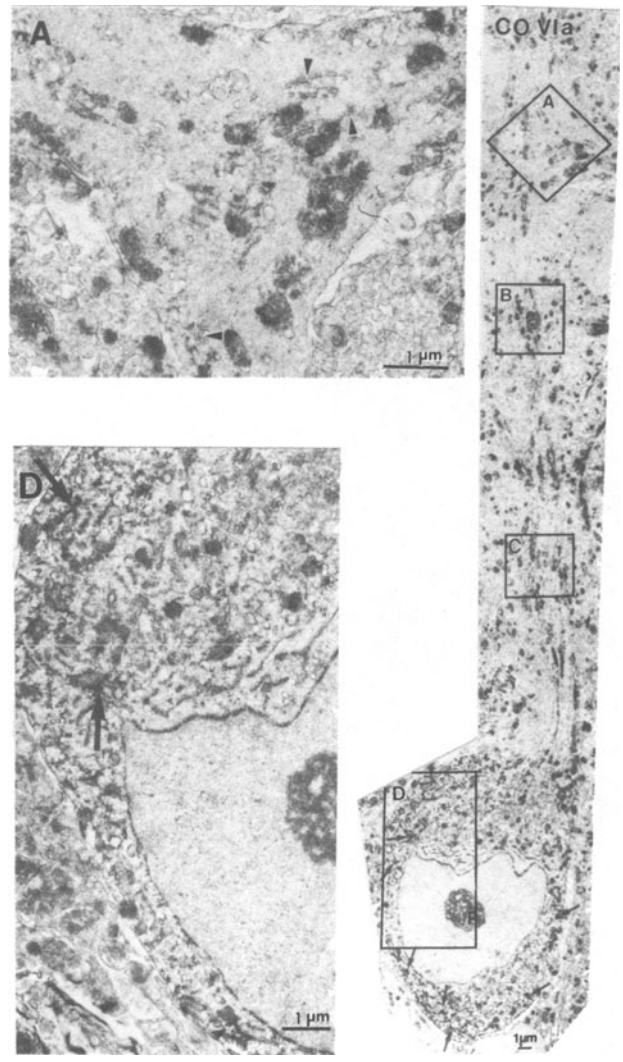

Figure 28. Ultrathin section of mouse cerebellum processed for EM *in situ* hybridization with CO VIa antisense riboprobes labeled with Digoxigenin-11-UTP. In contrast to mitochondrial-encoded CO III, nuclear-encoded CO VIa mRNAs were found in the extramitochondrial compartment, primarily associated with the cytoplasmic side of the rough endoplasmic reticulum (arrows) and the outer nuclear membrane of Purkinje cell body (P). An enlargement of a portion of the cell body (D) is seen to the lower left. Unlike CO III, the labeling of nuclear-encoded CO VIa message was confined exclusively to the cell bodies. In tracing the dendrites of this Purkinje cell from the proximal to the distal parts in the molecular layer (low magnification montage on the right, with the most distal portion (A) shown at a higher magnification on the upper left), no labeling was evident in the rough endoplasmic reticulum (arrowheads) or other organelles in the cytoplasm. The rest of the neuropil was also devoid of labeling. (Modified from Wong-Riley et al., 1997a).

10.3. Model of Cytochrome Oxidase Subunit Synthesis and Assembly

CO holoenzyme assembly is dependent upon subunit contributions from both mitochondrial and nuclear genomes (Wikstrom et al., 1981). The genes for the 3 mitochondrial CO subunits, which form the catalytic center of the enzyme, are present in their host organelles throughout the entire extent of the neuron, but are most abundant in regions of high energy demand, such as dendrites (Hevner and Wong-Riley, 1991). The expression of these genes, however, is most prevalent in neuronal cell bodies and less so in dendrites and axon terminals. On the other hand, the genes for the other ten CO subunits reside only in the nucleus, and the synthetic machinery of their gene products occurs only in the perikarya. Once synthesized, these nuclear-encoded CO subunit precursor proteins are delivered within the mitochondrial compartment to distal processes, where they form a precursor pool (Liu and Wong-Riley, 1994).

Our collective results support a model for CO subunit synthesis, assembly, and distribution in neurons as depicted in Figure 29. The synthesis of mitochondrial- and nuclear-CO subunit proteins (mCO and nCO) involves at least two processes: (1) Transcription in the nucleus and translation in the somatic cytoplasm of nCO as well as of mitochondrial gene expression proteins (mitochondrial transcription factors; Clayton, 1991); and (2) import of nCO precursor proteins and transcription factors into the somatic mitochondria, where the processing of nCO precursor proteins and the activation of mtDNA by transcription factors lead to the maturation of nCO, synthesis of mCO, and subsequent assembly of the holoenzyme. These processes are most pronounced within neuronal cell bodies. However, in dendrites and some axon terminals, transcription and translation of some mCO continue and provide the framework for the subsequent incorporation of nCO, whose precursors form a pool in these processes. In a typical multipolar neuron, such local reserve is both expedient and critical for sustaining and anticipating numerous local synaptic activi-

Figure 29. Schematic diagrams showing the subcellular localization of mitochondrial- and nuclear-encoded CO mRNAs (A) and a model for the synthesis, assembly, and distribution of CO in various compartments of neurons (B). Mitochondrial-encoded CO mRNAs are localized in mitochondria (**A**, top), being densest in the cell body, moderate in dendrites, and present also in some axon terminals. Nuclear-encoded CO mRNAs, on the other hand, are found exclusively in the somatic cytoplasm outside of the mitochondria, and associated mainly with the cytoplasmic side of the rough endoplasmic reticulum and the outer nuclear membrane (**A**, bottom). (**B**) The present model is based on our work up-to-date and represents a slight modification of our previous models (Hevner and Wong-Riley, 1991; Liu and Wong-Riley, 1994). It also incorporates some previously postulated mechanisms regarding nuclear-encoded transcription factors for the stimulation of mitochondrial DNA (mtDNA) transcription as well as mitochondrial transport along microtubules. Within the cell body (middle panel), nuclear-encoded CO mRNAs are transcribed in the nucleus and translated into specific CO subunit (n-CO) precursor proteins on RER and/or free ribosomes (1), and are subsequently imported into the mitochondria (2) (see also Maccecchini et al., 1979). Once inside, the precursor proteins (nCO precursor) are inserted into the inner mitochondrial membrane (3) either with their attached presequence or after the presequence has been cleaved by proteases (4). Following processing, nCO subunit proteins bind to existing mitochondrial subunit proteins (mCO) for assembly into CO holoenzyme (5). Meanwhile, nuclear-encoded transcription factors (n-TF) are also transcribed in the nucleus and translated in the somatic cytoplasm (6). They are then imported into the mitochondria (7), where they bind to mtDNA (8) and stimulate its gene expression (9). The newly synthesized mitochondrial CO subunit proteins (mCO) are then inserted into the inner mitochondrial membrane (10), where they form the catalytic core for holoenzyme assembly with nuclear-derived CO subunits (nCO mature) (5). These processes are most active in the cell bodies, but the expression and production of mCO continues in dendrites (top panel) and some axon terminals (bottom panel). The production of nCO precursors, on the other hand, occurs only in the cell body, but they form a precursor pool in the mitochondria of many dendrites and some axon terminals, where they await further processing and assembly with mCO to form functional holoenzymes to meet local energy demands. (Taken from Wong-Riley et al., 1997a).

ties. Holoenzyme assembly of mCO and nCO in neurons is governed by dynamic energy needs, often at a very local level. Thus, neurons have effective mechanisms for regulating the oxidative enzymes that are critical for their energy supply and functional integrity at cellular, subcellular, and molecular levels.

11. OTHER CONSIDERATIONS

Much remains to be learned about mechanisms that coordinate the expression of physically separated genomes for mitochondrial biogenesis and protein trafficking, as well as for the synthesis, assembly, and turnover of respiratory enzymes. As discussed above, these problems are compounded in multipolar neurons. The molecular signal that triggers the cascade of events from functional activation to coordinated dual gene expressions in neuronal somata and processes remains elusive.

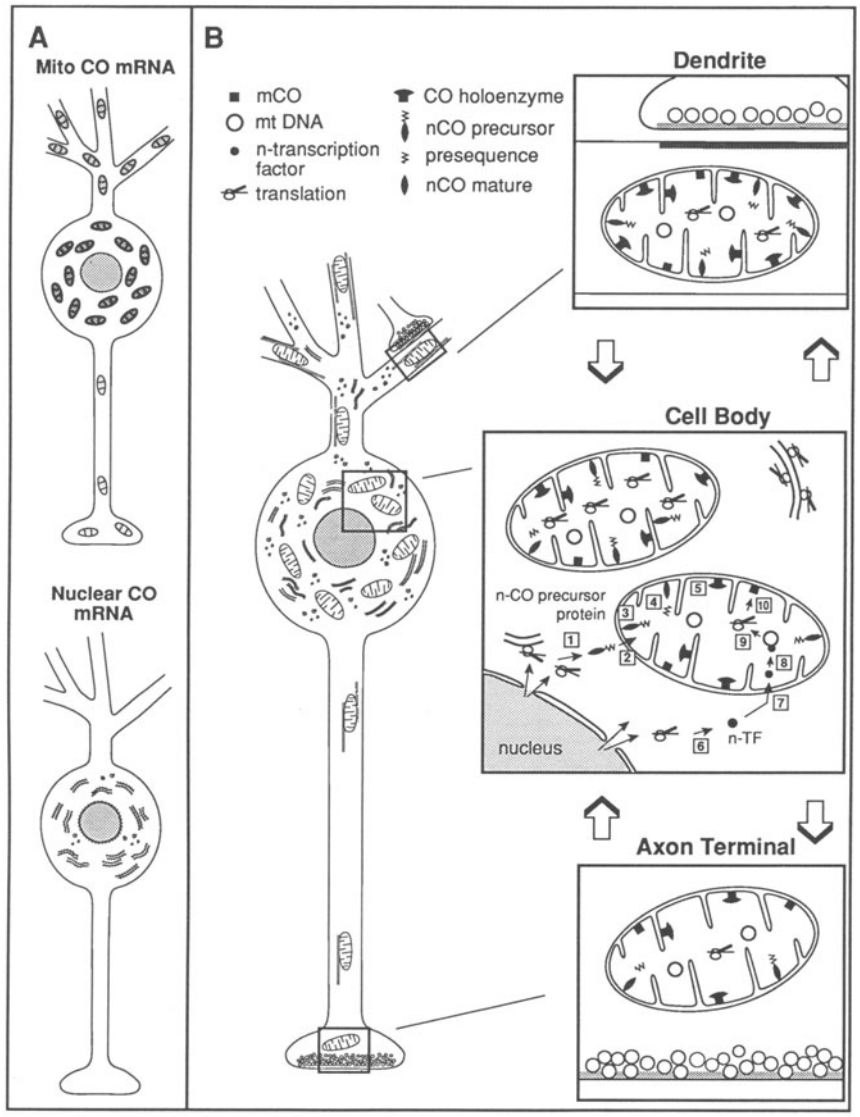

11.1. Nuclear Respiratory Factors

The recently discovered nuclear respiratory factors 1 and 2 (NRF-1 and NRF-2) show great promise in coordinating the two genomes by stimulating not only respiratory enzyme genes, including some CO subunit genes, but also mitochondrial transcription factors (mtTFA) that are necessary for both replication and transcription of mtDNA (Fisher et al., 1989; Evans and Scarpulla, 1990; Virbasius et al., 1993; Parisi et al., 1993; Virbasius and Scarpulla, 1994; Scarpulla, 1997). These transcription factors share a high degree of sequence identity with *Ets* domain activators of viral promoters, such as murine GA-binding protein (GABP) (Thompson et al., 1991; Virbasius et al., 1993). Our laboratory has begun examining activity-induced changes in GABP in cultured neurons (Zhang and Wong-Riley, 1997). More in-depth analysis of NRF's role in bigenomic regulation of cytochrome oxidase and other respiratory enzymes in neurons is also warranted.

11.2. Mitochondrial Diseases and Pathology

The symbiotic relationship between mitochondria and the nucleus has long been recognized as critical for normal workings of the cell. Dysfunction of one or the other, either genetically acquired or environmentally induced, could severely compromise the survival of the cell. A number of mitochondrial diseases have been recognized in the last three decades that impair energy metabolism and produce widespread clinical abnormalities (reviewed in Morgan-Hughes, 1986; Blass et al., 1988; Wallace, 1992; Ernster et al., 1995). Deficiency in cytochrome oxidase activity is often one of the diagnostic findings, even though the primary defect may not involve CO genes. In MERRF (myoclonic epilepsy and ragged red fibers) and MMC (maternally inherited myopathy and cardiopathy), the mutation is in the $tRNA^{Lys}$ gene and $tRNA^{Leu(UUR)}$ gene, respectively. Not surprisingly, they affect mainly the activities of complex I and complex IV, both of which have the most mitochondrial encoded subunits among the electron transport chain enzymes (reviewed in Wallace, 1992). In Leigh's syndrome (subacute necrotizing encephalomyelopathy), mutation in a nuclear-encoded CO subunit gene has been implicated in some of the patients (Munaro et al., 1997). In Kearns-Sayre syndrome, however, large-scale deletions of mtDNA, including CO subunit genes, induce a down-regulation of mitochondrial-, but not of nuclear-encoded CO subunit proteins (Mita et al., 1989). Mutations that directly affects CO I gene (a G7444A transition in the mtDNA) has been reported in a small number of patients with Leber's Hereditary Optic Neuropathy, a disease that typically targets one of the complex I genes (Brown et al., 1992). However, mitochondrial diseases are highly variable, and the same genotype does not always predict a set of phenotypes or vice versa (Wallace, 1995).

In recent years, attention has been paid to the relationship between mtDNA mutation and aging (reviewed in Wallace, 1995). With normal aging, mutant mtDNAs are expected to increase from cumulative attacks by reactive oxygen species. Tissues that are highly dependent on aerobic metabolism, such as brain and muscle, are particularly vulnerable to respiratory dysfunction. If sufficient defective mitochondria accumulate, pathology is expected to set in. Indeed, diseases of aging such as Alzheimer's, Huntington's, and Parkinson's diseases have exhibited defects in oxidative phosphorylation (reviewed in Wallace, 1992). The role of cytochrome oxidase in Alzheimer's Disease (AD) is particularly compelling, and this topic will be extensively discussed and reviewed in other chapters of this volume. Our own analysis of AD brains indicates that cytochrome oxidase levels determined biochemically, histochemically and immunohistochemically were significantly reduced in many brain regions (Wong-Riley et al., 1997b).

12. CONCLUSIONS

Cytochrome oxidase is one of the most ancient enzymes known; yet its importance as an indicator of neuronal functioning is only realized in the last two decades. Its heterogeneous distributions at the regional, laminar, cellular and subcellular levels reveal neurons' ingenuity in regulating their local energy metabolism. Its sensitivity in responding to functional perturbations bears testimony to the plastic properties of even mature neurons. Being bigenomically encoded, cytochrome oxidase serves as a useful model for probing the mechanisms of dual genomic regulation of an essential respiratory enzyme. In neurons, where the two genomes can be far apart, local enzyme activity appears to be controlled mainly by mitochondrial-encoded transcripts and subunit proteins, which form the catalytic core of the enzyme. Under normal conditions, neuronal activity regulates cytochrome oxidase activity, amount, subunit proteins, subunit mRNAs, and mitochondrial gene copy number.

ACKNOWLEDGMENTS

It is a distinct pleasure for M. Wong-Riley to thank all her past and present associates who have contributed valuable time, effort and talent to the projects. Special thanks go to Z. Huang, W. Liebl, C. Zhang and S. Holzman for their expert assistance in recent projects and in the preparation of the plates. Supported by NIH grant EY05439 to M. W-R.

REFERENCES

Attardi, G. and Schatz, G. (1988). Biogenesis of mitochondria. *Annu. Rev. Cell Biol.*, 4, 289–333.

Ausubel F.M., Brent R., Kingston R.E., Moore D.D., Seidman J.G., Smith J.A. and Struhl K. (1994). *Current Protocols in Molecular Biology*. John Wiley and Sons, New York.

Azzi, A. and Muller, M. (1990). Cytochrome c oxidase: polypeptide composition, role of subunits, and location of active metal centers. *Arch. Biochem. Biophys.*, 280, 242–251.

Bachelard, H.S. Energy utilized by neurotransmitters. In D.H. Ingvar and N.A. Lassen (Eds.), *Brain Work: The Coupling of Function, Metabolism, and Blood Flow in the Brain, Alfred Benzon Symposium VIII*. Academic Press, New York, 1975, pp. 79–81.

Basu, A. and Avadhani, N.G. (1991). Structural organization of nuclear gene for subunit Vb of mouse mitochondrial cytochrome c oxidase. *J. Biol. Chem.*, 266, 15450–15456.

Bereiter-Hahn, J., and M. Voth (1983). Metabolic control of shape and structure of mitochondria *in situ*. *Biol. Cell*, 47, 309–322.

Bibb, M.J., Van Etten, R.A., Wright, C.T., Walverg, M.W. and Clayton, D.A. (1981). Sequence and gene organization of mouse mitochondrial DNA. *Cell*, 26, 167–180.

Blass, J.P., Sheu, R.K.-F. and Cedarbaum, J.M. (1988). Energy metabolism in disorders of the nervous system. *Rev. Neurol. (Paris)*, 144, 543–563.

Borowsky, I.W. and Collins, R.C. (1989). Histochemical changes in enzymes of energy metabolism in the dentate gyrus accompany deafferentation and synaptic reorganization. *Neurosci.*, 33, 253–262.

Brown, G.C., Crompton, M. and Wray, S. (1991). Cytochrome oxidase content of rat brain during development. *Biochim. Biophys. Acta*, 1057, 273–275.

Brown, M.D., Yang, C.-C., Trounce, I., Torroni, A., Lott, M.T. and Wallace, D.C. (1992). A mitochondrial DNA variant, identified in Leber Hereditary Optic Neuropathy patients, which extends the amino acid sequence of cytochrome c oxidase subunit 1. *Am. J. Hum. Genet.*, 51, 378–385.

Capaldi, R.A. (1990). Structure and assembly of cytochrome c oxidase. *Arch. Biochem. Biophys.*, 280, 252–262.

Capaldi R.A., Takamiya S., Zhang Y.Z., Gonzalez-Halphen D. and Yanamura W. (1987). Structure of cytochrome-c oxidase. *Curr. Top. Bioenerg.*, 15, 91–112.

Carroll, E.W. and Wong-Riley, M.T.T. (1984). Quantitative light and electron microscopic analysis of cytochrome oxidase-rich zones in the striate cortex of the squirrel monkey. *J. Comp. Neurol.*, 222, 1–17.

Cohen, P.J. (1973). Effect of anesthetics on mitochondrial function. *Anesthesiology*, 39, 153–164.

Cohen, P. Well established systems of enzyme regulation by reversible phosphorylation. In P. Cohen (Ed.) *Recently Discovered Systems of Enzyme Regulation by Reversible Phosphorylation.* Elsevier/North-Holland Biomedical Press, Amsterdam, 1980a, pp. 1–10.

Cohen, P. Protein phosphorylation and the co-ordinated control of intermediary metabolism. In P. Cohen (Ed.) *Recently Discovered Systems of Enzyme Regulation by Reversible Phosphorylation.* Elsevier/North-Holland Biomedical Press, Amsterdam, 1980b, pp. 255–268.

Collingridge, G.L. and Singer, W. (1990). Excitatory amino acid receptors and synaptic plasticity. *Trends Pharm. Sci.* 11, 290–296.

Creutzfeldt, O.D. Neurophysiological correlates of different functional states of the brain. In D.H. Ingvar and N.A. Lassen (Eds.), *Brain Work. Alfred Benzon Symposium, VIII.* Academic Press, New York, 1975, pp. 21–46.

Darriet, D., Der T. and Collins, R.C. (1986). Distribution of cytochrome oxidase in rat brain: studies with diaminobenzidine histochemistry *in vitro* and [^{14}C]cyanide tissue labeling *in vivo*. *J. Cereb. Blood Flow Metab.*, 6, 8–14.

Dawson, T.M. and Snyder, S.H. (1994). Gases as biological messengers: Nitric oxide and carbon monoxide in the brain. *J. Neurosci.*, 14, 5147–5159.

DeYoe, E.A., Trusk, T.C. and Wong-Riley, M.T.T. (1995). Activity correlates of cytochrome oxidase-defined compartments in granular and supragranular layers of primary visual cortex of the macaque monkey. *Vis. Neurosci.* 12, 629–639.

Dimlich, R.V.W., Showers, M.J. and Shipley, M.T. (1990). Densitometric analysis of cytochrome oxidase in ischemic rat brain. *Brain Res.*, 516, 181–191.

DiRocco, R.J., Kageyama, G.H. and Wong-Riley, M.T.T. (1989). The relationship between CNS metabolism and cytoarchitecture: A review of ^{14}C-deoxyglucose studies with correlation to cytochrome oxidase histochemistry. *Comput. Med. Imag. and Graph.*, 13, 81–92.

Erecinska, M., and I.A. Silver (1989). ATP and brain function. *J. Cereb. Blood Flow Metab.*, 9, 2–19.

Ernster, L., Luft, R. and Orrenius, S. (1995). Mitochondrial Diseases. Proceedings of Nobel Symposium 90. *Biochim. Biophy. Acta*, 1271, 1–292.

Errede B., Kamen M. D. and Hatefi Y. (1978). Preparation and properties of complex IV (ferrocytochrome *c*: oxygen oxidoreductase EC 1.9.3.1). *Meth. Enzymol.*, 53, 40–47.

Evans, M.J. and Scarpulla, R.C. (1990). NRF-1: a *trans*-activator of nuclear-encoded respiratory genes in animal cells. *Genes & Devt.*, 4, 1023–1034.

Fagg, G.E. (1985). L-Glutamate, excitatory amino acid receptors and brain function. *Trends Neurosci.*, 8, 1–4.

Fisher, R.P., Parisi, M.A. and Clayton, D.A. (1989). Flexible recognition of rapidly evolving promoter sequences by mitochondrial transcription factor 1. *Genes & Devt.*, 3, 2202–2217.

Fonnum, F. (1984). Glutamate: a neurotransmitter in mammalian brain. *J. Neurochem.*, 42, 1–11.

Forsburg, S.L. and Guarente, L. (1989). Communication between mitochondria and the nucleus in regulation of cytochrome genes in the yeast Saccharomyces cerevisiae. *Annu. Rev. Cell Biol.*, 5, 153–180.

Garthwaite, J. (1991). Glutamate, nitric oxide and cell-cell signaling in the nervous system. *Trends Neurosci.*, 14, 60–67.

Gonzalez-Lima, F. Brain imaging of auditory learning functions in rats: Studies with fluorodeoxyglucose autoradiography and cytochrome oxidase histochemistry. In F. Gonzalez-Lima, T. Finkenstadt, and H. Scheich (Eds.), *Advances in Metabolic Mapping Techniques for Brain Imaging of Behavioral and Learning Functions.* NATO ASI Series D. Vol. 68, Kluwer Academic Publishers, Dordrecht/Boston/London, 1992, pp. 39–109.

Gonzalez-Lima, F. and Garrosa, M. (1991). Quantitative histochemistry of cytochrome oxidase in rat brain. *Neurosci. Lett.*, 123, 251–253.

Goto, Y., Naoki, A. and Taro, O. (1989). Nucleotide sequence of cDNA for rat brain and liver cytochrome c oxidase subunit IV. *Nucleic Acids Res.*, 17, 2851.

Grafstein, B. and Forman, D.S. (1980). Intracellular transport in neurons. *Physiol. Rev.*, 60, 1167–1283.

Gross, N.J., Getz, G.S. and Rabinowitz, M. (1969). Apparent turnover of mitochondrial deoxyribonucleic acid and mitochondrial phospholipids in the tissues of the rat. *J. Biol. Chem.*, 244, 1552–1562.

Grossman L.I., Rosenthal N.H., Akamatsu M. and Erickson R.P. (1995). Cloning, sequence analysis, and expression of a mouse cDNA encoding cytochrome c oxidase subunit VIa liver isoform. *Biochim. Biophys. Acta*, 1260, 361–364.

Harding, A.E. (1991). Neurological disease and mitochondrial genes. *Trends Neurosci.*, 14, 132–138.

Hartl, F.U., Pfanner, N., Nicholson, D.W. and Neupert, W. (1989). Mitochondrial protein import. *Biochim. Biophys. Acta*, 988, 1–45.

Hatefi, Y. (1985). The mitochondrial electron transport and oxidative phosphorylation system. *Annu. Rev. Biochem.*, 54, 1015–1069.

Hevner, R.F. and Wong-Riley, M.T.T. (1989). Brain cytochrome oxidase: Purification, antibody generation, and immunohistochemical/histochemical correlations in the CNS. *J. Neurosci.*, 9, 3884–3898.

Hevner, R.F. and Wong-Riley, M.T.T. (1990). Regulation of cytochrome oxidase protein levels by functional activity in the macaque monkey visual system. *J. Neurosci.*, 10, 1331–1340.

Hevner, R.F. and Wong-Riley, M.T.T. (1991). Neuronal expression of nuclear and mitochondrial genes for cytochrome oxidase (CO) subunits analyzed by in situ hybridization: Comparison with CO activity and protein. *J. Neurosci.*, 11, 1942–1958.

Hevner, R.F. and Wong-Riley, M.T.T. (1993). Mitochondrial and nuclear gene expression for cytochrome oxidase subunits are disproportionately regulated by functional activity in neurons. *J. Neurosci.*, 13, 1805–1819.

Hevner, R.F., Duff, R.S. and Wong-Riley, M.T.T. (1992). Coordination of ATP production and consumption in brain: Parallel regulation of cytochrome oxidase and Na^+,K^+-ATPase. *Neurosci. Lett.*, 138, 188–192.

Hevner, R.F., Liu, S. and Wong-Riley, M.T.T. (1993). An optimized method for determining cytochrome oxidase activity in brain tissue homogenates. *J. Neurosci. Meth.*, 50, 309–319.

Hevner, R.F., Liu, S. and Wong-Riley, M.T.T. (1995). A metabolic map of cytochrome oxidase in the rat brain: Histochemical, densitometric and biochemical studies. *Neurosci.*, 65, 313–342.

Hicks, T.P., Lodge, D. and McLennan, H. (1987). *Excitatory Amino Acid Transmission*. Alan R. Liss, New York.

Hood, D.A. (1990). Co-ordinate expression of cytochrome c oxidase subunit III and VIc mRNAs in rat tissues. *Biochem. J.*, 269, 503–506.

Hundt, E., Trapp, M. and Kadenbach, B. (1980). Biosynthesis of cytochrome c oxidase in isolated rat hepatocytes. *FEBS Lett.*, 115, 95–99.

Hyde, G.E. and Durham, D. (1990). Cytochrome oxidase response to cochlea removal in chicken auditory brainstem neurons. *J. Comp. Neurol.*, 297, 329–339.

Ignacio, P.C., Baldwin, B.A., Vijayan, V.K., Tait, R.C. and Gorin, F.A. (1990). Brain isozyme of glycogen phosphorylase: Immunohistological localization within the central nervous system. *Brain Res.*, 529, 42–49.

Isashiki, Y., Nakagawa, M. and Higuchi, I. (1991). Immunohistochemistry of the monkey retina with a monoclonal antibody against subunit V of cytochrome c oxidase. *ACTA Ophthal.*, 69, 321–326.

Jaussi, R., Sonderegger, P., Fluckiger, J. and Christen, P. (1982). Biosynthesis and topogenesis of aspartate aminotransferase isoenzymes in chicken embryo fibroblasts. The precursor of the mitochondrial isoenzyme is either imported into mitochondria or degraded in the cytosol. *J. Biol. Chem.*, 257, 13334–13340.

Jeffrey, P.L., James, K.A.C., Kidman, A.D., Richards, A.M. and Austin, L. (1972). The flow of mitochondria in chicken sciatic nerve. *J. Neurobiol.*, 3, 199–208.

Kadenbach B. and Merle P. (1981). On the function of multiple subunits of cytochrome c oxidase from higher eukaryotes. *FEBS Lett.*, 135, 1–11.

Kadenbach B., Hartmann R., Glanville R. and Buse G. (1982). Tissue-specific genes code for polypeptide VIa of bovine liver and heart cytochrome c oxidase. *FEBS Lett.*, 138, 236–238.

Kadenbach, B., Jaraush, S., Hartmann, R. and Merle, P. (1983). Separation of mammalian cytochrome c oxidase into 13 polypeptides by a sodium dodecyl sulfate- gel electrophoresis procedure. *Anal. Biochem.*, 129, 517–521.

Kageyama, G.H. and Wong-Riley, M.T.T. (1982). Histochemical localization of cytochrome oxidase in the hippocampus: Correlation with specific neuronal types and afferent pathways. *Neurosci.*, 7, 2337–2361.

Kageyama, G.H. and Wong-Riley, M.T.T. (1984). The histochemical localization of cytochrome oxidase in the retina and lateral geniculate nucleus of the ferret, cat, and monkey, with particular reference to retinal mosaics and ON/OFF-center visual channels. *J. Neurosci.*, 4, 2445–2459.

Kageyama, G.H. and Wong-Riley, M.T.T. (1985). An analysis of the cellular localization of cytochrome oxidase in the lateral geniculate nucleus of the adult cat. *J. Comp. Neurol.*, 242, 338–357.

Kaput, J., Goltz, S. and Blobel, G. (1982). Nucleotide sequence of the yeast nuclear gene for cytochrome c peroxidase precursor. *J. Biol. Chem.*, 257, 15054–15058.

Katz, L.C., Gilbert, C.D. and Wiesel, T.N. (1989). Local circuits and ocular dominance columns in monkey striate cortex. *J. Neurosci.*, 9, 1389–1399.

Krnjevic, K. Coupling of neuronal metabolism and electrical activity. In D.H. Ingvar and N.A. Lassen (Eds.), *Brain Work: The Coupling of Function, Metabolism, and Blood Flow in the Brain, Alfred Benzon Symposium VIII*. Academic Press, New York, 1975, pp. 65–78.

Krnjevic, K. Neurotransmitters in cerebral cortex: a general account, In E.G. Jones and A. Peter (Eds.), *Cerebral Cortex, Vol. 2. Functional Properties of Cortical Cells*. Plenum Press, New York, 1984, pp. 39–61.

Krnjevic, K. and S. Schwartz (1966). The action of gamma-aminobutyric acid on cortical neurons. *Exp. Brain Res.*, 3, 320–336.

LaManna, J.C., Kutina-Nelson, K.L., Hritz, M.A., Huang, Z. and Wong-Riley, M.T.T. (1996). Decreased rat brain cytochrome oxidase activity after prolonged hypoxia. *Brain Res.*, 720, 1–6.

Land, P.W. and Simons, D.J. (1985). Metabolic activity in SmI cortical barrels of adult rats is dependent on patterned sensory stimulation of the mystacial vibrissae. *Brain Res.*, 341, 189–194.

Livingstone, M.S., and Hubel, D.H. (1984). Anatomy and physiology of a color system in the primate visual cortex. *J. Neurosci.*, 4, 309–356.

Liu, S., Wilcox, D.A., Sieber-Blum, M. and Wong-Riley, M. (1990). Developing neural crest cells in culture: Correlation of cytochrome oxidase activity with SSEA-1 and dopamine beta-hydroxylase immunoreactivity. *Brain Res.*, 535, 271–280.

Liu, S. and Wong-Riley, M.T.T. (1994). Nuclear-encoded mitochondrial precursor protein: Intramitochondrial delivery to dendrites and axon terminals of neurons and regulation by neuronal activity. *J. Neurosci.*, 14, 5338–5351.

Lomax M.I. and Grossman L.I. (1989). Tissue-specific genes for respiratory proteins. *Trends Biochem. Sci.*, 14, 501–503.

Lorenz, T. and Willard, M. (1978). Subcellular fractionation of intra-axonally transported polypeptides in the rabbit visual system. *Proc. Natl. Acad. Sci. USA*, 75, 505–509.

Lowry, O.H. Energy metabolism in brain and its control. In D.H. Ingvar and N.A. Lassen (Eds.), *Brain Work: The Coupling of Function, Metabolism, and Blood Flow in the Brain, Alfred Benzon Symposium VIII*. Academic Press, New York, 1975, pp. 48–64.

Luo, X.G., Hevner, R.F. and Wong-Riley, M.T.T. (1989). Double labeling of cytochrome oxidase and gamma aminobutyric acid in central nervous system neurons of adult cats. *J. Neurosci. Meth.*, 30, 189–195.

Maccecchini M.L., Rudin Y., Blobel G. and Schatz G. (1979). Import of proteins into mitochondria: precursor forms of the extramitochondrially made F1-ATPase subunits in yeast. *Proc. Natl. Acad. Sci. USA*, 76, 343–347.

Malenka, R.C. and Nicoll, R.A. (1993). NMDA-receptor-dependent synaptic plasticity: multiple forms and mechanisms. *Trends Neurosci.*, 16, 521–527.

Mata, M., D.J. Fink, H. Gainer, C.B. Smith, L. Davidsen, H. Savaki, W.J. Schwartz, and L. Sokoloff (1980). Activity-dependent energy metabolism in rat posterior pituitary primarily reflects sodium pump activity. *J. Neurochem.*, 34, 213–215.

Mawe, G.M., and M.D. Gershon (1986). Functional heterogeneity in the myenteric plexus: Demonstration using cytochrome oxidase as a verified cytochemical probe of the activity of individual enteric neurons. *J. Comp. Neurol.*, 249, 381–391.

Mita, S., Schmidt, B., Schon, E.A., DiMauro, S. and Bonilla, E. (1989). Detection of "deleted" mitochondrial genomes in cytochrome-c oxidase-deficient muscle fibers of a patient with Kearns-Sayre syndrome. *Proc. Nail. Acad. Sci. USA*, 86, 9509–9513.

Mjaatvedt, A.E. and Wong-Riley M.T.T. (1986). Double-labeling of rat a-motoneurons for cytochrome oxidase and retrogradely transported [^{3}H]WGA. *Brain Res.*, 368, 178–182.

Mjaatvedt, A.E. and Wong-Riley M.T.T. (1988). Relationship between synaptogenesis and cytochrome oxidase activity in Purkinje cells of the developing rat cerebellum. *J. Comp. Neurol.*, 277, 155–182.

Mjaatvedt, A.E. and Wong-Riley, M.T.T. (1991). Effects of unilateral climbing fiber deafferentation on cytochrome oxidase activity in the developing rat cerebellum. *J. Neurocytol.*, 20, 2–16.

Morgan-Hughes, J.A. (1986). Mitochondrial diseases. *Trends Neurosci.*, 9, 15–19.

Mori, M., Morita, T., Ikeda, F., Amaya, Y., Tatibana, M. and Cohen, P.P. (1981). Synthesis, intracellular transport, and processing of the precursors for mitochondrial ornithine transcarbamylase and carbamoylphosphate synthetase I in isolated hepatocytes. *Proc. Natl. Acad. Sci.* USA, 78, 6056–6060.

Morris, R.L. and Hollenbeck, P.J. (1993). The regulation of bidirectional mitochondrial transport is coordinated with axonal outgrowth. *J. Cell Sci.*, 104, 917–927.

Munaro, M., Tiranti, V., Sandona, D., Lamantea, E., Uziel, G., Bisson, R. and Zeviani, M. (1997). A single cell complementation class is common to several cases of cytochrome c oxidase-defective Leigh's syndrome. *Hum. Mol. Genet.*, 6, 221–228.

Nakanishi, S. (1992). Molecular diversity of glutamate receptors and implications for brain function. *Science*, 258, 597–603.

Nie, F. and Wong-Riley, M.T.T. (1995). Double labeling of GABA and cytochrome oxidase in the macaque visual cortex: Quantitative EM analysis. *J. Comp. Neurol.*, 356, 115–131.

Nie, F. and Wong-Riley, M.T.T. (1996a). Differential glutamatergic innervation in cytochrome oxidase-rich and -poor regions of the macaque striate cortex: Quantitative EM analysis of neurons and neuropil. *J. Comp. Neurol.*, 369, 571–590.

Nie, F. and Wong-Riley, M.T.T. (1996b). Metabolic and neurochemical plasticity of g-aminobutyric acid-immunoreactive neurons in the adult macaque striate cortex following monocular impulse blockade: Quantitative electron microscopic analysis. *J. Comp. Neurol.*, 370, 350–366.

Nie, F. and Wong-Riley, M. (1996c). Mitochondrial- and nuclear-encoded subunits of cytochrome oxidase in neurons: Differences in compartmental distribution, correlation with enzyme activity, and regulation by neuronal activity. *J. Comp. Neurol.*, 373, 139–155.

Nobrega, J.N., Raymond, R., DiStefano, L. and Burnham, W.M. (1993). Long-term changes in regional brain cytochrome oxidase activity induced by electroconvulsive treatment in rats. *Brain Res.*, 605, 1–8.

Palay, S.L. and Chan-Palay, V. (1974). *Cerebellar Cortex*. Springer, New York.

Parisi, M.A., Xu, B. and Clayton, D.A. (1993). A human mitochondrial transcriptional activator can functionally replace a yeast mitochondrial HMG-box protein both in vivo and in vitro. *Mol. Cell. Biol.*, 13, 1951–1961.

Pfeiffer, B., Elmer, K., Roggendorf, W., Reinhart, P.H., and Hamprecht, B. (1990). Immunohistochemical demonstration of glycogen phosphorylase in rat brain slices. *Histochem.*, 94, 73–80.

Poyton R.O., Trueblood C.E., Wright R.M. and Farrell L.E. (1988). Expression and function of cytochrome c oxidase subunit isologues. *Ann. N.Y. Acad. Sci.*, 550, 289–307.

Reid, G.A., Yonetani, T. and Schatz, G. (1982). Import of proteins into mitochondria: import and maturation of the mitochondrial intermembrane space enzymes cytochrome b_2 and cytochrome c peroxidase in intact yeast cells. *J. Biol. Chem.*, 257, 13068–13074.

Reimann, A., Huther, F.-J., Berden, J.A. and Kadenbach, B. (1988). Anions induce conformational changes and influence the activity and photoaffinity-labeling by 8-azido-ATP of isolated cytochrome c oxidase. *Biochem. J.*, 254, 723–730.

Rosevear, P., VanAken, T., Baxter, J. and Ferguson-Miller, S. (1980). Alkyl glycoside detergents: a simpler synthesis and their effects on kinetic and physical properties of cytochrome c oxidase. *Biochem.*, 19, 4108–4115.

Ruscak, M., and Whittam, R. (1967). The metabolic response of brain slices to agents affecting the sodium pump. *J. Physiol.*, 19, 595–610.

Sambrook J., Fritsch E.F. and Maniatis T. (1989). *Molecular cloning: a laboratory manual*, 2d ed. Cold Spring Harbor Press, Cold Spring Harbor, New York.

Sanger F., Nicklen S. and Coulson A.R. (1977). DNA sequencing with chain-terminating inhibitors. *Proc. Natl. Acad. Sci. USA*, 74, 5463–5467.

Scarpulla, R.C. (1997). Nuclear control of respiratory chain expression in mammalian cells. *J. Bioenerg. Biomemb.*, 29, 109–119.

Schimke, R.T. and Doyle, D. (1970). Control of enzyme levels in animal tissues. *Annu. Rev. Biochem.*, 39, 929–976.

Schlerf A., Droste M., Winter M. and Kadenbach B. (1988). Characterization of two different genes (cDNA) for cytochrome c oxidase subunit VIa from heart and liver of the rat. *EMBO J.*, 7, 2387–2391.

Schwartz, W.J. and Sharp, F.R. (1978) Autoradiographic maps of regional brain glucose consumption in resting, awake rats using [^{14}C]2-deoxyglucose. *J. Comp. Neurol.*, 177, 335–360.

Schwartz, W.J., C.B. Smith, L. Davidsen, H. Savaki, L. Sokiloff, M. Mata, D.J. Fink, and H. Gainer (1979). Metabolic mapping of functional activity in the hypothalamo-neurohypophyseal system of the rat. *Science*, 205, 723–725.

Schwerzmann, K., Hoppeler, H., Kayar, S.R. and Weibel, E.R. (1989). Oxidative capacity of muscle and mitochondria: Correlation of physiological, biochemical, and morphometric characteristics. *Proc. Natl. Acad. Sci. USA*, 86, 1583–1587.

Siegel, G., Agranoff, B., Albers, R.W. and Molinoff, P. (1989). *Basic Neurochemistry*. 4th ed. Raven Press, New York.

Smith, L. and Camerino, P.W. (1963). The reaction of particle-bound cytochrome c oxidase with endogenous and exogenous cytochrome c. *Biochem.*, 2, 1432–1439.

Sokoloff, L. Changes in enzyme activities in neural tissues with maturation and development of the nervous system. In F.O. Schmitt and F.G. Worden (Eds.), *The Neurosciences: Third Study Program*. MIT Press, Cambridge, 1974, pp. 885–898.

Sokoloff, L. (1981). Localization of functional activity in the central nervous system by measurement of glucose utilization with radioactive deoxyglucose. *J. Cereb. Blood Flow Metab.*, 1, 7–36.

Sokoloff, L., Reivich, M., Kennedy, C., Des Rosiers, M.H., Patlak, C.S., Pettigrew, K.D., Sakurada. O. and Shinohara, M. (1977). The [^{14}C]deoxyglucose method for the measurement of local cerebral glucose utilization: theory, procedure, and normal values in the conscious and anesthetized albino rat. *J. Neurochem.*, 28, 897–916.

Suske, G., Enders, C., Schlerf, A. and Kadenbach, B. (1988). Organization and nucleotide sequence of two chromosomal genes for rat cytochrome c oxidase subunit VIc: a structural and a processed gene. *DNA*, 7, 163–171.

Taanman J.-W., Turina P. and Capaldi R.A. (1994). Regulation of cytochrome c oxidase by interaction of ATP at two binding sites, one on subunit VIa. *Biochem.*, 33, 11833–11841.

Thompson, C.C., Brown, T.A. and McKnight, S.L. (1991). Convergence of Ets- and notch-related structural motifs in a heteromeric DNA binding complex. *Science*, 253, 762–768.

Trembleau A., Morales M. and Bloom F.E. (1994). Aggregation of vasopressin mRNA in a subset of axonal swellings of the median eminence and posterior pituitary: Light and electron microscopic evidence. *J. Neurosci.*, 14, 39–53.

Vale, R.D., Schnapp, B.J., Reese, T.S. and Sheetz, M.P. (1985). Movement of organelles along filaments dissociated from the axoplasm of the squid giant axon. *Cell*, 40, 449–454.

Vanneste, W.H., Ysebaert-Vanneste, M. and Mason, H.S. (1974). The decline of molecular activity of cytochrome oxidase during purification. *J. Biol. Chem.*, 249, 7390–7401.

Viebrock, A., Perz, A. and Sebald, W. (1982). The imported preprotein of the proteolipid subunit of the mitochondrial ATP synthase from *Neurospora crassa*. Molecular cloning and sequencing of the mRNA. *EMBO J.*, 1, 565–571.

Vik, S.B. and Capaldi, R. (1980). Conditions for optimal electron transfer activity of cytochrome c oxidase isolated from beef heart mitochondria. *Biochem. Biophys. Res. Comm.*, 94, 348–354.

Virbasius, J.V. and Scarpulla, R.C. (1990). The rat cytochrome c oxidase subunit IV gene family: tissue-specific and hormonal differences in subunit IV and cytochrome c mRNA expression. *Nucleic Acids Res.*, 18, 6581–6586.

Virbasius, J.V. and Scarpulla, R.C. (1994). Activation of the human mitochondrial transcription factor A gene by nuclear respiratory factors: a potential regulatory link between nuclear and mitochondrial gene expression in organelle biogenesis. *Proc. Natl. Acad. Sci. USA*, 91, 1309–1313.

Virbasius, J.V., Virbasius, C.A. and Scarpulla, R.C. (1993). Identity of GABP with NRF-2, a multisubunit activator of cytochrome oxidase expression, reveals a cellular role for an ETS domain activator of viral promoters. *Genes Dev.*, 7, 380–392.

Wallace, D.C. (1992). Diseases of the mitochondrial DNA. *Annu. Rev. Biochem.*, 61, 1175–1212.

Wallace, D.C. (1995). 1994 William Allan Award Address: Mitochondrial DNA variation in human evolution, degenerative disease, and aging. *Am. J. Hum. Genet.*, 57, 201–223.

Warren, R., Tremblay, N. and Dykes, R.W. (1989). Quantitative study of glutamic acid decarboxylase-immunoreactive neurons and cytochrome oxidase activity in normal and partially deafferented rat hindlimb somatosensory cortex. *J. Comp. Neurol.*, 288, 583–592.

Wharton D. C. and Tzagoloff A. (1967). Cytochrome oxidase from beef heart mitochondria. *Meth. Enzymol.*, 10, 245–250

Wikstrom M., Krab K. and Saraste M. (1981). *Cytochrome Oxidase. A synthesis*. Academic Press, New York.

Williams, R.S. (1986). Mitochondrial gene expression in mammalian striated muscle: evidence that variation in gene dosage is the major regulatory event. *J. Biol. Chem.*, 261, 12390–12394.

Williams, R.S. and Harlan, W. (1987). Effects of inhibition of mitochondrial protein synthesis in skeletal muscle. *Am. J. Physiol.*, 253, C866–871.

Williams, R.S., Salmons, S., Newsholme, E.A., Kaufman, R.E. and Mellor, J. (1986). Regulation of nuclear and mitochondrial gene expression by contractile activity in skeletal muscle. *J. Biol. Chem.*, 261, 376–380.

Williams, R.S., Garcia-Moll, M., Mellor, J., Salmons, S. and Harlan, W. (1987). Adaptation of skeletal muscle to increased contractile activity: expression of nuclear genes encoding mitochondrial proteins. *J. Biol. Chem.*, 262, 2764–2767.

Wong-Riley, M. (1979). Changes in the visual system of monocularly sutured or enucleated cats demonstrable with cytochrome oxidase histochemistry. *Brain Res.*, 171, 11–28.

Wong-Riley, M.T.T. (1989). Cytochrome oxidase: An endogenous metabolic marker for neuronal activity. *Trends Neurosci.*, 12, 94–101.

Wong-Riley, M.T.T. Primate Visual Cortex: Dynamic metabolic organization and plasticity revealed by cytochrome oxidase. In A. Peters and K. Rockland (Eds.), *Cerebral Cortex*, Vol. 10, Primary Visual Cortex in Primates. Plenum Press, New York, 1994, pp. 141–200.

Wong-Riley, M.T.T. and Carroll, E.W. (1984a) Quantitative light and electron microscopic analysis of cytochrome oxidase-rich zones in V II prestriate cortex of the squirrel monkey. *J. Comp. Neurol.*, 222, 18–37.

Wong-Riley, M., and Carroll, E.W. (1984b). The effect of impulse blockage on cytochrome oxidase activity in the monkey visual system. *Nature*, 307, 262–264.

Wong-Riley, M.T.T. and Kageyama, G.H. (1986). Localization of cytochrome oxidase in the spinal cord and dorsal root ganglia, with quantitative analysis of ventral horn cells in monkeys. *J. Comp. Neurol.*, 245, 41–61.

Wong-Riley, M.T.T. and Norton, T.T. (1988). Histochemical localization of cytochrome oxidase activity in the visual system of the tree shrew: Normal patterns and the effect of retinal impulse blockage. *J. Comp. Neurol.*, 272, 562–578.

Wong-Riley, M., and Riley, D.A. (1983). The effect of impulse blockage on cytochrome oxidase activity in the cat visual system. *Brain Res.*, 261, 185–193.

Wong-Riley, M.T.T. and Welt, C. (1980). Histochemical changes in cytochrome oxidase of cortical barrels following vibrissal removal in neonatal and adult mice. *Proc. Natl. Acad. Sci.*, 77, 2333–2337.

Wong-Riley, M.T.T., Merzenich, M.M. and Leake, P.A. (1978). Changes in endogenous enzymatic reactivity to DAB induced by neuronal inactivity. *Brain Re.*, 141, 185–192.

Wong-Riley, M.T.T., Walsh, S.M., Leake-Jones, P.A., and Merzenich, M.M. (1981). Maintenance of neuronal activity by electrical stimulation of unilaterally deafened cats demonstrable with the cytochrome oxidase technique. *Ann. Otol. Rhinol. Laryngol.* 90, Suppl. 82, 30–32.

Wong-Riley, M.T.T., Tripathi, S.C., Trusk, T.C., and Hoppe, D.A. (1989a). Effect of retinal impulse blockage on cytochrome oxidase-rich zones in the macaque striate cortex. I. Quantitative EM analysis of neurons. *Vis. Neurosci.*, 2, 483–497.

Wong-Riley, M, Trusk, T.C., Tripathi, S.C. and Hoppe, D.A. (1989b). Effect of retinal impulse blockage on cytochrome oxidase-rich zones in the macaque striate cortex. II. Quantitative EM analysis of neuropil. *Vis. Neurosci.*, 2, 499–514.

Wong-Riley, M.T.T., Hevner, R.F., Cutlan, R., Earnest, M., Egan, R., Frost, J. and Nguyen, T. (1993). Cytochrome oxidase in the human visual cortex: Distribution in the developing and the adult brain. *Vis. Neurosci.*, 10, 41–58.

Wong-Riley, M.T.T., Trusk, T.C., Kaboord, W., and Huang, Z. (1994). Effect of retinal impulse blockage on cytochrome oxidase-poor interpuffs in the macaque striate cortex: quantitative EM analysis of neurons. *J. Neurocytol.*, 23, 533–553.

Wong-Riley, M.T.T., Mullen, M.A., Huang, Z. and Guyer, C. (1997a). Brain cytochrome oxidase subunit complementary DNAs: Isolation, subcloning, sequencing, light and electron microscopic in situ hybridization of transcripts, and regulation by neuronal activity. *Neurosci.*, 76, 1035–1055.

Wong-Riley, M., Antuono, P., Ho, K.-C., Egan, R., Hevner, R., Liebl, W., Huang, Z., Rachel, R. and Jones, J. (1997b). Cytochrome oxidase in Alzheimer's Disease: Biochemical, histochemical, and immunohistochemical analyses of the visual and other systems. *Vision Research*, Special issue on Alzheimer's Disease and the Visual System, in press.

Wong-Riley, M., Anderson, B., Liebl, W. and Huang, Z. (1998a). Neurochemical organization of the macaque striate cortex: Correlation of cytochrome oxidase with Na^+K^+ATPase, NADPH-diaphorase, nitric oxide synthase, and NMDA receptor subunit 1. *Neurosci.*, in press.

Wong-Riley, M.T.T., Huang, Z., Liebl, W., Nie, F., Xu, H. and Zhang, C. (1998b). Neurochemical organization of the macaque retina: Effect of TTX on levels and gene expression of cytochrome oxidase and nitric oxide synthase, and on the immunoreactivity of Na^+K^+ATPase and NMDA receptor subunit 1. *Vis. Res.*, in press.

Woodford, B.J. and Blanks, J.C. (1989). Uptake of tritiated thymidine in mitochondria of the retina. *Invest. Ophthalmol. Vis. Sci.*, 30, 2528–2532.

Woodward, D.J., Hoffer, B.J., Siggins, G.R. and Bloom, F.E. (1971) The ontogenetic development of synaptic junctions, synaptic activation and responsiveness to neurotransmitter substances in rat cerebellar Purkinje cells. *Brain Res.*, 34, 73–79.

Yamada, M., Amuro, N., Goto, Y. and Okazaki, T. (1990). Structural organization of the rat cytochrome c oxidase subunit IV gene. *J. Biol. Chem.*, 265, 7687–7692.

Yip, V.S., Zhang, W.-P., Woolsey, T.A. and Lowry, O.H. (1987). Quantitative histochemical and microchemical changes in the adult mouse central nervous system after section of the infraorbital and optic nerves. *Brain Res.*, 406, 157–170.

Zhang, C. and Wong-Riley, M.T.T. (1996). Do nitric oxide synthase, NMDA receptor subunit R1 and cytochrome oxidase co-localize in the rat central nervous system? *Brain Res.*, 729, 205–215.

Zhang, C. and Wong-Riley, M.T.T. (1997). Effect of depolarization on cytochrome oxidase gene expression in primary neuronal culture of rat cortex. *Soc. Neurosci. Abstr.*, 23, 89.

2

QUANTITATIVE HISTOCHEMISTRY OF CYTOCHROME OXIDASE ACTIVITY

Theory, Methods, and Regional Brain Vulnerability

F. Gonzalez-Lima and A. Cada

Institute for Neuroscience and Department of Psychology
The University of Texas at Austin
Mezes 330
Austin, Texas 78712

ABSTRACT

This chapter explains the theory and methods for the mapping of cytochrome oxidase activity in the brain using quantitative histochemistry. Cytochrome oxidase catalyzes the electron transfer from cytochrome *c* to oxygen in all higher forms of living organisms. cytochrome oxidase activity can be measured histochemically using diaminobenzidine as the electron donor to reduce cytochrome *c*. This histochemical reaction is performed in fresh-frozen brains under conditions of linearity, using internal activity standards and quantitative densitometry, to allow quantification of enzymatic activity units. During cellular respiration, this reaction is necessary for ATP synthesis because of its coupling with oxidative phosphorylation. Cytochrome oxidase is critically important to neurons because they depend on oxidative metabolism for energy production. This chapter also reviews the regional brain effects of cytochrome oxidase inhibition. Enhanced vulnerability to cytochrome oxidase inhibition is found in brain regions most often engaged in associative memory functions. It is proposed that this vulnerability may depend on the sustained neuronal metabolic demands that long-term learning and memory imposes on these regions.

1. INTRODUCTION

Cytochrome oxidase (C.O.) is the oxygen-activating enzyme for the respiration of all animal cells, enabling cells to use oxygen to oxidize food materials (Wikstrom, Krab & Saraste, 1981). Seligman, Karnovsky, Wasserkrug and Hanker (1968) introduced a diami-

Cytochrome Oxidase in Neuronal Metabolism and Alzheimer's Disease,
edited by Gonzalez-Lima, Plenum Press, New York, 1998.

nobenzidine histochemical technique that delineated the localization of C.O. in mitochondria of heart, liver and kidney. Wong-Riley (1979) successfully modified this technique for the study of nervous tissue. Hevner and Wong-Riley (1989) showed that the optical density of histochemically labeled sections closely correlates with the amount of C.O. in nervous tissue. Since mammalian neurons normally obtain their energy from aerobic metabolism, the mapping of C.O. activity provides an elegant approach to visually display the oxidative metabolic capacity of various regions of the nervous system (Wong-Riley, Nie, Hevner & Liu, this volume).

Since C.O. catalyzes the electron transfer from cytochrome c to molecular oxygen in all eukaryotes, this enzyme is pivotal to the functioning of nervous tissue which critically depends on oxidative metabolism for energy production. C.O. is essential for aerobic metabolism in the brain because the brain normally derives almost all of its energy from aerobic metabolism of glucose (Sokoloff, 1992). C.O. catalyzes the reaction necessary for ATP synthesis by its coupling with oxidative phosphorylation. It constitutes the site where energy is conserved for subsequent ATP synthesis (Wikstrom *et al.*, 1981). In principle, all energy-consuming mechanisms that deplete the ATP produced in neurons should lead to up-regulation in the synthesis of C.O. to meet sustained metabolic demands.

Cytochrome oxidase histochemistry has demonstrated that the regional metabolic capacity of the brain is distributed unevenly. For example, in the auditory system C.O. has been mapped qualitatively in several avian species (Braun, Scheich, Schachner & Heizmann, 1985; Brauth, 1990; Hyde & Durham, 1990), cats (Hovda, Chugani, Villablanca, Badie & Sutton, 1992; Wong-Riley, Merzenich & Leake, 1978), guinea pig's superior olivary nuclei (Schofield & Cant, 1991), and rats (Harley & Bielajew, 1992). Auditory nuclei are characterized by greater C.O. labeling compared to other regions in the nervous system; a finding consistent with their higher metabolic use of glucose (Gonzalez-Lima & Scheich, 1984). If C.O. histochemistry could be quantitatively measured to obtain enzyme activity, it would provide a major advantage over other C.O. measuring techniques because it would have cellular anatomical resolution throughout the entire brain.

Gonzalez-Lima and Garrosa (1991) introduced the use of internal standards of known C.O. activity combined with computerized image analysis as a method to quantify enzyme activity from histochemically stained brain sections. Gonzalez-Lima and Cada (1994) incorporated the use of internal activity standards and quantitative densitometry together with a histochemical procedure (Silverman & Tootell, 1987) found more sensitive than other available protocols. The level of sensitivity and quantification of the resulting method was adequate to detect subtle differences in regional brain metabolic capacity (e.g. Poremba, Jones & Gonzalez-Lima, this volume).

2. THEORY

2.1. Theoretical Model of the Cytochemical Reaction

C.O. (ferrocytochrome *c*: O_2 oxidoreductase, EC 1.9.3.1) is also called cytochrome c oxidase, cytochrome aa_3, or the respiratory enzyme. C.O. is an integral transmembrane protein of the inner mitochondrial membrane. Figure 1 illustrates how electrons donated from diaminobenzidine (DAB) reduce cytochrome *c* (Cyt C). The heme units of C.O. (Cyt a-a_3) catalyze the transfer of electrons from Cyt C to molecular oxygen to form water. The staining in the cytochemical reaction is produced when DAB is oxidized to an indamine polymer (OXIDIZED DAB). Since continuous reoxidation of Cyt C by C.O. is required

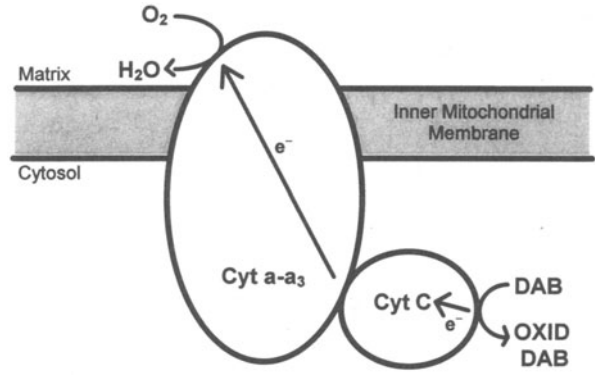

Figure 1. Schematic of the theoretical model of the diaminobenzidine (DAB) cytochemical reaction adapted from Seligman *et al.* (1968) and Wong-Riley (1989).

for the accumulation of the visible OXIDIZED DAB, this reaction serves to visualize C.O. activity. The staining of the reaction product is further intensified by the addition of cobalt to the preincubation solution (Gonzalez-Lima & Jones, 1994).

Each catalytic unit (a-a_3 monomer) of C.O. is made of two heme groups (a and a_3) and two copper ions bound to protein. The a and a_3 hemes differ mainly in spin and reactivity to various ligands in the ferrous and ferric states, and in their attachment to different polypeptide chains. Ligands bind the sixth axial position of heme a_3 (Wikström et al 1981). The two copper ions can be differentiated spectroscopically as A and B. The A copper is detectable and is in rapid redox equilibrium with heme a. The B copper is usually undetectable and is in contact with heme a_3. Spectroscopic methods take advantage of the different optical spectra of reduced and oxidized C.O. For instance, fully oxidized C.O. shows a large band at 820–840 nm which is primarily (85%) due to copper A and a weak band at 655 nm presumably due to copper B (Wikström *et al.,* 1981).

Spectrophotometric assay of C.O. is based on the rate of oxidation of cytochrome c measured by following the decrease in absorbance at 550 nm (Wharton & Tzagoloff 1967). A modification of this method is used for the spectrophotometric assay of C.O. activity in the internal standards of our quantitative histochemical technique. The reaction occurring at sites containing C.O. activity is the electron transfer from cytochrome *c* to oxygen, where at physiological pH cytochrome c is a pure electron donor and water is formed:

$$\text{cytochrome } c \text{ (Fe II)} + 1/4\ O_2 + H^+ \rightarrow \text{cytochrome } c \text{ (Fe III)} + 1/2\ H_2O$$

At physiological pH in an oxygenated medium, this reaction leads to transfer of electrons across a redox potential of 500 mV, with energy generation of about 23 kcal per electron pair transfer that is conserved for ATP synthesis at the C.O. site of oxidative phosphorylation in the inner mitochondrial membrane (Wikström *et al.,* 1981). These observations derived *in vitro* are in principle relevant to histochemical C.O. experiments. Thus in addition to pH, the oxygen and cytochrome *c* concentrations of the incubation medium influence the overall reaction.

Oxygen primarily binds the sixth position of Fe II in heme a_3, and then heme a_3 and copper B form together a binuclear center that catalyzes the reduction of oxygen to water. Therefore, saturation of the reaction medium with oxygen in C.O. histochemistry increases staining by increasing C.O. oxidation, which oxidizes cytochrome *c*, which in turn oxidizes the chromogen (DAB) that forms the reaction product (Silverman & Tootell 1987). The addition of an optimal amount of cytochrome *c* to the incubation medium is

also important, as substrate concentrations too high or too low may inhibit the reaction (Kugler, Vogel, Volk & Schiebler, 1988).

2.2. C.O. as an Endogenous Marker for Neuronal Function

The functional activity of regional, cellular and subcellular compartments of nervous tissue is tightly coupled with oxidative energy metabolism. C.O. is a mitochondrial enzyme used as an endogenous marker of local tissue metabolic capacity, because of its pivotal role in cellular respiration. C.O. is the oxygen-activating enzyme for the respiration of all animal and plant cells (eukaryotes) and some bacteria (prokaryotes), and it is the site of oxidative phosphorylation where energy is conserved for synthesis of ATP (Wikström *et al.*, 1981). ATP is used for all energy-consuming functions of neurons.

The main consumer of ATP in neurons is the Na^+/K^+ pump that maintains ion balance, sustaining the resting membrane potential that is depolarized in the electrical firing of neurons (Hevner, Duff & Wong-Riley, 1992). For a steady resting membrane potential, the ionic gradients across the membrane must be maintained using metabolic energy derived from the hydrolysis of ATP. Since the Na^+/K^+ pump moves these ions against their electrochemical gradients, ATP must be hydrolyzed to provide the energy to actively transport these ions to maintain the charge separation across the membrane constant. An increased neuronal electrical activity will ultimately lead to increased cellular aerobic respiration and obligatory C.O. activity to generate ATP. The role of mitochondria in intracellular calcium homeostasis is also important because as a result of synaptic activity neurons are subjected to transient elevations in intracellular calcium (Miller, 1991).

This coupling between C.O. activity and the energy-demanding ionic pumps related to the electrical activity of neurons is what led Wong-Riley (1989) to postulate that the level of C.O. activity within neurons should be coupled with their functional level of activity. Thus the more active neurons in a brain region have increased C.O. content in their mitochondria (Hevner & Wong-Riley, 1989). Increased neuronal electrical activity leads to increased cellular respiration and C.O. activity to produce more ATP. Although this is true under physiological conditions, there are exceptions in pathological states (Hyde & Durham, 1994).

In addition, the more active compartments within a neuron contain more mitochondria and C.O. activity (Wong-Riley 1989). Tonically active neurons are those with more C.O. activity to maintain a greater capacity for energy production needed to fuel ionic pumps and other ATP-dependent processes required for proper electrical activity. Experimental manipulations that increase or decrease the activity of neurons over a period of days result in corresponding increase or decrease of C.O. activity inside their mitochondria (Wong-Riley, 1989). The precise location of C.O. reactivity can be determined at regional, cellular, and subcellular compartments using light and electron microscopy. Therefore, there is anatomical certainty of how an increase in C.O. activity is represented subcellularly in response to physiological neuronal activity (Hevner & Wong-Riley 1989).

Histochemistry of C.O. activity has shown that the metabolic capacity of the brain can change in response to alterations in neuronal functional activity. For example, C.O. has been applied as a metabolic marker in the auditory system (e.g. Braun *et al.*, 1985; Brauth 1990; Hyde & Durham 1990; Gonzalez-Lima & Cada, 1994), the visual system (e.g. Wong-Riley, 1989), and brain regions outside primary sensory systems (e.g. Kugler, Vogel, Volk & Schiebler, 1988; Di Rocco, Kageyama & Wong-Riley, 1989). Although most experimental manipulations have focused on invasive procedures aimed at decreasing C.O. levels, there is also evidence of increases in C.O. activity (Nobrega, Raymond, DiStefano & Burnham, 1993).

Using our recent studies as examples, local cerebral C.O. activity has been increased with various genetic (Papa, Sadile, Sergaent & Gonzalez-Lima, this volume), hormonal (Crews, Coomber, Baldwin, Azad & Gonzalez-Lima, 1996; Jones, Gonzalez-Lima, Crews, Galef & Clark, 1997), environmental (Coomber, Crews & Gonzalez-Lima, 1997), and behavioral manipulations (Poremba, Jones & Gonzalez-Lima, 1997; Crews, Coomber & Gonzalez-Lima, 1997). Moreover, we have been able to demonstrate that some learning-related increases in neuronal memory functions are related to increases in C.O. activity (Poremba *et al.*, this volume), using the sensitive histochemical and quantitative imaging procedures explained below.

2.3. Rationale for Using Quantitative C.O. Histochemistry

Mapping of C.O. activity in nervous tissue is based on specific methodological considerations that determine the sensitivity as well as the possibility of quantification of the C.O. staining method in terms of enzyme activity units. The enzymatic activity of C.O. can be measured by biochemical spectrophotometric assay (Wharton & Tzagaloff 1967), differential reflectance spectroscopy (Wikström *et al.*, 1981), immunohistochemistry (Hevner & Wong-Riley 1989), cytochemistry (Wong-Riley, 1989), or histochemistry (Wong-Riley 1979; Kugler *et al.*, 1988). Biochemical assays and spectroscopy provide accurate quantification of C.O. activity, but they lack the precise anatomical localization achieved by cytochemical or histochemical staining. For learning and memory studies aimed at mapping changes in brain activity at regional and systems levels, the light microscopic resolution of C.O. histochemistry is required (Poremba *et al.*, 1997). Electron microscopic resolution is not needed for learning studies interested in regional mapping. However, if subcellular resolution is of interest, then the reader is referred to the cytochemical methods of Wong-Riley (1989).

When C.O. histochemistry is quantitatively measured to obtain enzyme activity, it offers a major advantage over other C.O. measuring techniques. Biegon and Wolff (1986) introduced the use of computerized image analysis with internal standards of known enzymatic activity as a method to achieve quantification of acetylcholinesterase activity from histochemically stained brain sections. A similar approach has been developed by Gonzalez-Lima and Garrosa (1991) to quantify C.O. activity by histochemical staining using a technique that is compatible with autoradiography.

Gonzalez-Lima and Cada (1994) adopted a C.O. procedure like that of Silverman and Tootell (1987) that was found more sensitive than the other available protocols, and incorporated the use of internal standards and quantitative densitometry. The present level of sensitivity and quantification of our technique appears to be adequate to detect learning effects produced by chronic training paradigms (e.g. Poremba *et al.*, this volume). C.O. methods with higher threshold for detecting C.O. reactivity may be adequate for other applications but may fail to detect small activity changes that are demonstrated by a more sensitive and quantitative procedure. The reasons for C.O. staining sensitivity are many, as discussed by Silverman and Tootell (1987), but some factors are purely empirical and can not be fully explained at this time. For example, the addition of acetone fixing of the section, the cobalt preincubation, the oxygenation and increase in temperature of the reaction medium, and inclusion of DMSO, all improve the C.O. staining reaction. In the following sections, factors that affect C.O. histochemical sensitivity and quantification will be briefly discussed.

2.3.1. Calibration with Internal Activity Standards. The quantitative approach is based on the use of internal standards of C.O. activity measured spectrophotometrically

together with quantitative image analysis of reaction product optical density (O.D.). Both internal standards and quantitative densitometric analysis are routinely used in other metabolic mapping techniques such as 2-deoxyglucose (2-DG) or fluorodeoxyglucose (FDG) autoradiography (Gonzalez-Lima, 1992). One problem with C.O. histochemical stains is some variability of O.D. from different incubation reactions. This problem can be controlled by the inclusion of complete sets of standards of known C.O. activity together with each preincubation and incubation medium and by faithfully reproducing tissue processing procedures. Any uncontrolled factors affecting O.D. will affect both the standards and brain sections. O.D. readings of reaction product can then be compared across incubation reactions by converting the O.D. to an internal calibration curve relating O.D. to C.O. activity.

2.3.2. Preincubation vs. Postincubation Fixation. Chalmers and Edgerton (1989) have shown that quantification of C.O. activity after perfusion-fixation provides an imprecise estimate of enzyme activity in fresh-frozen tissue. They found that after perfusion with a mixture of 2.5% paraformaldehyde and 1.5% glutaraldehyde, C.O. activity in the spinal cord was 10.5% of the level found in fresh-frozen tissue. Furthermore, all neurons were not equally affected. Whereas some cell types retained their activity, others were 90% below their activity in fresh-frozen tissue. Nobrega (1992) also reported decreased C.O. reactivity after perfusion-fixation. These findings suggest that a decreased enzymatic activity makes perfusion-fixation inadequate for quantitative studies. In addition, it appears that the qualitative patterns of C.O. reactivity in different cell types may also be altered in different ways.

The need for perfusion-fixation in quantitative light microscopy of C.O. histochemistry can be eliminated by repeated washing of the tissue sections in changes of phosphate buffer before and after the preincubation step. This effectively removes red blood cells that may later become stained with DAB during the incubation step. One needs to seek a balance between optimal enzyme activity and good tissue preservation. While it is true that preincubation fixation would affect the activity of C.O., a totally unfixed brain may be more prone to structural distortion and other artifacts. Therefore, postincubation fixation of the tissue sections after the C.O. incubation step has taken place, and the reaction product has been formed, provides a better alternative than initial perfusion-fixation. In this way, the deleterious effects of perfusion-fixation on enzymatic activity may be avoided, and the sections can effectively be post-fixed before light microscopic examination.

Ideally, brains should be extracted without perfusion or fixation, as these procedures affect both 2-DG autoradiography and C.O. quantitative histochemistry. 2-DG is washed out by the perfusion (Sokoloff, 1989), and C.O. activity is diminished by the standard fixation used in Wong-Riley's protocol (1979), as demonstrated by Nobrega (1992). Before preincubation, however, a brief on-the-slide fixation of the frozen sections can be done with cold acetone. Pretreatment of cryostat sections with acetone produces a significant increase in demonstrable C.O. activity (Silverman & Tootell 1987). According to Kugler *et al.* (1988), an explanation for this positive effect may be that acetone increases the permeability of mitochondrial membranes and facilitates penetration of the chromogen (DAB) to the site of the respiratory chain. This suggestion is supported by electron microscopic C.O. cytochemical studies (Kugler *et al.*, 1988).

With brains of reptiles (Figure 2A) the quantitative C.O. histochemical procedure explained below is as effective as in rodents (Figure 2B). With smaller brains of some amphibians, we have used perfusion and fixation prior to brain removal to facilitate handling

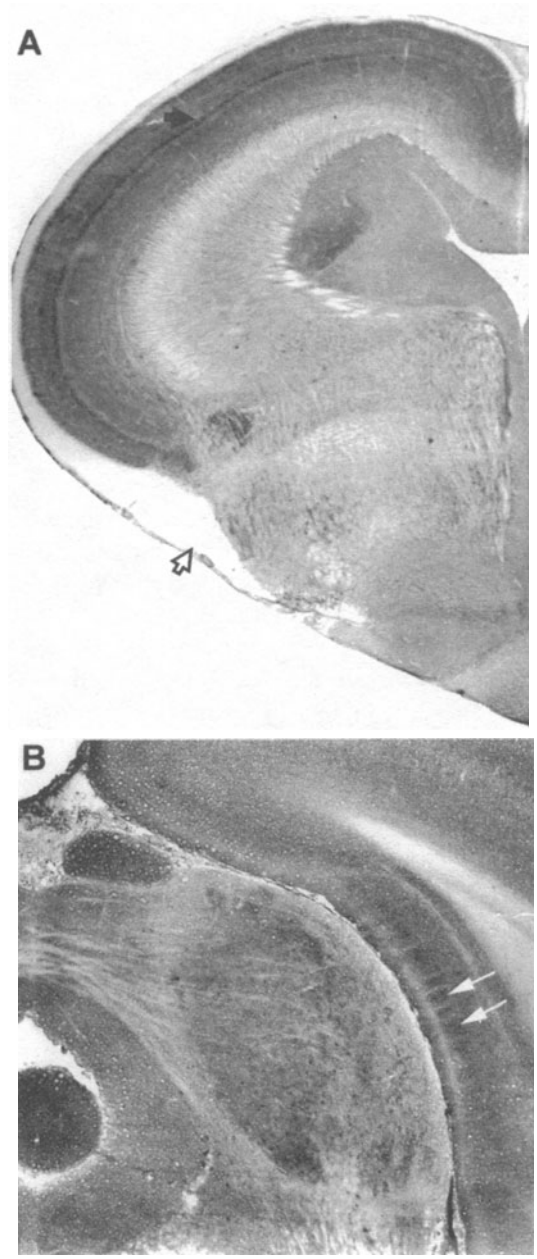

Figure 2. *A.* Example of C.O. stained brain of a reptile. The section was taken from the midbrain of the ground lizard *Ameiva exsul.* The bulk of the dorsal midbrain in lizards consists of the optic tectum. It can be seen in great detail with C.O. staining as a highly laminated cortical structure (filled arrow pointing to thin layer with darkest staining). The white matter of the optic tract around the optic tectum can also be clearly distinguished due to its minimal labeling (open arrow). *B.* Example of C.O. stained brain of a rodent. The section was taken from the midbrain and adjacent cortical regions of the hooded rat. The inferior colliculus appears in the center as a large egg-shaped structure, with lightly stained commissural axons running medio-laterally and darker dorso-ventral patches consisting of the terminal synaptic field of the lateral lemniscus. The white arrows point to C.O.-rich blobs or puffs in the presubiculum, a neuroanatomical pattern not previously described. This modular organization in the presubiculum may be analogous to the well known examples of C.O.-rich puffs discovered by Wong-Riley in the primary visual cortex of primates (see Fig. 4A).

of small brains (Marler, Wilczynski, & Gonzalez-Lima, 1992). But this considerably slows the entire reaction to obtain comparable reaction product. Furthermore, when using very small brain sections or some paste standards, the cold acetone step may impair adherence to the slide. This can be corrected by preincubation fixing of the sections with 0.5% glutaraldehyde solution. Although a brief exposure of a few minutes to low concentration glutaraldehyde may have no significant effect on the C.O. reaction, a more prolonged exposure will decrease C.O. activity resulting in a longer reaction time for adequate staining (Silverman & Tootell 1987).

2.3.3. Optimal Tissue Sectioning and Storage. Handling of fresh-frozen tissue for quantitative measures is facilitated by precision cryosectioning, picking up sections on slides, and the use of an on-the-slide staining procedure that minimizes distortion and misalignment problems. For light microscopic studies, cryostat sections of nervous tissue have been found superior to vibratome sections because the freezing step appears to increase the permeability of mitochondrial membranes for DAB. Kugler *et al.* (1988) determined that cryostat sections are superior to vibratome sections of hippocampus, because in frozen sections all mitochondria contained C.O. reaction product, whereas in vibratome sections there were many mitochondria without reaction product.

For the C.O. technique to be compatible with FDG or 2-DG autoradiography, the brains need to be removed and cryosectioned using the same procedures. Animals are killed by decapitation; the use of anoxia (such as in carbon dioxide euthanasia) should be avoided because of its adverse effect on the redox C.O. reaction done postmortem. It is also possible, but unsettled at this time, that some anesthetics used for euthanasia may affect enzymatic reactivity.

To prevent loss of C.O. activity once frozen tissue is cut, the sections should not be air-dried or stored at room temperature, or dried on a hotplate as done for sections used for FDG autoradiography. Rather, sections should be kept frozen in the cryostat while sectioning, and then stored in a freezer at –40°C. Cooler storage temperatures tend to dehydrate the sections, while warmer storage for prolonged periods decreases C.O. activity. Although Silverman & Tootell (1987) used heat drying for about 20 sec, this is needed only when both C.O. and FDG (or 2-DG) techniques are going to be performed on the same section. When adjacent sections are used for C.O. and FDG techniques, the C.O. sections should be kept frozen until staining. Heating of tissue, even briefly, reduces C.O. activity.

2.3.4. Preincubation Metal Intensification with Tris Buffer and DMSO. Metal intensification with cobalt chloride, nickel ammonium sulfate or manganese chloride has been shown to enhance the sensitivity of detecting benzidine reaction products in HRP histochemistry (Adams, 1977; DeOlmos & Heimer, 1977). Ten minutes with a preincubation solution of 0.05M Tris buffer at pH 7.6, containing cobalt chloride and DMSO similar to that of Adams (1977) and DeOlmos and Heimer (1977), has increased the sensitivity of C.O. histochemistry over that of Wong-Riley's (1979) protocol without loss of specificity (Silverman & Tootell, 1987). We confirmed this enhanced sensitivity in C.O. staining of rat brains when incorporating this preincubation step in our original quantitative histochemical procedure (Gonzalez-Lima & Garrosa, 1991).

The positive action of preincubation with cobalt chloride is seen in the formation of a darker reaction product, which may involve polymerization of the initial DAB reaction catalyzed by cobalt chloride. Excess precipitate is eliminated by repeated changes in phosphate buffer to remove the cobalt salts not incorporated into the mitochondrial reaction product (Silverman & Tootell, 1987). We have repeatedly confirmed this cobalt-enhanced sensitivity and specificity in the C.O. staining of brains from many different species, such as humans (Gonzalez-Lima, Valla & Matos-Collazo, 1997), lizards (Crews *et al.*, 1996; 1997; Coomber *et al.*, 1997), amphibians (Marler *et al.*, 1992), mice (Cada & Gonzalez-Lima, 1993; Gonzalez-Lima, Helmstetter & Agudo, 1993), gerbils (Gonzalez-Lima & Jones, 1994), rats (Cada, Gonzalez-Lima, Rose & Bennett, 1995), and rabbits (e.g. Figure 3).

This improved sensitivity results in more contrast and reduced incubation time for reaction product formation without loss of specificity, as demonstrated by the complete elimination of reaction product formation in the presence of potassium cyanide or in the absence of DAB in the incubation medium. Although a simple blue filter (Kodak Wratten

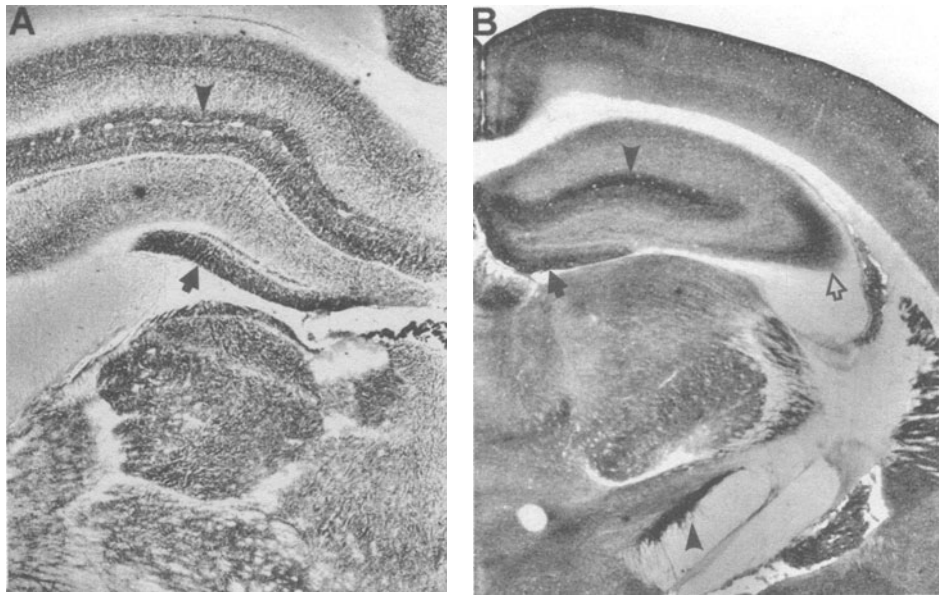

Figure 3. Hippocampal formation and thalamus stained with the quantitative C.O. histochemical method. *A.* Example from a rabbit brain showing the detailed laminar pattern of the hippocampal formation. The darker layers correspond to synaptic fields of dendritic spines and axon terminals, whereas the lighter layers correspond to cell bodies and nonsynaptic neuropil. *B.* Example from a gerbil brain showing the high contrast in C.O. labeling patterns. Cortical layers as well as subcortical nuclei can be distinguished. For instance, the subthalamic nucleus shows up as a darkly labeled diagonal band over the white matter of the cerebral peduncle (arrowhead in the lower third of section B). In adult rabbit and gerbil as well as in other mammals, the darkest C.O.-rich layers of the hippocampal formation correspond to a central band (arrowheads) comprised of the lacunosum moleculare layer of the hippocampus and the molecular layer of the inner blade of the dentate gyrus. The outer blade of the dentate gyrus also shows a dark ventral band corresponding to the molecular layer (arrows). The CA3 pyramidal cell layer shows the greatest C.O. activity among the hippocampal CA fields (open arrow in B).

#47) could enhance the contrast of photographs of C.O. sections, metal intensification is necessary to obtain an adequate contrast in the original sections (not just the photographs) so that regions of interest could be more easily delineated for the quantification of absolute O.D. units in the tissue.

DMSO is presumed to involve enhancing penetration of the reagents into the neurons (DeOlmos & Heimer 1977). DMSO can be added during the preincubation phase with favorable results. But these additives are effective only in the preincubation step (i.e., before the C.O. incubation reaction). Addition to the incubation reaction medium of DMSO (Kugler *et al.,* 1988), and cobalt (Nobrega, 1992) offers little gains. Furthermore, metal intensification during incubation affects conditions necessary for quantification of C.O. activity. It is possible to maximally intensify the darkness of the DAB reaction product by introducing certain metal salts into the incubation solution, as shown by DeOlmos and Heimer (1977) in HRP histochemistry. This was useful for identification of HRP-stained axon collaterals morphologically. In the case of C.O. histochemistry, intensified C.O. labeling may be useful to identify morphologically the changing distribution of C.O. in developing brains (Wong-Riley, Hevner, Cutlan, Earnest, Egan, Frost & Nguyen, 1993) as well as numerous neuroanatomical patterns (Hevner, this volume). Examples of nickel-intensified C.O. histochemistry in the visual cortex of monkey and cat are shown in Figure 4.

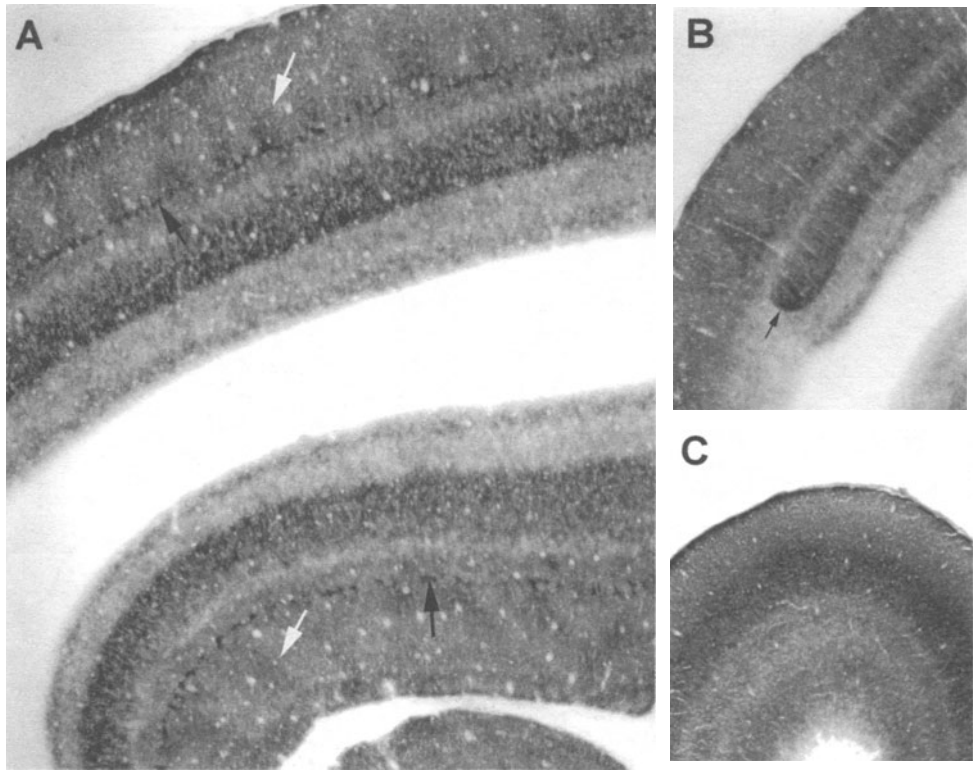

Figure 4. *A.* Macaque visual cortex (V1), showing C.O.-rich blobs in layers II and III (white arrows) and the darkly stained pyramidal cells of layer IVa (black arrows). *B.* Macaque visual cortex, showing the border between areas V1 and V2 (arrow). *C.* Cat visual cortex, showing definition of cortical layering. In all cases, magnification is 3x, and are 40 μm sections stained with nickel-enhanced C.O. histochemistry, with a method modified from that of Dyck and Cynader (PNAS 90: 9066–9069, 1993). A.M. Crane, R.A. Frazor and D.G. Albrecht.

The use of maximal metal intensification during the incubation reaction facilitates morphological visualization of reaction product in all neurons (Kageyama & Robertson, 1993; Liu, Gu & Cynader, 1993). However, using metal intensification procedures during incubation invalidate the quantitative requirements of graded reaction product reactivity proportional to C.O. enzymatic activity. That is because maximal intensification results in saturation of reaction product formation and similar dark staining of cells with low and high C.O. activities. If the objective of the C.O. stain is to obtain a quantitative functional index of C.O. activity, rather than a morphological index with saturated staining, then metal intensification is better used as a preincubation step rather than during incubation. In this manner, the incubation reaction can proceed undisturbed using parameters that result in nonsaturated reaction product formation in a rate of reaction linear with respect to increasing incubation time. For the same reason, C.O. histochemical procedures which yield reaction rates different during the first minutes and subsequent period of incubation (e.g. Kugler *et al.,* 1988) are also invalid for quantitative C.O. histochemistry.

2.3.5. Temperature, pH, Oxygenation, and Duration of the C.O. Incubation Reaction. DeOlmos and Heimer (1977) were able to increase the sensitivity of HRP histochemistry by manipulating intrinsic factors of the incubation reaction such as pH and temperature.

Silverman and Tootell (1987) similarly improved C.O. staining intensity by increasing pH, temperature, and adding oxygen to the incubation medium. The standard spectrophotometric assay of C.O. developed by Wharton and Tzagoloff (1967) uses pH 7 at 37°C for optimal C.O. activity *in vitro*. Although pH 7 appears optimal for biochemical assays of C.O. activity in separated mitochondria *in vitro*, pH 7.6 improves the histochemical staining facilitating entry of the reagents by swelling of tissue mitochondria *in situ* (Silverman and Tootell, 1987). Higher temperatures can also accelerate the C.O. reaction, but when using internal activity standards in our quantitative method, a 37°C temperature showed the best linearity between densitometric measures of staining intensity and incubation time.

Silverman and Tootell (1987) also found that oxygen saturation of the incubation medium improved C.O. staining by increasing DAB oxidation to form the colored reaction product. However, we have found that saturation is best done before the introduction of the rack of slides with the sections. This is because oxygen bubbling during the reaction causes a differential distribution of bubbles in the solution that results in nonuniform staining of adjacent slides (Gonzalez-Lima, 1992). Gentle agitation with a stirrer bar throughout the reaction and ample circulation between, above, and below the slides prevents the formation of a staining gradient by circulating the oxygen and reagents thoroughly. Exposure of the reaction medium to intense light needs to be avoided because it may produce spontaneous DAB oxidation leading to nonspecific staining.

With 40 micron sections, we conduct the reaction in a closed oven at 37°C (measured inside the incubation solution) for 60 minutes for optimal quantitative results in rodent and reptilian brains. But in other animal species longer reaction times are needed. For example, better staining intensity and linearity for quantification may be obtained with incubation times of 90 minutes in monkeys and 120 minutes in humans (Figure 5).

2.4. Definition of C.O. Activity Units

Besides differences in the preincubation and incubation histochemical protocols, there are factors such as temperature and pH related to the conditions used during biochemical enzymatic determination and the calculation of C.O. activity units that result in differences between laboratories. These relevant factors, however, are usually not all reported in previous enzymatic activity studies (Benzi, Arrigoni, Dagani, Marzatico, Curti, Manzini & Villa, 1979; Curti, Giangare, Redolfi, Fugaccia & Benzi, 1990; Darriet, Der & Collins, 1986; Hess and Pope, 1953; Van Raamsdonk, Smit-Onel, Donsellaar & Diegenbach, 1987) making comparisons of absolute activity units complicated. The temperature of the reaction medium, for instance, would influence the speed of C.O. reaction product formation and calculated rate of activity.

We have reported C.O. units measured spectrophotometrically at both 22°C (standard room temperature) (Gonzalez-Lima & Cada, 1994) as well as at 37°C (Gonzalez-Lima & Garrosa, 1991; Cada *et al.,* 1995). For routine measures, solutions at 22°C are more stable; that is, they show little auto-oxidation as compared to 37°C, which facilitates reproducibility of multiple triplicate assays from the same stock solutions. While Hess and Pope (1953) have also measured activity at 22°C, they have converted activity to 37°C by multiplying units by a factor of 3, assuming C.O. activity to be doubled per each 10°C rise in temperature. We have not found this assumption to be valid. The definition of C.O. activity units using optimal reaction conditions for spectrophotometry, such as pH 7 at 37°C, may be preferable for studies evaluating absolute C.O. activity, rather than simpler routine assays (Hess & Pope, 1953) done at room temperature in which C.O. units can be defined reliably but at below maximal levels (Gonzalez-Lima & Cada, 1994).

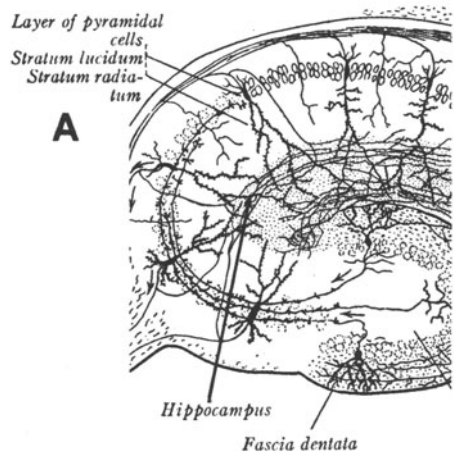

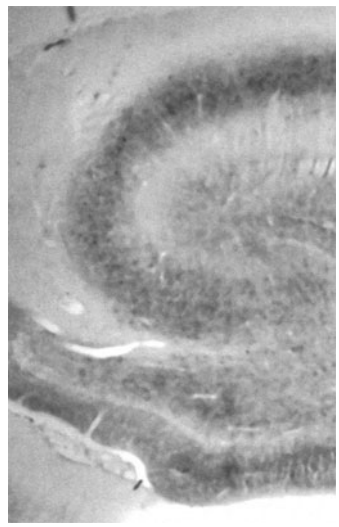

Figure 5. Section of the human hippocampal formation. *A.* Diagram showing the cellular morphology and connections based on Golgi stains by Cajal. *B.* Section of 40 microns stained for 120 minutes using the described C.O. method. The darkest C.O. staining in *B* corresponds to a central band (pointed by arrow labeled Hippocampus in *A*). This C.O.-rich band is where the apical dendrites of the pyramidal cells and the granule cells receive the afferent axon terminals, i.e. the input field of axodendritic synaptic interactions in the hippocampus. This comprises a stratum moleculare of tangential axons from the subiculum and perforant fibers, and a deeper stratum known as the stratum lacunosum. Similarly dark staining is found in the molecular layer of the dentate gyrus (labeled Fascia dentata in *A*) where the dendrites of granule cells synapse with the incoming axon terminals. Note that the lowest staining is shown by the layer of pyramidal cell bodies, stratum lucidum, and stratum radiatum. (Frozen tissue kindly provided by K. Hatanpää from the NIH).

An ideal situation is for all investigators to use the same conditions to define a unit of activity, and to consistently report data under these conditions. Alternatively, the activity from a whole-brain homogenate or a similar reference may be reported to provide a relative index of the enzymatic activity obtained under different measurement conditions. For example, homogenates of fresh-frozen rat brains showed an average C.O. activity of 175 units (μmol/min/g tissue w/w) in our assay conditions reported below. This average C.O. activity units in our control brains was very similar to the average C.O. activity in the whole rat brain (158 ± 5) reported by Hevner, Liu and Wong-Riley (1993). Our somewhat higher value may be attributed to the fact that our C.O. units were defined at pH 7 and 37°C, as in our original method (Gonzalez-Lima & Garrosa, 1991), as opposed to pH 6 and 30°C as done by Hevner *et al.* (1993). The agreement between these control brain C.O. values suggests that both assays were optimal in unmasking enzyme activity to maximal or near maximal levels (Hevner *et al.*, 1993). Whether the units are defined based on tissue wet weight (w/w) or dry weight needs also to be specified (Nobrega *et al.*, 1993). Our activity units showed good agreement with values reported in the literature when similar conditions were used to measure and define the units of C.O. activity.

For those interested in reporting a relative C.O. quantification, without measurement of enzyme activity units, comparisons using relative indexes such as whole-brain or white matter as references may be useful. Reporting relative densitometric ratios, such as is done in 2-DG studies (e.g. Gonzalez-Lima & Scheich, 1984) is a useful approach that may suffice for many C.O. applications (e.g. Jones *et al.,* 1997). It is valid to quantify relative values, as long as one does not presume that they represent absolute values. However, it should be cautioned that if a C.O. histochemical procedure fails to meet the quantitative requirements of linearity of reaction product formation with respect to incubation time and section thickness, it can not be used as a valid quantitative method with relative measures (Stoward, 1980).

3. METHODS

3.1. Detailed Procedures for C.O. Quantitative Histochemistry

3.1.1. Brain Removal, Freezing, and Sectioning. Activity of C.O. is quantified postmortem. Rats are decapitated and their unfixed brains are quickly removed, frozen, and sectioned. The minimal time necessary to remove the brain should be used. In rats, this is usually a couple of minutes but in monkeys much longer periods may be used without apparent significant loss of C.O. activity. We have obtained reliable quantitative results in humans with the average postmortem time interval before freezing of brain of less than 7 hours (Gonzalez-Lima *et al.,* 1997). A critical requirement is to keep constant the time from death to brain freezing in all subjects that will be compared within an experiment.

Freezing of the brain may be done by immersing it into 2-methylbutane (isopentane) for about 30 seconds. The isopentane is kept at –40°C in a chest freezer where the brain is slowly immersed and subsequently stored. Rodent brains can also be frozen on electrical freezing stages that take a couple of minutes to completely freeze the brain. These slower freezing procedures are preferred to rapid submerging of the brain in cooler media such as liquid nitrogen. They minimize cracking freezing artifacts and improve the quality of tissue sections without loss of C.O. activity. The frozen brain is wrapped in cellophane, sealed with tape, and stored at –40°C. Brains stored in this way can be kept for several months. These procedures when standardized serve to minimize drying of the brain prior to cutting and improve tissue quality without affecting C.O. quantitative histochemistry. Sections are cut at 40 μm on a cryostat at –20°C, picked up with clean slides, and stored inside sealed slide boxes at –40°C. Adjacent sections may be used for other techniques, such as FDG and others described by Papa *et al.* (this volume).

3.1.2. Preparation of C.O. Tissue Standards. This technique requires utmost care to ensure consistency of quantitative determinations. Standards are prepared with homogenized brain tissue. A fully active rat brain homogenate does not contain adequate C.O. activity to cover the upper end of the C.O. range of activity found in the most active regions of the rat brain. Thus we have shown that C.O. activity is linear with respect to time of incubation, thickness, and optical density. This demonstrates that standards of varying thicknesses can be used to increase the optical density, and thus activity, for as long as this relationship remains linear. We have found that sections up to 160 μm remain optically linear in our 60 minute incubation reaction. Routinely we use standards sectioned at five thicknesses (i.e. 10, 20, 40, 60 & 80 μm) and mounted on a slide as illustrated in Figure 6.

Generally, brain tissue from the species studied should be used given that it has not been perfused or exposed to anesthetics. There are instances in which anesthetics cannot

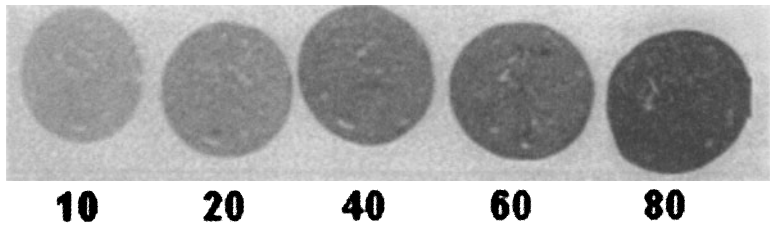

Figure 6. Example of stained C.O. standards mounted on a slide, showing increasing levels of reactivity proportional to the increasing thicknesses (10, 20, 40, 60 & 80 μm).

be avoided, but it should be noted that they variably decrease enzyme activity. At least 10 g of tissue are needed to make several tubes of standards. It may not be feasible to use neural tissue from very small subjects such as some amphibians and reptiles. In those cases we have found that rodent neural tissue is an acceptable substitute with similar optical density per unit activity.

Harvest tissue quickly, remove meninges and trim spinal cord to about 0.5 cm and store in 4°C phosphate buffer (pH 7.4) until all tissue is collected. Transfer tissue to chilled clear glass/glass homogenizer tubes and hand homogenize on ice for 2–3 minutes, or until uniform. Fill 1.5 ml o-ring microtubes 3/4 full of tissue paste and spin briefly at low rpm (1000 rpm, 5–10 sec) to remove air bubbles. Then freeze in the same manner as the experimental tissue. a reliable method for freezing is like that used for the brains; i.e., to slowly submerge microtubes with tissue in isopentane chilled to –40°C in an ultrafreezer. The tubes are then stored at –40°C. To section for histochemistry, mount on the cryostat chuck in the same manner as the experimental tissue and section at 5 to 6 thicknesses on the same day as the histochemical procedure. We have found that storing thaw-mounted sections of the tissue standards will result in poor tissue adherence as well as cracking and other artifacts.

3.1.3. Biochemical Spectrophotometric Assay of C.O. Activity. C.O. activity in the standards is spectrophotometrically measured with methods adapted from Hess and Pope (1953), Wharton and Tzagoloff (1967), Hevner *et al.* (1993) and Cada *et al.* (1995). Activity units are defined at pH 7 and 37°C as 1 unit oxidizes 1 μmol of reduced cytochrome c per min (μmol/min/g tissue wet weight).

Materials:

1) Cytochrome *c* (Sigma, from horse heart, minimum 95% purity based on molecular weight of 12,384, prepared using TCA)
2) Sodium ascorbate
3) Potassium phosphate buffer (0.05 M, pH 7.0)
   11.24 g potassium phosphate monobasic (KH_2PO_4)
   16.66 g sodium phosphate dibasic (Na_2HPO_4)
   distilled water to 4 liters
4) Brain paste standards
5) Isolation buffer:
   109.5 g sucrose (MW 342.3)
   0.38 g EDTA (MW 380.2)
   1.58 g Trizma hydrochloride (MW 157.6)
   distilled water to 1 liter
6) 10% sodium deoxycholate in distilled water

Procedure:

1. A 1% solution of cytochrome *c* in 0.05 M potassium phosphate buffer is made and reduced with sodium ascorbate per 10 ml. About 3–5 ml of this cytochrome *c* solution is sufficient for most assays. A change from dark red to light pink will be seen as the protein in the solution changes from an oxidized to a primarily reduced state. Once a definitive color change is seen, a few more sodium ascorbate crystals are added to ensure that an excess exists in the solution. The reduced cytochrome *c* is dialyzed against chilled potassium phosphate buffer changed with 3.5 liters of fresh buffer every 8 hours for a total of 24 hours in a refrigerator. A dialysis cassette or tubing with a molecular cutoff pore membrane size of 3,500 or 7,000 MW is appropriate, as the MW of cytochrome *c* is about 12,400 which allows the free exchange of unbound sodium ascorbate.
2. After excess sodium ascorbate is removed, the solution is diluted from 1% to 0.07% using reserved cold potassium phosphate buffer. The ratio of absorbance (optical density) of the diluted solution is measured at 550 and 565 nm in the spectrophotometer. The ratio of 550/565 nm should be greater than 6. If it is not, the solution is further reduced using 0.01 g sodium hydrosulfite per 40 ml dilute solution.
3. Tissue homogenate preparation: An aliquot of brain tissue paste standard is homogenized in cold isolation buffer (1 g per 4 ml buffer).
4. Assay working solution preparation: The solution of tissue homogenate from #3 is diluted from 20% with 10% sodium deoxycholate (a detergent, in distilled water) and cold isolation buffer to result in final concentrations of 0.25% tissue and 0.50% sodium deoxycholate. This final assay solution is then swirled thoroughly or mixed in a vortex and is allowed to stand at room temperature for 5 min to solubilize the cell membranes. It is then mixed with a vortex again briefly before placing on ice for assay. This working assay solution should be used within 30 min while the tissue homogenate from #3 is stable for hours on ice. We have found that it is necessary to increase tissue concentration to 2.5% and sodium deoxycholate to 2% when assaying monkey or human brain tissues due to their increased amount of white matter.
5. Place 1.0 ml of the reduced cytochrome *c* (0.07%) in a 10 mm cuvette and warm to 37°C. The spectrophotometer should be set to 550 nm.
6. Add 10 µl of the assay working solution, cover with a clean gloved finger and turn over three times, put into the spectrophotometer, and record absorbance at least every 15 seconds for the first minute of the reaction (0, 15, 30, 45 and 60 seconds).
7. Repeat steps 5 and 6 twice to check consistency.

3.1.4. Worked Example of Biochemical Assay.

1. Cytochrome c substrate. To 3 ml of cold 0.05 M potassium phosphate buffer add 0.03 g cytochrome *c*; swirl to mix. Add ~0.03 g sodium ascorbate and swirl to mix, noting the color change from dark red to lighter pink. If the color change occurs, add several more crystals of sodium ascorbate to ensure an excess exists in the solution. If the reduction of the cytochrome *c* appears to be incomplete, add sodium ascorbate 0.01 g at a time until the change no longer occurs. Place the reduced solution into a pre-soaked (with excess water removed) piece of Spectra-Por 3 (MW cutoff 3,000) dialysis tubing, tie or clip closed, and dialyze unbound sodium ascorbate out of the medium against 3,500 ml of cold 0.05 M

potassium phosphate buffer on a magnetic stirrer for 24 hours in a refrigerated environment. Dilute the reduced cytochrome *c* solution from 1% to 0.07% by mixing together 2.8 ml of the 1.0% solution and 37.5 ml of cold 0.05 M potassium phosphate buffer reserved from the original 4 liters of buffer made. Measure the absorbance of this solution in a spectrophotometer at 550 and 565 nm using the potassium phosphate buffer as a reference. The ratio of 550/565 should be greater than 6. If it is greater than 6, then divide among capped vials and place on ice for the assay, making sure that the solution does not freeze. If the ratio is less than 6, the solution can be further reduced with sodium hydrosulfite. Add ~0.01 g to the ~40 ml of solution and place into a container with a cap. Shake vigorously for 3 min and re-measure the absorbance. Repeat if necessary.

2. Tissue homogenate. Record the weight of a small weigh boat, then zero the balance and quickly add ~0.5 g of frozen tissue standard. Immediately transfer the tissue to a 10–15 ml capacity glass/glass hand homogenizer. Re-weigh the weigh boat to ascertain the exact amount of tissue that went into the homogenizer. Add 2 ml of cold isolation buffer and homogenize slowly but thoroughly (20–25 times), then transfer to a capped vial and place on ice, but do not allow the mixture to freeze.
3. Assay solution. Prepare 5 ml of a 10% sodium deoxycholate (detergent) solution by putting 5 ml of distilled water into a snap top 15 ml vial and adding 0.5 g of sodium deoxycholate. For the assay solution, the final percentages of tissue and detergent are 0.25% and 0.5% respectively. Therefore, in a small flask, add 37.5 ml of cold isolation buffer and 2 ml of the 10% sodium deoxycholate. Swirl to mix then add 0.5 ml of the cold tissue homogenate and mix thoroughly. Allow to stand at room temperature for 5 minute to solubilize cell membranes, then mix in vortex briefly, divide among capped vials, and place onto ice.
4. Running the assay. Set the spectrophotometer at 550 nm and 37°C. If a heater element is not available, the reaction may be run at room temperature, ensure that the cytochrome c solution has warmed to room temperature from its original 4°C temperature before running the reaction. To a 1.5 ml, 10 mm pathlength cuvette, add 1 ml of potassium phosphate buffer and place into the reference cell holder, or "zero" the absorbance at 550 nm with the buffer. Remove the cuvette and replace it with one containing 1 ml of the reduced, diluted and dialyzed cytochrome *c* solution. Allow to warm to the reaction temperature. Remove the cuvette containing the warmed cytochrome *c* solution and quickly add 10 µl of the assay solution mixture. Cover with a gloved finger, turn over 3 times to mix, and place into the spectrophotometer. Measure absorbance at 0, 15, 30, 45 and 60 seconds. The change in absorbance between 0 and 60 seconds will be used to calculate the activity.

3.1.5. Worked Calculation of C.O. Activity in the Example. Amount of tissue in the 10 µl sample:

1. 0.5 g tissue + 2.0 ml buffer = 2.5 ml total volume (1 g of neural tissue can be assumed to equal 1 ml). 0.5 g/2.5 ml total volume = 0.2 g/ml.
2. $\frac{0.2\text{g}}{\text{ml}} \times \frac{0.5\text{ml tissue homogenate used for dilution}}{40\text{ml total volume of assay solution}} = 0.0025\text{g / ml in assay solution}$
3. $\frac{0.0025\text{ g}}{1\text{ ml}} \times \frac{1\text{ ml}}{1000\ \mu\text{l}} = 2.5 \times 10^{-6}\text{ g / µl}$

$(2.5 \times 10^{-6}\ \text{g}/\mu\text{l}) \times (10\ \mu\text{l aliquot used in reaction}) = 2.5 \times 10^{-5}\ \text{g}/10\ \mu\text{l sample}$

$$\text{C.O. activity} = \frac{\text{change in absorbance for the first minute / extinction coefficient}}{\text{grams of tissue in the 10 } \mu\text{l}}$$

$$= \frac{0.086 \text{ change in the first minute} / 19.6\ \mu\text{mol} / \text{cm (1 cm pathlength)}}{2.5 \times 10^{-5}\ \text{g tissue in the 10 } \mu\text{l sample}}$$

$$= 0.004387755 / 0.000025$$

= 175.5 μmol/min/g tissue wet weight (typical value for a whole-brain homgenate of an adult male rat)

3.1.6. C.O. Histochemical Staining Procedure. This procedure follows Silverman and Tootell (1987) with some modifications.

Materials:

1. Phosphate buffer from stock solutions (0.1 M monobasic and dibasic) in a ratio of 100 ml monobasic to 900 ml dibasic, and adjusted until pH 7.4.
2. Tris buffer is a mixture of 500 ml 0.2 M Tris base, 774 ml 0.1 N HCl and H_2O to 2 l. To this add 550 mg cobalt chloride, 200 g sucrose and 10 ml DMSO.

The phosphate and Tris buffers can be kept refrigerated for several days if color does not change.

3. The DAB solution for a 100 ml bath is made with 50 mg DAB (3,3′-diaminobenzidine tetrahydrochloride, Sigma), 7.5 mg cytochrome *c* (from horse heart, 95% minimum purity, prepared using TCA, Sigma), 5 g sucrose, 2 mg catalase (from bovine liver, 2,000–5,000 units activity/mg protein, Sigma), 0.25 ml DMSO, and phosphate buffer added to make 100 ml. Care must be taken with the DAB because it is a carcinogen. Gloves and mask are to be worn when handling DAB, and contaminated surfaces should be cleaned with a bleach, but extreme care is required not to contaminate the incubation solution or any of the staining dishes with bleach as this will lead to artifacts (bluish decolored regions).The DAB incubation solution must be made fresh each time. Both the preincubation and incubation solutions must be renewed after each rack of slides is run through them.
4. The staining baths can be done conveniently in large glass staining dishes with a rack of slides. This is important to try to stain the same brain regions for all groups of animals in a single incubation to minimize inter-staining variation.
5. Two or more complete sets of C.O. standards should be stained in each incubation bath.

Procedure:

Sections should be kept frozen until placing in the sequence of baths and times listed below:

1. Cold buffered 0.5% glutaraldehyde in 0.1 M pH 7.4 phosphate buffer (4°C) to affix sections, 5 min.
2. 0.1 M phosphate buffer with 10% sucrose (in four changes), 5 min each
3. Preincubation with Tris buffer and additives, 10 min.
4. 0.1 M phosphate buffer rinse
5. Incubation with DAB solution (preceded by 5 min. of oxygen bubbling) at 37°C with automatic stirring in a dark oven, 60 min. for rodents and reptiles

6. Buffered formalin (10%) with 10% sucrose, 30 min.
7. Dehydration baths of 30, 50, 70, 90, 95 (2 changes), 100% (3 changes) ethanol, 5 min. each
8. Xylene (3 changes), 5 min. each
9. Coverslip slides with Permount

3.1.7. Frequently Asked Practical Questions about the Described Histochemical and Spectrophotometric Procedures.

Q. How do you reduce the cytochrome *c* solution with sodium ascorbate? What if we add too much? How long do we wait before we begin dialysis? Are there any other compounds that can be used for reduction?

A. One percent cytochrome *c* is reduced by adding the sodium salt of ascorbic acid in small amounts to the solution until a definitive color change is seen-approximately 0.1 grams per 10 ml. The solution will turn from a dark red to a much lighter pink when most of the molecules are reduced. At that point add a slight excess of sodium ascorbate; unless a very large excess is added (~3–4 g extra) the dialysis procedure will effectively remove all unbound ascorbate molecules so that they will not interfere with the reaction in the spectrophotmetric assay. As soon the solution is visibly reduced, put it into the dialysis tubing against the same buffer used to make the cytochrome *c* solution. Sodium hydrosulfite will also reduce cytochrome *c*, but the reaction is not as stable as that of sodium ascorbate, which is why it is used only as a last resort measure.

Q. Why is catalase (Sigma) used in the histochemical procedure?

A. Catalase is a heme-containing protein that catalyzes the dismutation of hydrogen peroxide into water and molecular oxygen. Hydrogen peroxide is a normal product of oxygen respiration; thus the breakdown of these molecules has a two-fold advantage of preventing both interference by the free-radical in enzyme activity as well as the addition of molecular oxygen to the substrate.

Q. In the C.O. histochemical protocol, the final step is to use 10% sucrose phosphate buffer (PB) with 4% formalin (v/v). What does v/v mean? I am used to 4% paraformaldehyde; is that okay to use?

A. v/v means volume/volume. Formaldehyde is a colorless gas, which due to its reactivity, cannot be handled easily. Hence, formaldehyde is normally dissolved in water and sold as a 37–40% aqueous solution called formalin. Formalin is then diluted to ~4%, such that each 90 ml of 10% sucrose PB is mixed with 10 ml of formalin. Paraformaldehyde is the white solid (polymer) left after evaporation of formalin (formalin heated by steam for about 30 min).

Q. When we were preparing the tissue homogenate standards we spun a 1.5 ml cryovial of tissue in order to remove air bubbles. The result was separation of the tissue (production of a pellet). How can I prevent this from occurring?

A. If you produce a pellet when you spin a tube of brain paste, then it was spun for too long and too many revolutions per minute (RPM). Using 5–10 sec at 1,000–2,000 RPM is quite sufficient. If you do produce a pellet, rehomogenizing is not recommended as significant packing off the tissue has occurred; discard and spin the remaining tubes BRIEFLY before freezing evenly and rapidly in the same manner as the experimental tissue.

Q. We cut one of our brain paste standards and it looked quite fragmented. Is it supposed to look solid without chatter in it? We cut it at –20°C, 40 μm thick.

A. The brain paste standards need to be equilibrated in the cryostat for longer than brain tissue. Some batches of standards can be cut at –20°C, but most somewhat warmer; –12°C to –15°C.

Q. We are putting the range of thicknesses of standards on several different slides. If we try to put all the homogenate sections of different thicknesses on one slide, the slide sometimes get so much condensation on it that the sections melt (especially the thick sections). Do you put them all on one slide?

A. We utilize a 3" × 3" aluminum plate attached to the knife holder in our cryostat. Sections of 10–160 μm can be cut and moved onto the plate so that all standards of different thicknesses can be mounted onto the room-temperature slide at the same time. Alternatively, several sections could be moved to the edge of the knife so that 4–6 could be mounted simultaneously. After thaw-mounting the sections, the slide is immediately put in a rack kept inside of the cryostat to refreeze. When mounted in this fashion we have little problem with adherence of the standards during the histochemical procedure. It is important to note that best adherence of the standards will also occur when they are sectioned no more than 24 hours before the histochemical procedure is done.

Q. How can I determine if my C.O. standards are linear?

A. A linear relationship should exist between homogenate cryostat section thickness and optical density following staining. Optimally, there should be less than 5% variation in measured optical density in several sets of standard slides (if not, uneven homogenization or variations in temperature in different incubations were probably the cause). In most cases, the range of optical density in the standards exceeds the range of that found in regions of interest in the tissue sections.

Q. In C.O. spectrophotometry, my initial absorbance reading is 0.5 and the change in absorbance over one minute is at least 50% lower than expected based on published activities. What could have gone wrong?

A. Without adequate reduced substrate (cytochrome *c*), the enzyme activity cannot be measured accurately and will always appear low. Oxidized cytochrome *c* is a competitive inhibitor of reduced cytochrome *c*. Your absorbance readings indicate that you do not have sufficient reduced substrate as the initial optical density should be 0.8 or greater.

Additionally:

1. Make sure you have cuvettes with a 1.0 cm path length that are optical quality.
2. Make sure cuvettes are oriented properly. Call the manufacturer if necessary.
3. To zero the spectrophotometer, place ferricyanide-oxidized cytochorme *c* solution as a reference (use a saturated potassium ferricyanide solution). Your absorbance reading should be 0.800–1.000.
4. Look at the cytochrome *c* in your sample (reduced) and reference (oxidized) cuvettes. Are they different colors? If not, then the cytochrome *c* in your sample cuvette is probably not adequately reduced. The ratio of the absorbance at 550 to 565 nm should be at least 6, indicating a sufficient amount of reduced cytochrome *c* in the substrate.
5. Are all tissue extracts and reagents kept on ice until used?
6. Do you allow time for the cold cytochrome c substrate to warm to 37°C in the spectrophotometer prior to adding tissue extract?
7. Is your spectrophotometer set to 550 nm?

8. What is the condition of the tissue that you are using? Was it obtained fresh and homogenized immediately? Were drugs used for euthanasia? (They variably inhibit cytochrome oxidase activity.)

Q. In your protocol for C.O. spectrophotometry you use dipotassium EDTA in the solution to dilute the tissue suspension. Can I use a sodium EDTA, or are you avoiding Na for some reason? If so, why?

A. Sodium EDTA can be substituted; the extremely low concentration in which it is used does not significantly affect the molarity or pH of the solution.

Q. What about using other methods of enzyme activity analysis such as oxygen electrode–polarography?

A. We have used the oxygen electrode method to measure cytochrome oxidase activity. Although somewhat easier than the spectrophotometry method, it uses 50–100 times more tissue and substrate, is more expensive to set up and maintain due to the constant replacement of oxygen permeable membranes, and consistently results in suboptimal enzyme activities compared to the spectrophotometric method.

3.2. Densitometry and Image Analysis

The densitometric analysis is the same as described for FDG autoradiography (Gonzalez-Lima, 1992), except that the calibration is based on the optical density (OD) of stained standards with the units of C.O. activity measured spectrophotometrically in the same standards. The imaging system is calibrated with the C.O. standards by measuring the OD of each standard and entering the corresponding C.O. units of activity. Any region of interest in the digitized image can be defined and the system provides mean, range, and standard deviation of gray levels which are transformed to C.O. activity units per gram of tissue.

The most critical factor in image analysis is the human factor. Considerable time should be spent examining the sections before any densitometry, to carefully select all the regions of interest and note any focal patterns of labeling. The densitometric data are only as good as the neuroanatomical experience and care of the investigator, and this cannot be replaced by any degree of sophistication of the imaging system or transformation of the data. When selecting images and regions of interest make completely sure, by use of adjacent sections stained with Nissl or fiber techniques, that you delineate each brain region at equivalent levels for each subject. Negative and even misleading results can happen if you select sections that do not precisely correspond between brains.

3.2.1. Macroscopic Image Analysis. For measuring C.O. activity in regions of interest, artifact-free sections are placed on a DC-powered light box with a stable and uniform illumination field (Meyers Instruments, Houston) and captured through a high resolution black-and-white camera (Javelin JE2362) with a macro lens. The analog signal from the camera is transmitted to a frame grabber (Targa) mounted in a computer (Everex) where the image is digitized. There are other commercially available systems that incorporate similar components. Great care should be taken to calibrate the set up to optimize imaging at the range of darkness of the sections. The best imaging environment is a dark room with dim and stable indirect lighting positioned so as not to project shadows on the illumination of the sections. The system should include the capability of image subtraction. The slide background needs to be subtracted from each image to correct optical distortions from illumination, the lens, and camera before proceeding with densitometry. A calibration

curve is generated for each batch by using its set of C.O. standards, and the results are verified to ensure a linear relationship between C.O. concentration and OD in the imaging system. When properly calibrated, the above system using JAVA software (Jandel Scientific) yields accurate densitometric values automatically expressed as C.O. units. The effects of the experimental manipulation on changes in regional C.O. activity units are evaluated statistically using repeated measure analysis of variance with "brain region" operating as the within-subjects factor. The omnibus analysis is followed by tests for simple effects (SPSS-PC software).

3.2.2. Microscopic Image Analysis. For quantitative C.O. cytochemistry of individual neurons, analysis can be done of neuronal compartments at the light microscopic level (Gonzalez-Lima *et al.,* 1997). Stained tissue slides are mounted on a light microscope (Olympus model BX40) connected to an image processing system. The same microscope lamp intensity level is set and verified densitometrically throughout the study, and condenser centration is performed prior to each imaging session to ensure that illumination levels were equivalent for the measurement of optical density. A high resolution CCD video camera (Javelin JE7442) is mounted on the microscope to capture the images and transmit them to a frame grabber (Targa) mounted in a computer (Dell) where the image is digitized. Analysis is completed through the use of JAVA (Jandel Scientific) imaging software.

The recommendations of Chieco, Jonker, Melchiorri, Vanni and Van Noorden (1994) were followed to avoid photometric errors in image cytometry. A clear background from a mounted slide was subtracted from each image to correct for lens and camera anomalies and shading distortion. An interference glass filter was interposed in the microscope light path to correct for white light distortion. The brightest pixel of the image was maintained few gray levels below saturation to correct for blooming caused by excessive light. On the video camera, the automatic gain was switched off and the gamma control was switched on to obtain gray levels linear with transmission. A 40x objective was used and sections were stained lightly to avoid distributional error, glare, and diffraction errors. Pixel spacing was calibrated with a stage micrometer separately for vertical and horizontal dimensions. For spatial calibration, the JAVA software was used in the computer to load conversion values into look-up tables. A calibration strip containing various gray levels of known optical densities (Kodak) was imaged at the beginning of each session and was used to construct a calibration curve for the conversion of gray levels to optical density for that session. Each imaging session was thereby independently calibrated to optical density.

3.3. Methodological Validation of Quantitative C.O. Histochemistry

3.3.1. Quantitative Methodological Findings. For the validation of activity standards, samples of each standard were assayed for calculation of specific activity spectrophotometrically. Percent weight of standards was related to assessed activity. The relationships between time of incubation, section thickness, and activity of dissected regions, with their reaction product measured densitometrically were demonstrated. After systematically varying parameters for the assays, brain standards were developed which showed a linear relationship ($r = 0.99$) between C.O. activity (activity units) and C.O. reactivity (OD units) (Figure 7).

Thickness standards of known C.O. activity (measured spectrophotometrically) were included in each staining batch and were imaged on a DC-powered light box using JAVA. The optical density and activity measurements of these standards were then used to construct a regression equation. The change in optical density showed linear relationships

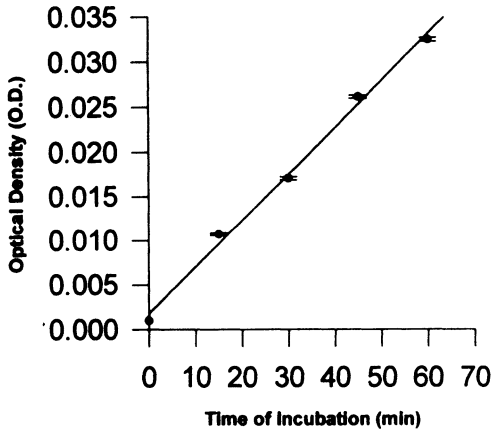

Figure 7. Calibration curve showing the linear relationship between C.O. activity and optical density in the cytochemical tissue standards. Activity units were measured spectrophotometrically and are expressed as μmol/min/g tissue wet weight. Optical density of brain tissue standards was measured with an imaging system calibrated with an optical density step tablet. Standard error bars of mean measures are shown, but in most cases are smaller than the size of the symbols.

with respect to tissue activity, incubation time, and section thickness in each of the staining batches (r = 0.99) as illustrated in Figures 7, 8 and 9. Optical density measures of the sections were thereby independently converted to C.O. activity units using the calibration curves generated with the standards' optical density and activity units.

A rat brain homogenate did not have as much C.O. activity as the most active regions of the brain, including auditory nuclei. Therefore, when using standards with less activity than whole-brain homogenates, it is necessary to extrapolate C.O. activity units above the range of observations made to include the brain structures with the most activity. To avoid the need to extrapolate, brain homogenate standards cut in increasing thicknesses served to obtain increasing proportions of C.O. reactivity. This was the most

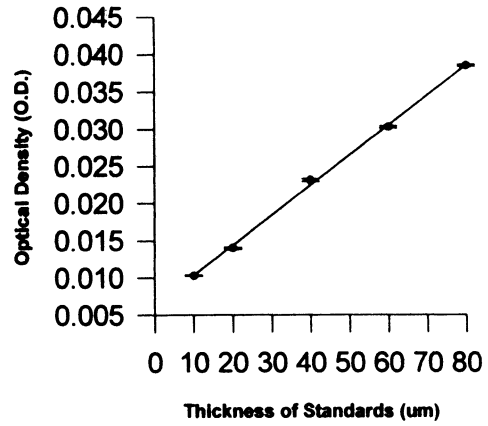

Figure 8. Effect of cytochemical incubation time on optical density of 40 μm brain sections. The increase in optical density was linear with respect to increasing time in the 37°C incubation medium. Standard error bars of mean measures are shown, but in most cases are smaller than the size of the symbols.

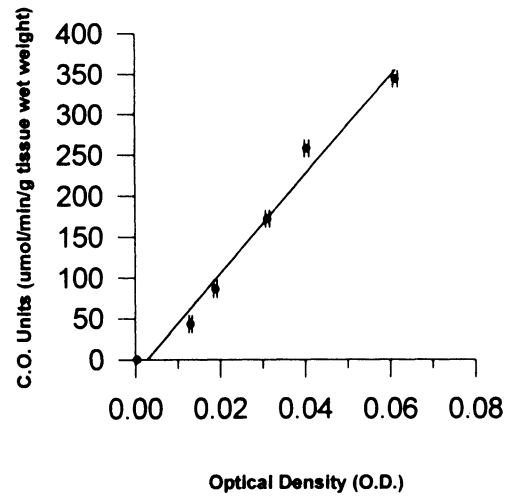

Figure 9. Effect of section thickness on optical density of standard brain homogenate sections incubated for 60 min at 37°C. The increasing optical density was linear with respect to increased section thickness of the paste standards. Standard error bars of mean optical density are shown, but in most cases are smaller than the size of the symbols.

convenient method when used with the C.O. cytochemical procedure described above because it resulted in a rate of reaction linear with respect to increasing incubation time (Fig. 8) and section thickness (Fig. 9).

The calibration procedure for the conversion of densitometric measures of reaction product (OD) to spectrophotometric measures of enzyme activity units was further verified by comparison of dissected brain regions analyzed spectrophotometrically with the converted units obtained in stained tissue sections. The measured activity units were linearly correlated (r = 0.96) with the OD of histochemical stain (Gonzalez-Lima & Jones, 1994), similar to the findings with the tissue standards.

3.3.2. Effect of Preincubation Fixation. The quantitative cytochemical method as proposed here provides a good indicator of fresh tissue C.O. enzymatic activity (i.e. without a substantial fixation inhibition) because preincubation fixation is limited to 5 min with 0.5% glutaraldehyde. We have directly assessed the effect of this preincubation fixation step by comparing adjacent sections from the same tissue standards that either remained totally unfixed (n = 14) or that were fixed with 0.5% glutaraldehyde for 5 min (n = 14). All sections were stained together on the same baths side-by-side. The mean OD units of the unfixed sections (10 readings/section) was 0.039 (± 0.002 standard deviation), while the mean for the fixed sections was 0.038 (± 0.002 standard deviation). This difference (2.52%) was not statistically significant ($p = 0.30$, $t = 1.07$, $df = 13$). It was determined that only a very small decrease in C.O. reactivity was produced by our brief fixation step before the preincubation and incubation baths. This step is done only for convenience, to affix the sections onto the slides to prevent sections from floating off during subsequent staining baths.

3.3.3. Interassay Variability and Linearity for Group Comparisons. To determine the interassay variability and linearity of the quantitative C.O. method, separate sets of standards of known C.O. activity were stained using new solutions in 26 experiments. The optical density readings have standard errors below 5% of the means, and under the above conditions, the activity units of the C.O. standards were correlated with gray levels at −0.97 (n = 26) with a linear function.

The present C.O. cytochemical procedure demonstrated that it fulfills general quantitative methodological requirements detailed by Stoward (1980). First, there needs to be a way to subtract any nonspecific staining. This was done in our method by image subtraction of the OD background of unreactive tissue standards. Second, the change in OD must be linear during the incubation period (Fig. 8). Third, the enzyme activity must increase in proportion to tissue section thickness (Fig. 9). Finally, there needs to be a conversion procedure (Fig. 7) by comparison of data measured biochemically to provide a way to express measures in OD as actual enzyme units. The validity of the conversion procedure was verified also using dissected brain regions. The method presented here fulfilled these quantitative criteria and thus provides a superior histochemical approach for regional and neuronal mapping studies of C.O. activity.

4. COMPARISON WITH DEOXYGLUCOSE AUTORADIOGRAPHY

A fully quantitative approach to C.O. histochemistry can be readily applied with the use of C.O. internal standards of known activity together with the application of quantitative image analysis. Both internal standards and quantitative densitometry are routinely used in FDG and 2-DG autoradiographic techniques. The main problem to control with C.O. histochemistry is the variability of staining from different experiments. This problem is greatly alleviated by the introduction of slides with complete sets of tissue paste standards of known amounts of C.O. activity with each staining experiment. Experimental factors affecting stain intensity will then affect both the C.O. standards and the brain sections. In this manner gray levels of stain intensity converted to an internal standard curve can be compared across baths. In many cases, the regions of interest from all the brains in one experiment can be stained together in the same bath when using large staining dishes, to further minimize variability.

The theoretical chemical processes responsible for the observed C.O. reaction product are better understood and localized than in FDG and 2-DG autoradiography. For example, 2-DG is trapped primarily in glia as opposed to neurons (Magistretti & Pellerin, 1996). In contrast, C.O. reactivity is primarily localized to labeled neurons because of their dominant oxidative aerobic metabolism (Gonzalez-Lima et al., this volume). Glia show only minimal C.O. reactivity because of their dominant glycolytic anaerobic metabolism. This dichotomy in C.O. staining between darkly reactive neurons and lightly reactive glia is analogous to the dichotomy observed in skeletal muscle fibers between "red" and "white" fibers. That is, skeletal muscle contains darkly C.O. reactive fibers called "red fibers" which are rich in mitochondrial enzymes and depend primarily on oxidative energy metabolism. It also contains lightly C.O. reactive "white fibers" which are poor in mitochondrial enzymes and are dependent on glycolytic anaerobic metabolism.

A major advantage of C.O. histochemistry over FDG and 2-DG autoradiography is its cellular resolution at the light microscopic level that allows accurate delineation of brain regions of interest and identification of individual neuronal populations with high levels of oxidative metabolic capacity (Figure 10).

Note also in Figure 10 that the red nucleus (arrows) is darkly stained with C.O. in *A*, whereas it shows background labeling with FDG autoradiography in *B*. This difference between C.O. activity and glucose utilization is characteristic of many brain regions under baseline conditions. Generally in rodents, subcortical motor regions show relatively greater C.O. staining than subcortical visual and somatosensory regions. For example, in Figure 10A the rat oculomotor complex, red nucleus and interpeduncular nucleus show

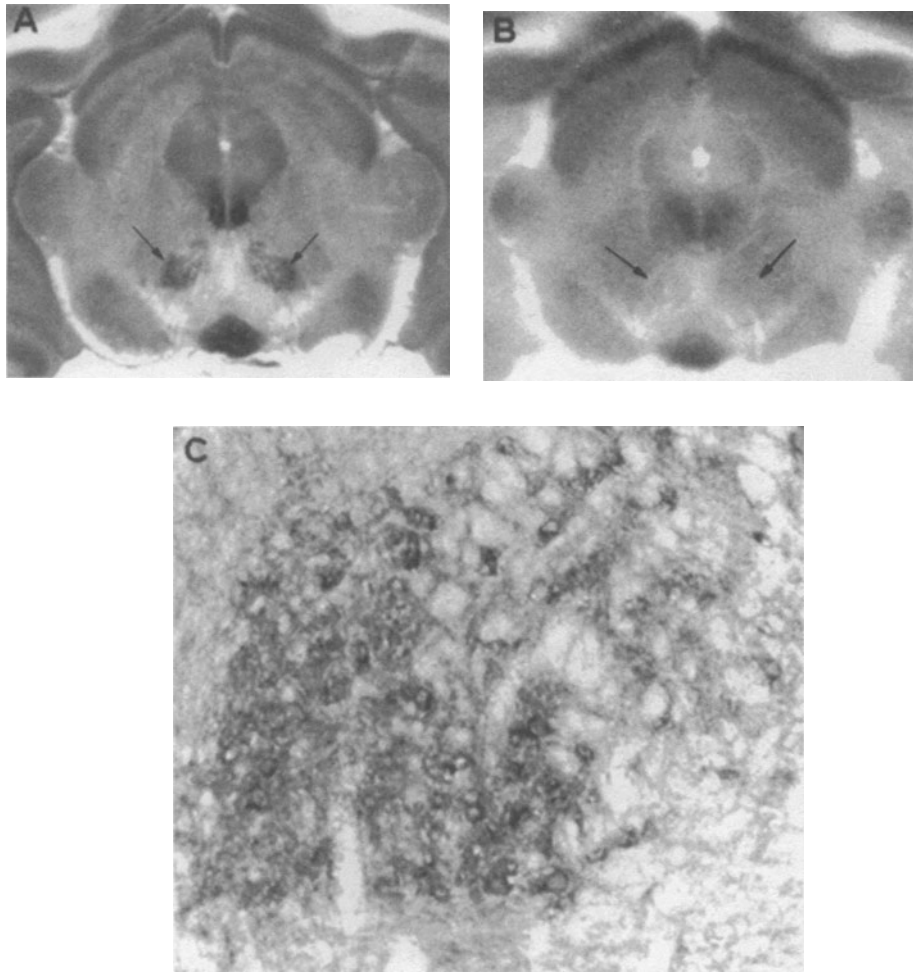

Figure 10. Examples of adjacent rat brain sections processed with C.O. and FDG techniques are illustrated in *A* and *B* respectively. Using the described C.O. procedure it is possible to resolve individually stained neurons in the red nucleus (*C*). These neurons show darkly stained perikaria around their unstained cell nuclei, providing a dark ring appearance that is characteristic of neurons with dominant axosomatic excitatory synapses, found in many brain regions.

greater C.O. staining than the superficial layer of the superior colliculus. The opposite is the case of FDG labeling in Figure 10B, where the predominant labeling is in the superficial layer of the superior colliculus that receives the sensory input from the retina. Such differences are expected under resting conditions in an illuminated testing environment, because C.O. staining primarily reflects the baseline oxidative metabolic capacity of neurons, whereas FDG uptake visualizes ongoing nonoxidative (glycolysis) metabolism of glucose in glia as well as oxidative glucose use by light-activated neurons.

As compared with glucose metabolism, the C.O. modifications in the tissue after prolonged stimulation or training reach a more stabilized state of oxidative metabolism (Wong-Riley, 1989). This produces an inherently less variable outcome than FDG and 2-DG studies that reflect a more acute state of energy metabolism during animal testing. In cases involving chronic training conditions, the C.O. technique is more likely to reveal

changes than 2-DG or FDG or similar acute metabolic markers (Poremba et al., this volume). This is because an acute state may not reflect cumulative changes in baseline metabolism unless the testing conditions are such that the modified neurons are metabolically activated (Nobrega, 1992).

An additional advantage of the described C.O. procedure is the use of an on-the-slide staining technique. This facilitates handling of tissue sections because the same (or adjacent) frozen sections can be autoradiographed for FDG (or other tracer) and subsequently stained for C.O. while attached to the original slide. This minimizes distortion and misalignment problems, and helps to maintain a more uniform treatment of the sections during staining procedures.

4.1. Different Goals of C.O. and Deoxyglucose Experiments

The goals of using quantitative C.O. histochemistry are different from those for studies with FDG or 2-DG. Poremba et al. (this volume) described in more detail these differences for the neuroimaging of learning and memory functions. Briefly, the main goal of the C.O. experiment is to visualize a long-lasting change in brain metabolic *capacity* produced by a learning paradigm. Changes in C.O. activity revealed by histochemistry reflect underlying changes in the endogenous long-term metabolic capacity of the brain (Wong-Riley, 1989; Silverman & Tootell, 1987). Thus while FDG is used to assess short-term changes in metabolic activity evoked by the stimulation during the post-injection survival period, C.O. is used to assess long-term alterations in enzymatic content that develop slowly during the entire period of the experiment. Changes in C.O. activity in learning paradigms may require several days of training, and lead to alterations of this endogenous metabolic marker that are linked to the prolonged metabolic demand on certain brain regions throughout training. Therefore, the goal of C.O. experiments is not to assess acute changes in functional activity over a period of minutes in response to a stimulus like in the case of FDG or 2-DG. The C.O. technique is suited for assessing the effects of chronic training over days or weeks on the alterations of activity levels linked to the sustained metabolic demands on the brain regions involved in the training.

FDG and C.O. techniques can complement each other by measuring different metabolic processes produced by short-term presentation of a stimulus (FDG) vs. long-term presentation (C.O.). The possibility of discriminating the immediate effects of a stimulus (FDG) from the carry-over prolonged effects of a stimulus (C.O.) is of special significance for learning and memory studies. For example, learning to differentiate conditioned sounds for several days (such as in experiments described in Poremba et al., this volume) may lead to significant changes in the metabolic capacity (C.O.) of brain regions due to protein and synaptic membrane synthesis that may be involved in long-term memory processes. That is, without having any stimulation with the conditioned sounds on the day the brain is removed, the postmortem analysis of C.O. activity would reveal baseline changes in comparison with control unconditioned subjects. This means that the goals of C.O. experiments of associative learning include controlling the stimuli throughout training in the experimental and control groups to match the number and history of stimulation, with the only difference being the temporal pairing relationship between the stimuli. In the case of FDG, however, the most critical concern is to match the stimuli during the FDG post-injection period when the on-going metabolic activity is being assessed.

In combined FDG and C.O. experiments, to achieve the full quantitative potential of C.O. mapping it is necessary to consider the specific aims in each stage of an experiment (Gonzalez-Lima, 1992). First, care must be given to the training duration to permit suffi-

cient time for the process of enzyme up-regulation or down-regulation, depending on the metabolic demands of the specific task on neurons. Second, tissue processing requires procedures compatible with FDG autoradiography to examine the same brains for both C.O. and FDG. Third, internal calibration standards of known C.O. activity should provide a way to compare sections stained in different batches to minimize variability. Fourth, the sensitivity and specificity of the staining reaction should be maximized to detect subtle changes without reaching saturation or nonlinear reactivity. Fifth, the preparation of the sections should preserve the location of the reaction product and FDG. Finally, analysis should be based on quantitative densitometry calibrated with standards showing linearity so as to yield reliable units of C.O. enzyme activity and FDG incorporation.

5. EXPERIMENTAL CYTOCHROME OXIDASE INHIBITION

Brain energy failure based on C.O. enzymatic inhibition was produced with a pharmacological model in azide-treated rats (Bennett & Rose, this volume) to address three fundamental questions: 1) Which brain regions are more vulnerable to inhibition of C.O. activity? 2) What behavioral and brain deficits are common among this model and other models of compromised brain energy metabolism? and 3) Do C.O. deficits in this model parallel cellular oxidative metabolism changes in Alzheimer's brains? (Gonzalez-Lima et al., this volume).

In order to test the hypothesis that direct C.O. inhibition will result in similar neural metabolic and behavioral deficits to those found in aged rats with chronic ischemia (Abdollahian, Cada, Gonzalez-Lima & de la Torre this volume), sodium azide, which specifically inhibits C.O. activity, was administered to 4 month old rats. The brains of rats treated for 2 weeks with sodium azide or saline vehicle, via subcutaneously implanted osmotic minipumps, were analyzed for C.O. histochemistry as previously described (Cada *et al.*, 1995).

Briefly, each rat is anesthetized with secobarbital (40 mg/kg) and implanted subcutaneously with an Alzet 2ML4 osmotic minipump containing either sodium azide solution (160 g/L) or the 0.9% saline vehicle. The Alzet 2ML4 minipump has a 2 ml reservoir and provides a constant infusion rate of 2.5 µl/hr for 28 days; therefore, the dose of sodium azide delivered is 400 µg/hr. This treatment regimen has been shown to decrease C.O. activity by 35% in mitochondria extracted from rat forebrain homogenates (Bennett, Diamond, Stryker, Parks & Parker Jr., 1992b).

We found that this treatment regimen decreases overall brain C.O. activity by about 30%, with significant variability in degree between some brain regions (Cada *et al.*, 1995). Since this model selectively impairs spatial memory and the expression of hippocampal long-term potentiation, we could relate C.O. deficits with behavioral deficits. Commonly affected brain regions where the amount of C.O. inhibition was consistently correlated with the degree of spatial memory deficits were identified for future detailed cellular comparisons with the Alzheimer's disease brains.

5.1. Background and Rationale for Using Sodium Azide to Inhibit C.O. Activity

Analyses of C.O. histochemical measures across many species have shown that there is heterogeneity in the distribution of regional metabolic capacity (Wong-Riley, 1989 for review). In addition to its interregional heterogeneity, C.O. activity can be altered by

manipulating neuronal activity. For example, C.O. activity in the auditory nuclei can be inhibited by blocking auditory input for a period of days (Wong-Riley *et al.*, 1978). A similar inhibition of C.O. activity has been demonstrated in the visual system of cats by a variety of techniques that block neural input from one eye (Wong-Riley & Riley, 1983). Nobrega *et al.* (1993) induced an increase in C.O. activity restricted to limbic areas of rat brains measured 28 days after a series of electroconvulsive treatments. Taken together, these results imply that C.O. activity is positively correlated with neuronal activity.

Bennett and colleagues developed a rat model of persistent systemic C.O. inhibition (Bennett, Diamond, Parker, Stryker & Rose, 1992a; Bennett *et al.*, 1992b). Continuous subcutaneous infusion of sodium azide (NaN_3) in rats produced a chronic partial inhibition (35–39%) of cytochrome oxidase activity in mitochondrial fractions of whole brain homogenates, without significantly affecting other enzymes of the respiratory chain (complexes I, II, and III). This azide treatment impaired spatial learning and memory and the expression of hippocampal long-term potentiation (LTP), a physiological model of long-lasting synaptic plasticity (Bennett *et al.*, 1992ab; Bennett & Rose, 1992). Thus, there is *a priori* evidence to assume that particular regions related to spatial memory functions will be more sensitive to C.O. inhibition than others; for example the hippocampal formation, the amygdala and the frontal cortex have been implicated in numerous studies (reviewed by Aggleton, 1992; Olton, Wible, Pang & Sakurai, 1989). Azide-induced C.O. inhibition also leads to formation of reactive free radicals and oxidative damage (Partridge, Monroe, Parks, Johnson, Parker Jr., Eaton & Eaton, 1994).

It has been shown that C.O. is more vulnerable to insult in Alzheimer's disease than are other enzymes of the respiratory chain (Beal, Hyman & Koroshetz, 1993; Kish, Bergeron, Rajput, Dozic, Mastrogiacomo, Change, Wilson, DiStefano & Nobrega, 1992; Mecocci, MacGarvey & Beal, 1994; Mutisya, Bowling & Beal, 1994; Parker, Filley & Parks 1990; Parker, Mahr, Filley, Parks, Hughes, Young & Cullum, 1994a; Parker, Parks, Filley & Kleinschmidt-DeMasters, 1994b). The clinical finding that a C.O. defect in Alzheimer's disease occurs in the periphery as well as in the brain suggests that a defect in metabolism in Alzheimer's disease might be widespread (Blass, Sheu & Cedarbaum, 1988; Blass, 1993). Yet the genetic studies on differences between C.O. subunits in different brain regions suggest that systemic inhibition of C.O. activity may still be associated with selective regional vulnerability within the brain (Chandrasekaran, Stoll, Giordano, Atack. Matocha, Brady & Rapoport, 1992).

The goals of our experiment were to quantify histochemically the effects of sodium azide treatment on C.O. activity in rat brain and to determine whether there is differential vulnerability among brain regions in response to this treatment. The goal was to select a sampling of regions from telencephalic, diencephalic, and mesencephalic levels to test the hypothesis that regional effects of systemic azide are heterogeneous in the brain. The main findings are discussed in the context of how preferential sodium azide inhibition of C.O. in some brain regions could contribute to the learning and memory deficits that are induced by this treatment. These results were reported in more detail in Cada *et al.* (1995).

5.2. Methodological Histochemical Considerations

Calibration curves were generated using histochemically measured OD of the brain paste standards and the spectrophotometrically determined C.O. activity units of the brain paste thickness standards. The three sets of standards, though reacted in separate incubation media, showed no significant differences (t-tests, $p > 0.21$) between their optical densities. The interassay coefficient of variation (standard deviation × 100 / mean) was

0.82% for the three staining batches. For each one of the paste standards, its average value showed a standard error (S.E.) below 0.5% of the mean measured across the batches. A regression equation generated using the activity of the thickness standards from separate incubations and the OD of the brain paste standards resulted in a linear function: $r = 0.978$, $y = 6377.24x - 29.89$. Using this regression equation, the OD obtained from each structure was converted to activity units (micromol/min/g tissue wet weight).

In the image analysis of regions, the central part of each region was located and measured by two experimenters. The intra- and inter-rater reliability for this sampling technique was assessed by comparing 15 measures made twice from the same 15 loci, separated by a three-month interval. For the intra-rater reliability, the same experimenter made the measures, and this resulted in a mean coefficient of variation of 5.41% and a correlation of $r = 0.93$. For the inter-rater reliability, a second experimenter made the second measures, and this resulted in a coefficient of variation of 5.81% and a correlation of $r = 0.87$ between measures of the same regions.

Using calibration standards of known C.O. activity together with quantitative image analysis of histochemical sections formed the basis for the applied quantitative approach (Gonzalez-Lima & Garrosa, 1991). Both of these tools are commonly used in 2-deoxyglucose autoradiography (Gonzalez-Lima, 1992; Gonzalez-Lima *et al.*, 1993) and other metabolic mapping techniques (Biegon & Wolff, 1986; Nobrega, 1992; Nobrega *et al.*, 1993). Histochemical techniques such as the one used here contain some variability between tissue processed in different incubation reactions. However, if tissue processing procedures are strictly reproduced and complete sets of standards of known C.O. activity are included with each incubation medium—as was done in the present study—the problem of inter-assay variability is largely resolved. Thus the percent differences found between the various brain regions in response to azide treatment could not be accounted for simply by variability between assays or paste standards. The important point is not that the tissue level of C.O. activity is different among brain regions (Wong-Riley, 1989, for review); but rather that the between-group percent decreases produced by azide treatment are significantly larger in some regions.

5.3. Regional Effects of Sodium Azide on Brain C.O. Activity

The total C.O. activity was 170.43 ± 0.1 units (mean ± S.E.) for the control brains, and 121.06 ± 0.1 units for the azide-treated brains. This corresponded to an overall –29% difference between the groups. The maximal activity among the regions sampled was 228 units in the occipital cortex (Area 18) of the control brains. The maximal activity in the azide-treated brains was below 180 units, found in the basolateral amygdaloid nucleus (BlA).

An expected finding was that all brain regions examined showed a reliable decrement in C.O. activity after sodium azide treatment. The regional evaluation of C.O. activity was performed in two steps, from a more general evaluation of integrated activity at three rostrocaudal levels to a more specific evaluation of a sample of 22 separate regions. In both evaluations, the C.O. activities measured in the sodium azide treated rats were significantly lower than those found in the control rats ($p < 0.01$, ANOVA followed by subsequent comparisons with corrected t-tests).

The first regional analysis showed that in addition to the between-groups reduction in C.O. activity at each level, there was indication of the mesencephalic level being more strongly affected than the others. The mean percent reductions (± S.E.) for each level were: 27.31 ± 0.77 for the telencephalic, 29.27 ± 1.18 for the diencephalic, and 35.70 ± 0.33 for

Table 1. Regional activity of cytochrome oxidase in the brains of azide-treated and control rats[a]

Structure	Control Mean ± S.E.	Experimental Mean ± S.E.	Difference %
Deep mesencephalic nucleus (DpMe)	143.75 ± 1.96	90.41 ± 1.07	−37.11
Central amygdaloid nucleus (CeA)	182.12 ± 0.85	114.70 ± 2.57	−37.02
Superior colliculus-deep (SCDp)	164.59 ± 1.46	106.87 ± 0.87	−35.07
Central gray (CG)	162.79 ± 1.38	106.89 ± 1.12	−34.34
Ventral tegmental area (VTA)	109.28 ± 1.01	75.68 ± 1.22	−30.75
Subiculum (Sub)	165.77 ± 1.90	115.10 ± 1.13	−30.57
Medial amygdaloid nucleus (MeA)	183.83 ± 0.58	129.27 ± 2.36	−29.68
CA1 of hippocampus (CA1)	182.22 ± 1.73	128.29 ± 1.32	−29.60
Basolateral amygdaloid nucleus (B1A)	198.69 ± 1.09	140.40 ± 2.38	−29.34
CA2 of hippocampus (CA2)	176.28 ± 1.88	125.43 ± 1.15	−28.85
Auditory cortex (Aud)	157.41 ± 2.71	112.13 ± 1.62	−28.77
CA3 of hippocampus (CA3)	171.58 ± 1.81	122.65 ± 1.24	−28.52
Area 18 (A18)	180.11 ± 1.93	128.92 ± 1.07	−28.42
Area 18a (A18a)	178.81 ± 1.84	130.30 ± 1.54	−27.13
Retrosplenial cortex (Rs)	179.43 ± 1.96	131.09 ± 0.97	−26.94
Medial frontal cortex (MFC)	178.83 ± 0.90	136.64 ± 0.95	−26.90
Sulcal frontal cortex (SFC)	196.32 ± 1.20	143.58 ± 0.79	−26.86
Area 17 (A17)	180.86 ± 1.81	132.35 ± 1.29	−26.82
Red nucleus (Red)	166.74 ± 0.90	122.46 ± 1.18	−26.56
Lateral frontal cortex (LFC)	187.71 ± 1.26	138.36 ± 0.53	−26.29
Superior colliculus-superior (SCSu)	172.39 ± 1.56	127.55 ± 1.24	−26.01
Entorhinal cortex (Ent)	147.32 ± 1.25	109.54 ± 0.96	−25.64

[a]Mean ± standard error (S.E.) units in μmol/min/g tissue wet weight were obtained by averaging measurements from five control and four treated rats. In each rat, a given structure was measured in three consecutive sections. Percent differences between groups were calculated as 100 × (Experimental − Control) / Control. ANOVA followed by subsequent comparisons with corrected t-tests were used to assess differences statistically. Each structure's mean was significantly lower in the experimental group at $p < 0.01$ (from Cada *et al.*, 1995).

the mesencephalic levels. In the sodium azide treated rats, the percentages of C.O. activity reduction in the sections (n = 12 / level) at the mesencephalic levels were significantly greater than those at the telencephalic levels when compared using nonparametric tests (Mann-Whitney U–Wilcoxon Rank Sum W tests: U = 10, W = 88, $p < 0.01$). But no significant differences in percent reduction were found between telencephalic and diencephalic levels ($p > 0.9$).

The more specific regional analysis involved measuring C.O. activities in 22 brain regions (Table 1). This evaluation served to confirm the inhibitory effect of azide treatment on a region-by-region basis and allowed the identification of the regions with the highest decrement in activity, corresponding to the deep mesencephalic reticular area (−37.11%) and the central amygdala (-37.02%). These regions showed decrements which were significantly greater than the other decrements found in the telencephalic (U = 28, W = 106, $p < 0.05$) and diencephalic (U = 28, W = 106, $p < 0.05$) levels, but not significantly greater than mesencephalic levels (U = 53, W = 131, $p > 0.29$). Other activity decrements at the regional telencephalic and diencephalic levels showed statistically comparable means.

5.4. Differential Vulnerability of Brain Regions to C.O. Inhibition

Three main observations were made. First, there was a general decrement in C.O. activity following sodium azide treatment. This decrement ranged from 27% to 35% in the

integrated activities measured at telencephalic, diencephalic and mesencephalic levels, and between 25% and 37% in the individual regions analyzed. This decrement measured histochemically is consistent with a previous report of 35–39% decrease in biochemically assayed mitochondrial C.O. activity in brain homogenates from rats given the same azide treatment (Bennett *et al.*, 1992b). Second, midbrain reticular formation and central amygdala appeared more vulnerable than other regions to the sodium azide effects. Third, differences in regional vulnerability were manifested as different patterns of interregional activity correlations found in control and treated brains (Cada *et al.*, 1995).

The brain is especially vulnerable to sodium azide treatment because of its disproportionate aerobic energy requirement, thus making it strongly dependent on oxidative phosphorylation (Wong-Riley, 1989). Impairments of aerobic respiration have the potential for limiting the activity of the brain (Wikström *et al.*, 1981). Decreases of 25–37% in C.O. activity may be of potential functional significance for brain processes affected by aging such as learning and memory (Bennett *et al.*, 1992a,b). For example, in a comparison of C.O. activity in mitochondria isolated from brains of 4-month-old and 30-month-old rats, a significant age-related decrease of 25% in C.O. activity was observed in the parietotemporal cortex (Curti *et al.*, 1990). A C.O. activity decrease of 25% or more may be associated with a reduced capacity for ATP production, as suggested by a parallel regulation of C.O. and Na^+, K^+-ATPase activities in brain (Hevner, *et al.*, 1992).

A possible explanation for the regional effects of azide on C.O. activity may be differences in access of azide to different regions, but there is presently no experimental support for this mechanism. Systemic infusion of sodium azide produced heterogeneity both in the degree of C.O. inhibition and in the correlations of C.O. activity among brain regions. Whether all brain regions presumably had equal access to this highly diffusible compound is unknown. Another possible explanation for the selective vulnerability of some brain regions may be related to the differential expression of C.O. genes in different brain regions. Chandrasekaran *et al.* (1992) have provided evidence that this is the case in monkey brain. For example, cDNA clones for the three C.O. subunits encoded by mitochondrial DNA showed higher levels of mRNA in frontal pole, dorsal lateral frontal cortex, and hippocampus than in the primary visual or somatosensory cortices, in agreement with heterogeneous C.O. histochemistry in these regions. Chandrasekaran *et al.* (1992) concluded that such differences may be related to differences in the distribution of neuropil versus cell bodies in the brain regions investigated; and they further suggested that these genetically-mediated regional differences may be relevant to selective regional vulnerability in Alzheimer's disease.

In a subsequent study, Chandrasekaran, Giordano, Brady, Stoll, Martin & Rapoport, (1994) investigated the expression of C.O.-related genes in the temporal cortex and motor cortex of Alzheimer's brains, and found significantly more decreased mitochondrial RNA levels in the temporal region as compared to the motor region or the same regions in healthy age-matched controls. The studies of Chandrasekaran *et al.* (this volume) provide evidence to suggest that the selective vulnerability of C.O. inhibition may be linked to genetically-inherent capabilities of some regions particularly relevant for memory. This evidence may be relevant for the observed regional heterogeneity in C.O. inhibition after sodium azide treatment.

To our knowledge, no studies on C.O. activity in Alzheimer's brains have been done in the mesencephalic reticular formation or the central amygdala where C.O. inhibition was greatest in the present study after azide treatment. The fact that histopathological plaques and tangles may or may not be abundant in these regions in humans, is not a sufficient argument to discount the potential role of mitochondrial pathophysiological events in

these regions in relation to some memory deficits of Alzheimer's patients (Mecocci *et al.*, 1994). The deep mesencephalic reticular formation and the central amygdaloid nucleus exhibited the largest overall decreases in C.O. activity in response to the azide treatment. The ascending reticular input from the mesencephalic reticular formation represents an important pathway in the reticular activating system linked to behavioral arousal (Gonzalez-Lima & Scheich, 1985) and memory consolidation (Bloch, 1976); and the central amygdala has a well-established role in memory modulation and behavioral dysfunction (Aggleton, 1992).

5.5. Effects of C.O. Inhibition on Memory Functions

The hippocampal formation, the deep mesencephalic reticular formation and the central amygdala are disproportionately affected by sodium azide. The hippocampus is a preferential target of damage in Alzheimer's brains (Ball, Fisman, Machinski, Blume, Fox, Pral, Kirshen, Fox & Merskey, 1985) and is typically associated with some memory functions in humans and other mammals. Cada *et al.* (1995) found that the interregional positive correlations between C.O. activity in the hippocampal formation and other brain regions, which existed in control brains, disappeared after sodium azide treatment. This functional uncoupling may affect primarily associative memory functions which are the product of interactions between different brain regions (Gonzalez-Lima & McIntosh, 1996).

This azide treatment has been shown to produce learning and memory deficits on appetitively- and aversively-motivated tasks that are highly impaired by hippocampal dysfunction (Bennett *et al.*, 1992a,b; Bennett & Rose, 1992). Indeed, this azide treatment impairs the functional organization of long-term potentiation in the hippocampal formation (Bennett *et al.*, 1992a). Inhibition of C.O. activity can produce some of the symptoms commonly associated with Alzheimer's disease, such as deficits in spatial memory and orientation. Bennett *et al.* (1992a,b) chronically administered sodium azide to rats and found that the subjects showed difficulty with associative learning and memory tasks (two-way shuttle box and radial maze). These memory impairments did not appear to be secondary to any significant sensory or motor impairments.

Further examination by Bennett and Rose (1992; this volume) found that sodium azide administration impairs performance in the Morris water maze task in rats, another spatial learning task. Again without showing motor impairment, the subjects demonstrated difficulty in both acquisition and retention of the maze task, strengthening the hypothesis that azide infusion produces learning and memory deficits similar to those found in Alzheimer's disease. This evidence seems to indicate that sodium azide treatment could be a useful animal model of the kind of memory impairment found in Alzheimer's disease. It also provides experimental evidence consistent with the theory advocating a C.O. defect as a key producer of memory symptoms in Alzheimer's disease (Gonzalez-Lima *et al.*, this volume).

In conclusion, the enhanced vulnerability to C.O. inhibition of brain regions most often engaged in associative memory functions, may depend on the sustained neuronal metabolic demands imposed by associative learning and memory in these regions. Neural regions with learning and memory-related neuronal activity, increase their C.O. activity to meet the sustained energy utilization required for long-term neuronal and synaptic plasticity (Poremba *et al.*, this volume). This would render memory-related regions more vulnerable to C.O. inhibition and oxidative damage, resulting in preferential atrophy of their more metabolically active neuronal populations.

ACKNOWLEDGMENTS

Supported by Texas Advanced Technology Program grant 003658-361, NSF grant IBN9222075, and NIH grant RO1 MH43353 to FGL, and by NIH grant T32 MH18837 to AC. We thank Dr. A. Poremba, D. Jones, J. Valla and H.P. Nair for valuable assistance and comments. We are also grateful for the sections supplied by A.M. Crane, R.A. Frazor, and D.G. Albrecht, and the human tissue provided by Dr. K. Hatanpää.

REFERENCES

Adams, J. C., 1977, Technical considerations on the use of horseradish peroxidase as a neuronal marker. *Neurosci.* 2: 141–145.

Aggleton, J. P., ed., 1992, The Amygdala: Neurobiological Aspects of Emotion, Memory, and Mental Dysfunction, Wiley-Liss, New York.

Ball, M.J., Fisman, M., Hachinski, V., Blume, W., Fox, A., Kral, V.A., Kirshen, A.J., Fox, H., and Merskey, H., 1985, A new definition of Alzheimer's disease: A hippocampal dementia, *Lancet* 1: 14–16.

Beal, M. F., Hyman, B. T., and Koroshetz, W., 1993, Do defects in mitochondrial energy metabolism underlie the pathology of neurodegenerative disorders?, *TINS* 16(4): 125–131.

Bennett, M. C., Diamond, D. M., Parker, Jr. W. D., Stryker, S. L., and Rose, G. M., 1992a, Inhibition of cytochrome oxidase impairs learning and hippocampal plasticity: A novel animal model of Alzheimer's disease. In Simpkins, J., Crews, F. T., and Meyer, E. M. (eds.), Alzheimer's Disease Therapy: A New Generation of Progress, Plenum Press, New York, pp. 485–501.

Bennett, M. C., Diamond, D. M., Stryker, S. L., and Parker, Jr. W.D., 1992b, Cytochrome oxidase inhibition: A novel animal model of Alzheimer's disease, *J. Geriat. Psychiat. Neurol.* 5: 93–101.

Bennett, M. C., and Rose, G. M., 1992, Chronic sodium azide treatment impairs learning of the Morris water maze, *Behav. Neur. Biol.* 58: 72–75.

Benzi, G., Arrigoni, E., Dagani, F., Marzatico, F., Curti, D., Manzini, A., and Villa, R.F., 1979, Effect of chronic treatment with some drugs on the enzymatic activities of the rat brain, *Biochem. Pharmacol.* 28: 2703–2708.

Biegon, A., and Wolff, M., 1986, Quantitative histochemistry of acetylcholinesterase in rat and human brain postmortem, *J. Neurosci. Meth.* 16: 39–45.

Blass, J. P., 1993, Pathophysiology of aging, *Neurol. Suppl.* 4: 25–38.

Blass, J. P., Sheu, R. K. F., and Cedarbaum, J. M., 1988, Energy metabolism disorders of the nervous system, *Revue Neurologique* 144: 543–563.

Bloch, V., 1976, Brain activation and memory consolidation. In Rosenzweig, M. R. and Bennett, E. L. (eds.), Neural Mechanisms of Learning and Memory, MIT Press, Cambridge, Massachusetts, pp. 582–590.

Braun, K., Scheich, H., Schachner, M., and Heizmann, C.W., 1985, Distribution of parvalbumin, cytochrome oxidase activity and ^{14}C-2-deoxyglucose uptake in the brain of the zebra finch I. auditory and vocal motor systems, *Cell Tissue Res.* 240: 101–115.

Brauth, S.E., 1990, Investigation of central auditory nuclei in the budgerigar with cytochrome oxidase histochemistry, *Brain Res.* 508: 142–146.

Cada, A., Gonzalez-Lima, F., Rose, G.M., and Bennett, M.C., 1995, Regional brain effects of sodium azide treatment on cytochrome oxidase activity: A quantitative histochemical study, *Metab. Brain Disease* 10: 303–319.

Chalmers, G.R., and Edgerton, V.R., 1989, Marked and variable inhibition by chemical fixation of cytochrome oxidase and succinate dehydrogenase in single motoneurons, *J. Histochem. Cytochem.* 3: 899–901.

Chandrasekaran, K., Giordano, T., Brady, D.R., Stoll, J., Martin, L.J., and Rapoport, S.I., 1994, Impairment in mitochondrial cytochrome oxidase gene expression in Alzheimer's disease, *Molec. Brain Res.* 24: 336–340.

Chandrasekaran, K., Stoll, J., Giordano, T., Atack, J. R., Matocha, M. F., Brady, D. R., and Rapoport, S. I., 1992, Differential expression of cytochrome oxidase (COX) genes in different regions of monkey brain, *J. Neurosci. Res.* 32: 415–423.

Chieco, P., Jonker, A., Melchiorri, C., Vanni, G., and Van Noorden, C.J.F., 1994, A user's guide for avoiding errors in absorbance image cytometry: A review with original experimental observations, *Histochem. J.* 26: 1–19.

Coomber, P., Crews, D., and Gonzalez-Lima, F., 1997, Independent effects of incubation temperature and gonadal sex on the volume and metabolic capacity of brain nuclei in the leopard gecko (*Eublepharis macularius*), a lizard with temperature-dependent sex determination, *J. Comp. Neurol.* 380: 409–421.

Crews, D., Coomber, P., Baldwin, R., Azad, N., and Gonzalez-Lima, F., 1996, Brain organization in a reptile lacking sex chromosomes: effects of gonadectomy and exogenous testosterone, *Hormones and Behav.* 30: 474–486.

Crews, D., Coomber, P., and Gonzalez-Lima, F., 1997, Effects of age and sociosexual experience on the morphology and metabolic capacity of brain nuclei in the leopard gecko (*Eublepharis macularius*), a lizard with temperature-dependent sex determination, *Brain Res.* 758: 169–179.

Curti, D., Giangare, M. C., Redolfi, M. E., Fugaccia, I., and Benzi, G., 1990, Age-related modifications of cytochrome c oxidase activity in discrete brain regions, *Mech. Ageing and Dev.* 55: 171–180.

Darriet, D., Der, T., and Collins, R.C., 1986, Distribution of cytochrome oxidase in rat brain: studies with diaminobenzidine histochemistry in vitro and [^{14}C]cyanide tissue labeling in vivo, *J. Cereb. Blood Flow Metab.* 6: 8–14.

De Olmos, J., and Heimer, L., 1977, Mapping of collateral projections with the HRP-method, *Neurosci. Lett.* 6: 107–114.

Di Rocco, R.J., Kageyama, G.H., and Wong-Riley, M.T.T., 1989, The relationship between CNS metabolism and cytoarchitecture: A review of 14C-deoxyglucose studies with correlation to cytochrome oxidase histochemistry, *Computerized Medical Imaging Graphics,* 13: 81–92.

Gonzalez-Lima, F., 1992, Brain imaging of auditory learning functions in rats: Studies with fluorodeoxyglucose autoradiography and cytochrome oxidase histochemistry. In Gonzalez-Lima, F., Finkenstaedt, Th., and Scheich, H. (eds.), Advances in Metabolic Mapping Techniques for Brain Imaging of Behavioral and Learning Functions, Kluwer Academic Publishers, Dordrecht/Boston/London NATO ASI Series D, Vol. 68: pp 39–109.

Gonzalez-Lima, F., and Cada, A., 1994, Cytochrome oxidase activity in the auditory system of the mouse: A qualitative and quantitative histochemical study, *Neuroscience* 63: 559–578.

Gonzalez-Lima, F., and Garrosa, M., 1991, Quantitative histochemistry of cytochrome oxidase in rat brain, *Neuroscience Lett.* 123: 251–253.

Gonzalez-Lima, F., Helmstetter, F. J., and Agudo, J., 1993, Functional mapping of the rat brain during drinking behavior: A fluorodeoxyglucose study, *Physiol. Behav.* 54: 605–612.

Gonzalez-Lima, F., and Jones, D., 1994, Quantitative mapping of cytochrome oxidase activity in the central auditory system of the gerbil: A study with calibrated activity standards and metal-intensified histochemistry, *Brain Res.* 660: 34–49.

Gonzalez-Lima, F., and McIntosh, A.R., 1996, Conceptual and methodological issues in the interpretation of brain-behavior relationships. In R.W. Thatcher, G. Reid Lyon, J. Ramsey and N. Krasnegor (Eds.), *Developmental Neuroimaging: Mapping the Devlopment of Brain and Behavior:* Academic Press, Orlando, FL, pp. 235–253.

Gonzalez-Lima, F., and Scheich, H., 1985, Ascending reticular activating system in the rat: A 2-deoxyglucose study, *Brain Res.* 344: 70–88.

Gonzalez-Lima, F., and Scheich, H., 1984, Functional activation in the auditory system of the rat produced by arousing reticular stimulation: A 2-deoxyglucose study, *Brain Res.* 299: 201–214.

Gonzalez-Lima, F., Valla, J., and Matos-Collazo, S., 1997, Quantitative cytochemistry of cytochrome oxidase and cellular morphometry of the human inferior colliculus in control and Alzheimer's patients, *Brain Res.* 752: 117–126.

Harley, C.A., and Bielajew, C.H., 1992, A comparison of glycogen phosphorylase and cytochrome oxidase histochemical staining in rat brain, *J. Comp. Neurol.* 322: 377–389.

Hess, H. H., and Pope, A., 1953, Ultramicrospectrophotometric determination of cytochrome oxidase for quantitative histochemistry, *J. Biol. Chem.* 204: 295–306.

Hevner, R. F., Duff, R. S., and Wong-Riley, M. T. T., 1992, Coordination of ATP production and consumption in brain: parallel regulation of cytochrome oxidase and Na+, K+-ATPase, *Neurosci. Lett.* 138: 188–192.

Hevner, R.F., Liu, S., and Wong-Riley, M.T.T., 1993, An optimized method for determining cytochrome oxidase activity in brain tissue homogenates, *J. Neurosci. Meth.* 50: 309–319.

Hevner, R. F., and Wong-Riley, M. T. T., 1989, Brain cytochrome oxidase: Purification, antibody production, and immunohistochemical/histochemical correlations in the CNS, *J. Neurosci.* 9: 3884–3898.

Hovda, D.A., Chugani, H.T., Villablanca, J.R., Badie, B., and Sutton, R.L., 1992, Maturation of cerebral oxidative metabolism in the cat: a cytochrome oxidase histochemistry study, *J. Cereb.. Blood Flow Metab.* 12: 1039–1048.

Hyde, G.E., and Durham, D., 1990, Cytochrome oxidase response to cochlea removal in chick auditory brainstem neurons, *J. Comp. Neurol.* 297: 329–339.

Hyde, G.E., and Durham, D., 1994, Rapid increase in mitochondrial volume in nucleus magnocellularis neurons following cochlea removal, *J. Comp. Neurol.* 339: 27–48.

Jones, D., Gonzalez-Lima, F. Crews, D., Galef, B.G., and Clark, M.M., 1997, Effects of intrauterine position on the metabolic capacity of the hypothalamus of female gerbils, *Physiol. Behav.* 61: 513–519, 1997.

Kageyama, G.H., and Robertson, R.T., 1993, Relationships between neuromorphogenesis and cytochrome oxidase (C.O.) activity in rat auditory and visual cortices, hippocampus and cerebellum as demonstrated with metal-intensified C.O. histochemistry, *Soc. Neurosci. Abstr.* 19: 1711.

Kish, S.J., Bergeron, C., Rajput, A., Dozic, S., Mastrogiacomo, F., Chang, L., Wilson, J.M., DiStefano, L.M., and Nobrega, J.N., 1992, Brain cytochrome oxidase in Alzheimer's disease, *J. Neurochem.* 59: 776–779.

Kugler, P., Vogel, S., Volk., H., and Schiebler, T.H., 1988, Cytochrome oxidase histochemistry in the rat hippocampus: A quantitative metholodological study, *Histochem.* 89: 269–275.

Liu, Y., Gu', Q., and Cynader, M.S., 1993, An improved staining technique for cytochrome C oxidase, *J. Neurosci. Meth.* 49: 181–184.

Magistretti, P.J., and Pellerin, L., 1996, Cellular bases of brain energy metabolism and their relevance to functional brain imaging: evidence for a prominent role of astrocytes, *Cerebral Cortex* 6: 50–61.

Marler, C.A., Wilczynski, W., and Gonzalez-Lima, F., 1992, Metabolic mapping using cytochrome oxidase histochemistry in frog brain areas associated with auditory processing and reproductive behavior, *Soc. Neurosci. Abstr.* 18: 882.

Mecocci, P., MacGarvey, U., and Beal, M. F., 1994, Oxidative damage to mitochondrial DNA is increased in Alzheimer's disease, *Ann. Neurol.* 36: 747–751.

Miller, R.J., 1991, The control of neuronal Ca^{2+} homeostasis, *Prog. Neurobiol.* 37: 255–285.

Mutisya, E.M., Bowling, A.C., and Beal, M.F., 1994, Cortical cytochrome oxidase activity is reduced in Alzheimer's disease, *J. Neurochem.* 63: 2179–2184.

Nobrega, J. N., 1992, Brain metabolic mapping and behaviour: Assessing the effects of early developmental experiences in adult animals. In Gonzalez-Lima, F., Findenstaedt, Th., and Scheich, H. (eds.), Advances in Metabolic Mapping Techniques for Brain Imaging of Behavioral and Learning Functions, Kluwer Academic Publishers, Dordrecht/Boston/London, NATO ASI Series D, Vol. 68: pp. 125–149.

Nobrega, J. N., Raymond, R., DiStefano, L., and Burnham, W. M., 1993, Long-term changes in regional brain cytochrome oxidase activity induced by electroconvulsive treatment in rats, *Brain Res.* 605: 1–8.

Olton, D. S., Wible, C. G., Pang, K., and Sakurai, Y., 1989, Hippocampal cells have mnemonic correlates as well as spatial ones, *Psychobio.* 17: 228–229.

Parker, W.D., Jr., Filley, C.M., and Parks, J.K., 1990, Cytochrome oxidase deficiency in Alzheimer's disease, *Neurol.* 40: 1302–1303.

Parker, W.D., Jr., Mahr, N.J., Filley, C.M., Parks, J.K., Hughes, M.A., Young, D.A. and Cullum, C.M., 1994a, Reduced platelet cytochrome c oxidase activity in Alzheimer's disease, *Neurol.* 44: 1086–1090.

Parker, W.D., Jr., Parks, J., Filley, C.M., and Kleinschmidt-DeMasters, B.K., 1994b, Electron transport chain defects in Alzheimer's disease brain, *Neurol.* 44: 1090–1096.

Partridge, R.S.; Monroe, S.M.; Parks, J.K.; Johnson, K.; Parker, W.D. Jr.; Eaton, G.R., and Eaton, S.S., 1994, Spin trapping of azidyl and hydroxyl radicals in azide-inhibited submitochondrial particles, *Arch. Biochem. and Biophysics* 310(1): 210–217.

Poremba, A., Jones, D., and Gonzalez-Lima, F., 1997, Metabolic effects of blocking tone conditioning on the rat auditory system, *Neurobiol. Learning Mem.* 68: 154–171.

Schofield, B.R., and Cant, N.B., 1991, Organization of the superior olivary complex in the guinea pig. I. Cytoarchitecture, cytochrome oxidase histochemistry, and dendritic morphology, *J. Comp. Neurol.* 314: 645–670.

Seligman, A.M., Karnovsky, M.J., Wasserkrug, H.L., and Hanker, J.S., 1968, Nondroplet ultrastructural demonstration of cytochrome oxidase activity with a polymerizing osmiophilic reagent, diaminobenzidine (DAB), *J. Cell Biol.* 38: 1–14.

Silverman, M. S., and Tootell, R. B. H., 1987, Modified technique for cytochrome oxidase histochemistry: Increased staining intensity and compatibility with 2-deoxyglucose autoradiography, *J. Neurosci. Meth.* 19: 1–10.

Sokoloff, L., 1989, Circulation and energy metabolism of the brain. In G.J. Siegel, B.W. Agranoff, R.W. Albers, & Molinoff, P., (Eds.), *Basic Neurochemistry.* (pp. 471–495). Boston: Little Brown.

Sokoloff, L., 1992, Imaging techniques in studies of neural functions. In Gonzalez-Lima, F., Finkenstaedt, T., and Scheich H., (Eds.), *Advances in Metabolic Mapping Techniques for Brain Imaging of Behavioral and Learning Functions. NATO ASI Series, Vol. D68.* (pp. 1–37). Dordrecht/Boston/London: Kluwer Academic Publishers.

Stoward, P.J., 1980, Criteria for the validation of quantitative histochemical enzyme techniques. In *Trends in Enzyme Histochemistry and Cytochemistry*, Ciba Foundation, Excerpta Medica, Amsterdam, pp. 11–31.

Van Raamsdonk, W., Smit-Onel, M., Donsellaar, Y., and Diegenbach, P., 1987, Quantitative cytochemical analysis of cytochrome oxidase and succinate dehydrogenase activity in spinal neurons, *Acta Histochem.* 81: 129–141.

Wharton, D.C., and Tzagoloff, A., 1967, Cytochrome oxidase from beef heart mitochondria, *Methods of Enzymology* 10: 245–250.

Wikström, M., Krab, K., and Saraste, M., 1981, Cytochrome Oxidase: A Synthesis, Academic Press, New York.

Wong-Riley, M.T., Hevner, R.F., Cutlan, R., Earnest, M., Egan, R., Frost, J., and Nguyen, T., 1993, Cytochrome oxidase in the human visual cortex: distribution in the developing and the adult brain, *Vis. Neurosci., 10:* 41–58.

Wong-Riley, M.T.T., 1989, Cytochrome oxidase: an endogenous metabolic marker for neuronal activity, *TINS,* 12: 94–101.

Wong-Riley, M. T. T., 1979, Changes in monocularly sutured or enucleated cats demonstrable with cytochrome oxidase histochemistry, *Brain Res.* 171: 11–28.

Wong-Riley, M. T. T., Merzenich, M. M., and Leake, P. A., 1978, Changes in endogenous enzymatic reactivity to DAB induced by neuronal inactivity, *Brain Res.* 141: 185–192.

Wong-Riley, M. T. T., and Riley, D. A., 1983, The effect of impulse blockage on cytochrome oxidase activity in the cat visual system, *Brain Res.* 261: 185–193.

3

CYTOCHROME OXIDASE AND NEUROANATOMICAL PATTERNS

What Is the Connection?

Robert F. Hevner

Nina Ireland Laboratory of Developmental Neurobiology
University of California-San Francisco
San Francisco, California 94143-0984

ABSTRACT

Cytochrome oxidase (C.O.) histochemistry has proved to be an excellent method for the identification of neuroanatomical patterns. In some cases, C.O. staining has led to the discovery of completely novel patterns; the best known examples are the puffs (or blobs) in primate visual area V1, and the stripes in visual area V2. In other cases, C.O. staining has revealed modules associated with cytoarchitectural patterns that were previously known but whose modular organization was not fully appreciated, such as the periodic cell clusters in entorhinal cortex layers 2–3. In developmental neuroanatomy, C.O. histochemistry has been used to demonstrate emerging patterns (the barrelettes of the brainstem trigeminal complex) before they become visible by other methods. In addition, C.O. is a useful marker for detecting neuroanatomical changes caused by environmental manipulations, or by genetic defects in spontaneous or targeted mutant animals. Since C.O. is present in all brain cells, the sensitivity of the histochemical method for showing neuroanatomical patterns may seem paradoxical. In this chapter, I will attempt to explain the remarkable correspondence between C.O. activity and patterns in the brain by delineating the links between C.O. activity, neuronal functional activity, synaptic inputs, parallel pathways, and modular processing.

1. INTRODUCTION

Throughout the history of neuroanatomy, advances in our knowledge of brain structure (and implications for function) have depended as much on the development of suit-

Cytochrome Oxidase in Neuronal Metabolism and Alzheimer's Disease,
edited by Gonzalez-Lima, Plenum Press, New York, 1998.

able new histological techniques, as on the diligence of scientists using the techniques. For example, the elegant dendritic and axonal structure of individual neurons could only be discerned after the Golgi method became available; without it, Cajal would never have made his great achievements. Likewise, the fine structure of the synapse could not be examined until the advent of electron microscopy. More recently, neurochemistry and gene expression have become amenable to histological analysis using the techniques of immunohistochemistry and in situ hybridization. The introduction of C.O. histochemistry to brain studies (Wong-Riley, 1976, 1979) brought a new histological method into use, which has found much wider application than the obvious use of studying energy metabolism.

The potential of C.O. histochemistry for anatomical studies was not widely recognized at its introduction, principally because of the understandable but mistaken belief that such a ubiquitous mitochondrial enzyme would show few neuroanatomical features of interest, much less reveal new patterns relevant to the function of cortex and other areas. But such initial skepticism gave way to greater enthusiasm as the usefulness and success of the method became well-known. The first part of this chapter will be devoted to reviewing some of the neuroanatomical successes of C.O. histochemistry, with particular attention to C.O. staining patterns related to modular units in the brain, and their correlates such as afferent inputs, physiological activity, and processing mechanisms.

The second part of this chapter will explore in greater detail the reasons why C.O. activity correlates with so many neuroanatomical patterns. The essential theme will be that this correlation is a reflection of the fundamental and well-established linkage between neuronal functional activity and oxidative energy metabolism (Erecinska and Silver, 1989), a linkage which is maintained over different spatial scales in brain tissue from the regional, to the cellular, to the subcellular (Wong-Riley, 1989; Hevner et al., 1995). On the basis of this linkage, if one simplistically regards C.O. histochemistry as a window for viewing the organization of neuronal functional activity in histological sections (with some caveats), it becomes plausible—even predictable—that C.O. staining should show interesting neuroanatomical patterns. However, the exact significance of C.O. histochemical patterns remains controversial. In particular, it is unclear whether modular arrays—of which several types have been demonstrated by C.O. staining—are really important for processing in the brain, or merely consequences of developmental rules and thus epiphenomena (Purves et al., 1992). Arguments favoring each view will be discussed.

The underlying metabolic linkage between C.O. enzyme levels and neuronal functional activity has been studied in great depth, and need not be reviewed here. Suffice it to say that in general, the levels of C.O. in any neuronal compartment are a reliable indicator of past and continuing energy demands, as determined by requirements for ion pumping and other ATP-consuming reactions associated with electrical and synaptic activity in neurons. More complete discussions of this linkage can be found in the review by Wong-Riley (1989), and in the chapter by Wong-Riley et al. in this volume.

2. METHODS

2.1. C.O. Histochemistry

The staining method for light microscopy of the central nervous system (Wong-Riley, 1979) is simple and robust, and details of the staining reaction can be found in other chapters of these proceedings. Most pertinent to exploring neuroanatomical patterns of

C.O. activity, are methods for the proper orientation and sectioning of tissue specimens. Most experienced neuroanatomists will be familiar with these issues, but for the nonspecialist, details of specimen preparation are provided.

2.2. Section Orientation: Optimizing Pattern Visualization

Most brain patterns are unfortunately not visible from all angles, and can be viewed optimally only in nonstandard planes of section. The best approach for most areas is to familiarize oneself with the anatomy beforehand, perform pilot studies in one or more standard planes (coronal, sagittal, or horizontal), and then examine nonstandard planes of section as necessary for optimal results.

2.2.1. Special Planes of Section. Special planes of section are usually necessary for fully appreciating patterns of C.O. activity. In the cerebral cortex, the planes parallel (i.e., tangential) and perpendicular to the pial surface are usually best. Ideally, the tangential plane cuts horizontally through a single layer of the cortex, and thus shows intralaminar variations of enzyme activity, which may be correlated with modular patterns. Due to the curvature of the cortical surface, tangential sections through large areas can only be obtained by flattening the cortex prior to sectioning (see below). The perpendicular plane is best for showing enzyme activity differences between layers. Brain regions other than cortex may also require nonstandard orientation. For example, in the thalamus, the barreloids of the rodent trigeminal system are seen best in oblique sections oriented approximately 5° downward anteriorly, and 20° downward laterally from the horizontal plane (Van der Loos, 1976).

2.2.2. Flattening the Cortex for Tangential Sections. Very large cortical regions from gyrencephalic brains necessitate complicated procedures such as those described by Tootell and Silverman (1985) and by Olavarria and Van Sluyters (1985). For less convoluted regions of cortex from lissencephalic brains, or exposed portions of gyrencephalic brains (such as the monkey opercular cortex, which includes much of visual area V1) a simpler approach can be used. After perfusion or immersion fixation, the region of interest (which may include the entire neocortex of the mouse or rat) is dissected free of the rest of the brain. The tissue should be cryoprotected as usual with 20–30% sucrose or other appropriate treatment. A blade or scraper is then used to carefully remove underlying brain tissue until a curved sheet of roughly even thickness (usually 2–5 mm) is obtained, with the cortical surface on the convex side. The entire sheet of tissue is then gently flattened between two glass slides (standard size or larger, as needed), each of which should be covered with Parafilm to prevent the brain tissue from sticking to the glass. Rubber bands or metal clips can then be used to maintain gentle pressure which is needed to keep the cortex flat. The sandwich of cortex and slides is then covered completely with powdered dry ice to promote rapid freezing. After several minutes, the flat-frozen cortex can be removed from between the glass slides, mounted on a base of near-frozen mounting medium (such as OCT) with the cortical surface facing up, and again covered with powdered dry ice, taking care that the cortex is not allowed to thaw (since repeated freeze-thaw causes excessive morphological artifact). The block can then be sectioned on a cryostat or freezing sliding microtome. If the sections are thawed for free-floating incubations, they will tend to assume their original curved shape, but can be coaxed back to flatness using a fine paintbrush when the sections are mounted on slides.

2.3. Photographic Reproduction and Imaging

The most important step for obtaining high-quality images of C.O.-stained sections is to react the tissue in C.O. histochemical staining solution for the proper amount of time so that contrast between different structures is maximized. However, additional methods can be very useful for enhancing contrast among regions of interest. For photography with black-and-white film, the specimen should be illuminated with light passed through a blue filter (Kodak Wratten #47) which selectively transmits wavelengths absorbed by the yellow-brown diaminobenzidine reaction product. Alternatively, metals such as nickel or cobalt may be added to the C.O. reaction solution (Silverman and Tootell, 1987) to yield a blue-black reaction product that absorbs all wavelengths; however, the metals seem to increase nonspecific precipitation of aggregates which may stick to sections and thus mar the results.

My preferred method for imaging of C.O.-stained sections is color slide photography, which provides pleasing esthetic results and, with modern scanning devices and computers equipped with the appropriate software, is easily converted to high-contrast color or black-and-white images. For presentations, the color slides can be projected directly. For prints, the slides can be scanned with a laser scanner connected to a personal computer (e.g., Nikon CoolScan LS-1000 scanner connected to a Power Macintosh), and then adjusted digitally using image processing software such as Adobe Photoshop. The scanning hardware is critical for obtaining high-resolution raw images with a broad range of brightness and color values, whereas the software is critical for modifying the image appropriately. For example, using Photoshop one can select only the blue channel of the color image, and convert that to a black-and-white image, effectively achieving the equivalent of passing the illuminating light through a blue filter. Or, color can be balanced to correct for any mismatch between the spectrum of illuminating light and color response of the film (which differs between films optimized for Daylight and Tungsten light). Other useful software features include brightness and contrast adjustment. A little time invested in familiarizing oneself with these eletronic tools pays high dividends for presenting C.O. histochemistry results, as well as other types of images.

3. NEUROANATOMICAL PATTERNS REVEALED BY C.O. HISTOCHEMISTRY

Some idea of the variety of patterns shown by C.O. histochemistry can be obtained by reference to the following examples. The following list is by no means exhaustive, but includes a sampling of cortical and subcortical regions in which C.O. patterns have been linked to disparate anatomical pathways and functional subdivisions.

3.1. Parallel Pathways through the Primate Visual Cortex

The modular arrays of C.O. staining in the primate visual cortex are the best-understood examples of correlation between C.O. activity and brain systems for processing. They are also the best-known regions where C.O. histochemistry has revealed neuroanatomical features that were previously unknown, and which led to fundamental advances in the field.

3.1.1. Area V1. The discovery of C.O. histochemical patterns in primate visual areas V1 and V2 had a major impact because these were the first clues to the presence of parallel pathways through early stages of the visual cortex. In the late 1970s, Margaret Wong-Riley

first observed regions of increased C.O. activity in layers 2–3 of area V1, which seemed to form regular repeating units as seen in sections cut perpendicular to the cortex. This information was communicated to David Hubel who regarded the results with some skepticism; his extensive and pioneering physiological studies with Torsten Wiesel had shown no obvious evidence of neuronal activity patterns in striate cortex that might correspond to the C.O.-rich repeats. As recounted in his book (Hubel, 1988), Hubel initially discounted Wong-Riley's puffs as possibly an effect of environmental conditions (e.g., rearing under conditions of selective exposure to lines with particular orientations). Nevertheless, Hubel and his graduate student, Jonathan Horton, went on to examine C.O. activity in sections of striate cortex cut tangential to the cortical surface. This plane of section revealed the striking regular array of C.O. puffs (alternatively known as patches, blobs, and various other appellations), which could hardly be dismissed or ignored as an artifact (Fig. 1A). Horton and Hubel reported their description of C.O. puffs in the striate cortex in Nature in 1981 (Horton and Hubel, 1981). Wong-Riley's contribution was not mentioned in their paper, but her studies done in conjunction with postdoctoral fellow Ed Carroll were subsequently published in 1984 (Carroll and Wong-Riley, 1984). Hubel subsequently acknowledged Wong-Riley as the first to discover the C.O. puffs in striate cortex (Hubel, 1988).

Since their discovery, a panoply of methods has been used to examine physiological and anatomical properties of the C.O. puffs, with the goal of elucidating their significance for visual processing. Studies have shown that the puffs receive axonal inputs selectively from specific cell groups in the lateral geniculate nucleus; are centered over ocular dominance columns; and respond selectively to color information in visual stimuli (reviewed by Livingstone and Hubel, 1988). One of the more fundamental results has been the association of C.O. puffs with a distinct anatomical pathway through the visual system, which is specialized for color processing and is maintained separately through higher-order cortical regions. Excellent reviews delineating the role of C.O. puffs in the context of visual processing have been written by DeYoe and Van Essen (1988), and by Livingstone and Hubel (1988).

A second pattern of interest in the striate cortex is the reticulated network of high enzyme activity in layer 4A (Figs. 1A, 1B). The dark staining in this layer appears as a broken line in sections cut perpendicular to the cortical surface, but its reticulated pattern is obvious in sections cut tangential to the surface. The C.O. pattern is correlated with an identical reticulated pattern of axonal input from the lateral geniculate nucleus as demonstrated by tract-tracing methods.

3.1.2. Area V2. The discovery of puffs in area V1 obviously suggested the possibility that C.O.-related patterns might be found in other cortical areas, and attention was quickly turned to the next hierarchical level of visual cortex, area V2. This region was indeed found to contain a modular array of C.O.-rich zones (Tootell et al., 1983; Wong-Riley and Carroll, 1984a), defining a much more complex pattern than the simple repetition of puffs seen in V1. Instead, V2 contains irregular, somewhat globular zones of increased C.O. reactivity which are larger than V1 puffs, and which are arranged in nearly linear groups (as seen in tangential section) suggestive of stripes (Fig. 1C). Interpretation of the C.O. pattern in V2 was difficult and required careful observation of C.O.-stained sections as well as correlation with other physiological and anatomical data (DeYoe and Van Essen, 1985).

Ultimately, two different types of darkly C.O.-reactive stripes were recognized, on the basis of their relative width and other properties: thick stripes and thin stripes. The two types of stripes alternate with each other, and are separated by C.O.-poor interstripes, thus repeating the sequence thick, inter, thin, inter, thick, inter, thin, inter, and so on (Fig.1C).

As mentioned previously, each of the V2 stripes is in turn comprised of large C.O.-rich globular zones linked to each other like beads on a string.

As in V1, the C.O.-defined modules in V2 appear to belong to different visual processing streams or pathways. Moreover, each modular subdivision in V2 is interconnected with V1 modules that subserve related processing functions. Specifically, the thick stripes

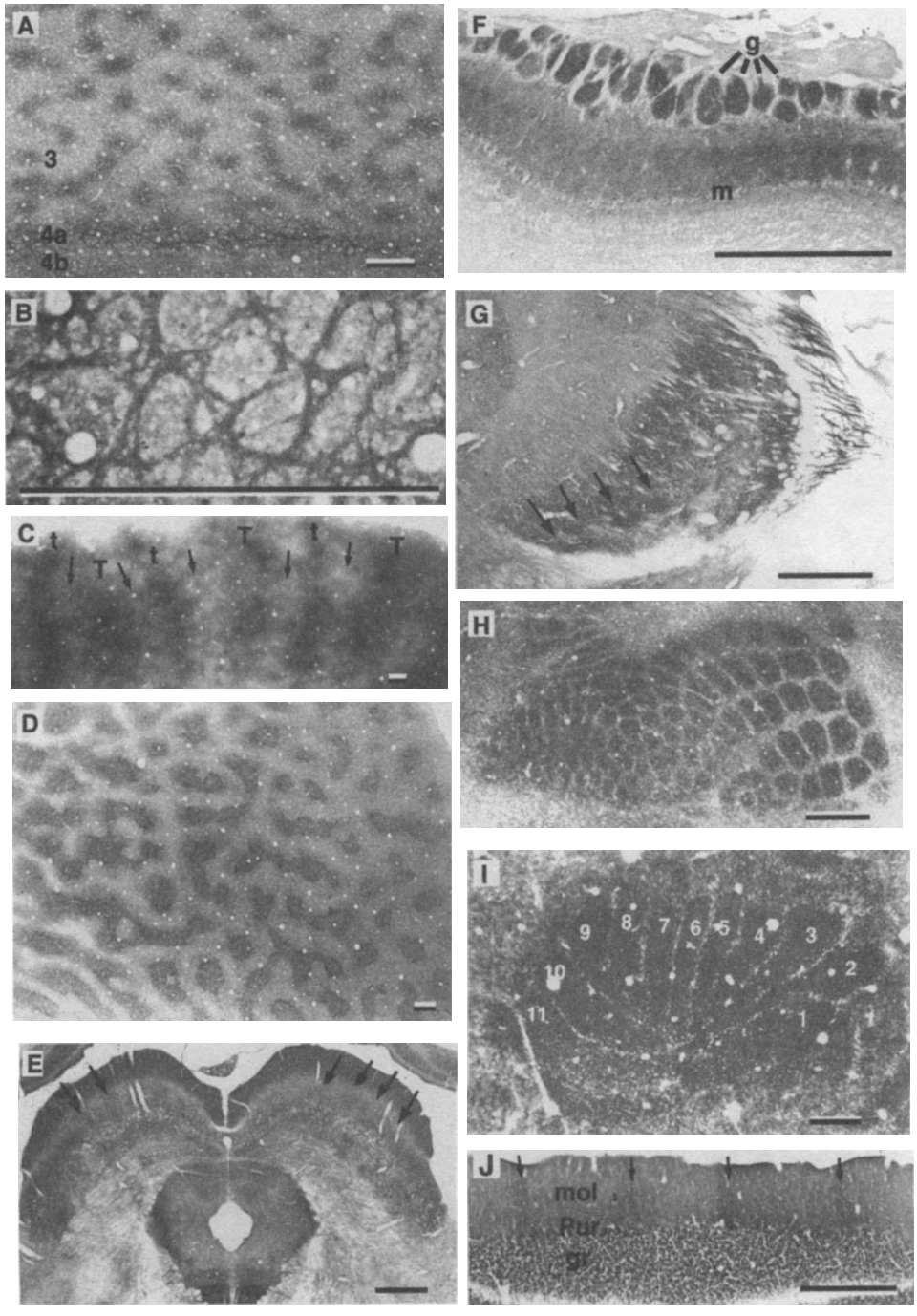

in V2 are generally associated with motion processing, and receive input from layer 4b of area V1. The thin stripes are specialized for color processing and receive major inputs from the puffs in V1. The interstripes seem to process information about stereopsis and object orientation, and receive inputs from the similarly C.O.-pale interpuffs of area V1 (reviewed by DeYoe and Van Essen, 1988; Van Essen and Gallant, 1994). These parallel pathways through V1 and V2, respectively known as the MD (magno-dominated), BD (blob-dominated), and ID (interblob-dominated) streams (Van Essen and Gallant, 1994), converge and diverge in higher level visual areas, ultimately giving rise to two major cortical subdivisions of visual processing, the parietal stream specialized for motion and spatial relationship processing, and the inferotemporal stream specialized for form and color processing (Ungerleider and Mishkin, 1982; Van Essen and Gallant, 1994).

The possibility remains that other, higher-order areas of visual cortex may also have C.O.-related modular organization, but studies have revealed no obvious C.O. patterns to date.

3.2. Isomorphic Representations in the Somatosensory System

The mouse and rat somatosensory system contains prominent modules, some of which were identified by cytoarchitectural methods years before the introduction of C.O. histochemistry. However, C.O. histochemistry has greatly facilitated the study of these prototypical modules and their development, plasticity, and circuitry (see Yuste and Simons, 1997, for references and a review of current research).

3.2.1. Barrels and Related Structures. The trigeminal somatosensory pathway in rats and mice (and some other animals) receives massive inputs from the facial whiskers known as mystacial vibrissae, which serve as important tactile sensory organs. As might be expected, central representations of the vibrissae—located in the brainstem, thalamus, and cortex—are proportionately large and prominent.

Figure 1. Neuroanatomical patterns demonstrated by C.O. histochemistry. (A) Puffs in monkey primary visual cortex area V1 (tangential section). The puffs are found in layers 2–3, and appear as periodic patchy regions of increased C.O. staining in this section (mostly through layer 3). The section also passes through layers 4a (shown at higher magnification in panel B) and 4b. (B) Reticulated network of dark C.O. reactivity in layer 4a of monkey visual cortex area V1 (tangential section). (C) Thick and thin stripes in macaque monkey visual cortex area V2 (tangential section). Alternating darkly-reactive thin (t) and thick (T) stripes are separated by pale interstripes (arrows). Within stripes, C.O. activity is variable and broken up into large globular zones. (D) Islands and stripes in human entorhinal cortex (tangential section). The darkly C.O.-reactive structures correlate with cell clusters in layer 2, but also bridge gaps between the clusters and extend upwards into layer 1. (E) Patches of dark C.O. staining in the rat superior colliculus (coronal section). These columnar regions of high enzyme activity (arrows) are most prominent in the intermediate layers of the superior colliculus, but extend into deeper layers. (F) Synaptic glomeruli (g) in rat olfactory bulb (coronal section). The glomeruli generally have high C.O. activity, although individual glomeruli differ in their staining intensity. In contrast, the major output cells of the olfactory bulb—the mitral (m) cells—have low C.O. activity in their somata. (G) Barreloids (arrows) in rat ventrobasal thalamus (coronal section). Only a few barreloids are visible in this plane; a nonstandard oblique plane is optimal for viewing these modules. (H) Barrels in mouse somatosensory cortex (tangential section). The largest barrels are arranged in five rows corresponding isomorphically to the five rows of mystacial vibrissae on the animal's upper face. (I) Ray-like stripes in the somatosensory cortex of the star-nosed mole, isomorphically representing the 11 fleshy rays surrounding one side of the animal's nose. (J) Parasagittal stripes of dark C.O. reactivity (arrows) in rat cerebellar vermis (horizontal section). The stripes are more obvious in the molecular layer (mol) than in the Purkinje (Pur) or granule (gr) cell layers in this example. Scale bars 0.5 mm. Photograph in (C) provided courtesy of Dr. M. Wong-Riley. Panel (I) adapted from Catania et al. (1993) with permission.

The cortical representation of vibrissae in primary somatosensory area S1, known as the barrel field, consists of distinct barrel-shaped (in cross section) modules that can be identified using classical stains such as cresyl violet (Woolsey and van der Loos, 1970), or more easily by histochemistry for C.O. (Wong-Riley and Welt, 1980) or succinate dehydrogenase (e.g., Riddle et al., 1992). Each barrel processes sensory inputs from a single vibrissa. The total number of barrels and barrel-related structures (which process information from smaller facial hairs and portions of the paws) has been counted at about 200 per mouse hemisphere (Woolsey and Van der Loos, 1970). The spatial organization of barrels in the cortex, as observed most clearly in flattened sections of cerebral cortex (Fig. 1H), is isomorphic (somatotopic) to the pattern of vibrissae on the face.

Subsequent to description of the cortical barrels, similar isomorphic representations were identified at lower levels of processing in the somatosensory brainstem and thalamus. The thalamic modules, known as barreloids, are seen well in Nissl- or C.O.-stained horizontal sections, though the optimal plane for viewing them is tilted about 5° downward anteriorly, and 20° downward laterally (Van der Loos, 1976). They can also be observed in coronal sections, though this plane reveals only a few barreloids in each section (Fig. 1G). Even sections cut with optimal orientation do not show all of the barreloids, since this field has a dome-shaped curvature.

Vibrissae representations in the brainstem (barrelettes) are the most recently identified of the modular fields in the barrel-related pathway, and present the most complex organization (Belford and Killackey, 1979; Ma, 1991a). The brainstem trigeminal complex comprises four distinct subnuclei, which presumably perform different types of afferent processing, although the functional differences between them remain unclear. Of these four subnuclei, three contain anatomically recognizable (by Nissl staining, C.O. histochemistry, and other methods) isomorphic representations of vibrissae: the trigeminal subnuclei principalis (nVp), interpolaris (nVo), and caudalis (nVc). The fourth subnucleus, oralis (nVo), displays no evidence of barrelettes (Ma, 1991a). Brainstem barrelettes have been found in several species in addition to rat and mouse, including the cat (Nomura et al., 1986). In development, the three barrelette formations are visible by C.O. histochemistry prior to their cytoarchitectonic formation (Ma, 1991b).

To summarize, the rodent somatosensory system contains five isomorphic representations of the vibrissae at three different hierarchical levels of the afferent pathway, all of which can be identified readily by C.O. histochemistry. This system has been attractive for experimental studies of development and plasticity, and C.O. histochemistry has been a mainstay of these studies, as will be discussed further below.

3.2.2. Ray-like Stripes in the Cortex of the Star-Nosed Mole. The star-nosed mole, as its name suggests, has a specialized array of fleshy, digit-like rays projecting around its nose. These rays are important sensory organs for finding food, as the animals apparently use them for exploring the underground environment. The rays are innervated by unique receptor/nerve ending structures known as Eimer's organs. Catania et al. (1993) hypothesized that these rays might, like the mouse and rat facial whiskers, have distinct modular representations in the somatosensory cortex. They furthermore predicted that the shape of each module would be elongated, reflecting the shape of the nose rays, in contradistinction to the round-to-oval barrels, which reflect the evenly spaced, punctate distribution of hair follicles.

Flattened sections of cortex stained by C.O. histochemistry revealed an array of 11 stripes of dark enzyme reactivity, apparently isomorphic to the 11 rays on each side of the nose (Fig. 1I). Microelectrode studies with lesion mapping of cells responsive to ray

stimulation showed an isomorphic correlation between the ray being stimulated, and the cortical stripe where responses were elicited (Catania et al., 1993). This confirmation of their hypothesis including the number and shape of cortical stripes, represents evidence favoring the concept that modules may be important processing units in the brain, especially in the cortex—a concept to be explored in greater detail below.

3.3. Modules in the Entorhinal Cortex

The vertebrate entorhinal cortex (EC), a large cortical area with strong connections to hippocampus, has been known at least since the days of Cajal to contain prominent clusters of neurons in its upper layers. These neuron clusters are most obvious in layer 2, but are also seen readily in layer 3 of higher species, especially primates. Since other areas with nonhomogeneous distributions of neurons (such as the barrel field) are organized into processing modules, we hypothesized that the EC cell clusters likewise indicated modular organization.

To further test this idea and study the possible modular organization of EC in more detail, we stained sections of rat, monkey and human EC by C.O. histochemistry and immunohistochemistry (Hevner and Wong-Riley, 1992). In all three species the layer 2 cell clusters, which project via the perforant pathway to the dentate gyrus and hippocampus, were intensely C.O.-reactive. Layer 3, which also sends projections via the perforant pathway albeit to portions of the hippocampus distinct from those innervated by layer 2, likewise demonstrated high C.O. levels, especially in neuron clusters.

In some portions of the human EC, columns of high C.O. activity extended from layer 2 neuron clusters upwards into layer 1, reaching the pial surface. In addition, strips of darkly C.O.-reactive neuropil within layer 2 connected some of the neuron clusters. These data suggested that neuron clusters in layer 2 were components of larger modules that also included regions of neuropil in layers 1 and 2.

Tangential sections through layers 1–3 of monkey and human EC demonstrated a striking pattern of C.O.-reactive islands and stripes (Fig. 1D). The EC from one human hemisphere contained between 200–250 such modules in layer 2.

The functional and physiological basis of this modular organization in the upper EC layers remains unclear, but there are some intriguing clues. Golgi preparations have shown that the apical dendrites of layer 2 and layer 3 neurons are segregated into separate tangential domains within layers 1–2, which presumably correspond to the C.O.-defined dark and light modules (Amaral et al., 1987; Carboni et al., 1990). Furthermore, tract-tracing studies have shown that different cortical areas and subcortical structures selectively project to layer 2 neuron clusters, or to the interstitial neuropil between clusters (Insausti et al., 1987a, 1987b; Saunders and Rosene, 1988).

These findings, combined with the fact that layers 2 and 3 send efferent projections to distinct portions of the dentate gyrus and hippocampus (Steward and Scoville, 1976; Witter and Amaral, 1991), suggest the possibility that two separate processing streams pass through the EC and hippocampal formation, and are anatomically segregated so as to give rise to the modular pattern observed by Nissl and C.O. staining methods. This hypothesis would be analogous to the segregation of separate pathways through primate visual cortex (see above), although three visual streams have been identified whereas only two are postulated through the EC and hippocampus. Furthermore, the visual processing streams have been associated with distinct physiological responses and functions, whereas the possible physiological significance of the putative two pathways through EC and hippocampus remains completely unknown.

The EC and hippocampus have been implicated in memory processing, and together form part of the medial temporal lobe memory system (Squire and Zola-Morgan, 1991). If two distinct pathways do pass through the EC and hippocampus, then it will be very interesting to find out how each of them contributes to overall memory functions.

3.4. The Olfactory Bulb and Odorant Processing

The olfactory bulb is unique among cortex-related structures in that it receives direct sensory innervation from peripheral sensory neurons. These inputs arise from the olfactory neuroepithelium located in the nasal cavity, and end in the olfactory glomeruli, where they synapse with central neurons, in particular the mitral cells which relay olfactory inputs to the piriform and entorhinal cortices.

The glomeruli are distinct morphological modules that appear cell-sparse in Nissl-stained sections, but are intensely C.O.-reactive in histochemical preparations (Fig. 1F). Individual glomeruli differ in their C.O. enzyme activity, indicating that different glomeruli maintain somewhat variable levels of functional activity (Hevner and Wong-Riley, 1989). In contrast, the mitral cell bodies are all generally low in C.O. activity (Fig. 1F).

Recent studies using molecular biological techniques (reviewed by Dulac, 1997) have led to rapid advances in the understanding of olfactory glomeruli and their inputs from receptor neurons, which provide a framework for interpreting the different C.O. levels among glomeruli. The receptor neurons detect odorant molecules by their interaction with olfactory receptor proteins located on the cell surface. Genetic analysis has shown that the olfactory receptor proteins are encoded by a family of more than one thousand genes, conferring sensitivity to a wide variety of odorants. Each receptor neuron expresses only one odorant receptor protein, which defines the type of odorant molecules to which the neuron will respond. However, since there are many thousands of receptor neurons, the same olfactory receptor protein is expressed by more than one (generally several) receptor neurons.

One of the most remarkable findings to emerge in recent years is that all receptor neurons expressing the same particular odorant receptor protein converge on the same few glomeruli. Thus, the olfactory bulb essentially acts as a chemotopic map, in which each glomerulus responds to specific odorants, and the perceived smell is determined by the combination of activated glomeruli. Since each glomerulus only responds to a particular odorant class, its overall functional activity will be determined by how frequently and intensely the animal is exposed to that odorant. Therefore, C.O. activity levels can be assumed to reflect the odorant environment of the animal. According to this model, selective exposure to a particular odorant should lead to selective stimulation of enzyme levels in the glomeruli responsive to that odorant, and conversely deprivation of an odorant should lead to down-regulation of C.O. activity in specific glomeruli.

3.5. Patches in the Superior Colliculus

The intermediate layers of the superior colliculus demonstrate patchy, somewhat columnar variations in C.O. reactivity (Fig. 1E). These patches were first described in the mouse by Wiener (1986) and Wallace (1986) independently but are also seen in the rat (Hevner et al., 1995). Other histochemical markers and afferent inputs likewise show patchiness in the same layers, but none of those markers or inputs seems to be well correlated with C.O. activity (Sefton and Dreher, 1995). Thus, the significance of the C.O. patches is unclear at present.

3.6. Stripes in the Cerebellar Vermis

The cerebellar cortex in the vermis of rats contains four longitudinal stripes of dark C.O. reactivity, two stripes in each hemivermis (Fig. 1J). A similar pattern is observed in the monkey cerebellum. All cerebellar cortical layers display the C.O. stripes, though their relative prominence in different layers varies among species (Hess and Voogd, 1986; Leclerc et al., 1990; Hevner et al., 1995). Numerous other markers also display longitudinal zonation, most dramatically the proteins zebrin I and zebrin II (aldolase C), as well as acetylcholinesterase (Voogd, 1995). The boundaries between darkly and lightly C.O.-reactive zones are the same ones defined by zebrin-1-positive and negative zones (Leclerc et al., 1990). The zebrin-1 pattern has been correlated with parasagittal stripes receiving selective inputs from particular subdivisions of the inferior olivary nuclei (Gravel et al., 1987). Despite the abundant anatomical evidence of longitudinal modules in the cerebellum, their functional significance is entirely unknown.

4. PRINCIPLES UNDERLYING THE CORRELATION BETWEEN CYTOCHROME OXIDASE ACTIVITY AND NEUROANATOMICAL PATTERNS

The examples cited above illustrate the point that C.O. histochemistry is a remarkably robust method for demonstrating functionally significant neuroanatomical patterns. In some cases it is the best or only method available, e.g. for showing the puffs in primate V1, the stripes in primate V2, and the barrelettes in early postnatal rodents. What accounts for this surprising correlation between C.O., a "housekeeping" enzyme, and patterns in the brain?

I will suggest that three simple principles can explain this correlation: (1) C.O. enzymatic activity is tightly linked to neuronal functional activity; (2) different pathways in the brain sustain distinct levels of neuronal functional activity; and (3) brain pathways are frequently, if not usually organized into processing modules.

4.1. C.O. Enzymatic Activity Is Tightly Linked to Neuronal Functional Activity

The concept of "neuronal functional activity" is easily understood on an intuitive level, but unfortunately is difficult to define in rigorous terms. Major components include ion fluxes across the neuronal plasma membrane (e.g., action potential currents and postsynaptic currents); synaptic vesicle assembly, transport, release, and recycling; and neurotransmitter synthesis and reuptake. Although there is no way to measure neuronal functional activity in absolute terms, relative comparisons can be made. For example, in the ocular dominance column system of macaque monkey visual area V1, selective monocular input blockage (e.g., by monocular tetrodotoxin treatment) results in decreased physiological activity in columns driven by the treated eye, as detected by a variety of methods including electrode recording of action potentials (DeYoe et al., 1995), 2-deoxyglucose (2-DG) uptake (Kennedy et al., 1976), and optical recording (Lieke et al., 1989).

The tight linkage between neuronal functional activity and C.O. activity has already been extensively documented; the reader is referred to reviews by Wong-Riley (1989) and Wong-Riley et al. (this volume). Neuronal activity requires large amounts of ATP, mainly for ion pumping to maintain transmembrane gradients discharged by synaptic potentials, and to a much lesser extent action potentials (Erecinska and Silver, 1989). Neurons rely

almost entirely on oxidative metabolism for supplying their ATP, and C.O. is a key enzyme catalyzing the final step in the mitochondrial electron transport chain. Experimental manipulations have shown that C.O. activity is regulated according to the functional demands of neurons. Thus, C.O. levels increase or decrease with stimulation or inhibition of neuronal activity, respectively. The genetic regulation of C.O. is beginning to be understood (reviewed by Wong-Riley et al., this volume), though the molecular mechanisms linking C.O. gene expression and neuronal functional activity remain obscure.

4.2. Different Pathways Sustain Distinct Levels of Neuronal Functional Activity

As discussed above, there is no absolute measure of neuronal functional activity. Practical approaches for studying overall neuronal functional activity are the 2-DG method, first developed by Sokoloff and co-workers (Sokoloff et al., 1977), and the more recent innovation of optical imaging (Lieke et al., 1989).

Extensive studies of visual cortex by Tootell and co-workers (Tootell et al., 1988a, 1988b, 1988c; Tootell et al., 1989) have shown that the V1 puffs and V2 stripes identified by C.O. histochemistry, have higher levels of 2-DG uptake than do interpuff and interstripe regions under most conditions. Furthermore, stimuli appropriate to specific modular processing functions of the V1 puffs (color) and V2 stripes (thick stripes: motion; thin stripes: color) enhance 2-DG uptake in the appropriate modules, whereas other stimuli enhance uptake in other module types. These findings are but one example of neuronal activity differences that are pathway- and function-specific. A 2-DG survey of the rat brain revealed differences among many various pathways (Sokoloff et al., 1977).

Our map of C.O. activity in the rat brain also demonstrated many pathway-specific differences (Hevner et al., 1995), most of which parallelled those observed in the 2-DG map (Sokoloff et al., 1977). However, the 2-DG uptake and C.O. activity maps were not perfectly concordant, for reasons discussed in our paper (Hevner et al., 1995). Since C.O. enzymatic activity is tightly linked to neuronal functional activity (see above), it is easy to understand why pathways differ in their C.O. activity.

The neurochemical and electrophysiological basis for pathway-specific differences in neuronal functional activity are under investigation. Action potential frequency is one parameter that may differ among pathways; for example, cells in the puffs in primate area V1 reportedly have higher spontaneous activity than do those in the interpuff regions (Livingstone and Hubel, 1984). In both the V1 puffs (Nie and Wong-Riley, 1996) and the hippocampus (Kageyama and Wong-Riley, 1982), high levels of C.O. activity are associated with strong excitatory and glutamatergic afferent input. Since most C.O. is located within dendrites (Wong-Riley, 1989), it is likely that postsynaptic electrical activity driven by strong excitation is a major determinant of overall neuronal functional activity, and accounts for much of the variation among pathways.

4.3. Many Brain Pathways Are Anatomically Organized into Patterned Modules

Modular patterns are found in many brain areas, especially the cerebral cortex. However, there is controversy over both the general prevalence of modules and their importance for processing functions.

There is no question that modular organization is widespread in the brain. Virtually every region from the forebrain to the hindbrain displays some modular patterns: glomeruli

in the olfactory bulb; V1 puffs and S1 barrels in sensory cortex; entorhinal islands and stripes in association cortex; patch and matrix compartments in the striatum (Gerfen, 1992); barreloids in the thalamus; patches in the superior colliculus; interconnected inferior olive subdivisions and longitudinal stripes in the cerebellum; and barrelettes in ascending pathways of the brainstem. Catania et al. (1993) predicted that modules for processing nose-ray sensation were present in the star-nosed mole somatosensory cortex, and even predicted the stripe-like shape of those modules. Many modular patterns have been identified in the past 20 years, and it may be anticipated that additional examples will be forthcoming.

The significance of modular (or "iterated") patterns has been discussed at length in a provocative article by Purves et al. (1992). They concluded that, whereas modules are certainly a prominent feature of the cortex and other brain regions, "such patterns arise as an incidental consequence of the developmental rules that govern the formation of synaptic connections." They argued that since it is neuronal connections and activity patterns that are important for processing, their organization into modular units is not fundamentally necessary. They also pointed out that specialized modules appear to be lacking from many cortical areas and other brain regions.

The arguments set forth by Purves et al. (1992) strike at the heart of the issue of how structure is related to function. Their same arguments might just as well be applied (and in the past, have been applied) to the division of the cortex into areas. Are distinct cortical areas with different morphological characteristics required for functional specialization? On a theoretical, information-processing level perhaps not; but since the brain is a biological machine, perhaps areal and modular specializations are necessary.

An interesting case in point is the mouse mutant *barrelless* (*brl*), in which the cytoarchitectural parcellation of the somatosensory cortex is lost as an autosomal recessive trait (Welker et al., 1996). These mice also show poorly defined barreloids in the thalamus, but no other cytoarchitectural abnormalities (including cortical lamination and size of the whisker representation). In *brl* homozygotes, thalamocortical inputs to the somatosensory cortex are not confined to barrel-like zones as they are in normal mice, but instead are evenly distributed within layers 4 and 6. Nevertheless, the topography of cortical activation from the periphery (as determined by the 2-DG method) remains normal. However, the spatial and temporal discrimination of whisker stimulation are decreased, as determined by single cell electrophysiological recording. The authors concluded that "the functional operation of the cerebral cortex depends on the pattern of thalamocortical connectivity"—in this case, a modular pattern.

I would not argue that modular organization is an absolute requirement in all brain regions or cortical areas, only that modules are useful and probably necessary for certain types of processing. They may be particularly important for the segregation of separate pathways through the same cortical area—as is the case in primate V1 and V2, and probably in the entorhinal cortex. In any case, regardless of whether modules are fundamentally important or merely incidental, they are prevalent and generally show distinct levels of C.O. enzymatic activity.

5. C.O. HISTOCHEMISTRY IN THE ANALYSIS OF PATTERN PLASTICITY AND DEVELOPMENT

Since C.O. histochemistry is a simple method for revealing neuroanatomical patterns, it has been widely used in developmental studies, and for studying the brain's response to altered inputs (i.e., plasticity).

5.1. Developmental Changes in the Number of Modular Units

The intriguing question of whether the number of modular units in particular brain areas remains constant or changes during postnatal development has been investigated in a few systems by Purves and co-workers. Using C.O. histochemistry, they found that the number of puffs (or blobs) in the macaque monkey visual cortex remains the same from birth to maturity (Purves and LaMantia, 1993). Likewise, in the mouse somatosensory cortex (studied with succinate dehydrogenase histochemistry), the number of barrels and barrel-like structures does not change postnatally, although there is differential growth among individual modules in this system (Riddle et al., 1992). In contrast, the number of glomeruli in the mouse olfactory bulb increases by approximately four- to five-fold from birth to sexual maturity (Pomeroy et al., 1990). Since inputs from the olfactory epithelium to the glomeruli are genetically specified and constant among animals (reviewed by Dulac, 1997), it is likely that this last difference reflects protracted maturation of olfactory bulb morphology.

5.2. Plasticity of Modular Patterns

The response of modular patterns to experimental manipulations such as deafferentation varies according to brain area and age of the animal. For example, in the mouse barrel fields, early (postnatal) loss of whisker input results in fusion and decreased size of barrels as examined by C.O. histochemistry, but later (adult) deprivation of whisker stimulation results only in decreased C.O. activity without disruption of the modular pattern (Wong-Riley and Welt, 1980). This dependence on animal age accords with the large body of evidence showing that there are critical periods in development, during which connectional patterns are most sensitive to experimental alterations. However, the puffs in primate area V1 are not as sensitive to early deprivation. They still have a virtually normal appearance in animals treated to completely remove photoreceptor influences on the thalamus or cortex prior to cortical innervation (Kuljis and Rakic, 1990). This indicates that developmental sensitivity to afferent input may differ widely among modular systems, probably depending on whether their assembly is driven more by genetic or activity-dependent factors.

In adult animals, data from C.O. histochemical studies are quite consistent in showing that module number and pattern do not change as a result of altered afferentation. Rather, the intensity of C.O. histochemical staining changes in parallel with the change in neuronal functional activity in modules. This is true in the rodent somatosensory cortex (Wong-Riley and Welt, 1980) as well as in the primate visual cortex (Wong-Riley and Carroll, 1984b; Trusk et al., 1990).

5.3. Modular Patterns in Genetic Mutants

A variety of spontaneous and targeted mutations result in altered development and/or plasticity of regions with modular patterns. The barrel fields in mouse somatosensory cortex, and the subcortical barreloids and barrelettes, are all accessible to examination by C.O. histochemistry and have been of particular interest to developmental biologists. The mouse is a convenient mammalian system and is amenable to genetic techniques. One mouse mutant, the spontaneous mutant *barrelless*, was mentioned above. This mutant fails to develop cytoarchitectural barrels, and has altered thalamocortical inputs and somatosensory processing in the barrel fields (Welker et al., 1996).

Various mouse lines with targeted mutations of particular genes ("knockout" mice) display altered barrel patterning as well. For example, we have found that mice with targeted mutation of the *Tbr-1* gene, which encodes a putative transcription factor expressed in the embryonic cerebral cortex (Bulfone et al., 1995), lack any indication of barrels or barrel-like patterns in tangential sections of cortex stained by C.O. histochemistry (Hevner et al., 1996). We subsequently observed that these mice fail to establish any connections between thalamus and cortex, which would account for their lack of barrels (Hevner et al., 1997).

Another genetically altered mouse line that lacks barrels as determined by C.O. histochemistry, is the transgenic mouse line Tg8. Mutants in this line have a deficiency of monoamine oxidase A, an enzyme that catabolizes monoamines including serotonin. An excess of serotonin during the critical period is apparently responsible for the lack of barrels, since administration of a drug (parachlorophenylalanine) that blocks serotonin synthesis restores formation of barrels, whereas an inhibitor of catecholamine synthesis does not (Cases et al., 1996).

6. CONCLUSIONS

C.O. histochemistry is a simple method that has had a surprising impact, far beyond what could have been imagined at its introduction. Some of the most important (and surprising) advances to come from using this method have concerned neuroanatomical patterns. Who could have anticipated that C.O., a mitochondrial enzyme found throughout all cells of the nervous system, would reveal important new modular pathways such as those related to the puffs of primate area V1 and the stripes of area V2? In particular, V1 had already been subjected to intense scrutiny by other anatomical and physiological techniques and was hardly expected to yield new secrets to a mitochondrial enzyme. Other neuroanatomical patterns also proved to be easily demonstrable by C.O. histochemistry, and their study has been greatly facilitated by the addition of this technique to the neuroanatomical armamentarium.

In retrospect, and after two decades of continuous investigations into the relation between C.O. and neuronal functional activity, we can now discern the principal reasons why C.O. histochemistry is able to reveal the modular arrays that it does. My main goal in this chapter has been to clearly delineate these reasons, summarized in the three principles enumerated in section 4: (1) C.O. histochemistry is tightly linked to neuronal functional activity; (2) different pathways sustain distinct levels of neuronal functional activity; and (3) many pathways are anatomically organized into patterned modular processing units. With these principles in mind, it becomes predictable that C.O. histochemistry should reveal many neuroanatomical patterns throughout the brain. Not all areas with modular organization will necessarily show interesting patterns of C.O. histochemical staining; but conversely, it is probably true that any region with an interesting pattern of C.O. staining is likely to contain one or more pathways divided into modular units. Furthermore, modular organization may sometimes imply multiple pathways through a particular region. This has been observed in the visual areas V1 and V2, and may be true in the entorhinal cortex.

An important collateral benefit of C.O. histochemistry's ability to reveal neuroanatomical patterns has been the facilitation of research into the modular and parallel organization of brain pathways. Studies of pattern development and plasticity, studies involving localization of cells with certain electrophysiological characteristics to particular modules, and studies correlating modules with other markers such as 2-DG uptake

(e.g., Tootell et al., 1988a) and Na^+,K^+-ATPase activity (Hevner et al., 1992) have all advanced more quickly because of C.O. histochemistry. And for this, we all owe a debt of gratitude to Dr. Margaret Wong-Riley, in whose honor this volume is dedicated.

ACKNOWLEDGMENTS

Dr. M. Wong-Riley provided the photograph of V2 stripes used in Figure 1C. The illustration of ray-related stripes in the star-nosed mole cortex (Figure 1I) was taken from Catania et al. (1993) with permission from the publisher. I thank Dr. Francisco Gonzalez-Lima for his editorial encouragement and patience. Finally, I thank Dr. Margaret Wong-Riley for her exemplary commitment to excellence in research, her strength in the face of adversity, her devotion to education, and her unfailing sense of humor which have all been an inspiration to me ever since I was her student.

REFERENCES

Amaral, D. G., Insausti, R., and Cowan, W. M. (1987). The entorhinal cortex of the monkey: I. Cytoarchitectonic organization. *J. Comp. Neurol.*, 264, 326–355.

Belford, G. R., and Killackey, H. P. (1979). The development of vibrissae representation in subcortical trigeminal centers of the neonatal rat. *J. Comp. Neurol.*, 188, 63–74.

Bulfone, A., Smiga, S. M., Shimamura, K., Peterson, A., Puelles, L., and Rubenstein, J. L. R. (1995). *T-brain-1*: A homolog of *Brachyury* whose expression defines molecularly distinct domains within the cerebral cortex. *Neuron*, 15, 63–78.

Carboni, A. A., Lavelle, W. G., Barnes, C. L., and Cipolloni, P. B. (1990). Neurons of the lateral entorhinal cortex of the rhesus monkey: A Golgi, histochemical, and immunocytochemical characterization. *J. Comp. Neurol.*, 291, 583–608.

Carroll, E. W., and Wong-Riley, M. T. T. (1984). Quantitative light and electron microscopic analysis of cytochrome oxidase-rich zones in the striate cortex of the squirrel monkey. *J. Comp. Neurol.*, 222, 1–17.

Cases, O., Vitalis, T., Seif, I., De Maeyer, E., Sotelo, C., and Gaspar, P. (1996). Lack of barrels in the somatosensory cortex of monoamine oxidase A-deficient mice: Role of a serotonin excess during the critical period. *Neuron*, 16, 297–307.

Catania, K. C., Northcutt, R. G., Kaas, J. H., and Beck, P. D. (1993). Nose stars and brain stripes. *Nature*, 364, 493.

DeYoe, E. A., and Van Essen, D. C. (1985). Segregation of efferent connections and receptive field properties in visual area V2 of the macaque. *Nature*, 317, 58–61.

DeYoe, E. A., and Van Essen, D. C. (1988). Concurrent processing streams in monkey visual cortex. *Trends Neurosci.*, 11, 219–226.

DeYoe, E. A., Trusk, T. C., and Wong-Riley, M. T. T. (1995). Activity correlates of cytochrome oxidase-defined compartments in granular and supragranular layers of primary visual cortex of the macaque monkey. *Vis. Neurosci.*, 12, 629–639.

Dulac, C. (1997). How does the brain smell? *Neuron*, 19, 477–480.

Erecinska, M., and Silver, I. A. (1989). ATP and brain function. *J. Cerebr. Blood Flow Metab.*, 9, 2–19.

Gerfen, C. R. (1992). The neostriatal mosaic: multiple levels of compartmental organization. *Trends Neurosci.*, 15, 133–139.

Gravel, C., Eisenman, L. M., Sasseville, R., and Hawkes, R. (1987). Parasagittal organization of the rat cerebellar cortex: Direct correlation between antigenic Purkinje cell bands revealed by mabQ113 and the organization of the olivocerebellar projection. *J. Comp. Neurol.*, 265, 294–310.

Hess, D. T., and Voogd, J. (1986). Chemoarchitectonic zonation of the monkey cerebellum. *Brain Res.*, 369, 383–387.

Hevner, R. F., and Wong-Riley, M. T. T. (1989). Brain cytochrome oxidase: purification, antibody production, and immunohistochemical/histochemical correlations in the CNS. *J. Neurosci.*, 9, 3884–3898.

Hevner, R. F., and Wong-Riley, M. T. T. (1992). Entorhinal cortex of the human, monkey, and rat: metabolic map as revealed by cytochrome oxidase. *J. Comp. Neurol.*, 326, 451–469.

Hevner, R. F., Duff, R. S., and Wong-Riley, M. T. T. (1992). Coordination of ATP production and consumption in brain: parallel regulation of cytochrome oxidase and Na^+,K^+-ATPase. *Neurosci. Lett.*, 138, 188–192.

Hevner, R. F., Liu, S., and Wong-Riley, M. T. T. (1995). A metabolic map of cytochrome oxidase in the rat brain: histochemical, densitometric, and biochemical studies. *Neuroscience*, 65, 313–342.

Hevner, R. F., Smiga, S., Bulfone, A., Meneses, J. J., Pedersen, R. A., and Rubenstein, J. L. R. (1996). Targeted mutation of the Tbr-1 gene causes abnormal development of the cerebral cortex and olfactory bulb. *Soc. Neurosci. Abstr.*, 22, 1011.

Hevner, R. F., Smiga, S., Bulfone, A., Meneses, J. J., Pedersen. R. A., and Rubenstein, J. L. R. (1997). Cerebral cortex lamination and extrinsic connections are disrupted in mice with targeted mutation of *Tbr-1* gene. *Soc. Neurosci. Abstr.*, 23, 80.

Horton, J. C., and Hubel, D. H. (1981). Regular patchy distribution of cytochrome oxidase staining in primary visual cortex of macaque monkey. *Nature*, 292, 762–764.

Hubel, D. H. (1988). *Eye, Brain, and Vision*. Scientific American Library, W. H. Freeman and Co., New York.

Insausti, R., Amaral, D. G., and Cowan, W. M. (1987a). The entorhinal cortex of the monkey: II. Cortical afferents. *J. Comp. Neurol.*, 264, 356–395.

Insausti, R., Amaral, D. G., and Cowan, W. M. (1987b). The entorhinal cortex of the monkey: III. Subcortical afferents. *J. Comp. Neurol.*, 264, 396–408.

Kageyama, G. H., and Wong-Riley, M. T. T. (1982). Histochemical localization of cytochrome oxidase in the hippocampus: correlation with specific neuronal types and afferent pathways. *Neuroscience*, 7, 2337–2361.

Kennedy, C., Des Rosiers, M. H., Sakurada, O., Shinohara, M., Reivich, M., Jehl, J. W., and Sokoloff, L. (1976). Metabolic mapping of the primary visual system of the mokey by means of the autoradiographic [^{14}C]deoxyglucose technique. *Proc. Natl. Acad. Sci. USA*, 73, 4230–4234.

Kuljis, R. O., and Rakic, P. (1990). Hypercolumns in primate visual cortex can develop in the absence of cues from photoreceptors. *Proc. Natl. Acad. Sci. USA*, 87, 5303–5306.

Leclerc, N., Doré, L., Parent, A., and Hawkes, R. (1990). The compartmentalization of the monkey and rat cerebellar cortex: zebrin I and cytochrome oxidase. *Brain Res.*, 506, 70–78.

Lieke, E. E., Frostig, R. D., Arieli, A., Ts'o, D. Y., Hildesheim, R., and Grinvald, A. (1989). Optical imaging of cortical activity: real-time imaging using extrinsic dye-signals and high resolution imaging based on slow intrinsic-signals. *Annu. Rev. Physiol.*, 51, 543–559.

Livingstone, M. S., and Hubel, D. H. (1984). Anatomy and physiology of a color system in the primate visual cortex. *J. Neurosci.*, 4, 309–356.

Livingstone, M., and Hubel, D. (1988). Segregation of form, color, movement, and depth: Anatomy, physiology, and perception. *Science*, 240, 740–749.

Ma, P. M. (1991a). The barrelettes—architectonic vibrissal representations in the brainstem trigeminal complex of the mouse. I. Normal structural organization. *J. Comp. Neurol.*, 309, 161–199.

Ma, P. M. (1991b). Barrelettes—architectonic vibrissal representations in the brainstem trigeminal complex of the mouse. II. Normal post-natal development. *J. Comp. Neurol.*, 327, 376–397.

Nie, F., and Wong-Riley, M. T. T. (1996). Differential glutamatergic innervation in cytochrome oxidase-rich and -poor regions of the macaque striate cortex: quantitative EM analysis of neurons and neuropil. *J. Comp. Neurol.*, 369, 571–590.

Nomura, S., Itoh, K., Sugimoto, T., Yasui, Y., Kamiya, H., and Mizuno, N. (1986). Mystacial vibrissae representation within the trigeminal sensory nuclei of the cat. *J. Comp. Neurol.*, 253, 121–133.

Olavarria, J., and Van Sluyters, R. C. (1985). Unfolding and flattening the cortex of gyrencephalic brains. *J. Neurosci. Meth.*, 15, 191–202.

Pomeroy, S. L., LaMantia, A. S., and Purves, D. (1990) Postnatal construction of neural circuitry in the mouse olfactory bulb. *J. Neurosci.*, 10, 1952–1966.

Purves, D., and LaMantia, A. (1993). Development of blobs in the visual cortex of macaques. *J. Comp. Neurol.*, 334, 169–175.

Purves, D., Riddle, D. R., and LaMantia, A.-S. (1992). Iterated patterns of brain circuitry (or how the cortex gets it spots). *Trends Neurosci.*, 15, 362–368.

Riddle, D., Richards, A., Zsuppan, F., and Purves, D. (1992). Growth of the rat somatic sensory cortex and its constituent parts during postnatal development. *J. Neurosci.*, 12, 3509–3524.

Saunders, R. C., and Rosene, D. L. (1988). A comparison of the efferents of the amygdala and the hippocampal formation in the rhesus monkey: I. Convergence in the entorhinal, prorhinal, and perirhinal cortices. *J. Comp. Neurol.*, 271, 153–184.

Sefton, A. J., and Dreher, B. Visual system. In G. Paxinos (Ed.), *The Rat Nervous System, 2d ed.*, Academic Press, San Diego, 1995, pp. 833–898.

Silverman, M. S., and Tootell, R. B. H. (1987). Modified technique for cytochrome oxidase histochemistry: increased staining intensity and compatibility with 2-deoxyglucose autoradiography. *J. Neurosci. Meth.*, 19, 1–10.

Sokoloff, L., Reivich, M., Kennedy, C., Des Rosiers, M. H., Patlak, C. S., Pettigrew, K. D., Sakurada, O., and Shinohara, M. (1977). The [^{14}C]deoxyglucose method for the measurement of local cerebral glucose utilization: theory, procedure, and normal values in the conscious and anesthetized albino rat. *J. Neurochem.*, 28, 897–916.

Squire, L. R., and Zola-Morgan, S. (1991). The medial temporal lobe memory system. *Science*, 253, 1380–1386.

Steward, O., and Scoville, S. A. (1976). Cells of origin of entorhinal cortical afferents to the hippocampus and fascia dentata of the rat. *J. Comp. Neurol.*, 169, 347–370.

Tootell, R. B. H., and Silverman, M. S. (1985). Two methods for flat-mounting cortical tissue. *J. Neurosci. Meth.*, 15, 177–190.

Tootell, R. B., Silverman, M. S., DeValois, R. L., and Jacobs, G. H. (1983). Functional organization of the second cortical visual area (V2) in the primate. *Science*, 220, 737–739.

Tootell, R. B. H, Hamilton, S. L., Silverman, M. S., and Switkes, E. (1988a). Functional anatomy of macaque striate cortex. I. Ocular dominance, binocular interactions, and baseline conditions. *J. Neurosci.*, 8, 1500–1530.

Tootell, R. B. H., Silverman, M. S., Hamilton, S. L., DeValois, R. L., and Switkes, E. (1988b). Functional anatomy of macaque striate cortex. III. Color. *J. Neurosci.*, 8, 1569–1593.

Tootell, R. B. H., Hamilton, S. L., and Switkes, E. (1988c). Functional anatomy of macaque striate cortex. IV. Contrast and magno-parvo streams. *J. Neurosci.*, 8, 1594–1609.

Tootell, R. B. H., and Hamilton, S. L. (1989). Functional anatomy of the second visual area (V2) in the macaque. *J. Neurosci.*, 9, 2620–2644.

Trusk, T. C., Kaboord, W. S., and Wong-Riley, M. T. T. (1990). Effects of monocular enucleation, tetrodotoxin, and lid suture on cytochrome-oxidase reactivity in supragranular puffs of adult macaque striate cortex. *Vis. Neurosci.*, 4, 185–204.

Ungerleider, L. G., and Mishkin, M. Two cortical visual systems. In D. G. Ingle, M. A. Goodale, and R. J. Q. Mansfield (Eds.), *Analysis of Visual Behavior*, MIT Press, Cambridge, MA, 1982, pp. 549–586.

Van der Loos, H. (1976). Barreloids in mouse somatosensory thalamus. *Neurosci. Lett.*, 2, 1–6.

Van Essen D. C., and Gallant, J. L. (1994). Neural mechanisms of form and motion processing in the primate visual system. *Neuron*, 13, 1–10.

Voogd, J. Cerebellum. In G. Paxinos (Ed.), *The Rat Nervous System, 2d ed.*, Academic Press, San Diego, 1995, pp. 309–350.

Wallace, M. N. (1986). Spatial relationship of histochemically demonstrable patches in the mouse superior colliculus. *Exp. Brain Res.*, 62, 241–249.

Welker, E., Armstrong-James, M., Bronchti, G., Ourednik, W., Gheorghita-Baechler, F., Dubois, R., Guernsey, D. L., Van der Loos, H., and Neumann, P. E. (1996). Altered sensory processing in the somatosensory cortex of the mouse mutant barrelless. *Science*, 271, 1864–1867.

Wiener, S. I. (1986). Laminar distribution and patchiness of cytochrome oxidase in the mouse superior colliculus. *J. Comp. Neurol.*, 244, 137–148.

Witter, M. P., and Amaral, D. G. (1991). Entorhinal cortex of the monkey: V. Projections to the dentate gyrus, hippocampus, and subicular complex. *J. Comp. Neurol.*, 307, 437–459.

Wong-Riley, M. T. T. (1976). Endogeous peroxidatic activity in brain stem neurons as demonstrated by their staining with diaminobenzidine in normal squirrel monkeys. *Brain Res.*, 108, 257–277.

Wong-Riley, M. (1979). Changes in the visual system of monocularly sutured or enucleated cats demonstrable with cytochrome oxidase histochemistry. *Brain Res.*, 171, 11–28.

Wong-Riley, M. T. T. (1989). Cytochrome oxidase: an endogenous metabolic marker for neuronal functional activity. *Trends Neurosci.*, 12, 94–101.

Wong-Riley, M., and Carroll, E. W. (1984a). Quantitative light- and electron-microscopic analysis of cytochrome oxidase-rich zones in V II prestriate cortex of the squirrel monkey. *J. Comp. Neurol.*, 222, 18–37.

Wong-Riley, M., and Carroll, E. W. (1984b). Effect of impulse blockage on cytochrome oxidase activity in monkey visual system. *Nature*, 307, 262–264.

Wong-Riley, M. T. T., and Welt, C. (1980). Histochemical changes in cytochrome oxidase of cortical barrels after vibrissal removal in neonatal and adult mice. *Proc. Natl. Acad. Sci. USA*, 77, 2333–2337.

Woolsey, T. A., and van der Loos, H. (1970). The structural organization of layer IV in the somatosensory region (S I) of mouse cerebral cortex: The description of a cortical field composed of discrete cytoarchitectonic units. *Brain Res.*, 17, 205–242.

Yuste, R., and Simons, D. (1997). Barrels in the desert: the Sde Boker workshop on neocortical circuits. *Neuron*, 19, 231–237.

4

FUNCTIONAL MAPPING OF LEARNING-RELATED METABOLIC ACTIVITY WITH QUANTITATIVE CYTOCHROME OXIDASE HISTOCHEMISTRY

Amy Poremba, Dirk Jones, and F. Gonzalez-Lima

Department of Psychology and Institute for Neuroscience
University of Texas at Austin
330 Mezes
Austin, Texas 78712

ABSTRACT

Utilizing quantitative histochemistry to view increases or decreases in the activity of the mitochondrial enzyme cytochrome oxidase (C.O.) affords a new functional neuroimaging technique for examining baseline changes in activity which have taken place over a period of time, as opposed to evoked activity alone. Cytochrome oxidase is the pivotal mitochondrial oxidative enzyme for energy production in cells. The amount of this enzyme is tightly coupled to aerobic oxidative energy metabolism in cells. This chapter will describe how the recent advances in histochemical quantification of this enzymatic activity have been used to look at even relatively small changes resulting from learning experiences to map the functional circuitry of associative learning. All three studies described here demonstrate how acoustic stimuli can modify the activity of the auditory system and create distinct patterns of functional metabolic activity when the auditory stimulus acquires different behavioral roles through learning. The cytochrome oxidase mapping technique can provide functional images of how the metabolic capacity of intact neural systems change in response to external stimuli.

1. INTRODUCTION

1.1. Brain Imaging with Cytochrome Oxidase Quantitative Histochemistry

Mapping the functional circuitry underlying behavior has long been a goal of neuroscience and biopsychology. "In recent years new techniques have been developed that now

Cytochrome Oxidase in Neuronal Metabolism and Alzheimer's Disease,
edited by Gonzalez-Lima, Plenum Press, New York, 1998.

allow the imaging of properties of the nervous system that are more related to its functional activity than to its structure or morphology. These techniques have made it possible to measure quantitatively the regional rates of physiological and biochemical processes within the brain and to reconstruct images of the brain in which these rates are displayed quantitatively and spatially distributed exactly where they occur in the brain" (Sokoloff, 1992). The quantitative C.O. histochemical method is one such technique. It provides a novel approach to determine whether tissue alterations in oxidative metabolic capacity are produced by learning and, if so, to map the neural circuits where these changes occur.

While many neuroimaging tools are now available, histochemical quantification of C.O. activity is a methodology that holds promise for delineating learning circuits in use over relatively long periods of time, such as those required for conditioning, as opposed to memory retrieval. Postmortem assessment of C.O. enzymatic activity, an endogenous metabolic marker, can be utilized to view long-term changes in metabolic capacity resulting from the entire training period, whereas markers of glucose utilization (e.g., 2-deoxyglucose, 2-DG, and fluoro-deoxyglucose, FDG) are used to assess short-term cellular energy demands in response to stimulus-evoked neuronal activity during an acute testing period (Gonzalez-Lima, 1992).

The metabolic capacity of neurons is primarily determined by their ability to use ATP for the high energy-requiring membrane potentials involved in synaptic communication (Wong-Riley, 1989). The rate-limiting respiratory enzyme for the oxidative energy metabolism of neurons coupled to ATP production is the mitochondrial enzyme C.O. (Wong-Riley, 1989). Since the capacity of a neuron to communicate with others in a network is coupled to its mitochondrial capacity for producing energy, a sustained increase in the energy demand of the cell requires increased production of the C.O. enzyme. C.O. enzymatic changes in the tissue after prolonged training reach a more stabilized state of oxidative metabolism as compared to glucose metabolism (Wong-Riley, 1989). Thus, measurement of the activity of the respiratory enzyme C.O. allows identification of regions with long-term training-dependent changes.

Assessment of C.O. enzymatic activity in the brain has mainly been used to investigate relatively large metabolic changes in neuronal activity. For example, changes due to reduced sensory stimulation after eye enucleation or retinal impulse blockage (Wong-Riley *et al.*, 1997; Wong-Riley, 1979, 1989; Wong-Riley *et al.*, 1989), Alzheimer's disease (Gonzalez-Lima *et al.*, 1997; Schapira, 1996; Parker, *et al.*, 1994; Simonian and Hyman, 1994; Kish *et al.*, 1992), disruption of blood circulation or hypoxia (de la Torre *et al.*, 1997; LaManna *et al.*, 1996), aging (Takai *et al.*, 1995), and electroconvulsive treatment (Nobrega *et al.*, 1993). The addition of a quantitative histochemical approach (Gonzalez-Lima and Jones, 1994; Gonzalez-Lima and Cada, 1994), has now made it possible to begin investigating the more subtle learning-related neuronal changes in C.O. activity.

One simple way to illustrate the usefulness of C.O. histochemistry is to draw an analogy between this technique and muscle size. As the demand on a muscle increases with sustained use, the muscle grows, reflecting its greater mechanical capacity (potential energy). Similarly, as the energy demand on brain cells is increased by sustained use, C.O. activity increases. Thus the C.O. increase reflects a greater metabolic capacity of brain cells. If prolonged training involves exercising the right arm more than the left, the right muscles become enlarged making it possible to tell which arm was more engaged during the exercise training by measuring the increase in muscle size. On the other hand, if we observed the movement of the arms at the end of the training period, we would be able to identify which muscles were being utilized at that particular moment in time (glucose metabolic markers, 2-DG or FDG), but not which muscles had been repeatedly used (C.O.

metabolism changes). The C.O. measure allows identification of regions with training-dependent changes. The studies reviewed in this chapter confirm quantitative C.O. histochemistry as a new technique that can be used to reveal the neural effects of learning. This metabolic mapping approach is important because it enables us to place associative learning effects in intact neural networks in behaving animals.

1.2. Differences between FDG/2-DG Autoradiography and C.O. Quantitative Histochemistry as Applied to Neuroimaging of Learning

This section will discuss the differences between mapping metabolic activity with FDG/2-DG autoradiography and with C.O. quantitative histochemistry when considering studies of learning. Both imaging techniques, C.O. and FDG/2-DG (DG) operate on the basis that electrical activity of brain cells is tightly coupled to oxidative energy metabolism. Although both are whole-brain mapping techniques which assess metabolic activity, the techniques are qualitatively different in what they measure.

The primary fuel for the brain is glucose, which is ultimately oxidized to carbon dioxide and water. The mitochondrial enzyme cytochrome oxidase is essential for aerobic glucose metabolism because it catalyzes the terminal step in cellular oxidation of glucose (Wong-Riley, 1989). It is the oxygen-activating enzyme for the respiration of all animal cells (Wikström et al., 1981). C.O. catalyzes the electron transfer from cytochrome c to oxygen, therefore this enzyme is central to the functioning of organs like the brain that critically depend on oxidative metabolism for energy production. C.O. constitutes the site of oxidative phosphorylation where energy is conserved for subsequent synthesis of adenosine triphosphate (ATP) (Wikström et al., 1981). ATP is used for energy-consuming functions of neurons. Thus, increased neuronal electrical activity leads to increased cellular respiration and CO activity to produce more ATP. C.O. catalyzes the reaction necessary for the synthesis of ATP by its coupling with oxidative phosphorylation.

Wong-Riley (1979) recognized the potential of C.O. as a metabolic marker and introduced her histochemical method as an elegant approach to visually display changes in the metabolic capacity of nervous tissue. This coupling between C.O. activity and the energy-demanding electrical activity of neurons is what led Wong-Riley (1979) to postulate that the level of C.O. activity within neurons should be coupled with their functional level of activity. Neurons that are more active have increased C.O. content in their mitochondria and increased numbers of mitochondria. Tonically active neurons have more C.O. activity in order to maintain a greater capacity for energy production to fuel their electrical activity (Wong-Riley, 1989). Experimental manipulations that increase or decrease the activity of neurons over a period of days result in a corresponding increase or decrease in C.O. activity (Wong-Riley *et al.*, 1989). The anatomical resolution obtained with C.O. histochemistry cannot be matched by other C.O. measuring techniques or standard autoradiography. In addition, the use of internal C.O. standards and computerized image analysis makes it possible to quantify regional differences in brain C.O. activity, which is coupled to sustained neural functional activity. This is of particular interest for learning and memory studies.

Electrical activity of neurons is generated by membrane potentials and maintained by the sodium/potassium pump, driven by ATP, which in turn is provided by the mitochondria as they metabolize glucose. Thus the metabolism of glucose analogs such as DG primarily demonstrate membrane electrical activity changes maintained by the operation of the sodium/potassium pump. For this reason, DG mapping is not limited to a single electrical event such as postsynaptic action potentials recorded by single unit techniques

(Theurich *et al.*, 1984). Thus it follows that dominant DG uptake is concentrated on the regions of the cellular membrane with the most active sodium/potassium pumps, i.e., in electrically excited membrane regions with the highest sodium load. Since glucose analogs indicate electrical activity changes throughout the brain, they are ideally suited for obtaining comprehensive functional maps of regions affected by a particular stimulation.

Experiments using DG measure glucose utilization in the brain, which, during stimulation, is mainly the result of an acute metabolic need. DG is taken up as glucose in both the oxidative and glycolytic pathways to produce energy (ATP) for the metabolic needs associated with the sodium/potassium pump (Erecinska and Silver, 1989). The goal of experiments studying learning is the identification of brain sites involved in the particular paradigm used. One way to do this is to assess changes in long-term metabolic capacity of the brain.

Most metabolic processes ultimately depend on the energy provided by ATP (Figure 1). These processes include supporting the ionic concentration gradients of Na^+, K^+, and Ca^{2+} as well as the synthesis of proteins, e.g. neurotransmitters and mRNA; lipid synthesis; phosphorylation reactions; fast axonal and dendritic transport; packaging and transport of neurotransmitters; and active transport of substances across the plasma membrane and the maintenance of structural integrity of the cell (Erecinska and Silver, 1989). The energy required for the sodium/potassium pump and for the calcium pump accounts for 50–60% of the ATP produced by mitochondrial oxidative processes which require C.O., while the numerous other energy requirements listed above account for the remaining

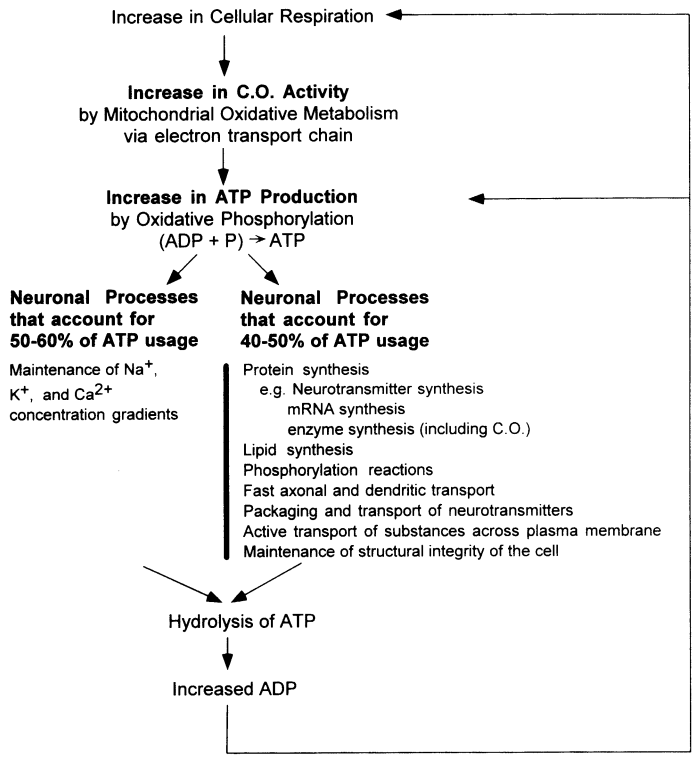

Figure 1. Flow chart outlining the cellular responses that may result from increased neuronal activity and a subsequent increase in metabolism. ATP usage supplies 90% of the total energy requirements for the cell. Increases in ATP usage may upregulate the production of C.O., which can be mapped with quantitative histochemistry.

40–50% (Erecinska and Silver, 1989). The neuroimaging provided by quantitative C.O. histochemistry reflects the need for ATP.

Thus, FDG is used to assess short-term changes in metabolic activity attributable to an increased need for ATP to supply energy for the sodium/potassium pump evoked by the stimulation during the standard 45–60 minute post-injection survival period. On the other hand, C.O. is used to assess longer-term alterations in enzymatic levels that develop during the entire period of the experiment (possible several days) to supply ATP for a variety of cellular energy needs. Therefore, metabolic mapping of C.O. is qualitatively different from DG. Increased C.O. activity during learning may be the result of more than just an increased metabolic need due to an increased need to supply ATP for the sodium/potassium pump. The results of conjoint studies may overlap and C.O. mapping will likely show increases in most of the same structures shown by DG. However, C.O. mapping may identify additional structures involved in longer-term metabolic changes, such as sustained increases in enzyme or neurotransmitter levels, membrane synthesis or morphological changes, in addition to increased neuronal electrical activity.

While DG uptake primarily represents the activity within the first stages of oxidative metabolism, C.O. histochemistry isolates the final stages of the process (Wong-Riley, 1989) and may therefore measure the metabolic needs of a wider array of processes. After injection of radiolabeled DG, glucose is taken up during the presentation of sensory stimuli, due to an immediate increase in the need for ATP. Levels of C.O. are probably modified during the training session and for some time thereafter due to increased energy needs even during resting times. Increased energy demands may be brought about by functional processes possibly occurring throughout training; these require changes in cellular energy consumption even between conditioning sessions. These processes may include increased firing due to reverberatory circuits, as well as evoked firing patterns that persist beyond the experimental period optimal for uptake of radiolabeled DG. In addition, factors which may be involved in learning and memory, such as increased protein synthesis due to upregulation of neurotransmitters, production of enzymes such as C.O. itself, long-term potentiation (LTP), and synaptic plasticity requiring morphological changes, may all be potential contributors to these energy demands.

One explanation for different patterns of activation between C.O. and DG techniques in the same experimental animal is that two cells (A and B) might have the same firing rate but the long-term effects differ. The similar firing rate may produce similar uptake of labeled DG and result in no mean differences between experimental groups. However, as in the case of LTP, a different pattern of inputs from two cells to target cell A can lead to the same firing pattern as in cell B, which receives input from only one other cell. Even though the firing rate for the target cells A and B may be the same, cell A that receives the input from two different cells may have a change in the cellular cascading messenger system. This may lead to long-term changes which may include an increased need for C.O. due to an increasing need for ATP which may result from increases in protein synthesis (synaptic modification), neurotransmitter synthesis, etc. in addition to the increase in firing rate above baseline.

Thus, C.O. is similar to FDG in that it does reflect and positively correlate with increases in firing rate. However, FDG mainly reflects an increased need for the Na^+/K^+ pump since that is the primary energy demand occurring during the main uptake time of the FDG (the bulk in the first 10–15 minutes after injection and the remainder to about 45 minutes) (Mata et al., 1980). Other ATP-requiring processes generally take longer (minutes to hours) to initiate and are initiated by cascading messenger systems (Fride et al, 1989; Freeman et al., 1995). Changes in C.O. activity may be an accurate reflection of

these other ATP-requiring processes in the cell. The hypothesis that the additional 40–50% of ATP produced in the mitochondria used for processes such as protein synthesis are critical during learning is a testable assumption. In fact, protein synthesis has been directly implicated in learning processes (for review see Ponomarenko and Kamyshev, 1997). For example, Fride et al. (1989) have shown that mitochondrial protein synthesis starts approximately 25 minutes after active avoidance training in rats and this protein synthesis is dependent upon newly formed mRNA.

A combination of DG and CO techniques on the same brain is entirely feasible (Braun et al., 1985ab, Silverman and Tootell, 1987, Gonzalez-Lima and Garrosa, 1991). It is desirable because the two methods provide different metabolic information: DG is related to a short-term and more transient functional effects of the stimulus during testing, and CO is related to long-term and more permanent effects on metabolic capacity developed during training. Both types of information are potentially of great value in understanding how learning and memory functions are organized in the brain. For example, the functional increase in metabolic activity (revealed by DG) in a given brain region during presentation of a conditioned stimulus may derive from a pre-existing modification in metabolic capacity (revealed by C.O.), or it may be a transient effect relayed to that region from another site where there is a more permanent effect of the conditioning training. The use of these two techniques in conjunction may make it possible to discriminate between the immediate effects of a stimulus (DG) from those initiated in the longer-term, such as protein synthesis which might lead to synaptic plasticity (C.O.). These prolonged effects of a stimulus (C.O.) may be of special significance for learning and memory studies.

Some learning processes may require a number of days while others may only take a few hours. Theoretically, an increase in the production of C.O. could occur in less than one hour, due to the time necessary for protein synthesis to occur after stimulation or training (Rose, 1991). Changes in C.O. activity may not necessarily entail several days of training, although this would in all likelihood enhance the signal to noise ratio of the critical changes, increasing the probability of detecting them. On the other hand, examination of C.O. activity within a few hours of training may not yield a measurable change in enzymatic activity.

An example of the differences between the mapping techniques of C.O. and FDG from the same experimental groups can be seen from work done in our laboratory (Figure 2). A detailed description of the behavioral methods for this experiment is given in this chapter, Section 3.1. Subjects in the Blocking group were first conditioned with light-shock pairings and exhibited virtually no behavioral expression of conditioning to a tone CS when the tone was part of a compound stimulus (tone and light) paired with shock. Although all subjects received the same tone-shock contiguity, conditioning to the tone was remarkably different due to previous experience. Subjects in the Control group who had no prior pairings with the light CS did not demonstrate impaired conditioning to the compound tone/light stimulus. Although all subjects received the same tone-shock contiguity, conditioning to the tone was remarkably different due to previous experience.

The results show a different pattern of results for mean C.O. activity between the groups in the auditory system, specifically the dorsal cochlear nucleus (DCN), inferior colliculus (IC) and secondary auditory cortex (TE2), (Figure 2, second and third rows show differences in the inferior colliculus). However, there were no mean differences in FDG uptake between the Blocking and Control groups in the auditory system (Figure 2, last row, IC). Both groups in the FDG experiment show increased uptake in the approximate tonotopic region of the inferior colliculus corresponding to the tone stimulus, but there was no difference in this mean uptake between the groups, nor differences in other structures of the auditory system. Thus in this experiment, hearing the auditory tone

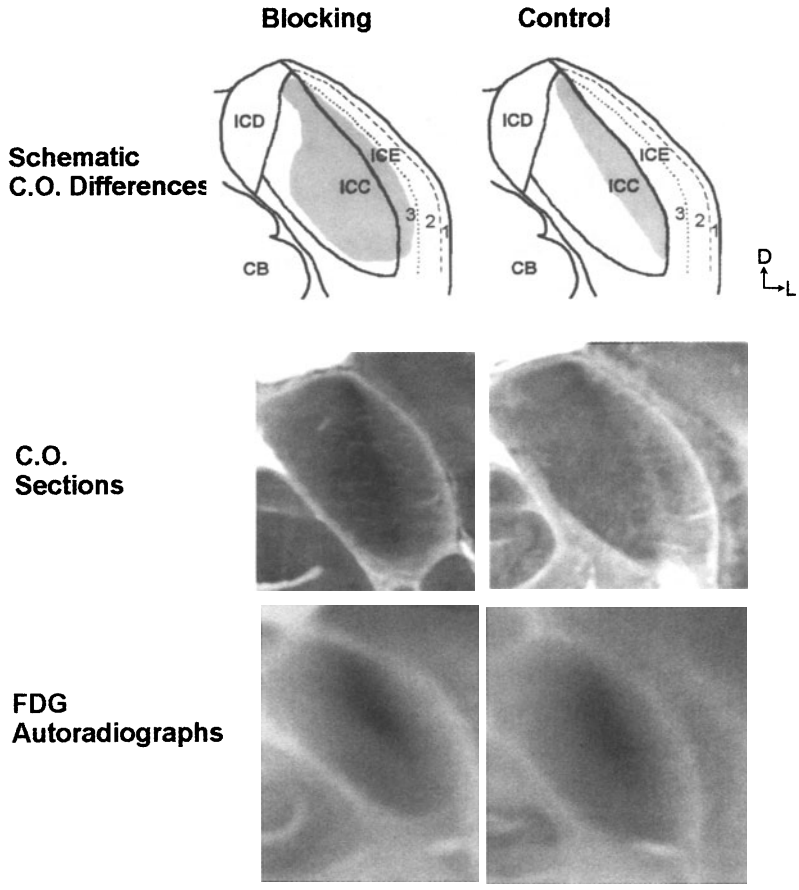

Figure 2. Individual examples of cytochrome oxidase (C.O.) labeling patterns and FDG uptake patterns in the inferior colliculus for the Blocking and Control groups. Schematic representations of the same sections are shown in the first row, where the gray-shaded area outlines the approximate areas of higher C.O. activity for the respective groups. Particularly noticeable is the larger area of strong C.O. activation in the Blocking group compared with the Excitor Control group (second row). The Excitor Control group's C.O. activation does not extend past the lateral boundary of the ICC, whereas the Blocking group's C.O. activation clearly extends into the third layer of the ICE. In contrast to these differences seen with C.O., there were no differences between groups in the FDG autoradiographs (third row). ICD, dorsal nucleus of the inferior colliculus; ICC, central nucleus of the inferior colliculus; ICE external nucleus of the inferior colliculus; 1, first layer of the ICE; 2, second layer of the ICE; 3, third layer of the ICE; CB cerebellum. Original magnification factor, 18. Top is dorsal (D) and right is lateral (L).

stimulus produced the same acute metabolic need (no mean group differences) in the auditory system as assessed by FDG, but produced measurable changes in sustained metabolic need as evidenced by the differences in C.O. activity between the groups. This difference in C.O. activity may be accounted for by long-term activation of certain structures due to the energy demand for maintenance of ionic concentration gradients in the cell, as well as other energy-requiring cellular mechanisms.

Assessment of C.O. activity is better suited for identification of the functional demands of processing during the entire conditioning experience than DG, a technique which better reflects online responses to a specific stimulus during a finite experimental period. Therefore, C.O. is an important tool for identification of brain structures in which both evoked activity and long-term cellular modifications have taken place. C.O. enzy-

matic activity could be up-regulated as the result of a number of different energy requiring mechanisms in the cell reflecting learning-induced plasticity. These changes may eventually result in modifications in the morphology, synapse formation or a change in the number of synapses. It has been proposed that such synaptic changes are the result of learning (Kleim et al., 1997). Whereas DG measures the acute increased need for glucose, C.O. is a cumulative marker for increased metabolic capacity.

1.3. Considerations for the Quantitative Cytochrome Oxidase Technique

There are several positive aspects to using quantitative C.O. histochemistry as a general mapping tool. 1) This procedure is inexpensive and relatively easy to accomplish with a small number of equipment requirements (average cost per histochemical staining batch is about $100/batch). The imaging system to analyze the data once obtained is the more expensive part of the experiment but is a one time cost. 2) Any procedure that can be done with frozen sections, or that can be combined with post-fixing can also be done on sections adjacent to those stained for C.O. (autoradiography, immunohistochemistry, various types of morphological staining, and in-situ hybridization). Using a combination of techniques in the same experimental animals allows one to look at general metabolic increases as well as other measures of interest. For example, the expression and distribution of specific immediate early genes can be combined to provide a very powerful experimental approach. 3) The C.O. technique assesses the cumulative changes in baseline metabolic activity associated with the entire learning experience; it is not a measure of on-going evoked activity. After prolonged training, C.O. changes in the tissue reach a more stabilized state of oxidative metabolism as compared with glucose metabolism (Wong-Riley, 1989). This seems to provide a more stable representation of the metabolic state than FDG and 2-DG studies which reflect rapidly changing metabolic activity during short-term behavioral testing of the animal. The acute state (as measured by FDG and 2-DG) may not reflect changes in baseline metabolism unless the testing conditions are such that the appropriate structures are engaged. As demonstrated by Nobrega (1992) this activational condition is not always obvious in experiments assessing the effect of experience on brain function. In cases involving chronic training conditions, C.O. may be a better metabolic marker than other metabolic markers (2-DG or FDG; Nobrega, 1992). This is due to the ability of C.O. histochemistry to reveal baseline cumulative changes in metabolic capacity, as opposed to a stimulus-evoked effect during an acute testing phase. 4) While this technique allows investigation of changes in metabolic activity in any part of the brain, as do FDG, 2-DG, positron emission tomography (PET) and functional magnetic resonance imaging (fMRI), cytochrome oxidase histochemistry has the additional advantage of single-cell resolution at both the electron (Wong-Riley *et al.*, 1994, 1997) and light (Gonzalez-Lima *et al.*, 1997) microscopy levels. 5) Quantitative C.O histochemistry is an excellent general mapping tool to assess the entire brain and to use as a first-pass inspection of the functional neuroanatomy of any learning situation.

However, as with all techniques there are also limitations associated with C.O. histochemistry. In order to design and interpret C.O. studies accurately, the following issues must be taken into account. 1) Quantitative C.O. histochemistry is intended to be a used as a general mapping tool and as such, is not a measure of evoked activity. It is indicative of the changes taking place over the entire training period and does not have the time resolution that studies involving electrophysiology and/or other currently available imaging techniques (such as optical imaging, FDG, fMRI, etc.) have. 2) C.O. histochemistry pro-

vides no information about physical anatomical connections; current neuroanatomical information from additional studies are needed for that. 3) A final major issue is that just as with other techniques looking at energy use in some way (FDG, fMRI, etc.), one does not know if the observed increases or decreases in C.O. activity are the result of electrophysiological excitatory or inhibitory postsynaptic potentials, or increases or decreases in action potentials. Presumably all electrical changes requiring oxygen-derived energy will lead to increases in C.O. activity (Wong-Riley et al., this volume).

In order to use this technique to its full potential, when designing an experiment involving C.O. mapping it is necessary to consider the specific aims in each stage of an experiment. First, consideration must be given to the duration of the training paradigm to allow sufficient time for protein synthesis of C.O. and its build-up linked to the metabolic demands of the specific task on the brain. Second, internal standards of known C.O. activity should be used to provide a means of comparing sections stained at different times. This will minimize variability and allow for comparisons across animals. Third, the sensitivity of the staining reaction should be maximized to detect learning related changes. Fourth, the histological procedures in preparing the sections for analysis should preserve the locations of the reaction product. Finally, analysis should be based on reliable quantitative densitometry calibrated with standards so as to yield enzyme activity as with the quantitative methods discussed in this volume (Gonzalez-Lima and Cada, 1998).

In the studies described in this chapter, significant learning related changes in C.O. activity between experimental and control conditions could be seen with as few as 12 pairings of CS (conditional stimulus) and US (unconditional stimulus) spread over three training days. This is less training than we had originally envisioned would be needed to view learning-related changes with C.O. activity. Since the quantitative method has increased the sensitivity of the measurement of C.O. activity perhaps a strong, acute stimulus is also sufficient to increase C.O. activity in a highly salient condition. Although more extensive parametric studies of the time course of the enzymatic changes need to be done, this technique holds promise as a new way to map long-term learning related changes across the entire brain, at both the whole structure level and at the level of the individual neuron. The chances of observing specific learning-related changes will increase after those pathways have been activated a number of times, increasing the signal to noise ratio.

To successfully map learning related changes with C.O. histochemistry experimental and control groups need to be matched for number and history of stimulation. The only difference between the experimental and controls groups should be the temporal pairing relationship between the stimuli. Experiments of associative learning necessitate equating the stimuli throughout training to match the experimental and control groups, with the only difference being the temporal pairing relationship between the stimuli. If the parameters set forth here can be met then quantitative C.O. histochemistry can be utilized as an excellent general mapping tool to be used as a first pass procedure in conjunction with more reductionistic techniques or in comparison with functional maps from many other similar training paradigms.

2. APPLICATION OF QUANTITATIVE C.O. HISTOCHEMISTRY TO THE STUDY OF CONDITIONED SUPPRESSION TO AN AUDITORY STIMULUS

First, we wanted to apply the C.O. histochemistry technique to a simple behavioral paradigm to assess learning effects on a relatively circumscribed system, the auditory sys-

tem. Conditioned fear in rats is one of the most commonly used excitatory behavioral paradigms for investigating Pavlovian conditioning (Miller and Spear, 1985). Suppression of normal drinking behavior (conditioned suppression or conditioned emotional response) is a common measure of conditioned fear. A water-deprived rat is placed in an operant chamber and trained to lick a tube in order to obtain a reward of sweetened water. When the rat is responding at a steady, high rate, Pavlovian conditioning trials are introduced. A compound stimulus of light and tone (CS) is presented periodically, followed by a brief electric footshock (US). As paired presentations of tone and footshock continue, the rat stops drinking while the light and tone are on. The presentation of the CS, signaling footshock, results in suppression of drinking, i.e., the conditioned response (CR).

This study focused on the learning-induced plasticity of the auditory system (Poremba et al., 1998). The conditioned suppression paradigm has generated a large number of behavioral studies (for review see Domjan, 1996) but fewer studies assessing the sensory neural basis of conditioned suppression (McIntosh and Gonzalez-Lima, 1993, 1994, 1995; Dantzer and Delacour, 1972) or conditioned fear (LeDoux, 1995; Davis, 1994).

Learning-related patterns of plasticity in the auditory system have been demonstrated by several neuronal recording and glucose-imaging studies. Learning-related neuronal plasticity has been reported in the medial geniculate nucleus (MGN; e.g. Gabriel *et al.*, 1975, 1976; Edeline and Weinberger, 1992), auditory cortex (AC; e.g. Edeline *et al.*, 1993), and dorsal cochlear nucleus (DCN) and inferior colliculus (IC; McIntosh and Gonzalez-Lima, 1993). The validity of using cytochrome oxidase enzymatic activity to view learning-related changes was tested. We hypothesized that changes in C.O. activity related to learning would be observed in the auditory system after conditioning.

2.1. Experimental Design and Methods for Conditioned Excitor Experiment

Subjects were 24 male Long-Evans, black-hooded rats weighing an average of 100g (approx. 33 days old). There were 7 rats in the Conditioned Excitor group, 11 rats in the Pseudorandom group, and 6 rats in the Naive group which were never trained. The subjects in the Conditioned Excitor group also serve as the control group in the blocking study described in Section 3.

Methodological details of the training paradigm have been reported previously (Poremba et al., 1997). Training was conducted in standard sound attenuated operant conditioning chambers where animals had access to a 10% sucrose water solution. A photo source module placed an infrared beam in front of the drinking tube to monitor drink time and latency. The acoustic stimulus was a low frequency modulated (FM) tone (1–2 kHz 500 msec upward sweep at 2 sweeps/sec, 15 sec total CS duration, 65 dB sound pressure level measured at the center of the chamber). The visual stimulus was provided by two flashing white lights (15 sec duration, intensity of 200 footcandles measured 2 cm from the source). Background illumination was provided by a red light mounted outside the opposite side of the chamber at the rear. The grid floor of the chamber was wired to a Lafayette Instruments Master Shocker in order to deliver a 0.5 mA scrambled footshock, 0.75 sec in duration. Presentation of stimuli and collection of latency and duration of the drink response were controlled by computer programs created using MED-PC behavioral programming language (MED Associates).

A conditioned suppression paradigm was used for all training, wherein the degree of conditioning is assessed by determining if the normally ongoing drinking behavior is interrupted by a conditioned stimulus (CS) presentation. Following 24 h of water deprivation,

subjects began daily baseline sessions of 15 min. of free access to a 10% sucrose water solution in the operant chamber. A measure of baseline drinking was established on four consecutive days before training began and animals were randomly assigned to the Conditioned Excitor or Pseudorandom groups. Each rat in these two groups received 27 tone CS presentations (1–2 kHz) and 28 unconditioned stimulus (US) presentations. The total number of other experimental stimuli across all training days was also comparable between the two groups [36–40 light presentations and 4–6 comparator tone presentations (10–20 kHz)].

Light and footshock pretraining for the Conditioned Excitor group consisted of separate sessions over four days with 15 unpaired light and footshock presentations and one pairing of light with footshock to match the number of presentations in the Pseudorandom group. Tone conditioning for the Conditioned Excitor group consisted of four pairings on each of three days of the CS (tone/light compound) paired with a mild footshock (US) for a total number of 12 paired presentations (Table 1). All training sessions were approximately 20 min long with ITIs that ranged randomly from 60 to 180 sec.

The Pseudorandom group received, equivalent to the Conditioned Excitor group, pseudorandom presentations of the tone, light, and footshock with a probability of tone being paired with footshock at 0.037, i.e., one light/footshock pairing and one tone/footshock pairing over seven training days spanning a 2-week period, to prevent the stimuli from acquiring a reliable predictive value of shock delivery. At least one hour after each daily session was completed, the animals were given 45 min. free access to water in their home cages.

Behavioral testing was done for three days before the last day of training. The first day of testing consisted of exposure to the context while measures of grooming, freezing, mobility, rearing and drinking were taken by the same trained, "blind" observer for each session to assess any contextual conditioning for both experimental groups. The second and third days of testing consisted of behavioral probe trials where unreinforced presentations of each stimulus, the light, tone, compound stimulus of the light and tone, and a high frequency FM tone (10–20 kHz, 65 dB, used as a comparison stimulus) were presented to both experimental groups. Time spent drinking and latency to drink were measured.

Drinking was monitored for 15 seconds prior to the onset of the CS as well as during the CS presentation for the computation of suppression ratios, $CS_{\text{drink time}}/(\text{pre-}CS_{\text{drink time}} + CS_{\text{drink time}})$; (Kamin, 1969). Suppression ratios range from 0 to 0.5. A value of zero indicates that the animal suppressed drinking when the CS was presented and 0.5 indicates no change in drinking behavior with the presentation of the CS. A low suppression ratio indicates a higher degree of conditioned fear.

Upon completion of the training the rats were sacrificed, complete unfixed brains were extracted, frozen in isopentane at –40°C, and cut into serial 40 μm sections in a Reichert-Jung cryostat at –20°C. Sections were picked up on clean glass slides and processed by the quantitative C.O. histochemical procedure described in this volume (Gonzalez-Lima and Cada, 1998). A set of C.O. standards, preparation of which is also

Table 1. Behavioral design

Groups	Phase 1	Phase 2
Conditioned excitor	L, S	TL→S
Pseudorandom	L, S	T, L, S

Note: This table outlines the basic behavioral design used. L = flashing light, TL = low-frequency tone/flashing light compound, S = footshock.

described in this volume (Gonzalez-Lima and Cada, 1998), was sectioned at varying amounts of thicknesses (10, 20, 40, 60 and 80 μm). A set of standards was included with each batch of incubation medium for the generation of a single regression equation between C.O. activity and optical density of the sections for the subsequent comparison of all tissue in the present experiment. The brain homogenate was spectrophotometrically measured and activity units were defined at pH 7 and 37°C where 1 unit oxidizes 1 μmol of reduced cytochrome c per min (μ mol/min/g tissue wet weight).

Using the adjacent sections stained for Nissl substance, representative sections of the eleven auditory regions of interest from each brain were chosen. A stereotaxic atlas of the rat brain (Paxinos and Watson, 1986) was used to select rat brain sections that approximately matched the auditory system structures: the dorsal and ventral cochlear nuclei (DCN and VCN; Bregma −11.3 mm); external (ICE), central (ICC), and dorsal (ICD) nuclei of the inferior colliculus (IC; Bregma −8.3 mm); the medial (MGM), dorsal (MGD), and ventral (MGV) divisions of the medial geniculate nucleus (MGN; Bregma −5.8 mm); and three divisions of auditory temporal cortex (TE1, TE3; Bregma −5.8 mm and TE2; Bregma -8.3mm; Brodmann's areas 41, 20 and 36, respectively).

The optical density (O.D.) in the C.O. stained sections was analyzed using an image-processing system as described in this volume (Gonzalez-Lima and Cada, 1998). The system was calibrated using an O.D. step tablet (Kodak) and the histochemical reaction product (chromatic indicator of C.O.) was measured in O.D. units. The images were corrected for optical distortions from the camera through subtraction of the background (a slide coverslipped with Permount without brain tissue). Using a single regression equation between C.O. activity and O.D., a calibration curve was created using the C.O. standards (Gonzalez-Lima and Jones, 1994; Gonzalez-Lima and Cada, 1998). These standards were linear in the range of thicknesses described above. Subsequent densitometric measures taken from brain images were then automatically expressed in terms of C.O. activity units (μmol/min/g tissue wet weight).

Analysis of each structure involved taking four readings per section from three sections per brain (i.e., 12 readings per region per brain) for each brain region of interest. Readings were taken from both hemispheres of the brain to avoid artifacts. For each region measured, the size of the densitometer window was set to approximately one quarter the size of the whole region, and four adjacent sites were measured to cover the region. The size of this window was held constant across subjects. For example, a window of 7 × 7 pixels (approx. 250 × 250 microns) was used for the IC. Thus, for all animals, in each of three sections, four separate sites of a preset sample window were measured in such a way that the majority of each structure was measured, falling within the borders of the anatomical region of interest, and held constant across animals. Analysis of variance (ANOVA) and post-hoc tests [Tukey's Honest Significant Difference Test (HSD)] were used to test the statistical significance of the results at $p < 0.05$.

2.2. Behavioral and Neuronal Effects of Excitatory Conditioning

Conditioned suppression was ascertained during three probe trials one hour before decapitation of the rats by measuring the amount of conditioned suppression of drinking to tone only presentations (Figure 3). A repeated measures ANOVA (group by trials) indicated that the tone mean conditioned suppression ratio for the main effect of group was significant ($F[1,16] = 7.61$, $p < 0.02$). The Conditioned Excitor group mean suppression ratio was significantly lower overall than the Pseudorandom group. These ratios indicate that, as predicted, the Conditioned Excitor group did learn to suppress drinking behavior

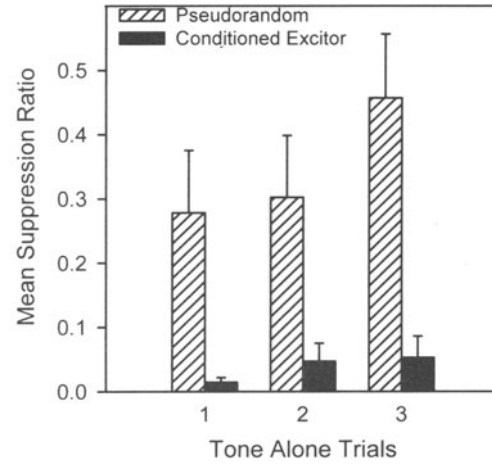

Figure 3. Mean ± standard error (SE) of conditioned suppression to drinking during tone only presentations in Pseudorandom (hatched bars) and Conditioned Excitor (solid bars) groups. Suppression to drink is expressed as a ratio of time spent drinking during the tone presentation (A) divided by the sum of time spent drinking before (B) and during the tone (A/[A + B]). Three trials of the target tone were presented in an altered context to reduce excitatory cues external to the tone. There was significantly more suppression to the tone in the Conditioned Excitor group than in the Pseudorandom group supporting the prediction that the Conditioned Excitor group would acquire excitatory conditioning to the tone while the Pseudorandom group would not.

during the tone presentation, whereas the Pseudorandom group did not suppress. No behavioral data are shown for the naive group, since they had no exposure to the test stimuli.

2.2.1. Conditioned Excitor: Cytochrome Oxidase Activity for the Lower Auditory Structures. The lower auditory structures (cochlear nuclei and inferior colliculus) exhibited higher C.O. activity in the Pseudorandom group than the Conditioned Excitor group (Figure 4). An ANOVA of the three groups for each lower auditory structure indicated significant mean differences in each of the following areas: DCN ($F[2,23] = 5.52$, $p < 0.02$); VCN ($F[2,22] = 3.69$, $p < 0.05$); ICC ($F[2,23] = 13.53$, $p < 0.001$); ICD ($F[2,23] = 20.93$, $p < 0.001$); ICE ($F[2,23] = 13.59$, $p < 0.001$). Specifically, post-hoc analyses (HSD, $p < 0.05$; see Table 2) showed that the Pseudorandom group had significantly higher overall C.O. activity than the Naive group, and also higher C.O. activity than the Conditioned Ex-

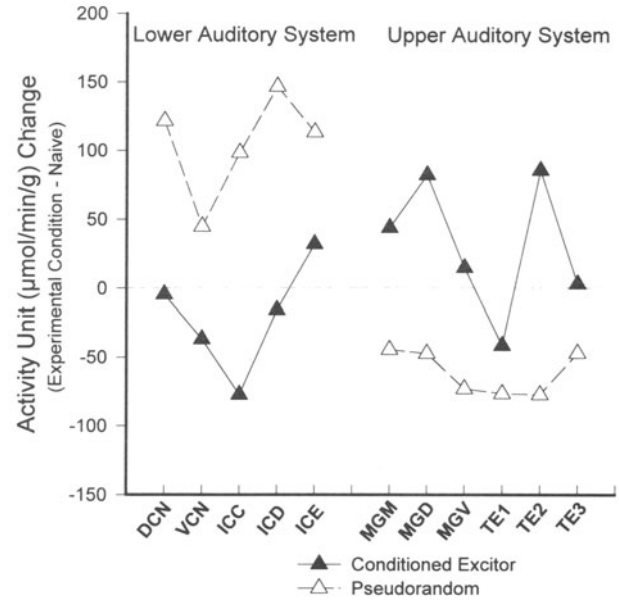

Figure 4. Graph of activity unit changes expressed as µmol/min/g tissue wet wt in the auditory system for the Conditioned Excitor group and the Pseudorandom group. The change in activity units are expressed as the difference in mean C.O. activity of the Naive group from experimental condition. The lower auditory structures (cochlear nuclei and inferior colliculus) exhibited relatively higher C.O. activity in the Pseudorandom group than the Conditioned Excitor group, while the upper auditory structures (medial geniculate and auditory cortex) had the opposite pattern. See Table 2 for explanation of the abbreviations.

Table 2. Regional activity of cytochrome oxidase in the brains of Conditioned Excitor, Pseudorandom, and Naive groups of animals

Structure	Conditioned (I) Mean ± S.E.	Pseudorandom (II) Mean ± S.E.	Naive (III) Mean ± S.E.	Post-hoc comparisons I vs II	I vs III	II vs III
Lower auditory system						
Dorsal cochlear nucleus (DCN)	430.76 ± 25.34	556.78 ± 34.34	435.26 ± 24.01	+		+
Ventral cochlear nucleus (VCN)	306.02 ± 12.78	387.78 ± 26.00	343.04 ± 25.97	+		
Central N. inferior colliculus (ICC)	229.07 ± 3.77	404.69 ± 25.22	306.39 ± 34.16	+		+
Dorsal N. inferior colliculus (ICD)	230.04 ± 2.57	392.47 ± 23.39	245.85 ± 19.91	+		+
External N. inferior colliculus (ICE)	273.15 ± 4.00	354.47 ± 16.37	241.13 ± 22.29	+		+
Upper auditory system						
Medial N. medial geniculate (MGM)	231.39 ± 4.35	143.11 ± 13.43	187.68 ± 15.99	+	+	
Dorsal N. medial geniculate (MGD)	268.12 ± 8.10	138.78 ± 10.20	186.15 ± 15.89	+	+	+
Ventral N. medial geniculate (MGV)	269.67 ± 9.95	181.85 ± 16.97	254.97 ± 22.76	+		+
Primary auditory cortex (TE1)	247.02 ± 4.35	212.11 ± 13.43	288.73 ± 16.00			+
Secondary auditory cortex (TE2)	353.24 ± 8.10	190.63 ± 10.20	268.01 ± 15.89	+	+	+
Tertiary auditory cortex (TE3)	251.10 ± 9.95	200.83 ± 16.97	248.12 ± 22.76	+		

Mean ± standard error (S.E.) units in μmol/min/g tissue wet weight were obtained by averaging measurements from three consecutive brain sections per neuronal area for each subject. Results of post-hoc comparison tests (+ indicates $p < .05$) for each ANOVA are summarized for each brain structure shown in the right three columns.

citor group for all lower auditory structures. An exception was the VCN for which the Pseudorandom group was higher than the Conditioned Excitor group alone, but was not significantly different from the Naive group.

The C.O. pattern of activity found for the Pseudorandom group in the present study is comparable to the findings of two previous metabolic studies using similar paradigms. Both paradigms result in a lack of behavioral responding as does the Pseudorandom group. First, in a study investigating long-term habituation to tone stimuli, increases in 2-DG uptake were evident in the IC and the DCN as well as other lower auditory structures (Gonzalez-Lima *et al.*, 1989), corresponding well with the results of the current study where presentation of random stimuli occurred over several training days. Second, in another experiment when conditioning to a tone stimulus was prevented due to prior associative conditioning to a visual stimulus paired with footshock, i.e. blocking phenomenon (Poremba *et al.*, 1997a), lower auditory structures again showed increased C.O. metabolic activity. These results are relevant because blocking produces a lack of responding to the tone stimulus, that may be similar to the pseudorandom presentations of this study and long-term habituation in a previous 2-DG study (Gonzalez-Lima *et al.*, 1989).

In these cases, similar behavioral responses resulted in similar patterns of metabolic activity with the two different methods (C.O. and 2-DG). However, 2-DG/FDG is a measure of evoked activity and as such we would not expect, in all cases, to mirror the changes in baseline metabolic activity observed with C.O. histochemistry (for an extended discussion of the differences between the FDG and C.O. techniques see Section 1.2., this chapter). Although long-term habituation involves a decline of overt behavioral responding implemented by a decrease in synaptic transmission in invertebrate sensory neurons (Castellucci *et al.*, 1978), the previous (Gonzalez-Lima *et al.*, 1989) and current findings, wherein lower auditory structures show an increase in C.O. activity in the pseudorandom condition, suggest that in the lower auditory system in rats, long-term habituation is an active metabolic process.

2.2.2. Conditioned Excitor: Cytochrome Oxidase Activity for the Upper Auditory Structures. In contrast to the results with the lower auditory structures, the upper auditory structures (MGN and auditory cortices) exhibited higher C.O. activity in the Conditioned Excitor group than the Pseudorandom and Naive groups (Figure 4). In some areas, the Pseudorandom group had decreased C.O. activity in comparison to the Naive group. An ANOVA of the three groups indicated significant mean differences in each of the following areas: MGM ($F[2,21] = 13.68$, $p < 0.001$); MGD ($F[2,21] = 35.32$, $p < 0.001$); MGV ($F[2,21] = 8.34$, $p < 0.01$); TE1 ($F[2,23] = 4.59$, $p < 0.05$); TE2 ($F[2,23] = 25.51$, $p < 0.001$; TE3 ($F[2,23] = 3.52$, $p < 0.05$). Specifically, post-hoc analyses (HSD, $p < 0.05$; see Table 2) showed significantly higher overall C.O. activity in the Conditioned Excitor group than in the Pseudorandom group for all upper auditory structures except for primary auditory cortex (TE1). Furthermore, the only auditory regions with significantly greater C.O. activity in the Conditioned Excitor group as compared to the Naive group were MGM, MGD and TE2 (Table 2). These later structures form the so-called lemniscal-adjunct thalamo-cortical auditory system, which has been linked to the associative memory of sounds by electrophysiological studies (Gabriel *et al.*, 1975, 1976).

The increased metabolic enzymatic activity in the MGN of the Conditioned Excitor group in this study is supported by previous findings in other paradigms showing learning-related changes in neuronal firing patterns in response to associative auditory conditioning (McEchron *et al.*, 1996; Edeline and Weinberger, 1992; Edeline *et al.*, 1990; Weinberger, 1982; Ryugo and Weinberger, 1978; Gabriel *et al.*, 1976; Olds *et al.*, 1972; Buchwald *et al.*, 1966). Lesions of the MGN also disrupt the acquisition of other types of fear conditioning (Poremba and Gabriel, 1997; Romanski and LeDoux, 1992; Iwata *et al.*, 1986; Jarrell *et al.*, 1986; LeDoux *et al.*, 1986a,b). The pattern of results for the auditory cortex in this experiment are also in agreement with previous findings of robust receptive field changes in the auditory cortex specific to a behaviorally conditioned tone, particularly in secondary auditory cortex (Weinberger, 1995; Diamond and Weinberger, 1986). Teich *et al.* (1988) describes evidence that also suggests a long-term role for the auditory cortex in tone-signaled heart rate conditioning; rabbits with lesions of the auditory cortex did not have impaired acquisition of the behavior but had difficulty maintaining their behavioral performance on subsequent training days compared to controls.

There were also significant decreases in metabolic activity associated with the pseudorandom experimental condition compared to the Naive group in some of the same upper auditory system structures (MGD, MGV, TE1, TE2) that showed increases in the Conditioned Excitor group. This suggests that metabolic activity in the upper auditory structures may be more closely correlated with whether or not the experimental subject is making a tone-signaled learned behavioral response. Furthermore, the memory associated with the conditioned sound is more likely to be represented by the regions showing greater metabolic capacity in the Conditioned Excitor group as compared to both Naive and Pseudorandom groups. These regions were the MGM, MGD and TE2, which may encode the associative memory of the CS by increased protein synthesis of C.O. Long-term enhancement of neuronal metabolic capacity may be critical to memory function as suggested by studies implicating C.O. inhibition in Alzheimer's disease (this volume, Gonzalez-Lima et al., 1998).

2.2.3. Examples of C.O. Enzymatic Activity in Inferior Colliculus and Medial Geniculate Nucleus. The patterns of reactivity in the IC and MGN are illustrated in Fig. 5. Darker labeling of the IC for the Pseudorandom group compared to the Conditioned Excitor group and the opposite pattern in the MGN of darker labeling in the Conditioned Excitor group than the Pseudorandom group is visible in these photomicrographs. However,

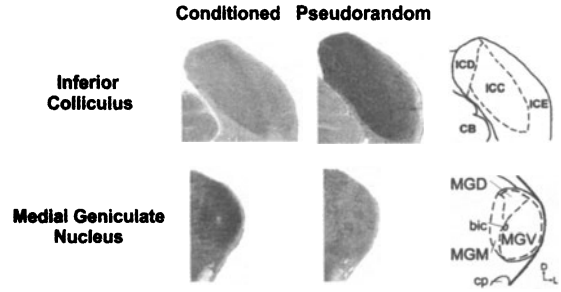

Figure 5. Photomicrographs of the inferior colliculus (IC) and medial geniculate nucleus (MGN) illustrating examples of C.O. reactivity patterns for the Conditioned Excitor (left column) and Pseudorandom (middle column) groups. Darker labeling of the IC in the Pseudorandom group compared to the Conditioned Excitor group is consistent with higher CO reactivity in the lower auditory structures of the Pseudorandom group. The opposite pattern in the upper auditory system is shown for the MGN with darker labeling in the Conditioned Excitor group than the Pseudorandom group. Levels correspond approximately to –8.8 mm and –5.8 mm posterior to Bregma (Paxinos and Watson, 1986). Group differences are based on computerized densitometry of the stained tissue as the photomicrographs may show contrast differences due to processing. Schematic drawing represents divisions of the two nuclear groups (right column). Top is dorsal (D), right is lateral (L).

such cursory inspection of photomicrographs is inadequate to evaluate the data because photomicrographs may show contrast differences due to developing and processing factors and other merely incidental differences. The effects reported here are based on reproducible differences determined by direct densitometric analysis of C.O. stained sections from each structure in every subject and found to be statistically reliable for each group.

2.3. Assessment of C.O. Metabolic Activity in the Auditory System Shows a Clear Distinction between the Conditioned and Pseudorandom Groups

These results support the hypothesis that tone CS processing is metabolically enhanced during associative conditioning at the upper auditory structures (MGN and auditory cortices). On the other hand, metabolic activation of the lower structures (DCN, VCN and IC) in the Pseudorandom group suggest that these areas may be activated during habituation to tone stimuli, when the system is required to filter out possibly less meaningful or meaningless stimuli (Figure 6). There is a clear distinction between thalamocortical and lower divisions of the auditory system based on the differences in metabolic activity evoked by classical conditioning, which leads to an overt learned behavioral response, versus pseudorandom stimulus presentations, which lead to behavioral habituation. The lower auditory system may be engaged in active inhibition of the sensory response to non-predictive sound stimuli during non-associative conditions, whereas the upper auditory system may be coding for whether or not the animal is making a conditioned response signaled by an auditory cue.

The present results show that separate patterns of long-term activation occur at different levels of the auditory system based on specific learning experiences (e.g. paired trials versus pseudorandom stimuli presentations). The once-held view of non-plastic sensory neurons that are exclusively concerned with detection of physical stimulus properties is being replaced with the more inclusive view that sensory neurons are also involved in behavioral stimulus properties acquired by learning. This view is supported by the present C.O. study, previous neuronal recording studies (see 2.1., this chapter), as well as

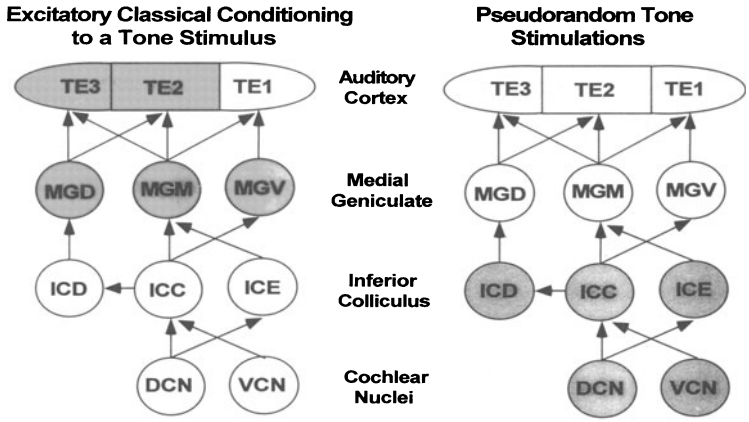

Figure 6. Schematic diagram of the auditory regions showing the metabolic changes (higher regional group differences in C.O. activity indicated in dark gray) for the Conditioned Excitor group (left) and Pseudorandom group (right). Major ascending connections within the auditory system of the rat brain are depicted with arrows. Abbreviation explanations can be found in Table 2.

FDG metabolic studies (Cahill *et al.*, 1996; McIntosh and Gonzalez-Lima, 1993, 1995; Scheich *et al.*, 1993; Gonzalez-Lima, 1992; Gonzalez-Lima *et al.*, 1989; Gonzalez-Lima and Agudo, 1990; Gonzalez-Lima and Sheich, 1984a,b, 1986).

3. APPLICATION OF C.O. HISTOCHEMISTRY TO THE STUDY OF BLOCKING TONE CONDITIONING

In this second experiment (Poremba, Jones and Gonzalez-Lima, 1997), we were interested in exploring the metabolic mapping of a more complex learning situation. Kamin (1969) described the phenomenon of blocking and referred to it as the lack of behavioral expression of conditioning to a novel stimulus due to the presence of a previously conditioned stimulus. The subjects showing this effect differed only in their history prior to conditioning of the tone/light compound paired with footshock. Subjects in the Blocking group first conditioned with light-shock pairings exhibited virtually no behavioral expression of conditioning to a tone CS when the tone was part of a compound stimulus (tone and light) paired with shock. Subjects in the Control group who had no prior pairings with the light CS did not demonstrate impaired conditioning to the compound tone/light stimulus. Although all subjects received the same tone-shock contiguity, conditioning to the tone was remarkably different due to previous experience.

The blocking paradigm has generated a large number of behavioral studies and inspired a number of theories about conditioning (e.g. Holland, 1985; Mackintosh, 1983; Pearce & Hall, 1980; Rescorla & Wagner, 1972). Several of these theories suggest that blocking affects CS processing in neural sensory systems (Kamin, 1969; Mackintosh, 1983; Pearce & Hall, 1980). The available neurobiological studies have assessed the effects of lesions to the hippocampus or the amygdala (Gallo & Candido, 1995; Holland & Gallagher, 1993; Rickert, Bennet, Land & French, 1978; Solomon, 1977), or electrical recordings in the visual system during the blocking phenomenon (Kinkaide & Walley, 1974; Walley, 1982). Lesions of the dorsal hippocampus prevented blocking whereas lesions of the amygdala did not (Holland & Gallagher, 1993; Rickert, et al., 1978; Solomon, 1977).

In this experiment, intact subjects were presented with the same tone stimuli but neural CS processing is presumably different in the blocking condition than in the simple excitatory conditioning. Identifying the neuronal circuits utilized may answer whether the sensory processing of the tone is the same under both behavioral learning conditions. The main hypothesis was that the blocking paradigm's effects on brain activity were consistent with effects linked to changes in CS processing in the auditory system.

3.1. Experimental Design and Methods for the Blocking Experiment

Subjects were 23 male Long-Evans, black-hooded rats weighing an average of 100 g (approx. 33 days old). Seven subjects did not meet the learning criterion and were excluded from the study. Two other animals had inadequate tissue preparation and were also excluded. For the final data analysis there were 7 rats in the Blocking group and 7 rats in the Control group (previously discussed as Conditioned Excitor group). Explicit details of the training and processing of the brain tissue are explained in Section 4.1.

All training was done with the conditioned suppression paradigm, where the degree of conditioning is assessed through interruption of the normally ongoing drinking behavior. The Blocking group was expected to exhibit little or no suppression of drinking during the test phase while the Control group was expected to show a significant suppression of their drinking.

During Phase 1 training the Blocking group received pairings of a light stimulus with the footshock so that the light stimulus was conditioned as an excitor. During Phase 1 training the Control group was given random presentations of both the light and the footshock. Both groups received a compound stimulus of the light and tone paired with the footshock during Phase 2 training (Table 3). Intertrial intervals randomly ranged from 1 to 3 min. During probe trials, the light, tone, compound stimulus of the light and tone, and a high frequency FM tone (10–20 kHz, 65 dB, used as a comparison stimulus) were presented.

The number of stimuli was equated in the two groups so that neural effects could be linked to different kinds of training rather than to different number of stimuli presentations. Both groups received 16 presentations of the light and of the footshock in Phase 1. In the Blocking group, this excitatory training consisted of pairing the flashing light with a mild footshock, four trials a day for four days. In the Control group, 15 light and shock presentations were explicitly unpaired in separate sessions across four days of training. In addition to the 15 unpaired presentations, one paired presentation of the light and shock occurred after two days of training, resulting in a probability for light/shock pairing of 0.0625. This was done to minimize any potential for the light in the Control group to become habituated or to acquire properties consistent with conditioned excitation or conditioned inhibition. Phase 2 proceeded identically for both groups. The tone/light compound was paired with footshock four times a day for three days for a total number of 12 paired presentations. The first probe session day consisted of exposure to the context while meas-

Table 3. Behavioral design

Groups	Phase 1	Phase 2
Blocking	L→S	TL→S
Control	L, S	TL→S

Note: This table outlines the basic behavioral design used. L = flashing light, TL = low-frequency tone/flashing light compound, S = footshock.

ures of grooming, freezing, mobility, rearing and drinking were taken to access any contextual conditioning. The second and third probe session days consisted of 3 unreinforced presentations of each stimulus. Time spent drinking and latency to drink were measured.

Drinking was monitored for 15 seconds prior to the onset of the CS as well as during the CS presentation for the computation of suppression ratios, $CS_{drink\ time}/(pre\text{-}CS_{drink\ time} + CS_{drink\ time})$; (Kamin, 1969). Suppression ratios range from 0 to 0.5. A value of zero indicates that the animal suppressed drinking when the CS was presented and 0.5 indicates no change in drinking behavior with the presentation of the CS. A low suppression ratio indicates a higher degree of conditioned fear.

Upon completion of the training the rats were sacrificed, complete unfixed brains were extracted, frozen in isopentane at –40°C, and cut into serial 40 μm sections in a Reichert-Jung cryostat at –20°C. Sections were picked up on clean glass slides and processed by the quantitative C.O. histochemical procedure described in this volume (Gonzalez-Lima and Cada, 1998). A set of C.O. standards, preparation of which is also described this volume (Gonzalez-Lima and Cada, 1998), was sectioned at varying amounts of thicknesses (10, 20, 40, 60 and 80 μm). A set of standards was included with each batch of incubation medium for the generation of a single regression equation between C.O. activity and optical density of the sections for the subsequent comparison of all tissue in the present experiment. The brain homogenate was spectrophotometrically measured and activity units were defined at pH 7 and 37°C where 1 unit oxidizes 1 μmol of reduced cytochrome c per min (μ mol/min/g tissue wet weight).

The DCN, VCN, IC, and MGN were each analyzed in two ways, whole structure and tonotopically. The AC was analyzed in two ways as well, whole structure and by cell layer. Whole structure analysis involved taking four readings per section from three sections per brain (i.e., 12 readings per region per brain) for each region. Readings were taken from both hemispheres of the brain to avoid artifacts. For each region measured, the size of the measuring window of the densitometer was set to approximately one quarter the size of the whole region, and four adjacent sites were measured to cover the region. The size of this window was held constant across subjects. For example, a window of 7x7 pixels was used for the IC. Thus, for all animals, in each of three sections, four separate sites of a preset sample window were measured in such a way that the majority of each structure was measured, falling within the borders of the anatomical region of interest, and held constant across animals. For the tonotopic analysis, the structures were divided into isofrequency divisions based on the tonotopic organization, delineated by our fluorodeoxyglucose (FDG) studies (Gonzalez-Lima, 1992; Gonzalez-Lima & Agudo, 1990; Gonzalez-Lima & Scheich, 1984a,b, 1986) and O.D. measurements were taken from the low frequency 1–2 kHz tonotopic region corresponding to the CS and from a high frequency 10–20 kHz unstimulated tonotopic region for comparison. Laminar cortical analysis for the AC entailed taking three readings from each cell layer division (II/III, IV, V and VI) in each of three sections. Layer I was not quantified to avoid artifacts on the surface of the sections. The statistical significance of the results was tested with one-way analysis of variance (ANOVA), except where otherwise noted.

3.2. Behavioral and Neuronal Effects of the Blocking Phenomenon

Blocking of the tone conditioning was ascertained during three probe trials one hour before decapitation by measuring the amount of conditioned suppression of drinking to tone only presentations (Figure 7). A repeated measures ANOVA (group by trials) indicated that the tone mean conditioned suppression ratio for the Blocking group was significantly higher

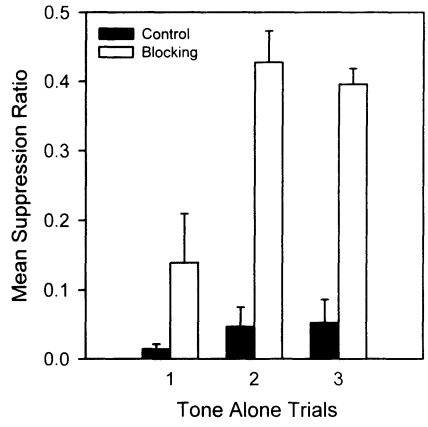

Figure 7. Mean ± standard error (SE) of conditioned suppression to drink during tone only presentations in Blocking (open bars) and Control (solid bars) groups. Suppression to drink is expressed as a ratio of time spent drinking during the tone presentation (A) divided by the sum of time spent drinking before (B) and during the tone (A/A+B). Low suppression ratios indicate strong excitatory control of behavior. The significantly higher suppression ratios in the Blocking group compared to the Control group support the prediction of little or no behavioral control by the tone in the Blocking group (From Poremba *et al.*, 1997).

than the Control group ($F[1,12] = 101.47$, $p < 0.0001$). These ratios indicate that, as predicted, the Blocking group did not suppress drinking behavior during the tone presentation, whereas the Control group did. As anticipated, the novel high frequency tone without any conditioning failed to produce significant conditioned suppression responses in the Blocking group. The high tone produced a mean ± SE suppression ratio of 0.28 ± 0.05 as would be expected of a novel tone without training presented in the excitatory context. Behavioral responding to the low tone (paired with footshock) was similar to that of the novel high frequency tone (not paired with footshock) used as comparator, suggesting that the small decrease in suppression ratios to the low tone were due to blocking during tone/light pairings with footshock. Behaviorally, both groups showed conditioned suppression responses to the light alone (mean ± S.E., Control = 0.14 ± 0.04, Blocking = 0.03 ± 0.02) and to the tone/light compound (mean ± S.E., Control = 0.06 ± 0.02, Blocking = 0.03 ± 0.01).

3.2.1. Blocking Phenomenon: Cytochrome Oxidase Activity in the Auditory System. When each whole auditory structure was assessed the ICC showed significantly higher overall C.O. activity in the Blocking group (mean ± S.E. = 251 ± 9 AU) than in the Control group (mean ± S.E. = 229 ± 3 AU; $F[1,12] = 5.20$, $p < 0.05$). Additionally, in the Blocking group the tonotopic stimulated 1–2 kHz frequency band in the IC was expanded from the ICC to the ICE as shown in Fig. 2, and mean C.O. activity was significantly higher for the Blocking group than for the Control group (11% increase, $F[1,12] = 5.89$, $p < 0.04$). The other auditory regions did not show significant overall C.O. activity changes.

To further investigate changes across the medial to lateral extent of the right IC for each subject, a vertical average measurement profile, consisting of average intensity for each column of approximately 100 pixels within a rectangular area, was measured. The rectangular area was subdivided into five equal divisions. This type of analysis yielded additional information about the changes in C.O. activation patterns elicited by the experimental conditions in the ICE. A repeated measures ANOVA of the profile analysis resulted in a significant interaction of group with division of the IC ($F[4,44] = 2.53$; $p < 0.05$). Post-hoc analysis indicated that the Blocking group had significantly greater C.O. activity in the ICE (most lateral division) relative to the Control group ($p < 0.05$). This increased C.O. activation in the Blocking group located in the ICE was mainly confined to the third layer which is composed of large multipolar neurons (Figure 2, upper and middle rows, Section 1.2.).

3.2.2. Tonotopic Ratios of C.O. Activity for Blocking and Control Groups. A ratio of the mean C.O. activity for the tone-stimulated (1–2 kHz) to unstimulated frequency bands

(10–20 kHz), within subjects, was estimated in auditory nuclei. Tonotopic low and high regions in the auditory nuclei could be easily separated based on comparable FDG autoradiographs of the effects of the two tone frequencies (Gonzalez-Lima & Scheich, 1984a,b; Ryan, Furlow, Woolf & Keithly, 1988; Gonzalez-Lima & Agudo, 1990; Gonzalez-Lima, 1992). This analysis included the low frequency tonotopic space (1–2 kHz) divided by the a high frequency tonotopic representation (10–20 kHz), in DCN, VCN, IC and MGN, irrespective of nuclear subdivisions (Figure 8). This tonotopic analysis revealed that for the DCN, the Blocking group mean ratio (26.60) was larger than the Control group (5.35; Mann-Whitney U test for ratios, $p < 0.05$). The other regions were not significantly different between groups for these relative tonotopic ratios.

3.2.3. Laminar Cortical Analysis for the Blocking Experiment. The primary, secondary, and tertiary areas of auditory cortex (Brodmann's areas 41, 36 and 20, respectively) were further analyzed by taking the density readings from cortical layers II and III together, and layers IV, V, and VI separately (Figure 9). This layer-by-layer comparison was done because C.O. activity was greater in the midlayers than in superficial and inner layers of the cortex. This laminar analysis revealed that in the secondary auditory cortex, layers II/III and IV of the Control group had significantly higher mean C.O. activity than the corresponding layers of the Blocking group (layers II/III: $F[1,12] = 6.4$, $p < 0.03$; layer IV: $F[1,12] = 6.09$, $p < 0.03$).

3.2.4. Discussion of C.O. Activity Results for the Blocking Experiment. The major findings of this study show that blocking tone conditioning modifies tissue metabolic responses in the auditory system. These findings support the hypothesis that tone CS processing is

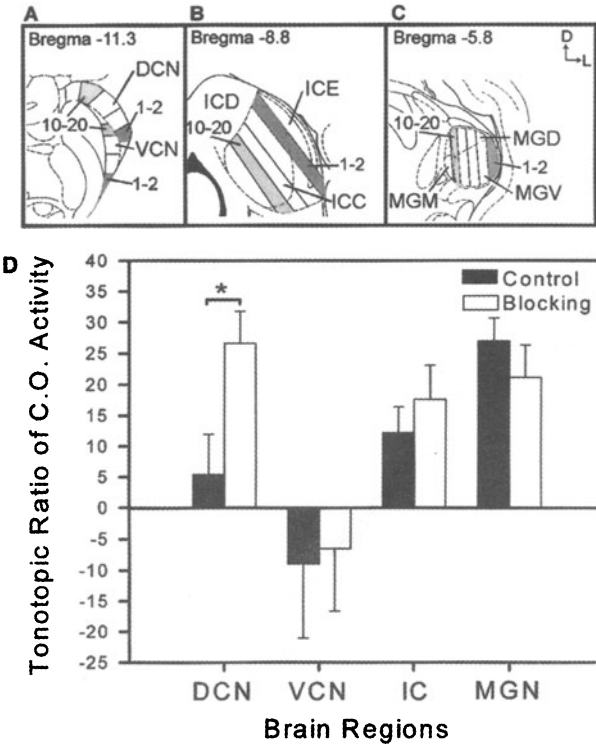

Figure 8. A–C) Schematic representations of the tonotopic frequency bands in the DCN, VCN, IC, and MGN. The bands (1–2 kHz and 10–20 kHz), from which mean activity values were collected to calculate tonotopic ratios of C.O. activity, are indicated for each brain region. D) Mean ± SE tonotopic ratios of C.O. activity are reported as tone-stimulated (dark-shaded areas in A–C) divided by unstimulated frequency bands (light-shaded areas in A–C) by brain region for the Control group (dark bars) and the Blocking group (open bars). The asterisk indicates a significant group difference of $p < 0.05$. DCN, dorsal cochlear nucleus; VCN, ventral cochlear nucleus; IC, inferior colliculus; MGN, medial geniculate nucleus (From Poremba *et al.*, 1997).

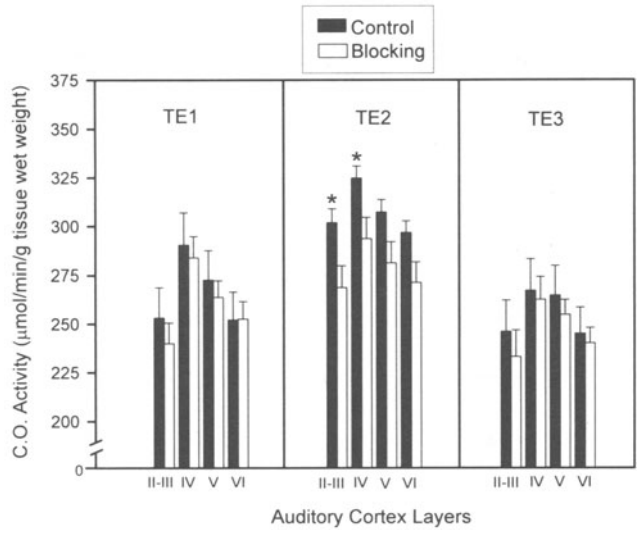

Figure 9. Mean ± SE C.O. activity (µmol/min/g tissue wet wt) for primary (TE1), secondary (TE2), and tertiary (TE3) auditory cortex by layer for the Control group (dark bars) and the Blocking group (open bars). Analysis of layer I is omitted due to folding problems that arise at the edge of the tissue. The asterisks indicate significant group differences at the $p < 0.03$ level (From Poremba *et al.*, 1997).

altered during blocking. These blocking effects are localized to regions with CS-US interactions, and these results can be used to help explain various behavioral effects of blocking proposed by learning theorists.

This blocking study focused on the plasticity of the auditory neural system. If blocking is strictly an order of "higher" functioning than the auditory system, then C.O. activity levels should have been similar for the Blocking group and the Control group. However, the results show a different pattern of auditory system C.O. activity between the groups (Figure 10).

The Blocking effects were localized to regions that allow for CS-US interactions. The auditory regions showing metabolic differences between Blocking and Control groups (DCN, IC and secondary auditory cortex) are the only auditory structures in the rat brain known to receive direct anatomical connections from somatosensory structures that carry tactile US information (Figure 11). Only two auditory structures receive direct somatosensory input from the dorsal column nuclei, DCN and IC (Weinberg & Rustioni, 1987; Aitken, Dickhaus, Schult & Zimmerman, 1978; Blomqvist & Wiberg, 1985; Bull & Berkley, 1984; RoBards, 1979; Willard & Martin, 1984). These overlapping anatomical inputs al-

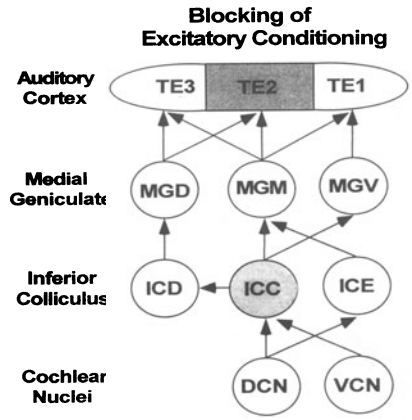

Figure 10. Schematic diagram of the auditory regions showing metabolic changes for the Blocking group. Higher regional C.O. activity in the Blocking group compared to the Control group are highlighted in gray. Major ascending connections within the auditory system of the rat brain are depicted with arrows. Abbreviation explanations can be found in Table 2.

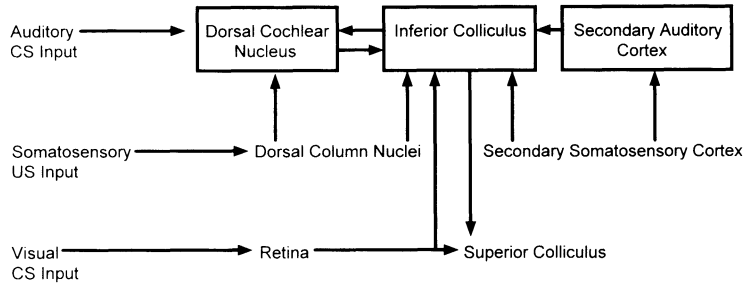

Figure 11. Schematic diagram of the auditory regions showing metabolic changes (enclosed in boxes) between the Blocking and Control groups. Anatomical connections (arrows) with somatosensory and visual structures in the rat brain are shown for the significant areas. Metabolic changes shown are for significant group differences in mean C.O. activity (inferior colliculus and secondary auditory cortex) and tonotopic ratios (dorsal cochlear nucleus) (From Poremba *et al.*, 1997).

low direct functional interactions between CS (auditory) and US (footshock) pathways at the DCN and IC levels. These two lower auditory structures are also the only two that receive descending information from non-auditory higher processing cortical structures (Beyerl, 1978; Coleman & Clerici, 1987; Shore, Helfert, Bledsoe, Altshuler & Godrey, 1991). The IC also receives auditory system feedback, from auditory cortex (Beyerl, 1978; Coleman & Clerici, 1987). These unique inputs to the DCN and IC may allow for integration of somatosensory US information with auditory CS information at a very early stage of tone processing.

In the particular case of tone conditioning blocked by previous conditioning to light stimulus, the IC may also play a key functional role for specific anatomical reasons. First, it is the obligatory site of convergence for ascending and descending auditory pathways that carry the CS information. Second, the IC is the only auditory structure in the rat that receives direct visual input, via retinal projections (Itaya & van Hoesen, 1982). Thus, in our blocking paradigm this intermodal pattern of connectivity in the IC allows a direct interaction between auditory, visual and somatosensory inputs during compound tone/light pairing with the US. The IC provides a central location where CS-US interaction, between the tone CS and the footshock US pathways, is anatomically linked to the light CS pathways.

The mild US footshock used in this study may evoke more general pain responses mediated by spinothalamic and reticular systems in addition to specific tactile somatosensory information mediated by the dorsal column system. The MGM receives inputs from the spinal cord (LeDoux, Ruggerio, Forest, Stornetta & Reis, 1987). Although a tone excitor can increase MGM activity as compared to an unpaired tone (Edeline & Weinberger, 1992; Gabriel, Saltwick & Miller, 1976), our tone blocking and excitor groups produced similar effects on the MGM. This suggests that blocking effects may not be mediated by spinothalamic pathways. In the case of the reticular system, ascending pathways influence the metabolic responses in all the auditory nuclei (Gonzalez-Lima & Scheich, 1984b). Therefore, it appears that only auditory nuclei with direct dorsal column inputs, carrying US tactile information, showed a greater metabolic response during blocking (DCN and IC).

The specificity of US tactile vs. pain information may be related to the greater metabolic response during blocking in some areas. Aversive stimuli may produce pain responses in spinothalamic and reticular systems, but perhaps the dorsal column convey the somatosensory pattern unique to the US footshock present during CS-US training in the blocking paradigm. A different, yet unique, somatosensory pattern may need to be evoked

by the US in addition to the pain input in order for conditioning to occur to a new stimulus in the tone/light compound. Support for this idea is strong when considering that previous behavioral experiments demonstrate that blocking is greatly reduced when the locus or intensity of the US is changed (Stickney & Donahoe, 1983; Wagner et al., 1980).

The pattern of results for auditory cortex is in agreement with findings demonstrating robust receptive field changes in auditory cortex specific to a behaviorally conditioned tone (Diamond & Weinberger, 1986; Weinberger, 1995). In this experiment, secondary auditory cortex is the one auditory system structure which showed a greater metabolic capacity for the Control (Conditioned Excitor) group compared with the Blocking group. In the Control group, layers II/III and IV of secondary auditory cortex exhibited significantly higher levels of mean C.O. activity compared with the Blocking group. This increase in auditory cortex may be due to the fact that only in the Control group does the tone presentation elicit a cued behavioral conditioned suppression response (Figure 11). These auditory cortex results are similar to those of Kinkaide and Walley (1974) in which recordings from visual cortex showed increased evoked potentials when the visual stimulus solely predicted the aversive event compared to when conditioning to the visual stimulus was blocked. Both experiments demonstrated increased activity in the sensory cortices of the Control groups. These Control groups both learned that a particular sensory signal came to predict an aversive event, compared with the Blocking groups, which presumably learned that the same particular sensory signal was irrelevant. This suggests that the cortical plasticity is related to the behavior, in this case, learned conditioned suppression. Interestingly, Walley (1982) did not find a specific effect related to blocking of the visual stimulus in lateral geniculate nucleus which is in agreement with our negative findings in medial geniculate nucleus.

The pattern of C.O. activity for the Blocking group may be compared to the findings of a previous study which investigated 2-deoxyglucose (2-DG) uptake during short- and long-term habituation to tone stimuli. Increased 2-DG uptake during long-term habituation was observed in the IC and DCN as well as other lower auditory structures (Gonzalez-Lima, Finkenstaedt & Ewert, 1989). These findings correspond well with the results of this study and may be relevant because long-term habituation produces a lack of responding to the habituated auditory stimulus, i.e., a kind of behavioral inhibition, similar to the blocking effects.

The previous long-term habituation data, further analyzed using a functional interactions approach, also demonstrated that the descending influence of the auditory cortex to the ICE was prominently involved during long-term habituation (McIntosh & Gonzalez-Lima, 1992). In the present study, the third layer of the ICE showed significantly higher mean C.O. activity for the Blocking group compared to the Control group. Long-term habituation to the sensory stimulus may be analogous to the metabolically active process of the blocking phenomenon in the auditory system. The subjects exhibiting the blocking phenomenon are, in effect, showing behavioral inhibition to the tone, similar to repeated tone alone stimulus presentations which result in behavioral habituation. This descending influence from auditory cortex to ICE may reduce the signal component associated with the tone since the ICE is part of the descending corticofugal extra-lemniscal system (McIntosh & Gonzalez-Lima, 1992). The extra-lemniscal system is proposed to relay non-tonotopic qualities of the auditory stimulus, and may be related to stimulus signal value.

The results of this blocking study have important implications regarding the learning theory behavioral hypotheses of blocking. Behavioral observations of the blocking phenomenon have inspired a number of theories about conditioning (Mackintosh, 1983, Pearce & Hall, 1980; Rescorla & Wagner, 1972). Our neural mapping results may help to

resolve a specific issue surrounding this phenomenon. While the Rescorla-Wagner model (1972) emphasizes US processing in establishing the CS-US associations, Mackintosh (1983) and others (Holland & Gallagher, 1993; Solomon, 1977) emphasize CS attentional and information processes. We propose that blocking is related to the spatio-temporal interaction of CS-US pathways in the brain. Since blocking takes place at central points where interaction between CS and US inputs in the brain are occurring, independent changes in either CS or US parameters would be sufficient, but not necessary to produce the blocking effect. What appears necessary for blocking to occur is a change in the processing of the CS-US interactions in the brain. Such a change can also be accomplished by altering the temporal relationship between the CS and the US from Phase 1 to Phase 2 (see Table 1) of training (Barnet, Grahame & Miller, 1993), without the need to independently modify CS or US parameters. Similarly, changing excitatory time cues during training is sufficient to block conditioned responses to the tone CS (Williams & LoLordo, 1995).

Holland and Gallagher (1993) state that it is the processing of the CS, a shift in attention, that changes during blocking, which our results partially support. However, the metabolic changes in the auditory system are not consistent with a simple lack of "attention" to the blocked tone, as could be argued if the tone had generally resulted in lower metabolism in the auditory system of tone blocked as compared to tone excitor animals. Instead, the metabolically active changes related to the neural processing of the CS occur in auditory structures where the US signal interacts with the tone signal. Alterations in the US signal by behavioral manipulations would therefore be expected to affect the blocking phenomenon, as demonstrated by previous behavioral experiments (Goddard, 1996) and theoretically by the Rescorla-Wagner model (1972). Our neural findings are more consistent with explanations of blocking based on the interaction of the CS with the US, rather than independent CS or US effects. Anatomical convergence of CS and US sensory pathways in the auditory system (DCN and IC) permits the functional interaction of auditory (tone CS) and somatosensory (footshock US) sensory effects, i.e., auditory-somatosensory stimuli association. Therefore, our findings are more in line with blocking hypotheses based on altered CS-US interactions, such as the hypothesis of temporal coding proposed by Barnet, et al., (1993), which is based on behavioral blocking studies with simultaneous and forward CS-US pairings.

4. APPLICATION OF QUANTITATIVE C.O. HISTOCHEMISTRY TO THE STUDY OF DIFFERENTIAL INHIBITION

The last experiment involved assessing whether or not there is learning related neural plasticity in the auditory system in response to a safety signal, i.e., a negative conditioned stimulus (CS-) that is never paired with an aversive US during conditioning (Shin et al., 1997). Although a negative contingency between the CS^- and the US does not produce a conditioned fear response, associative learning does occur. The training of the differential inhibitor involved intermingling CS alone presentations with excitatory training. In a differential inhibition protocol involving an aversive event as the US, the trained inhibitor becomes a signal of safety. The experimental group training and the control condition (pseudorandom stimuli presentations) are nearly identical throughout training. Because there is no discrete reinforcer paired with the CS in either the experimental or control conditions, this paradigm was instrumental in determining if the C.O. technique could distinguish learning related maps between these highly similar training conditions.

4.1. Experimental Design and Methods for Differential Inhibition Experiment

Naive age-matched male Long Evans, black-hooded rats weighing an average of 100g (aprox. 33 days old) from the supplier (Harlan) were used. All animals were weighed daily for one week prior to training, to adapt to their new surroundings and to being handled. Subjects were housed under standard laboratory conditions (12:12, light:dark cycle), 2 to 3 to a cage and given food ad libitum. There were 11 rats in the Differential Inhibitor group and 11 rats in the Pseudorandom group.

A conditioned emotional response (CER) procedure was used to ascertain the amount of associative control acquired by the stimulus. Changes in baseline drinking in response to test stimulus presentations were used as an indication of conditioning. Training in the Differential Inhibition group consisted of reinforced presentation of a light stimulus intermingled with unreinforced presentations of a tone stimulus (Table 4). Subjects in the Pseudorandom group received the same number and type of stimulus presentations, but in a pseudorandom order.

Behavioral testing was done for three days between the second and third training sessions. The first day of testing consisted of exposure to the context while measures of grooming, freezing, mobility, rearing and drinking were taken by the same trained, "blind" observer for each session to assess any contextual conditioning for both experimental groups. The second and third days of testing consisted of behavioral probe trials where unreinforced presentations of each stimulus, the light, tone, compound stimulus of the light and tone, and a high frequency FM tone (10–20 kHz, 65 dB, used as a comparison stimulus) were presented to both experimental groups. Time spent drinking and latency to drink were measured.

Drinking was monitored for 15 seconds prior to the onset of the CS as well as during the CS presentation for the computation of suppression ratios, $CS_{\text{drink time}}/(\text{pre-}CS_{\text{drink time}} + CS_{\text{drink time}})$; (Kamin, 1969). Suppression ratios range from 0 to 0.5. A value of zero indicates that the animal suppressed drinking when the CS was presented and 0.5 indicates no change in drinking behavior with the presentation of the CS. A low suppression ratio indicates a higher degree of conditioned fear.

Upon completion of the training the rats were decapitated, complete unfixed brains were extracted, frozen in isopentane at –40°C, and cut into serial 40 μm sections in a Reichert-Jung cryostat at –20°C. Sections were picked up on clean glass slides and processed by the quantitative C.O. histochemical procedure described in this volume (Gonzalez-Lima and Cada, 1998). A set of C.O. standards, preparation of which is also described in this volume (Gonzalez-Lima and Cada, 1998), was sectioned at varying amounts of thicknesses (10, 20, 40, 60 and 80 μm). A set of standards was included with each batch of incubation medium for the generation of a single regression equation be-

Table 4. Behavioral design

Groups	Phase 1	Phase 2
Differential	L→S	L→S
Inhibition		T
Pseudorandom	L, S	T, L, S

Note: This table outlines the basic behavioral design used. L = flashing light, TL = low-frequency tone/flashing light compound, S = footshock.

tween C.O. activity and optical density of the sections for the subsequent comparison of all tissue in the present experiment. The brain homogenate was spectrophotometrically measured and activity units were defined at pH 7 and 37°C where 1 unit oxidizes 1 μmol of reduced cytochrome c per min (μ mol/min/g tissue wet weight).

Using the adjacent sections stained for Nissl substance, representative sections of the eleven auditory regions of interest from each brain were chosen. A stereotaxic atlas of the rat brain (Paxinos & Watson, 1986) was used to select rat brain sections that approximately matched the auditory system structures: the dorsal and ventral cochlear nuclei (DCN and VCN; Bregma −11.3 mm); trapezoid nucleus and olivary complex (Bregma −9.8 mm); nuclei of the dorsal and lateral lemniscus (Bregma −8.3 mm); external (ICE), central (ICC), and dorsal (ICD) nuclei of the inferior colliculus (IC; Bregma −8.3 mm); the medial (MGM), dorsal (MGD), and ventral (MGV) divisions of the medial geniculate nucleus (MGN; Bregma −5.8 mm); and three divisions of auditory temporal cortex (TE1, TE3; Bregma −5.8 mm and TE2; Bregma −8.3 mm; Brodmann's areas 41, 20 and 36, respectively).

The optical density (O.D.) in the C.O. stained sections was analyzed using an image-processing system as described in this volume (Chapter by Gonzalez-Lima and Cada, 1998). The system was calibrated using an O.D. step tablet (Kodak) and the histochemical reaction product (chromatic indicator of C.O.) was measured in O.D. units. The images were corrected for optical distortions from the camera through subtraction of the background (a slide coverslipped with Permount without brain tissue). Using a single regression equation between C.O. activity and O.D., a calibration curve was created using the C.O. standards (Gonzalez-Lima and Jones, 1994). These standards were linear in the range of thicknesses described above. Subsequent densitometric measures taken from brain sections were then expressed in terms of C.O. activity units (μmol/min/g tissue wet weight).

For the tonotopic analysis, the structures were divided into isofrequency divisions based on the tonotopic organization, delineated by our fluorodeoxyglucose (FDG) studies (Gonzalez-Lima, 1992; Gonzalez-Lima & Agudo, 1990; Gonzalez-Lima & Scheich, 1984a,b, 1986) and O.D. measurements were taken from the low frequency 1–2 kHz tonotopic region corresponding to the CS- and from a high frequency 10–20 kHz unstimulated tonotopic region for comparison. Laminar cortical analysis for the auditory cortex entailed taking three readings from each cell layer division (II/III, IV, V and VI) in each of three sections for all primary, secondary and tertiary auditory cortices. Layer I was not quantified to avoid artifacts on the surface of the sections. Analysis of variance (ANOVA) and post-hoc tests [Tukey's Honest Significant Difference Test (HSD)] were used to test the statistical significance of the results at $p < 0.05$.

The Differential Inhibition group received one day of four pairings of a light (CS+, flashing at 10 Hz) with a mild footshock (US). This resulted in the light becoming a conditioned excitor (CS+). Following CS+ training were four days of paired L-US trials intermingled with tone (CS-, 1–2 kHz) presentations unpaired with the shock. The Pseudorandom group received pseudorandom presentations of the light, tone and shock stimuli in equal number to the Differential Inhibition group.

4.2. Behavioral and Neural Effects of Differential Inhibition

Assessment of conditioning to the tone showed distinct behaviors in the two groups. A ratio of 0.5 indicates little associative control, while a ratio of 0.1 indicates strong control. In the group trained with the light as a CS+ and the tone as a CS– significantly more suppression was seen to the light than to the tone ($p < 0.001$). In the Pseudorandom group

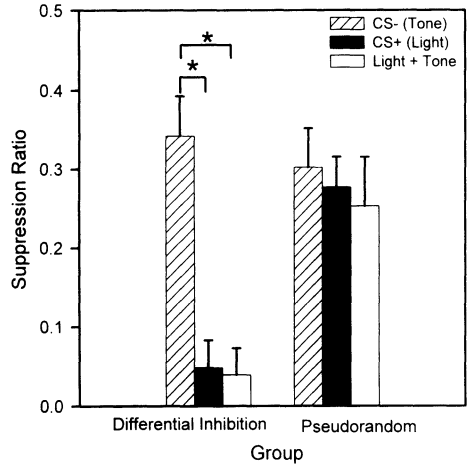

Figure 12. Mean ± standard error (SE) of conditioned suppression to drink during stimuli presentations in the Differential Inhibition (left) and Pseudorandom (right) groups. Assessment of conditioning to the tone showed distinct behaviors in the two groups. In the Differential Inhibition group, trained with the light as a CS+ and the tone as a CS–, significantly more suppression was seen to the light than to the tone. In the Pseudorandom group no significant differences were seen. This supports the prediction that explicitly unpaired presentations produce inhibitory control, while random presentations do not result in significant control. The asterisks indicate significant group differences at the $p < 0.001$ level.

no significant differences were seen. This supports the prediction that explicitly unpaired presentations produce inhibitory control, while random presentations do not result in significant control (Fig. 12).

When each whole auditory structure was assessed five neuronal areas showed mean differences in C.O. activity between the Differential Inhibitor group and the Pseudorandom control group. Specifically, the dorsal nucleus of the lateral lemniscus (LLD), medial nucleus of the medial geniculate nucleus (MGM), dorsal nucleus of the medial geniculate nucleus (MGD), primary auditory cortex (TE1), and secondary auditory cortex (TE2) showed significantly higher overall C.O. activity in the Differential Inhibition group than in the Pseudorandom group (Table 5). The other auditory regions did not show significant overall C.O. activity changes.

Table 5. Regional enzymatic activity of cytochrome oxidase in the brains of Differential Inhibitor and Pseudorandom groups of animals

Structure	Differential inhibitor Mean ± S.E.	Pseudorandom Mean ± S.E.
Dorsal cochlear N. (DCN)	562.10 ± 25.87	556.78 ± 34.34
Ventral cochlear N. (VCN)	397.16 ± 21.74	387.78 ± 26.00
Medial superior olivary N. (MSO)	347.09 ± 27.59	317.52 ± 30.14
Lateral superior olivary N. (LSO)	403.03 ± 31.44	372.30 ± 28.65
Trapezoid body N. (TBN)	161.03 ± 6.60	156.01 ± 3.81
Dorsal N. lateral lemniscus (LLD)	323.51 ± 22.49	270.20 ± 11.00*
Ventral N. lateral lemniscus (LLV)	453.96 ± 26.11	447.74 ± 25.56
Central N. inferior colliculus (ICC)	421.47 ± 31.81	404.69 ± 25.22
Dorsal N. inferior colliculus (ICD)	355.87 ± 27.61	392.47 ± 23.39
External N. inferior colliculus (ICE)	321.88 ± 28.87	354.47 ± 16.37
Medial N. MGN (MGM)	208.24 ± 15.59	144.93 ± 15.09*
Dorsal N. MGN (MGD)	181.14 ± 12.90	144.48 ± 9.58*
Ventral N. MGN (MGV)	234.28 ± 19.25	181.85 ± 16.97
Primary auditory cortex (TE1)	242.73 ± 11.97	212.11 ± 13.43*
Secondary auditory cortex (TE2)	220.39 ± 13.64	190.63 ± 10.20*
Tertiary auditory cortex (TE3)	222.85 ± 11.71	200.83 ± 16.97

Mean ± standard error (S.E.) units in μmol/min/g tissue wet weight were obtained by averaging measurements from three consecutive brain sections per neuronal area for each subject. An asterisk denotes a significant difference between the two groups ($p < 0.05$).

Tonotopic ratios revealed differences in processing of the tone stimulus. A within-subjects ratio of the mean C.O. activity for the tone-stimulated (1–2 kHz) to unstimulated frequency bands (10–20 kHz) was estimated in auditory nuclei where tonotopic low and high regions could be easily separated based on comparable FDG autoradiographs of the effects of the two tone frequencies (Gonzalez-Lima & Scheich, 1984a,b; Ryan, Furlow, Woolf & Keithly, 1988; Gonzalez-Lima & Agudo, 1990; Gonzalez-Lima, 1992). Ratios were computed by dividing CO activity in the tonotopic representation of the CS- by the activity in the tonotopic representation of a non CS frequency. Tonotopic ratios revealed differences in processing of the tone stimulus. Both the VCN and the IC had a relatively higher ratio of activity when the tone was a differential inhibitor than when it was a pseudorandom tone (Figure 13; Mann-Whitney U test for ratios, $p < 0.05$).

4.3. Discussion of C.O. Activity Results for the Differential Inhibition Experiment

Although the auditory stimulus was not paired with the reinforcing footshock in either the experimental or control groups, conditioning to the tone signal (CS–) occurred in the Differential Inhibition group when the CS– and US were unpaired in a predictable manner even though the CS- was not paired with a reinforcing footshock. Rather, the absence of the footshock paired with the tone in the same training session where light was paired with footshock was sufficient for the tone to become a differential inhibitor. The animals in the Pseudorandom group did not acquire significant behavioral control to the light or tone signals when they had no predictable relationship with the US.

In addition to the difference in behavioral learning between the Differential Inhibition group and the Pseudorandom group, significant differences in the oxidative metabolic capacity of the auditory system were evident (Figure 14). The Differential Inhibitor group showed increased mean C.O. activity in the nuclei of the dorsal lateral lemniscus and medial geniculate and in the primary and secondary auditory cortex in comparison to the

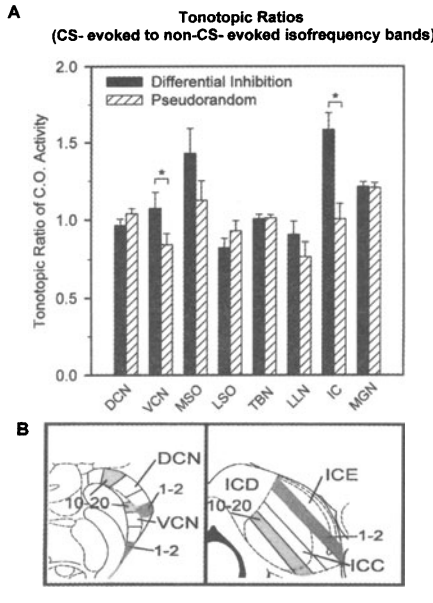

Figure 13. A) Tonotopic ratios revealed differences in processing of the tone stimulus as a result of training. B) Ratios were computed by dividing C.O. activity in the tonotopic representation of the CS– by the activity in the tonotopic representation of a non CS frequency. Both the VCN and the IC had relatively higher activity when the tone training was for differential inhibition (dark bars) than when it was as a pseudorandom tone (hatched bars).

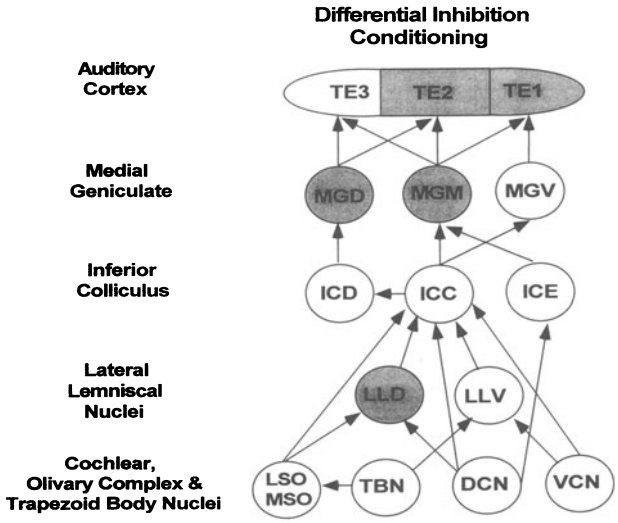

Figure 14. Schematic diagram of the auditory regions showing the metabolic changes for the Differential Inhibition group. Areas shaded in gray indicate regions with significantly higher C.O. activity in the Differential Inhibition group compared to the Pseudorandom group. Major ascending connections within the auditory system of the rat brain are depicted with arrows.

Pseudorandom group. Further analyses showed changes in the tonotopic representation of the auditory stimulus between groups. Tonotopic ratios of CS– to non-CS– representation showed increased metabolic capacity in the Differential Inhibition group compared to the Pseudorandom group in the ventral cochlear nucleus and inferior colliculus.

These findings suggest that differential inhibition may not simply be stimulus habituation, although behaviorally these two conditions look similar. In the conditioned suppression paradigm, differential inhibition entails conditioning of a safety signal rather than habituation to the tone stimulus. These metabolic imaging results show that processing of an auditory stimulus conditioned as a differential inhibitor is qualitatively different from processing of a pseudorandom tone, even though the behavioral response to the tone was similar in both groups throughout training.

5. GENERAL DISCUSSION OF THE THREE LEARNING SITUATIONS FUNCTIONALLY MAPPED IN THE AUDITORY SYSTEM WITH C.O. QUANTITATIVE HISTOCHEMISTRY

The findings of these three studies suggest that excitatory conditioning, inhibitory conditioning and the blocking phenomenon produce changes in auditory processing that are qualitatively different (Figure 15). The results of the three experiments reviewed in this chapter can now be considered in relationship to each other since the number of stimuli presented was the same for all three experiments.

One general conclusion that can be drawn from all three experiments is that the once-held view of non-plastic sensory neurons that are exclusively concerned with detection of physical stimulus properties needs to be replaced with a more inclusive view that sensory neurons are involved in behavioral stimulus properties acquired by learning. This view is supported by the present C.O. studies as well as previous FDG metabolic studies (Gonzalez-Lima & Sheich, 1984a,b, 1986; Gonzalez-Lima, Finkenstaedt & Ewert, 1989; Gonzalez-Lima & Agudo, 1990; Gonzalez-Lima, 1992; Gonzalez-Lima & McIntosh, 1994, 1996; McIntosh & Gonzalez-Lima, 1991, 1993, 1995; Cahill, Ohl & Scheich, 1996; Scheich, Simonis, Ohl, Tillein & Thomas, 1993), and electrophysiological studies showing

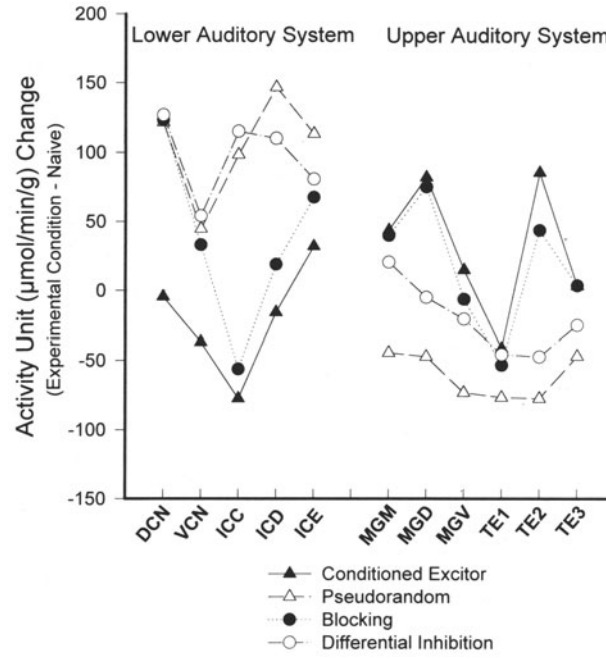

Figure 15. Summary graph of auditory system regional deviations in C.O. activity from Naive baseline for the Conditioned Excitor (Control), Pseudorandom, Blocking, and Differential Inhibition groups. Values are expressed as the difference in mean C.O. activity of the Naive group from the mean C.O. activity for each experimental condition.

the development of auditory system learning-related plasticity (Buchwald, Halas & Schramm, 1966; Gabriel, et al., 1976; Weinberger, 1995).

In excitatory conditioning a CS comes to elicit responses that are related to the US whereas in blocking that conditioning is not seen due to previous learning; while in differential inhibition, the CS comes to control or elicit a response opposite to that of an excitor. Interesting comparisons can be made across all these groups to reveal differences in auditory processing due to such aspects of training as CS-US contiguity and CS associative control of the US.

Cytochrome oxidase activity levels for Conditioned Excitor and Blocking groups are similar in their patterns for the lower and upper auditory systems whereas the Differential Inhibition and Pseudorandom groups are similar in a reversed pattern (Figure 15). The Conditioned Excitor and the Blocking group may have similar activity patterns because in both of these groups the tone is paired with footshock US; whereas in the Differential Inhibition and Pseudorandom groups the tone is not generally paired with the footshock US. Additionally, as compared to naive rats (baseline on Figure 15), enhanced C.O. activity in MGM, MGD and TE2 was a common finding shared by the two groups trained with tone CS-US contiguity. This suggests that these upper auditory structures may participate in the contiguity aspect of Pavlovian conditioning, independently of whether a conditioned response is present (Conditioned Excitor group) or absent (Blocking group).

Cytochrome oxidase activity in the DCN is elevated above naive levels for all groups except for the Conditioned Excitor group (Figure 15). One commonality among the other three groups, Pseudorandom, Blocking and Differential Inhibition, is that these animals do not display a tone-contingent fear response throughout training, but the Conditioned Excitor group does. The increased C.O. activity in the DCN for these three groups may be the result of normal processing due to hearing a tone repeatedly, whereas the DCN may be actively inhibited due to encoding of the fear associated with the tone in the Conditioned Excitor group. In the case of the Conditioned Excitor group animals freeze to the

tone throughout the training experience and this response continues with later presentations of the tone. In the case of the Blocking group, during training the animals also freeze to tone presentations because the tone is part of the compound stimulus of tone and light paired with footshock. However, when the tone is presented alone to these animals the freezing behavior is not seen indicating that blocking has occurred. In the other two groups, Differential Inhibition and Pseudorandom, tone was not consistently paired with the footshock and freezing did not consistently occur after tone presentations. The DCN activity values for all groups are not separated by whether or not the animal is experiencing CS-US contiguity or freezing during training. The groups are separated by whether or not that condition results in a conditioned freezing response to the tone CS alone; that is, the tone becomes an excitor and elicits the conditioned response.

In general, the Pseudorandom group has decreased C.O. activity in the upper auditory system in relation to the groups where some type of learning to the tone is seen (Conditioned Excitor, Blocking and Differential Inhibitor groups). The notable exceptions to this are MGV, TE1 and TE3, where the learning groups are similar or lower in C.O. activity as compared to the naive rats (Figure 15). TE1 processing seems more similar to a random tone than a tone with learned significance. This is consistent with findings that lemniscal neurons have narrow frequency tuning whereas non-lemniscal neurons generally have broader tuning and greater response plasticity, including modification of frequency receptive fields during learning (Lennartz and Weinberger, 1992). Modification of interactions in non-lemniscal pathways have been proposed to mediate the learned signal value of auditory stimuli (McIntosh and Gonzalez-Lima, 1993). Auditory cortical area TE1 appears to be processing strictly the tone information, with no significant differences due to specific training conditions. This contrasts with the non-lemniscal auditory region, TE2, which shows increased C.O. activity when the tone is paired with the US.

The cytochrome oxidase histochemistry has allowed us to view different patterns in the auditory system even when behavioral outcomes of conditioning were the same (eg. Pseudorandom vs Differential Inhibition). This is a powerful technique for the initial identification of the areas which may be learning-related before attempting more reductionistic studies such as neuronal recordings, electron-microscopy, synaptic modification, etc.. Collectively, these findings illustrate that mapping the metabolic activity of C.O. with quantitative histochemistry can be successfully used to reveal learning effects on the brain.

ACKNOWLEDGMENTS

We thank Alison Crane for reading and editing drafts of this chapter. Supported by NIH grant MH43353 and NSF grant IBN9222075 to F.G.L. and NIH grant T32 MH18837 to A.P.

REFERENCES

Aitken, L.M., Dickhaus, H., Schult, W., and Zimmermann, M. (1978). External nucleus of inferior colliculus: Auditory and spinal somatosensory afferents and their interactions. *J. Neurphysiol.*, 41, 837–846.

Barnet, R.C., Grahame, N.J., and Miller, R.R. (1993). Temporal encoding as a determinant of blocking. *J. Exp. Psychol.*, 19, 327–341.

Beyerl, B.D. (1978). Afferent projections to the central nucleus of the inferior colliculus of the rat. *Brain Res.*, 145, 209–223.

Blomquist, A., and Wiberg, M. Some aspects of the anatomy of somatosensory projections to the cat midbrain. In M. Rowe and W.D. Willis (Eds.), *Development, Organization, and Processing in Somatosensory Pathways:*

The proceedings of a satellite symposium of the International Congress of Physiological Sciences. Liss., New York, 1985, pp. 215–222.

Braun, K., Scheich, H., Schachner, M., and Heizmann, C.W. (1985a). Distribution of parvalbumin, cytochrome oxidase activity and ^{14}C-2-deoxyglucose uptake in the brain of the zebra finch I. Auditory and vocal motor systems. *Cell Tissue Res.*, 240, 101–115.

Braun, K., Scheich, H., Schachner, M., and Heizmann, C.W. (1985b). Distribution of parvalbumin, cytochrome oxidase activity and ^{14}C-2-deoxyglucose uptake in the brain of the zebra finch II. Visual system. *Cell Tissue Res.*, 240, 117–127.

Buchwald, J.S., Halas, E.S., and Schramm, S. (1966). Changes in cortical and subcortical unit activity during behavioral conditioning. *Physiol. Behav.,* 1, 11–22.

Bull, M.S., and Berkley, K.J. (1984). Differences in the neurons that project from the dorsal column nuclei to the diencephalon, pretectum and tectum in the cat. *Somatosens. Res.,*1, 281–300.

Cahill, L., Ohl, F., and Scheich, H. (1996). Alteration of auditory cortex activity with a visual stimulus through conditioning: A 2-deoxyglucose analysis. *Neurobio. Learn. Mem.,* 65, 213–222.

Castellucci, V.F., Carew, T.J., and Kandel, E.R. (1978). Cellular analysis of long-term habituation of the gill-withdrawal reflex of Aplysia californica. *Science* 202, 1306–1308.

Coleman, J.R., and Clerici W.J. (1987). Source of projections to subdivisions of the inferior colliculus in the rat. *J. Comp. Neurol.,* 262, 215–226.

Dantzer, R. and Delacour, J. (1972). Modification of a phenomenon of conditioned suppression by a thalamic lesion. *Physiol. Behav.,* 8, 997–1003.

Davis, M. (1994). The role of the amygdala in emotional learning. *Int. Rev. Neurobiol.,* 36, 225–66.

de la Torre, J.C., Cada, A., Nelson, N., Davis, G., Sutherland, R.J., and Gonzalez-Lima, F. (1997). Reduced cytochrome oxidase and memory dysfunction after chronic brain ischemia in aged rats. *Neurosci. Lett.,* 223, 165–168.

Diamond, D.M. and Weinberger, N.M. (1986). Classical conditioning rapidly induces specific changes in frequency receptive fields of single neurons in secondary and ventral ectosylvian auditory cortical fields. *Brain Res.,* 372, 357–360.

Domjan, M. (1996). *The essentials of conditioning and learning*, Brooks/Cole Publishing Company, Pacific Grove, CA.

Edeline, J.M., Neuenschwander-el Massioui, N., and Dutrieux, G. (1990). Discriminative long-term retention of rapidly induced multiunit changes in the hippocampus, medial geniculate and auditory cortex. *Behav. Brain Res.*, 39, 145–155.

Edeline, J.M., Pham, P., and Weinberger, N.M. (1993). Rapid development of learning-induced receptive field plasticity in the auditory cortex. *Behav. Neurosci.*, 107, 539–51.

Edeline, J.M., and Weinberger, N.M. (1992). Associative retuning in the thalamic source of input to the amygdala and auditory cortex: Receptive field plasticity in the medial division of the medial geniculate body. *Behav. Neurosci.,* 106, 81–105.

Freeman, F.M., Rose, S.P., and Scholey, A.B. (1995). Two time windows of anisomycin-induced amnesia for passive avoidance training in the day-old chick. *Neurobiol. Learning & Mem.*, 63, 291–295.

Fride, E., Ben-Or, S., and Allweis, C. (1989). Mitochondrial protein synthesis may be involved in long-term memory formation. *Pharm. Biochem. & Beh.*, 32, 873–878.

Gabriel, M., Miller, J.D., and Saltwick, S.E. (1976). Multiple-unit activity of the rabbit medial geniculate nucleus in conditioning, extinction, and reversal. *Physiol. Psychol.,* 4, 124–134.

Gabriel, M. Saltwick, S.E., and Miller, J.D. (1975). Conditioning and reversal of short-latency multiple-unit responses in the rabbit medial geniculate nucleus. *Science*, 189(4208), 1108–1109.

Gallo, M., and Candidio, A. (1995). Dorsal hippocampal lesions impair blocking but not latent inhibition of taste aversion learning in rats. *Behav. Neurosci.*, 109, 413–425.

Goddard, M.J. (1996). Effect of US signal value on blocking of a CS-US association. *J. Exp. Psychol. Anim. Behav. Process.,* 22, 258–264.

Gonzalez-Lima, F. Brain imaging of auditory learning functions in rats: Studies with fluorodeoxyglucose autoradiography and cytochrome oxidase histochemistry. In F. Gonzalez-Lima, T. Finkenstädt, and H. Scheich (Eds.), *Advances in Metabolic Mapping Techniques for Brain Imaging of Behavioral and Learning Functions.* NATO ASI Series D Vol. 68, Kluwer Academic Publishers, Dordrecht/Boston/London, 1992, pp. 39–109.

Gonzalez-lima, F., and Agudo, J. (1990). Functional reorganization of neural auditory maps by differential learning. *Neuroreport*, 1, 161–164.

Gonzalez-Lima, F., and Cada, A. (1994). Cytochrome oxidase activity in the auditory system of the mouse: A qualitative and quantitative histochemical study. *Neuroscience,* 63, 559–578.

Gonzalez-lima, F., Finkenstädt, T., and Ewert, J.-P. (1989). Neural substrates for long-term habituation of the acoustic startle reflex in rats: A 2-deoxyglucose study. *Neurosci. Letters,* 96, 151–156.

Gonzalez-Lima, F., Finkenstädt, and T., Ewert, J.P. (1989). Learning-related activation in the auditory system of the rat produced by long-term habituation: A 2-deoxyglucose study. *Brain Res.*, 489, 67–79.

Gonzalez-Lima, F. and Garrosa, M. (1991). Quantitative histochemistry of cytochrome oxidase in rat brain. *Neurosci. Lett.*, 123, 251–253.

Gonzalez-Lima, F., and Jones, D. (1994). Quantitative mapping of cytochrome oxidase activity in the central auditory system of the gerbil: A study with calibrated activity standards and metal-intensified histochemistry. *Brain Res.*, 660, 34–49.

Gonzalez-Lima, F., and McIntosh, A.R. (1994). Neural network interactions related to auditory learning analyzed with structural equation modeling. *Hum. Brain Mapping*, 2, 23–44.

Gonzalez-Lima, F., and McIntosh, A.R. Conceptual and methodological issues in the interpretation of brain-behavior relationships. In R.W. Thatcher, G.R. Lyon, J. Rumsey, and N. Krasnegor (Eds.), *Developmental Neuroimaging: Mapping the Development of Brain and Behavior.* Academic Press, New York, 1996, pp. 235–253.

Gonzalez-lima, F., and Scheich, H. (1986). Classical conditioning of tone-signaled bradycardia modifies 2-deoxyglucose uptake patterns in cortex, thalamus, habenula, caudate-putamen and hippocampal formation. *Brain Res.*, 363, 239–256.

Gonzalez-Lima, F., and Scheich, H. (1984a). Classical conditioning enhances auditory 2-deoxyglucose patterns in the inferior colliculus. *Neurosci. Ltrs.*, 51, 79–85.

Gonzalez-Lima, F., and Scheich, H. (1984b). Neural substrates for tone-conditioned bradycardia demonstrated with 2-deoxyglucose. I. Activation of auditory nuclei. *Behav. Brain Res.*, 14, 213–233.

Gonzalez-Lima, F., Valla, J., and Matos-Collazo, S. (1997). Quantitative cytochemistry of cytochrome oxidase and cellular morphometry of the human inferior colliculus in control and Alzheimer's patients. *Brain Res.*, 752, 117–126.

Holland, P.C., and Gallagher, M. (1993). Effects of amygdala central nucleus lesions on blocking and unblocking. *Behav. Neurosci.*, 107(2), 235–245.

Iwata, J., LeDoux, J.E., Meeley, M.P., Arneric, S. and Reis, D.J. (1986) Intrinsic neurons in the amygdaloid filed projected to by the medial geniculate body mediate emotional responses conditioned to acoustic stimuli. *Brain Res.*, 383, 195–214.

Itaya, S.K., and van Hoesen, G.W. (1982). WGA-HRP as a transneuronal marker in the visual pathways of monkey and rat. *Brain Res.*, 236, 199–204.

Jarrell, T.W., Gentile, C.G., McCabe, P.M., and Schneiderman, N. (1986). The role of the medial geniculate region in differential Pavlovian conditioning of bradycardia in rabbits. *Brain Res.*, 374, 126–136.

Kamin, L.J. Predictability, surprise, attention, and conditioning. In B. A. Campbell and R. M. Church (Eds.), *Punishment and Aversive Behavior.* Appleton-Century-Crofts, New York, 1969, pp. 242–259.

Kinkaide, P.S., and Walley, R.E. (1974). Visual evoked potentials during stimulus selection in eyelid conditioning in the rabbit (*oryctolagus cuniculuc*). *J. Comp. Physiol. Psychol.*, 87(3), 481–494.

Kleim, J.A., Vij, K., Ballard, D.H., and Greenough, W.T. (1997) Learning-dependent synaptic modifications in the cerebellar cortex of the adult rat persist for at least four weeks. *J. Neurosci.*, 17, 717–721.

Mackintosh, N.J. (1983). *Conditioning and associative learning.* Oxford University Press, New York.

Kish, S.J., Bergeron, C., Rajput, A., Dozic, S., Mastrogiacomo, F., Chang, L., Wilson, J.M., DiStefano, L.M., and Nobrega, J.N. (1992). Brain cytochrome oxidase in Alzheimer's disease. *J. Neurochem.*, 59, 776–779.

LaManna, J.C., Kutina-Nelson, K.L., Hritz, M.A., Huang, Z., and Wong-Riley, M.T. (1996). Decreased rat brain cytochrome oxidase activity after prolonged hypoxia. *Brain Res.*, 720, 1–6.

LeDoux, J.E. (1995). Emotion: clues from the brain. *Ann. Rev. Psychol.* 46, 209–35.

LeDoux, J.E., Iwata, J., Pearl, D., and Reis, D.J. (1986a). Disruption of auditory but not visual learning by destruction of intrinsic neurons in the medial geniculate body of the rat. *Brain Res.*, 371, 395–399.

LeDoux, J.E., Sakaguchi, A., Iwata, J., and Reis, D.J. (1986b). Interruption of projections from the medial geniculate body to an archineostriatal field disrupts the classical conditioning of emotional responses to acoustic stimuli. *Neuroscience*, 17, 615–627.

LeDoux, J.E., Ruggerio, D.A., Forest, R., Stornetta, R., and Reis, D.J. (1987). Topographic organization of convergent projections to the thalamus from the inferior colliculus and spinal cord in the rat. *J. Comp. Neurol.*, 264, 123–146.

Mata, M., Fink, D.J., Gainer, H., SMith, C.B., Davidsen, L., Savaki, H., Schwartz, W.J. and Sokoloff, L. (1980). Activity-dependent energy metabolism in rat posterior pituitary primarily reclects sodium pump activity. *J. Neurochem.*, 34, 213–215.

McEchron, M.D., Green, E.J., Winters, R.W., Nolen, T.G., Schneiderman, N., and McCabe, P.M. (1996). Changes of synaptic efficacy in the medial geniculate nucleus as a result of auditory classical conditioning. *J. Neurosci.*, 16, 1273–83.

McIntosh, A.R., and Gonzalez-Lima, F. (1995). Functional network interactions between parallel auditory pathways during Pavlovian conditioned inhibition. *Brain Res.*, 683, 228–241.

McIntosh A.R., and Gonzalez-Lima, F. (1991). Structural modeling of functional neural pathways mapped with 2-deoxyglucose: Effects of acoustic startle habituation on the auditory system. *Brain Res.*, 547, 295–302.

McIntosh, A.R. and Gonzalez-Lima, F. (1993). Network analysis of functional auditory pathways mapped with fluorodeoxyglucose: Associative effects of a tone conditioned as a Pavlovian excitor or inhibitor. *Brain Res.*, 627, 129–140.

McIntosh, A.R., and Gonzalez-Lima, F. (1994). Network interactions among limbic cortices, basal forebrain and cerebellum differentiate a tone conditioned as a Pavlovian excitor or inhibitor: Fluorodeoxyglucose mapping and covariance structural modeling. *J. Neurophysiol.*, 72, 1717–1733.

Miller, R.R., and Spear, N.E. (Eds). (1985). *Information Processing in Animals: Conditioned Inhibition.* L. Erlbaum Associates, New Jersey.

Nobrega, J.N., Raymond, R., DiStefano, L., and Burnham, W.M. (1993). Long-term changes in regional brain cytochrome oxidase activity induced by electroconvulsive treatment in rats. *Brain Res.*, 605, 1–8.

Olds, J., Disterhoft, J., Segal, M., Kornblith, D.L, and Hirsh, R. (1972). Learning centers of rat brain mapped by measuring latencies of conditioned unit responses. *J. Neurophysiol.* 35, 202–219.

Parker, Jr., W.D., Parks, J., Filley, C.M, and Kleinschmidt-DeMasters, B.K. (1994). Electron transport chain defects in Alzheimer's disease brain. *Neurology* 44, 1090–1096.

Paxinos, G., and Watson, C. (1986). *The Rat Brain in Stereotaxic Coordinates.* Academic Press, San Diego.

Pearce, J.M., and Hall, G. (1980). A model for Pavlovian learning: Variations in the effectiveness of conditioned but not of the unconditioned stimuli. *Psychol. Rev.*, 87(6), 532–552.

Ponomarenko, V.V. and Kamyshev, N.G. (1997). Genetic aspects of the mechanisms of learning. *Neurosci. & Behavioral Physiology,* 27, 245–249.

Poremba, A., Jones, D., and Gonzalez-Lima, F. (1997). Metabolic effects of blocking tone conditioning on the rat auditory system. *Neurobiol. Learn. Mem.*, 68, 154–171.

Poremba, A., Jones, D. and Gonzalez-Lima, F. (1997). Classical conditioning modifies cytochrome oxidase activity in the auditory system. *submitted.*

Poremba, A., and Gabriel, M. (1997). Lesions of the medial geniculate nucleus block development of amygdalar and cingulothalamic training-induced neuronal activity in rabbits. *J. Neurosci.* 17, 8645–8655.

Rescorla, R.A., and Wagner, A.R.. A theory of Pavlovian conditioning: Variations in the effectiveness of reinforcement and nonreinforcement. In A. H. Black and W. F. Prokasy (Eds.), *Classical Conditioning II.*. Appleton-Century-Crofts, New York, 1972, pp. 64–98.

Rickert, E.J., Bennett, T.L., Lane, P., and French, J. (1978). Hippocampectomy and the attenuation of blocking. *Behav. Biol.*, 22, 147–160.

RoBards, M.J. (1979). Somatic neurons in the brainstem and neocortex projecting to the external nucleus of the inferior colliculus: An anatomical study in the opposum. *J. Comp. Neurol.*, 184, 547–566.

Romanski, L.M., and LeDoux, J.E. (1992). Equipotentiality of thalamo-amygdala and thalamo-cortico-amygdala circuits in auditory fear conditioning. *J. Neurosci.*, 12, 4501–4509.

Rose, S.P. (1991) How chicks make memories: the cellular cascade from c-fos to dendritic remodelling. *TINS.* 14, 390–397.

Ryan, A.F., Furlow, Z., Woolf, N.K., and Keithly, E.M. (1988). The spatial representation of frequency in the rat dorsal cochlear nucleus and inferior colliculus. *Hearing Res.*, 36, 181–190.

Ryugo, D.K., and Weinberger, N.M. (1978). Differential plasticity of morphologically distinct neuron populations in medial geniculate body of the cat during classical conditioning. *Behav. Biol.*, 22, 275–301.

Schapira, A.H. (1996). Oxidative stress and mitochondrial dysfunction in neurodegeneration. *Curr. Opin. Neurol.*, 9, 260–264

Scheich, H., Simonis, C., Ohl, F., Tillein, J., and Thomas, H. (1993). Functional organization and learning-related plasticity in auditory cortex of the Mongolian gerbil. *Prog. Brain Res.*, 97, 135–143.

Shin, S., Poremba, A., Jones, D., and Gonzalez-Lima, F. Sensory learning: Safety signal induced auditory system metabolic plasticity during differential inhibition of conditioned fear. *Soc. Neurosci. Abstr.*, 1997, 23, 2119.

Silverman, M.S., and Tootell, R.B.H. (1987). Modified technique for cytochrome oxidase histochemistry: Increased staining intensity and compatibility with 2-deoxyglucose autoradiography. *J. Neurosci. Methods,* 19, 1–10.

Simonian, N.A., Hyman, B.T. (1994). Functional alterations in Alzheimer's disease: selective loss of mitochondrial-encoded cytochrome oxidase mRNA in the hippocampal formation. *J. Neuropathol. Exp. Neurol.*, 53, 508–512.

Sokoloff, L. (1992). Imaging techniques in studies of neural functions. In F. Gonzalez-Lima, T. Finkenstädt, and H. Scheich (Eds.), *Advances in Metabolic Mapping Techniques for Brain Imaging of Behavioral and Learning Functions.* NATO ASI Series D Vol. 68, Kluwer Academic Publishers, Dordrecht/Boston/London, 1992, pp. 1–38.

Solomon, P.R. (1977). Role of the hippocampus in blocking and conditioned inhibition of the rabbit's nictitating membrane response. *J. Comp. Physiol. Psychol.*, 91, 407–417.

Stickney, K.J., and Donahoe, J.W. (1983). Attenuation of blocking by a change in US locus. *Anim. Learn. Behav.* 11, 60–66.

Takai, D., Inoue, K., Shisa, H., Kagawa, Y., and Hayashi, J. (1995). Age-associated changes of mitochondrial translation and respiratory function in mouse brain. *Biochem. Biophys. Res. Commun.*, 217, 668–674.

Teich, A.H., McCabe, P.M., Gentile, C.G., Jarrell, T.W., Winters, R.W., Liskowsky, D.R., and Schneiderman NS (1988). Role of auditory cortex in the acquisition of differential heart rate conditioning. *Physio. Behav.*, 44, 405–412.

Theurich, M., Muller, C.M., and Scheich, H. (1984). 2-deoxyglucose accumulation parallels extracellularly recorded spike activity in the avian auditory neostriatum. *Brain Res.*, 322, 157–161.

Wagner, A.R., Mazur, J.E., Donegan, N.H., and Pfautz, P.L. (1980). Evaluation of blocking and conditioned inhibition to a CS signaling a decrease in US intensity *J. Exp. Psychol. Anim. Behav. Process.*, 6, 376–385.

Walley, R.E. (1982). Specific and Nonspecific changes in visual evoked potentials during eyelid conditioning in the rabbit (*Oryctolagus cuniculus). J. Comp. Physiol. Psychol.*, 96(1), 12–25.

Weinberger, N.M. (1995). Dynamic regulation of receptive fields and maps in the adult sensory cortex. *Ann. Rev. Neurosci.*, 18, 129–158.

Weinberger, N.M . Sensory plasticity and learning: The magnocellular medial geniculate nucleus of the auditory system. In C.D. Woody (Ed.), *Conditioning: Representation of Involved Neural Function*, Plenum Publications, New York, 1982, pp 697–710.

Weinberg, R.J., and Rustioni, A. (1987). A cuneocochlear pathway in the rat. *Neuroscience*, 20, 209–219.

Wikström, M., Krab, K., and Saraste, M. (1981). *Cytochrome Oxidase : A synthesis*. Academic Press, New York.

Willard, F.H., and Martin, G.F. (1984). Collateral innervation of the inferior colliculus in the North American opossum: a study using fluorescent markers in a double-labeling paradigm. *Brain Res.*, 303, 172–182.

Williams, D.A., and LoLordo, V.M. (1995). Time cues block the CS, but the CS does not block time cues. *Q. J. Exp. Psychol.*, 48, 97–116.

Wong-Riley, M.T.T. (1989). Cytochrome oxidase: An endogenous metabolic marker for neuronal activity. *Trends Neurosci.*, 12, 94–101.

Wong-Riley, M.T., Mullen, M.A., Huang, Z., and Guyer, C. (1997). Brain cytochrome oxidase subunit complementary DNAs: isolation, subcloning, sequencing, light and electron microscopic in situ hybridization of transcripts, and regulation by neuronal activity. *Neuroscience,* 76, 1035–1055.

Wong-Riley, M. (1979). Changes in the visual system of monocularly sutured or enucleated cats demonstrable with cytochrome oxidase histochemistry. *Brain Res.*, 171, 11–28.

Wong-Riley, M.T., Tripathi, S.C., Trusk, T.C., and Hoppe, D.A. (1989). Effect of retinal impulse blockage on cytochrome oxidase-rich zones in the macaque striate cortex: I. Quantitative electron-microscopic (EM) analysis of neurons. *Visual Neurosci.*, 2, 483–497.

Wong-Riley, M.T., Trusk, T.C., Kaboord, W., and Huang, Z. (1994). Effect of retinal impulse blockage on cytochrome oxidase-poor interpuffs in the macaque striate cortex: quantitative EM analysis of neurons. *J. Neurocytol.*, 23, 533–553.

5

FUNCTIONAL IMAGING PROBES TO STUDY THE NEURAL BASES OF BEHAVIOR IN GENETIC ANIMAL MODELS OF ADHD

A Comparative Analysis of Short and Long-Term Markers of Neuronal Activity

Michele Papa,[1] Adolfo G. Sadile,[1] Joseph A. Sergeant,[2] Jason Shumake,[3] and F. Gonzalez-Lima[3]

[1]Institute of Human Anatomy
Laboratory Neurophysiology of Behaviour and Neural Networks
Department of Human Physiology "F. Bottazzi"
Second University of Naples (SUN)
Naples, Italy
[2]Department of Clinical Psychology
University of Amsterdam
Amsterdam, The Netherlands
[3]Institute for Neuroscience and Department of Psychology
University of Texas at Austin
Austin, Texas 78712

ABSTRACT

The following studies used molecular imaging techniques to trace the neural substrates of behavior in two genetic models of hyperactivity in rats. Additionally, the studies compared differences between markers sensitive to short-term changes and markers sensitive to long-term changes in neuronal activity. The first series of experiments used adult male Spontaneously Hypertensive Rats (SHR) with Wistar-Kyoto Normotensive (WKY) rats as controls. The second series used Naples-High Excitability (NHE) rats and Naples Low-Excitability (NLE) rats with random-bred (NRB) rats as controls. The following techniques were used to analyze the brains of these animals: (i) quantitative autoradiography of dopamine receptors, (ii) Ca^{2+}/calmodulin-dependent protein kinase II (CaMKII) immunohistochemistry, (iii) transcription factors such as *c-FOS,* and (iv) quantitative cytochrome oxidase (C.O.) histochemistry. In Series 1 experiments, light microscope and computer assisted image analysis

Cytochrome Oxidase in Neuronal Metabolism and Alzheimer's Disease,
edited by Gonzalez-Lima, Plenum Press, New York, 1998.

showed that the SHR had a higher density of binding sites for D-1/D-5 dopamine receptors and a reduced expression of CaMKII and *c-FOS,* but not *JUN-B,* in the most rostral portions of the caudate-putamen, the nucleus accumbens, and the olfactory tubercle. SHR also had a lower C.O. activity in the medial and lateral prefrontal cortices, compared to WKY controls. Furthermore, regional correlative analyses among different areas with different markers revealed that under basal conditions, SHR had reduced interregional correlations. In Series 2 experiments, C.O. metabolic differences between the NLE and NHE were found in the granular cell layer of the outer blade of the dentate gyrus. In addition, NLE showed greater C.O. activity than NRB in medial frontal cortex, and lower activity in perirhinal cortex (dorsal region). NHE showed greater C.O. activity than NRB in entorhinal cortex (superficial layers) and lower activities in perirhinal cortex and cortical amygdala. These data support the hypothesis that NLE/NHE rats may be an appropriate model for studying genetically altered limbic regions related to impaired emotional processing. Altogether, the results support the involvement of limbic cortico-striatal circuits in the anterior basal forebrain in attentive processes and impulsiveness, and support the use of the SHR and NHE strains as animal models of attention deficit hyperactivity disorder (ADHD) in children.

1. INTRODUCTION

Animal models of attention are important for both basic research questions addressing the neurobiological correlates of attention and applied research questions addressing Attention Deficit Hyperactivity Disorder (ADHD) (Gunning & Sergeant, 1994). ADHD is a syndrome which affects mostly male children and is characterized by attention problems accompanied by impulsiveness, hyperkinesis, restlessness, and disturbances in timing (DSM-IV, 1994; Frick & Lahey, 1991; Gunning & Sergeant, 1994; Swanson *et al.*, 1998). Attention deficits have been elicited in animals through lesion models and genetic models. In the lesion strategy, neuroanatomical structures thought to be critically involved in attention processing are disabled, either through surgical or pharmacological manipulation. Researchers then compare the performance of the lesioned group to a control group on performance measures assumed to assess attention, such as the five-choice serial reaction task (Robbins & Everitt, 1994). Any deficits detected are assumed to be due to the area lesioned. The genetic models presented here work in the reverse way.

Attentional abilities are assumed to vary across a population, and the researcher then, through selective breeding, produces two strains of rats—one that expresses attention deficits and one that does not. Then the two groups are subjected to neuroimaging analyses and the results compared. In both the lesion models and the genetic models, the researcher may introduce an additional pharmacological manipulation, such as giving the animals a dopamine (DA) agonist, in an attempt to alleviate the performance deficit. If the drug works, the animal model is assumed to have additional construct validity with attention deficit disorders in humans, which also respond favorably to DA agonists (Safer & Krager, 1988; Seiden, Sabol, & Ricaurte, 1993). Furthermore, the animal model may be used to test future drug developments.

1.1. Neural Bases of Behavior in Genetic Animal Models of ADHD

This chapter discusses an investigation of the neural substrates of hyperactivity and attention deficits of two genetic models, the Spontaneously Hypertensive rat (SHR) (Sagvolden, 1996), and the Naples High-Excitability (NHE) rats (Cerbone, Pellicano, & Sadile, 1993b). Both strains of rats are hyperactive and show attention deficits in behavioral paradigms (Barkley, DuPaul, & McMurray, 1991; Goodyear & Hynd, 1992). The

Naples High-Excitability and Low-Excitability rat lines were thus named for their respective behavior on spatial novelty tasks, such as a Lát maze, a hexagonal tunnel maze and an asymmetric radial arm maze. These rats' reactivity to novelty cannot be attributed to general motor hyperactivity as baseline motor activity between strains is not significantly different (Cerbone, Patacchioli, & Sadile, 1993a).

Functional imaging techniques allow the mapping of the spatial distribution of changes which occur in the short-term, as well as in the long-term, at the level of markers sensitive to changes in activity induced in neural networks. The studies reported here attempt to analyze the emerging profile from several different functional imaging markers to compare it with cytochrome oxidase (C.O.) quantitative histochemistry (Gonzalez-Lima & Cada, this volume). C.O. has been demonstrated to reflect long-lasting changes in tissue metabolic capacity induced by neuronal activity and learning and memory processes (Poremba, Jones & Gonzalez-Lima, this volume). The functional probes we compared are (i) dopamine receptors of the D-1 and D-2 families, (ii) the enzyme Ca^{2+}/calmodulin-dependent protein kinase II (CaMKII), (iii) transcription regulators of gene expression, and (iv) the respiratory chain enzyme cytochrome oxidase (C.O.).

1.2. Dopamine Receptors

The "dopamine hypothesis" is the most widely accepted working hypothesis of ADHD. It is based on the amelioration of symptoms by psychostimulant drugs acting at DA synapses, such as methylphenidate, amphetamine and pemoline (Safer & Krager, 1988; Seiden, Sabol, & Ricaurte, 1993). Therefore, it has been suggested that the mesocorticolimbic dopamine system (Dahlstrom & Fuxe, 1964) is involved in the expression of ADHD. The mesocorticolimbic system, which originates in the ventral tegmental area (VTA), innervates forebrain limbic structures, such as the prefrontal cortex, the nucleus accumbens, and the olfactory tubercle. Mesocorticolimbic circuits are a major component of a multiple attentional network system (Marrocco, Witte, & Davidson, 1994; Posner & Dehane, 1994; Robbins & Everitt, 1994).

The neurotransmitter DA binds to multiple synaptic and extra-synaptic receptors, which are coded by five distinct genes (D-1 to D-5). The D-1 receptor subfamily is composed of molecular D-1 (Dearry *et al.*, 1990) and D-5 (Grandy *et al.*, 1991; Sunahara *et al.*, 1991), whereas the D-2 subfamily is composed of molecular D-2 (Bunzow *et al.*, 1988), D-3 (Sokoloff *et al.*, 1990) and D-4 (Van Tol *et al.,* 1991) subtypes. The D-1 group leads to activation of adenylate cyclase, while the D-2 group either inhibits or does not affect adenylate cyclase activity (Kebabian & Caine, 1979). In addition, the signal transduction pathways for DA also involve phospholipase C, and the regulation of K^+ and Ca^{2+} channels (Liu *et al.*, 1996).

Brain slice perfusion experiments have shown an impaired DA release in the SHR model of ADHD under basal conditions (Russel *et al.*, 1996; Russel *et al.,* 1995). In addition, the blockade of the DA re-uptake system by methylphenidate (MP) improves ADHD in children and animal models (Safer & Krager, 1988; Seiden, Sabol, & Ricaurte, 1993).Genetically, a higher than expected number of Variable Number Tandem Repeats (VNTR) of sequences coding for DA transporter (DAT) has been shown in ADHD children (Cook, *et al.*, 1995).

1.3. Ca^{2+}/Calmodulin-Dependent Protein Kinase II

Ca^{2+}/calmodulin-dependent protein kinase II (CaMKII) (Papa *et al.*, 1996a) is one of the major molecular devices in signal transduction (Hanson & Schulman, 1992) and repre-

sents the major protein of the postsynaptic density (Kelly, McGuinness, & Greengard, 1984), but it is also present at the presynaptic level (Popoli *et al.*, 1995). There are several isoforms of this kinase unevenly distributed across the brain (Rostas & Dunkley, 1992). All of these isoforms utilize phosphorylation (McGlade-McCulloh, 1993) to regulate the assembly of cytoskeletal components (Drewes *et al.*, 1992), receptors of the ionotropic glutamate type (McGlade-McCulloh, 1993), subunits of the GABA receptors (Machu, Firestone, & Browning, 1993), and the adenylate cyclase type III (Wayman, Impey, & Storm, 1995). CaMKII is a multifunctional protein on which the cross-talk between different second messenger systems converge. It is thought to be involved in the induction, but not the expression, of long-term potentiation (Malinow, Schulman, & Tsein, 1989), neuronal plasticity (Hanson & Schulman, 1992), and learning and memory processes (Silva *et al.*, 1992).

1.4. Transcription Factors

The expression of several target proteins (such as receptor subunits, ion channels, and membrane constituents) is regulated by the orchestration of several transcription factors (TF), which are coded by a numerous and heterogeneous gene superfamily, also referred to as immediate early genes [IEG] (Morgan & Curran, 1991). They code for proteins which mediate many of the neurons' long-term responses to trans-synaptic signals (Sheng & Greenberg, 1990). They dimerize and enter the nucleus where they bind to specific DNA binding sites, such as the *AP-1* site (Morgan & Curran, 1991) for *Fos* and *Jun*, or the *SP-1* site (Christy & Nathans, 1989) for the zinc finger family member *Zif-268* (also known as *NGF-1A*, *KROX-24* or *egr-1*) (Rhodes & Klug, 1993), thus increasing or decreasing gene expression.

1.5. Cytochrome Oxidase

Cytochrome oxidase (C.O.) is an integral transmembrane protein of the inner eukaryotic mitochondrial membrane. It acts as a terminal enzyme in the electron transport chain which catalyses transfer of electrons from its reduced substrate, ferrocytochrome *c*, to molecular oxygen to form water. C.O. is coupled to the process of oxidative phosphorylation, which is responsible for the generation of ATP. This energy device is then used for active ion pumping to maintain the resting membrane potential, fast axoplasmic transport, and synthesis of macromolecules and neurotransmitters. The maintenance of ion balance constitutes the major energy-consuming function of neurons. In fact, increased neuronal activity promotes heightened cellular respiration in order to generate more ATP for the accelerated activity of Na/K transporting ATPase (Wikstrom, Krab, & Saraste, 1981) .

Wong-Riley (1979, 1989) postulated that the level of neuronal C.O. activity should correlate positively with the functional activity level of neurons. Much evidence shows a correlation between C.O. activity and functional activity of various nuclear groups under normal conditions, and there are adaptive adjustments of C.O. activity in response to experimentally induced changes in neuronal functional activity (Gonzalez-Lima & Jones, 1994; Hyde & Durham, 1990; Robbins & Everitt, 1994; Wong-Riley, 1979, 1989; Wong-Riley *et al.*, 1993; Gonzalez-Lima, 1992).

The preset molecular microscopic imaging analysis focused on areas in the anterior forebrain because they are the target sites of the nigrostriatal and mesocorticolimbic dopaminergic systems, which are thought to be involved in the control of attentional processes along with other systems (Marrocco, Witte, & Davidson, 1994; Posner & Dehsne, 1994; Robbins & Everitt, 1994).

Quantitative receptor autoradiography, immunocytochemistry for CaMKII and the transcription factors c-FOS and JUN were carried out under baseline conditions on serial sections of the anterior forebrain of male SHR and WKY rats. In the SHR/WKY as well as in the Naples lines, quantitative C.O. histochemistry was carried out under comparable conditions to monitor long-lasting changes in neural networks. Baseline (unstimulated) conditions were chosen because hyperactive rodent models as well as ADHD children show attentional deficits at low motivational levels (van der Meere, Vreeling, & Sergeant, 1992).

2. MATERIALS AND METHODS

2.1. Animals

SHR and WKY male rats were obtained from Charles River (Italy), whereas male rats of the NHE, NLE and random-bred controls (NRB) were from our animal colony in Naples. The experiments on SHR/WKY rats were carried out on juvenile (six weeks old) rats for dopamine receptor autoradiography, and for immunocytochemistry for alpha-CaMKII and transcription factors. The experiments on cytochrome oxidase on SHR/WKY and NHE/NLE/NRB rats were carried out on adult (six months old) animals. Rats were housed in groups of two in standard makrolon cages and put under standard conditions on a 12:12 light-dark cycle. The whole brain was removed and frozen in cold isopentane and stored at −80°C. The brains of Naples lines were air-freight shipped in dry ice to Austin, TX, for C.O. quantitative histochemical analysis.

2.2. Dopamine Receptor Binding Assays

The assays were carried out according to the procedure described by Kirouac and Ganguly (1993). Briefly, pilot assays to establish radioligand concentrations and incubation conditions for the assays of D-1 and D-2 receptor subtypes were performed on brains of normal Wistar rats. A saturation analysis (maximal binding capacity and affinity) was performed using 7 concentrations of the radioactive DA antagonist [^{3}H]-SCH 23390 (Spec. Act. 60–87 Ci/mM; 0.1–5.0 nM). D-1 excess unlabelled antagonist SCH 23390 was used to control for non-specific binding. For D-2 receptor subfamily two competition studies were carried out using 4.2 nM ^{3}H-raclopride and 5 nM ^{3}H-quinpirole with unlabelled spiperone (0.1 nM–1 μM) and 7-OH-DPAT (0.1 nM–10 μM) as unlabelled displacers. In both series of binding assays, ketanserin (1 μM) was added to resolve the DA and serotonin components of the binding (List & Seeman, 1981).

2.2.1. Quantitative Autoradiography. The anterior forebrain was serially sectioned and randomly assigned to different experiments. The slides with tissue sections were incubated using optimized conditions and exposed to [^{3}H]-sensitive films (Amersham). Exposure time was 18 days for SCH 23390, 8 weeks for raclopride and 3 months for quinpirole. Films were developed and optical densities (OD) of sections were analyzed with reference to co-exposed standard [^{3}H]-microscale (calibration curve to convert OD to receptor concentration). The OD readings were taken by a CCD camera (Hamamatsu Photonics, Italy), and converted to a 640 × 480 pixel file by an acquisition board and a computer-assisted image analysis system (MCID-M4; Imaging Res. Inc, Canada). The recognition of forebrain structures was accomplished by inspection of Nissl-stained adjacent sections and an atlas of the rat brain (Paxinos & Watson, 1986).

2.2.2. Data Analysis and Statistics. In the saturation analysis the values of maximal binding capacity (B_{max}) and dissociation constant (K_D) were obtained by non-linear regression analysis with an hyperbolic model using the PRISM software 2.0 version (Graph-Pad, CA). Whenever the saturation was not achieved, a correction algorithm was used, as described elsewhere (Zilles *et al.*, 1986) by adding the K_D value to the total free ligand concentration and dividing the sum by the free ligand concentration. The values of binding at about the dissociation constant were assumed to index high-affinity binding sites and were used for the rostro-caudal gradient. Values of high-affinity sites across rat lines were tested by two-tailed Student's t-test for unpaired data.

In competition studies, the plots were computed by non-linear regression analysis with a sigmoidal curve. The specific binding for D-2, D-3, and D-4 receptors was obtained by subtracting non-specific binding from the total ^{3}H-quinpirole binding. The K_i, defined as the concentration of cold displacer which inhibited 50% of the binding, was obtained by the computed EC_{50} values by the algorithm of Cheng and Prussoff (1973), i.e. Ki = EC_{50} divided by the concentration of the ligand plus KD. ^{3}H-quinpirole specific binding in the absence of and in the presence of 10 nM 7-OH-DPAT allows the estimation by Gaddum's equation of 17% of D-2 and 15% of D-3 subtypes. Similarly, ^{3}H-quinpirole specific binding in presence of 10 nM 7-OH-DPAT allows the estimation of 34% of D-2 and 14% of D-4 subtypes. ^{3}H-raclopride specific binding in presence of 1 μM spiperone allows estimation of 70% of the D-2 and 54% of the D-3 subtypes.

Two-way factorial analysis of variance (ANOVA; 2 × n) line × rostro-caudal level was used for each area, and planned comparisons between rat lines were made by the t-test for unpaired data. In order to analyze neural network interactions, regional cross-correlation analyses were made by Pearson product × moment between individual DA receptor binding sites, averaged out for each animal across sections within the sampled area. The correlation coefficients were transformed to "z-scores," and planned comparisons were made using Student's t-test for unpaired data (Edwards, 1967). The rejection level was set at 2p equal or above 0.05.

2.3. CaMKII and Transcription Factor Antibodies

The primary antibody was a mouse monoclonal antibody towards the alpha-subunit of the CaMKII (Boehringer, Mannheim) or a rabbit polyclonal antibody against the *c-FOS* and *JUN-B* (Santa Cruz Biotechnologies, CA). For transcription factors the corresponding control peptides were used to test specificity. The secondary antibody was a goat anti-mouse serum and the revealing system was the avidin-biotin complex (ABC; Vector Laboratories, Burlingame, CA).

2.3.1. Perfusion-Fixation. At the age of 6 weeks, rats were deeply anesthetized by continuous exposure to ether and perfused transcardially with physiological saline followed by 4% paraformaldehyde in 0.1 M phosphate buffer (PB, pH 7.3). Brains were post-fixed in the same fixative for 2 h, washed in phosphate-buffered saline (PBS), soaked in 30% sucrose for cryoprotection, frozen in isopentane on dry ice and stored at –80°C.

2.3.2. Immunocytochemistry. 50 μm-thick cryostat coronal sections were collected in ice-cold PBS containing 0.1% sodium azide. Sections were free-floating immunostained for the detection of the alpha-subunit of CaMKII (Papa *et al.*, 1996a) or the transcription factors cited above, as previously described (Papa *et al.*, 1996c). The dilution of the antibody was 1:500. The sections were exposed to diaminobenzidine (DAB, 100 mg in 200 ml

buffer), and a Nickel-Cobalt intensification procedure was performed. To assess the specificity of labeling, control experiments were performed by incubating overnight the primary antibody with a ten-fold excess of peptide antigen in PBS. The sections were mounted on poly-L-lysine coated slides and coverslipped.

2.3.3. Data Acquisition. Images were taken by a CCD camera (Hamamatsu Photonics, Italy) mounted on a Zeiss Axioskop microscope and analyzed quantitatively with an image analysis system (MCID-M4; Imaging Research Inc., Canada). The nucleus accumbens (ACB) was outlined for each section, divided into subterritories according to Nissl-stained adjacent sections and calbindin-treated sections, and analyzed (Zahm & Brog, 1992). The pole was defined as the rostral portion of the ACB at its fusion with the dorsal striatum. The core was divided from the shell throughout the posterior horn of the anterior commissure. Immunoreactive elements for the α-CaMKII, which labels mainly neuronal somata and dendrites (Schulman, 1993), or the transcription factors, which are nuclear, were considered positive when they fell into the range between 0 and 140/160 (grey levels 0–255).

2.3.4. Data Analysis and Statistics. Since no satisfactory erosion/dilation algorithm solves the de-agglomeration problem, field measurements were used instead of object measurement. Thus, the area of each of the three n.accumbens subterritories covered by immunoreactive elements, expressed as percent of the total area (*proportional area*), was the dependent variable. Data were submitted to a 3-way ANOVA (Edwards, 1967) line x subterritory x level (as covariate). Between-line planned comparisons were made by two-tailed t-test for unpaired data. Left-to-right differences were analyzed by t-test for paired data. The rejection level was set at $p \geq 0.05$.

2.4. Quantitative C.O. Histochemistry

2.4.1. SHR and WKS Rats. Coronal cryostat sections (20 micron thick) were serially taken across the brain. They were processed by the method of Gonzalez-Lima and Jones (1994). Images were taken by a CCD camera (Hamamatsu Photonics, Italy) mounted on an Axioskop Zeiss microscope and loaded to a file through an acquisition board and a PC-assisted image analysis system (MCID-M4; Imaging Res., Canada). Optical densities were transformed in units of enzyme activity by a standard curve using heart tissue as a source of C.O. in presence of different amounts of brain tissue. Data were analyzed using ANOVA and Students *t* comparing mean C.O. activity units (micromol/min/g tissue) between the different strains of rats, and interregional correlations were done as described above.

2.4.2. Naples Lines. Brains were taken from 15 naive rats selectively bred for activity level on maze tasks (Sprague-Dawley derived). The animals were decapitated, and the brains removed without perfusion or fixation and frozen in isopentane. The brains were sectioned with a cryostat at 40 μm sections. The sections were thaw-mounted to slides and kept frozen until staining.

The staining procedure first required a series of chemical exposures: 0.1 M phosphate buffer with 10% sucrose (4 changes, 5 min. each), a preincubation with Tris buffer (10 min. each), and a 0.1 M phosphate buffer rinse. Then the slides were incubated for 60 minutes with DAB (preceded by bubbling oxygen into DAB for 5 min.) at 37°C while stirring. The slides then sat in buffered formalin (10%) with 10% sucrose for 30 min before a

series of dehydration baths in 30, 50, 70, 90, 95 (two baths) and 100 (three baths) percent ethanol, with 5 min in each bath. The slides then went through a series of three xylene baths of 5 min each before being permounted and coverslipped. (For details, see Gonzalez-Lima and Cada, this volume.)

C.O. reactivity was measured in optical density (OD) units using an image-processing system: high-gain camera, Targa image capture board, computer running JAVA software (Jandel Scientific), Sony color monitor and DC-powered illuminator. C.O. activity was measured spectrophotometrically at 37°C, pH 7, using calibration standards with brain tissue homogenates, and transformation of OD into C.O. activity units (Cada et al., 1995). Three data points were taken in each region of interest for each of the three sections selected per brain region. A vertical OD reading was taken through the layers of the hippocampus giving average sample readings for those layers.

3. RESULTS

3.1. D-1 Receptor Family Autoradiography

A saturation analysis using different concentrations (0.1–5.0 nM) of the DA D-1/D-5 antagonist ^{3}H-SCH23390 revealed that a single receptor model best fit the data. Under basal conditions, significant differences were found between WKY and SHR rats in the maximal number of binding sites and in the dissociation constant. In fact, a 2-way ANOVA line x region on B_{max} and K_D gave a significant main effect of line ($F = 7.91$; $p < 0.006$) and region ($F = 404.4$; $p < 0.0001$). In addition, the dissociation constants indicate that under basal conditions SHR have a higher K_D in all the accumbal subterritories and olfactory tubercle, and a lower K_D in the globus pallidus.

3.1.1. Rostro-caudal Level. Analysis of binding sites in the rostro-caudal plane (Figure 1 upper row) revealed that under baseline conditions there were significantly different receptor levels. In fact, in the CPU of both lines, there was a gradient with higher density of binding sites in the anterior than in the posterior levels, as shown by the line x level interaction effect ($F = 3.44$; $p < 0.001$). However, in the most rostral portions of the CPU, there was a significant strain effect consisting of a higher number of sites in the SHR than in the WKY ($p < 0.025$).

A picture similar to the CPU (dorsal striatum) was evident also in the accumbal complex (ventral striatum). In fact, a rostro-caudal negative gradient was demonstrated by the level effect of ANOVA in the core ($F = 42.73$; $p < 0.00001$) and the shell ($F = 38.28$; $p < .00001$) of both strains, and a positive gradient ($F = 4.68$; $p = 0.038$) in the pole of the nucleus accumbens in WKY only. Thus, SHR showed a higher density of binding sites in the accumbal pole. In the olfactory tubercle, there was a higher number of high-affinity binding sites in the most rostral portions of SHR only, as shown by the strain x level interaction effect ($F = 3.45$; $p = 0.003$).

3.2. D-2 Receptor Family Autoradiography

3.2.1. Raclopride Binding. The affinity of the ligand for D-2 is twice as much as for D-3, as the K_i value is 1.8 nM for D-2 and 3.5 nM for D-3. Thus, total binding represents 3/4 of the high-affinity binding sites for D-3, being at about the K_i, and half of the D-2 sites.

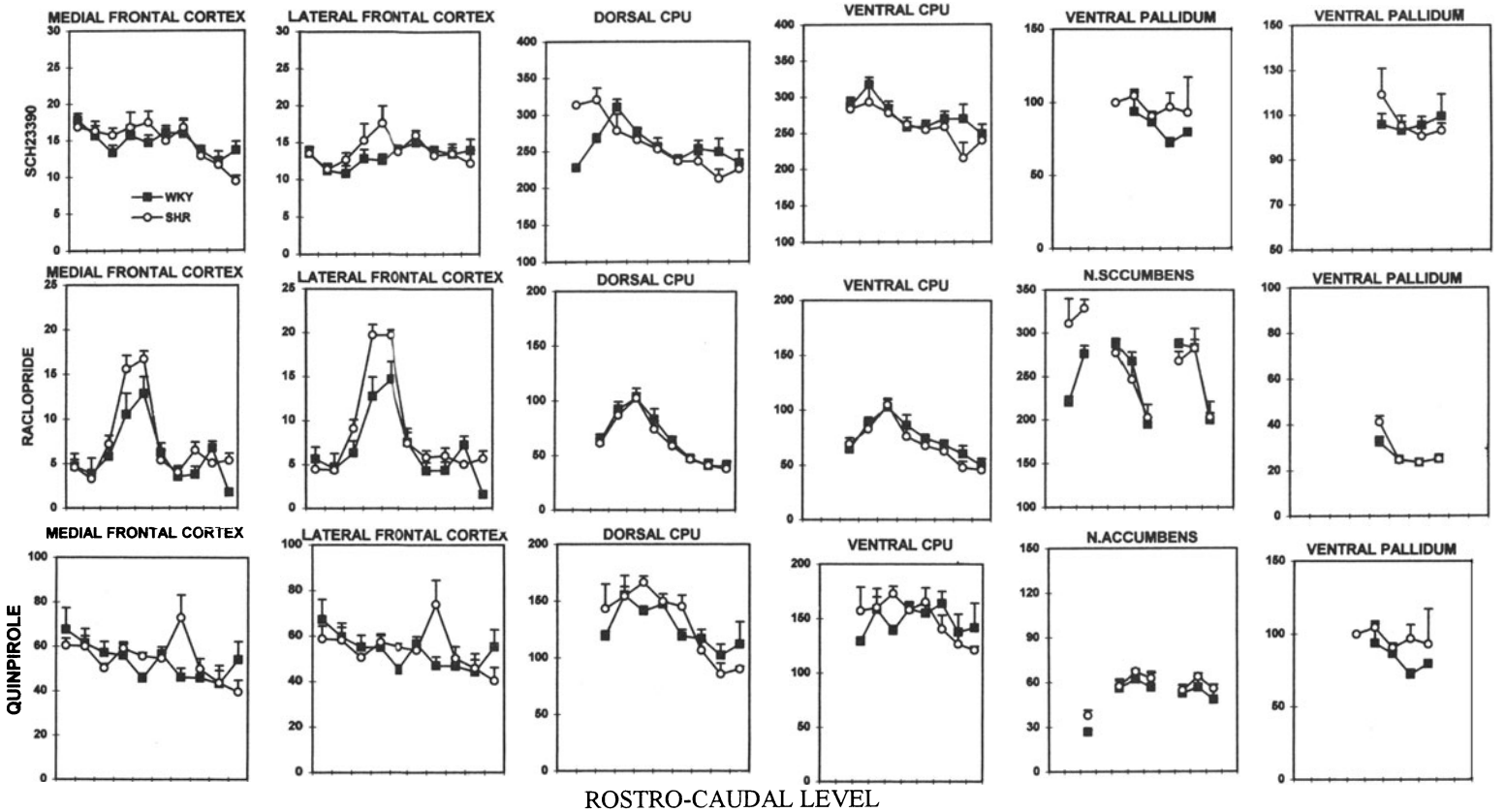

Figure 1. Rostro-caudal gradients in the high-affinity D-1/D-5 receptor binding sites (upper row), as measured at about the dissociation constant (K_D), and D-2 receptor subtypes, as monitored by raclopride (middle row) or quinpirole binding (lower row) in WKY and SHR rats under basal conditions. Values are femtomoles/mg of protein (Mean ± SEM). The rostro-caudal plane has been arbitrarily divided into sublevels with reference to bregma, according to atlas (Paxinos & Watson, 1986) and Nissl-stained adjacent sections. Bregma sublevels were between +3.40 and −2.80 for the caudate-putamen (CPU). For the accumbal complex, they were between +3.40 and +2.10 for the pole, +2.70 and 0.00 for both core and shell, and between +1.20 and −1.40 for the ventral pallidum. The nucleus accumbens core and shell have been arbitrarily plotted on different planes.

3.2.2. Quinpirole Binding. The ^{3}H-QB specific binding labels mainly the high-affinity binding sites for the DA D-2, D-3 and D-4 receptor subtypes, all of which are around the K_i value. While no significant line difference was detected across the sampled areas ($F = 2.95$; $0.05 < p < 0.10$), the treatment effect was highly significant ($F = 12.34$; $p < 0.001$), as it was the region effect ($F = 45.28$; $p < 0.0001$). No significant left-to-right difference in the level of D-2/D-4 nor D-2/D-3 receptor binding sites was found, as tested by two-tailed t-test for paired data between left and right hemispheres. Moreover, the inhibition constants (Ki) for 7-OH-DPAT were higher in the caudate-putamen, the accumbal core and shell, the ventral pallidum and the septal nuclei of the SHR, compared to the WKY, under basal conditions.

3.2.3. Rostro-caudal Levels. Figure 1 shows the region-specific patterns of D-2 family binding by raclopride (middle row) and quinpirole (lower row). Two-way ANOVA line x level showed no main effect nor line interaction in any of the sampled areas. There was only a highly significant effect of rostro-caudal level by raclopride in both frontal cortices, the caudate-putamen and the ventral pallidum, whereas by quinpirole binding there was a significant negative gradient in the CPU and the accumbens core and shell.

3.2.4. Regional Intercorrelation Analysis. Within each group, pairwise correlations of the levels of DA receptor binding sites among the sampled brain areas can be an indirect measure of regional interactions ("cross-talk"). These average correlation coefficients, after "z" transformation, revealed that SHR have an average score for D-1 binding sites lower than that in WKY rats (WKY: 0.2593 ± 0.170; SHR: -0.111 ± 0.201; $df = 109$; $2p < 0.01$ by t-test for non paired data). For D-2 family measured by ^{3}H-raclopride binding, the degree of intercorrelations was similar in the two rat lines (WKY: 0.5539 ± 0.041; SHR: 0.450 ± 0.047; $df = 380$; n.s). For D-2 receptor family, as measured by $^{3H\text{-quin-}}$ pirole binding, WKY and SHR were very similar in the cross-correlation score (WKY: 0.633 ± 0.022; SHR: 0.452 ± 0.028; $df = 420$; n.s.).

3.3. Ca^{2+}/Calmodulin-Dependent Protein Kinase II (CaMKII)

Representative computer overlay reconstructions of the nucleus accumbens complex of WKY and SHR rats are reported in Figure 2.

3.3.1. Rostro-caudal Levels. The expression of alpha-CaMKII in computer overlay reconstructions of the ACB subterritories showed a lower level in the rostral pole and the shell in the SHR compared to the WKY (Figure 3, upper graph). In addition, while both WKY and SHR had a higher expression in the pole and shell, the WKY, but not the SHR, showed a negative rostro-caudal gradient with higher levels in the most rostral levels of the shell. Thus, the SHR showed a lower expression in the anterior 2/5 of the shell, but not of the core, where both groups demonstrated a similar, less steep rostro-caudal gradient. The CaMKII levels in the SHR were 84.7% and 62.4% of the control level in the rostral pole and the shell, respectively, but they did not change in the core.

Three-way factorial ANOVAs line (WKY and SHR) × ACB subterritory (pole, core and shell) × rostro-caudal level (7 arbitrary levels, as dependent variable, two for the pole and five for the core and shell) revealed a significant main effect of ACB subterritory ($F = 15.32$; $p < 0.001$), level ($F = 10.71$; $p < 0.005$) and a strain x level interaction effect ($F = 5.26$; $p < 0.01$). No left-to-right difference was detected by t-test for paired data.

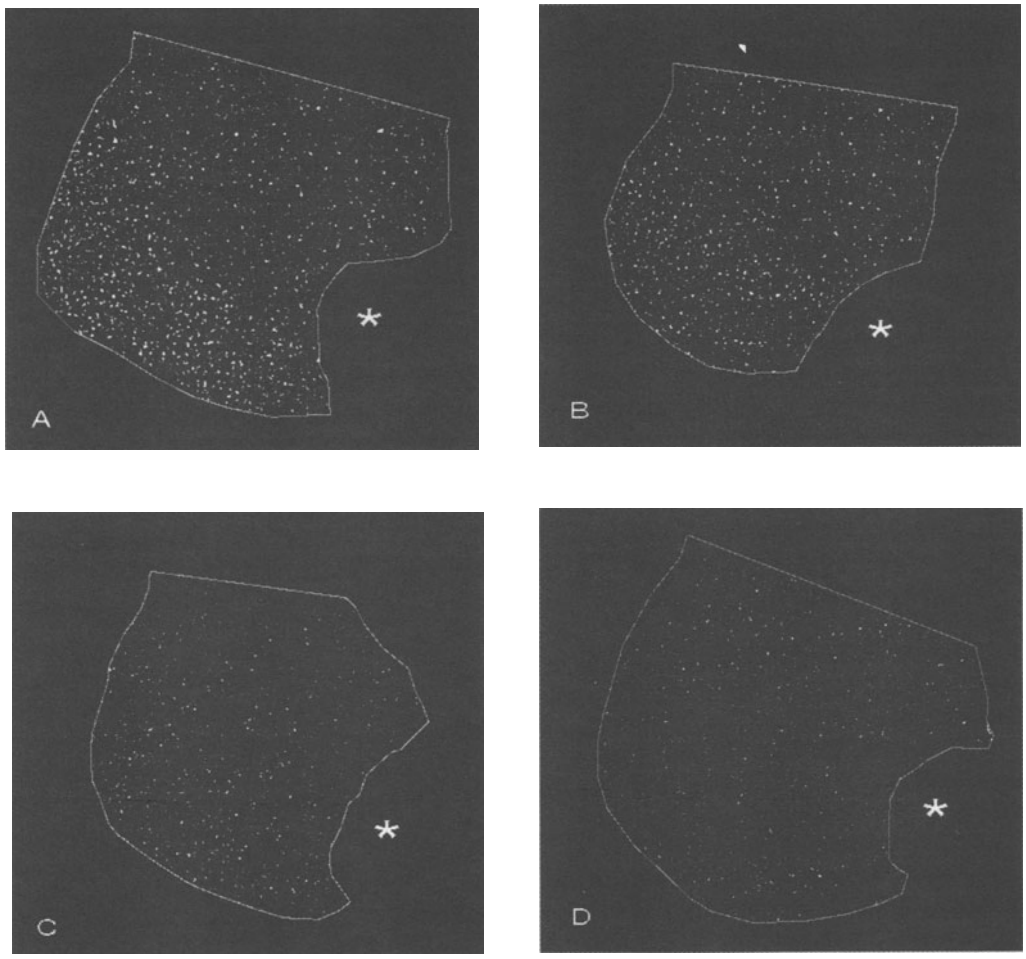

Figure 2. Computer overlay reconstructions of representative coronal sections of the nucleus accumbens of WKY (left column) and SHR (right column) rats showed labeling for the α-isoform of CaMKII (upper row) and *c-FOS* (lower row). The staining for α-CaMKII pertains to neuronal somata and dendrites, whereas the staining for *c-FOS* is nuclear. The asterisks mark the anterior commissure close to the external capsule, which indicates the medial portion of the structure.

3.3.2. Regional Intercorrelation Analysis. By correlating within each group inter-regional levels of CaMKII, the degree of cross-talk was higher in the WKY than in the SHR rats (WKY: 0.707 ± 0.051; SHR:0.188 ± 0.049; df = 134; $2p < 0.01$ by t-test for non-paired data).

3.4. *c-FOS* Transcription Factor

The expression of *c-FOS* was lower in the rostral pole, core and shell of the SHR accounting for 60%, 54.5% and 55% of the WKY level, respectively (Figure 3 middle graph).

3.4.1. Rostro-caudal Level. A 3-way factorial ANOVA line x ACB subterritory x antero-posterior levels (as dependent variable) revealed a significant main effect of ACB

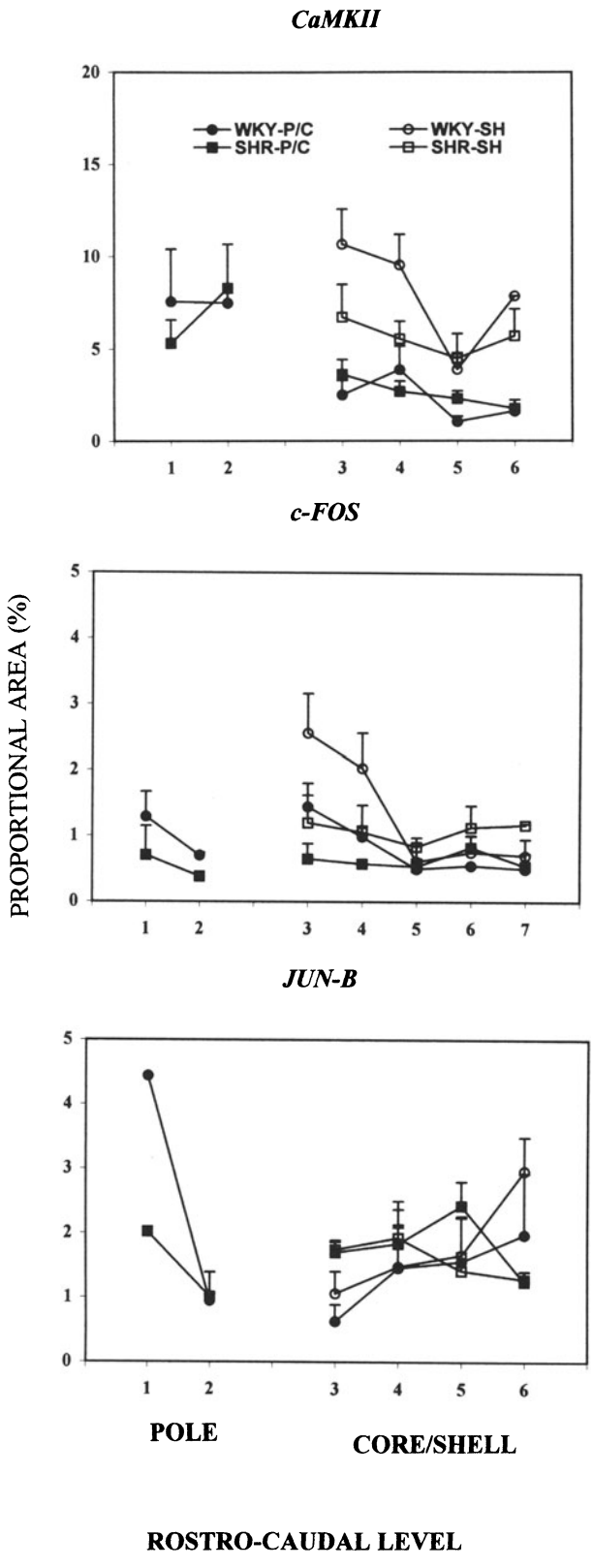

Figure 3. Alpha-isoform of CaMKII and transcription factors *c-FOS* and *JUN-B* in the rostro-caudal plane of the anterior forebrain of WKY and SHR. Values are proportional areas expressed as percent of total area covered by positive elements (Mean ± SEM). The rostro-caudal plane has been divided in arbitrary sublevels between +2.70 and +2.10 for the pole, +2.70 and 0.00 for both core and shell, with reference to bregma, according to Paxinos and Watson's atlas (1986) and inspection under the microscope of Nissl-stained adjacent sections. P/C, accumbens pole and core; SH, accumbens shell. Significance levels refer to between-line planned comparisons by two-tailed t-test for unpaired data following 3-way ANOVA (see Methods).

subterritory ($F = 10.05$; $p < 0.01$) and level ($F = 9.42$; $p < 0.01$) and a strain x level interaction effect ($F = 5.76$; $p < 0.025$).

3.4.2. Regional Intercorrelation Analysis. The cross-correlation score measured by this marker was higher in the SHR than in the WKY rats (WKY: 0.253 ± 0.058; SHR: 0.449 ± 0.063; $df = 205$; $p < 0.023$).

3.5. *JUN-B* Transcription Factor

The expression of *JUN-B* was lower in the rostral pole and shell of the SHR than in the WKY, as it accounted for 65% and 80% of the WKY level. In the core the labeling shows an increase to 128.6% in the SHR compared to WKY-rats.

3.5.1. Rostro-caudal Level. A 3-way factorial ANOVA line x ACB subterritory x antero-posterior level (as dependent variable) showed significant main effects of ACB subterritory ($F = 10.54$; $p < 0.005$) and level ($F = 5.88$; $p < 0.01$) and a strain x level interaction effect ($F = 4.78$; $p < 0.05$).

3.6. Cytochrome Oxidase Activity in SHR and WKY Rats

3.6.1. Standards. The standard curve for the transformation of units of optical density into activity units, expressed as μmoles/min/g wet weight tissue, was performed by the Gonzalez-Lima method (Gonzalez-Lima & Jones, 1994). Representative pastes containing different concentrations of C.O. activity are reproduced in Figure 4. The interpolation of data was linear.

Examples of coronal sections of the anterior forebrain of WKY and SHR rats are shown in Figure 5.

As shown in Table 1, rats of the SHR line showed a lower C.O. activity level in the medial (FR-2) and lateral (FR-1) frontal cortices. In fact, a 3-way 2 × 8 × 2 factorial ANOVA rat line (SHR vs. WKY) × area × brain side (as dependent variable) revealed significant main effects for line ($F = 10.21$; $p < 0.001$) and area ($F = 8.56$; $p < 0.005$) but not for brain side nor interaction effects.

3.6.2. Rostro-caudal Level. The level of metabolic capacity in the rostro-caudal plane in the sampled areas of WKY and SHR is reported in Figure 6 (lower row) for the

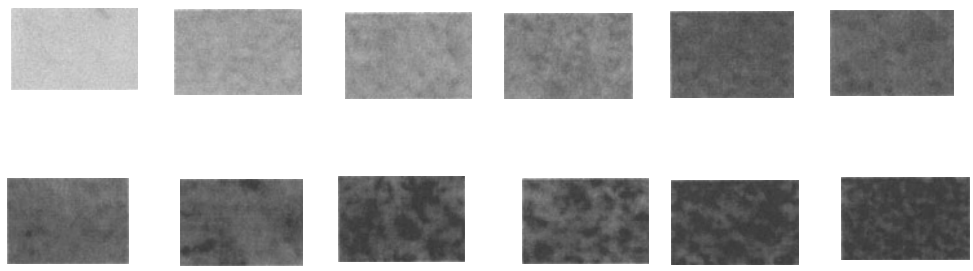

Figure 4. Cytochrome oxidase standards. Representative pastes showing different concentrations of cytochrome oxidase which allowed the formation of a standard reference curve for the conversion of optical density units into C.O. activity.

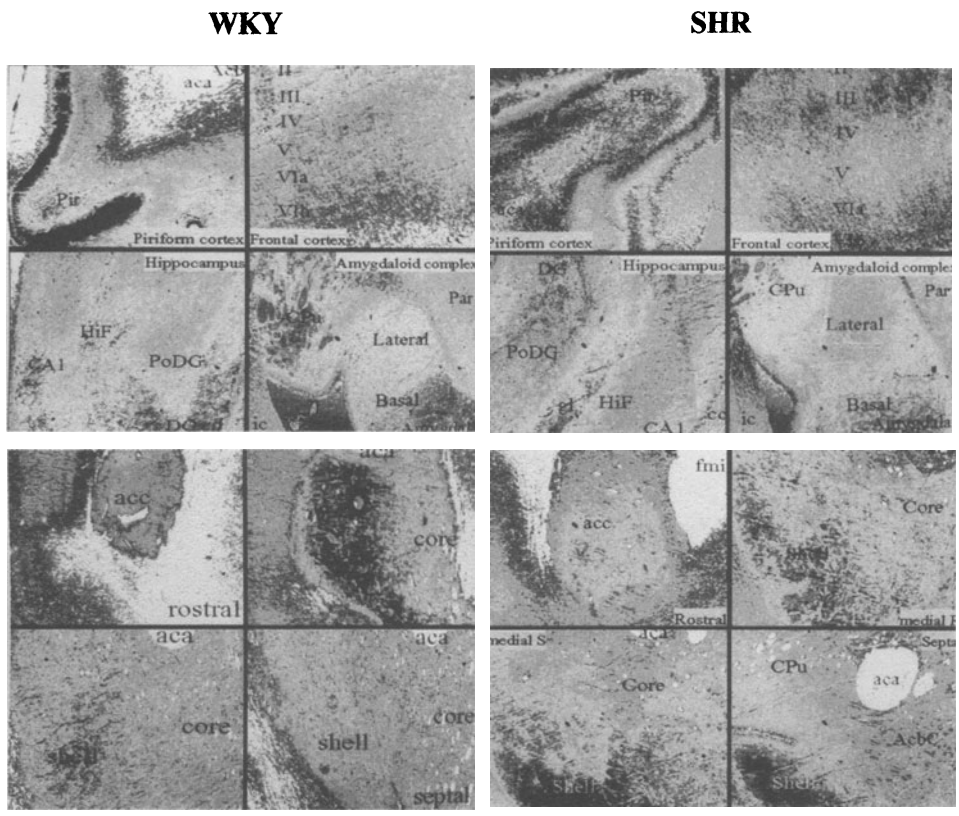

Figure 5. Representative images of brain areas mapped by cytochrome oxidase in WKY (left column) and SHR (right column) rats under basal conditions. The sampled areas are the pyriform cortex; the frontal cortex and its layers; the hippocampus; the amygdal complex with lateral and basal nuclei; aca, anterior commisure; acc, nucleus accumbens septal; core and shell; CA1, hippocampal region CA1; CPu, caudate-putamen; FMI, forceps minus of the corpus callosum; HiF, hippocampal formation; Pir, pyriform cortex; PoDGr, polyform layer of hippocampal dentate gyrus.

accumbal subterritories and the ventral pallidum, and in Figure 6 (upper row) for medial and lateral frontal cortices and the dorsal and ventral portions of the caudate-putamen.

A 2-way ANOVA rat line (WKY vs. SHR) x level (as dependent variable) revealed significant main effects for line in the rostral pole of the accumbens [$F = 4.049$, $p = 0.049$] and a highly significant effect for level in the core ($F = 10.459$; $p < 0.001$) and shell of the ACB

Table 1. Cytochrome oxidase activity in basal forebrain structures of naive SHR and WKY rats

Group	FR-1	FR-2	CPU-D	CPU-V	Pole	Core	Shell	VP
WKY-M								
L	14.7±0.78	14.2±0.55	18.4±0.34	18.4±0.49	18.8±0.41	17.0±1.06	18.2±1.32	10.6±1.02
R	14.7±0.72	14.7±0.34	18.1±0.54	18.2±0.44	20.9±1.70	16.3±0.80	17.7±1.29	10.5±1.44
SHR-M								
L	12.6±0.48[a]	12.8±0.59	17.6±1.46	17.4±1.26	16.1±1.55	16.4±0.79	17.4±0.85	10.5±0.56
R	12.8±0.50[a]	12.7±0.46	17.1±1.07	16.9±1.03	18.2±1.57	16.5±0.48	17.7±0.67	10.2±0.44

[a] $P < 0.01$. Figures are the mean ± SEM C.O. activity expressed as μM/min/g wet weight tissue. L, left side; R, right side; FR1, lateral frontal cortex; FR2, medial frontal cortex; CPU, caudate-putamen; D, dorsalis; V, ventralis; pole, core and shell, accumbal subregions; VP, ventral pallidum. There were no significant left-to-right differences, as tested by 2P t-test for paired data. significance symbols refer to WKY/SHR comparisons by 2P t-test for unpaired data.

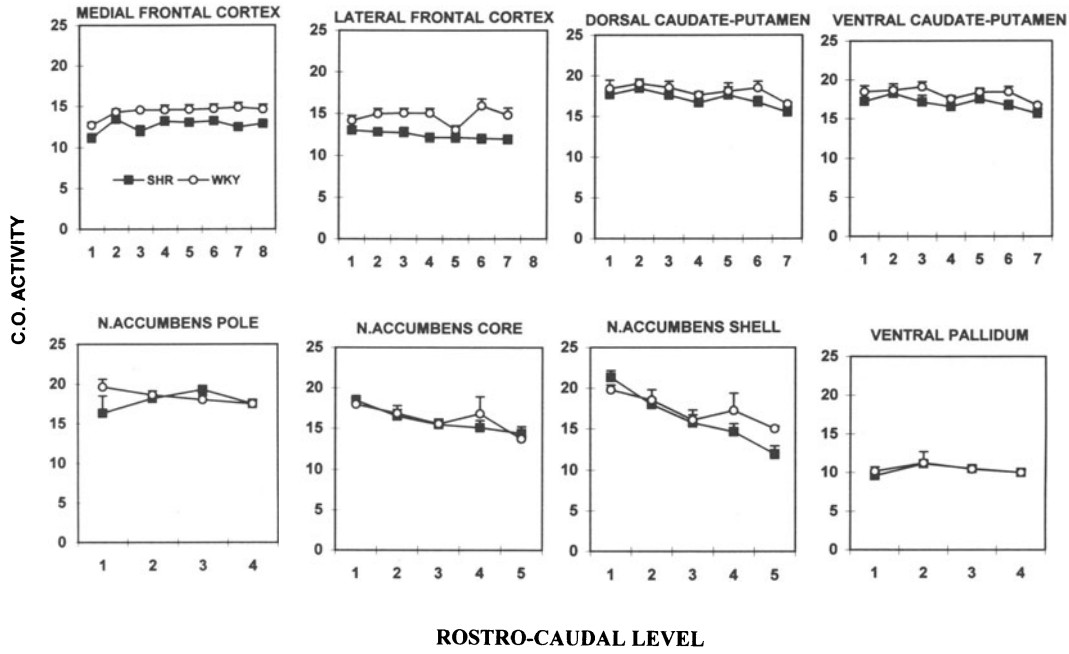

Figure 6. Rostro-caudal gradients in cytochrome oxidase activity (Mean ± SEM) in WKY and SHR rats in anterior forebrain sites, such as the medial (FR-2) and lateral (FR-1) frontal cortices, the dorsal and ventral caudate-putamen, the nucleus accumbens subterritories (pole, core and shell), and the ventral pallidum. The rostro-caudal plane has been arbitrarily divided in sublevels +4.20 and −2.80 for FR-1 and FR-2, +2.80 and −2.80 for both dorsal and ventral portions of caudate-putamen, between +3.40 and +2.10 for the pole, +2.70 and 0.00 for both core and shell, and between +2.00 and −1.40 for the ventral pallidum, with reference to bregma.

($F = 22.46$; $p < 0.001$) but not in the ventral pallidum. The line effect in the accumbal pole was due to a decreased level in SHR in the most rostral level. In the core and shell of ACB the level effect was due to higher metabolic capacity in the rostral than in the caudal portions.

In the ventral portion of the CPU there was a lower metabolic capacity in the SHR as revealed by a significant main effect for line ($F = 4.566$, $p = 0.034$). In the medial and lateral frontal cortices, SHR showed a lower metabolic capacity than WKY rats, as indicated by significant main effects for line ($F = 6.76$ and 16.84; $p < 0.01$ and 0.001, respectively). In the lateral frontal cortex only, there was an effect of the level due to a lower metabolic capacity in the most rostral portions of both rat lines ($F = 2.272$, $p = 0.028$).

3.6.3. Regional Intercorrelation Analysis. Correlating within each group individual levels of activity among different brain areas should give a hint about their interactions or "cross-talk", as previously described by Cada *et al.* (1995), which is shown in Table 2 and in Figure 7.

The average cross-correlation score was higher in the SHR than in the WKY (WKY: 0.420 ± 0.102; SHR: 0.782 ± 0.041; $t = 2.333$; $df = 54$; $0.025 < 2p < 0.05$ by t-test for non-paired data). Further, the WKY differed from the SHR mainly in the cross-correlations between the medial and lateral frontal cortices and the dorsal and ventral portions of the CPU, and between the latter and the ventral pallidum. Despite mostly positive scores, the SHR showed a smaller score of cross-correlations between the core and the shell of the accumbens and the ventral pallidum. These effects can be seen by careful examination of Figure 7, which demonstrates the discriminative power of this analysis when implemented by the method of Cada *et al.* (1995).

Table 2. Regional correlations of cytochrome oxidase activity in basal forebrain structures of SHR and WKY rats

Area	Group	FR2	CPU-D	CPU-V	Pole	Core	Shell	VP
FR1	WKY	0.978[a]	−0.625[d]	−0.653[d]	0.503	0.395	0.371	0.959[a]
	SHR	0.909[a]	0.932[a]	0.887[b]	0.735[c]	0.668[d]	0.571	0.896[b]
FR2	WKY		−0.690[c]	−0.717[c]	0.503	0.343	0.339	0.950[a]
	SHR		0.798[c]	0.728[c]	0.743[c]	0.909[b]	0.861[c]	0.584
CPU-D	WKY			0.999[a]	0.536	0.566	0.647[d]	−0.094
	SHR			0.994[a]	0.949[b]	0.652[d]	0.978[a]	1.000[a]
CPU-V	WKY				0.504	0.535	0.618[d]	−0.131
	SHR				0.978[a]	0.565	0.978[a]	1.000[a]
Pole	WKY					0.984[a]	0.981[a]	0.742[c]
	SHR				0.733[c]	0.576	0.848[b]	
Core	WKY						0.995[a]	0.615[d]
	SHR						0.978[a]	0.320
Shell	WKY							0.604[d]
	SHR							0.124

[a]P < 0.005; [b]P < 0.01; [c]P < 0.025; [d]P < 0.05. Figures are the 2P Pearson's correlation coefficients.

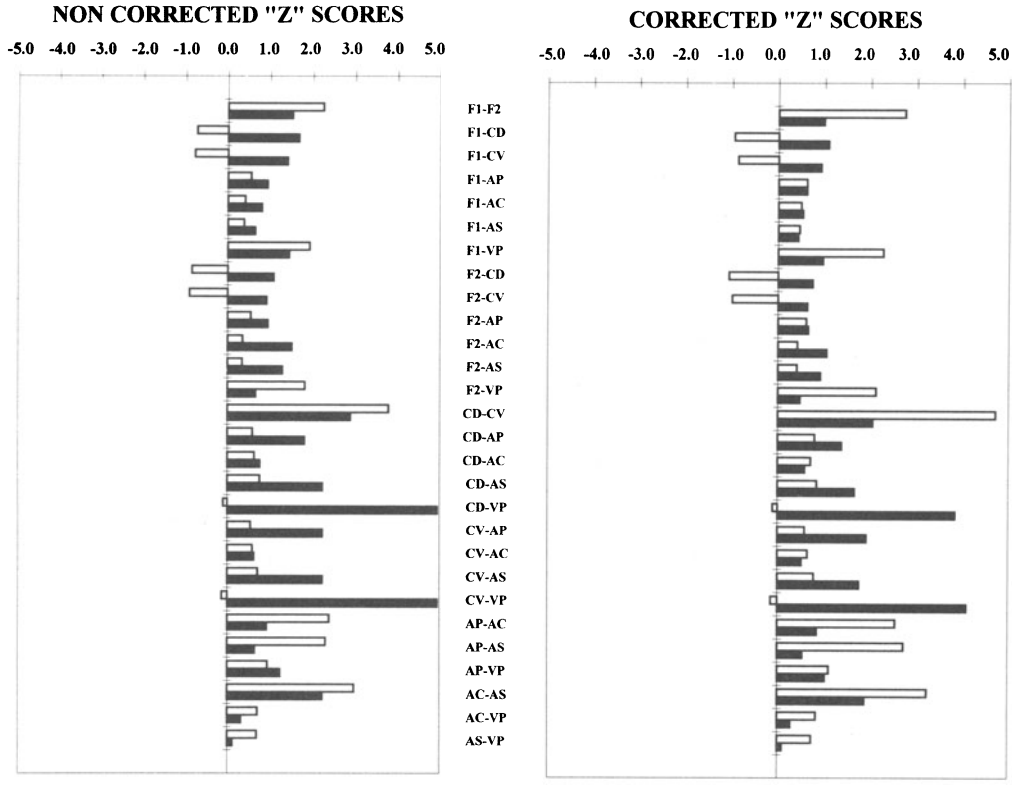

Figure 7. Regional covariations between cytochrome oxidase activity in the brain of WKY (open columns) and SHR (filled columns) rats under basal conditions. Figures are the "z" transformations of correlation coefficients by Pearson's product x moment method. The left panel shows the correlation between pairs of areas as "z" scores, whereas the right panel shows data corrected as "z" scores divided by the average "z" score among areas within brain by the Cada *et al.* method (1995). F1, lateral frontal cortex (area 1); F2, medial frontal cortex (area 2); C, caudate-putamen; D, dorsalis; V, ventralis; AP, AC, AS, nucleus accumbens pole, core and shell; VP, ventral pallidum.

3.7. Cytochrome Oxidase Activity in Naples NHE, NLE, and NRB Rats

The results are summarized in three tables, corresponding to regions of the hippocampal formation (Table 3), cerebral cortex (Table 4), and subcortical nuclei (Table 5). In Table 3, the outer granular cell layer of the dentate showed significant differences between the NLE and NHE groups. In fact, this was the only region showing a significant difference between these groups. This difference was mainly due to the outer granular cell layer of the dentate showing a localized decrease in C.O. activity in NLE. In addition, the entorhinal cortex (outer layers) showed an increased C.O. activity in NHE vs. NRB.

In Table 4, the medial frontal cortex showed an increased C.O. activity in NLE vs. NRB. The posterior parietal cortex (outer and middle layers) showed a decreased C.O. activity in NHE. The perirhinal cortex (in dorsal, middle and ventral parts) showed decreased C.O. activities in NHE vs. NRB. The dorsal perirhinal cortex also showed a decreased C.O. activity in NLE vs. NRB. Note that all differences in the cerebral cortex are in comparison with the NRB group. In NLE, the increase in C.O. activity was only in medial frontal cortex, a region implicated in depressive behavior.

In Table 5, most subcortical nuclei showed no differences, including nucleus accumbens and caudate-putamen. However, the cortical amygdala showed a decreased C.O. activity in NHE vs. NRB, corresponding to a region whose dysfunction is traditionally linked to increased emotionality.

These results in the Naples lines suggest that the neural basis for the hyperactivity of SHR rats is not mediated by the same neural systems differentiating the NHE and NLE rats. The NHE rats are not hyperactive under basal (nonincentive) conditions lacking novelty such as running wheel activity. Instead, NHE and NLE rats are hyperreactive and hyporeactive to spatial novelty, respectively. These results show that quantitative C.O. his-

Table 3. Group mean ± standard error of C.O. activity units in the hippocampal formation

Regions	NRB	NLE	NHE
Hippocampus, field CA1	199.26 ± 8.71	186.42 ± 7.39	185.45 ± 8.78
Hippocampus, field CA2	217.26 ± 10.33	198.36 ± 7.43	201.18 ± 8.15
Hippocampus, field CA3	215.71 ± 10.69	210.18 ± 11.03	198.12 ± 7.96
Hippocampus, field CA4	193.33 ± 11.19	180.84 ± 7.03	176.90 ± 8.74
Dentate gyrus, inner blade	223.00 ± 6.50	206.95 ± 5.63	206.66 ± 7.68
Dentate gyrus, outer blade	221.49 ± 6.17	223.99 ± 5.82	228.65 ± 4.97
Dentate outer molecular layer	247.55 ± 7.95	243.83 ± 6.49	237.85 ± 7.69
Hilus, fascia dentata	205.18 ± 11.74	193.28 ± 8.01	185.58 ± 9.28
Dentate inner molecular layer	233.81 ± 8.57	217.88 ± 4.17	214.18 ± 7.82
Stratum lacunosum-moleculare	221.49 ± 6.61	212.16 ± 5.20	217.10 ± 10.20
Stratum radiatum	191.30 ± 7.75	178.76 ± 6.24	175.71 ± 10.19
Stratum oriens	196.96 ± 7.77	183.93 ± 5.97	186.21 ± 9.27
Granular cell layer, outer[3]	187.91 ± 12.32	157.26 ± 3.32	174.88 ± 4.73
Granular cell layer, inner	176.99 ± 10.79	163.90 ± 5.57	163.60 ± 3.72
Pyramidal cell layer	187.96 ± 8.68	163.77 ± 8.71	170.15 ± 7.65
Presubiculum	221.48 ± 9.68	258.35 ± 22.31	209.16 ± 12.44
Dorsal subiculum	230.54 ± 6.32	277.55 ± 26.28	232.92 ± 11.72
Entorhinal cortex, outer[2]	182.09 ± 6.44	218.64 ± 14.92	201.60 ± 4.10
Entorhinal cortex, middle	185.98 ± 6.80	221.40 ± 16.67	201.46 ± 6.12
Entorhinal cortex, inner	191.32 ± 9.40	228.13 ± 16.90	213.09 ± 7.17
Ventral subiculum	246.64 ± 6.95	347.83 ± 44.04	286.12 ± 33.47

1, 2 and 3 indicate significant group difference at $p < 0.05$ (t-test), 1: NRB vs NLE, 2: NRB vs NHE, 3: NLE vs NHE.

Table 4. Group mean ± standard error of C.O. activity units in the cerebral cortex

Regions	NRB	NLE	NHE
Medial frontal cortex[1]	231.04 ± 8.00	285.23 ± 19.29	257.42 ± 45.21
Dorsal frontal cortex	238.98 ± 11.94	308.76 ± 31.11	260.89 ± 42.92
Lateral frontal cortex	240.70 ± 9.55	343.75 ± 48.27	267.30 ± 39.15
Sulcal frontal cortex	242.46 ± 11.62	317.12 ± 38.85	273.98 ± 47.58
Anterior cingulate cortex, dorsal	257.57 ± 8.17	330.90 ± 53.75	318.91 ± 38.91
Anterior cingulate cortex, middle	256.15 ± 12.40	337.69 ± 59.64	324.62 ± 45.52
Anterior cingulate cortex, ventral	264.51 ± 14.25	340.04 ± 53.42	328.70 + 65.10
Posterior cingulate cortex, dorsal	234.05 ± 5.76	217.29 ± 4.72	206.21 ± 10.51
Posterior cingulate cortex, middle	233.09 ± 6.48	211.76 ± 4.40	211.81 ± 8.95
Posterior cingulate cortex, ventral	228.37 ± 3.05	220.66 ± 8.04	211.30 ± 6.81
Primary motor cortex, outer	244.77 ± 7.17	303.95 ± 53.11	276.98 ± 33.10
Primary motor cortex, middle	246.82 ± 7.81	292.29 ± 35.90	298.46 ± 48.02
Primary motor cortex, inner	230.16 ± 7.74	269.09 ± 28.69	268.04 ± 27.29
Primary somatosensory cortex, outer	241.49 ± 11.02	329.23 ± 42.07	298.17 ± 49.58
Primary somatosensory cortex, middle	254.73 ± 15.80	326.41 ± 38.73	332.50 ± 71.57
Primary somatosensory cortex, inner	216.74 ± 10.76	244.67 ± 11.23	260.10 ± 25.78
Primary olfactory cortex	268.63 ± 20.84	339.20 ± 36.97	326.54 ± 75.72
Posterior parietal cortex, outer[2]	231.25 ± 11.75	212.29 ± 7.76	188.14 ± 9.66
Posterior parietal cortex, middle[2]	220.60 ± 6.44	199.78 ± 8.68	189.96 ± 8.12
Posterior parietal cortex, inner	202.54 ± 4.46	180.38 ± 9.50	184.64 ± 9.03
Perirhinal cortex, dorsal[1,2]	212.42 ± 6.59	188.96 ± 6.54	173.75 ± 6.31
Perirhinal cortex, middle[2]	200.03 ± 6.22	187.30 ± 7.75	164.77 ± 8.16
Perirhinal cortex, ventral[2]	186.11 ± 5.95	175.59 ± 7.40	156.57 ± 7.32
Retrosplenial cortex, outer	229.31 ± 10.91	274.08 ± 23.85	226.57 ± 12.68
Retrosplenial cortex, middle	235.64 ± 10.56	307.22 ± 35.60	226.72 ± 15.71
Retrosplenial cortex, inner	234.38 ± 15.33	319.48 ± 39.10	220.89 ± 15.32
Visual cortex, outer	229.94 ± 8.99	254.40 ± 12.36	227.38 ± 18.16
Visual cortex, middle	257.70 ± 16.06	310.31 ± 28.90	256.52 ± 28.83
Visual cortex, inner	231.02 ± 7.57	271.18 ± 20.80	232.62 ± 13.76
Auditory cortex, outer	230.67 ± 4.35	290.55 ± 21.18	196.28 ± 46.99
Auditory cortex, middle	262.72 ± 10.98	371.44 ± 41.35	261.13 ± 26.32
Auditory cortex, inner	230.84 ± 6.93	278.67 ± 23.30	224.31 ± 10.73

1, 2 and 3 indicate significant group difference at $p < 0.05$ (t-test), 1: NRB vs NLE, 2: NRB vs NHE, 3: NLE vs NHE.

tochemistry can successfully discriminate the neural substrates mediating different behaviors in genetic animal models.

4. DISCUSSION

These studies investigated within the anterior forebrain the neural substrates of behavior in the SHR and the Naples strains. We compared data obtained across different techniques such as radioligand binding studies and quantitative dopamine receptor autoradiography, immunocytochemistry for CaMKII, transcriptional regulators of gene expression, and cytochrome oxidase histochemistry, which monitor short-term and long-term changes in neuronal activity in neural networks.

4.1. Dopamine Receptors

Quantitative autoradiography for DA-receptors detected differences in the density of binding sites for D-1/D-5, but not for D-2 binding sites. In spite of the lack of cellular

Table 5. Group mean ± standard error of C.O. activity units in subcortical nuclei

Regions	NRB	NLE	NHE
Medial septal nu.	241.42 ± 12.45	274.57 ± 19.53	281.57 ± 46.77
Lateral septal nu., dorsal	220.60 ± 7.77	286.99 ± 40.42	258.05 ± 23.87
Lateral septal nu., middle	229.90 ± 9.13	310.89 ± 44.39	283.50 ± 44.14
Lateral septal nu., ventral	236.44 ± 8.37	301.17 ± 31.94	304.35 ± 57.54
Accumbens nu., core	235.72 ± 11.74	272.38 ± 24.66	250.24 ± 31.07
Accumbens nu., shell	189.25 ± 6.35	209.71 ± 9.98	201.16 ± 16.47
Habenular nu.	210.13 ± 7.26	205.33 ± 3.76	199.77 ± 7.70
Lateral habenular nu.	252.76 ± 16.07	233.26 ± 3.66	240.43 ± 9.40
Parafascicular thalamic nu.	204.11 ± 8.41	192.16 ± 4.20	183.31 ± 8.83
Ventroposterior thalamic nu.	209.88 ± 6.57	197.48 ± 3.21	186.71 ± 10.85
Caudate-putamen, rostral	233.30 ± 10.76	250.86 ± 11.82	245.55 ± 23.17
Caudate-putamen, caudal	233.25 ± 4.21	233.40 ± 6.36	220.40 ± 9.78
Basolateral amygdaloid nu.	198.29 ± 8.01	184.32 ± 8.93	177.94 ± 8.80
Lateral amygdaloid nu.	179.43 ± 7.50	159.56 ± 9.26	148.90 ± 7.66
Central amygdaloid nu.	187.26 ± 7.26	195.28 ± 8.97	175.01 ± 8.10
Medial amygdaloid nu.	172.04 ± 6.55	170.59 ± 9.92	152.11 ± 6.30
Cortical amygdaloid nu.[2]	174.64 ± 9.00	153.85 ± 11.77	142.22 ± 5.88
Vertical diagonal band nu.	206.39 ± 9.63	225.87 ± 13.24	223.80 ± 23.53

1, 2 and 3 indicate significant group difference at $p < 0.05$ (t-test), 1: NRB vs NLE, 2: NRB vs NHE, 3: NLE vs NHE.

resolution, receptor autoradiography allowed the assessment of dissociation constants following ex-vivo in-vitro analysis of the dynamics of binding in presence of increasing concentrations of the D-1/D-5 receptor antagonist, tritiated SCH23390. A discrete alteration was found by the measurement of binding sites for D-1 and D-2 receptor families at about the dissociation constant. This effect occurred across the entire rostro-caudal plane in serial sections including the frontal cortex; the caudate-putamen complex, both dorsalis and ventralis; the nucleus accumbens pole, core, and shell; and the ventral pallidum.

While DA receptors could have been measured also by immunocytochemistry using specific antibodies with the advantage of a cellular resolution, the higher spatial resolution would have replaced a quantitative profile with a qualitative profile. This would have overlooked the dynamic function of ligand-receptor interaction and the finding of different binding site densities with altered dissociation constants in a restricted coronal segment of the anterior forebrain. Alternatively, in-situ hybridization could have dealt with this problem. In fact, messenger RNA (mRNA) for protein subunits of the DA receptor complex could be detected, thus allowing a quantitative estimate of mRNAs using riboprobes or oligoprobes. However, since different proteins can be formed from the same mRNA molecule as a result of alternative splicing or posttranslational modifications, in-situ hybridization could be misleading in that it allows the detection of the mRNA, but not of the protein products derived from that single RNA molecule.

4.2. CaMKII and Transcription Factors

The immunocytochemical determination of the alpha-isoform of the enzyme CaMKII is at the level of high resolution light-microscopy. This enzyme is a coincidence detector device of spatio-temporal contingencies, not only at the cellular level, but also in dendrites and in presynaptic terminals. The alpha-isoform could also have been measured by in-situ hybridization but considerations similar to those made above would apply in the case of CaMKII as well.

Similarly, the immunocytochemical detection of transcription factors allowed the cellular-level visualization of nuclei elements, which were immunolabeled for the peptide product of *c-FOS*. Higher specificity could have been attained by using in-situ hybridization of the messenger RNA coding for the protein *c-FOS*. However, the same considerations about in-situ hybridization apply to *c-FOS* as they did to CaMKII and DA-receptors (see above).Moreover, a rostro-caudal gradient could be detected, which would have been otherwise overlooked if few sections had been sampled and analyzed by in-situ hybridization, immunocytochemistry or western blot analysis.

In contrast to CaMKII, which is present in the neuropil labeling of mostly postsynaptic sites and to a lesser extent presynaptic terminals, *c-FOS* exclusively labels nuclei. Thus, the two markers monitor different aspects of functional circuits, namely the neurons of origin and the dendritic/axonic connections, respectively.

Both CaMKII and transcription factors monitor short-lasting events, the time constants of which are minutes to hours. It is widely accepted that c-*FOS* is a neuronal marker that is part of a complex orchestration that eventually leads to changes in gene expression. However, when a component of the FOS-family dimerizes with a component of the JUN-family, it can either activate or inhibit gene expression. In fact, in three-fourths of cases, FOS/JUN dimers activate gene expression, whereas in one-fourth of cases, when a FOS member dimerizes with *JUN-B*, gene expression is inhibited instead. Furthermore, in the cases of activating gene expression, late genes of the FOS-family, such as *FOS-B* and FOS-related antigen 1 and 2 (FRA-1 and FRA-2) can be expressed, thus influencing gene expression in a time-dependent-manner. This is just one example of how a time variable can be coded in neural circuits as a spatial variable.

4.3. Cytochrome Oxidase

The first outcome of the C.O. study demonstrated that under basal conditions the medial and lateral frontal cortices of the SHR expressed a lower metabolic capacity than those of WKY controls. This lower activity is in agreement with previous data from the literature on animal models and ADHD children. However, the frontal cortex findings are somewhat contradictory, as some studies show impairment and some do not (Filipek *et al.*, 1996). Interestingly, there is discordance also in animals models, as for instance the Naples High-Excitability (NHE) rats do not differ in metabolic capacity, as monitored by the same C.O. method, in the medial and lateral frontal cortex under basal, naive conditions (Gonzalez-Lima *et al.*, 1996). In the same experiment, another genetic model, the Naples Low-Excitability (NLE) rats, characterized by low behavioral arousal and increased non-selective attention to spatial novelty (Aspide *et al.*, 1998), showed an increased metabolic capacity in the medial and lateral frontal cortices.

Another finding from the C.O. study on the SHR model is the difference in the rostro-caudal plane in the accumbal core and shell and in the caudate-putamen, but not in the medial and lateral frontal cortices nor in the ventral pallidum. This finding correlates well with similar gradients in the distribution of dopamine receptors of the D-1 and D-2 subfamilies (Carey *et al.*, 1997). In other words, the C.O. enzyme appears as the end product of the chain of events which are triggered by the D-1 and D-2 receptors, and leads to activation or inhibition of adenylate cyclase in GABA neurons to form cAMP in the caudate-putamen and the accumbal complex. These regions are interconnected with the substantia nigra pars compacta, ventral tegmental area (VTA) and ventral pallidum (Dahlstrom & Fuxe, 1964).

The most rostral portions of both the caudate-putamen and the accumbal complex show a lower activity in the SHR model than in control rats by all markers except C.O. activity. This apparent discrepancy can perhaps be explained by the consideration that, while C.O. activity is the result of a complex integration among different signals of different origin, dopamine receptor autoradiography reflects the interplay of a smaller number of signals converging on dopaminergic synapses. Therefore, what can be found at a single receptor level does not necessarily extend to all other markers, as each of them monitors activity at different cellular levels and with a different time constant.

The different interregional correlative profile in the brains of SHR and WKY indicates a different cross-talk in these animals, as revealed by a procedure conceptually similar to the cross-correlation analysis used by electrophysiologists (Brazier, 1961). By indicating the areas which are correlated and those which are not correlated and to what extent, it is clear that the WKY make different brain operations than the SHR. In fact, the average correlation score and the regional profile indicate that under basal conditions there was a simultaneous low level of activation across almost all sampled areas, as demonstrated by the lack of difference at the population level. Within groups, individual differences within each sampled area covaried to the point that the covariation was high but no deviation from this "choral", "unison" activity could be detected.

Thus, this comparative imaging approach has allowed the detection and mapping of differences in the cortico-striato-pallidal neural network under basal conditions. The low cross-talk as indirectly measured by the high degree of covariance or synchronization demonstrates that the brains of SHR rats are poorly modulated. The low basal expression of transducer systems such as the Ca^{2+}/calmodulin-dependent protein kinase II (Papa *et al.*, 1996a) or transcriptional regulators of gene expression such as peptides of the immediate early gene families *FOS*, *JUN* and *zif-268* in the accumbal core and shell of SHR rats (Papa *et al.*, 1998) point to basic failures in the neuronal machinery leading eventually to plastic changes.

The major outcome of the experiments with the Naples lines, is that they differ in metabolic capacity in areas which are thought to be involved in the processing of limbic and spatial information. Interestingly, of all the 71 regions analyzed (including sensory and motor regions) only prefrontal and limbic regions showed C.O. metabolic differences. Hippocampal metabolic differences between the NLE and NHE were found in the granular cell layer of the outer blade of the dentate gyrus. This was the only region with a significant difference between the experimental strains (NLE vs. NHE) and supports the conclusion that these strains differ in hippocampal function (Cerbone *et al.*, 1993). Granule cells of the dentate gyrus show postnatal cell division in rats, and are particularly vulnerable to manipulations such as X-irradiation in infancy (Altman, 1986). Indeed, granule cell hypoplasia in the X-irradiated infant rat leads to hyperreactivity and learning deficits which have been hypothesized to simulate deficits found in ADHD children (Diaz-Granados *et al.*, 1994).

Greater metabolic capacity of entorhinal cortex was found in the high behavioral reactivity NHE group as compared to NRB controls. Entorhinal influences on hippocampal function may be related to hyperreactivity (Cerbone *et al.*, 1993). Genetic selection led to greater metabolic capacity in the medial frontal cortex correlated to low behavioral reactivity. This region has been related to depressive behavior in 2-deoxyglucose studies (Caldecott-Hazard & Weissman, 1992). Lower metabolism in the posterior parietal cortex, the perirhinal cortex, and the cortical amygdala of both NHE and NLE suggests a potential learning impairment because these regions are related to the differentiation of associative effects of conditioned stimuli in rats (Gonzalez-Lima & Scheich, 1986; McIntosh & Gonzalez-Lima, 1994).

4.4. Neural Bases of Behavior in Genetic Animal Models of ADHD

As the ADHD syndrome in children has been described with variants showing prevailing attention or activity deficits (Barkley, DuPaul, & McMurray, 1991; Goodyear & Hynd, 1992), similarly, animal models can reproduce and feature the main aspects of the clinical heterogeneity. In fact, NLE and NHE rat lines show altered non-selective attention, as measured by the duration of rearing episodes, but NHE are hyperreactive and NLE are hyporeactive. Therefore, the NHE might model the ADD-plus variants of ADHD (Aspide *et al.*, 1997).

The finding of a discrete defect in the anterior forebrain is particularly relevant, on theoretical grounds, given the strategic role of the anterior caudate-putamen, corresponding to the head of the caudate nucleus in humans, which is thought to be involved in higher order cognitive functions (Graybiel *et al.*, 1994), and given its relationships with orbito-frontal cortex and limbic structures (Zahm & Brog, 1992). First, the most rostral portion of the caudate-putamen has been demonstrated by functional imaging techniques to have abnormal activity related to some neuropsychiatric disorders (Benkelfat *et al.*, 1990; Rapoport, 1988), and to ADHD as well (Filipek, 1996). Second, the lower neuronal activity level is associated with a higher density of dopamine receptors of the D-1/D-5 subfamily (Carey, 1997). Third, subchronic treatment with methylphenidate, a drug which blocks to different degrees the transporter systems for biogenic amines [serotonin, dopamine, norepinephrine, epinephrine and histamine (Gatley, 1996)], has been shown to reverse the altered dopamine D-1/D-5 receptor distribution in the most rostral portions of the caudate-putamen but not in the accumbal core and shell (Diewald *et al.*, in preparation). Thus, it is plausible to hypothesize that such a segmental defect is due to disintegration between transcription factors with restricted spatial domains and environmental signals during critical organizational phases of the anterior forebrain.

In conclusion, the molecular imaging techniques used in these studies allowed us to investigate the neural substrates of brain operations made in neural networks in two animal models of ADHD, the SHR and the NHE/NLE rats. While ADHD children do not benefit in the long run by treatment with the blockers of the dopamine re-uptake system, these experiments should be pursued in an attempt to verify the possibility that the segmental defect could be partially modified in rats following behavioral training and drug therapy.

ACKNOWLEDGMENTS

This research has been supported by EU Human Capital and Mobility contract ERBCHRXCT930303, by Telethon-Italy grant #E513, by NIH grant MH43353, and by NSF grant IBN9222075. The technical assistance of D. Hu and K. Nixon is gratefully acknowledged.

REFERENCES

Altman, J. (1986). An animal model of minimal brain dysfunction. In M. Lewis (ed.), *Learning disabilities and prenatal risk.* Urbana and Chicago: Univ. of Illinois Press.

American Psychiatric Association (1994) *Diagnostic and Statistical Manual of Mental Health, Fourth Edition.* Washington, DC.

Aspide, R., Gironi Carnevale, U.A., Sergeant, J.A., and Sadile, A.G. (1998) Impaired non-selective attention in two animal models of Attention-Deficit Hyperactivity Disorder. *Behav. Brain Res.* (in press).

Barkley, R.A., DuPaul, G.J. and McMurray, M.B. (1991) Attention deficit disorder with and without hyperactivity: Clinical response to three different doses of methylphenidate. *Pediatrics 87*, 519–531.

Benkelfat, C., Nordahl, T.E., Semple, W.E., King, A.C., Murphy, D.L. and Cohen, R.M. (1990) Local cerebral glucose metabolic rates in obsessive-compulsive disorder. Patients treated with clomipramine. *Arch. Gen. Psychiatry 47*, 840–848.

Brazier, M.A.B. (1961) *Computer techniques in EEG analysis.* 18, 1–68.

Bunzow, J.R., Van Tol, H.H.M., Grandy, D.K., Albert, P., Salon, J., Christie, J., Machida, C.A., Neve, K.A., and Civelli, O. (1988) Cloning and expression of a rat dopamine D2 receptor cDNA. *Nature 336,* 783–787.

Cada, A., Gonzalez-Lima, F., Rose, G.M., and Bennett, C. (1995) Regional brain effects of sodium azide treatment on cytochrome oxidase activity: a quantitative histochemical study. *Metabolic Brain Disease 10,* 303–320.

Caldecott-Hazard, S. and Weissman, A.D. (1992) Brain systems involved in depressed behaviors: Corroboration from different metabolic studies. In *Advances in metabolic mapping techniques for brain imaging of behavioral and learning functions. NATO ASI Series D, Vol. 68.* eds Gonzalez-Lima F., Finkenstaedt T. and Scheich H. pp. 39–109. Kluwer Academic Publishers, Dordrecht.

Carey, M.P., Diewald, L., Papa, M., Gironi Carnevale, U.A., Pellicano, M.P., Esposito, F., Sagvolden, T., Sergeant, J.A., and Sadile, A.G. (1998) Differential distribution of D-1 and D-2 dopamine receptors in the target sites of the mesolimbic system in an animal model of ADHD. *Behav. Brain Res.* (in press).

Cerbone, A., Patacchioli, F.R., and Sadile, A.G. (1993a) A neurogenetic and morphogenetic approach to hippocampal functions based on individual differencews and neurobehavioral covariations. *Behav. Brain Res. 55,* 1–16.

Cerbone, A., Pellicano, M.P., and Sadile, A.G. (1993b) Evidence for and against the Naples High and Low-Excitability rats as genetic model to study hippocampal functions. *Neurosci. Biobehav. Rev. 17,* 295–303.

Cheng, Y. and Prusoff, W.H. (1973) Relationship between the inhibition constant (Ki) and the concentration of inhibitor which causes 50 per cent inhibition (I50) of an enzymatic reaction. *Biochem. Pharmacol. 22,* 3099–3108.

Christy, B. and Nathans, D. (1989) DNA binding site of the growth factor-inducible protein Zif268. *Proc. Natl. Acad. Sci. U. S. A. 86,* 8737–8741.

Cook, E.H., Jr., Stein, M.A., Krasowski, M.D., Cox, N.J., Olkon, D.M., Kieffer, J.E., and Leventhal, B.L. (1995) Association of attention-deficit disorder and the dopamine transporter gene. *Am. J. Hum. Genet. 56,* 993–998.

Dahlstrom, A. and Fuxe, K. (1964) Evidence for the existence of monoamine-containing neurons in the central nervous system. I. Demonstration of monoamines in cell bodies of brain stem neurons. *Acta Physiol. Scand. 62, Suppl. 232,* 1–55.

Dearry, A., Gingrich, J.A., Falardeau, P., Fremeau, R.T., Bates, M.D., and Caron, M.G. (1990) Molecular cloning and expression of the gene for a human D1 dopamine receptor. *Nature 347,* 72–76.

Diaz-Granados, J.L., Greene, P.L., & Amsel, A. (1994). Selective activity enhancement and persistence in weanling rats after hippocampal x-irradiation in infancy: Possible relevance for ADHD. *Behavioral and neural biology 61,* 251–259.

Drewes, G., Lichtenberg-Kraag, B., Doring, F., Mandelkow, E.M., Biernat, J., Goris, J., Doree, M., and Mandelkow, E. (1992) Mitogen activated protein (MAP) kinase transforms tau protein into an Alzheimer-like state. *Eur. Mol. Biol. Org. J. 11,* 2131–2138.

Edwards, A.L. (1967) *Statistical Methods for the Behavioral Sciences.* Holt, Rinehart and Winston, New York.

Filipek, P A; Semrud-Clikeman, M; Steingard, R J; Renshaw, P F; *et al.* (1997) Volumetric MRI analysis comparing subjects having attention-deficit hyperactivity disorder with normal controls. *Neurology 48,* 589–601.

Frick, P.J. and Lahey, B.B. (1991) Nature and characteristics of attention-deficit hyperactivity disorder. *School Psychol. Rev. 20,* 163–173.

Gatley, S.J., Pan, D.F., Chen, R.Y., Chaturvedi, G. and Ding, Y.S. (1996) Affinities of methylphenidate derivatives for dopamine, norepinephrine and serotonin transporters. *Life Sci. 58,* PL231-PL239.

Gonzalez-Lima F. (1992) Brain imaging of auditory learning functions in rats: studies with fluorodeoxyglucose autoradiography and cytochrome oxidase histochemistry. In *Advances in metabolic mapping techniques for brain imaging of behavioral and learning functions. NATO ASI Series D, Vol. 68.* eds Gonzalez-Lima F., Finkenstaedt T. and Scheich H. pp. 39–109. Kluwer Academic Publishers, Dordrecht.

Gonzalez-Lima, F., Hu, D., Nixon, K., Sagvolden, T., Sergeant, J.A., and Sadile, A.G. (1996) Altered metabolic capacity of frontal and limbic regions in rats genetically selected for low and high behavioral reactivity to spatial novelty. *Proc. IBNS, Cancun, Mexico. 5,* 39

Gonzalez-Lima, F. and Jones, D. (1994) Quantitative mapping of cytochrome oxidase activity in the central nervous system of the gerbil: a study with calibrated activity standards and metal-intensified histochemistry. *Brain Res. 660,* 34–49.

Goodyear, P. and Hynd, G.W. (1992) Attention-deficit disorder with (ADD/H) and without (ADD/WO) hyperactivity: behavioral and neuropsychological differentiation. *J. Clin. Child Psychol. 21,* 273–305.

Gonzalez-Lima, F. and Scheich, H. (1986) Classical conditioning of tone-signaled bradycardia modifies 2-deoxyglucose uptake patterns in cortex, thalamus, habenula, caudate-putamen and hippocampal formation. *Brain Res. 363,* 239–256.

Grandy, D.K., Zhang, Y., Bouvier, C., Zhou, Q., Johnson, R.A., Allen, L., Buck, K., Bunzow, J.R., Salon, J., and Civelli, O. (1991) Multiple D5 dopamine receptor genes: A functional receptor and two pseudogenes. *Proc.Natl.Acad.Sci.USA 88,* 9175–9179.

Graybiel, A.M., Aosaki, T., Flaherty, A.W., and Kimura, M. (1994) The basal ganglia and adaptive motor control. *Science 265*, 1826–1831.

Gunning, W.B., and Sergeant, J.A. (1994) Attention deficit disorder: from concept to treatment. *State Art 1,* 4–15.

Hanson, P.I. and Schulman, H. (1992) Neuronal Ca^{2+}/Calmodulin-dependent protein kinases. *Annu. Rev. Biochem. 61,* 559–601.

Hyde, G.E. and Durham, D. (1990) Cytochrome oxidase response to cochlea removal in chicken auditory brainstem neurons. J. *Comp. Neurol. 297*, 329–339.

Kebabian, J.W. and Caine, D.B. (1979) Multiple receptors for dopamine. *Nature 277,* 93–96.

Kelly, P.T., McGuinness, T.L., and Greengard, P. (1984) Evidence that the major postsynaptic density protein is a component of a Ca2+/Calmodulin-dependent protein kinase. *Proc.Natl.Acad.Sci.USA 81,* 945–949.

Kirouac, G.J. and Ganguly, P.K. (1993) Up-regulation of dopamine receptors in the brain of the spontaneously hypertensive rat: an autoradiographic analysis. *Neuroscience 52*, 135–141.

List, S.J. and Seeman, P. (1981) Resolution of dopamine and serotonin receptor components of [^{3}H]spiperone binding to rat brain regions. *Proc. Natl. Acad. Sci. U. S. A. 78,* 2620–2624.

Liu, L.X., Monsma, F.J., Sibley, D.R., and Chiodo, L.A. (1996) D2L, D2S, and D3 dopamine receptors stably transfected into NG108–15 cells couple to a voltage-dependent potassium current via distinct G protein mechanisms. *Synapse 24,* 156–164.

Machu, T.K., Firestone, J.A., and Browning, M.D. (1993) Ca^{2+}/Calmodulin-dependent protein kinase II and protein kinase C phosphorylate a synthetic peptide corresponding to a sequence that is specific for the gamma-2L subunit of the GABA-A receptor. *J. Neurochem. 61,* 375–377.

Malinow, R., Schulman, H., and Tsien, R.W. (1989) Inhibition of postsynaptic PKC or CaMKII blocks induction but not expression of LTP. *Science 245,* 862–866.

Marrocco, R.T., Witte, E.A., and Davidson, M.C. (1994) Arousal systems. *Curr. Opin. Neurobiol. 4,* 166–170.

McGlade-McCulloh, E., Yamamoto, H., Tan, S.E., Brickey, D.A., and Soderling, T.R. (1993) Phosphorylation and regulation of receptors by calcium/calmodulin-dependent protein kinase II. *Nature 362*, 640–642.

McIntosh, A.R. & Gonzalez-Lima, F. (1994) Network interactions among different limbic cortices, basal forebrain, and cerebellum differentiate a tone conditioned as a Pavlovian excitor or inhibitor: Fluorodeoxyglucose mapping and covariance structural modeling. *Journal of neurophysiology, 72,* 1717–1733.

Morgan, J.I. and Curran, T. (1991) Stimulus-transcription coupling in the nervous system: involvement of the inducible proto-oncogenes fos and jun. *Annu. Rev. Neurosci. 14,* 421–451.

Papa, M., Sergeant, J.A., and Sadile, A.G. (1998). Reduced transduction mechanisms in the accumbal interface of an animal model of ADHD. *Behav. Brain Res.* (in press).

Papa, M., Sagvolden, T., Sergeant, J.A., and Sadile, A.G. (1996a) Reduced CaMKII-positive neurones in the accumbal shell of an animal model of Attention-Deficit Hyperactivity Disorder. *Neuroreport. 7,* 3017–3020.

Papa, M., Sagvolden, T., Sergeant, J.A., and Sadile, A.G. (1996b) Reduced transduction mechanisms in the accumbal interface of an animal model of ADHD. *Behav. Brain Res.* (in press).

Papa, M., Sergeant, J.A., and Sadile, A.G. (1996c) Differential expression of transcription factors in the accumbal complex of an animal model of ADHD. *NeuroReport 8,* 1607–1612.

Paxinos, G. and Watson, C. (1986) *The Rat Brain in Stereotaxic Coordinates.* Academic Press, London.

Popoli, M., Vocaturo, C., Perez, J., Smeraldi, E., and Racagni, G. (1995) Presynaptic Ca^{2+}/calmodulin-dependent protein kinase II: autophosphorylation and activity increase in the hippocampus after long-term blockade of serotonin reuptake. *Mol. Pharmacol. 48,* 623–629.

Posner, M.I. and Dehane, S. (1994) Attentional Networks. Trends Neurosci. 17, 75–79.

Rapoport, J.L. (1988) The neurobiology of obsessive-compulsive disorder [clinical conference]. *JAMA 260,* 2888–2890.

Rhodes, D. and Klug, A. (1993) Zinc fingers. *Sci. Am. 268,* 56–62.

Robbins, T.W. and Everitt, B.J. (1994) Arousal systems and attention. In *The Cognitive Neurosciences* ed Gazzaniga M.S. pp. 703–720. The MIT Press, Cambridge, MA.

Rostas, J.A.P. and Dunkley, P.R. (1992) Multiple forms and distribution of Calcium/Calmodulin-stimulated protein kinase II in brain. J. *Neurochem. 59,* 1191–1202.

Russell, V., de Villiers, A., Sagvolden, T., Lamm, M., and Talijaard, J.J.F. (1996) Differences between electrically-, ritalin-, and d-amphetamine-stimulated release of [^{3}H]-dopamine from brain slices suggest impaired vesicu-

lar storage of dopamine in an animal model of attention-deficit hyperactivity disorder. *Behav. Brain Res.* (in press).

Russell, V.A., de Villiers, A.S., Sagvolden, T., Lamm, M.C.L., and Taljaard J.J.F. (1995) Altered dopaminergic function in the prefrontal cortex, nucleus accumbens and caudate-putamen of an animal model of Attention-Deficit Hyperactivity Disorder - the spontaneously hypertensive rat. *Brain Res. 676,* 343–351.

Safer, D.J. and Krager, J.M. (1988) A survey of medication treatment for hyperactive/inattentive students. *JAMA 260,* 2256–2258.

Sagvolden, T. (1996) The Attention Deficit Disorder might be a reinforcement deficit disorder. In *Contemporary Psychology in Europe: Theory, Research and Application* eds Georgas, J., Manthouli, M., Besevegis, E., and Kokkevi, A. pp. 132–143. Hogrefe and Huber, Gottingen.

Schulman H. (1993) The multifunctional Ca^{2+}/Calmodulin-dependent protein kinases. *Curr. Opin. Cell Biol. 5,* 247–253.

Seiden, L.S., Sabol, K.E., and Ricaurte, G.A. (1993) Amphetamine: effects on catecholamine systems and behaviour. *Annu. Rev. Pharmachol. Toxicol. 32,* 639–677.

Sheng, M. and Greenberg, M.E. (1990) The regulation and function of c-fos and other immediate early genes in the nervous system. *Neuron 4,* 477–485.

Silva, A.J., Paylor, R., Wehner, J.M., and Tonegawa, S. (1992) Impaired spatial learning in alpha-Calcium-Calmodulin Kinase II mutant mice. *Science 257,* 206–211.

Sokoloff, P., Giros, B., Martres, M.P., Bouthenet, M.L. and Schwartz, J.C. (1990) Molecular cloning and characterization of a novel dopamine receptor (D3) as a target for neuroleptics. *Nature 347,* 146–151.

Sunahara, R.K., Guan, H.C., O'Dowd, B.F., Seeman, P., Laurier, L.G., Ng, G., George, S.R., Torchia, J., Van Tol, H.H.M., and Niznik, H.G. (1991) Cloning of the gene for a human dopamine D5 receptor with higher affinity for dopamine than D1. *Nature 150,* 614–619.

Swanson, J.M.. Sergeant, J.A., Taylor, E., Sonuga-Barke, E.J.S., Jensen, P.S., and Canwell, D.P. (1998) Attention-deficit hyperactivity disorder and hyperkinetic disorder. *The Lancet 351,* 429–433.

van der Meere, J., Vreeling, H.J., and Sergeant, J. (1992) A motor presetting study in hyperactive, learning disabled and control children. *J. Child Psychol. Psychiatry 33,* 1347–1354.

Van Tol, H.H.M., Bunzow, J.R., Guan, H.C., Sunahara, R.H., Seeman, P., Niznik, H.B., and Civelli, O. (1991) Cloning of the gene for a human dopamine D4 receptor with high affinity for the antipsychotic clozapine. *Nature 350,* 610–614.

Wayman, G.A., Impey, S., and Storm, D.R. (1995) Ca^{2+} inhibition of type III adenylyl cyclase in vivo. *J.Biol.Chem. 270,* 21480–21486.

Wikstrom, M., Krab, K., and Saraste, M. (1981) *Cytochrome oxidase: a synthesis.* Academic Press, New York.

Wong-Riley, M.T.T. (1979) Changes in the visual system of monocularly sutured or enucleated cats demonstrated with cytochrome oxidase histochemistry. *Brain Res. 17,* 111–128.

Wong-Riley, M.T.T. (1989) Cytochrome oxidase: an endogenous metabolic marker for neeuronal activity. *Trends Neurosci. 12,* 94–101.

Wong-Riley, M.T.T., Hevner, R.F., Cutlan, R., Earnest, M., Egan, R., Frost, J., and Nguyen, T. (1993) Cytochrome oxidase in the human visual cortex: distribution in the developing and adult brain. *Visual Neurosci. 10,* 41–58.

Zahm, D.S. and Brog, J.S. (1992) On the significance of subterritories in the "Accumbens" part of the rat ventral striatum. *Neuroscience 50,* 751–767.

Zilles, K., Schleicher, A., Rath, M., Glaser, T., and Traber, J. (1986) Quantitative autoradiography of transmitter binding sites with an image analyzer. *J. Neurosci. Meth. 18,* 207–220.

6

CYTOCHROME OXIDASE INHIBITION IN ALZHEIMER'S DISEASE

F. Gonzalez-Lima, J. Valla, and L. Jorandby

Institute for Neuroscience and Department of Psychology
The University of Texas at Austin
Mezes 330
Austin, Texas 78712

ABSTRACT

There is a compelling need to understand neuronal oxidative metabolism in Alzheimer's brains in order to unequivocally diagnose and treat Alzheimer's disease patients successfully. This disease may be affecting one of every three families in the US. Although rare familial types of Alzheimer's disease follow Mendelian genetics, most cases appear after age 65 and have no clearly identifiable nuclear genetic defects. It is in this majority of late-onset, sporadic cases that defects in cytochrome oxidase activity have been linked to mitochondrial DNA mutations. Recent mounting evidence suggests that a cytochrome oxidase catalytic defect with mitochondrial DNA oxidative damage is a reliable marker of sporadic Alzheimer's disease. With advancing age, chronic inhibition of cytochrome oxidase activity produces neuronal metabolic failure and memory dysfunction. Cytochrome oxidase inhibition leads to senile dementia and neurodegeneration in late-onset Alzheimer's disease in a cascade of multiple intracellular events, initiated primarily by neuronal aerobic energy depletion, mitochondrial formation of reactive oxygen species and disruption of intracellular calcium homeostasis. Quantitative cytochemical methods for assessing cytochrome oxidase activity in individual cells are described in detail. Cytochemical findings are discussed in relationship to the selective vulnerability of metabolically active larger projection neurons in Alzheimer's brains. Additional results are presented that suggest that muscle biopsy may be used as an early diagnostic aid in living subjects suspected of sporadic Alzheimer's disease. The data support the hypothesis that sporadic Alzheimer's disease is a systemic mitochondrial disease, characterized by cytochrome oxidase inhibition. Early in sporadic Alzheimer's disease the inhibition of neuronal cytochrome oxidase activity is caused by a systemic cytochrome oxidase defect. The brain is proposed to be the most vulnerable organ to show primary oxidative pathogenesis as a result of systemic cytochrome oxidase inhibition. Possible treatments for neuronal oxidative stress in Alzheimer's disease are proposed.

Cytochrome Oxidase in Neuronal Metabolism and Alzheimer's Disease,
edited by Gonzalez-Lima, Plenum Press, New York, 1998.

1. INTRODUCTION

Whether genetic or environmental, the pathogenesis of Alzheimer's disease involves a cascade of multiple intracellular events, eventually resulting in failure of oxidative energy metabolism and neuronal death. Although much attention has been devoted to Alzheimer's disease, relatively little has been devoted to the role of oxidative energy metabolism in this disease. Recent studies indicate that mitochondrial electron transport dysfunction is involved in various neurodegenerative diseases, including Alzheimer's disease (Beal *et al.*, 1997).

1.1. Alzheimer's Disease as a Metabolic Brain Disease

There is a compelling need to develop biological markers to confirm a clinical diagnosis of Alzheimer's disease (A.D.) during life in order to unequivocally identify A.D. patients for emerging therapeutic interventions (Arai, 1996). A.D. is characterized by initial memory loss, followed by progressive loss of neurons leading to dementia and loss of all nervous functions, and eventually death. A.D. is now the fourth-largest killer of adults 65 and older, and this disease may be affecting one of every three families in the United States (Gonzalez-Lima & Gonzalez-Lima, 1987).

Population studies indicate that the United States is an aging country. Estimates show that 17–20% of the United States population, about 50 million people, will be over age 65 by the year 2030 (Leon *et al.*, 1996). The number of elderly is increasing with the approach of the millennium. Therefore elderly afflictions, such as A.D., have become subjects of intense focus. There are two types of A.D., familial and sporadic. Familial A.D. has been linked to nuclear genetic defects that follow Mendelian organization but this constitutes only a small number of known A.D. cases. Familial A.D. has been correlated with early onset of A.D. and is generally thought to be an autosomal dominant trait. Sporadic A.D., which accounts for the majority of the A.D. cases, is associated with late-onset of the disease and has not been linked to nuclear genetic defects but rather defects in mitochondrial deoxyribonucleic acid (DNA) (Parker & Davis, 1997). The main purpose of mitochondrial energy metabolism in cells is to produce adenosine triphosphate (ATP), the main chemical energy source of the cell. However, mitochondrial metabolism has also been implicated in the production of free radicals within the cell. This free radical production can cause protein and lipid peroxidation as well as oxidative mitochondrial DNA (mtDNA) damage. Due to the fact that not only nuclear DNA but also mtDNA encode for the mitochondrial enzymes responsible for metabolism, any damage to mtDNA can lead to abnormal operations in energy metabolism. Disruption in cell energy metabolism can lead to dysfunction in microtubule assembly, synaptic degeneration, and cell pathology (Chandrasekaran *et al.*, 1994).

A.D. is characterized by selective neuronal cell death in its earlier stages and this selective death could possibly be explained by mitochondrial genomic defects causing the respiratory abnormalities. It has also been shown that energy metabolism is impaired in the A.D. brain (Parker & Davis, 1997). This paper will propose possible therapies available for treatment of defective mitochondrial respiration caused by mtDNA damage via free radicals. Accumulation of free radicals leads to further defective mitochondrial respiration and cell death. Therapies discussed will focus on the oxidative stress imposed on cells via mitochondrial respiration. The main types of therapies to be discussed will include antioxidant vitamins, estrogens, nitrone traps, and acetyl-L-carnitine.

1.2. Neuronal Oxidative Metabolism

Cytochrome *c* oxidase (C.O., also known as cytochrome aa_3, ferrocytochrome *c:* oxygen oxidoreductase, EC 1.9.3.1) is the mitochondrial enzyme responsible for the utilization of oxygen for aerobic energy metabolism. In the final step of the cellular electron transport chain (respiratory chain), molecules of C.O. pass their electrons to molecular oxygen. An estimated 95% of the oxygen used by cells reacts in this single process (Wikstrom, Krab & Saraste, 1981).

The brain uses glucose as its main source of energy. There are three main processes involved in glucose metabolism: glycolysis, the tricarboxylic acid cycle, and oxidative phosphorylation. Glycolysis is an anaerobic process; that is, it does not require oxygen. It is not efficient at ATP production, producing only 2 ATP per molecule of glucose. Glycolysis, however, produces nicotinamide adenine dinucleotide (NADH, reduced form), a co-enzyme, as well as two pyruvate molecules for every glucose molecule that enters glycolysis. NADH, which is easily oxidized, makes an excellent electron carrier/donor and pyruvate acts as the substrate for aerobic metabolism. Aerobic (oxygen-dependent) metabolism, which takes place in the inner mitochondrial membrane, involves a cycle of enzymes (known as the citric acid cycle, the Krebs cycle, or tricarboxylic acid cycle, TCA) which with every turn of the cycle allows re-arrangement of the pyruvate molecules and generation of carbon dioxide and water. Other products of TCA are NADH and FADH (flavin adenine dinucleotide, a co-enzyme in reduced form) which in turn transfer their electrons to the electron transport chain (ETC) in order to drive the last major metabolic energy process, oxidative phosphorylation (Becker *et al.*, 1996). The ETC is a series of proteins bound within the inner mitochondrial membrane and contains four complexes, each which accepts electrons from the lower complex in order to ultimately donate electrons to the last electron acceptor, oxygen, to generate water (Figure 1). This electron transfer chain also drives the transport of protons into the inner mitochondrial space and allows separation of charges. The protons then run down their electrochemical gradient and enter the inner mitochondrial membrane through F1 ATPase, an inner mitochondrial membrane enzyme. F1 ATPase acts to phosphorylate ADP to ATP by using the energy generated from the electrochemical gradient of the protons (Parker & Davis, 1997).

1.3. Quantitative Cytochemistry of Cytochrome Oxidase in Alzheimer's Disease

Although rare familial types of A.D. follow traditional Mendelian genetics, the great majority of A.D. cases appear late in life and have no clearly identifiable nuclear genetic defects. It is in this majority of late-onset cases that defects in C.O. activity have been linked to mitochondrial DNA mutations (Davis *et al.*, 1997). An understanding of the C.O. defect in A.D. may facilitate a more effective medical treatment for this majority of cases. Monitoring of C.O. activity and oxidative DNA damage may also serve to evaluate the success of early treatments in reversing this enzymatic defect to prevent oxidative stress leading to neurodegeneration.

Among the initial events in A.D., patients exhibit decreased C.O. activity as well as spatial memory deficits. Therefore, we modeled these particular aspects of A.D. in animals by experimentally compromising brain energy metabolism in ways expected to decrease C.O. activity and affect spatial memory (Gonzalez-Lima & Cada, this volume). We then assessed cellular changes in C.O. activity in the experimental brains and in A.D. brains

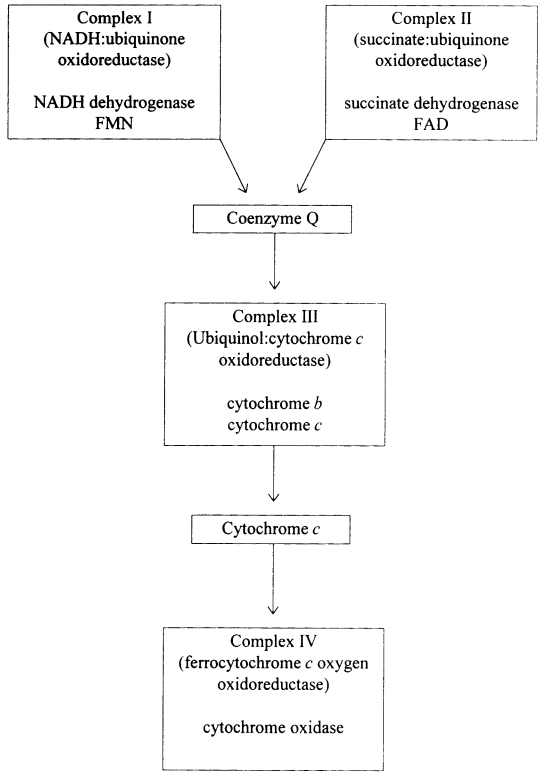

Figure 1. The components of the electron transport chain. Cytochrome oxidase catalyzes the reaction by which oxygen forms water.

with a quantitative C.O. histochemical method developed in our laboratory (Cada *et al.*, 1995; Gonzalez-Lima & Cada, 1994; Gonzalez-Lima *et al.*, 1997). It was concluded that C.O. inhibition is the major source of oxygen free radicals that lead to oxidative stress and neurodegeneration in A.D. (Gonzalez-Lima *et al.*, 1998).

Histochemistry has become the tool of choice for displaying visually the regional oxidative metabolic capacity of the nervous system. Seligman, Karnovsky, Wasserkroug and Hanker (1968) developed a histochemical technique based on the oxidative polymerization of diaminobenzidine (DAB) to a reaction product that chromatically labeled C.O. in heart, liver and kidney. Wong-Riley (1979) modified this DAB technique, applying it to the nervous system and later demonstrating that the optical density of histochemically stained sections is closely correlated with the concentration of C.O. in the tissue (Hevner & Wong-Riley, 1989). Gonzalez-Lima and Garrosa (1991) introduced a more sensitive method to quantify changes in regional cerebral C.O. activity within histochemically stained sections, utilizing internal tissue standards of known C.O. activity together with computerized image analysis. This quantitative method has been further validated, refined and applied to various tissues and animal species (Coomber *et al.*, 1997; Gonzalez-Lima, 1992; Gonzalez-Lima & Cada, 1994; Gonzalez-Lima & Jones, 1994; Gonzalez-Lima & Cada, this volume). Gonzalez-Lima *et al.* (1997) reported the first successful quantitative cytochemical study of C.O. activity in normal humans and A.D. patients. This more sensitive cytochemical method used in postmortem brains was able to detect C.O. activity decreases of about 18% in overall cell bodies and neuropil, and of 10% in peak neuropil activity in midbrain neurons of A.D. patients.

2. QUANTITATIVE CYTOCHEMISTRY OF CYTOCHROME OXIDASE IN ALZHEIMER'S BRAINS

Inhibition of C.O. activity in late-onset Alzheimer's disease brain tissue has been confirmed independently by several laboratories in the U.S. and Canada, including our lab (Chagnon *et al.*, 1995; Gonzalez-Lima *et al.,* 1997; Kish *et al.*, 1992; Mutisya *et al.*, 1994; Parker *et al*, 1994b; see Kish, 1997 for review). Since the brain relies almost exclusively on the aerobic metabolism of glucose for its energy, C.O. function is essential for normal brain function. Parker and colleagues found C.O. activity decreases of 17% to 50% in platelet mitochondria isolated from patients with A.D (Parker *et al.*, 1990; Parker *et al.*, 1994a). This systemic deficiency is also supported by the finding of mutations in mitochondrial C.O. genes found in A.D. (Davis *et al.*, 1997), and the mounting evidence cited below that a C.O. catalytic defect is a primary event in A.D. leading to cellular oxidative damage.

The clinical significance of experimental models of C.O. inhibition using sodium azide (Bennett & Rose, this volume) and cerebrovascular insufficiency (de la Torre, this volume) was assessed by considering them in relation to C.O. changes in Alzheimer's brains. Frozen tissue samples from A.D. cases, confirmed histopathologically and clinically diagnosed as demented, were compared to control cases matched by age, sex and postmortem time. Although not every regional effect found in the animal models (Gonzalez-Lima & Cada, this volume) may have a homologous counterpart in A.D. brains, it is hypothesized that C.O. deficits involve similar cellular groups and cellular compartments that are more vulnerable to A.D. histopathology. Based on our first study, limited to nuclei of the inferior colliculus, we anticipate cellular alterations in C.O. metabolism in specific groups of larger projection neurons with the highest oxidative metabolism that are predominantly affected by A.D., while neighboring neurons are spared (Gonzalez-Lima *et al.,* 1997).

C.O. is an essential enzyme for brain function because C.O. is a mitochondrial enzyme responsible for the activation of oxygen for aerobic metabolism in all animal cells, and the brain relies almost exclusively on the aerobic metabolism of glucose for its energy. Moreover, since C.O. is intimately tied to the ATP production, the energy molecule of cells, sustained changes in the demand for ATP energy are reflected in histochemical changes in C.O. activity (Hevner *et al.*, 1992; Wong-Riley, 1979; Wong-Riley, 1989). Therefore, C.O. activity assessed postmortem can be used as an endogenous marker of long-term change in oxidative metabolic energy capacity (Nobrega *et al.*, 1993). The histochemical method developed by Gonzalez-Lima and Garrosa (1991) for quantification of C.O. enzymatic activity using calibrated C.O. activity standards allows a cytochemical extension for use with human tissue and cellular microimaging at the light microscope level (Gonzalez-Lima *et al.*, 1997).

A.D. is a pathophysiological state which seems to have a C.O. metabolic alteration. Various researchers have described a C.O. deficit in blood platelets (Parker *et al.*, 1994a; Parker, 1991; Parker *et al.*, 1990) as well as in brain homogenates (Kish *et al.*, 1992; Mutisya, Bowling & Beal, 1994; Parker *et al.,* 1994b) from A.D. patients. Administration of substances known to antagonize C.O. activity, such as sodium azide, have been shown to produce behavioral deficits in animals, such as spatial learning deficits in the Morris water maze, similar to some symptoms of A.D. patients (Bennett *et al.*, 1992ab).

The central auditory system, although extensively mapped and relatively well-defined, has been subjected to little scrutiny in regard to A.D. Our laboratory specialization in auditory learning and memory (Gonzalez-Lima, 1992) led us to begin examining the auditory system of A.D. patients. Ohm and Braak (1989) examined the auditory brainstem nuclei of A.D. patients and in 3 out of 7 cases found "considerable neuritic plaque

formation" in the inferior colliculus (IC), whereas no plaques were found in the other auditory brainstem nuclei. Sinha and colleagues examined the auditory system in A.D. more thoroughly in 9 A.D. cases and 8 age-matched controls (Sinha *et al.*, 1993). They located numerous plaques and neurofibrillary tangles in the IC, all contained within the central nucleus of A.D. patients, and no changes in the controls. Therefore, it was predicted based on these studies that C.O. activity differences between A.D. patients and age-matched controls would be found in the central nucleus of the IC rather than in the other IC nuclei (dorsal and external). It is also possible that initial alterations in the IC may contribute to functional impairments found early in the auditory system of A.D. patients (Grimes *et al.*, 1985).

We studied C.O. activity patterns in the auditory system, specifically in the IC, to quantify cellular metabolic changes which may occur as part of the pathophysiology of A.D. We tested the hypothesis that C.O. metabolic alterations in auditory neurons in A.D. would be specific to the larger projection neurons in the central nucleus. This specific prediction is in line with the greater vulnerability of some larger projection neurons found in A.D., for example in cortical layers III and V (Van Hoesen, 1990) of cytoarchitecture Type 3 cortex of von Economo (Ranson & Clark, 1959), and in nucleus basalis (Arendt *et al.*, 1983), and the hypothesis that A.D. affects predominantly specific groups of larger projection neurons with the highest oxidative metabolism (Sinha *et al.*, 1993).

2.1. Overview of Methods for Quantitative C.O. Cytochemistry

Tissues were stained for C.O. activity using the quantitative C.O. cytochemical technique of Gonzalez-Lima *et al.* (1997) which has the advantage that it provides cellular spatial resolution at the light microscope level. Briefly, our current method producing results illustrated in the Figure 2 plates involved 3 steps.

2.1.1. Human Tissue Processing and Staining. Frozen tissue was sectioned and picked up on clean slides in a cryostat. Slides were processed for C.O. quantitative histochemistry as described in Gonzalez-Lima and Cada (1994). Preincubation was followed by incubation.

2.1.2. Spectrophotometry of C.O. Activity. C.O. activity standards were made from the brains of rats. The brains were homogenized at 4°C and aliquots were frozen and sectioned at varying thickness to develop a gradient of C.O. activity in the sections used as standards. Standards were stained together with tissue sections to generate a calibration curve between standard C.O. activity and optical density in the tissue. C.O. activity in the standards was spectrophotometrically measured with methods adapted from Wharton and Tzagoloff (1967) and Hevner, Liu and Wong-Riley (1993) as reported in Cada *et al.* (1995). Activity units were defined at pH 7 and 37°C as 1 unit oxidizes 1 μmol of reduced cytochrome c per min (μmol/min/g tissue wet weight).

2.1.3. Microscopic Image Analysis. Stained tissue slides were mounted on a light microscope or DC-powered light box connected to an imaging system. A high resolution CCD video camera captured the images and transmitted them to a frame grabber in a computer where the image was digitized. Analysis was completed with JAVA (Jandel Scientific) imaging software. A calibration strip containing known optical densities (Kodak) was imaged at the beginning of each session and was used to construct a calibration curve for the conversion of gray levels to optical density for that session. Each imaging session was thereby independently calibrated to optical density. Thickness standards of

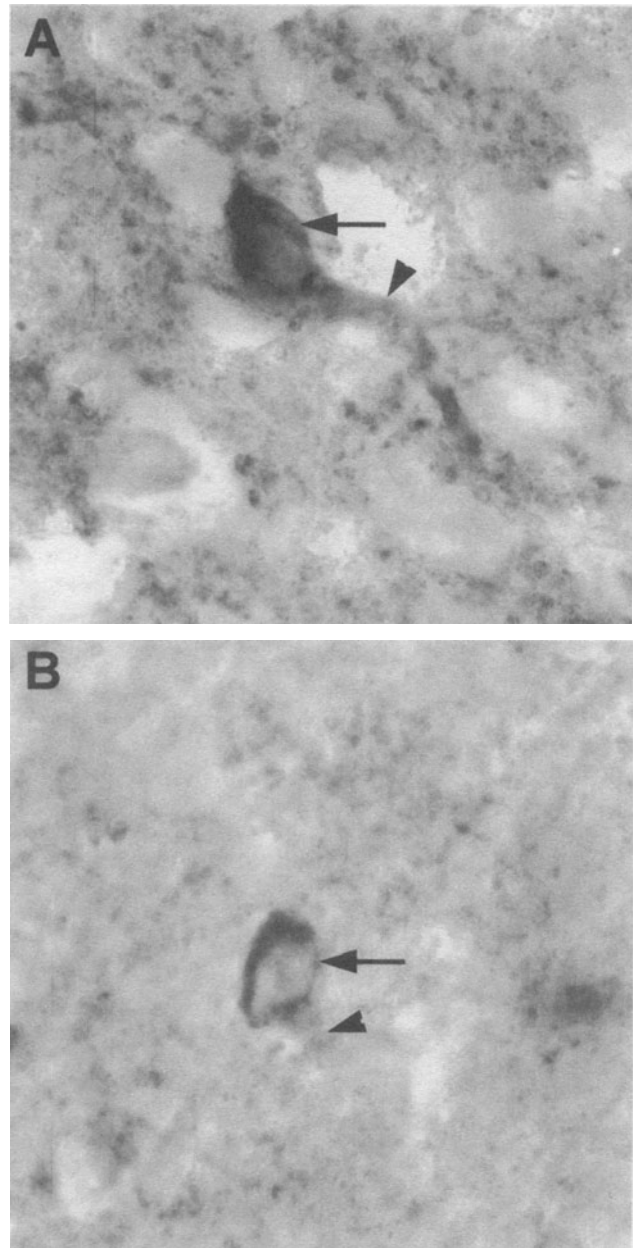

Figure 2. Light microscope image captures of central nucleus of the inferior colliculus (ICC) neurons stained for C.O. (arrows). A. Neuron from aged control. B. Neuron from Alzheimer's patient. Note the dendritic processes extending down and to the right (arrowheads). Neurons are for illustrative purposes and group differences are shown in Table 1.

known C.O. activity (measured spectrophotometrically) were included in each staining batch and were imaged on the DC-powered light box using JAVA. The change in optical density showed linear relationships with respect to tissue activity, section thickness, and incubation time in each of the staining batches. The optical density and activity measurements of these standards were then used to construct a regression equation. Optical density measures of the sections were thereby independently converted to C.O. activity units using a calibration curve generated with the standards' optical density and activity units.

2.2. Detailed Methodological Cytochemical Considerations in A.D. Brains

Frozen brain samples were obtained from the Alzheimer's Disease Research Center Neuropathology Core at the University of Southern California School of Medicine and from the Brain Bank of the Michigan Alzheimer's Disease Research Center at the University of Michigan Medical Center. Tissue samples were stored at −40°C until processing. The non-A.D., non-demented control group consisted of 5 males and 3 females with a mean age of 79.6 ± 3.1 years, a mean post-mortem interval of 6.9 ± 1.6 hours, and a mean brain weight of 1287.5 ± 39.8 grams. The A.D. group consisted of 7 males and 1 female with a mean age of 78.3 ± 2.9 years, a mean post-mortem interval of 6.5 ± 1.3 hours, and a mean brain weight of 1175.0 ± 50.9 grams. Patients' reports included years since diagnosis of A.D. dementia (mean = 8.6 ± 1.1 years) and confirmation of A.D. histopathology. The available drug histories showed no neuroleptic use. Student's two-tailed *t* tests demonstrated no significant differences between the control group and the A.D. group in age ($p > 0.75$), post-mortem interval ($p > 0.84$), and brain weight ($p > 0.10$).

Brain tissue was sectioned at 40 μm in the transverse plane and picked up on clean slides in a Frigocut 2800 cryostat at −15°C. Slides were processed for C.O. quantitative cytochemistry as in our previously described histochemical procedures (Gonzalez-Lima, 1992; Gonzalez-Lima & Cada, 1994; Gonzalez-Lima & Garrosa, 1991; Gonzalez-Lima & Jones, 1994). Preincubation was followed by incubation at 37°C for 120 min. Adjacent sections were stained with Cresyl violet to delineate the cytoarchitecture of the IC.

Tissue standards of C.O. activity were made from the brains of 12 adult male rats. Each rat was decapitated, its brain rapidly removed and stored in 4°C sodium phosphate buffer (pH 7.4) until all 12 brains were collected. The brains were homogenized at 4°C and aliquots were frozen in 1.5 mL microtubes and sectioned at varying thicknesses to develop a gradient of C.O. activity in the sections used as standards. Sections of the standards were stained together with the IC sections for the generation of a regression equation between standard C.O. activity and optical density in the tissue in each staining batch. C.O. enzyme activity was spectrophotometrically measured using a method adapted from Wharton and Tzagoloff (1967) and Hevner *et al.* (1993) as reported in Cada *et al.* (1995). Activity units were defined at pH 7 and 37°C as in our original quantitative method where 1 unit oxidizes 1 μmol of reduced cytochrome c per min (μmol/min/g tissue wet weight). Activity units can also be expressed in terms of grams of protein content (Lowry *et al.*, 1951) by multiplying the reported values by 10 since our brain standards contained an average of 10% protein (Gonzalez-Lima & Cada, 1994).

After C.O. staining, slides were mounted on an Olympus light microscope connected to an image processing system. A 40x objective was used and sections were stained lightly to avoid distributional error, glare, and diffraction errors. Pixel spacing was calibrated with a stage micrometer separately for vertical and horizontal dimensions. For spatial calibration, the JAVA software was used in the computer to load conversion values into look-up tables. The optical density and activity measurements of these standards were then used to construct a regression equation. The change in optical density showed linear relationships with respect to tissue activity and section thickness in each of the three staining batches done ($r = 0.96$, 0.97, and 0.97). Optical density measures of the IC sections were thereby independently converted to C.O. activity units using the calibration curves generated with the standards' optical density and activity units.

The sample consisted of a total of 480 neurons, with 30 cells per subject for 16 subjects. The inferior colliculus was subdivided into three separate nuclei: the central (ICC),

dorsal (ICD) and external (ICE). To avoid mistakenly sampling from outside the intended nucleus, observations were restricted to the central part of the IC subdivisions. Ten cells were sampled randomly per nuclear subdivision per subject from up to 8 sections, with sections sampled separated by at least a 120 μm interval. Other selection criteria for sampling were that tissue was free from artifacts of staining and tissue processing (such as cracks, folds, and foreign particles) and that cells showed no obvious signs of morphological abnormalities (such as vacuolations, dendritic swellings, eccentric nuclei, etc.). A total of eight densitometric and six morphometric measures were taken from each cell; for these measurements, the cell body was oriented in the center of the image area (Figure 3).

2.3. Findings with Quantitative C.O. Cytochemistry in Control and A.D. Brains

Large and small cell subgroups were compared across the entire inferior colliculus. The larger than average cells (>12.1 μm in diameter) contained higher C.O. activity as revealed in their perikaryon average ($p < 0.001$), perikaryon peak ($p < 0.002$), and primary branch peak ($p < 0.02$) measures (one-way ANOVA). This is consistent with the view that large cell bodies in the IC tend to be of projection neurons supporting greater processes that require higher oxidative metabolic demands.

The same morphometric and C.O. activity measurements were completed with 8 controls ($n = 240$ cells) and 8 A.D. subjects ($n = 240$ cells), matched by age and postmortem time, and the results were statistically compared for each measure. No morphometric differences were found between A.D. and control neuronal measures. The activity measurements from the A.D. tissue did not differ significantly from the controls when large and small cells were combined in the analysis (one-way ANOVA). However, the large A.D. cells in the ICC ($n = 35$), as compared to the control cells ($n = 37$), were deficient in C.O. activity in the overall average ($p < 0.032$) and neuropil peaks ($p < 0.012$) measures (Table 1). This corresponded to a 17.7% decrement in overall average activity and a 10.3% decrement in peak neuropil activity. No significant activity differences were found in the smaller than average cell subgroup.

All measurements were taken using JAVA (Jandel) software, as follows: *Overall Average*: With the cell body in the center of the image area, the C.O. activity was averaged across the entire rectangular image area (165 × 130 μm). This area included primarily the neuropil that surrounded each single cell sampled, the cell body, and capillary space. *Neuropil Peaks*: The three highest points of peak activity in the neuropil of each rectangular image area of 165 × 130 μm were selected and measured. Each peak was measured by averaging an area contained within a 13 × 13 pixel (5 × 5 μm) window. *Perikaryon Average*: The average activity of the cell body, excluding the nucleus and any processes. This was measured by outlining the perimeter of the cell body and nucleus and averaging the interior of that outline. *Perikaryon Peak*: The point of highest activity in the perikaryon; the average of a 5 × 5 pixel (2.4 × 2.4 μm) window. *Primary Branch Peak*: The point of highest activity in the primary branch of the largest arborizing process; the average of a 5 × 5 pixel window. *Primary Branch Average*: The average activity of the above primary branch, measured by outlining the branch from the cell body to the first visible secondary branch and averaging the activity within. *Secondary Branch Peak*: The point of highest activity in a secondary branch of the largest arborizing process; the average of a 3 × 3 pixel (1.7 × 1.7 μm) window. *Secondary Branch Average*: The average activity of the above secondary branch, measured by outlining the branch from the primary branch to the first visible tertiary branch and averaging the activity within.

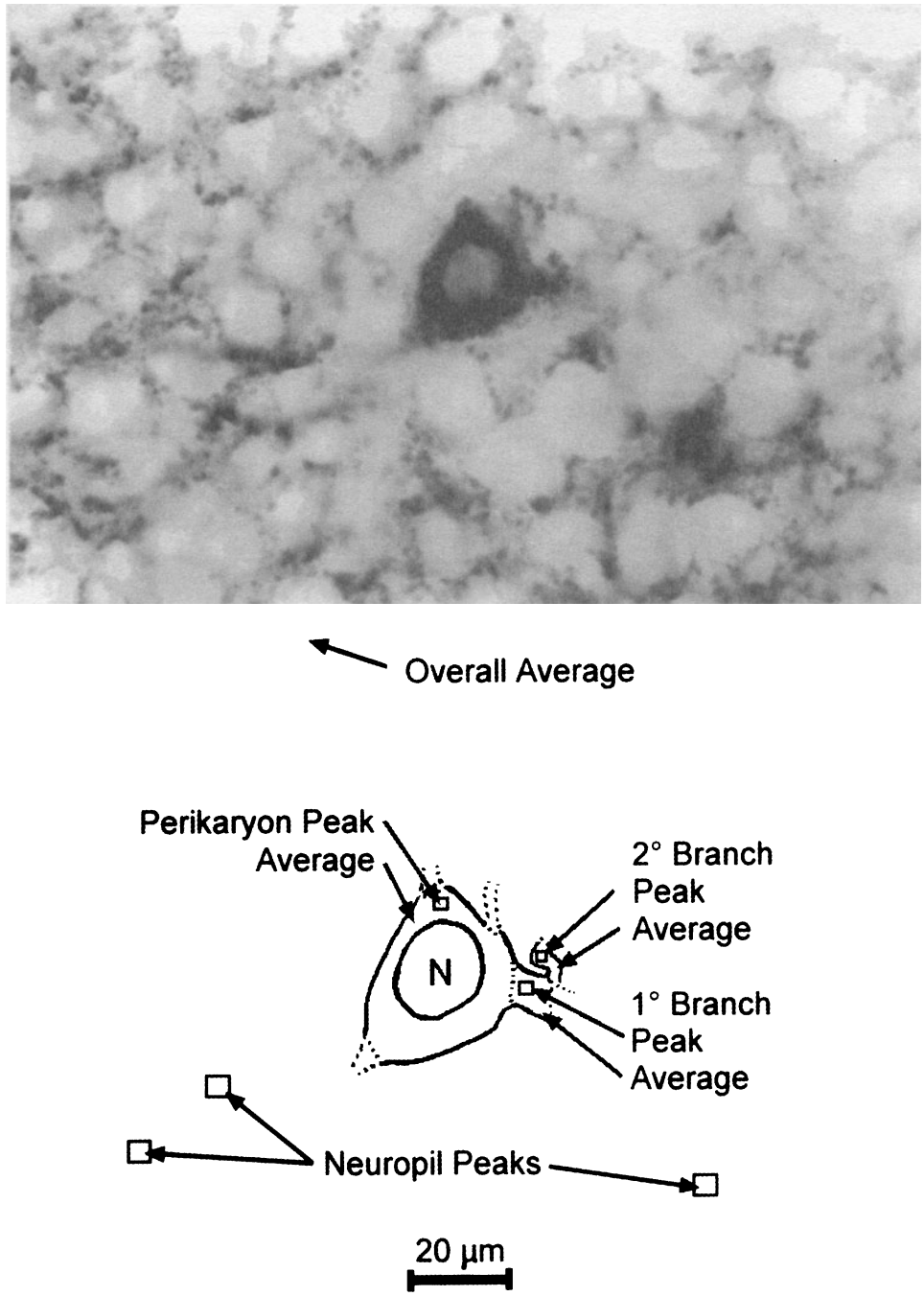

Figure 3. Top: A large cell of the ICC stained for C.O. and captured in JAVA. Bottom: The same cell outlined for measurement as listed. Averaged C.O. measurements are shown as borders; peak measurements are shown as boxes approximating the size of the sampled peak area. N = nucleus of cell. Scale bar equal for top and bottom figures.

Table 1. Comparison of the larger than average cells of the ICC between A.D. and control[a]

Measures	Control	A.D.
Overall average*	182.85 ± 9.60	150.49 ± 11.31
Neuropil peaks*	690.93 ± 20.88	620.02 ± 18.49
Perikaryon average	769.99 ± 43.46	740.32 ± 33.56
Perikaryon peak	1084.98 ± 59.48	1083.50 ± 53.44
1° branch peak	816.37 ± 56.45	764.25 ± 39.34
1° branch average	630.29 ± 48.70	569.80 ± 38.24
2° branch peak	701.56 ± 59.62	576.91 ± 56.16
2° branch average	501.99 ± 47.48	441.67 ± 50.79

[a]The controls showed significantly more C.O. activity in the overall average and neuropil peaks measures (*$p < 0.05$). This may reflect the heightened vulnerability to A.D. of the larger projection neurons.

2.4. Implications of the C.O. Activity Defect Found in A.D. Neurons

This study used the first quantitative cytochemical method developed which allows microdensitometric cellular measures to be expressed as actual C.O. enzyme activity units. Quantitative C.O. cytochemistry may be one of the most appropriate metabolic mapping techniques for examining postmortem neural tissue from human subjects. C.O. is an endogenous respiratory enzyme which, when assessed cytochemically, can illustrate the effect of heightened or lessened metabolic demands on individual neurons over an extended period of time. Therefore, cytochemical examination of C.O. activity levels, and thereby, long-term neuronal activity patterns, provides a method for quantifying cellular metabolic differences across groups of subjects and various pathophysiological states.

The cytochemical C.O. deficit found in our comparison of individual neurons could not be accounted for simply by a nonspecific effect, such as loss of neurons, as may be the case of C.O. activity biochemical measures in tissue homogenates (Kish, 1997). The larger than average cells of the ICC suffered a C.O. decrement in A.D., but there were no other C.O. alterations or morphometric differences in the inferior colliculus of A.D. patients that would indicate any generalized metabolic change. This finding supports the hypothesis that A.D. affects mainly specific groups of larger projection neurons while neighboring neurons are spared (Sinha *et al.*, 1993). Also, a greater abundance of neurofibrillary tangles and neuritic plaques in A.D. is found in cortical layers III and V, which contain larger projection neurons than the other layers (Van Hoesen, 1990).

However, not all the larger neurons in the inferior colliculus were affected. When the larger cells were examined across all three inferior colliculus nuclei, no significant effects were found because the group differences were specific to the ICC sample, which showed the largest C.O. activity in control brains. This specific metabolic effect is consistent with the A.D. study of Sinha *et al.* (1993), which showed that the anatomic histopathology in the inferior colliculus was all contained within the ICC. Since the C.O. deficit in A.D. may precede the anatomic histopathology, it is of little value to try to correlate the number of tangles and plaques with the C.O. activity in the same tissue sample. For example, a good correlation between both measures may simply mean that a nonspecific decrease in C.O. activity may result from loss of neurons or damage in the sample. Conversely, one may find a poor correlation between C.O. and A.D. histopathology measures when there are C.O. deficits in areas in which anatomic changes have not yet developed. Therefore, the important correlation is not that they coexist at the same time in a

tissue sample, rather it is that the same regions and cell types selectively impaired in C.O. metabolism match those that are more vulnerable to develop A.D. histopathology.

The selective vulnerability to A.D. histopathology of some brain regions is related to their differential expression of C.O. genes (Chandrasekaran *et al.*, 1992). Differences in the distribution of neuropil versus cell bodies in these regions may be related to genetically-mediated C.O. differences relevant to selective histopathological vulnerability in A.D. (Chandrasekaran *et al.*, 1992). This conclusion was supported by another study of the expression of C.O. genes in the temporal and motor cortex of A.D. patients. Chandrasekaran *et al.* (1994) found significantly more decreased C.O. mitochondrial RNA levels in the temporal cortex as compared to the motor cortex, or in A.D. as compared to the same regions in age-matched controls. These studies suggest that the selective histopathological vulnerability of some regions in A.D. may be linked to genetically-inherent C.O. differences in these regions. This evidence may be relevant for the observed C.O. deficit in the ICC.

A metabolic role of a C.O. mitochondrial defect in A.D. may take place even in the absence of subsequent anatomic histopathology. It has been shown consistently that C.O. activity is more vulnerable in A.D. than are other enzymes of the respiratory chain (Beal *et al.*, 1993; Kish *et al.*, 1992; Mecocci *et al.*, 1994; Mutisya, *et al.*, 1994; Parker *et al.*, 1990; Parker *et al.*, 1994ab; Kish, 1997). The evidence that a C.O. defect in A.D. occurs in the periphery, as well as in the brain, suggests that a C.O. defect in A.D. may be widespread. Yet our findings, together with studies showing regional brain differences in C.O. activity and gene expression, suggest that systemic impairment of C.O. activity in A.D. may still be associated with selective vulnerability. Particularly vulnerable for hypometabolism in A.D. are certain cortical regions (Reiman *et al.*, 1996) which match von Economo's Type 3 cortex based on cytoarchitectonic criteria (inferior parietal, superior and middle temporal, and parts of prefrontal cortex). These Type 3 cortical areas may share certain cytoarchitectonic features, such as neuropil adjacent to larger neurons which show the highest C.O. activity in projection cortical layers and some subcortical nuclei.

In conclusion, neurons which are subjected to greater metabolic demands seem to develop more C.O. in order to produce and maintain heightened levels of activity. These neurons can be visualized for examination and quantification through our C.O. staining and image processing procedures. Reductions in C.O. activity due to pathology can also be measured, making these techniques especially relevant to study the pathophysiology of A.D.

3. CONSEQUENCES OF CYTOCHROME OXIDASE INHIBITION IN A.D. BRAINS

Although the etiology of sporadic A.D. is as yet unknown, the evidence reviewed here suggests that late-onset A.D. patients share a common pathophysiology: a systemic mitochondrial C.O. inhibition affecting the electron transport chain and producing reactive oxygen species that lead to oxidative damage and neurodegeneration. This defect seems to be selective to C.O., the fourth and final complex of the electron transport chain.

C.O. activity inhibition is the proper measure in these studies, not simply the loss of enzymes due to neuronal death. In a study utilizing A.D. patients in conjunction with aged and diseased controls, Parker *et al.* (1994b) pointed out that assays of brain mitochondria for measurement of peptide concentrations showed that the amounts of C.O. (cytochrome aa_3) were not significantly different between groups, indicating that C.O. was present in normal levels in the A.D. brain mitochondria, but in a catalytically abnormal state. This C.O. defect provides the foundation for the proposed C.O. neuropathophysiologic model of A.D. (Gonzalez-Lima *et al.*, 1998).

Our findings, together with the cited literature showing the existence of a C.O. defect in A.D., indicate generally that a mitochondrial defect is present during the course of this disorder. We have integrated this defect into a mitochondrial pathophysiologic model of A.D. based on C.O. inhibition leading to oxidative energy hypometabolism, oxidative damage and disrupted calcium homeostasis (Figure 4).

There are a number of very plausible arguments being put forth which can implicate a C.O. defect with A.D. (Parker & Davis, 1997). A discussion of some of these follows, beginning with the reduction of cellular energy metabolism, and following with our emphasis on the oxidative damage effects of the increased generation of free radicals due to a C.O. defect. Finally, there will be a discussion linking the C.O. defect to other A.D. features, namely the amyloid plaque and neurofibrillary tangle, as well as neuronal death in A.D.

3.1. Hypometabolism Due to C.O. Inhibition

An obvious consequence of a C.O. defect is that cellular energy output will be reduced due to C.O.'s placement in the electron transport chain that produces ATP by oxidative phosphorylation. Some researchers have suggested that A.D. is a hypometabolic brain

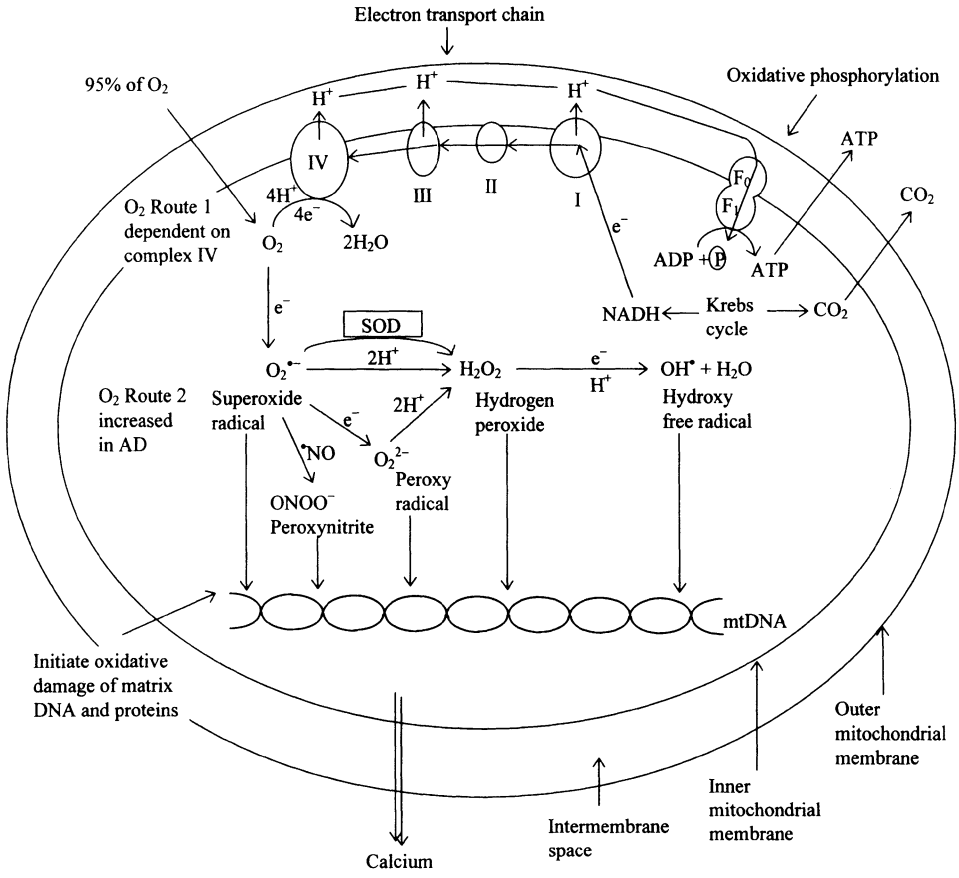

Figure 4. Schematic diagram of the proposed pathophysiologic model of Alzheimer's disease based on mitochondrial C.O. inhibition leading to oxidative damage (Route 2) and loss of calcium homeostasis (after Gonzalez-Lima *et al.*, 1998).

disease (Blass, 1993; Landin *et al.*, 1993; Meier-Ruge & Bertoni-Freddari, 1997). However, this energy use factor is difficult to tease out through the typical whole-brain blood flow and glucose use methods due to the confounding loss of brain cells and correspondingly lowered glucose uptake. One could predict the effects of reduced cellular energy: decreased ability to control ionic flow and resting potential (Beal *et al.*, 1993), increased vulnerability to insult (Bennett & Rose, 1992), and other impairments of cellular function, many of which could be additionally detrimental to the health of the cell and lead to its eventual demise. Again, the energy decline model is likely an effect of C.O. inhibition, but there are other features of A.D. which can be more directly related to the pathogenic effects of a C.O. defect.

3.2. Generation of Reactive Oxygen Species and Free Radicals in Neurons Due to C.O. Inhibition

In the mitochondria, free radicals are continually formed within the electron transport chain in a process driven by donated electrons. A free radical is defined as a species with one or more unpaired electrons. These unpaired electrons make the radical very unstable and therefore very reactive. Free radicals often are highly reactive as they "steal" electrons from other molecules. Free radicals have been implicated in a number of biological conditions from inflammation to normal aging (Harman, 1988) and are part of the body's normal physiological processing. Typically, the body uses several mechanisms to ensure that free radical levels remain controlled; e.g., free radical "scavengers" roam the system and tightly controlled reactions usually prevent the release of radicals before they are neutralized.

During oxidative phosphorylation, electron transport complexes I, III and IV pump protons (H+) for the production of ATP through the reduction of molecular oxygen to water controlled by cytochrome oxidase (complex IV), a process involving four electrons (Figure 4, Route 1). This is the major pathway for most oxygen consumption in mammals (Partridge *et al.*, 1994). However, another route exists, which reduces oxygen to superoxide ($O_2^{\bullet -}$), a potent free radical, in a one-electron process without the involvement of cytochrome oxidase in electron transport (Figure 4, Route 2). It has been estimated that 2% of oxygen utilized is converted to this or other free radicals during oxidative phosphorylation (Boveris & Chance, 1973).

In neurons, Route 2 oxidative stress is likely to be greater than in other cells because the proportion of oxygen consumption by the brain is over tenfold higher than in the rest of the body. For example, although the adult brain has 2% of the total body weight at least 20% of the total oxygen intake is consumed by the brain at rest (Sokoloff, 1989).

If the other respiratory chain complexes remain active in A.D. (as is suggested by Parker *et al.*, 1994ab), impairment of cytochrome oxidase could increase levels of $O_2^{\bullet -}$ by forcing more O_2 to be reduced through the secondary, one-electron route. Most of this $O_2^{\bullet -}$ is efficiently converted to hydrogen peroxide (H_2O_2) by membrane-bound superoxide dismutase (SOD). The level of H_2O_2 subsequently increases, and in most cells it is largely deactivated by glutathione peroxidase. However, neurons are particularly vulnerable to oxidative stress because they contain low levels of glutathione (Smith *et al.*, 1995a). For this reason glutathione peroxidase is not shown in Figure 4 as an important antioxidant defense that could prevent accumulation of hydrogen peroxide in neurons.

More H_2O_2 in neurons can be a substrate which leads to the formation of a highly reactive hydroxyl radical. In the presence of ferrous or cupric ions, H_2O_2 can participate in the Fenton reaction which results in the formation of the hydroxyl radical ($OH^{\cdot}$). Hydroxyl

radical can also be formed in a Haber-Weiss type of reaction when $O_2^{\bullet -}$ and H_2O_2 interact in the presence of an iron catalyst. Hydroxyl radical is probably the most damaging radical in that it will react with whatever biologic molecule is in its vicinity—proteins, lipids, etc.—and its substrate, H_2O_2, can cross cellular membranes into the extracellular space, where few antioxidant defense mechanisms exist (Southorn & Powis, 1988). Partridge *et al.* (1994) demonstrated this sequence of events in rat brain submitochondrial particles. Using the spin-trapping method of radical detection, they found that sodium azide inhibition of cytochrome oxidase does indeed lead to the increased production of H_2O_2 and, subsequently, the hydroxyl radical.

The hydroxyl radical, being intensely reactive, has a very short life span and mean effective radius; however, upon reacting with a stable molecule, hydroxyl can form other free radicals, thus initiating a chain reaction that could be thousands of events long. This seems to be the case in lipid membrane peroxidation, a common free radical effect which leads to a loss of fluidity, breakdown of membrane secretory functions, and loss of transmembrane ionic gradients. Neuronal membranes are likely to suffer more peroxidative damage than other cellular membranes because they contain a higher amount of polyunsaturated fatty acids susceptible to free radical damage (Smith *et al.*, 1995a). Hydroxyl radicals can also damage proteins, carbohydrates, and nucleic acids, both in the mitochondria and the nucleus (Southorn & Powis, 1988).

Unrestrained free radical production due to C.O. inhibition is sufficient to cause the neuronal degeneration and synaptic loss which in turn may cause the dementia and memory loss of A.D. patients. The defect in C.O. in A.D. can lead to increased free radical production, and free radicals may severely damage or kill a neuron via lipid peroxidation and by attacking mitochondrial and nuclear DNA. Mecocci *et al.* (1994) found significant threefold increases in oxidative damage to mitochondrial DNA in A.D. brains relative to age-matched controls. Neurons in A.D. also show widespread oxidative damage mediated by peroxynitrite (Smith *et al.*, 1997). Peroxynitrite ($ONOO^-$) is a strong oxidant formed from the reaction of superoxide with nitric oxide (NO).

3.3. Disruption of Intracellular Calcium Homeostasis Due to C.O. Inhibition

One important function of mitochondria is to maintain the homeostasis of calcium levels within the cell, a task accomplished by sequestration of excess calcium (Beal, 1992a; Gunther & Pfeiffer, 1990). When this ability is impaired due to C.O. inhibition, i.e., by free radical damage to the mitochondrial membrane or decreased ATP production, the cytosolic calcium level may rise (Richter & Kass, 1991). A potential result of this increased calcium level is calcium-dependent activation of calpain, an intracellular protease known to be involved in the degradation of cytoskeletal proteins (Schlaepfer *et al.*, 1985). Loss of the capacity for calcium incorporation in synaptic mitochondria during aging has been associated with impaired working memory in old animals (Huidobro *et al.*, 1993).

Impairment of neuronal C.O. metabolism resulting in decreased ATP production can have varied effects, such as decreasing the ability of the cell to maintain ionic potentials, as mentioned above. If the repolarization of a neuronal membrane is inhibited, prolonged or inappropriate opening of some voltage-gated calcium channels may result, increasing the cytosolic calcium level—this increase can cause a dysfunction of NMDA channels (Beal *et al.*, 1993). NMDA channels typically regulate calcium and sodium influx, are gated by magnesium and glutamate-activated NMDA receptors, and have been linked to synaptic plasticity and memory formation (Beal, 1992b).

Decreasing the ability of magnesium to gate NMDA channels could result in the opening of the channels by endogenous glutamate—thus increasing the flow of both sodium and calcium into the cell (Beal, 1992a; Beal *et al.*, 1993). Further attempts by the cell to mediate this influx of positively-charged ions in order to regain the resting potential will increase the demand for ATP and quickly deplete the cell of energy. Also, the mitochondria will preferentially absorb the excess calcium instead of produce ATP (Beal *et al.*, 1993), further reducing cellular energy output while also increasing the possibility of further mitochondrial damage due to mitochondrial calcium overload (Nicotera *et al.*, 1990). Neuronal damage resulting from a number of subsequent excitotoxic mechanisms can also kill the neurons (see Beal, 1992a,b; Beal *et al.*, 1993, for a review).

3.4. Relationship between C.O. Inhibition and Tau and Amyloid Beta Proteins in A.D.

Free radical damage resulting from C.O. inhibition may also mediate the toxicity implicating protein aggregates, such as paired helical filament tau and amyloid beta proteins, in A.D. and neuronal cell death (Smith *et al.*, 1995a,b). Neurofilament and cytoskeletal proteins with high proportion of lysine residues, such as tau, are especially vulnerable to oxidative damage and the formation of advanced glycation end products that generate reactive oxygen intermediates (Yan *et al.*, 1994). Furthermore, the oxygen free radicals generated by C.O. inhibition and by subsequent products such as glycated tau may induce the release of amyloid beta-peptide (Yan *et al.*, 1995).

Calpain has been found to be involved with the A.D.-characteristic amyloid plaques, perhaps facilitating their formation by improperly breaking down amyloid precursor protein, preventing its normal function and causing it to build up into the insoluble plaques (Iwamoto *et al.*, 1991; Shimohama *et al.*, 1991; Siman *et al.*, 1990). Neurofibrillary tangles may also be related to calpain-induced degradation of or interference with the fibril proteins (Iwamoto *et al.*, 1991; Nixon & Cataldo, 1994).

Amyloid may have other roles in the pathogenesis of A.D., such as that of a trophic factor responding to neural degeneration (Ihara, 1988; Saitoh *et al.*, 1989; Uchida *et al.*, 1988). This is a reasonable conclusion given that beta-amyloid precursor protein (APP) is used for cell membrane repair in many body regions, including the brain (Meier-Ruge *et al.*, 1994). Meier-Ruge *et al.*(1994) take this further by suggesting that the reduction in glucose turnover and ATP in the cells (possibly as a result of C.O. inhibition and free radical damage) prevents the proper utilization of APP (for membrane repair), leading to the buildup and subsequent senile plaques.

Increased membrane repair and synthesis has been associated with a recapitulation of developmental events in A.D. brains. For example, high levels of phosphomonoesters, growth factors, phosphotyrosine, pancreatic thread protein, C-series gangliosides, and other parameters reviewed by Pettegrew *et al.* (1997) have been documented. Increased membrane synthesis requires increased ATP use, which would be already compromised due to C.O. inhibition. Pettegrew *et al.* (1997) have shown changes in oxidative metabolism in *in vivo* studies with ^{31}P magnetic resonance spectroscopy consistent with the conclusion that the A.D. brain is under energetic stress.

3.5. Cerebrovascular Pathophysiology and C.O. Inhibition in A.D.

Ischemic cerebrovascular disease can produce vascular dementia and is a significant risk factor for A.D. Cerebrovascular pathophysiology may not only aggravate the ener-

getic stress in A.D. but it may also affect the blood-brain barrier and lead to C.O. inhibition. The relationship between C.O. inhibition and cerebrovascular pathophysiology will be discussed in detail in the chapter by Abdollahian, Cada, Gonzalez-Lima and de la Torre (this volume). A surgical model of chronic cerebrovascular insufficiency that demonstrates consistent spatial memory deficits in aged rats was used by us to study C.O. inhibition (de la Torre, Cada, Nelson, Davis, Sutherland & Gonzalez-Lima, 1997). The objective was to compare 19 month old rats subjected to bilateral ligation of the carotid arteries with sham-operated controls. Subjects were tested in the Morris water maze memory tasks weekly for four weeks following surgery. Brains were analyzed with C.O. histochemistry. Our data suggest that chronic cerebrovascular insufficiency leads to metabolic and memory impairments in these rats; hippocampal and posterior parietal regions particularly showed C.O. inhibition in the absence of the morphological histopathology that characterizes more severe ischemia (de la Torre *et al.*, 1997). In A.D., the effects of C.O. inhibition may interact with the decreased supply of oxygen and glucose due to vascular disease to produce the clinical picture of dementia.

4. NEURONAL OXIDATIVE DAMAGE IN ALZHEIMER'S DISEASE

Mitochondria are the major intracellular sources of reactive oxygen species. Increasing evidence indicates that oxidative damage is one of the important changes in the development of neuronal injury in A.D. (Sayre *et al.*, 1997; Smith *et al.*, 1995ab; Smith *et al.*, 1996ab; Smith *et al.*, 1997; Yan *et al.*, 1994; Yan *et al.*, 1995). Measurement of the degree of DNA damage is important for assessing toxicity of a C.O. defect in A.D. or the effectiveness of a treatment as an inhibitor of oxidative stress. Mitochondrial DNA is subject to severe oxidative damage, much more than nuclear DNA. Damage is assessed by the detection of various base modifications, particularly 8-hydroxy-deoxy-guanosine, which can lead to point mutations because of mispairing (reviewed by Richter, 1995). A chronic defect in C.O. activity in A.D. leads to oxidative damage to mitochondrial DNA and cell death in the brain (Mecocci *et al.*, 1994).

Mitochondrial dysfunction in neurodegenerative processes in A.D. involves three main features: an increase in free radical production, a decrease in the ATP/ADP ratio, and genetic defects in the mtDNA components (Sohal, 1997). These three main mechanisms are involved in a positive feedback loop within the mitochondria. A decrease in efficiency of antioxidant defenses and an increase in the production of free radicals is unbalanced in mitochondria that are at risk for oxidative stress. Mitochondria with a higher rate of production of free radicals will have an increased rate in oxidant damage to lipids, proteins, and mtDNA. This damage then continues the cycle by provoking further the production of free radicals and free radical damage. Additionally, a low ATP/ADP ratio leads to cellular inefficiency in production of energy and this can enhance the free radical production (Sohal, 1997).

Approximately 98% of the oxygen consumed by normal operating mitochondria is converted to water via the C. O. terminal complex of the electron transport chain. However, approximately 2% of the oxygen is not used by C.O. but is reduced into superoxide free radicals (Dykens, 1997). High reactivity allows free radicals to react with many components within the cell, the most common of which are lipid, protein, and DNA. Oxidation of the lipids in the plasma membrane usually involves unsaturated lipids which are most easily oxidized. This oxidation can damage the integrity, fluidity, and permeability of the plasma membrane. A chain reaction is induced with lipid oxidation and this amplifies and

propagates the assault of the radicals (Dykens, 1997). In protein oxidation, the complexes of the ETC themselves can be damaged or altered in function. Evidence from Parker, Parks, Filley, and Kleinschmidt-DeMasters (1994) has shown that there is depressed activity of all the ETC complexes in the A.D. brain but cytochrome oxidase activity is the most markedly depressed. The results of the investigation support the theory that a defect in C.O. activity is involved in mitochondrial dysfunction in the A.D. brain. Additionally, altered C.O. activity can exacerbate free radical production, mtDNA damage, and consequently further C.O. alteration (Gonzalez-Lima *et al.*, 1998).

Mitochondrial DNA damage is generally the most serious type of oxidative damage. Mitochondria with genetic damage due to oxidation are likely to have a decrease in oxidative metabolism and an increase in neuronal susceptibility to degeneration and death. Mutations in the mtDNA are more damaging than mutations in nuclear DNA due to a few pertinent reasons. There is a lack of DNA packing proteins called histones on the mtDNA. These histones are found on nuclear DNA and help in protecting the DNA against damage. The mtDNA is also located very close to the inner mitochondrial membrane allowing for easier access to free radicals. The mtDNA does not contain as many repair enzymes as do nuclear DNA, therefore mutation rates are ten-fold higher in mtDNA versus nuclear DNA. Additionally, there is an absence of introns, or intervening non-encoding sequences in mtDNA that occur in nuclear DNA. Introns in nuclear DNA are removed during splicing and if mutations exist in introns, they are not expressed in the final mRNA product (Dykens, 1997).

There are a number of endogenous antioxidants available to neutralize the free radical threat to the mitochondria and their neurons. These include superoxide dismutase (SOD), catalase, and glutathione peroxidase (GSH). SOD works on the superoxide radical to convert it to hydrogen peroxide (H_2O_2) which is then catalyzed by peroxisomes. However, H_2O_2 can react with lone electrons to produce hydroxy radicals (•OH) which are the most reactive and therefore the most dangerous oxidant radical (Radi *et al.*, 1997). GSH is available in the cytosol and mitochondrial compartments and converts H_2O_2 to an oxidized form of GSH and water. Catalase has been found in brain and heart mitochondria and converts H_2O_2 to molecular oxygen and water. Therefore, there are mechanisms available to transmute not only the superoxide radicals but also the resulting H_2O_2 which can form the •OH radical. The superoxide radical has also been found to interact with nitric oxide, which is present in the mitochondria, to produce the peroxynitrite radical ($ONOO^-$) which can also cause oxidative damage. Consequently, the free radicals that can be generated in the mitochondria are numerous, but vary in the degrees of damage they can inflict on the lipid, protein, and mtDNA (Radi *et al.*, 1997).

The pathophysiologic link to A.D. through mitochondrial respiration and electron transport has been theorized to be C.O. (Parker & Davis, 1997). Abnormal C.O. function has been linked to the increase in production of free radicals and this production, as outlined above, leads to cellular and DNA damage as well as further free radical production and problems with the electron transport chain (Gonzalez-Lima *et al.*, 1998). Evidence has supported the theory that C.O. is a valid metabolic marker of brain metabolic dysfunction in A.D. Cerebral oxidative metabolism has been measured with C.O. and it has been hypothesized that C.O. activity levels are good indications of the levels of brain aerobic metabolic capacity (Gonzalez-Lima *et al.*, 1998). Parker *et al.* (1994), have shown that content of C.O. protein in A.D. mitochondria is not significantly different from the levels in the control mitochondria but that the function of the enzyme is inhibited or abnormal. This abnormality has been linked to the production of free radicals and the continued cycling of cellular damage.

5. EARLY DIAGNOSIS OF A.D. USING PERIPHERAL TISSUE BIOPSY

Since the brain relies almost exclusively on the aerobic metabolism of glucose for its energy (Sokoloff 1989), C.O. function is essential for normal brain function. But C.O. is the terminal rate-limiting enzyme for cellular respiration in all eukaryote cells, suggesting that a systemic C.O. deficiency may be detected in A.D. nonneural cells. Parker *et al.* (1990, 1994) found a C.O. deficiency in platelet mitochondria isolated from patients with A.D. This systemic deficiency is also supported by the finding of Davis *et al.* (1997) of mutations in mitochondrial C.O. genes found in A.D., and the mounting evidence that a C.O. catalytic defect is a primary event in A.D. leading to cellular oxidative damage.

The diagnostic utility of the peripheral tissue C.O. measuring method used by Parker *et al.* (1990, 1994) is very limited due to its complex plateletpheresis-based technique. Simpler routine biochemical procedures for measuring C.O. activity in blood are insensitive to detect changes in A.D. patients (Van Zuylen *et al.,* 1992). The quantitative cytochemical method by Gonzalez-Lima *et al.* (1997) has the advantage that it could be used in peripheral tissues other than blood, where the C.O. activity of individual cells from biopsies could be accurately quantified using simpler cytochemical procedures and automated image analysis. Therefore, the quantitative C.O. method can be applied in a laboratory biopsy assay for diagnosis of late-onset, sporadic A.D. in a peripheral tissue.

Skeletal muscle was studied first because of its rich supply of mitochondria and well-established use in diagnostic enzyme histochemistry of neuromuscular diseases (Bauserman & Heffner, 1984). Apolipoprotein E (ApoE)-epsilon 4 allele, associated with familial A.D., has been found in skeletal muscle (Akaaboune *et al.,* 1994). It has also been documented that C.O. reactivity decrements can be detected in muscle with routine histochemistry in some childhood genetic diseases caused by C.O. deficiencies that lead to neurodegeneration, such as Leigh's (subacute necrotizing encephalomyelopathy) and Alper's (progressive infantile poliodystrophy) diseases (Sarnat, 1983). So it is reasonable to assume that our more sensitive histochemical method used in older patients, with clinical manifestations of dementia, may serve as a differential diagnostic aid for sporadic A.D. This could be done by confirming that the suspected patients have peripheral tissue C.O. activity decreases such as the 17% to 50% found in A.D. platelets (Parker *et al.,* 1990, 1994).

Samples from deltoid muscle are particularly well-suited to examine C.O. activity because they normally contain a predominance of Type I fibers. The two basic muscle fiber types in humans are Type I or red fibers and Type II or white fibers. The red fibers are primarily oxidative, while the white fibers are primarily glycolytic. As compared to white fibers, red fibers contain many more mitochondria and higher concentrations of oxidative enzymes (Sarnat, 1983). Thus, red fibers stain dark and white fibers stain light with our C.O. histochemical method.

Gonzalez-Lima & Valla (unpublished data) studied deltoid muscle samples from 12 subjects using quantitative C.O. histochemistry. Six of the subjects were late-onset A.D. cases with histopathologically confirmed A.D., and the other six subjects were aged normal controls. There were four females and two males in each group. Their mean (± standard error) age was 83 (± 2.4) and the postmortem time before freezing of the samples was 5 ± 0.8 hours. There were no significant ($p < 0.05$) group differences in age and postmortem time. But the groups showed clear significant differences in mean C.O. activity. The aged controls had 51.30 ± 6.57 units of C.O. activity, whereas the A.D. subjects had 29.18 ± 5.22 units. This corresponded to a significant (t-test, $p = 0.0249$) mean decrease of 43% in the A.D. subjects. Additionally, none of the A.D. cases showed C.O. activity values greater than

the mean of the aged controls. These results suggest that muscle biopsy may be used as an early diagnostic aid in living subjects suspected of sporadic A.D. An early diagnostic lab test of A.D. may facilitate a more effective medical treatment for the majority of A.D. cases, which are of the sporadic type. Monitoring of C.O. activity using muscle needle biopsies may also serve to evaluate the success of early treatments in reversing this enzymatic defect to prevent oxidative stress leading to neurodegeneration.

These data also support the hypothesis that sporadic A.D. is a systemic mitochondrial disease, characterized by C.O. inhibition. Furthermore, the finding of C.O. inhibition in peripheral tissues of A.D. patients has implications for the pathogenesis of A.D. For example, it may be possible to argue that a decrease in C.O. activity observed in neurons is a nonspecific consequence of any neurological disease leading to cerebral hypometabolism (e.g. Chandrasekaran *et al.*, this volume). However, a condition such as cerebral vascular changes, brain trauma, or other causative factors of brain hypometabolism are unlikely to explain a peripheral defect in C.O. activity as found in platelets by Parker *et al.* (1994) or in muscle by us. The most parsimonious explanation is that early in sporadic A.D. the inhibition of neuronal C.O. activity is caused by a systemic C.O. defect, rather than by nonspecific hypometabolic conditions following ischemia or other neurodegenerative processes. In this context, the brain would be the most vulnerable organ to show primary pathogenesis as a result of systemic C.O. inhibition. As indicated above, neurons are more vulnerable to show C.O.-dependent pathophysiology than other tissues. As reviewed by Dykens (1997), the brain is rich in lipids vulnerable to peroxidation and it has higher oxygen consumption, but the brain has less antioxidant defenses than other tissues that are less active aerobically.

6. POSSIBLE THERAPIES FOR OXIDATIVE STRESS IN A.D.

The life span of an individual is considered by some to be an expression of the control of oxygen consumption and metabolism (Gabbita *et al.*, 1997). Mitochondria act as the main source of oxygen consumption and specifically, the increase in oxygen consumption also brings an increase in free radicals. Therefore, available therapies, with endogenous and exogenous substances, are being investigated in order to slow the production of or neutralize the free radicals. Metabolic therapies for A.D. do not fit the mold for the typical A.D. therapy. Until recently, A.D. therapy has consisted mainly of boosting acetylcholine levels within the brain. However, new evidence within the area of free radicals offers some hopeful new therapies for A.D.

6.1. Antioxidants, Vitamins, CoQ, and Melatonin

An antioxidant is often thought of as a chain breaking inhibitor of lipid oxidation. Small molecular antioxidants such as vitamins C and E act to slow the rate of free radical production. Vitamin E, present in brain mitochondria, acts to break the chain reactions of lipid oxidation and also acts to neutralize certain free radicals. Vitamin E has also been found to inhibit cell death induced by amyloid beta protein (Behl *et al.*, 1992).

Vitamin C (ascorbic acid) is found in the gray and white matter of the brain and can act to recycle vitamin E radicals which are formed when vitamin E acts to break the chain reactions of oxidation within the cell. However, vitamin C can also act as a pro-oxidant in the presence of certain metal ions and produce a deleterious effect on lipids, proteins, and DNA within the cell. Therefore, vitamin C and its benefits to the cell depend on the concentration of itself and other metals and radicals within the cell (Gabbita *et al.*, 1997).

Other endogenous antioxidants such as coenzyme Q (CoQ) and melatonin have been proven effective in fighting lipid peroxidation as well. CoQ is an electron transport protein in the electron transport chain. When CoQ is reduced to ubiquinol, it has been found to cause inhibition of lipid peroxidation. Additionally, melatonin, a neuro-hormone, passes through the blood brain barrier because it is both lipid and water soluble and therefore is an advantageous possible therapy. Melatonin can distribute into compartments within the mitochondria and act as a direct free radical scavenger to also prevent lipid oxidation (Gabbita *et al.*, 1997). It has been hypothesized that the heterogeneous distribution of melatonin in the brain may be linked to the differential vulnerability of certain brain regions to oxidative damage in A.D. (Maurizi, 1997).

6.2. Estrogen

Estrogen therapy for treating A.D., aging, and dementia is under investigation as well. More women than men are afflicted with A.D., and women with A.D. have also been shown to have greater impairment in semantic and naming memory (Henderson, 1997). Evidence has linked brain areas such as the hippocampus cell sector CA1 to estrogens, specifically estradiol, and dendritic spine density has been shown to change during the estrous cycle of female rats (McEwen *et al.*, 1997). Therefore, it has been hypothesized that the circulating estrogens, estradiol and estrone, as well as progesterone, which start their decline at around age 40 and reach a nadir at approximately age 51, may have a link to an increased risk for A.D. in women (Sherwin, 1997). Sherwin (1997) has further linked estrogen with enhanced memory in women who have had menopause surgically induced. Epidemiological studies have found decreased risks for A.D. in post-menopausal women treated with estrogen replacement therapy (ERT). One study conducted by Kawas *et al.* (1996) identified a sample of 472 women participating in the Baltimore Longitudinal Study of Aging over a period of sixteen years. Use of estrogen replacement therapy, both oral and transdermal, was documented at each visit and 45% of the women were found to be using ERT. The women using ERT were found to have a lower risk of developing A.D. versus those not on ERT. The authors suggested further clinical trials using ERT as a possible therapy for A.D.

Paganini-Hill and Henderson (1996) also conducted an epidemiological study on the effects of estrogen therapy on the risk of A.D. Different estrogen dosages, preparations, and duration of therapy were also examined in relation to the risk of A.D. Paganini-Hill and Henderson (1996) examined 2,592 women in a Southern California retirement community. Of the 2,592 women, 138 were assessed with A.D. or other dementia by using death certificates and records. Each of 138 were matched to controls without identification of dementia or A.D. Estrogen users were found to have a decreased risk of A.D. by 30%. The investigators discuss the possible misclassification of diagnoses of A.D. by use of death certificates and therefore suggest a conservative conclusion on the findings of A.D. risks. Additionally, a correlation was found between increased dose and risk of A.D. The investigators found a significant reduction in risk of A.D. with an increase in dose of oral estrogen preparation and increased duration of use of estrogens (Paganini-Hill & Henderson, 1996).

These findings linking estrogen use with a reduced risk of A.D. in peri- and post-menopausal women have spurred further research into the benefits of estrogen, particularly in discerning the mode of action and possible link of estrogen with the reduction of free radicals in aging and A.D. Behl *et al.*, (1995) investigated the role of estrogen in protection against oxidative stress in neural tissue *in vitro*. Oxidative stress was induced in a clonal cell

mouse hippocampal line HT22 by amyloid beta protein, hydrogen peroxide, and glutamate. The investigators found that 17-beta estradiol, a common preparation of estrogen, prevented cellular damage and death due to the production of free radicals. This was assessed by cell counting and DNA labels to differentiate between dead and living cells. Cell lines that received a 20 hour pre-treatment with 17-beta estradiol before the toxins were used to induce oxidative stress were found to have a higher concentration of living cells.

A more recent study examined the neuroprotective effects of 17-beta estradiol as well as 17-alpha estradiol, a non-biologically active steroid, both of which have been found to prevent peroxidation buildup (Behl *et al.*, 1997). This study by Behl and colleagues used rat and mouse hippocampal neurons which were or were not pre-treated with either 17-beta estradiol, estrone, estriol, or 17-alpha estradiol. Accumulation of hydrogen peroxide within cells induced by glutamate, H_2O_2, and amyloid beta protein was measured by a 2,7-dichlorofluorescein diacetate assay previously developed (Behl *et al.*, 1997). Cells which were pre-treated with steroids with an OH group on the "A" ring of the structure were afforded protection from H_2O_2 and amyloid protein toxicity.

6.3. Progesterone Antagonist, RU486

Behl *et al.* (1997) have also conducted further studies with a progesterone antagonist, RU486, as a neuroprotective agent against A.D. Previous evidence has shown that progesterone initially increases estrogen-induced dendritic spine formation within the brain hippocampal CA1 sector and then acts to trigger down-regulation of the spine density. With estrogen withdrawal, down-regulation of the spines was slow but with progesterone involvement occurred more rapidly, within 8–12 hours. Additionally, RU38486, an antagonist of progesterone, acts to block down-regulation of the dendritic spines (McEwen *et al.*, 1997). Behl *et al.* (1997) also found that RU486 has potential to act as a neuroprotective agent against cell death due to oxidative stress. Behl *et al.* (1997) used in vitro hippocampal cell lines and organotypic hippocampal cell lines, which still contain the connections and differentiation regionally, and therefore are considered close parallels to *in vivo* cells. Oxidative stress was induced in these cells by use of amyloid beta (Aβ), glutamate, and H_2O_2. These substances are known to induce free radical production, promote oxidation of lipids and accumulation of peroxides, precursors of the •OH radical. Behl and colleagues (1997) found that pre-treatment of the cell lines with RU486 prevented peroxidation accumulation and cell death within the *in vitro* cells used.

Additionally, RU486 was thought to be more effective as a free radical scavenger than vitamin E. Only 10^{-5} M of RU486 was needed for the same neuroprotection as 2.3×10^{-4} M of vitamin E. The investigators further promoted the theory that RU486 acts independent of receptor mechanisms. Neuroprotective activity of RU486 was found to be independent of the time of administration to the cells. Additionally, the presence of progesterone and glucocorticoid receptors, which are activated by RU486, did not change the neuroprotection afforded by RU486. In fact, cells without these receptors were also afforded protection. Also, receptor saturation was reached at the 10^{-5} level of RU486; this level was the minimum level of substance needed for neuroprotection of cell lines (Behl *et al.*, 1997).

6.4. Acetyl-L-carnitine

An additional therapy involving the metabolic aspects of mitochondria is treatment with acetyl-L-carnitine. Acetyl-L-carnitine is an endogenous substance in various organs in the body as well as in the brain. It is synthesized by acetyl-L-carnitine transferase in the

mitochondria (Spagnoli *et al.*, 1991). Acetyl-L-carnitine is involved in taking up long chain fatty acids for building of membranes within the mitochondria. Acetyl-L-carnitine was originally used as a method of up-regulating the acetylcholine levels in A.D. brain. It has also been theorized that acetyl-L-carnitine may play a role as a precursor for acetylcholine and was originally investigated for A.D. treatment because of this property (Terwel *et al.*, 1995). Recently, the metabolic benefits of acetyl-L-carnitine have been investigated in possible A.D. treatment. Acetyl-L-carnitine has been found to modulate the level of acetyl CoA within the mitochondria. Acetyl CoA is a main substrate of the TCA cycle occurring within the mitochondria. This increase in acetyl CoA is considered indicative of a regulation of metabolism (Terwel *et al.*, 1995).

There have been studies investigating the benefits of acetyl-L-carnitine treatment *in vivo* in rats and in humans. Terwel and colleagues conducted a study examining the effects of pre-treatment of acetyl-L-carnitine on the enzymatic activities within the rat hippocampus and septum after injection of streptozotocin into areas of the rat brain. The investigators examined the activity of choline acetyltransferase, acetyl-L-carnitine transferase, and glutarate dehydrogenase, all of which are reduced in A.D. brains (Terwel *et al.*, 1995). The levels of activity were tested within the septum and hippocampus of rats treated with acetyl-L-carnitine over a period of two weeks and those not treated with acetyl-L-carnitine. Both groups received streptozotocin injections. The investigators found that activity levels of all the enzymes except choline acetyltransferase were reduced in the septum. Within the hippocampus, however, activity levels of choline acetyltransferase were affected. Acetyl-L-carnitine showed preservation of cholinergic neurons and activity within the hippocampus and selectively within the septum. Additionally, the use of streptozotocin as an animal model of A.D. is limited in the changes that it brings enzymatically within the brain. Therefore, although investigators theorized that acetyl-L-carnitine had a neuroprotective benefit toward cholinergic neurons, the mechanism of that effect is not readily apparent nor is the validity of the effects on streptozotocin treated rats.

A study by Spagnoli *et al.* (1991) has given evidence of the benefits of acetyl-L-carnitine treatment in human A.D. subjects. The study was conducted over a period of one year in a double blind placebo treatment. A group of 130 A.D. diagnosed patients were used and were assessed on the Blessed Dementia Scale (BDS), the Organic Brain Syndrome Scale, and the DSM III criteria for dementia to appraise the cognitive and functional impairment of each patient. Those treated with acetyl-L-carnitine showed a slower rate of impairment on the Blessed Dementia Scale in 13 out of 14 factors in as early as three months into the treatment. Spagnoli *et al.* (1991), however, warn that measures on the BDS before treatment were very low and could not theoretically reach a lower level of memory and cognition. This consideration may impair interpretation of the benefits of the acetyl-L-carnitine on cognition in dementia.

Another study by Pettegrew *et al.* (1995) also supports the evidence that treatment with acetyl-L-carnitine over a period of one year can slow the deterioration of cognitive function in probable A.D. patients. This cognitive function was assessed by the Mini Mental Status Exam and the Alzheimer's Disease Assessment Scale. Pettegrew *et al.* (1995) also found a normalization in the originally low phosphomonoester (PME) levels of the acetyl-L-carnitine treated patients but not the placebo patients. PME is considered as a measure of membrane phospholipid and synapse generation and high energy phosphate metabolism. Low levels that were observed in A.D. patients before treatment with acetyl-L-carnitine were thought to be a sign of membrane and synapse degeneration as well as decreased metabolism. The investigators theorized a link may exist in the energy and metabolic boost that acetyl-L-carnitine may give to A.D. patients and this may be measurable

in the changes in levels of PME. Pettegrew and colleagues call for further studies with larger sample sizes in order to accurately assess acetyl-L-carnitine's benefits in the A.D. brain (Pettegrew *et al.*, 1997).

6.5. Nitrones

Nitrone agents were originally developed and used in free radical chemistry. Only recently, has nitrone related therapeutics been shown to have beneficial use in stroke, aging, and A.D. Nitrone based therapies can and have been found to inhibit lipid oxidation. Free radicals can add to the carbon nitrogen double bond in the nitrone compound to form a spin adduct species, which engages in a rapid kinetic reaction. The most dangerous radical, the hydroxy radical, is a classic example of a free radical used in the spin adduct reaction. Alpha-phenyl-tert-butyl nitrone (PBN) is one of the main nitrones used in ischemia and A.D. research. When •OH reacts with PBN, the PBN-OH spin adduct that results is more stable than the •OH radical.

Carney and Floyd (1991) tested the treatment of PBN on ischemia induced injuries by ligation of the carotid arteries in gerbils. Deprivation of oxygen by ligation of the carotids resulted in neuronal death in the hippocampus. However, with the reintroduction of oxygen (reperfusion) into the brain, Carney and Floyd (1991) found that most neuronal death occurred during the reperfusion rather than during the initial ligation of carotids. Pre-treatment with PBN prior to ischemia and reperfusion prevented approximately 50% of the normal protein oxidation that occurs during ligation and reperfusion. Carney and Floyd (1991) also found that intra-peritoneal injection of PBN to 15–18 month old gerbils over the course of two weeks restored brain oxidative protein levels and increased spatial memory, as assessed by the radial arm maze. Additionally, animals with the 14 day PBN treatment showed fewer errors in the radial arm maze than older untreated gerbils. These nitrone studies not only appear to support PBN success in treating oxidative stress, but even more importantly, they support the theory that oxidative stress is a main factor in aging.

Hensley *et al.* (1997) have suggested a more elaborate mechanism for the neuroprotective aspects of nitrones other than free radical scavenging. These investigators have found evidence that nitrones may be inhibiting or suppressing gene transcription of events associated with oxidative stress. One particular event would be the transcription of nitric oxide synthase (NOS). NOS is the enzyme responsible for synthesizing nitric oxide (NO). It has been shown that if NO is available within the mitochondria it can react with the superoxide radicals to form the peroxynitrite free radical ($ONOO^-$) which is also a cause of free radical damage to the cell (Smith *et al.*, 1997). The transcription factor NFχB responds to changes within the cell and promotes gene expression by sending two of its subunits to the nucleus of the cell to bind the proper genes in order to induce NOS transcription. Studies reviewed by Hensley *et al.* (1997) have found that with the addition of H_2O_2 or other pro-oxidants to cells *in vitro* activates the NFχB transcription factor. Treatment with antioxidants, such as nitrones, has shown to block the transcription of genes under NFχB control, such as NOS (Hensley *et al.*, 1997).

There is evidence which supports further the involvement of nitrones in inhibiting the expression of NOS. Studies inducing endotoxemia by using lipopolysaccharide (LPS) from bacteria in cells in vitro support this theory. These cells suffer from elaboration of cytokine and macrophage production, a feature involved in bacterial inflammation. Macrophages, when activated, have been implicated in the generation of superoxide radicals. Pre-treatment with PBN however, showed an increase in cell survival and down regulation of the NOS induction caused by macrophages and cytokines (Hensley *et al.*, 1997).

In summary, metabolic therapies for A.D. with substances such as estrogens and acetyl-L-carnitine have produced promising results in human clinical trials. *In vitro* treatment with estrogen has also produced new insight into the possible mechanisms of estrogens and its derivatives in free radical modulation. Additionally, evidence of acetyl-L-carnitine involvement in phospholipid membrane production has been uncovered. Although the actual mechanism of acetyl-L-carnitine in the A.D. brain is still unclear, evidence points to an up-regulation of oxidative metabolism. Nitrones prove to be the most hopeful new free radical treatment and its application to A.D. is positive. However, nitrone mechanisms are still unclear; control of gene transcription competes with the free radical scavenging hypothesis. Until the mechanisms of nitrones can be clearly parsed out, their treatment value for A.D. is limited.

The treatments discussed in this review focus on moderating the oxidative stress produced from impaired C.O. metabolism. However, among the main three discussed, all appear to act at different levels of free radical inhibition. Estrogen and nitrones are thought of generally as free radical scavengers whereas acetyl-L-carnitine as a metabolic up-regulator. Although these treatments act to modulate and inhibit the damage caused by oxidative stress, they do not address the theoretical crux of the problem. They do not work at the level of the electron transport chain where defects in the mtDNA and C.O. activity may be occurring. An examination of this area may further reveal a more direct therapy that addresses not only the symptoms but the origin of C.O. inhibition in A.D. There is a compelling need to investigate C.O. as a biological marker to unequivocally identify A.D. patients for emerging therapeutic interventions (Arai, 1996).

7. CONCLUSIONS

1. A.D. is characterized by initial memory loss, progressive atrophy of neurons leading to dementia and loss of all nervous functions, and eventually death. A.D. is now the fourth-largest killer of adults 65 and older, and this disease may be affecting one of every three families in the United States (Gonzalez-Lima & Gonzalez-Lima, 1987). Although rare familial types of A.D. follow traditional Mendelian genetics, the great majority of A.D. cases appear late in life and have no clearly identifiable nuclear genetic defects. It is in this majority of late-onset, sporadic cases that defects in C.O. activity have been linked to mitochondrial DNA mutations (Davis *et al.*, 1997).
2. Neuronal C.O. inhibition in the mitochondrial electron transport chain is sufficient to initiate the pathophysiology associated with A.D. Memory deficits in A.D. may result from the metabolic consequences of C.O. inhibition on brain function before the accumulation of morphologic pathology, such as senile plaques and neurofibrillary tangles.
3. Decreased C.O. activity leads to neuronal damage, atrophy and death in A.D. mainly as a result of increased free radical production. The proposed pathophysiology of Alzheimer's disease will lead to a cascade of multiple intracellular events, resulting from failure of oxidative energy metabolism. For example, proteins such as tau will be particularly vulnerable to oxidative damage. Increases in amyloid plaques in A.D. nervous tissue and blood vessels may be promoted by an energy-underfunded attempt to repair free radical damage and by a calcium-mediated calpain interaction due to the instability of the mitochondrial membrane. Neurofibrillary tangles could also be promoted by calpain activation, and the vulnerability of the neuron to glutamate excitotoxicity may increase.

4. Early in sporadic A.D. the inhibition of neuronal C.O. activity is caused by a systemic C.O. defect that may be detected in peripheral tissues. Therefore, muscle biopsy may be used as an early diagnostic aid in living subjects suspected of sporadic A.D. The brain is proposed to be the most vulnerable organ to show primary oxidative pathogenesis as a result of systemic C.O. inhibition. Cytochemistry of C.O. activity and monitoring of oxidative mtDNA damage may also serve to evaluate the success of early treatments in reversing the consequences of the C.O. systemic defect in A.D. This research may serve as the basis for testing therapeutic agents for improving C.O. metabolism aimed at reversing brain energy failure and oxidative damage in animal models and ultimately in demented patients.
5. The reviewed therapies to prevent oxidative stress leading to neurodegeneration are a positive step towards not only developing treatments of A.D. but also development of a new model of A.D. The systemic C.O. inhibition hypothesis of sporadic A.D. has provided a new focus on the etiology of the disease. This is a step away from the neurotransmitter hypothesis of A.D. involving acetylcholine levels and receptors in the brain. The metabolic theory has produced promising evidence of a mitochondrial and genetic link and this calls for further study and validation.

ACKNOWLEDGMENTS

Supported by Texas Advanced Technology Program grant 361 to FGL. We thank the Alzheimer's Disease Research Center Neuropathology Core, USC School of Medicine, Los Angeles, California 90033, which is funded by AG05142, National Institute for Aging; and the Brain Bank of the Michigan Alzheimer's Disease Research Center at the University of Michigan, Ann Arbor, Michigan 48104, which is funded by AG08671, National Institute for Aging, for the tissue used in these studies.

REFERENCES

Aggleton, J.P. (Ed.), 1992, *The Amygdala: Neurobiological Aspects of Emotion, Memory, and Mental Dysfunction.* New York: Wiley-Liss.

Akaaboune, M., Villanova, M., Festoff, B.W., Verdiere-Sahuque, M., & Hantai, D., 1994, Apolipoprotein E expression at neuromuscular junctions in mouse, rat and human skeletal muscle, *FEBS Letters, 351,* 246–248.

Arai, H., 1996, Biological markers for the clinical diagnosis of Alzheimer's disease. *Tohoku Journal of Experimental Medicine, 179,* 65–79.

Arendt, T., Bigl, V., Arendt, A., & Tennstedt, A., 1983, Loss of neurons in the nucleus basalis of Meynert in Alzheimer's disease, paralysis agitans and Korsakoff's disease. *Acta Neuropathologica, 61,* 101–108.

Ball, M.J., Fisman, M., Hachinski, V., Blume, W., Fox, A., Kral, V.A., Kirshen, A.J., Fox, H., & Merskey, H., 1985, A new definition of Alzheimer's disease: A hippocampal dementia. *Lancet, 1,* 14–16.

Bauserman, S.C. & Heffner, R.R., 1984, Mitochondrial myopathies. In Heffner, R.R. (Ed.), *Muscle Pathology,* L.W. Roth, Series Ed., Churchill-Livingstone, Inc., New York.

Beal, M.F., 1992a, Does impairment of energy metabolism result in excitotoxic neuronal death in neurodegenerative illnesses? *Annals of Neurology, 31,* 119–130.

Beal, M.F., 1992b, Mechanisms of excitotoxicity in neurologic diseases. *The FASEB Journal, 6,* 3338–3342.

Beal, M.F.; Howell, N.; Bodis-Wollner, I. (Eds.), 1997, *Mitochondria and Free Radicals in Neurodegenerative Diseases.* New York: Wiley-Liss.

Beal, M.F., Hyman, B.T., & Koroshetz, W., 1993, Do defects in mitochondrial energy metabolism underlie the pathology of neurodegenerative disorders? *Trends in Neurosciences, 16,* 125–131.

Becker, W., Reece, J.B., & Peonie, M.F., 1996, *The World of the Cell.* Menlo Park: Benjamin/Cummings Publishing Company.

Behl, C., Davis, J., Cole, G.M., & Schubert, D., 1992, Vitamin E protects nerve cells from amyloid beta protein toxicity. *Biochemical & Biophysical Research Communications, 186,* 944–950.

Behl, C., Widmann, M., Trapp, T., & Holsboer, F., 1995, 17-beta estradiol protects neurons from oxidative stress-induced cell death in vitro. *Biochemical & Biophysical Research Communications, 216,* 473–482.

Behl, C., Trapp, T., Skutella, T., & Holsboer, F., 1997, Protection against oxidative stress-induced neuronal cell death--a novel role for RU486. *European Journal of Neuroscience, 9,* 912–920.

Behl, C., Skutella, T., Lezoualc'h, F., Post, A., Widmann, M., Newton, C.J., & Holsboer, F., 1997, Neuroprotection against oxidative stress by estrogens: structure-activity relationship. *Molecular Pharmacology, 51,* 535–541.

Bennett, M.C., & Rose, G.M., 1992, Chronic sodium azide treatment impairs learning of the Morris water maze task. *Behavioral and Neural Biology, 58,* 72–75.

Bennett, M.C., Diamond, D.M., Parker, W.D., Jr., Stryker, S.L., & Rose, G.M., 1992a, Inhibition of cytochrome oxidase impairs learning and hippocampal plasticity: a novel animal model of Alzheimer's disease. In J. Simpkins, F.T. Crews, & E.M. Meyer (Eds.), *Alzheimer's Disease Therapy: A New Generation of Progress,* pp. 485–501, New York: Plenum Press.

Bennett, M.C., Diamond, D.M., Stryker, S.L., Parks, J.K., & Parker, W.D., Jr., 1992b, Cytochrome oxidase inhibition: a novel animal model of Alzheimer's disease. *Journal of Geriatric Psychiatry & Neurology, 5,* 93–101.

Biegon, A., & Wolff, M., 1986, Quantitative histochemistry of acetylcholinesterase in rat and human brain post-mortem. *Journal of Neuroscience Methods, 16,* 39–45.

Blass, J.P., Sheu, R.K.F., & Cedarbaum, J.M., 1988, Energy metabolism in disorders of the nervous system. *Revue Neurologique, 144,* 543–563.

Blass, J.P., 1993, Metabolic alterations common to neural and non-neural cells in Alzheimer's disease. *Hippocampus, 3 Spec No,* 45–53.

Bloch, V., 1976, Brain activation and memory consolidation. In M.R. Rosenzweig & E.L. Bennett (Eds.), *Neural Mechanisms of Learning and Memory,* pp. 582–590, Cambridge, Massachusetts: MIT Press.

Boveris, A., & Chance, B., 1973, The mitochondrial generation of hydrogen peroxide: General properties and the effect of hyperbaric oxygen. *Biochemical Journal, 134,* 707–716.

Cada, A., Gonzalez-Lima, F., Rose, G.M., & Bennett, M.C., 1995, Regional brain effects of sodium azide treatment on cytochrome oxidase activity: A quantitative histochemical study. *Metabolic Brain Disease, 10,* 303–319.

Carney, J.M., & Floyd, R.A., 1991, Protection against oxidative damage to CNS by alpha-phenyl-tert-butyl nitrone, PBN) and other spin-trapping agents: a novel series of nonlipid free radical scavengers. *Journal of Molecular Neuroscience, 3,* 47–57.

Chagnon, P., Betard, C., Robitaille, Y., Cholette, A., Gauvreau, & D., 1995, Distribution of brain cytochrome oxidase activity in various neurodegenerative diseases. *Neuroreport, 6,* 711–715.

Chandrasekaran, K., Stoll, J., Giordano, T., Atack, J.R., Matocha, M.F., Brady, D.R., & Rapoport, S.I., 1992, Differential expression of cytochrome oxidase, COX) genes in different regions of monkey brain. *Journal of Neuroscience Research, 32,* 415–423.

Chandrasekaran, K., Giordano, T., Brady, D.R., Stoll, J., Martin, L.J., & Rapoport, S.I., 1994, Impairment in mitochondrial cytochrome oxidase gene expression in Alzheimer's disease. *Molecular Brain Research, 24,* 336–340.

Coomber, P., Crews, D., & Gonzalez-Lima, F., 1997, Independent effects of incubation temperature and gonadal sex on the volume and metabolic capacity of brain nuclei in the leopard gecko, *Eublepharis macularius*), a lizard with temperature-dependent sex determination. *Journal of Comparative Neurology, 380,* 409–421.

Curti, D., Giangare, M.C., Redolfi, M.E., Fugaccia, I., & Benzi, G., 1990, Age-related modifications of cytochrome *c* oxidase activity in discrete brain regions. *Mechanisms of Ageing and Development, 55,* 171–180.

Davis, R.E., Miller, S., Herrnstadt, C., Ghosh, S.S., Fahy, E., Shinobu, L.A., Galasko, D., Thal, L.J., Beal, M.F., Howell, N., & Parker, W.D., 1997, Mutations in mitochondrial cytochrome *c* oxidase genes segregate with late-onset Alzheimer disease. *Proceedings of the National Academy of Sciences, 94,* 4526–4531.

de la Torre, J.C., Cada, A., Nelson, N., Davis, G., Sutherland, R.J., & Gonzalez-Lima, F., 1997, Reduced cytochrome oxidase and memory dysfunction after chronic brain ischemia in aged rats. *Neuroscience Letters, 223,* 165–168.

de Leon, M.J., Convit, A., George, A.E., Golomb, J., de Santi, S., Tarshish, C., Rusinek, H., Bobinski, M., Ince, C., Miller, D., & Wisniewski, H., 1996, In vivo structural studies of the hippocampus in normal aging and in incipient Alzheimer's disease. *Annals of the New York Academy of Sciences, 777,* 1–13.

Dykens, J.A., 1997, Mitochondrial free radical production and oxidative pathophysiology: implications for neurodegenerative diseases. In M.F. Beal, N. Howell, & I. Bodis-Wollner (Eds.), *Mitochondria and Free Radicals in Neurodegenerative Diseases,* pp. 29–56, New York: Wiley-Liss.

Gabbita, S.P., Butterfield D.A., & Carney, J.M., 1997, Neurodegeneration and potential antioxidant-based therapeutic approaches. In M.F. Beal, N. Howell, & I. Bodis-Wollner (Eds.), *Mitochondria and Free Radicals in Neurodegenerative Diseases,* pp. 497–512, New York: Wiley-Liss.

Gonzalez-Lima, E.M., & Gonzalez-Lima, F., 1987, Sources of stress affecting caregivers of Alzheimer's disease patients. *Health Values, 11,* 3–10.

Gonzalez-Lima, F., & Scheich, H., 1985, Ascending reticular activating system in the rat: A 2- deoxyglucose study. *Brain Research, 344,* 70–88.

Gonzalez-Lima, F., & Garrosa, M., 1991, Quantitative histochemistry of cytochrome oxidase in rat brain. *Neuroscience Letters, 123,* 251–253.

Gonzalez-Lima, F., 1992, Brain imaging of auditory learning functions in rats: Studies with fluorodeoxyglucose autoradiography and cytochrome oxidase histochemistry. In F. Gonzalez-Lima, T. Finkenstadt, & H. Scheich (Eds.), *Advances in Metabolic Mapping Techniques for Brain Imaging of Behavioral and Learning Functions,* NATO ASI Vol. D68, pp. 39–109, The Netherlands: Kluwer Academic Publishers.

Gonzalez-Lima, F., Helmstetter, F.J., & Agudo, J., 1993, Functional mapping of the rat brain during drinking behavior: A fluorodeoxyglucose study. *Physiology & Behavior, 54,* 605–612.

Gonzalez-Lima, F., & Jones, D., 1994, Quantitative mapping of cytochrome oxidase activity in the central auditory system of the gerbil: A study with calibrated activity standards and metal-intensified histochemistry. *Brain Research, 660,* 34–49.

Gonzalez-Lima, F., & Cada, A., 1994, Cytochrome oxidase activity in the auditory system of the mouse: A qualitative and quantitative histochemical study. *Neuroscience, 63,* 559–578.

Gonzalez-Lima, F., & McIntosh, A.R., 1996, Conceptual and methodological issues in the interpretation of brain-behavior relationships. In R.W. Thatcher, G.R. Lyon, J. Ramsey, & N. Krasnegor (Eds.), *Developmental Neuroimaging: Mapping the Development of Brain and Behavior,* pp. 235–253, Orlando, Florida: Academic Press.

Gonzalez-Lima, F., Valla, J., & Matos-Collazo, S., 1997, Quantitative cytochemistry of cytochrome oxidase and cellular morphometry of the human inferior colliculus in control and Alzheimer's patients. *Brain Research, 752,* 117–126.

Gonzalez-Lima, F., Valla, J., & Cada, A., 1998, Brain cytochrome oxidase activity and how it relates to the pathophysiology of memory and Alzheimer's disease. In T. Ozben (Ed.), *Free Radicals, Oxidative Stress and Antioxidants: Pathological and Physiological Significance.* New York: Plenum Press.

Grimes, A.M., Grady, C.L., Foster, N.L., Sunderland, T., & Patronas, N.J., 1985, Central auditory function in Alzheimer's disease. *Neurology, 35,* 352–358.

Gunther, T.E., & Pfeiffer, D.R., 1990, Mechanisms by which mitochondria transport calcium. *American Journal of Physiology, 258,* c755-c786

Harman, D., 1988, Free radicals in aging. *Molecular and Cellular Biochemistry, 84,* 155–161.

Henderson, V.W., 1997, The epidemiology of estrogen replacement therapy and Alzheimer's disease. *Neurology, 48,* S27-S35

Hensley, K., Carney, J.M., Stewart, C.A., Tabatabaie, T., Pye, Q., & Floyd, R.A., 1997, Nitrone-based free radical traps as neuroprotective agents in cerebral ischaemia and other pathologies. *International Review of Neurobiology, 40,* 299–317.

Hess, H.H., & Pope, A., 1953, Ultramicrospectrophotometric determination of cytochrome oxidase for quantitative histochemistry. *Journal of Biological Chemistry, 204,* 295–306.

Hevner, R.F., & Wong-Riley, M.T.T., 1989, Brain cytochrome oxidase: purification, antibody production, and immunohistochemical/histochemical correlations in the CNS. *Journal of Neuroscience, 9,* 3884–3898.

Hevner, R.F., Duff, R.S., & Wong-Riley, M.T.T., 1992, Coordination of ATP production and consumption in brain: parallel regulation of cytochrome oxidase and NA+, K+-ATPase. *Neuroscience Letters, 138,* 188–192.

Hevner, R.F., Liu, S., & Wong-Riley, M.T.T., 1993, An optimized method for determining cytochrome oxidase activity in brain tissue homogenates. *Journal of Neuroscience Methods, 50,* 309–319.

Huidobro, A., Blanco, P., Villalba, M., Gomez-Puertas, P., Villa, A., Pereira, R., Bogonez, E., Martinez-Serrano, A., Aparicio, J.J., & Satrustegui, J., 1993, Age-related changes in calcium homeostatic mechanisms in synaptosomes in relation with working memory deficiency. *Neurobiology of Aging, 14,* 479–486.

Ihara, Y., 1988, Massive somatodendritic sprouting of cortical neurons in Alzheimer's disease. *Brain Research, 459,* 138–144.

Iwamoto, N., Thangnipon, W., Crawford, C., & Emson, P.C., 1991, Localization of calpain immunoreactivity in senile plaques and in neurones undergoing neurofibrillary degeneration in Alzheimer's disease. *Brain Research, 561,* 177–180.

Kawas, C., Resnick, S., Morrison, A., Brookmeyer, R., Corrada, M., Zonderman, A., Bacal, C., Lingle, D.D., & Metter, E., 1997, A prospective study of estrogen replacement therapy and the risk of developing Alzheimer's disease: the Baltimore Longitudinal Study of Aging. *Neurology, 48,* 1517–1521.

Kish, S.J., Bergeron, C., Rajput, A., Dozic, S., Mastrogiacomo, F., Chang, L., Wilson, J.M., DiStefano, L.M., & Nobrega, J.N., 1992, Brain cytochrome oxidase in Alzheimer's disease. *Journal of Neurochemistry, 59,* 776–779.

Kish, S.J., 1997, Brain energy metabolizing enzymes in Alzheimer's disease: alpha-ketoglutarate dehydrogenase complex and cytochrome oxidase. In J.C. de la Torre & V. Hachinski (Eds.), *Cerebrovascular Pathology in Alzheimer's Disease,* pp. 218–228, New York: New York Academy of Sciences.

Landin, K., Blennow, K., Wallin, A., & Gottfries, C.G., 1993, Low blood pressure and blood glucose levels in Alzheimer's disease: Evidence for a hypometabolic disorder? *Journal of Internal Medicine, 233,* 257–363.

Lowry, O.H., Rosebrough, N.J., Farr, A.L., & Randall, R.J., 1951, Protein measurement with the folin phenol reagent. *Journal of Biological Chemistry, 193,* 295–275.

Maurizi, C.P., 1997, Loss of intraventricular fluid melatonin can explain the neuropathology of Alzheimer's disease. *Medical Hypotheses, 49,* 153–158.

McEwen, B.S., Alves, S.E., Bulloch, K., & Weiland, N.G., 1997, Ovarian steroids and the brain: implications for cognition and aging. *Neurology, 48,* S8-S15

Mecocci, P., MacGarvey, U., & Beal, M.F., 1994, Oxidative damage to mitochondrial DNA is increased in Alzheimer's disease. *Annals of Neurology, 36,* 747–751.

Meier-Ruge, W., Bertoni-Freddari, C., & Iwangoff, P., 1994, Changes in brain glucose metabolism as a key to the pathogenesis of Alzheimer's disease. *Gerontology, 40,* 246–252.

Meier-Ruge, W.A., & Bertoni-Freddari, C., 1997, Pathogenesis of decreased glucose turnover and oxidative phosphorylation in ischemic and trauma-induced dementia of the Alzheimer type. In J.C. de la Torre & V. Hachinski (Eds.), *Cerebrovascular Pathology in Alzheimer's Disease,* pp. 229–241, New York: New York Academy of Sciences.

Mutisya, E.M., Bowling, A.C., & Beal, M.F., 1994, Cortical cytochrome oxidase activity is reduced in Alzheimer's disease. *Journal of Neurochemistry, 63,* 2179–2184.

Nicotera, P., Bellomo, G., & Orrenius, S., 1990, The role of Ca2+ in cell killing. *Chemical Research in Toxicology, 3,* 484–494.

Nixon, R.A., & Cataldo, A.M., 1994, Free radicals, proteolysis, and the degeneration of neurons in Alzheimer disease: How essential is the b-amyloid link? *Neurobiology of Aging, 15,* 463–469.

Nobrega, J.N., 1992, Brain metabolic mapping and behavior: Assessing the effects of early developmental experiences in adult animals. In F. Gonzalez-Lima, T. Finkenstaedt, & H. Scheich (Eds.), *Advances in Metabolic Mapping Techniques for Brain Imaging of Behavioral and Learning Functions,* NATO ASI Vol. D68, pp. 125–149, Dordrecht/Boston/London: Kluwer Academic Publishers.

Nobrega, J.N., Raymond, R., DiStefano, L., & Burnham, W.M., 1993, Long-term changes in regional brain cytochrome oxidase activity induced by electroconvulsive treatment in rats. *Brain Research, 605,* 1–8.

Ohm, T.G., & Braak, H., 1989, Auditory brainstem nuclei in Alzheimer's disease. *Neuroscience Letters, 96,* 60–63.

Olton, D.S., Wible, C.G., Pang, K., & Sakurai, Y., 1989, Hippocampal calls have mnemonic correlates as well as spatial ones. *Psychobiology, 17,* 228–229.

Paganini-Hill, A., & Henderson, V.W., 1996, Estrogen replacement therapy and risk of Alzheimer disease. *Archives of Internal Medicine, 156,* 2213–2217.

Parker, W.D., Jr., Filley, C.M., & Parks, J.K., 1990, Cytochrome oxidase deficiency in Alzheimer's disease. *Neurology, 40,* 1302–1303.

Parker, W.D., Jr., 1991, Cytochrome oxidase deficiency in Alzheimer's disease. *Annals of the New York Academy of Sciences, 640,* 59–64.

Parker, W.D., Jr., Mahr, N.J., Filley, C.M., Parks, J.K., Hughes, M.A., Young, D.A., & Cullum, C.M., 1994a, Reduced platelet cytochrome c oxidase activity in Alzheimer's disease. *Neurology, 44,* 1086–1090.

Parker, W.D., Jr., Parks, J., Filley, C.M., & Kleinschmidt-DeMasters, B.K., 1994b, Electron transport chain defects in Alzheimer's disease brain. *Neurology, 44,* 1090–1096.

Parker, W.D., Jr., & Davis, R.E., 1997, Primary mitochondrial DNA defects as a causative event in Alzheimer's disease. In M.F. Beal, N. Howell, & I. Bodis-Wollner (Eds.), *Mitochondria and Free Radicals in Neurodegenerative Diseases,* pp. 319–334, New York: Wiley-Liss.

Partridge, R.S., Monroe, S.M., Parks, J.K., Johnson, K., Parker, W.D., Jr., Eaton, G.R., & Eaton, S.S., 1994, Spin trapping of azidyl and hydroxyl radicals in azide-inhibited submitochondrial particles. *Archives of Biochemistry and Biophysics, 310,* 210–217.

Pettegrew, J.W., Klunk, W.E., Panchalingam, K., Kanfer, J.N., & McClure, R.J., 1995, Clinical and neurochemical effects of acetyl-L-carnitine in Alzheimer's disease. *Neurobiology of Aging, 16,* 1–4.

Pettegrew, J.W., Klunk, W.E., Panchalingam, K., McClure, R.J., & Stanley, J.A., 1997, Magnetic resonance spectroscopic changes in Alzheimer's disease. In J.C. de la Torre & V. Hachinski (Eds.), *Cerebrovascular Pathology in Alzheimer's Disease,* pp. 282–306, New York: New York Academy of Sciences.

Radi, R., Castro, L., Rodriguez, M., Cassina, A., & Thomson, L., 1997, Free radical damage to mitochondria. In M.F. Beal, N. Howell, & I. Bodis-Wollner (Eds.), *Mitochondria and Free Radicals in Neurodegenerative Diseases,* pp. 57–90, New York: Wiley-Liss.

Reiman, E.M., Caselli, R.J., Yun, L.S., Chen, K., Bandy, D., Minoshima, S., Thibodeau, S.N., & Osborne, D., 1996, Preclinical evidence of Alzheimer's disease in persons homozygous for the epsilon 4 allele for apolipoprotein E. *New England Journal of Medicine, 334,* 752–758.

Richter, C., & Kass, G.E.N., 1991, Oxidative stress in mitochondria: its relationship to cellular Ca2+ homeostasis, cell death, proliferation, and differentiation. *Chemico-Biological Interactions, 77,* 1–23.

Richter, C., 1995, Oxidative damage to mitochondrial DNA and its relationship with aging. *International Journal of Biochemistry and Cell Biology, 27,* 647–653.

Saitoh, T., Sundsmo, M., Roch, J., Kimura, N., Cole, G., Schubert, D., Oltersdorf, T., & Schenk, D.B., 1989, Secreted form of amyloid protein precursor is involved in the growth regulation of fibroblasts. *Cell, 58,* 615–622.

Sarnat, H.B., 1983, *Muscle Pathology and Histochemistry*, Chicago: American Society of Clinical Pathologists Press.

Sayre, L.M., Zelasko, D.A., Harris, P.L., Perry, G., Salomon, R.G., & Smith, M.A., 1997, 4-Hydroxynonenal-derived advanced lipid peroxidation end products are increased in Alzheimer's disease. *Journal of Neurochemistry, 68,* 2092–2097.

Schlaepfer, W.W., Lee, C., Lee, V., & Zimmerman, U.J., 1985, An immunoblot study of neurofilament degradation in situ and during calcium-activated proteolysis. *Journal of Neurochemistry, 44,* 502–509.

Seligman, A.M., Karnovsky, M.J., Wasserkrug, H.L., & Hanker, J.S., 1968, Nondroplet ultrastructural demonstration of cytochrome oxidase activity with a polymerizing osmiophilic reagent, diaminobenzidine, DAB, *Journal of Cell Biology, 38,* 1–14.

Sherwin, B.B., 1997, Estrogen effects on cognition in menopausal women. *Neurology, 48,* S21-S26

Shimohama, S., Suenaga, T., Araki, W., Yamaoaka, Y., Shimizu, K., & Kimura, J., 1991, Presence of calpain II immunoreactivity in senile plaques in Alzheimer's disease. *Brain Research, 558,* 105–108.

Siman, R., Card, J.P., & Davis, L.G., 1990, Proteolytic processing of B-amyloid precursor by calpain I. *Journal of Neuroscience, 10,* 2400–2411.

Sinha, U.K., Hollen, K.M., Rodriguez, R., & Miller, C.A., 1993, Auditory system degeneration in Alzheimer's disease. *Neurology, 43,* 779–785.

Smith, M.A., Lawrence, S.M., Monnier, V.M., & Perry, G., 1995a, Radical ageing in Alzheimer's disease. *Trends in Neuroscience, 18,* 172–176.

Smith, M.A., Rudnicka-Nawrot, M., Richey, P.L., Prapotnik, D., Mulvihill, P., Miller, C.A., Sayre, L.M., & Perry, G., 1995b, Carbonyl-related posttranslational modification of neurofilament protein in the neurofibrillary pathology of Alzheimer's disease. *Journal of Neurochemistry, 64,* 2660–2666.

Smith, M.A., Perry, G., Richey, P.L., Sayre, L.M., Anderson, V.E., Beal, M.F., & Kowall, N., 1996a, Oxidative damage in Alzheimer's. *Nature, 382,* 120–121.

Smith, M.A., Sayre, L., & Perry, G., 1996b, Is Alzheimer's a disease of oxidative stress? *Alzheimer's Disease Review, 1,* 63–67.

Smith, M.A., Richey-Harris, P.L., Sayre, L.M., Beckman, J.S., & Perry, G., 1997, Widespread peroxynitrite-mediated damage in Alzheimer's disease. *Journal of Neuroscience, 17,* 2653–2657.

Sohal, R.S., 1997, Role of mitochondria and oxidative stress in the aging process. In M.F. Beal, N. Howell, & I. Bodis-Wollner (Eds.), *Mitochondria and Free Radicals in Neurodegenerative Diseases,* pp. 91–108, New York: Wiley-Liss.

Sokoloff, L., 1989, Circulation and energy metabolism of the brain. In G.J. Siegel, B.W. Agranoff, R.W. Albers, & P. Molinoff (Eds.), *Basic Neurochemistry,* pp. 471–495, Boston: Little Brown.

Southorn, P.A., & Powis, G., 1988, Free radicals in medicine. *Mayo Clinic Proceedings, 63,* 381–408.

Spagnoli, A., Lucca, U., Menasce, G., Bandera, L., Cizza, G., Forloni, G., Tettamanti, M., Frattura, L., Tiraboschi, P., & Comelli, M., 1991, Long-term acetyl-L-carnitine treatment in Alzheimer's disease. *Neurology, 41,* 1726–1732.

Terwel, D., Prickaerts, J., Meng, F., & Jolles, J., 1995, Brain enzyme activities after intracerebroventricular injection of streptozotocin in rats receiving acetyl-L-carnitine. *European Journal of Pharmacology, 287,* 65–71.

Uchida, Y., Ihara, Y., & Tomonaga, M., 1988, Alzheimer's disease brain extract stimulates the survival of cerebral cortical neurons from neonatal rats. *Biochemical and Biophysical Research Communications, 150,* 1263–1267.

Van Hoesen, G.W., 1990, The dissection by Alzheimer's disease of cortical and limbic neural systems relevant to memory. In J.L. McGaugh, N.M. Weinberger, & G. Lynch (Eds.), *Brain Organization and Memory: Cells, Systems, and Circuits,* pp. 234–261, New York: Oxford University Press.

Van Zuylen, A.J., Bosman, G.J., Ruitenbeek, W., Van Kalmthout, P.J., & De Grip, W.J., 1992, No evidence for reduced thrombocyte cytochrome oxidase activity in Alzheimer's disease. *Neurology, 42,* 1246–1247.

Wharton, D.C., & Tzagoloff, A., 1967, Cytochrome oxidase from beef heart mitochondria. *Methods of Enzymology, 10,* 245–250.

Wikstrom, M., Krab, K., & Saraste, M., 1981, *Cytochrome oxidase: A synthesis.* New York: Academic Press.

Wong-Riley, M.T.T., Merzenich, M.M., & Leake, P.A., 1978, Changes in endogenous reactivity to DAB induced by neuronal inactivity. *Brain Research, 141,* 185–192.

Wong-Riley, M.T.T., 1979, Changes in the visual system of monocularly sutured or enucleated cats demonstrated with cytochrome oxidase histochemistry. *Brain Research, 171,* 11–28.

Wong-Riley, M.T.T., & Riley, D.A., 1983, The effect of impulse blockage on cytochrome oxidase activity in the cat visual system. *Brain Research, 261,* 185–193.

Wong-Riley, M.T.T., 1989, Cytochrome oxidase: an endogenous metabolic marker for neuronal activity. *Trends in Neurosciences, 12,* 94–101.

Yan, S.D., Chen, X., Schmidt, A.M., Brett, J., Godman, G., Zou, Y.S., Scott, C.W., Caputo, C., Frappier, T., Smith, M.A., Perry, G., Yen, S.H., & Stern, D., 1994, Glycated tau protein in Alzheimer's disease: a mechanism for induction of oxidant stress. *Proceedings of the National Academy of Sciences, 91,* 7787–7791.

Yan, S.D., Yan, S.F., Chen, X., Fu, J., Chen, M., Kuppusamy, P., Smith, M.A., Perry, G., Godman, G.C., Nawroth, P., Zweier, J.L., & Stern, D., 1995, Non-enzymatically glycated tau in Alzheimer's disease induces neuronal oxidant stress resulting in cytokine gene expression and release of amyloid beta-peptide. *Nature Medicine, 1,* 693–699.

7

MOLECULAR MECHANISMS OF IMPAIRED MITOCHONDRIAL GENE EXPRESSION IN ALZHEIMER'S DISEASE

Krish Chandrasekaran,[1] Kimmo Hatanpää,[2] Li-Ing Liu,[2] and Stanley I. Rapoport[2]

[1]Department of Anatomy and Cell Biology
Uniformed University of Health Sciences
Bethesda, Maryland 20814
[2]Laboratory of Neurosciences
National Institute on Aging
National Institutes of Health
Bethesda, Maryland 20892

ABSTRACT

In vivo positron emission tomography imaging suggests that brain energy metabolism is reduced in patients with Alzheimer's disease. In vitro studies using postmortem brains from Alzheimer's disease patients show corresponding decreases in expression of mitochondrial genes encoding for enzymes of oxidative energy metabolism. Neurodegeneration and age-dependent deletions and mutations in mitochondrial DNA are among factors that have been proposed to be responsible for this reduction. Recent findings, however, suggest that reduced energy metabolism in Alzheimer's disease is coupled to reduced neuronal activity. It is proposed that in Alzheimer's disease, reduced synaptic input and downregulation of oxidative energy metabolism render neurons more vulnerable to sudden energy metabolic insults such as excitotoxicity and thereby hasten neurodegeneration.

1. INTRODUCTION

Positron emission tomography (PET) has shown decreased regional cerebral metabolic rates for glucose in brains of patients with Alzheimer's disease (A.D.).[57,66,68] The metabolic reductions are greater than expected from tissue loss alone.[57,66,68]

Cytochrome Oxidase in Neuronal Metabolism and Alzheimer's Disease,
edited by Gonzalez-Lima, Plenum Press, New York, 1998.

It remains unknown whether metabolic deficits documented with PET are secondary to other neuronal changes or are primary in the A.D. process. Current hypotheses proposed to account for the PET changes are:

1.1. Neuropathological Changes Characteristic of A.D. Such as Neurofibrillary Tangles (NFTs) and Neuritic Plaques (NPs) Could Interfere with Mitochondrial Oxidative Phosphorylation (OXPHOS) in A.D. Brain

In life, decreased cerebral glucose metabolism in A.D. is more evident in parietal, temporal and frontal association neocortex than in primary sensory and motor neocortex, corresponding to the distribution of neuropathological features observed postmortem.[54] Therefore, glucose metabolic deficits could reflect neuropathologic changes in A.D.

1.2. Increased Oxidative Damage to Mitochondrial DNA (mtDNA) Could Be a Primary Event in A.D. Leading to Reduced Oxidative Energy Metabolism in A.D. Brain

Independent studies have reported 15–30% decreases in activity of cytochrome oxidase (C.O., complex IV of the electron transport chain), the rate limiting enzyme complex of the OXPHOS.[8,37,53,61–64,71,75–77] We reported 50% decreases in levels of mRNA for C.O. subunits I and III, which are encoded by mitochondrial DNA (mtDNA), in mid-temporal cortex displaying A.D. pathology, but not in the relatively spared primary motor cortex.[14–17,28,37–39] The reductions in C.O. activity and in C.O. subunit mRNA were due to decreases in expression of genes of OXPHOS rather than loss of mitochondria, as mtDNA, mitochondrial rRNA, and other mitochondrial non-OXPHOS enzymes were unaltered in A.D. temporal cortex compared with control brain.[14–17] Complexes of mitochondrial OXPHOS, such as C.O., require gene products from the physically separated mitochondrial and nuclear genomes.[6,10,50] In mammals, the C.O. enzyme has 13 subunits, the three largest of which, C.O. I, II and III, are encoded by mtDNA. The remaining subunits are derived from nuclear DNA (nDNA).[4,6,10,50] It has been suggested that mtDNA is susceptible to age-dependent oxidative damage because of its proximity to the inner mitochondrial membrane where large amounts of reactive oxygen species are generated.[3,35,55,58,74,84] Therefore, reductions in OXPHOS in A.D. brain has been ascribed to mutations and deletions in mtDNA.

1.3. Reduced Neuronal Activity Due to Dysfunction and Loss of Synapses Could Lead to Reduced Metabolic Need and Decreased OXPHOS Markers in A.D. Brain

Changes in neuronal activity have been reported to be associated with changes in levels of markers of mitochondrial oxidative energy metabolism.[44,46,86,88,89] Therefore, observed decreases in markers of OXPHOS and in brain glucose metabolism in A.D. could reflect reduced functional activity[21,24,72] caused by reduced metabolic needs.

An examination of these hypotheses in A.D. brain using molecular approaches is summarized in this review.

2. METHODS

2.1. Brain Samples

Frozen samples from midtemporal and motor cortices of A.D. brains and of neuropathologically normal brains were obtained from the Laboratory of Neurosciences Brain Bank (NIA, NIH, Bethesda, MD). The samples had been dissected at autopsy, frozen in isopentane cooled in liquid nitrogen, and stored at –80°C. The diagnosis of AD had been confirmed in each case by a neuropathologist following the CERAD criteria.[52,60] Ages and postmortem intervals of A.D. and control cases were not significantly different. From all samples, 10-(μ-thick cryostat sections were cut perpendicular to the pial surface. Sections were stored at –80°C and used within one month of cutting.

2.2. Preparation and Labeling of Probes

DNAs encoding for COX subunit III and 12S rRNA were generated by polymerase chain reaction (PCR) from human genomic DNA using the following primers: COX III 5' primer (positions 9,207–9,225 in mtDNA[4]): 5'-ATGACCCACCAATCACATG-3', COX III 3' primer (9,986–9,969): 5'-CCCTCATCAATAGATGG-3', 12S rRNA 5' primer (700–720): 5'-GCATCCCCGTTCCAGTGAGT-3', 12S rRNA 3' primer (1,482–1,462): 5'-TGTGTACGCGCTTCAGGGCC-3'. A GeneAmp kit (Perkin-Elmer, Norwalk, CT) was used. The PCR conditions were: 94°C, 30 sec; 56°C, 1 min; 72°C, 1 min 35 sec; 20 cycles. The amplified DNA fragments were gel purified and labeled with [^{35}S] dATP using a Random Primed Labeling kit (Boehringer-Mannheim, Indianapolis, IN). The labeled probes were purified using Nuctrap probe purification columns (Stratagene, La Jolla, CA). Northern blots hybridized with either probe showed a single band of expected size, verifying the specificity of the probes. An oligonucleotide probe for polyadenylated mRNA (poly $(A)^+$ mRNA) was prepared by labeling oligo (dT) (17-mer, Promega, Madison, WI) with [^{35}S] dTTP using terminal transferase. The average length of the resulting probe was 24 nucleotides. The sense probe, oligo (dA), was prepared in a similar way, except that it was labeled with [^{35}S] dATP.

2.3. In Situ Hybridization (ISH)

ISH was performed as described,[11] with the following modifications. Before prehybridization, the sections were dehydrated in ethanol, delipidized in chloroform for 10 min, rinsed in 100% and 95% ethanol, and air dried. The hybridization temperature was 42°C for the COX III probe and 45°C for the 12S rRNA probe. When using the oligo (dT) probe, the following additional modifications were made. The hybridization buffer contained 10% formamide, 2X SSC, 0.05 M sodium phosphate buffer (NaPi), pH 6.5, 10% dextran sulfate, 1.5 mg/ml DTT, 2X Denhardt's solution, 0.25 mg/ml *E. coli* RNA, 0.1 mg/ml sheared ssDNA, and probe (5×10^6 cpm/ml). The sections were hybridized at 20°C for 3 h. They were then washed three times, 20 min each, at 30°C in 1X SSC with 5 mM NaPi. Pretreatment of the sections with RNAse prior to ISH with the COX III and 12S rRNA probes obliterated all signal. Oligo (dA), the sense probe for poly $(A)^+$ mRNA, did not produce any signal.

2.4. Immunohistochemistry

After ISH, the slides were post-fixed for 1 h in 10% formalin at 4°C. They were then rinsed in three changes of 1X PBS for a total of 10 min at room temperature. After incubating the slides in 3% (v/v) normal horse serum (HS) in PBS for 15 min, they were incu-

bated in a solution containing a 1:1000 dilution of the PHF-1 antibody (a generous gift from Dr. Sharon Greenberg, W.M. Burke Medical Research Institute, NY), 1.5% HS, and 1X PBS overnight at 4°C. Thereafter, a standard ABC protocol[31] was followed using a Vectastain Elite kit for mouse IgG antibody (Vector Laboratories, Burlingham, CA). The color was developed using a DAB kit (Vector Laboratories) without nickel enhancement. The PHF-1 antibody recognizes the abnormally phosphorylated serine residues 396 and 404 in the A.D. tau. No staining was visible when the primary antibody was omitted.

2.5. Emulsion Autoradiography

After immunohistochemistry, the slides were air dried, dipped in Kodak NTB2 emulsion, air dried 2 h in the dark, and stored protected from light at –20°C for 20–30 h (oligo(dT)), 1–2 d (12S rRNA), or 5–7 d (COX III). After developing the emulsions, the sections were counterstained with 0.1% cresyl violet for 2 min.

2.6. Grain Counting and Analysis

The slides were coded before they were examined. Levels of mRNA in neurons were determined by counting silver grains over neuronal cell bodies using a 100X oil immersion objective. Neuronal cell bodies with a longitudinal diameter of at least 10 (μ, as measured with an ocular scale, were selected for counting from random fields in the pyramidal cell layers III and V.

3. RESULTS AND DISCUSSION

3.1. Is Impaired Energy Metabolism Caused by Neurodegeneration?

In association neocortex of normal human and nonhuman primate brain, C.O. subunit mRNA and C.O. activity are most evident in pyramidal cell bodies with long cortico-cortical and cortico-fugal projections, and in their terminal fields.[12,13,44,45] High expression and activity likely reflect the high metabolic requirements of these neurons for maintaining feed-forward and feedback connections.[12,13,44,56,80,86] In the A.D. brain, neurofibrillary tangles (NFT) are found mainly in large pyramidal cortico-cortical and cortico-fugal projection neurons of layers III and V.[54] Thus, the formation of NFTs could contribute to the decrease in C.O. subunit mRNA in vulnerable regions in A.D. brain.

3.1.1. Neurofibrillary Tangles and C.O. Subunit mRNA. The relation between accumulation of neurofibrillary tangles and levels of mtDNA-encoded genes of C.O. subunit mRNA was investigated by combined in situ hybridization and immunohistochemistry.[38] Levels of mtDNA-encoded C.O. subunit III and 12S rRNA and of poly(A)$^+$ mRNA (representing total mRNA encoded by mtDNA and nDNA) were measured using appropriate in situ hybridization probes. The accumulation of NFTs, evidenced by tau protein abnormally phosphorylated at its 396 and 404 serine residues, also was quantified in the cytoplasm of these neurons using an antibody staining specific for paired helical filaments, PHF-1. The results obtained in the pyramidal neurons of the temporal association and primary motor cortices of A.D. and control brains suggest different stages of decrease in C.O. subunit mRNA in A.D. neurons.[38] The first stage, evident in pyramidal neurons without phosphorylated tau or NFTs, results in reduced C.O. subunit III mRNA compared to tangle-free neurons of control brains. The level of mtDNA-encoded 12S rRNA is unaffected. In the

second stage, in which NFTs fill less than 50% of the cytoplasm, C.O. subunit III mRNA is further decreased while the levels of 12SrRNA and poly(A)$^+$ mRNA levels remain unchanged. In the third stage, when the tangles fill more than 50% of the cytoplasm, C.O. subunit III mRNA is further reduced, and 12S rRNA and poly(A)$^+$ mRNA levels are reduced as well. These results suggest that a decrease in C.O. subunit mRNA occurs early and precedes the formation of NFTs in individual pyramidal neurons in the midtemporal cortex of AD brains, and that C.O. subunit mRNA further decreases as NFTs appear and as their formation progresses.[38]

In situ hybridization of the hippocampal formation of AD brains has demonstrated that the decrease in C.O. subunit mRNA extends beyond regions that show neuropathological changes in A.D.[75,76] In the hippocampus, C.O. subunit mRNA was decreased in regions with NFTs and neuronal loss such as CA1, as well as in regions that are relatively-spared such as CA3, CA4 and dentate gyrus granule cells.[75,76] The fact that C.O. subunit mRNA was decreased throughout the hippocampal formation suggests that the decrease was due to disconnection of input and output pathways of the hippocampal formation. Thus, neurons at risk (e.g. remain structurally intact without PHF expression) in the A.D. brain may nonetheless undergo substantial reductions in markers of oxidative metabolism.

3.1.2. Neuritic Plaques and C.O. Subunit mRNA. A competing hypothesis is that amyloid β-protein (Aβ), aggregated in neuritic plaques (NPs), is the major contributor to neurodegeneration in A.D. Aggregated Ab is neurotoxic and induces oxidative injury in cell culture.[36] Therefore, the observed decreases in C.O. subunit mRNA and C.O. activity in A.D. brain can be assumed to be sensitive indicators of impaired neuronal function that may be associated with NPs.

The relation between accumulation of NPs and levels of mRNA of subunits for mtDNA-encoded genes of C.O. was investigated by combined in situ hybridization and-immunohistochemistry.[39] Levels of mtDNA-encoded C.O. subunit III (Fig. 1) and of

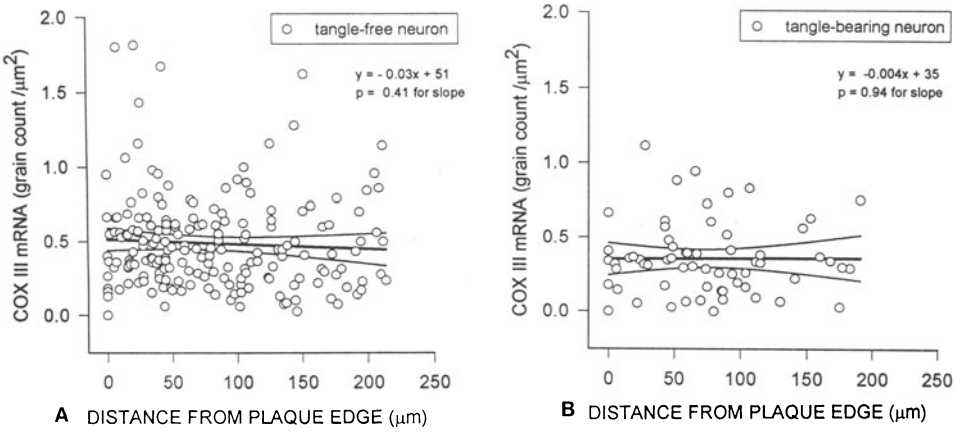

Figure 1. No significant gradient in C.O. III mRNA levels relative to distance from the closest plaques (NPs) in A.D. midtemporal cortex. Data is based on grain counting in A.D. brains to determine neuronal C.O. III mRNA levels in sections treated for in situ hybridization, followed by immunohistochemistry to detect NFTs and NPs. However, C.O. III mRNA is significantly reduced in tangle-bearing neurons (A) compared with tangle-free neurons (B). Regression line ± 95% confidence interval is shown. NFT, neurofibrillary tangle.

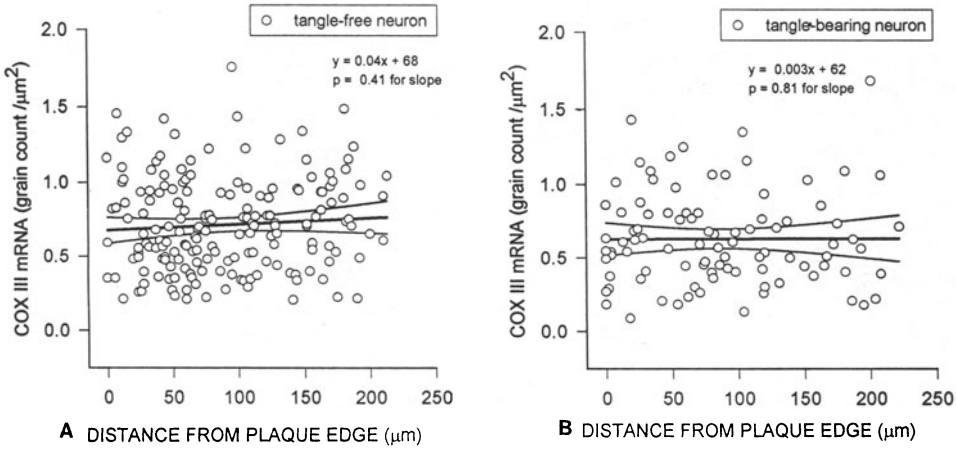

Figure 2. (A, B) No significant gradient in poly(A)$^+$ mRNA levels relative to distance from the closest plaques (NPs) in A.D. midtemporal cortex. Data is based on grain counting in A.D. brains to determine neuronal poly(A)$^+$ RNA levels in sections treated for in situ hybridization, followed by immunohistochemistry to detect NFTs and NPs. NFT, neurofibrillary tangle.

poly(A)$^+$ mRNA (Fig. 2) corresponding to total mRNA encoded by mtDNA and nDNA, were measured using appropriate in situ hybridization probes. The accumulation of NPs was identified using an antibody staining specific for paired helical filaments, PHF-1. The PHF-1 antibody recognizes the abnormally phosphorylated serine residues 396 and 404 in A.D. tau protein in NFTs and NPs. Levels of C.O. subunit mRNA in neuronal cell bodies relative to distance from NPs were examined. If NPs contributed to impaired neuronal function in A.D., either by being sites of oxidative damage or by being sources of harmful substances that diffuse from them, neurons closer to NPs would show less C.O. subunit mRNA and C.O. activity than neurons more distant.

It was found that levels of C.O. subunit III mRNA and C.O. enzyme activity were not related to proximity to NPs. Additionally, measurement of total C.O. subunit III mRNA and NP density, examined by analysis of northern blot and neuropathology, showed no significant correlation with NP density in midtemporal and primary motor cortex of A.D. and control brains.

Measurement of C.O. activity in hippocampal formation of AD brains has demonstrated that the decrease in C.O. activity extends beyond neurons that show neuropathological changes in A.D.[75,76] Decreases in C.O. activity are seen in areas with senile plaques (outer molecular layer of dentate gyrus) and in areas relatively free of plaques (CA4 and CA3). Moreover, De Carli et al. reported no correlation between the regional cerebral metabolic rate for glucose, as measured during life, and regional densities of NPs, determined postmortem in the same brains. These data suggest that the topographic expression of NPs is unrelated to impaired OXPHOS in A.D. brain.[23]

3.2. Is the Impairment in Energy Metabolism a Result of Primary Damage to Mitochondrial DNA?

One hypothesis holds that accumulation of oxidative damage of DNA is responsible for physiological changes associated with normal aging.[3,35,84] In this regard, mtDNA may

be particularly susceptible to age-dependent oxidative damage, due to its close proximity to the inner mitochondrial membrane where high amounts of reactive oxygen species are generated.[3,35,84] For example, in human brain, an age-dependent increase in oxidative damage to mtDNA has been observed.[3,35,49,84] The most important risk factor for A.D. is advanced age. Therefore, an increase in oxidative damage to mtDNA may contribute to reduced oxidative metabolism in A.D. brain.[48]

3.2.1. Oxidative Damage to mtDNA and C.O. Subunit mRNA. A 3-fold increase in the hydroxyl radical adduct, 8-oxo-2'-deoxyguanosine (oxo^{8}dG), has been reported in mtDNA of A.D. brain.[58] The increase was observed in regions which display A.D. pathology as well as in those with minimal pathology.[58] Conversion of guanosine to oxo^{8}dG also was demonstrated when the mitochondrial inner membrane was incubated with mtDNA in the presence of NADH and KCN, suggesting that inhibition of OXPHOS can contribute to increased oxo^{8}dG in mtDNA.[40] Thus, observed increases in oxo^{8}dG in A.D. brains might result from impaired mitochondrial function. Furthermore, sequencing of mtDNA from human retina has not shown an age-related accumulation of somatic mutations in mtDNA, even though retinal neurons are post mitotic, maintain high levels of oxidative metabolism and are constantly exposed to UV light.[9] Thus, reduced expression of OXPHOS genes in A.D. brain may not be entirely due to accumulation of oxidative damage in mtDNA.

3.2.2. Inherited Mutations in mtDNA and C.O. Subunit mRNA. In a recent study, Davis et al. reported increased levels of specific missense mutations in the mtDNA-encoded C.O. subunit I and II genes but not in the C.O. III gene in platelet from probable A.D. subjects as compared to controls.[22] It is unknown if the mutations in platelet reflect similar mutations in the brain. In addition, cybrids obtained by fusing mitochondria from platelet of probable A.D. patients with ρ° cells derived from SH-SY5Y neuroblastoma cells showed a decrease in C.O. activity but not in NADH dehydrogenase (complex I) activity.[22] However, in brains of patients with A.D., decreases in levels of mtDNA-encoded C.O. subunit III mRNA and NADH dehydrogenase subunit 1 and 4 mRNA have been observed.[15,17,28] Moreover, in patients with inherited mitochondrial diseases characterized by mutations and deletions,[32] with marked central nervous system involvement, PET studies have shown decreased molar ratio between cerebral oxygen and glucose utilization, suggesting metabolic uncoupling and increased glycolysis.[27] In contrast, in A.D., reductions occur in both cerebral oxygen and glucose utilization, but molar ratio is normal.[57,66] Further studies may are needed to understand the origin and the role of these mutations in A.D. pathogenesis and in OXPHOS deficits in A.D. brain.

3.2.3. Mitochondrial DNA Deletions and C.O. Subunit mRNA. Deletions of mtDNA have been observed in human brain, muscle and liver.[20,49,91] In particular, a 4977-base pair deletion of mtDNA (ΔmtDNA^{49,77}) was found to accumulate in these organs with increasing age.[20,49,91] These deletions were not detected by Southern blot analysis but could be demonstrated by the polymerase chain reaction (PCR) technique, which indicated only low levels of deletions in old subjects (0.005–0.1% of total mtDNA).[20,49,91]

Increased levels of ΔmtDNA^{49,77} in frontal cortex, detectable only by PCR, have been reported in A.D. patients.[19] However, the increases were present in patients younger but not older than 75 years.[19] We did not observe an increase in ΔmtDNA^{4977} in the temporal cortex of 6 A.D. patients who were older than 75 years, compared with 4 controls [0.026 ± 0.007% (mean ± SEM) in A.D. vs 0.020 ± 0.004% in controls]. Moreover, in in-

herited myopathies characterized by mutations and deletions in mtDNA, an increase rather than a decrease was seen in mitochondrial mRNA.[42] Clearly, additional studies are needed to elucidate the contribution if any, of mtDNA mutations and deletions to reduced expression of OXPHOS mRNA in A.D. brains.

3.3. Is the Impairment in Energy Metabolism the Result of Reduced Neuronal Activity?

Under normal conditions, glucose metabolism provides energy (ATP) to support ionic pumping and metabolic processes in the brain.[26] Most of this energy (up to 95%) is derived from oxidative metabolism of glucose, which occurs in mitochondria.[26] Measurement of local cerebral glucose utilization with the deoxyglucose technique supports the observed close coupling of energy metabolism to neuronal activity.[78]

Changes in neuronal activity have been shown to be associated with changes in levels of markers of mitochondrial oxidative energy metabolism.[25,47,86-89] Unilateral silencing of the cochlea in adult cats resulted in decreased C.O. activity in neurons in central auditory nuclei.[87] Removal of whiskers from adult mice induced a decrease in C.O. activity in contralateral cortical barrel neurons, two to three synapses removed from the periphery.[89] Similar correlations between reduced C.O. enzyme activity and reduced neuronal activity have been reported in visual and olfactory systems.[86]

Evidence that neuronal activity influences oxidative energy metabolism comes from a study by Hevner and Wong-Riley.[46] These authors measured C.O. activity, C.O. protein, mtDNA and mRNAs encoded by both mtDNA and nDNA in central visual areas of monkeys unilaterally blinded by intravitreal injection of tetrodotoxin.[46] After 3 days of tetrodotoxin, neurons in layers of the lateral geniculate nucleus (LGN) receiving input from the treated eye showed significantly decreased levels of all of the markers (Table 1). The largest decrease, 44% below control, was observed with mtDNA-encoded C.O. I mRNA. The decreases in C.O. activity and mtDNA were 9% and 18%, respectively. Nuclear DNA-encoded C.O. IV mRNA and C.O. VIII mRNA also showed decreases of 24% and 10%, respectively, compared with control. After 7 days of unilateral TTX exposure, the relative decreases in C.O. activity, mtDNA, C.O. IV mRNA and C.O. VIII mRNA approximated 25%, whereas the decrease in C.O. I mRNA remained at 50%.

In Table 1, we also present changes in different C.O. markers in the mid-temporal association cortex of A.D. compared with control subjects.[16,69] The pattern of changes are very similar to changes following TTX injection in the monkey, suggesting that reduced C.O. activity and reduced C.O. mRNA in A.D. reflect reduced metabolic demand. In other words, the simplest interpretation is that the A.D. data reflect downregulation in OXPHOS mRNA and enzyme expression in relation to reduced neuronal activity.

This interpretation is supported by observations that functional activation of depressed neuronal systems can increase energy metabolism and OXPHOS. In A.D. patients with mild-moderate dementia, functional activation can increase regional glucose metabolism and regional cerebral blood flow in association areas in which these parameters are reduced.[33,59,67] Similarly, in animals, activation of central neurons that have been depressed by chronic sensory deprivation can restore normal levels of markers of OXPHOS.[86,88] Electrical stimulation of the cochlear nerve after silencing of the cochlea was shown to reverse depressed C.O. activity in postsynaptic neurons in central auditory nuclei.[88] Likewise, a TTX-induced decrease in cortical C.O. activity was fully reversed after functional recovery.[86] If these interpretations are correct, we can ask the following question: What are the mechanisms which account for the coupling of OXPHOS and neuronal activity?

Table 1. Mitochondrial and nuclear DNA markers in vulnerable region in Alzheimer's disease and in lateral geniculate nucleus of monkey brain after intravitreal injection of tetrodotoxin

Marker	% Decrease in A.D. temporal cortex vs. control	% Decrease in LGN TTX treated vs. control monkey
OXPHOS markers		
C.O. enzyme activity	20–25	23 ± 1[a]
C.O. protein	ND	23 ± 2
mtDNA	n.s.	26 ± 4
C.O. I mRNA (mtDNA)[b]	58 ± 3	49 ± 3
C.O. III mRNA (mtDNA)	54 ± 5	ND
ND 1 mRNA (mtDNA)	50–60	ND
ND4 mRNA (mtDNA)	60 ± 8	ND
C.O. IV mRNA (nDNA)	40 ± 8	18 ± 3
C.O. VIII mRNA (nDNA)	ND	29 ± 3
ATP synthase β mRNA (nDNA)	50–60	ND
Non-OXPHOS markers		
12S rRNA (mtDNA)	n.s.	ND
28S rRNA (nDNA)	n.s.	ND
LDH-B mRNA (nDNA)	n.s.	ND
β actin mRNA (nDNA)	n.s.	ND

ND: not determined; n.s.: not significant; A.D. Alzheimer's disease; LGN: lateral geniculate nucleus; mtDNA: mitochondrial DNA; nDNA: nuclear DNA; C.O.: cytochrome oxidase; LDH-B: lactate dehydrogenase subunit B.
[a]Mean ± SEM; [b]parenthesis identify whether mRNA is encoded by mtDNA or nDNA.

3.4. Regulation of Expression of OXPHOS Genes

Table 1 shows that mtDNA-encoded mRNAs decreased by almost 50%, whereas both mtDNA and C.O. activity declined by 25% following TTX injection as well as in a pathological region of the A.D. brain. This two-fold difference in reductions implies that mtDNA copy number and rates of mitochondrial transcription and/or turnover are coupled to reduced neuronal demands in a similar way both in A.D. and in functional denervation.

Molecular mechanisms which control mitochondrial mRNA transcription and turnover are not fully understood, but some control mechanisms of gene expression have been identified.[6,29,30,51,73] The mammalian mitochondrial genome encodes polycistronic transcripts derived from heavy (H) and light (L) DNA strands.[6,51,73] The principal regulatory site, called the displacement loop (D-loop) region, contains sites for initiation of transcription of H and L strands as well as for originating H strand replication, so that transcription and replication may be regulated jointly.[6,51,73] However, gene expression in mitochondria is not self-contained, as protein and RNA components that are required for transcription and replication of mtDNA are encoded by nuclear genes.[6,51,73] Nuclear DNA-encoded factors (mtTFA and mtTFB) for mtDNA transcription have been identified.[73] Regulation of transcription of mtTFA and of nDNA-encoded C.O. and other OXPHOS genes in turn has been shown to be modulated by nuclear respiratory factors (NRF).[70,81–83] *Cis*-acting elements and DNA binding proteins common to mtDNA and nDNA-encoded genes of OXPHOS are known.[79] The importance of nuclear genes in regulating mitochondrial C.O. gene expression has been substantiated by a cell fusion experiment in which *in vivo* age-related reductions in C.O. activity in human skin fibroblasts were shown to recover completely following the introduction of ρ°-HeLa cell nuclei into the cells.[41] Nuclear genes responsible for restoration of C.O. activity are localized on several chromosomes.[41] Thus, a number of nuclear genes may regu-

late transduction of signals to the mitochondrial machinery. In addition, differential turnover of mature RNA species appears to play a role in determining the steady-state amounts of the mRNAs.[30] We postulated that ions may play a role in the regulation of mtDNA-encode C.O. subunit gene expression and/or turnover, because ATP in the brain is used primarily for ionic pumping during repolarizations.[18,43,85] Preliminary results obtained in cultured PC12 cells suggest that mtDNA-encoded C.O. subunit mRNA levels are regulated by changes in $[Na]_i$.[18] Further studies may elucidate the mechanism(s) by which neuronal activity regulates mtDNA-encoded gene expression and/or turnover.

3.5. Metabolic Downregulation and Neurotoxicity

Our findings that C.O. subunit mRNA is decreased in tangle-free neurons and that C.O. subunit mRNA is further decreased in neurons bearing early-stage tangles and even more in neurons bearing late-stage tangles suggest that tangle formation correlates with downregulation of oxidative energy metabolism at the level of individual neurons.[38]

We proposed that downregulation of energy metabolism renders neurons vulnerable to sudden energy demand associated with excitotoxicity or ischemia.[1,16,69] There is substantial evidence that inhibition of mitochondrial oxidative metabolism exacerbates toxicity mediated by excitotoxic glutamate receptors, particularly NMDA receptors.[7,34] Inhibition of mitochondrial oxidative metabolism or downregulation of metabolism followed by sudden energy demand may affect a variety of other cellular processes, including Ca^{2+} homeostasis, free radical production, and intracellular signaling and regulatory pathways.[1,7,16,34,69] Pharmacological stimulation of OXPHOS may be useful in A.D. because downregulation of OXPHOS enzymes may render neurons more vulnerable to sudden energy metabolic insults such as ischemia and excitotoxicity.

4. CONCLUSIONS

The pattern of impairment in markers of mitochondrial oxidative energy metabolism in affected regions of the A.D. brain is similar to the pattern observed following functional

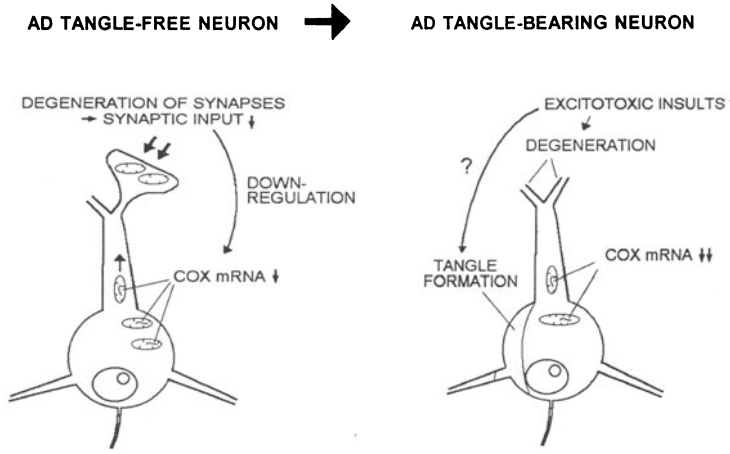

Figure 3. Suggested mechanism for decreased mitochondrial gene expression in brains of A.D. patients. We propose that impaired synaptic function leads to downregulation of oxidative energy metabolism. Downregulation of energy metabolism may render neurons more vulnerable to sudden energy metabolic insults such as excitotoxicity and thereby hasten neurodegeneration.

denervation in the nonhuman primate. This and the observation about the reduced OXPHOS extending beyond the regions which show pathology suggest that the reduced OXPHOS metabolism in A.D. may represent other neuronal changes that reduce energy needs. Activation of mitochondrial energy metabolism may be useful in A.D., because this may protect vulnerable neurons from sudden energy insults that may hasten neurodegeneration.

REFERENCES

1. Abe, K., Kawagoe, J., and Kogure, K. (1993) Early disturbance of a mitochondrial DNA expression in gerbil hippocampus after transient forebrain ischemia, *Neurosci Lett.*, 153, 173–176.
3. Ames, B.N., Shigenaga, M.K., and Hagen, T.M. (1995). Mitochondrial decay in aging. *Biochim. Biophys. Acta.*, 1271, 165–170.
4. Anderson, S., Bankier, A.T., Barrell, B.G., de Bruijn, M.H.L., Coulson, A.R., Drouin, J., Eperon, I.C., Nierlich, D.P., Roe, B.A., Sanger, F., Schreier, P.H., Smith, A.J.H., Staden, R. and Young, I.G. (1981) Sequence and organization of the human mitochondrial genome, *Nature*, 290, 457–465.
5. Attardi, G., Chomyn, A., King, M.P., Kruse, B., Polosa, P.L., and Murdter, N.N. (1989). Biogenesis and assembly of the mitochondrial respiratory chain: Structural, genetic and pathological aspects. *Biochem. Soc. Trans.*, 18, 509–513.
6. Attardi, G., and Schatz, G. (1988). Biogenesis of mitochondria. *Annu. Rev. Cell Biol.*, 4, 289–333.
7. Beal, M.F., Hyman, B.T. and Koroshetz, W. (1993). Do defects in mitochondrial energy metabolism underlie the pathology of neurodegenerative diseases? *Trends. Neurosci.*, 16, 125–131.
8. Blass, J.P., and Gibson, G.E. (1991). The role of oxidative abnormalities in the pathophysiology of Alzheimer's disease. *Rev. Neurol. (Paris).*, 147, 513–525.
9. Bodenteich, A., Mitchell, L.G. and Merril, C.R. (1991). A lifetime of retinal light exposure does not appear to increase mitochondrial mutations. *Gene*, 108. 305–310.
10. Capaldi, R.A. (1990) Structure and function of cytochrome c oxidase, *Annu. Rev. Biochem.*, 59, 569–596.
11. Chandrasekaran, K., Stoll, J., Giordano, T., Atack, J.R., Matocha, M.F., Brady, D.R. and Rapoport, S.I. (1992) Differential expression of cytochrome oxidase (COX) genes in different regions of monkey brain, *J. Neurosci. Res.*, 32, 415–423.
12. Chandrasekaran, K., Stoll, J., Brady, D.R., and Rapoport, S.I. (1992). Localization of cytochrome oxidase (COX) activity and cox mRNA in the hippocampus and entorhinal cortex in the monkey brain: Correlation with specific neuronal pathways. *Brain Res.*, 579, 333–336.
13. Chandrasekaran, K., Stoll, J., Rapoport, S.I., and Brady, D.R. (1993). Localization of cytochrome oxidase (COX) activity and COX mRNA in the perirhinal and superior temporal sulci of the monkey brain. *Brain Research.*, 606, 213–219.
14. Chandrasekaran, K., Giordano, T., Brady. D.R., Stoll, J., Hatanpää, K., Martin, L.J., and Rapoport, S.I. (1994). Impairment in gene expression of oxidative metabolism in vulnerable brain regions in Alzheimer's disease. *Neurobiol. Aging.*, 15: S125.
15. Chandrasekaran, K., Giordano,T., Brady, D.R., Stoll, J., Martin, L.J., and Rapoport, S.I. (1994). Impairment of mitochondrial cytochrome oxidase gene expression in Alzheimer's disease. *Mol. Brain Res.*, 24: 336–340.
16. Chandrasekaran, K., Hatanpää, K., Brady, D.R. and Rapoport, S.I. (1996) Evidence for physiological downregulation of brain oxidative phosphorylation in Alzheimer's disease, *Exp. Neurol.*, 142, 80–88.
17. Chandrasekaran, K., Hatanpää, K., Rapoport, S.I., and Brady, D.R. (1997) Decreased expression of nuclear and mitochondrial DNA-encoded genes of oxidative phosphorylation in association neocortex of Alzheimer's disease. *Mol. Brain Res.*, 44, 99–104.
18. Chandrasekaran, K., Li-Ing, L., Hatanpää, K. and Rapoport, S.I. (1997). Regulation of mitochondrial DNA-encoded cytochrome oxidase subunit gene expression in PC12 cells. *Soc. Neurosci. Abstr.*, 23, 1639.
19. Corral-Debrinski, M., Horton, T., Lott, M.T., Shoefner, J.M., Mcee, A.C., Beal, M.F., Garham, B.H., and Wallace, D.C. (1994). Marked changes in mitochondrial DNA deletion levels in Alzheimer's brains. *Genomics*, 23, 471–476.
20. Corral-Debrinski, M., Stepien, G., Shoefner, J.M., Lott, M.T. Kanter, K., Wallace, D.C. (1991). Hypoxemia is associated with mitochondrial DNA damage and gene induction. Implications for cardiac disease. *J. Am. Med. Assoc.*, 266, 1812–1816.
21. Davies, C.A., Mann, D.M.A., Sumpter, P.Q., and Yates, P.O. (1987). A quantitative morphometric analysis of the neuronal and synaptic content of the frontal and temporal cortex in patients with Alzheimer's disease. *J. Neurol. Sci.*, 78, 151–164.

22. Davis, R.E., Miller, J.S., Herrnstadt, C., Ghosh, S.S., Fahy, E., Shinobu, L.A., Galasko, D., Thal, L.J., Beal, M.F., Howell, N. And Parker Jr, W.D. (1997) Mutations in mitochondrial cytochrome c oxidase genes segregate with late-onset Alzheimer's disease, *Proc. Natl. Acad. Sci. USA*, 94, 4526–4531.
23. Decarli, C.S., Atack, J.R., Ball, M.J., Kaye, J.A., Grady, C.L., Fewster, P., Pettigrew, K.D., Rapoport, S.I., and Schapiro, M.B. (1992). Post-mortem regional neurofibrillary tangle densities but not senile plaque densities are related to regional cerebral metabolic rates for glucose during life in Alzheimer's disease patients. *Neurodegeneration.*, 1, 113–121.
24. DeKoky, S.T., and Scheff, S.W. (1990). Synapse loss in frontal cortex biopsies in Alzheimer's disease: Correlation with cognitive severity. *Ann. Neurol.*, 27, 457–464.
25. Dietrich, W.D., Durham, D., Dietrich, W.D., Durham, D., Lowry, O.H., and Woolsey, T.A. (1982). "Increased" sensory stimulation leads to changes in energy-related enzymes in the brain. *J. Neurosci.*, 2, 1608–1613.
26. Erecinska, M., Silver, I.A. (1989). ATP and brain function. *J. Cereb. Blood Flow Metab.*, 9, 2–19.
27. Frackowiak, R.S., Herold, S., Petty, R.K.H. and Morgan-Hughes, J.A. (1988). The cerebral metabolism of glucose and oxygen measured with positron emission tomography in patients with mitochondrial diseases. *Brain,* 111, 1009–1024.
28. Fukuyama, R.F., Hatanpää, K., Rapoport, S.I., and Chandrasekaran, K. (1996). Gene expression of ND4, a subunit of complex of oxidative phosphorylation in mitochondria, is decreased in temporal cortex of brains of Alzheimer's disease patients. *Brain Res.*, 713, 290–293.
29. Gadaleta, M.N., Petruzzella, V., Renis, M., Fracasso, F., and Cantatore, P. (1990). Reduced transcription of mitochondrial DNA in the senescent rat. Tissue dependence and effect of L-carnitine. *Eur. J. Biochem.*, 187, 501–506.
30. Gelfand, R., and Attardi, G. (1981). Synthesis and turnover of mitochondrial ribonucleic acid in HeLa cells: The mature ribosomal and messenger ribonucleic acid species are metabolically unstable. *Mol. Cell. Biol.*, 1, 497–511.
31. Gentleman, S.M., Roberts, G.W. (1995) Immunocytochemistry: a neuropathological perspective. Appendix: immunostaining protocol. In Roberts, G.W. and Polak, J.M. (Eds). *Molecular neuropathology*, Cambridge, England, Cambridge University Press. pp 72.
32. Goto, Y., Nonaka, I., and Horai, S. (1990). A mutation in the tRNA(Leu) (UUR) gene associated with the MELAS subgroup of mitochondrial encephalomyopathies. *Nature*, 248, 651–653.
33. Grady, C.L., Haxby, J.V., Horwitz, B., Gillette, J., Selerno, A., Gonzalez-Aviles, A., Ungerleider, L.E., Carson, R.E., Herscovitch, P., Schapiro, M.B., and Rapoport, S.I. (1993). Activation of cerebral blood flow during a visuoperceptual task in patients with Alzheimer's-type dementia. *Neurobiol. Aging.*, 14, 35–44.
34. Greene, J.G. and Greenamyre, J.T. (1996) Bioenergetics and excitotoxicity. *Prog. Neurobiol.*, 48(6) , 613–634.
35. Harman, D. (1992). Free radical theory of aging. *Mutation. Res.*, 275, 257–266.
36. Harris, M.E., Hensley, K., Butterfield, D.A., Leedle, R.A., and Carney, J.M. (1995). Direct evidence of oxidative injury produced by the Alzheimer's beta-amyloid peptide (1–40) in cultured hippocampal neurons. *Exp. Neurol.*, 131, 193–202.
37. Hatanpää, K., Brady, D.R., Stoll, J., Rapoport, S.I., and Chandrasekaran, K. (1994). Localization of the deficit in cytochrome oxidase (COX) activity and COX subunit mRNA within the cerebral cortex in Alzheimer's disease. *Soc. Neurosci. Abstr.*, 20, 1253.
38. Hatanpää, K., Brady, D.R., Stoll, J., Rapoport, S.I., and Chandrasekaran, K. (1996) Neuronal activity and early neurofibrillary tangles in Alzheimer's disease. *Ann. Neurol.*, 40, 411–420.
39. Hatanpää, K., Brady, D.R., Chandrasekaran, K. and Rapoport, S.I. (1996) Neuronal energy metabolism is not reduced by senile plaques in Alzheimer's disease. *Soc. Neurosci. Abstr.*, 22, 1174.
40. Hayakawa, K., Ozawa, T., Sugiyama, M., Tanaka, M., and Ozawa, T. (1991). Massive conversion of guanosine to 8-hydroxyguanosine in mouse liver mitochondrial DNA by administration of azidothymidine. *Biochem. Biophys. Res. Commun.*, 176, 87–93.
41. Hayashi, J.I., Ohta, S., Kagawa, Y., Kondo, H., Kaneda, H., Yonekawa, H., Takai, D., and Miyabayashi, S. (1994). Nuclear but not mitochondrial genome involvement in human age-related mitochondrial dysfunction. *J. Biol. Chem.*, 269, 6878–6883.
42. Heddi, A., Lestienne, P., Wallace, D.C., and Stepien, G. (1993). Mitochondrial DNA expression in mitochondrial myopathies and coordinated expression of nuclear genes involved in ATP production. *J. Biol. Chem.*, 268, 12156–12163.
43. Hevner, R.F., Duff, R.S., and Wong-Riley, M.T.T. (1992). Coordination of ATP production and consumption in brain: Parallel regulation of cytochrome oxidase and Na-,K-ATPase. *Neurosci. Lett.*, 138, 188–192.
44. Hevner, R.F., Liu, S., and Wong-Riley, M.T.T. (1995). A metabolic map of cytochrome oxidase in the rat brain: Histochemical, densitometric and biochemical studies. *Neuroscience*, 65, 313–342.

45. Hevner, R.F., and Wong-Riley, M.T.T. (1991). Neuronal expression of nuelear and mitochondrial genes for cytochrome oxidase (CO) subunits analyzed by in situ hybridization: Comparison with CO activity and protein. *J. Neurosci.* 11: 1942–1958.
46. Hevner, R.F., and Wong-Riley, M.T.T. (1993). Mitochondrial and nuelear gene expression for cytochrome oxidase subunits are disproportionately regulated by functional activity in neurons. *J. Neurosci.*, 13, 1805–1819.
47. Horton, J.C., and Hubel, D.H. (1981). Regular patchy distribution of cytochrome oxidase staining in primary visual cortex of macaque monkey. *Nature*, 292, 762–764.
48. Hutchin, T., and Cortopassi, G. (1995). A mitochondrial DNA clone is associated with increased risk for Alzheimer's disease. *Proc. Natl. Acad. Sci.*, 92, 6892–6895.
49. Ikebe, S., Tanaka, M., Ohno, K., Sato, W., Hattori, K., Kondo, T., Mizuno, Y., and Ozawa, T. (1990). Increase of deleted mitochondrial DNA in the striatum of Parkinson's disease and senescence. *Biochem. Biophys. Res. Commun.*, 179, 1044-1048.
50. Kadenbach, B., Kunh-Nentwig, L. and Buge, U.(1987) Evolution of a regulatory enzyme: cytochrome-c-oxidase (complex IV), *Curr. Top. Bioenerg.*, 15, 113–161.
51. Kagawa, Y., and Ohta, S. (1990). Regulation of mitochondrial ATP synthesis in mammalian cells by transcriptional control. *Int. J. Biochem.*, 22: 219–229.
52. Khachaturian, Z.S. (1985) Diagnosis of Alzheimer's disease. *Arch Neurol.*, 42, 1097–1105.
53. Kish, S.J., Bergeron, C., Rajput, A., Dozic, S., Mastrogiacomo, F., Chang, L-J., Wilson, J.M., Distefano, L.M., and Nobrega, J.N. (1992). Brain cytochrome oxidase in Alzheimer's disease. *J Neurochem.*, 59, 776–779.
54. Lewis, D.A., Campbell, M.J., Terry, R.D., and Morrison, J.H. (1987). Laminar and regional distributions of neurofibrillary tangles and neuritic plaques in Alzheimer's disease: A quantitative study of visual and auditory cortices. *J. Neurosci.*, 7, 1799–1808.
55. Linnane, A.W., Marzuki, W.S., Ozawa, T., and Tanaka, M. (1989). Mitochondrial DNA mutations as an important contributor to ageing and degenerative diseases. *Lancet*, 1, 642–645.
56. Liu, S., and Wong-Riley, M.T.T. (1994). Nuclear-encoded mitochondrial precursor protein: Intramitochondrial delivery to dendrites and axon terminals of neurons and regulation of neuronal activity. *J. Neurosci.*, 14, 5338–5351.
57. McGeer, P.L., Kamo, H., Harrop, R., McGeer, E.G., Martin, W.R.W., Pate, B.D., and Li, D.K.B. (1986). Comparison of PET, MRI, and CT with pathology in a proven case of Alzheimer's disease. *Neurology*, 36, 1569–1574.
58. Mecocci, P., MacGarvey, U., and Beal, M.F. (1994). Oxidative damage to mitochondria DNA is increased in Alzheimer's disease. *Ann. Neurol.*, 36, 747–751.
59. Mentis, M.J., Horwitz, B., Grady, C.L., Alexander, G.E., Vanmeter, J.W., Maisog, J.M., Pietrini, P., Schapiro, M.B. and Rapoport, S.I. (1996) Visual cortical dysfunction in Alzheimer's disease evaluated with a temporally graded "stress test" during PET, *Am. J. Psychiatry*, 153, 32–40.
60. Mirra, S.S., Hart, M.N. and Terry, R.D. (1993) Making the diagnosis of Alzheimer's disease. *Arch. Pathol. Lab. Med.*, 117, 132–144.
61. Mutsiya, E.M., Bowling, A.C., and Beal, M.F. (1994). Cortical cytochrome oxidase activity is reduced in Alzheimer's disease. *J. Neurochem.*, 63, 2179–2184.
62. Parker, W.D., Jr, Filley,C.M., and Parks, J.K. (1990). Cytochrome oxidase deficiency in Alzheimer's disease. *Neurology*, 40, 1302–1303.
63. Parker, W.D., Jr, Mahr, N.J., Filley, C.M., Parks, J.K., Hughes, D., Young, D.A., and Cullum, C.M. (1994). Reduced platelet cytochrome c oxidase activity in Alzheimer's disease. *Neurology*, 44, 1086-1090.
64. Parker, W.D., Jr, Parks, J., Filley, C.M., and Kleinschmidt-Demasters, B.K. (1994). Electron transport chain defects in Alzheimer's disease brain. *Neurology*, 44, 1090-1096.
65. Pietrini, P., Furey, M.L., Dani, A., Freo, U., Mentis, M.J., Alexander, G.E., and Rapoport, S.I. (1996). Functional response to audiovisual stimulation in Alzheimer's patients: Potential for therapeutic interventions. *Abstr. Soc. Neurosci.*, 22, 1176.
66. Rapoport, S.I. (1991). Positron emission tomography in Alzheimer's disease in relation to disease pathogenesis: A critical review. Cerebrovasc. *Brain Metab. Rev.*, 3, 297–335.
67. Rapoport, S.I., and Grady, C.L. (1993). Parametric in vivo brain imaging during activation to examine pathological mechanisms of functional failure in Alzheimer's disease. *Int. J. Neurosci.*, 70, 39–56.
68. Rapoport, S.I., Horwitz, B., Grady, C.L., Haxby, J.V., and Schapiro, M.B. Alzheimer's disease, a disease of the association neocortices and connected regions: Metabolic, cognitive and pathologic correlations.In H.J. Altman, and B. Altman (Eds), *Alzheimer's and Parkinson's diseases. Recent Aduances in Research and Clinical Management.* Plenum Press, New York. 1989, pp 115–136.

69. Rapoport, S.I., Hatanpää, K., Brady, D.R. and Chandrasekaran, K. (1997) Brain energy metabolism, cognitive function, and down-regulated oxidative phosphorylation in Alzheimer's disease, *J. Neurodegeneration*, 5, 473–476.
70. Scarpulla, R. (1996). Nuclear respiratory factors and the pathways of nuclear-mitochondrial interaction. *Trends Cardiovasc. Med.*, 6, 39–45.
71. Schagger, H., and Ohm, T.G. (1995). Human diseases with defects in oxidative phosphorylation. 2. F1FO ATP-synthase defects in Alzheimer's disease revealed by blue native polyacrylamide gel electrophoresis. *Eur J. Biochem.*, 227, 916–921.
72. Scheff, S.W., DeKosky, S.T., and Price, D.A. (1990). Quantitative assessment of cortical synaptic density in Alzheimer's disease. *Neurobiol. Aging.*, 11, 29–37.
73. Shadel, G.S., and Clayton, D.A. (1993). Mitochondrial transcription initiation. Variation and conservation. *J. Biol. Chem.*, 268, 16083–16086.
74. Shoffner, J.B., Brown, M.D., Torroni, A., Lott, M.T., abell, M.F., Mirra, S.S., Beal, M.F., Yang,C.C., Gearing, M., Salvo, R., Watts, R.L., Juncos, J.L., Hansen, L.A., Crain, B.J., Fayad, M., Reckord, .L., and Wallace, D.C. (1993). Mitochondrial DNA variants observed in Alzheimer's disease and Parkinson disease patients. *Genomics*, 17, 171–184.
75. Simonian, N.A., and Hyman, B.T. (1993). Functional alterations in Alzheimer's disease: Diminution of cytochrome oxidase in the hippocampal formation, *J. Neuropathol. Exp. Neurol.*, 52, 580–585.
76. Simonian, N.A., and Hyman, B.T. (1994). Functional alterations in Alzheimer's disease: selective loss of mitochondrial-encoded cytochrome oxidase mRNA in the hippocampal formation, *J. Neuropathol. Exp. Neurol.*, 53, 508–512.
77. Sims, N.R., Finegan, J.M., Blass, J.P., Bown, D., and Neary, D. (1987). Mitochondrial function in brain tissue in primary degenerative dementia. *Brain Res.*, 436, 30–38.
78. Sokoloff, L. (1991). Relationship between functional activity and energy metabolism in the nervous system: Whether, where and why. In N.A. Lassen, D.H. Ingvar, M.E. Raichle, and L. Friberg (eds). *Brain Work and Mental Activity. Quantitative Studies with Radioactive Tracers. Alfred Benson Symposium VIII.* Munksgaard. Copenhagen. pp. 52–67.
79. Suzuki, H., Hosokawa, Y., Nishikimi, M., and Ozawa, T. (1991). Existence of common homologous elements in the transcriptional regulatory regions of human nuclear genes and mitochondrial gene for the oxidative phosphorylation system. *J. Biol. Chem.*, 266, 2333–2338.
80. Vale, R.D., Schnapp, B.J., Reese, T.S., and Sheetz, M.P. (1985) Movement of organelles along filaments dissociated from the axoplasm of the squid giant axon, *Cell*, 40, 449–454.
81. Virbasius, C.A., Virbasius, J.V., and Scarpulla, R.C. (1993). NRF-1, an activator involved in nuclear-mitochondrial interactions, utilizes a new DNA-binding domain conserved in a family of developmental regulators. *Genes Dev.*, 7, 2431–2445.
82. Virbasius, J.V., and Scarpulla, R.C. (1994). Activation of the human mitochondrial transcription factor A gene by nuclear respiratory factors: A potential regulatory link between nuclear and mitochondrial gene expression in organelle biogenesis. *Proc. Natl. Acad. Sci. USA.*, 91, 1309–1313.
83. Virbasius, J.V., Virbasius, C.A., and Scarpulla, R.C. (1993). Identity of GABP with NRF-2, a multisubunit activator of cytochrome oxidase expression, reveals a cellular role for an ETS domain activator of viral promotors. *Genes Dev.*, 4, 380–392.
84. Wallace, D.C. (1992). Mitochondrial genetics: A paradigm for aging and degenerative diseases. *Science*, 256, 628–632.
85. Wolitzky, B.A., and Fambrough, D.M. (1986). Regulation of the (Na- + K-)-ATPase in cultured chick skeletal muscle. Modulation of expression by the demand for ion transport. *J. Biol. Chem.*, 261, 9990–9999.
86. Wong-Riley, M.T.T. (1989). Cytochrome oxidase: An endogenous metabolic marker for neuronal activity. *Trends Neurosci.*, 12, 94–101.
87. Wong-Riley, M.T.T. Merzenich, M.M., and Leake, P.A. (1978). Changes in endogenous enzymatic reactivity to DAB induced by neuronal inactivity. *Brain Res.*, 141, 185–192.
88. Wong-Riley, M.T.T., Walsh, S.M., Leake-Jones, P.A., and Merzenich, M.M. (1981). Maintenance of neuronal activity by electrical stimulation of unilaterally deafened cats, demonstrable with cytochrome oxidase technique. *Ann. Otol. Rhinol. Laryngol.*, 90 (Suppl.2): 30–32.
89. Wong-Riley, M.T.T., and Welt, C. (1980). Histochemical changes in cytochrome oxidase of cortical barrels after vibrissal removal in neonatal and adult mice. *Proc. Natl. Acad. Sci. USA.*, 77, 2333–2337.
90. Wragg, M.A., Talbot, C.J., Morris, J.C., Lendon, C.L., and Goate, A.M. (1995). No association found between Alzheimer's disease and a mitochondrial tRNA glutamine gene variant. *Neurosci. Lett.*, 201, 107–110.
91. Yen, T.-C., Su, J.-H., King, K.-L., Wei, Y.-H. (1991). Ageing associated 5 kb deletion in human liver mitochondrial DNA. *Biochem. Biophys. Res. Commun.*, 178, 124–131

8

BEHAVIORAL, ELECTROPHYSIOLOGICAL, AND BIOCHEMICAL CONSEQUENCES OF CHRONIC CYTOCHROME OXIDASE INHIBITION IN RATS

M. C. Bennett[1] and G. M. Rose[2]

[1]Experimental Therapeutics Branch
NINDS
[2]Neuroscience Drug Discovery
Bristol-Myers Squibb Co.

ABSTRACT

The mitochondrial enzyme cytochrome oxidase (C.O.) is an essential catalyst for electron transfer in oxidative phosphorylation. Recent clinical studies have shown that C.O. activity is reduced in both blood platelets and in the brains of patients with Alzheimer's disease (A.D.), suggesting that a decline in the efficiency of this enzyme could impair cognition. We explored this idea by chronically treating rats with sodium azide, using doses that inhibited C.O. but not other electron transport chain enzymes. Our initial studies demonstrated that selective C.O. inhibition produced deficits in learning tasks, including spatial learning, but did not alter basic sensorimotor function. Azide treatment also disrupted hippocampal long-term potentiation, a potential memory encoding mechanism. Both these effects may have been the consequence of a reduction in membrane bound protein kinase C activity that was observed in the hippocampus, but not in frontal or temporal cortex or cerebellum. Further work revealed that the stress hormone, corticosterone, potentiated azide-induced inhibition of C.O. and the resulting cognitive deficits. Thus, manipulation of C.O. activity in rats to mimic biochemical conditions observed in patients with A.D. caused impairments in learning and memory.

1. INTRODUCTION

The brain's enormous energy utilization renders it particularly vulnerable to conditions in which ATP generation is compromised. For example, damage to central neurons following hypoxia or ischemia occurs quickly, often causing irreversible damage. Oxidative phosphorylation, the major source of ATP in aerobic organisms, is catalyzed by a series of

Cytochrome Oxidase in Neuronal Metabolism and Alzheimer's Disease,
edited by Gonzalez-Lima, Plenum Press, New York, 1998.

mitochondrial enzymes. High-energy electrons generated by the oxidation of electron carrier species are transferred through these enzymes by a series of redox reactions, culminating with the reduction of molecular oxygen to water. Free energy released by these reactions is used to phosphorylate ADP to form ATP at three sites in the respiratory chain: complex I (NADH:ubiquinone oxidoreductase), complex III (ubiquinonol:ferricytochrome c oxidoreductase) and complex IV (ferrocytochrome c:oxygen oxidoreductase, also known as cytochrome c oxidase or C.O.). Electron transfer can be disrupted by inhibiting the activity of any of these enzymes.

Researchers have long sought to understand the mechanisms underlying neurodegenerative disorders such as Alzheimer's disease (A.D.). The high energy requirement of neurons has led to speculation that the accelerating process of neuron loss in early and mid-stage A.D. was the consequence of a defect in energy metabolism (Beal, 1995; Davis et al., 1997; Schapira, 1996). Furthermore, given the critical role of energy generation for keeping neurons alive, it is reasonable to assume that non-lethal perturbations in oxidative phosphorylation mechanisms would also be sufficient to impair normal brain function. Recent studies have shown that, of the electron transport chain enzymes, C.O. activity is preferentially reduced in blood platelets taken from patients with A.D. (Parker, Filley, & Parks, 1990; Parker et al., 1994a; Parker, Parks, Filley, & Kleinschmidt-DeMasters, 1994b). Other work has demonstrated that C.O. activity is also reduced in brain tissue taken post-mortem from A.D. patients (Chagnon, Betard, Robitaille, Cholette, & Gauvreau, 1995; Gonzalez-Lima, Valla, & Matos-Collazo, 1997; Kish et al., 1992; Mutisya, Bowling, & Beal, 1994; Reichmann, Florke, Hebenstreit, Schrubar, & Riederer, 1993; Simonian & Hyman, 1993; Simonian & Hyman, 1995), as is the mRNA for some C.O. subunits (Chandrasekaran, this volume; Chandrasekaran et al., 1994; Hatanpaa, Brady, Stoll, Rapoport, & Chandrasekaran, 1996; Simonian & Hyman, 1994; Simonian & Hyman, 1995). However, the finding of a decline in C.O. in the brain does not distinguish between a dysfunction of energy metabolism that is pathogenic and one that merely reflects cell death.

This issue led us to begin evaluating the effects of chronic C.O. inhibition in rats. The goal of this work was to develop a stable model system in which the consequences of chronic partial disruption of aerobic energy generation could be examined. Our hypothesis was that producing a condition of long-term mitochondrial insufficiency in the rat would model some of the elements of metabolic dysfunction that are present in age-related neurodegenerative diseases, such as A.D. Using the model, we hoped to be able to provide insight into the progression of such diseases, independent of whether mitochondrial dysfunction is part of the original pathogenesis. Here we offer a review of our progress and a perspective on the utility of the model.

2. METHODS

2.1. Azide Administration

Adult (4–6 month old) male Sprague-Dawley rats (Charles River) were used in all our studies. At the time of treatment, the rats were approximately 4 months of age and weighed 375–425 g. Under secobarbital anesthesia (50 mg/kg), rats were implanted subcutaneously with an Alzet 2ML4 osmotic minipump. For each subject, an incision of approximately 1 cm was made in the nape of the neck and the skin was retracted from the muscle and fascia to form a pocket of approximately 1 cm by 3 cm into which the

minipump was inserted. The incision was closed with wound clips. The Alzet 2ML4 minipump has a 2 ml reservoir and provides a constant infusion rate of 2.5 μg/hr for 28 days. The pumps were filled with either a solution of either 0.9% saline or concentrations of sodium azide (Aldrich Chemical, 99% purity) at 80, 120 or 160 μg/μl in the saline vehicle. These concentrations correspond to subcutaneous azide infusion rates of 200, 300 or 400 μg/hr. By weight, the target doses were 0.5, 0.75 or 1.0 mg/kg/hr.

Azide is a toxic substance (Klein-Schwartz et al., 1989), and must be treated appropriately. We have found that the 400 μg/hr dose of azide was lethal for approximately 10–20% of the treated rats, with death occurring within 48 hours of minipump implantation. The dose-response curves of sodium azide for both mortality and efficacy of C.O. inhibition are steep; therefore, careful titration of the dose delivered is essential. Mortality was very high when the dose of azide was raised to 500 μg/hr, but was negligible at the 300 μg/hr dose. However, the latter dose produced only a modest inhibition of C.O. activity, averaging 23% (Bennett, Mlady, Fleshner, & Rose, 1996a). Early post-surgical deaths can be reduced by careful attention to variables such as differences in the flow rates of the Alzet minipumps (which vary by lot, and also up to 10% within lots), and the use of a narrow range for the initial weights of the animals. We have found that young adult rats weighing at least 400 grams survive the treatment better than do lighter animals.

All of our studies were conducted using Alzet 2ML4 minipumps, because until recently this was the only option for infusion periods of longer than 14 days. A problem with this pump is its relatively large size, which seemed to hinder wound healing and sometimes altered natural locomotion or swimming in behavioral assessments. The Alzet corporation now offers a smaller pump, the model 2004, which also delivers agents continuously for a 28-day period. The difference in the displacement volume between the models 2004 and 2ML4 is substantial (1.0 versus 6.5 cubic centimeters). The smaller minipump is clearly advantageous from the perspective of size, and the excellent solubility of sodium azide easily permits the preparation of the higher solution concentrations that would be necessary. However, we have not yet had any experience using the smaller minipumps for azide administration. Nor have we explored intracerebroventricular administration of azide as a means of further inhibiting brain C.O. without increasing mortality. A potential caveat with this approach is the possible generation of motor seizures (Smith, Louis, Kruszyna, & Kruszyna, 1991), a phenomenon that we have not observed with our doses of peripherally administered azide.

2.2. Biochemistry

2.2.1. Mitochondrial Extraction. The materials used for the isolation of mitochondria from brain tissue consisted of the following: Isolation Buffer (10 mM Tris-base, 0.32 M sucrose, 2 mM K^+ EDTA, pH to 7.4 with HCl at 4°C); Modified Isolation Buffer (Isolation buffer with 0.3% w/v bovine serum albumin and 1 mM ATP, pH to 7.4 with HCl at 4°C); Ficoll Solutions, which were made up in modified isolation buffer (w/w) except 3% Ficoll, which is 6% Ficoll solution diluted 1:1 in deionized water, pH to 7.4 with HCl at 4°C; Alkaline Tris (6 mM Tris-base, pH to 8.1 with HCl at 4°C); Synaptic Ficoll Buffer (10 mM Tris-base, 0.24 M mannitol, 0.06 M sucrose, 50 μM K^+ EDTA, pH to 7.4 with HCl at 4°C; Oxygraph Buffer (10 mM potassium phosphate buffer, 0.225 M mannitol, 0.075 M sucrose, 10 mM Tris-base, 20 mM KCl, 50 μM K^+ EDTA, pH to 7.4 with HCl at 4°C).

Mitochondrial extraction and assays for C.O. activity were carried out as previously described (Bennett, Mlady, Kwon, & Rose, 1996b). To obtain brain tissue, the rats were given a lethal dose of sodium pentobarbital (100 mg/kg, i.p.). After the brains were ex-

tracted, they were placed on an ice-cold platform and a coronal slice was made at the level of the pons. The portion of the brain anterior to the cut was used to isolate cell body and synaptic mitochondria by a modification of the method of Lai and Clark (1979). The brain tissue was coarsely chopped, then homogenized in approximately 10 ml of cold modified isolation buffer in a Dounce homogenizer with a 0.1 mm clearance (12 passes). The homogenate was centrifuged for 3 min at 1300 x g. To maximize cell breakage, the pellet was resuspended in approximately 5 ml of the same buffer and the homogenization (6 passes) and centrifugation processes were repeated. The supernatants from both spins were combined, centrifuged for 10 min at 17,000 x g and the supernatant from this spin was discarded. The pellet was resuspended in approximately 5 ml of modified isolation buffer, which then was layered over a step gradient of 7.5% over 10% Ficoll solutions and centrifuged for 40 min at 4°C (Beckman ultracentrifuge, SW 28 rotor, 22,400 rpm, program 4 acceleration and deceleration) to separate cell body (somatic and dendritic) from synaptic terminal mitochondria. After this spin, the cell body mitochondria were in the pellet and the synaptosomes were in the second interface. The pellet was rinsed with isolation buffer, resuspended in 5–10 mls of this buffer and then centrifuged for 10 min at 9,800 x g. The new pellet, which contained isolated cell body mitochondria, was resuspended in a small volume (100–200 µl) of oxygraph buffer to a protein concentration of 5–10 mg/ml.

To isolate synaptic mitochondria, the second interface described above was diluted with approximately 3 volumes of modified isolation buffer. This suspension was centrifuged for 10 min at 9800 x g. The supernatant was discarded and the pellet was resuspended in approximately 5 ml of alkaline Tris in a Teflon-glass homogenizer (4 passes). An additional 10 ml of alkaline Tris was added and the suspension was centrifuged again for 10 min at 11,800 x g. After this spin, the pellet was resuspended in 5 ml of alkaline Tris as before and then centrifuged for 10 min at 8,300 x g. The resulting supernatant was decanted and the remaining lipid was gently washed away. The pellet, which contained the synaptosomal mitochondria, was resuspended in 5 ml of 3% Ficoll medium. The mitochondrial suspension was layered over 10 ml of 6% Ficoll medium and centrifuged for 30 minutes at 11,300 x g. The mitochondria-containing pellet was then gently washed with modified isolation buffer and resuspended in a small volume of this buffer to a protein concentration of 5–10 mg/ml. Mitochondria from both extractions were divided into smaller aliquots and stored at –70°C for later analysis.

2.2.2. Assay for Cytochrome Oxidase Activity. Cytochrome oxidase activity was measured spectrophotometrically as the rate at which the enzyme catalyzed the transfer of electrons from ferrocytochrome c to O_2. Initially, cytochrome c was reduced by an excess of ascorbic acid and separated over a Sephadex G50 swollen column. The concentration of ferrocytochrome c was determined spectro-photometrically, using $e_{550} = 18.5\ mM^{-1}cm^{-1}$. The volume of ferrocytochrome c that was used in the assay was calculated based upon a target assay concentration of 25 µM, which gives an absorbance reading of approximately 0.725.

To begin the assay, 20 µl of the detergent n-dodecyl beta-D-maltoside (10 mM) and the calculated volume of ferrocytochrome c were combined with sufficient buffer (20 mM potassium phosphate, pH = 7.0, room temperature) in a cuvette to yield 1 ml. The cuvette was then inserted in the spectrophotometer and equilibrated for 3 minutes at 30°C. The reaction was initiated with addition of mitochondrial protein, and the rate of oxidation of ferrocytochrome c was measured by following the decrease in absorbance at 550 nm for 2 minutes. To ensure that cytochrome c was completely oxidized at the end of the reaction, several crystals of potassium ferricyanide, a potent oxidant of ferrocytochrome c, were added to the cuvette and the minimum absorbance (A_∞) was noted to be around 0.22. Ab-

sorbance (A_t) was determined at 6 second intervals during the time of the reaction and the values of ln ($A_t - A_\infty$) were plotted against time. The k of the total reaction was calculated as the slope of this curve (D ln $[A_t - A_\infty]$/Dt). For each mitochondrial sample, replications of rate measurements were made using a range of 10–50 μg protein to confirm linearity. The k for cytochrome c oxidase is reported in units of sec^{-1} mg^{-1} mitochondrial protein as the average of these calculations.

3. RESULTS

3.1. Inhibition of C.O. by Azide

Our biochemical studies indicated that chronic subcutaneous infusion of sodium azide, at a dose of 400 μg/hr, caused a partial (40–50%) inhibition of whole brain mitochondrial C.O. activity. The observed variation in the degree of C.O. inhibition could be due to several factors, not the least of which is that sodium azide is a reversible inhibitor, and can become dissociated from C.O. during the activity assay (Hewitt & Hallas, 1959). Time course studies revealed that maximal inhibition of C.O. was not observed until seven days after the infusion was begun, but that this level of inhibition was maintained for the remaining 21 days of azide administration (Bennett et al., 1996b). Mitochondria isolated from synaptic terminals showed slightly greater peak inhibition of C.O. activity (approximately 47%) than was observed for mitochondria isolated from cell bodies (approximately 41%; Bennett et al., 1996b). These data are shown in Figure 1. The values for C.O. inhibition are somewhat greater than we reported in our initial studies (35–39%; Bennett, Diamond, Stryker, Parks, & Parker, 1992b), perhaps reflecting differences in time of administration or in the method of biochemical assessment. We have not performed complete dose-response studies of the inhibition of C.O. by azide. However, reducing the dose of azide by 25%, to 300 μg/hr, reduced the degree of C.O. inhibition by approximately half, to an average of only 23% (Bennett et al., 1996a). As was mentioned above, we have not been able to achieve greater C.O. inhibition, using sodium azide alone, without unacceptable mortality (but see Section 3.6).

In collaboration with the laboratory of Dr. Gonzalez-Lima (this volume), we performed an experiment using quantitative histochemical methods to determine whether there were differences in the amount of C.O. inhibition in different brain regions after chronic azide administration (Cada, Gonzalez-Lima, Rose, & Bennett, 1995). The rats in this experiment were treated with 400 μg/hr sodium azide for two weeks. This study demonstrated that the reduction of C.O. activity in the brain was fairly uniform across

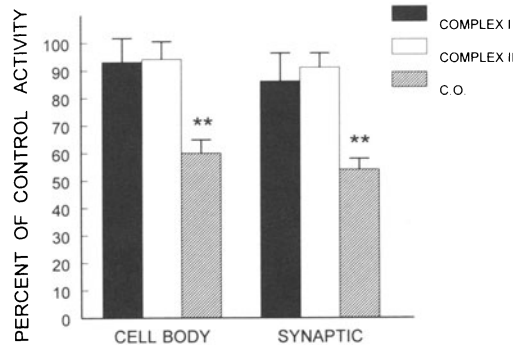

Figure 1. Effect of subcutaneous sodium azide infusion (400 μg/hr) on electron transport chain enzyme activities in whole rat brain. Data shown are taken from animals given 14 days of treatment. Azide infusion partially inhibited cytochrome oxidase (C.O.) activity in both cell body and synaptic mitochondria, but had no significant effect on the activity of complexes I or III. **$p < 0.01$ versus saline-treated control group.

the brain regions measured, ranging from a minimum inhibition of 26% (for entorhinal cortex, superior colliculus and lateral frontal cortex) to a maximum inhibition of 37% (in deep mesencephalic nucleus and central amygdaloid nucleus). Overall, the mean percent reductions in C.O. activity were slightly graded, with the inhibition in telencephalic regions (27%) being somewhat less that was observed in the diencephalon (29%) or mesencephalon (36%). These values compare favorably with those obtained using biochemical methods, given the different assay conditions and considering the reversible nature of the azide binding.

To begin to evaluate the specificity of azide treatment, we measured the effect of chronic administration (400 μg/hr) upon other electron transport chain enzymes. Detailed methods for these assays are given in Bennett et al. (Bennett et al., 1996b). We found that, in contrast to the inhibitory effect of azide on C.O., the activities of complexes I and III in whole brain mitochondrial samples were not significantly altered by up to four weeks of azide treatment (Bennett et al., 1996b). These data are shown in Figure 1.

Under some experimental conditions, azide has been reported to inhibit metalloenzymes, such as peroxidases, copper-containing superoxide dismutase (SOD) and catalase. We have not directly tested the activity of these other enzymes under our conditions of azide treatment. However, it is important to consider aspects of our in vivo model that differ from earlier work, which was often carried out in vitro under conditions different from those present in mammalian physiological systems. (These issues are discussed in detail in Bennett et al., 1996b). For example, azide is a potent inhibitor of various peroxidases at acidic pH, but has little or no effect on these enzymes at neutral or alkaline pH (Keilin, Hartree, Cecil, & Ogston, 1951). Furthermore, although azide has an avid affinity for enzyme copper, it produces only weak inhibition of copper-containing enzymes such as Zn-Cu SOD (Rotilio, Bray, & Fielden, 1972). In general, sodium azide is a far weaker inhibitor of both copper- and zinc-containing enzymes than is cyanide, the other major C.O. inhibitor (Malmstrom, Andreasson, & Reinhammar, 1975). At the concentrations we have used in our studies, we predict that azide would not significantly inhibit the activity of peroxidases or Zn-Cu SOD.

The catabolism of sodium azide presents other challenges to the specificity of our model of selective C.O. inhibition. Trace amounts of nitric oxide (NO) are produced from azide peroxidation in the presence of catalase (Keilin & Hartree, 1954). The potential effects of trace amounts of NO have not been specifically evaluated in our in vivo model. In addition, the azide-catalase complex is very sensitive to inhibition by NO (Keilin & Hartree, 1954). Catalase itself may therefore be somewhat inhibited in our model. It is not known what effect such inhibition could have on the anion and peroxide radical scavenging properties of catalase. A final issue regarding azide's specificity of action concerns the possible activation of guanylate cyclase as the consequence of NO generation. NO has been shown to be an inhibitor of mitochondrial enzyme complexes I and II (Nathan, 1992). Our observation that neither complex I (Bennett, Diamond, Stryker, Parks, & Parker Jr., 1992a; Bennett et al., 1996b) nor complex II (Bennett et al., 1996b) activity was altered by the doses of sodium azide we have employed suggests that NO is not being produced in amounts necessary to have a physiological effect. Nevertheless, it will be necessary to employ other techniques, such as antisense technology, to achieve truly selective and specific inhibition of C.O. However, our conclusion is that sodium azide, at the doses employed, is a good pharmacological tool with which to begin to examine the consequences of disrupting mitochondrial energy generation.

One consequence of an impairment of aerobic respiration in mitochondria is an increase in glycolysis, the anaerobic energy-yielding metabolic pathway. In glycolysis, glu-

cose is broken down to form pyruvate. If the aerobic pathways of the Kreb's cycle and the respiratory chain are available, pyruvate enters the Kreb's cycle and its metabolism proceeds aerobically. However, if there is an impairment of aerobic respiration, the equilibrium between pyruvate and lactate is shifted towards lactate, the anaerobic end-product. An increase in lactic acid is the earliest marker of a change in intermediary metabolism under anaerobic conditions (Siesjo & Zwetnow, 1970). If the reduction in energy-generating capacity induced by azide treatment was functionally important, it would be expected that the anaerobic conversion of glucose to lactate would be stimulated by low ATP. This increased anaerobic metabolism would be predicted to elevate serum lactate levels. We tested this hypothesis and found that, indeed, serum lactate concentrations were elevated in azide treated rats (Figure 2). Elevated lactate levels have also been reported in patients with a variety of neurodegenerative diseases, such as A.D. and Huntington's disease (Bowling & Beal, 1995; Kish et al., 1992; Koreshtz, Jenkins, Rosen, & Beal, 1997).

3.2. Effects of Azide Treatment on Behavior

As was mentioned above, mortality in the first two days after beginning sodium azide administration (at a dose of 400 μg/hr) was variable. However, animals that survived the initial treatment period recovered from surgery at the same rate as vehicle-treated animals. Once wound healing was complete, the rats' behavior in their home cages was indistinguishable from rats implanted with vehicle-containing pumps or unoperated controls. More formal evaluation of sensorimotor function by measuring activity in an open field and sensitivity to footshock demonstrated that azide-treated rats were not different from their control counterparts with respect to spontaneous exploratory/motor behavior or in their threshold to react to a painful stimulus (Bennett et al., 1992a).

Although azide-treated rats did not show impairments in sensorimotor function, they were impaired in tests of cognition. Our initial studies revealed deficits in two-way shuttle box avoidance and in the eight arm radial maze, a working memory task (Bennett et al., 1992a). Since these behavioral tasks are known to be modulated by many brain structures (Becker, Walker, & Olton, 1980; Fujimoto, Yoshida, Ikeguchi, & Niijima, 1989; Olton, Walker, & Gage, 1978), we next decided to focus our studies of the effects of azide upon cognition by testing the rats in the Morris water maze, a spatial learning task that is permanently disrupted by damage to the hippocampus (Moser, Moser, Forrest, Andersen, & Morris, 1995). Rats were given two weeks of sodium azide infusion at doses of either 200, 300 or 400 μg/hr prior to training, and drug treatment was continued throughout the testing period. Spatial learning was evaluated by testing the rats' ability to acquire a memory for location of an escape platform that was hidden in a pool of water (see Bennett et al., 1996a, for detailed methods).

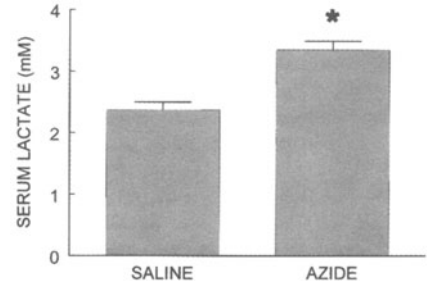

Figure 2. Sodium azide infusion (400 μg/hr) for two weeks caused a significant elevation in serum lactate levels. *$p < 0.05$ versus saline group.

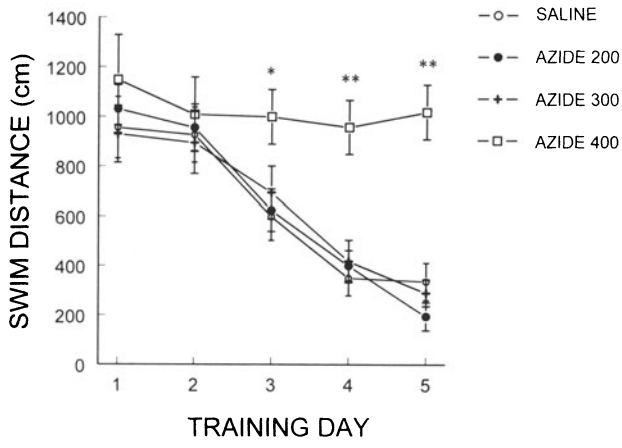

Figure 3. Dose-response evaluation of the effect of sodium azide infusion on spatial learning using the hidden platform version of the Morris water maze. Rats received saline or azide treatment for two weeks prior to beginning behavioral testing, and infusion continued throughout the testing period. Only the highest dose of azide (400 μg/hr) impaired spatial learning. *$p < 0.05$ versus all other groups; **$p < 0.01$ versus all other groups.

As can be seen in Figure 3, the highest dose of azide prevented learning over the five-day training period, while lower doses did not affect learning at all. Thus, the dose-response relationship for azide-induced spatial learning impairments was rather steep. However, similar limitations have been observed for other drugs that impair spatial learning, such as glutamatergic NMDA receptor antagonists (Robinson Jr., Crooks Jr., Shinkman, & Gallagher, 1989). In contrast to the deficit in spatial learning seen with 400 μg/hr azide treatment, no impairment was observed if the rats were trained to swim to a visible platform (Table 1). These data complement our previous work indicating that the doses of azide we employed did not induce general sensorimotor impairments.

Azide treatment at a dose of 400 μg/hr produced a significant impairment in spatial learning when the training procedure was performed while the drug was being administered. However, we found that this effect of azide did not persist beyond the treatment period. In a separate experiment, rats were given subcutaneous sodium azide (400 μg/hr) or saline for 28 days, after which the osmotic minipumps were removed and the wounds allowed to heal. When trained in the spatial version of the water maze two weeks later, all animals showed normal learning. This result suggests that the brain can recover function after a reasonably lengthy period of C.O. inhibition. Of course, the treatment period was much shorter than the many years of compromised energy metabolism that is likely to be experienced by humans with neurological diseases. It is also important to note that C.O. inhibition produced by long term partial ischemia may have irrecoverable consequences (Abdollahian et al., this volume).

Table 1. Visible platform training; time to swim to platform (sec)

Group	First two trials	Last two trials
Saline control	22.1 ± 2.6	9.3 ± 1.1
Azide, 200 μg/hr	18.3 ± 3.4	9.9 ± 2.4
Azide, 400 μg/hr	28.8 ± 5.9	11.1 ± 2.3

Results are presented as mean ± s.e.m. Rats were given six trials in a single training session. The visible platform's location was changed on every trial. There were no significant differences between groups for performance in this task (ANOVA). Comparisons of trial blocks 1 and 2 versus 5 and 6 showed significant differences within all the groups, indicating that they all learned this task.

3.3. Effect of Azide Treatment on Hippocampal Plasticity

Encoding information into memory very likely involves changing the strength of synaptic connections. A physiological process which provides a model for this phenomenon is called long-term potentiation (LTP) (Bliss & Collingridge, 1993; Maren & Baudry, 1995). LTP is a long lasting (hours to weeks) increase in synaptic strength induced by a brief period of intense activity. The capacity for LTP has been demonstrated in neocortical and other brain regions, but is especially well studied in the hippocampus (Malenka, 1994). Hippocampal LTP has been correlated with learning (e.g., Laroche, Doyere, & Bloch, 1989), and the decay of LTP has been correlated with the time course of behaviorally assessed forgetting (Barnes, 1979).

NMDA-type glutamate receptor antagonists, which, at appropriate doses, selectively impair spatial learning, also inhibit hippocampal LTP (Bannerman, Good, Butcher, Ramsay, & Morris, 1995; Walker & Gold, 1991). Since chronic infusion of sodium azide produced consequences similar to NMDA receptor antagonists at the behavioral level, we decided to evaluate the effect of azide on hippocampal plasticity. A particular problem with the idea that LTP represents an endogenous mechanism for memory formation is that the stimulation parameters typically used to induce it are not physiological (Maren & Baudry, 1995). However, we (Diamond, Dunwiddie, & Rose, 1988; Rose & Dunwiddie, 1986) and others (Greenstein, Pavlides, & Winson, 1988; Larson, Wong, & Lynch, 1986) have shown that stimuli patterned to mimic endogenous hippocampal activity markedly lowers the threshold for inducing LTP. We have also found that LTP induced by patterned stimulation, termed primed burst potentiation, was reduced in the hippocampus of aged rats, whereas LTP induced using conventional stimulation was not (Moore, Browning, & Rose, 1993; Rose, Heman, & Williams, 1996b). Thus, we used the primed burst potentiation paradigm to investigate the possible effect of sodium azide treatment on hippocampal plasticity.

Two weeks after chronic administration of azide (400 μg/hr) or the saline vehicle, rats were anesthetized with urethane and the population spike recorded from the CA1 pyramidal cell layer in response to stimulation of commissural/associational afferents. Responses recorded from saline- and azide-treated rats did not differ from each other in terms of their amplitudes or the stimulation current required to evoke them (Bennett et al., 1992a). After a baseline period, a train of stimulation, consisting of a single priming pulse, followed 170 ms later by a burst of four pulses at 200 Hz (all at twice the baseline stimulation current), was delivered to induce plasticity. The initial response to the primed burst train was a substantial increase in the population spike that decayed over a period of a few minutes to a lower, steady-state level. There were no differences between groups in the initial response, termed post-tetanic potentiation (PTP; Figure 4, left). PTP is regulated by

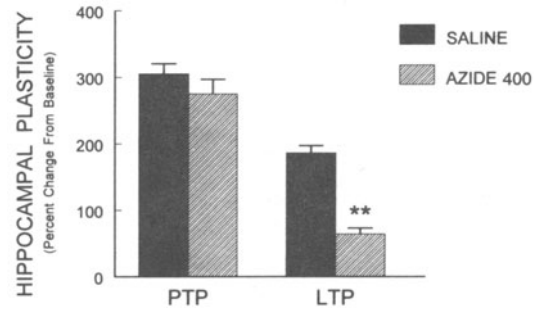

Figure 4. Effect of sodium azide infusion on hippocampal plasticity. Immediately evoked post-tetanic potentiation (PTP, measured during the first two minutes after the train) did not differ between groups. However, long-term potentiation (LTP, measured 26–30 minutes after the train) was significantly reduced in the hippocampus of azide-treated rats. **$p < 0.01$ versus saline group.

processes that are distinct from those that are responsible for the induction of longer lasting forms of plasticity (McNaughton, 1982). However, the amount of LTP evoked by the patterned stimulation train was significantly reduced by azide treatment (Figure 4, right). Thus, while azide treatment did not appear to disrupt normal synaptic transmission in the hippocampus, or to modify short-term plasticity processes, the mechanism for producing long term increases in synaptic strength was attenuated. Considered together with the detrimental effect of azide treatment upon learning, these electrophysiological results are consistent with the idea that the induction of long lasting plasticity is part of the neurobiological substrate for creating new long-term memories.

3.4. Azide Treatment and Protein Kinase C Activation

Protein kinase C (PKC) is the term applied to a family of serine/threonine isozymes that regulate many cellular processes (Casabona, 1997; Nishizuka, 1988). Of particular interest in the present context is evidence that activation of PKC is part of the memory encoding process (Van der Zee & Douma, 1997) and that PKC activation is necessary for the induction and maintenance of hippocampal LTP (Angenstein & Staak, 1997; Chen, Sweatt, & Klann, 1997). When PKC is activated, it is translocated from the cytosol to the cell membrane; thus, membrane-bound PKC can be measured to determine the degree of PKC activation. Since chronic treatment with sodium azide impaired spatial learning and LTP, we hypothesized that it would reduce hippocampal PKC activation. By measuring PKC activity in several brain regions, we hoped to gain insight into other types of behaviors that might be affected by azide treatment.

For this work, rats received subcutaneous administration of either sodium azide (400 μg/hr) or the saline vehicle for 14 days. At the end of this time period the animals were killed and tissue samples from frontal and temporal cortex, hippocampus and cerebellum were taken for biochemical assessment. Cytosolic and membrane-bound PKC activity were assayed using methods described in detail elsewhere (Bennett, Fordyce, Rose, & Wehner, 1995). As can be seen in Figure 5, a significant reduction in membrane-bound (activated) PKC was found in the hippocampus of azide-treated rats. No effect of azide treatment was observed in the cortical or cerebellar samples. In light of subsequent work (described below) revealing that the striatum appears to be particularly vulnerable to azide treatment (Bennett, 1995; Brouillet et al., 1995), it will be important to investigate the effect of chronic azide administration upon PKC activity in this brain region.

The inhibition of hippocampal PKC activity by azide was small (approximately 13 %), which raises the question of its biological significance. While this issue cannot be directly addressed, it is important to point out that PKC activation appears to be a tightly

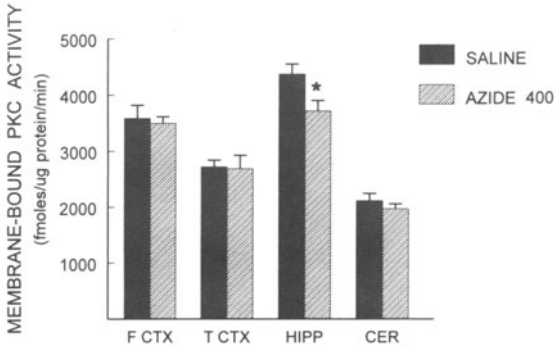

Figure 5. Membrane-bound protein kinase C (PKC) activity was significantly reduced in the hippocampus of rats that had received 14 days of sodium azide infusion (400 μg/hr) compared to saline-treated controls. In contrast, azide treatment had no effect on PKC activity in frontal or temporal cortex, or cerebellum. *$p < 0.05$ versus saline treatment.

regulated phenomenon, and that declines in PKC activity that occur during senescence in rats and mice (Fordyce & Wehner, 1993) (Battaini et al., 1995; Rose, Fordyce, & Wehner, 1996a) are of the same magnitude as were observed in the present experiment in which young rats were treated with azide. Thus, the finding of a reduction in hippocampal PKC activity is consistent with the observation of spatial learning impairment and reduced hippocampal plasticity after azide treatment.

3.5. Effects of Azide Treatment on Brain Morphology

A potential explanation for azide's behavioral and electrophysiological effects would be that chronic administration of this compound was neurotoxic, and that hippocampal neurons were more vulnerable than neurons in other brain regions. Our work to this point has not ruled out this possibility. However, using Nissl and silver stains, we have only rarely observed gross cell damage in the brain following up to four weeks of azide treatment at the 400 μg/hr dose. In more recent work, the combination of sodium azide with high doses of corticosterone was found to produce severe neuronal degeneration. In such cases, however, the primary target was the striatum, and no damage to limbic system structures was observed (Bennett, 1995). Selective striatal lesions have also been seen in studies in which high doses of sodium azide alone were given systemically, using a dosing regimen that permitted the rats to survive (Brouillet et al., 1994; Hicks, 1950).

Data from recent studies have forced a reevaluation of the question of whether neuron loss occurs with normal aging (Rapp & Gallagher, 1996; Rasmussen, Schliemann, Sorensen, Zimmer, & West, 1996). If neuronal loss does not occur, it is clear that gross neuropathology is not necessary for systems to become dysfunctional. Our experimental data with sodium azide provide further support for this idea. The future challenge will be to determine whether measurement of cytochrome oxidase activity can serve as a reliable diagnostic tool to predict the level of cognitive function.

3.6. Interaction between Sodium Azide and Corticosterone

While deficits in energy metabolism may be a prominent feature of age-related conditions such as Alzheimer's disease, they are not the only concomitant of the affliction. Serum cortisol levels are elevated in a substantial percentage of A.D. patients, a likely consequence of hippocampal neuron loss and the subsequent interruption of the feedback loop that terminates the secretion of adrenal glucocorticoid hormones following stressful events (Jacobson & Sapolsky, 1991). Since glucocorticoids have been shown to potentiate the negative consequences of a wide variety of acute metabolic insults (Harvey, Healing, Rees, Everett, & Cockburn, 1994; Sapolsky, 1986), we predicted that co-administration of corticosterone (the primary stress hormone in the rat) would potentiate the effects of sodium azide treatment.

We first tested this hypothesis at the behavioral level, using the Morris water maze task as was previously described. For this study, we employed the highest dose of azide that did not disrupt spatial learning (300 μg/hr), combined with a low dose of corticosterone (100 mg) administered in a slow-release pellet. Detailed methods for this study are given in Bennett et al. (Bennett et al., 1996a). As is shown in Figure 6, neither azide nor corticosterone affected spatial learning when administered alone. However, the combination treatment produced a learning deficit that was equivalent to that observed with 400 μg/hr azide treatment in previous studies. By contrast, learning in the visible platform version of the water maze was equivalent for all groups (Bennett et al., 1996a). Thus, com-

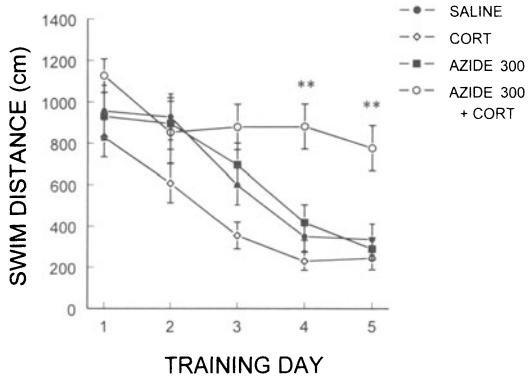

Figure 6. Synergy between sodium azide and corticosterone to impair spatial learning in the Morris water maze. Infusion of azide at a dose of 300 μg/hr, or chronic administration of a low dose of corticosterone, did not affect spatial learning. However, when these two treatments were given together a significant impairment was observed. **$p < 0.01$ versus all other groups.

bined treatment with corticosterone and sodium azide produced a selective impairment in spatial learning.

A finding of this study that was not predicted by previous research was that the combined treatment with corticosterone and sodium azide also potentiated the inhibition of C.O. activity over what was observed with azide alone. These data are shown in Figure 7. Corticosterone treatment alone did not have a significant effect on C.O. activity, although a 25% decrement was observed in the synaptic membrane fraction ($0.05 < p < 0.1$). However, the combination of corticosterone and sodium azide at 300 μg/hr produced equivalent, or greater, inhibition of C.O. than treatment with azide at the higher 400 μg/hr dose. What was noteworthy about the combination treatment was that this inhibition of C.O. was achieved without the mortality observed with higher doses of azide. Combined administration of a low dose of azide and corticosterone reduced C.O. activity to levels that were similar to what we previously observed with higher doses of azide alone. Thus, it is possible that the deficit in spatial learning observed with the combination treatment was simply a function of the enhancement of C.O. inhibition. Further work will be necessary to determine whether other mechanisms were involved.

4. CONCLUSIONS

Our work with the present rat model has shown that selective and stable partial inhibition of C.O. activity can be achieved through continuous subcutaneous infusion of

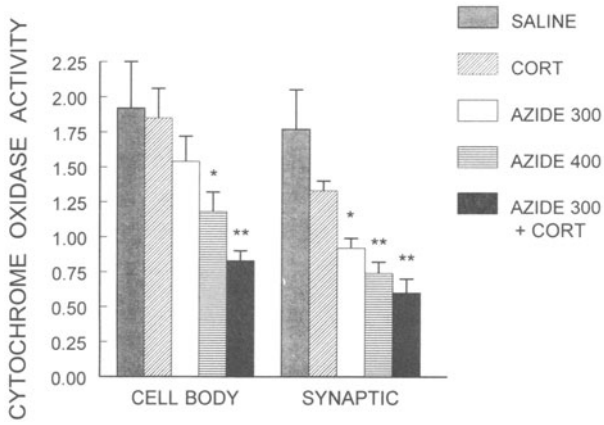

Figure 7. Combined treatment with azide (300 μg/hr) and corticosterone produced a significant reduction in C.O. activity in both cell body and synaptic mitochondria. Overall, synaptic fraction mitochondria appeared to be more sensitive to treatments than were cell body fraction mitochondria. *$p < 0.05$, **$p < 0.01$ versus saline-treated control group.

sodium azide. We have also demonstrated that chronic azide infusion impaired spatial learning, attenuated the amount of long-term plasticity that could be generated in the hippocampus, and decreased hippocampal protein kinase C activation. Furthermore, concurrent treatment with corticosterone potentiated both the degree of C.O. inhibition and the spatial learning deficit.

Many age-related neurodegenerative diseases, such as A.D. and Huntingtons's disease, often manifest both metabolic and endocrine dysregulation (Bowling & Beal, 1995; Jacobson & Sapolsky, 1991; Kish et al., 1992; Leblhuber et al., 1995; Mastrogiacoma, Lindsay, Bettendorff, Rice, & Kish, 1996). Our research has shown that when specific hormonal and metabolic conditions found in these disease states are experimentally induced in a rat model, similar biochemical, physiological and behavioral alterations are also observed. Thus, while the animal model clearly falls short of mimicking all the signs and symptoms of A.D., it has general utility for investigating possible bases or sequelae of this, or other, neurodegenerative diseases. However, it is important to note that the utility of the model does not require that the mitochondrial or endocrine defects be responsible for the pathogenesis of the diseases. Rather, our findings suggest that certain perturbations can exacerbate disease progression, regardless of whether they constitute primary etiological factors.

ACKNOWLEDGMENTS

This work was supported by grants from the National Institute on Aging and the Department of Veterans Affairs to G.M.R., and grants from the National Research Council and the Nancy and Imre Szabo Biomedical Foundation to M.C.B.

REFERENCES

Angenstein, F., & Staak, S. (1997). Receptor-mediated activation of protein kinase C in hippocampal long-term potentiation: facts, problems and implications [see comments]. *Progress in Neuropsychopharmacology and Biological Psychiatry, 21*(3), 427–54.

Bannerman, D. M., Good, M. A., Butcher, S. P., Ramsay, M., & Morris, R. G. M. (1995). Distinct components of spatial learning revealed by prior training and NMDA receptor blockade. *Nature, 378*, 182–186.

Barnes, C. A. (1979). Memory deficits associated with senescence: a neurophysiological and behavioral study in the rat. *Journal of Comparative and Physiological Psychology, 93(1)*, 74–104.

Battaini, F., Elkabes, S., Bergamaschi, S., Ladisa, V., Lucchi, L., Graa, D., PN, Schuurman, T., Wetsel, W. C., Trabucchi, M., & Govoni, S. (1995). Protein kinase C activity, translocation, and conventional isoforms in aging rat brain. *Neurobiology of Aging, 16*(2), 137–148.

Beal, M. F. (1995). Aging, energy, and oxidative stress in neurodegenerative diseases. *Annals of Neurology, 38*(3), 357–66.

Becker, J. T., Walker, J. A., & Olton, D. S. (1980). Neuroanatomical bases of spatial memory. *Brain Research, 200*, 307–320.

Bennett, M. C. (1995). Patterns of damage in rat brain produced by chronic sodium azide and corticosterone treatments. *Neuroscience Abstracts*, 751.

Bennett, M. C., Diamond, D. M., Stryker, S. L., Parks, J. K., & Parker Jr., W. D. (1992a). Cytochrome oxidase inhibition: A novel animal model of Alzheimer's disease. *Journal of Geriatric Psychiatry and Neurology, 5(2)*, 93–101.

Bennett, M. C., Diamond, D. M., Stryker, S. L., Parks, J. K., & Parker, W. D., Jr. (1992b). Cytochrome oxidase inhibition: a novel animal model of Alzheimer's disease. *Journal of Geriatric Psychiatry and Neurology, 5*(2), 93–101.

Bennett, M. C., Fordyce, D. E., Rose, G. M., & Wehner, J. M. (1995). Chronic sodium azide treatment decreases membrane-bound protein kinase C activity in the rat hippocampus. *Neurobiology of Learning and Memory, 64*, 187–190.

Bennett, M. C., Mlady, G. W., Fleshner, M., & Rose, G. M. (1996a). Synergy between chronic corticosterone and sodium azide treatments in producing a spatial learning deficit and inhibiting cytochrome oxidase activity. *Proceedings of the National Academy of Sciences of the United States of America, 93*(3), 1330–4.

Bennett, M. C., Mlady, G. W., Kwon, Y. H., & Rose, G. M. (1996b). Chronic in vivo sodium azide infusion induces selective and stable inhibition of cytochrome c oxidase. *Journal of Neurochemistry, 66*(6), 2606–11.

Bliss, T. V. P., & Collingridge, G. L. (1993). A synaptic model of memory: long-term potentiation in the hippocampus. *Nature, 361*, 31–39.

Bowling, A. C., & Beal, M. F. (1995). Bioenergetic and oxidative stress in neurodegenerative diseases. *Life Sciences, 56*(14), 1151–71.

Brouillet, E., Hantraye, P., Ferrante, R. J., Dolan, R., Leroy-Willig, A., Kowall, N. W., & Beal, M. F. (1995). Chronic mitochondrial energy impairment produces selective striatal degeneration and abnormal choreiform movements in primates. *Proceedings of the National Academy of Sciences of the United States of America, 92*(15), 7105–9.

Brouillet, E., Hyman, B. T., Jenkins, B. G., Henshaw, D. R., Schulz, J. B., Sodhi, P., Rosen, B. R., & Beal, M. F. (1994). Systemic or local administration of azide produces striatal lesions by an energy impairment-induced excitotoxic mechanism. *Experimental Neurology, 129*(2), 175–82.

Cada, A., Gonzalez-Lima, F., Rose, G. M., & Bennett, M. C. (1995). Regional brain effects of sodium azide treatment on cytochrome oxidase activity: a quantitative histochemical study. *Metabolic Brain Disease, 10*(4), 303–20.

Casabona, G. (1997). Intracellular signal modulation: a pivotal role for protein kinase C . *Progress in Neuropsychopharmacology and Biological Psychiatry, 21*(3), 407–25.

Chagnon, P., Betard, C., Robitaille, Y., Cholette, A., & Gauvreau, D. (1995). Distribution of brain cytochrome oxidase activity in various neurodegenerative diseases. *Neuroreport, 6*(5), 711–5.

Chandrasekaran, K., Giordano, T., Brady, D. R., Stoll, J., Martin, L. J., & Rapoport, S. I. (1994). Impairment in mitochondrial cytochrome oxidase gene expression in Alzheimer disease. *Brain Research. Molecular Brain Research, 24*(1–4), 336–40.

Chen, S. J., Sweatt, J. D., & Klann, E. (1997). Enhanced phosphorylation of the postsynaptic protein kinase C substrate RC3/neurogranin during long-term potentiation. *Brain Research, 749*(2), 181–7.

Davis, R. E., Miller, S., Herrnstadt, C., Ghosh, S. S., Fahy, E., Shinobu, L. A., Galasko, D., Thal, L. J., Beal, M. F., Howell, N., & Parker, W. D., Jr. (1997). Mutations in mitochondrial cytochrome c oxidase genes segregate with late-onset Alzheimer disease. *Proceedings of the National Academy of Sciences of the United States of America, 94*(9), 4526–31.

Diamond, D. M., Dunwiddie, T. V., & Rose, G. M. (1988). Characteristics of hippocampal primed burst potentiation *in vitro* and in the awake rat. *Journal of Neuroscience, 8(11)*, 4079–4088.

Fordyce, D. E., & Wehner, J. M. (1993). Effects of aging on spatial learning and hippocampal protein kinase C in mice. *Neurobiology of Aging, 14*, 309–317.

Fujimoto, K., Yoshida, M., Ikeguchi, K., & Niijima, K. (1989). Impairment of active avoidance produced after destruction of pedunculopontine nucleus areas in the rat. *Neuroscience Research., 6*, 321–328.

Gonzalez-Lima, F., Valla, J., & Matos-Collazo, S. (1997). Quantitative cytochemistry of cytochrome oxidase and cellular morphometry of the human inferior colliculus in control and Alzheimer's patients. *Brain Research, 752*(1–2), 117–26.

Greenstein, Y. J., Pavlides, C., & Winson, J. (1988). Long-term potentiation in the dentate gyrus is preferentially induced at a theta rhythm periodicity. *Brain Research, 438*, 331–334.

Harvey, P. W., Healing, G., Rees, S. J., Everett, D. J., & Cockburn, A. (1994). Glucocorticosteroid interactions with natural toxins: a mini review. *Natural Toxins, 2*(6), 341–6.

Hatanpaa, K., Brady, D. R., Stoll, J., Rapoport, S. I., & Chandrasekaran, K. (1996). Neuronal activity and early neurofibrillary tangles in Alzheimer's disease. *Annals of Neurology, 40*(3), 411–20.

Hewitt, E. J., & Hallas, D. G. (1959). Measurement of inhibition by azide in a biochemical assay system involving nitrite estimation by diazotization. *Nature, 184*, 1485–1487.

Hicks, S. P. (1950). Brain metabolism in vivo. II. The distribution of lesions caused by azide, malononitrile, plasmocid and dinitrophenol poisoning in rats. *Archives of Pathology, 49*, 545–563.

Jacobson, L., & Sapolsky, R. (1991). The role of the hippocampus in feedback regulation of the hypothalamic-pituitary-adrenocortical axis. *Endocrine Reviews, 12*, 118–134.

Keilin, D., & Hartree, E. F. (1954). Reactions of methaglobin and catalase with peroxidases and hydrogen donors. *Nature, 173*, 720–723.

Keilin, D., Hartree, E. F., Cecil, R., & Ogston, A. G. (1951). Purification of horseradish peroxidase and comparison of its properties with those of catalase and methaglobin. *Biochemical Journal, 49*, 88–106.

Kish, S. J., Bergeron, C., Rajput, A., Dozic, S., Mastrogiacomo, F., Chang, L. J., Wilson, J. M., DiStefano, L. M., & Nobrega, J. N. (1992). Brain cytochrome oxidase in Alzheimer's disease. *Journal of Neurochemistry, 59*, 776–779.

Klein-Schwartz, W., Gorman, R. L., Oderda, G. M., Massaro, B. P., Kurt, T. L., & Garriott, J. C. (1989). Three fatal sodium azide poisonings. *Medical Toxicology: Adverse Drug Experiences, 4*(3), 219–227.

Koreshtz, W. J., Jenkins, B. G., Rosen, B. R., & Beal, M. F. (1997). Energy metabolism defects in Huntington's disease and effects of coenzyme Q10. *Annals of Neurology, 41*, 160–165.

Lai, J. C. K., & Clark, J. B. (1979). Preparation of synaptic and non-synaptic mitochondria from mammalian brain. *Methods in Enzymology, 55*, 51–60.

Laroche, S., Doyere, V., & Bloch, V. (1989). Linear relation between the magnitude of long-term potentiation in the dentate gyrus and associative learning in the rat. A demonstration using commissural inhibition and local infusion of an N-methyl-D-aspartate receptor antagonist. *Neuroscience, 28*, 375–386.

Larson, J., Wong, D., & Lynch, G. (1986). Patterned stimulation at the theta frequency is optimal for the induction of hippocampal long-term potentiation. *Brain Research, 368*, 347–350.

Leblhuber, F., Peichl, M., Neubauer, C., Reisecker, F., Steinparz, F. X., Windhager, E., & Maschek, W. (1995). Serum dehydroepiandrosterone and cortisol measurements in Huntington's chorea. *Journal of Neurological Sciences, 132*, 75–79.

Malenka, R. C. (1994). Synaptic plasticity in the hippocampus: LTP and LTD. *Cell, 78*(4), 535–538.

Malmstrom, B. G., Andreasson, L. E., & Reinhammar, B. (1975). Copper-containing oxidases and superoxide dismutase. In P. D. Boyer (Ed.), *The Enzymes* (Vol. XII, pp. 507–579). New York: Academic Press.

Maren, S., & Baudry, M. (1995). Properties and mechanisms of long-term synaptic plasticity in the mammalian brain: relationships to learning and memory. *Neurobiology of Learning & Memory, 63*(1), 1–18.

Mastrogiacoma, F., Lindsay, J. G., Bettendorff, L., Rice, J., & Kish, S. J. (1996). Brain protein and alpha-ketoglutarate dehydrogenase complex activity in Alzheimer's disease. *Annals of Neurology, 39*(5), 592–8.

McNaughton, B. L. (1982). Long-term synaptic enhancement and short-term potentiation in rat fascia dentata act through different mechanisms. *Journal of Physiology, 324*, 240–262.

Moore, C. I., Browning, M. D., & Rose, G. M. (1993). Hippocampal plasticity induced by primed burst, but not LTP, stimulation is impaired in area CA1 of aged Fischer 344 rats. *Hippocampus, 3*, 57–66.

Moser, M.-B., Moser, E. I., Forrest, E., Andersen, P., & Morris, R. G. M. (1995). Spatial learning with a minislab in the dorsal hippocampus. *Proceedings of the National Academy of Sciences of the United States of America, 92*, 9697–9701.

Mutisya, E. M., Bowling, A. C., & Beal, M. F. (1994). Cortical cytochrome oxidase activity is reduced in Alzheimer's disease. *Journal of Neurochemistry, 63*(6), 2179–84.

Nathan, C. (1992). Nitric oxide as a secretory product of mammalian cells. *FASEB Journal, 6*, 3051–3064.

Nishizuka, Y. (1988). The molecular heterogeneity of protein kinase C and its implications for cellular regulation. *Nature, 334*, 661–665.

Olton, D. S., Walker, J. A., & Gage, F. H. (1978). Hippocampal connections and spatial discrimination. *Brain Research, 139*, 295–308.

Parker, W. D., Jr., Filley, C. M., & Parks, J. K. (1990). Cytochrome oxidase deficiency in Alzheimer's disease. *Neurology, 40*(8), 1302–3.

Parker, W. D., Jr., Mahr, N. J., Filley, C. M., Parks, J. K., Hughes, D., Young, D. A., & Cullum, C. M. (1994a). Reduced platelet cytochrome c oxidase activity in Alzheimer's disease [see comments]. *Neurology, 44*(6), 1086–1090.

Parker, W. D., Jr., Parks, J., Filley, C. M., & Kleinschmidt-DeMasters, B. K. (1994b). Electron transport chain defects in Alzheimer's disease brain [see comments]. *Neurology, 44*(6), 1090–1096.

Rapp, P. R., & Gallagher, M. (1996). Preserved neuron number in the hippocampus of aged rats with spatial learning deficits. *Proceedings of the National Academy of Sciences of the United States of America, 93*(18), 9926–30.

Rasmussen, T., Schliemann, T., Sorensen, J. C., Zimmer, J., & West, M. J. (1996). Memory impaired aged rats: no loss of principal hippocampal and subicular neurons. *Neurobiology of Aging, 17*(1), 143–7.

Reichmann, H., Florke, S., Hebenstreit, G., Schrubar, H., & Riederer, P. (1993). Analyses of energy metabolism and mitochondrial genome in post-mortem brain from patients with Alzheimer's disease. *Journal of Neurology, 240*(6), 377–80.

Robinson Jr., G. S., Crooks Jr., G. B., Shinkman, P. G., & Gallagher, M. (1989). Behavioral effects of MK-801 mimic deficits associated with hippocampal damage. *Psychobiology, 17(2)*, 156–164.

Rose, G. M., & Dunwiddie, T. V. (1986). Induction of hippocampal long-term potentiation using physiologically patterned stimulation. *Neuroscience Letters, 69*, 244–248.

Rose, G. M., Fordyce, D. E., & Wehner, J. M. (1996a). Hippocampal protein kinase C activtion correlates with spatial learning in aged male Fischer 344 rats. *International Behavioral Neuroscience Society Abstracts*(5), 53.

Rose, G. M., Heman, K. L., & Williams, L. R. (1996b). Chronic nerve growth factor administration enhances hippocampal primed burst potentiation in aged, but not young male Fischer 344 rats. *Neuroscience Abstracts, 22*, 752.

Rotilio, G., Bray, R. C., & Fielden, E. M. (1972). A pulse radiolysis study of superoxide dismutase. *Biochimica Biophysica Acta, 268*, 605–609.

Sapolsky, R. M. (1986). Glucocorticoid toxicity in the hippocampus: reversal by supplementation with brain fuels. *Journal of Neuroscience, 6*, 2240–2244.

Schapira, A. H. (1996). Oxidative stress and mitochondrial dysfunction in neurodegeneration. *Current Opinion in Neurology, 9*(4), 260–4.

Siesjo, B. K., & Zwetnow, N. N. (1970). The effect of hypovolemic hypotension on extra- and intracellular acid-base parameters and energy metabolites in the rat brain. *Acta Physiologica Scandinavica, 79*, 114–124.

Simonian, N. A., & Hyman, B. T. (1993). Functional alterations in Alzheimer's disease: diminution of cytochrome oxidase in the hippocampal formation. *Journal of Neuropathology and Experimental Neurology, 52*(6), 580–5.

Simonian, N. A., & Hyman, B. T. (1994). Functional alterations in Alzheimer's disease: selective loss of mitochondrial-encoded cytochrome oxidase mRNA in the hippocampal formation. *Journal of Neuropathology and Experimental Neurology, 53*(5), 508–12.

Simonian, N. A., & Hyman, B. T. (1995). Functional alterations in neural circuits in Alzheimer's disease. *Neurobiology of Aging, 16*(3), 305–9.

Smith, R. P., Louis, C. A., Kruszyna, R., & Kruszyna, H. (1991). Acute neurotoxicity of sodium azide and nitric oxide. *Fundamental and Applied Toxicology, 17*(1), 120–7.

Van der Zee, E. A., & Douma, B. R. (1997). Historical review of research on protein kinase C in learning and memory [see comments]. *Progress in Neuropsychopharmacology and Biological Psychiatry, 21*(3), 379–406.

Walker, D. L., & Gold, P. E. (1991). Effects of the novel NMDA antagonist, NRC 12626, on long-term potentiation, learning and memory. *Brain Research, 549*, 213–221.

9

CYTOCHROME OXIDASE

A Predictive Marker of Neurodegeneration

N. P. Abdollahian,[1] A. Cada,[2] F. Gonzalez-Lima,[2] and J. C. de la Torre[1]

[1]University of New Mexico
Division of Neurosurgery and Department of Neuroscience
Albuquerque, New Mexico 87106
[2]University of Texas, Austin
Institute for Neuroscience
Austin, Texas 78712

ABSTRACT

Cytochrome oxidase has been used in the past as a marker of neuronal activity. We propose that cytochrome oxidase may also serve as a useful marker for predicting potential neurodegeneration, particularly following chronic brain hypoperfusion. This proposal is based on a series of experiments in rats subjected to mild chronic brain hypoperfusion and tested at determined time points for regional cytochrome oxidase activity, visuo-spatial memory, reactive astrocytosis, neurodegenerative changes and microtubule associated protein 2 (MAP-2). The results of these experiments suggest the following scenario: four weeks following chronic brain hypoperfusion, regional cytochrome oxidase activity is reduced in parallel with spatial memory function although no neurodegenerative changes are seen anywhere in the brain, despite an increased density of astrocytes in the hippocampus. After 8 weeks of ischemia, neurodegenerative changes are still absent but spatial memory remains depressed while the postsynaptic dendritic marker MAP-2 shows loss of immunostaining in the apical dendrites of CA1 neurons (suggesting continued metabolic dysfunction of these neurons). Twelve weeks after brain hypoperfusion, some neurodegenerative signs begin to be seen in CA1 neurons with continued MAP-2 reduction and reactive gliosis. If rats with chronic brain hypoperfusion are kept for 25 weeks, neuronal loss and extended hippocampal neurodegeneration with cortical atrophy can be seen. Neuronal loss and extension of neurodegeneration 25 weeks after chronic brain hypoperfusion are dependent on factors: *age* of animal, *severity* of the chronic ischemic insult and of ischemia. We suggest that the chronologic progression of memory dysfunction, gliosis and MAP-2 loss following mild but chronic brain hypoperfusion are

Cytochrome Oxidase in Neuronal Metabolism and Alzheimer's Disease,
edited by Gonzalez-Lima, Plenum Press, New York, 1998.

due to lowered mitochondrial oxidative phosphorylation and reduced energy metabolism, initially in ischemic-sensitive neurons, such as in CA1. This energy metabolic down-regulation which is reflected by depressed cytochrome oxidase activity in the CA1 region, appears to precede neurodegenerative changes of CA1 neurons by many weeks. Cytochrome oxidase may be an important pathogenetic precursor of neurodegenerative pathology, particularly Alzheimer's disease which shares many of the anatomic and cognitive deficits seen in the rat model.

1. INTRODUCTION

The brain depends almost entirely on an adequate supply of glucose for all its energy needs [Erecinska & Silver, 1989]. In addition, the brain requires oxygen which together with glucose can generate 18 times the amount of ATP through mitochondrial oxidative phosphorylation as it can through glycolysis which does not use oxygen [Erecinska & Silver, 1989]. This concept becomes all the more critical when cerebral ischemia and/or hypoxia is able to reduce the delivery of glucose and oxygen to maintain normal neuronal function [de la Torre & Mussivand, 1993; de la Torre 1994; de la Torre, 1997a, b]. Consequently, in the absence of glucose and oxygen the brain can support metabolic activity via glycolysis for only a few minutes [Siesjo, 1978]. If only oxygen is reduced (hypoxia) and glucose delivery to brain continues normally, massive accumulation of lactate and a drop in brain pH can result in a condition that is extremely damaging to neurons which consume about 75% of all oxygen needed by the CNS [Siesjo, 1978]. Most of the ATP produced from oxidative phosphorylation is destined to support ionic gradients, particularly the Na^+,K^+-ATPase pump in neurono-glial membranes of gray matter [Albers et al., 1994; Astrup et al., 1981].

Cytochrome oxidase (C.O.) catalyzes the final reaction in the oxidative metabolism of glucose and as such, has become a useful marker of endogenous neuronal activity (Wong-Riley 1989).

In this chapter, we will review evidence that indicates local C.O. activity may also be an accurate *marker* of active neuronal dysfunction following chronic brain hypoperfusion, and that falling C.O. levels precede structural pathology in affected neurons.

There is a growing interest in the relationship between neuronal energy metabolism and neurodegenerative changes that occur in Alzheimer's disease (A.D.) [Mattson, 1997; Meier-Ruge & Bertoni-Freddari, 1994; Cheng & Mattson, 1992; Kish et al., 1992; Mutisya et al 1994; Hoyer, 1990; Hoyer, 1996]. This interest is partly motivated by changes in mitochondrial function which have been described in both A.D. and cerebral ischemia, a relationship that links two pathologic outcomes with a common energy metabolic organelle that can unchain a cascade of neurochemical reactions to produce neuronal dysfunction or death [Chagnon et al., 1995; Dimlich et al., 1990; Ozawa et al., 1967; Markesberry, 1997; Simonian & Hyman, 1995; Sims, 1996; Chandrasekaran et al., 1994]. The link is further reinforced by data showing that cerebral ischemia induced by stroke or head injury is associated with the deposition of b-amyloid, the protein commonly found in senile plaques in Alzheimer brains [Jendroska et al., 1993; Rasmusson et al., 1995; Roberts et al., 1994]. Similarly, apolipoprotein E, type 4 allele, a genetic risk factor in late-onset Alzheimer's disease, has been reported to be a major risk factor for ischemic stroke, atherosclerosis and vascular dementia, conditions known to present with varying degrees of cerebral hypoperfusion [Saunders et al., 1993; Davignon et al., 1988; Kosunen et al., 1995; Frisoni et al., 1994; Botet et al., 1992; Kalaria et al., 1996; Couderc et al., 1994; Venarucci 1994].

2. CHRONIC BRAIN HYPOPERFUSION

While representing only approximately 2 percent of the total body weight, the brain accounts for 20 percent of the total body oxygen consumption at rest [Clarke & Sokoloff, 1994]. This high metabolic activity of the brain is dependent on the continual supply of blood flow from the cerebral circulation which provides glucose, oxygen and other nutrients while removing carbon dioxide and other metabolic waste products [Clarke & Sokoloff, 1994]. The carotid and vertebral arteries are the sole inputs into the cerebrovasculature and provide the entire blood supply to the brain. Fluctuations or alterations in blood flow and hemodynamics through these arteries may have adverse effects upon brain physiology and function [de la Torre, 1997a,c; de la Torre & Mussivand, 1993].

The study of chronic brain hypoperfusion (CBH) is relevant to many clinical conditions such as stroke, head trauma, cerebrovascular disorders, coronary artery disease and dementia. Although substantial research and advancement in the fields of *acute* brain ischemia have occurred, not much attention has been given to how *chronic* ischemia produces memory impairment and neuronal dysfunction with advancing age.

Part of our work has been concerned with the physiologic, metabolic and cellular mechanisms whereby CBH produces progressive cognitive deficits and eventual neurodegeneration of ischemic-sensitive neurons. In studying this problem, we have characterized an aging rat model of CBH, using 2-VO (2-vessel occlusion), which mimics specific changes observed at the onset of dementia, particularly Alzheimer's disease. The 2-VO is a surgical procedure in which both common carotid arteries are permanently ligated subjecting the animal to chronic cerebrovascular insufficiency (Fig. 1). The hypothesis pro-

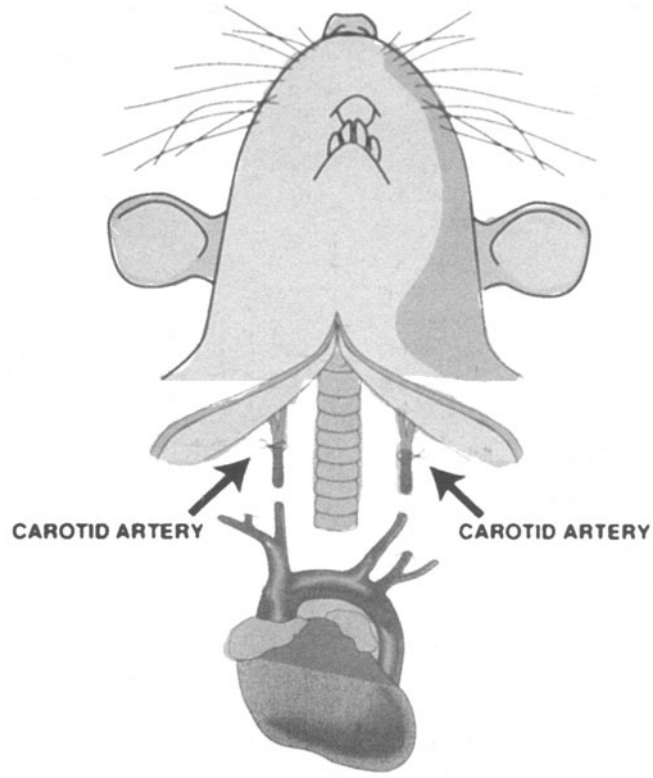

Figure 1. Surgical technique to induce chronic brain hypoperfusion by ligation of both common carotid arteries (2-vessel occlusion, 2-VO). The left subclavian artery can be ligated at the same time (3-VO) to accelerate neuropathologic changes observed in the CA1 sector.

posed here is that CBH initiates slow-evolving energy metabolic changes in ischemic sensitive brain regions, primarily hippocampal CA1 neurons, which alter normal neuronoglial homeostasis and produce cognitive impairment. The reduction of cerebral blood flow (CBF) generated by chronic cerebral ischemia, is reflected by diminished delivery of high energy substrates which in turn can disturb the localized energy metabolism in aged neurons, particularly those that are highly vulnerable to ischemia. This depression in energy production disrupts cellular and synaptic activities affecting memory function and eventually progresses into neuronal damage, atrophy, and death [de la Torre et al., 1995]. One of our objectives is to "model" some of the pathological and behavioral changes known to occur in A.D. and to study these changes in the aging rat subjected to CBH achieved by bilateral carotid artery occlusion or 2-vessel occlusion (2-VO). Since A.D. is the leading cause of dementia, our animal model may be useful not only for understanding the pathogenesis of A.D. but in developing a strategy to target novel treatments for this disorder.

2.1. Aging and CBF

Aging is associated with a complex set of processes which are difficult to isolate and define, but at least, their consequences are simple to understand. As we age, we become susceptible to degeneration in both structure and function in a variety of aspects ranging from the most basic molecular level, to the elaborate configuration of the organ system. This progressive and unbridled activity affects organs, tissues, and cells differently with varying degrees between individuals. Ultimately, it is the sum total of age-related changes upon the body and the intrinsic cell pathology it creates which ceases to support life.

Normal aging of the brain is best defined as an absence of organic brain disease with continued mental function well into the later decades of life. Although no signs of underlying disease may be observed, all aged individuals experience sporadic memory lapses. However, in some individuals, memory becomes more impaired and leads to a progressive deterioration of mental function, and intellectual skills that worsen with age. This condition is known as *dementia* [Duckett, 1991]. The most common form of dementia is Alzheimer's disease. Although the cause of A.D. is unknown, it is initiallly characterized by a progressive loss of visuo-spatial memory and later, by deterioration of intellectual functions that advances steadily into apathy, dissociation, stagnation, and ultimately to death [Blass, 1993]. Late-onset A.D. is primarily age-related and not an inevitable consequence of aging, however, it is a serious risk factor that will compromise the quality of life in the growing elderly population.

Throughout life, brain activity underlies simple motor skills such as walking, intricate cognitive behaviors such as the use of logic and abstraction, complex functions such as the expression of language and other processes which we are unaware but vitally depend upon. Thus, even small changes within the brain may have serious consequences in maintaining normal activity and supporting life.

In order to carry out these functions, the brain, like any other organ requires energy. Since the brain is completely dependent on the cerebrovasculature for energy substrates, it is highly vulnerable to alterations or disruptions if this supply is interrupted or reduced [Selmen et al., 1990; de la Torre & Hachinski, 1997]. Recent studies indicate that normal aging is accompanied by a progressive reduction in CBF and metabolism [Baron & Marchal, 1992; Kalaria, 1992; Shaw et al., 1984; Lassen & Ingvar, 1980]. This decline is most visible in the frontal, parietal, and inferior temporal regions; the latter two of which are involved in complex spatial configurations and memory performance characteristic of primates and higher vertebrates [Rogers et al., 1986; Smith, 1988; Squire et al., 1986]. Changes in CBF

and hemodynamics that are observed throughout aging are often independent of cerebrovascular disease and may only be associated with "benign forgetfulness" [Shaw et al., 1984].

Although age-related alterations in cerebral blood flow may have no immediate clinical significance, it may result in pathology by further reductions in CBF as a consequence of heart disease, head injury, or cerebrovascular ischemia [de la Torre, 1997a; Sparks et al., 1990; Graham, 1995; Jendrosca et al., 1990]. These risk factors can enhance or accelerate a predisposed decline in CBF seen in normal aging, further depressing the delivery of glucose and oxygen. Disturbances in the normal supply of glucose and oxygen to the brain are known to result in cognitive and behavioral dysfunction [Meier-Ruge & Bertoni-Freddari, 1996; Marcus et al., 1989; Grubb et al., 1987], but how this occurs is poorly understood. We have suggested that as the supply of these energy precursors gradually diminishes past a critical level needed to maintain functional activity, progressive alterations in cognition are observed and may lead to significant neurodegeneration in age-related vulnerable regions [de la Torre et al., 1997a,b; de la Torre et al 1992a,b; de la Torre et al., 1993]. Patients with both cerebrovascular disorders and late-onset Alzheimer's disease demonstrate marked reductions in CBF [Hachinski et al., 1975; Ingvar et al., 1978; Levy et al., 1978; Obrist et al., 1978; Rogers et al., 1986; Tachibana et al., 1984a; Yamaguchi et al., 1980], however, cerebrovascular disease produces more focal reductions in CBF which may lead to infarction [Erkinjuntti et al., 1988]. Conversely, studies show CBF is reduced more symmetrically, or globally, in Alzheimer's brains without cerebral infarction [Tachibana et al., 1984b; Zemcor et al., 1984], providing evidence that cerebral ischemia not only plays a role in cerebrovascular disease but also in the pathogenesis of A.D. [Ni et al., 1994; Tanaka et al., 1996]. PET studies have shown that A.D. patients have a relatively preserved cerebral metabolic rate of oxygen but a significant increase in the oxygen extraction factor (OEF), a phenomenon known as "misery perfusion" [Nagata et al., 1997].

2-VO, which is the mild form of CBH, permits experimental manipulation of CBF in order to investigate the slow and evolving neurophysiological consequences of reduced CBF on the brain. It has been shown that chronic 2-VO reduces CBF by 21% in the cortex and 32% in the hippocampus of middle-aged rats after 9 weeks of CBH [de la Torre et al., 1993]; however, CBF also varies with age and breed of rat. Wistar rats subjected to 2-VO show CBF reductions ranging from 25–49% of controls [Tsuchiya et al., 1993]. Moreover, studies measuring global CBF in both acute and chronic brain ischemia demonstrate reductions ranging from 25–75% of controls [Eklof & Siesjo, 1972; Jaspers et al., 1990; Sekhon et al., 1994; Sekhon, 1997].

It has not been experimentally determined if CBH reduces the delivery of glucose to neurons in the hippocampus or any other region. However, one study has shown that there is a distinct correlation between local CBF and local cerebral glucose utilization in the rat model of chronic carotid artery occlusion [Tsuchiya et al., 1993]. This relationship suggests that changes in cerebral function, or energy metabolism, can modify local cerebral blood flow to meet energy demands. Blood flow studies in Alzheimer's patients have shown that CBF parallel the progressive dementia, correlating with the depression in cognitive function [Hoyer, 1991a,b; Yamaguchi et al., 1980]. This raises the question of whether the reductions in glucose and oxygen which characterize this disorder, are pathogenic of A.D., and indicates chronic 2-VO may be an appropriate model in which to examine these issues.

2.2. Visuo-Spatial Memory

Chronic cerebrovascular ischemia produces progressive visuo-spatial memory deficits in young, middle-aged, and aged rats [de la Torre et al., 1997a; de la Torre et al., 1994; de la

Torre, 1992a; de la Torre et al., 1996; Pappas et al., 1996; Ni et al., 1994]. Although many studies have examined visuo-spatial memory in mammals, few studies provide a definition of this task in their experiments. Visuo-spatial memory has been functionally defined as an organism's ability to know or comprehend its location in the environment [Barnes et al., 1980; Smith et al., 1991]. Others suggest visuo-spatial memory not only involves retention of a spatial map relevant to an animal's position but continual update of this spatial representation is necessary for interaction with the environment [Barnes, 1988; O'Keefe & Nadel, 1978]. The common understanding of visuo-spatial memory in these studies is that animals use reference cues in their environment to form a spatial cognitive map to explore their environment. Thus, mammals rely on having an adequate representation of their environment in order to successfully navigate their surroundings, a behavior which is vital to survival [Barnes, 1988; Barnes et al., 1980; Zola-Morgan et al., 1986].

Aged rats and elderly humans have problems in performing spatial memory tasks compared to their younger counterparts [Cave & Squire, 1991; Ingram et al., 1981; Konigsmark & Murphy, 1970]. There is abundant evidence that old rats show deficits on tasks whose optimal solution requires the use of spatial processing [Barnes, 1988; Beatty et al., 1985; Landfeld, 1988], and is consistent with findings that older humans have less effective spatial representations of their environments than do young adults [Evans et al., 1984; Flicker et al., 1984]. However, these memory changes are subtle in the normal aging rat, and is predicted to be subtle in healthy older humans [Barnes, 1988]. Reduced CBF in both aged rats [Berman et al., 1988; Ohata et al., 1981; Yager et al., 1996] and humans [Lassen et al., 1980; Levy et al., 1978; Obrist, 1970] may underlie these mild changes in memory.

In mammals, studies indicate the medial temporal region, and particularly the hippocampus, are involved in visuo-spatial memory and other memory functions [Café et al., 1994; Squire et al 1986a; Zola-Morgan & Squire, 1989], establishing a link between memory function and the hippocampus. In humans, the severity of memory impairment resulting from medial temporal lobe surgery is correlated with the extent of hippocampal damage [Milner, 1974; Zola-Morgan & Squire, 1986a]. Models of memory impairment in monkeys have provided more support for this observation [Zola-Morgan, 1986b]. Following experimental chronic brain ischemia in rodents, performance on spatial tasks are more affected than other types of memory tasks [de la Torre et al., 1993; de la Torre et al., 1996; Ni et al., 1994; Park et al., 1996], indicating that the neural systems of the hippocampus involved in spatial memory are selectively impaired by cerebral ischemia [de la Torre & Fortin, 1994; Kiyota et al., 1991]. Visuo-spatial memory deficits induced by CBH have been shown to diminish in rats deoccluded two weeks after surgery, providing evidence that CBH is responsible for the progressive cognitive dysfunction in this rat model [de la Torre et al., 1993].

In aged rats, chronic brain hypoperfusion appears to confound the senescent decline in CBF with age and produce significant ongoing visuo-spatial memory dysfunction [de la Torre et al., 1992a,b; Pappas et al., 1996]. Likewise, memory deficits can result from CBH in humans, with memory function more vulnerable in aged individuals [Mayberg et al., 1995; Obrist et al., 1970]. As in rats, the biochemical substrate that produces memory dysfunction remains to be elucidated. Aged rats subjected to permanent occlusion of the common carotid arteries display a progressive impairment in the ability to solve spatial tasks which may begin as early as 1 week after occlusion [de la Torre, 1997b]. Visuo-spatial memory in rats is assessed by the Morris water maze (MWM), a spatial memory task which has been extensively used in behavioral research for examining changes in visuo-spatial memory after a variety of experimental insults [de la Torre et al., 1992a; Morris, 1984; Ordy et al., 1988; Olsen et al., 1994]. This device consists of a small cylindrical

pool which is filled with water and contains a submerged platform. Rats must use external cues located outside the pool to navigate and locate the submerged, non-visible platform in a given time. Performance in solving the task is dependent on hippocampal function and integrity [Landfeld, 1988].

The degree and onset of visuo-spatial deficits in our rat model depends on four factors including pre-training, severity of injury, duration of ischemia, and the animal's age. Pre-training rats on the MWM prior to experimental manipulation allows acquisition of the task to reference memory. When tested following acquisition, recall of reference information learned in training is used to solve the task. Pre-training is an experimental benefit because it allows direct examination of spatial behavior in response to the induced cerebral ischemia. In the 2-VO model, pre-trained middle aged 2-VO rats demonstrate spatial deficits which begin after several weeks of ischemia, whereas non-trained rats display spatial memory impairment as early as one week (de la Torre, 1997b; Sutherland et al., 1988). The emergence of visuo-spatial deficits in pre-trained 2-VO rats is slower, presumably because their recall of the pertinent information to solve the spatial task is substantially intact and not affected by a short duration of ischemia. In non-trained animals, the maze is a novel experience that tests working memory or the ability to acquire the task independent of previous reference memory [Barnes et al., 1980]. Thus, chronic cerebral hypoperfusion may adversely affect the consolidation process or limit recall of previous experience which may be applicable in solving spatial memory tasks. Short-term memory impairment in 2-VOs has also been demonstrated using the radial arm maze [Pappas et al., 1996].

Others have also shown that visuo-spatial memory impairment occurs in rats, 9 weeks to 9 months old, subjected to 2-VO [Ni et al., 1994; Tanaka et al., 1996]. However, the degree and length of memory impairment induced by 2-VO is dramatically decreased compared to studies on aged subjects [de la Torre, 1992b]. In these younger rats, behavioral deficits appear to be transient and time dependent. In middle-aged rats (13–15 months old), cognitive changes may take several weeks to develop, while spatial impairment is evident as early as one week after 2-VO in older (19–22 month old) rats. The relatively mild changes in young and middle age rats may be reflective of their higher CBF [Berman et al., 1988; Ohata et al., 1981; Yager et al., 1996]. Nevertheless, these previous studies indicate that aging is associated with an increased susceptibility to cognitive changes induced by 2-VO which further deteriorate with the duration of CVI.

2.3. Hippocampal Neurons

The hippocampal formation is a sea-horse shaped structure in the limbic system involved, among other things, in spatial memory function [Squire et al., 1986]. It is divided into 4 sectors known as; CA1-CA4 and the dentate gyrus. CA1 pyramidal neurons are excitatory and are interconnected with other hippocampal neurons and the perforant pathway from the entorhinal cortex [Fitzgerald, 1985]. The entorhinal cortex is richly interconnected with the cortical association areas and the limbic system, providing a link between the neocortex and the hippocampus [Papez, 1937; Kluver & Bucy, 1939]. Pyramidal CA1 neurons are especially vulnerable to ischemic insult [Ishimaru et al., 1995; Jones et al., 1981; Kirino, 1982; Pulsinelli et al., 1982] and demonstrate early and more severe damage compared with other brain regions [Landfeld, 1988]. CA1 neurons are of further interest because they are involved in the processes of learning and visuo-spatial memory function [Morris, 1984] and are sites of the earliest and most dramatic changes in Alzheimer's disease [Ball, 1977; Ordy et al., 1988; Terry & Wisniewski, 1972; Van Hoesen & Hyman, 1990; Wisniewski & Terry, 1973].

Chronic 2-VO in rats produces persistent memory deficits without notable histopathology for many weeks (Fig. 2) [de la Torre et al., 1992a; de la Torre & Fortin, 1994; Pappas et al., 1996; Sekhon et al., 1994]. Aged, Sprague-Dawley rats, not pre-trained on the MWM, display spatial memory deficits after one week (Fig. 3), but without significant structural damage and neuronal loss in the CA1 until 25 weeks following 2-VO [Pappas et al., 1996]. However, in this particular study, CA1 neurons were not examined for structural changes between weeks 9 and 25, suggesting that damage and loss of CA1 neurons may have occurred prior to week 25. In an unrelated study, it was shown that Wistar rats, 7 weeks to 9 months of age, display progressive loss and shrinkage of CA1 neurons after only 16 weeks [Ni et al., 1994]. However, Wistar rats appear to be more sensitive to 2-VO than Sprague-Dawley rats. Two days following carotid occlusion in Wistar rats, the mortality is as high as 21% (compared with less than 1% in Sprague-Dawley rats), with neuronal damage observed outside the CA1 of the hippocampus [Tsuchiya et al., 1992]. Post-surgical mortality in Sprague-Dawley rats is considerably reduced even when selective neuronal atrophy appears 12 weeks after CBH in middle-aged rats [de la Torre & Fortin, 1994]. This disparity has been reported by others [Sekhon et al., 1994; Tanaka et al., 1996] and indicates that age and breed of rat are two influential factors in the pathological and behavioral outcome induced by chronic brain hypoperfusion. Differences in CBF, cerebrovascular arborization, and extent of perfusion may be important conditions which vary with age and breed, and therefore may explain the differences in vulnerability to vascular insult.

If rats are subjected to 3-VO (3-vessel occlusion), involving ligation of both carotids and one vertebral artery, animals demonstrate the same structural changes in CA1 neurons after only 3 weeks and progressively worsen by 9 weeks (Fig. 4) [de la Torre et al., 1992a;

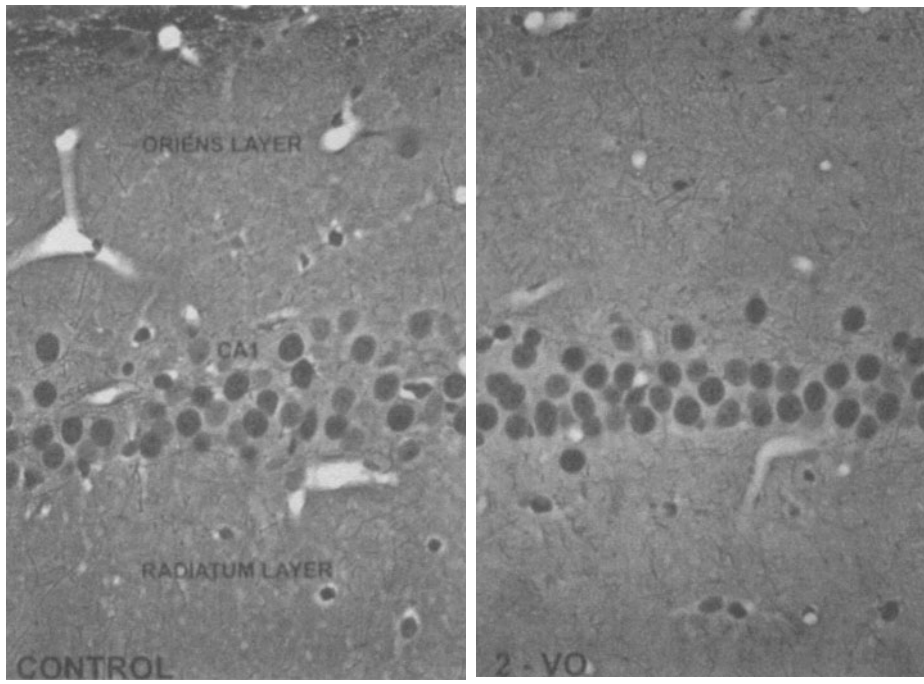

Figure 2. No structural pathology is seen in CA1 somata 8 weeks after chronic brain hypoperfusion obtained by 2-vessel (2-VO) occlusion of both common carotid arteries in aging rats. Normal CA1 somata (control) are shown on left panel. Presence of gliosis, regional cytochrome oxidase reduction and MAP-2 loss is however, present at this time point in 2-VO rats. Palmgren silver stain.

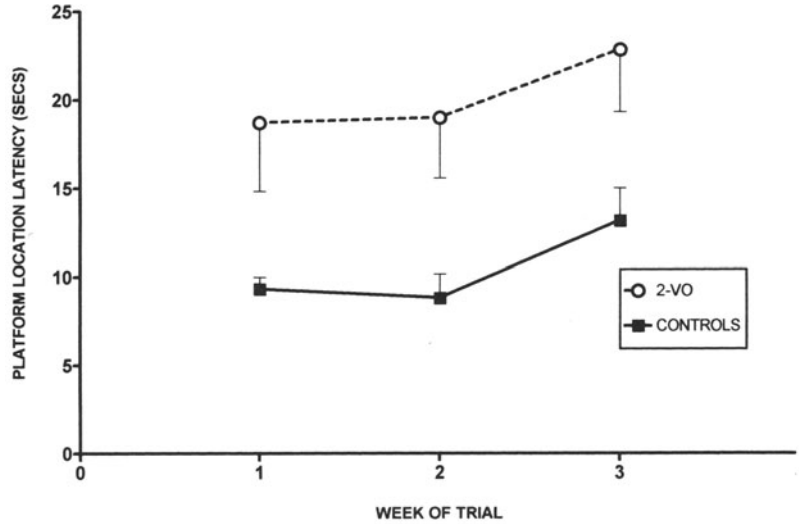

Figure 3. Mean platform location latencies at 1, 2, and 3 weeks after chronic brain hypoperfusion (2-vessel occlusion, 2-VO) is increased as compared to control rats, indicating lack of visuo-spatial ability in 2-VO aged rats. No neurodegenerative changes are seen in CA1 neurons or other regions of the brain. Bars are SEM; $p < 0.01$ comparing 2-VO with control values.

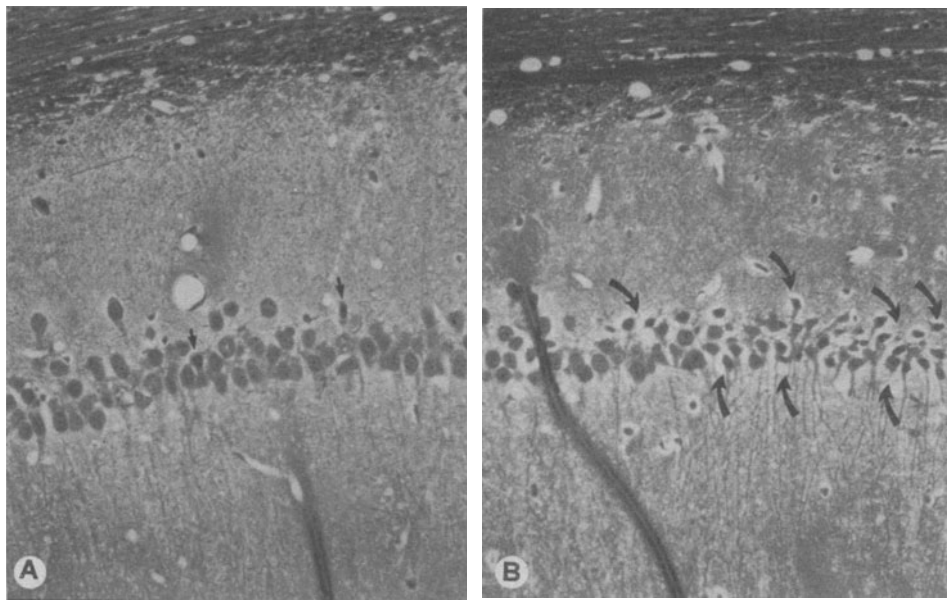

Figure 4. Progression of CA1 neurodegenerative changes (arrows) in middle aged rats subjected to 3-vessel occlusion (both carotids and subclavian artery) at 6 (A) and 12 weeks (B) of chronic brain hypoperfusion. Severe visuo-spatial memory impairment and loss of MAP-2 is present at both time points. These neurodegenerative changes after 3-vessel occlusion are in contrast with rats subjected to 2-vessel occlusion, which results in only a small percentage of neurodegeneration in CA1 neurons beginning 12 weeks after chronic brain hypoperfusion (see text for details).

de la Torre et al., 1996b]. By 25 weeks, 3-VO rats show extensive parietal cortex and hippocampal atrophy accompanied by ventriculomegaly [de la Torre et al., 1995]. This indicates that 2-VO produces a more mild injury than 3-VO, and rats are better able to withstand the low-level cerebral hypoperfusion, maintaining a certain degree of structural and functional integrity, compared to the more severe reduction in CBF produced by 3-VO. Thus, the extent of brain damage is dependent upon the *duration* and *severity* of hypoperfusion as well as on the *age* of the animal [de la Torre & Fortin, 1994; de la Torre et al., 1996b; Kaplan et al., 1991; Sekhon et al., 1997]. It is also of interest that memory acquisition is impaired as early as one week after surgery in 10 month old rats subjected to 3-VO, concurrent with more pronounced histopathological changes [de la Torre et al., 1992a]. From these findings, it appears that 3-VO in 10-month old rats is equivalent to 2-VO in 19 month old rats, indicating cognitive and neuronal changes are relative to the duration and severity of CBH, as well as age.

The visuo-spatial memory deficits achieved in these CBH studies are similar in nature to those following experimental lesioning of the hippocampus [Landfeld, 1988], yet 2-VO in aged rats does not produce significant neuronal damage and loss until 12–25 weeks [Pappas et al., 1996; de la Torre et al., 1996b]. Based upon the classic postulate that structure equates with function, it has been proposed that structural damage to CA1 neurons is responsible for the displayed memory deficits. However, 2-VO animals show spatial memory impairment well before any significant detectable structural changes in CA1 neurons such as hyperchromasia and pyknosis, which characterize the onset of neurodegeneration [de la Torre et al., 1996b; de la Torre et al., 1992a]. This discrepancy has been confirmed by others [Ni et al., 1995; Sekhon et al., 1994], implying that mechanisms other than cell damage or death may be responsible for the displayed memory impairment produced by chronic ischemia.

2.4. Neuronal Energy Metabolism and Cytochrome Oxidase

The brain is unique in that it depends almost entirely upon the aerobic metabolism of glucose for energy production under normal conditions [Erecinska & Silver, 1989]. Under special circumstances, the brain may use "ketone bodies" to fulfill its nutritional needs, but metabolism of D-b-hydroxybutyrate and acetoacetate formed from catabolism of fatty acids by the liver only significantly occurs during starvation, fat-feeding, or in diabetes [Owen et al., 1967]. Therefore, glucose can be considered the only source for energy production normally in the brain. In the neuron, the energy of glucose is shuttled through the glycolytic pathway to produce pyruvate, which is further converted into acetyl-CoA. Acetyl-CoA enters into the citric acid cycle, and oxidation of acetyl groups within this enzymatic pathway removes electrons which are funneled into the chain of mitochondrial electron carriers [Krebs et al., 1971].

The mitochondrial respiratory chain is located on the inner membrane of the mitochondria, the energy producing organelles of neurons and cells. Oxidative phosphorylation in the mitochondria produces carbon dioxide and water and is coupled to the production of high energy (~P) bonds stored as adenosine triphosphate (ATP). ATP is the universal source of chemical energy in all living organisms and it occupies a central position in brain function [Erecinska & Silver, 1989; Wong-Riley, 1989]. ATP is necessary for a broad range of neuronal functions including axonal and dendritic transport, transcription and translation, production of proteins and lipids, neurotransmitter synthesis and degradation, direct synaptic transmission, and ionic pumping [Hall, 1992; Clarke & Sokoloff, 1994]. Maintenance of the electrochemical gradient across neuronal membranes by ion pumping

is performed primarily by Na^+,K^+-ATPase which consumes approximately 60% of brain ATP [Hevner et al., 1992].

The process of oxidative phosphorylation is the culmination point of energy production and is catalyzed by cytochrome *c* oxidase (C.O.) in the mitochondrial respiratory chain. Electrons move from NADH or some other donor through several complexes including flavoproteins, ubiquinone, iron-sulfur proteins, and cytochromes. C.O. is the terminal enzyme (complex IV), in the mitochondrial respiratory chain. Approximately 95% of the energy derived from glucose is made available as ATP by oxidative metabolism [Clarke & Sokoloff, 1994]. Since there is a tight coupling between oxidative energy metabolism and energy utilization, C.O. has been used as a marker for neuronal activity [Wong-Riley, 1989].

As mentioned previously, cerebral blood flow is responsive to metabolic energy demands. However, the brain is not composed of a homogenous population of cells with equivalent physiological and morphological characteristics. Therefore, regional, cellular, and subcellular areas may not be equally sensitive to energy deprivation. Important questions are raised, in determining how chronic 2-VO produces cognitive and neuronal dysfunction. Are neurons that are involved in memory function more sensitive to changes in energy supply, and if so how does a mild, but persistent reduction in the supply of energy substrates affect neuronal function?

Histochemical C.O. analysis [Gonzalez-Lima & Garrosa, 1991], which can be translated into enzymatic activity, may be helpful in answering these questions. Differences in C.O. levels are observed not only between cellular populations and individual neurons, but also within the subcellular regions of a neuron [Wong-Riley, 1989]. C.O. levels appear to be highest in dendrites probably due to the large amount of excitatory synaptic input, and is regulated in parallel with the energy demanding Na^+,K^+-ATPase [Hevner et al., 1992].

Transient cerebral ischemia in rats and gerbils can result in energy dysfunction and reduced C.O. activity [Inoue et al., 1996; Ginsberg et al., 1977]. Initial evidence from our 2-VO model also shows that aged rats subjected to chronic cerebral ischemia demonstrate significant reductions in C.O. activity in the dorsal CA1 region and posterior parietal cortex (PPC) after 4 weeks [Fig. 5] [de la Torre et al., 1997b]. The CA1 and PPC have been reported to be a part of the neural system involved in memory function in the rat [Olton & Papas, 1979; DiMattia & Kesner, 1988]. These declines in C.O. activity were observed to occur prior to histological changes by light microscopy in CA1 pyramidal neurons, implying that C.O. may also be useful as a marker for neurodegeneration before any detectable

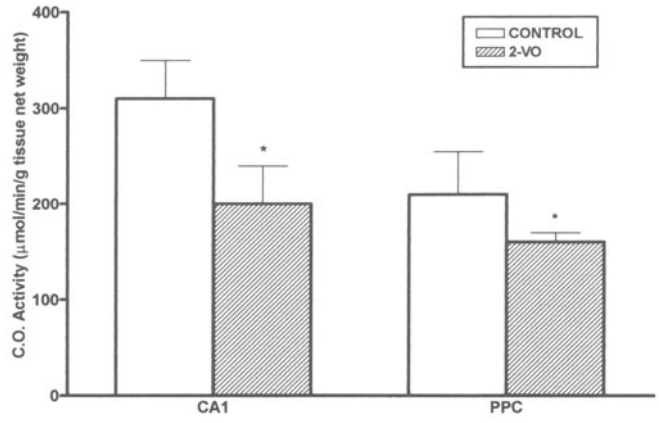

Figure 5. Regional C.O. activity following 4 weeks of chronic brain hypoperfusion (CBH) in CA1 and posterior parietal cortex (PPC) as compared to no CBH (controls). Note reduced C.O. activity that paralleled spatial memory dysfunction (see Fig. 3) only in CA1 and PPC but not in other brain regions examined. CA1 and PPC have been linked with visuospatial memory and learning. Bars are SEM; *$p < 0.05$.

cytostructural alterations are evident. Thus far, it is speculated that C.O. reductions following chronic CBH may localize primarily to dendrites, where Na^+,K^+-ATPase is located in highest concentrations along with C.O. [Hevner et al., 1992].

In A.D., oxidative energy metabolism, reflected by C.O. activity, is found diminished post-mortem and *in vivo* using positron emission tomography (PET) analysis [Chandrasekaran et al., 1996; Kish et al., 1992; Mutisya et al., 1994; Simonian & Hyman, 1994; Parker et al., 1990, 1994]. It has been proposed that these metabolic alterations precede the neuronal pathological changes [Swerdlow et al., 1993] and might contribute to the pathogenesis of A.D. However, it is not known whether declines in oxidative energy metabolism are primary to A.D. pathology or the result of some other etiological event.

2.5. Glia

Neuroglia are the largest class of nonexcitable cells found in the central nervous system (CNS), out-numbering neurons by about ten to one. Neuroglia are classified as macroglia (astrocytes and oligodendrocytes) or microglia, and are quite dynamic. Each type has its own array of channels, transmitters, surface molecules, receptors, and enzymes [Banati et al., 1996; Kettermann & Ransom, 1995]. They serve many different functions, such as regulation of extracellular K^+, maintaining the composition of the extracellular fluid of the brain, inactivation of neurotransmitters, formation of the blood-brain barrier, release of neuroactive amino acids, phagocytosis of injured synapses, and may be involved in the supply of energy substrates from the vasculature to neurons [Murphy, 1993].

Regions that undergo selective neuronal death characteristically demonstrate an increase in glial activation which appears well before any neuronal cell loss associated with ischemia [Petito et al., 1990]. Reactive astrocytes are characterized by hypertrophy, hyperplasia and an increase in glial fibrillary acidic protein (GFAP), an intermediate filament localized specifically to astrocytes [Kettermann & Ransom, 1995]. Cerebral ischemia may produce reactive astrogliosis in the hippocampus and cortex [Petito et al., 1990]. In 2-VO, astrocyte density in the stratum radiatum and oriens layer of the CA1 is increased between 2–25 weeks [Fig. 6] [Pappas et al., 1996; de la Torre et al., 1992a]. After 9 weeks of a more severe 3-VO insult, there is an increase in both density and hypertrophy of glial cells with mild pyramidal cell damage [de la Torre et al., 1992a]. It should be noted that increased GFAP immunoreactivity and proliferation of reactive astrocytes is observed in the hippocampus at the onset of A.D. and appears to precede extensive neuronal damage or mounting formation of senile plaques and neurofibrillary tangles [Delacourte, 1990; Duffy & Rapport, 1980].

The role of glia in response to ischemia is unclear, but research has produced two different viewpoints. First, it has been proposed that reactive glia either cause, influence, or aggravate ischemic injury [Banati et al., 1996]. Often the extent of reactive glial proliferation is an early indicator of subsequent changes in brain tissue [Wakiti et al., 1994]. One hypothesis suggests astrocyte acidosis following ischemia results in free-radical generation and injury to both astrocytes and surrounding tissue [Kettermann & Ransom, 1995], but much of this research has been limited to *in vitro* analysis where astrocytes never fully mature. Second, it is theorized that ischemic-activated glia act to promote neuronal resistance to ischemia and enhance neuronal survivability [Vibulsreth et al., 1987; Petito, 1990]. Glia can protect neurons from damage by releasing growth promoting cytokines [Giulian et al., 1993]. However, tissue culture experiments need to be carefully evaluated before extrapolating findings to whole-animal studies. Thus, the activation and functional role of reactive gliosis following cerebral ischemia is still speculative.

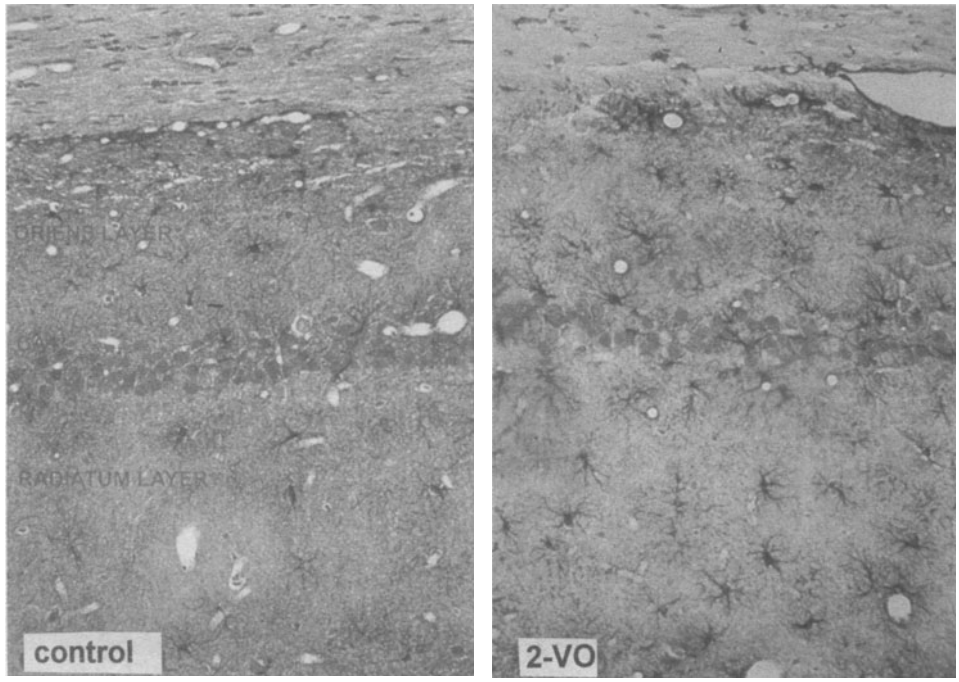

Figure 6. Hippocampal GFAP (glial fibrillary acidic protein) immunoreaction is significantly increased 4 weeks after chronic brain hypoperfusion obtained by bilateral carotid artery occlusion (2-VO). Control GFAP (no brain hypoperfusion) is seen on left side of picture. GFAP-positive astrocytes are seen invading oriens, pyramidal (CA1) and radiatum layer in 2-VO tissue but no CA1 neuronal degeneration is evident at this time point.

2.6. Cholinergic Neurons

Research on humans and animals suggests that the cholinergic system is important for learning, memory, and cognition [Perry, 1986]. Although they do not mediate memory directly, they appear to provide important modulatory input to hippocampal neurons.

A decrease in choline acetyltransferase and loss of cholinergic neurons is observed in the hippocampus and basal forebrain in A.D., but is of unknown origin [Dunnet, 1991]. Studies on chronic 2-VO rats (<9 months old) show a reduction in acetylcholine (ACh) levels in the cortex and hippocampus after 16 weeks [Tanaka et al., 1996]. In young rats (9 weeks), the degree of cognitive impairment correlates with the extent of cholinergic dysfunction. Moreover, dysfunction in hippocampal cholinergic neurons occurs after transient ischemia [Ishimaru et al., 1995]. Thus, progressive cognitive deficits produced by chronic cerebral hypoperfusion may also involve damage or loss of cholinergic neurons and terminals.

It is suggested that the reductions of CBF in A.D. and chronic 2-VO provide neurons with a reduced supply of glucose and oxygen for ATP generation. A decrease in ATP production reflects a decline in glycolysis, indicating a reduction in end products of glycolysis such as acetyl-CoA. Since acetyl-CoA is required for synthesis of acetylcholine (ACh), a loss of ACh synthesis may result from the diminished supply of glucose during cerebral ischemia leading to cholinergic dysfunction [Gibson & Peterson, 1984].

Additionally, CA1 neurons are both glutaminergic and ischemic-sensitive [Kirino, 1982], indicating a susceptibility to excitotoxic damage. Inhibition of Na^+,K^+-ATPase due to reduced energy substrates for ATP synthesis may disrupt ionic concentration gradients,

removing the Mg^{2+} block of N-methyl-D-aspartate (NMDA) receptors and permitting persistent activation by endogenous glutamate [Beal et al., 1993]. Although the mechanism by which glutamate is released is speculative [Szatkowski & Atwell, 1994], under these conditions free glutamate can persistently activate NMDA receptors resulting in Ca^{2+} influx and damage to CA1 neurons. Thus, glutamate excitotoxicity due to reduced energy substrates may play a pathogenic role in ischemic-induced neurodegeneration.

Chronic 2-VO in aged rats consequently produces changes similar to those observed at the onset of A.D. which include progressive deficits in spatial memory, proliferation of reactive astrocytes, changes in brain phospholipid synthesis, and neuronal damage specific to the hippocampus [de la Torre & Mussivand, 1993; Delacourte, 1990; Blass, 1993; Hoyer, 1990]. On the other hand, no changes in serum glucose, blood pressure, hematocrit, or blood gases have been observed to occur following CBH [de la Torre & Fortin, 1994]. Moreover, 2-VO does not produce any white matter changes or cortical infarcts which are representative of multi-infarct vascular dementia. Therefore, chronic 2-VO in aged rats is more reflective of the pathological and behavioral changes observed in A.D. than of cerebrovascular diseases, and consequently has become a useful animal model in which to analyze the underlying regional, cellular, and subcellular mechanisms of age-related dementia.

3. CYTOCHROME OXIDASE ACTIVITY FOLLOWING CBH

We have investigated neuronal energy metabolism following chronic CBH to determine if energy changes are pathogenic to the cognitive and neurodegenerative outcome. C.O., which provides 95% of brain energy as ATP [Erecinska & Silver, 1989], has been used as an endogenous marker for energy production [Wong-Riley, 1989] to ascertain if neuronal metabolism is disrupted following chronic cerebral ischemia. C.O. activity was examined histochemically after 4 weeks of persistent cerebrovascular ischemia in aging rats. A pattern of reduced C.O. activity was observed in the hippocampal CA1 after 4 weeks of CBH (Fig. 5).

C.O. activity was also examined in the subfields composing the CA1 region: the oriens, pyramidal, and radiatum layers. A reduction in C.O. activity was apparent in the radiatum layer of 2-VO brains at 12 weeks. The stratum radiatum and adjacent stratum laconosum-moleculare contain apical dendrites of CA1 neurons [Borowsky & Collins, 1989] and are the primary sites of excitatory synaptic input. Since C.O. is located in high levels in dendrites, indicating a high demand for ATP, the localized reduction in C.O. activity suggests dendrites may be early sites of alterations in oxidative energy metabolism due to CBH [Wong-Riley, 1989].

3.1. Effects of CBH on Memory and Neurons

Chronic 2-VO can produce visuo-spatial memory deficits from week 1 after CBH and these deficits progressively increase until 25 weeks. This impairment is not likely due to any sensory dysfunction linked to 2-VO, since 2-VO rats do not demonstrate notable difficulty on locating the visible platform. These results concur with previous work which has shown chronic 2-VO in aged rats produces visuo-spatial memory impairment in a progressive fashion [Pappas et al., 1996], however, the onset of memory impairment can occur later than expected. The late onset of visuo-spatial deficits, after 7 weeks of 2-VO, is reflective of the younger age of these rats compared to previous findings with 19–22

month old rats subjected to 2-VO [de la Torre et al., 1996b]. The discrepancy in onset of memory dysfunction indicates that middle-aged animals are not cognitively affected as early and severely as aged animals subjected to 2-VO, but unlike young rats they do not cognitively recover from this insult.

Although spatial memory performance was progressively impaired after 2-VO, we observed only negligible structural neuronal damage in CA1 neurons at 12 weeks. Structural damage is defined here as an increase in neuronal hyperchromasia and pyknosis visible by light microscopy. The cell damage produced by CBH is thought to represent the ongoing process of necrosis, a passive, pathological process leading to cell death. Recently, it has been proposed that ischemic-cell damage and death may be attributed to the physiological process of programmed cell death, or apoptosis [Schmidt-Kastner, 1997], but findings in rats subjected to 3-VO indicate neuronal damage is not an automated response to ischemia leading invariably to cell death. It was previously shown that if 3-VO rats, displaying mild neuronal damage after two weeks, are deoccluded and allowed to reperfuse, the characteristic staining properties of damaged neurons are diminished [de la Torre et al., 1993]. The recovery of damaged or dying neurons in the early stage of CBH indicates neuronal damage induced by chronic, low-grade ischemia does not involve activation of an intrinsic, irreversible death program [Schmidt-Kastner, 1997].

The memory deficits observed after CBH are similar to those induced by experimental lesioning of hippocampal CA1 neurons [Gionet et al., 1991], but 2-VO brains do not display moderate or widespread damage in the CA1. These results are consistent with other chronic 2-VO studies indicating a poor correlation exists between structural damage to CA1 pyramidal cells, or any other neurons in the rat brain, and cognitive impairment [de la Torre et al., 1992a; Ni et al., 1994; Pappas et al., 1996; Sekhon et al., 1994; Tanaka et al., 1996]. As a result, it appears that morphological neuronal damage in the CA1, or other brain regions, is not a necessary event for production of cognitive deficits in rats. However, CA1 neurons possess two unique characteristics that make them susceptible mediators of cognitive impairment following ischemia; they are highly ischemic-sensitive and they are involved in visuo-spatial memory function [de la Torre, 1997a]. Given the absence of structural neuronal damage in CA1 but progressive visuo-spatial impairment observed after 2-VO, it follows that disruption of the neuronal circuitry within these structurally intact neurons subjected to chronic CBH might occur, impairing neuronal function regulating cognition. Therefore, intraneuronal alterations which are not visible by light microscopy or external interactions between neurons and surrounding cells, may compromise overall function.

We have observed visible loss of MAP-2 immunostaining in CA1 apical dendrites after 8 and 12 weeks of CBH (Figs. 7, 8) Loss of MAP-2 reaction has been reported previously to occur after transient ischemia in gerbils, and was suggested to be a marker for early ischemic damage. [Kitagawa et al., 1989] MAP-2 is a protein involved in regulating microtubule assembly and polymerization, playing a role in providing and maintaining the structural framework of neurons [Kudo et al., 1990]. Concentrations of MAP-2 are highest in dendrites [Miyazawa et al., 1993], subsequently MAP-2 has been used as a postsynaptic marker for injury following brain ischemia and other insults [Park et al., 1996]. Data from our lab have revealed a loss of MAP-2 immunostaining in CA1 apical dendrites following 8–12 weeks of chronic 2-VO indicating microtubule structure in apical dendrites may have been altered, possibly compromising dendritic structure and function. However, eight weeks after CBH, no structural pathology of CA1 somata is apparent, yet we know these neurons are dysfunctional because CA1 apical dendrites show a loss of MAP-2 immunostaining and C.O. levels are reduced in this region (Fig. 7) and continue to be reduced

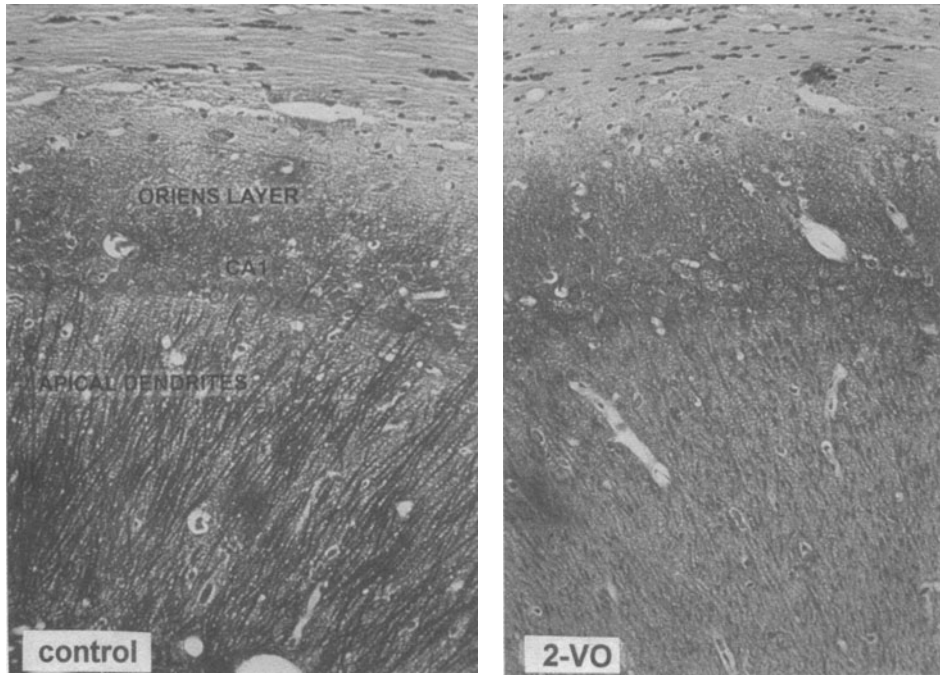

Figure 7. MAP-2 loss of immunoreaction in apical dendrites of CA1 neurons (as compared to control) 8 weeks after chronic brain hypoperfusion obtained by ligation of both common carotid arteries (2-VO). No structural pathology is seen in CA1 neurons at this time point but regional C.O. activity and spatial memory are reduced 4 weeks prior to MAP-2 changes (see Figs. 3 and 5) indicating CA1 neuronal dysfunction.

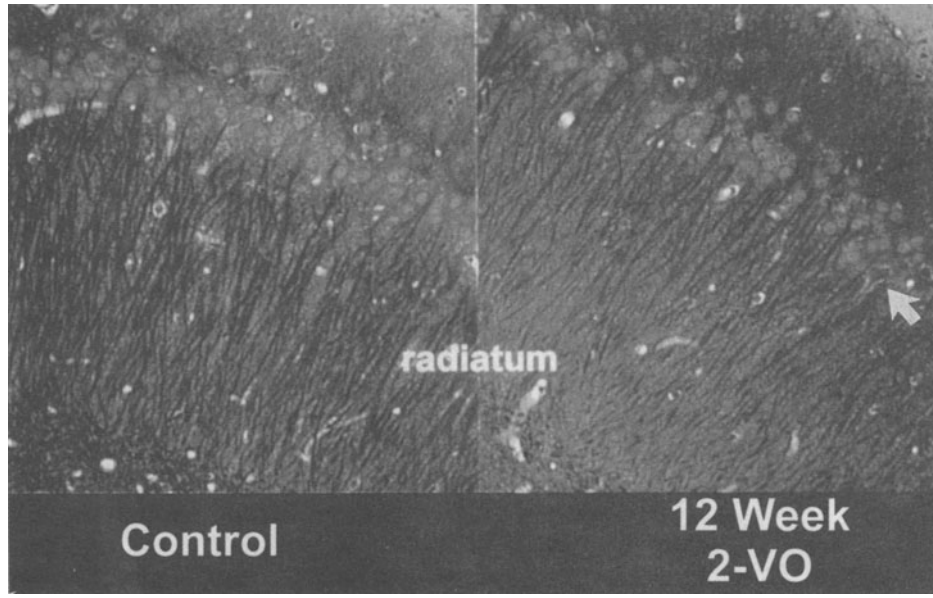

Figure 8. MAP-2 loss of immunoreaction (as compared to control) in apical dendrites of CA1 neurons 12 weeks after chronic brain hypoperfusion obtained with 2-vessel (2-VO) occlusion of the common carotid arteries. A small number of CA1 neurons (arrow) can be seen at this time point undergoing neurodegenerative changes. Regional cytochrome oxidase activity reduction (see Fig. 5) gliosis (Fig. 6) and spatial memory deficits (Fig. 3) were observed 8 weeks prior to the onset of neurodegeneration.

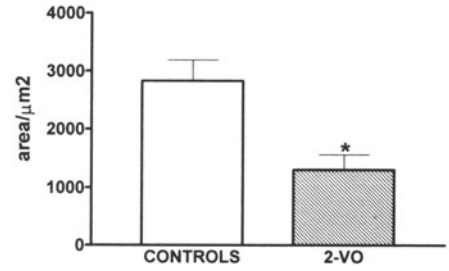

Figure 9. Percentage of MAP-2 immunostaining loss following 12 weeks of chronic brain hypoperfusion. MAP-2 is a dendritic marker of postsynaptic function. Bars are SEM; *$p < 0.01$.

after 12 weeks of CBH (Fig. 9). Yet, the structural changes in CA1 neurons become noticeable between 12–25 weeks after CBH, suggesting the following scenario:

After CBH, neurons begin to receive less glucose and oxygen due to the reduction in cerebral blood flow induced by CBH. Since glucose and oxygen are the main substrates for mitochondrial oxidative phosphorylation that yields the energy fuel ATP, their loss or decline after CBH can affect the activities of metabolic enzymes, notably C.O. which is located in the inner mitochondrial membrane and is highly distributed in dendrites and synaptic vesicles where energy demands are highest. Consequently, falling levels of C.O. not only reflect the ongoing neuronal activity but also presages impending neuronal failure, assuming the source of insult, CBH, continues. The decline in regional C.O. levels, for example in the CA1 sector, indicates that ion pumping generated by Na^+,K^+-ATPase is down-regulated since C.O. and Na^+,K^+-ATPase appear to change in parallel. [Hevner et al., 1992] The result of decreased Na^+,K^+-ATPase will have an adverse effect on dendritic function after 8 weeks of CBH, showing reductions in the cytoskeletal dendritic protein, MAP-2. This is what we see in many of our experimental designs. Consequently, glucose and oxygen reduced delivery stemming from CBH, lowers mitochondrial efficiency and oxidative phosphorylation, initially, only in the most ischemic-sensitive neuronal populations, such as CA1. This reduction in oxidative phosphorylation lowers neuronal energy metabolism as reflected by regional C.O. hypoactivity in the CA1 sector. Neurons whose energy input continue to be compromised, develop atrophic changes (12–25 weeks after CBH) and eventually die [Fig. 4] [de la Torre et al., 1997b; de la Torre et al., 1992a]. Pharmacologic manipulation of cerebral energy metabolism with selective inhibition of C.O. using sodium azide, reveals that severe spatial memory deficits and neurodegeneration are developed in rats within 1–4 weeks [Brouillet et al., 1994; Bennett et al., 1996a,b]. Moreover, regional inhibition of energy metabolism by stereotaxic injections of malonate into the striatum, result in retrograde loss of afferent substantia nigra neurons ipsilateral to the injection site [Sonsalla et al., 1997]. These studies demonstrate that regional disturbance of C.O. activity, by means other than cerebral ischemia, can result in cognitive and degenerative changes in the region of the metabolic disturbance. These findings further support our proposal that altered C.O. activity may be the *initial marker* for oxidative phosphorylation down-regulation and is a subsequent precursor of neurodegenerative pathology following CBH. A similar mechanism involving C.O. may be expressed prior to the onset of Alzheimer's disease [Chandrasekaran et al., 1996; de la Torre et al., 1997b].

3.2. Astrocyte Response to CBH

Astrocytes respond to ischemia by increasing their density and distribution [Banati et al., 1996], but how they are activated and why they respond to cerebral ischemia has remained elusive. We examined the hippocampus for a glial reaction using GFAP immu-

nodetection, a useful method in evaluating the distribution of reactive changes following brain injury or ischemia. GFAP immunoreactivity, denoting glial density, was significantly increased in the oriens layer of the CA1 following 7 and 12 weeks of 2-VO [Fig. 10], but with structural neuronal damage less than 5%. However, the results in glial density and neuronal damage were achieved in separate experimental groups and only an indirect comparison can be drawn. On the other hand, previous 2-VO studies have shown increases in glial density occur without apparent neuronal damage in the CA1 [de la Torre et al., 1992b; Pappas et al., 1996]. Hypertrophy of proliferated glia has been also observed at 7 and 12 weeks after CBH. Increases in GFAP are mainly due to glial hypertrophy and hyperplasia, indicating the glia observed in the oriens of the CA1 were ischemic-activated and became reactive [Fig. 6]. From the current results, reactive astrocytosis does not appear to be a response provoked by structural neuronal damage following ischemia, but may result from an alarm reaction by neurons undergoing C.O. decline, such as the CA1 population subjected to CBH, which signal for glial proliferation. Astrocytosis is a well-known reaction in the brain following physical injury or vascular insult.

3.3. C.O. and Reactive Astrocytosis

Reactive astrocytosis is well documented to occur following cerebral ischemia [Petito et al., 1990], but it is not understood what factor(s) or signals stimulate astrocytes to hypertrophy and proliferate early after this insult. Astrocytic hypertrophy may be a defensive tool used by neurons to resist cerebral ischemia [Petieto et al., 1990]. Extensive proliferation of these astrocytes may however, lead to neuronal injury [Petito et al., 1990]. Microglial activation is tightly controlled [Banati et al., 1996] which suggests glia activation may be a general non-specific immune response. Nevertheless, it still remains unclear how glia become activated in cerebral ischemia. Since the extent of glial proliferation following ischemia has been shown to predict subsequent neuronal damage [Wakiti et al., 1994], glia appear to become reactive independent of neuronal structural damage. For example, chronic CBH induces reactive gliosis in the hippocampus well before any detectable structural neuronal damage is observed using light microscopy [de la Torre et al., 1992b]. The consistent appearance of reactive glia following chronic 2-VO leads us to believe that glia may be responding to the decreased oxidative energy supply addressed by reduced C.O. activity [de la Torre et al., 1997b]. The localized energy changes induced by chronic ischemia may be a profitable environment for the primarily anaerobic astrocyte [Hsu et al., 1993]. Neurons depend highly upon oxidative energy supply to remain functionally active [Erecinska & Silver, 1989] whereas glia, drawing little from oxidative energy supply, rely mainly upon anaerobic metabolism [Wong-Riley, 1989]. Therefore, we

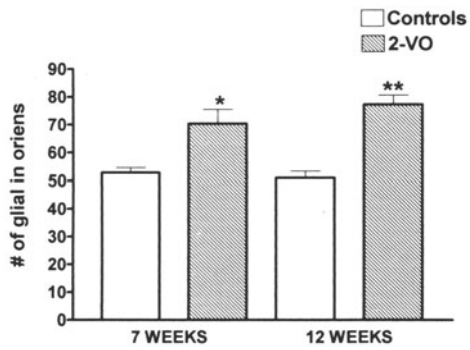

Figure 10. Number of glial fibrillary acidic protein (GFAP) proliferation in the oriens layer of the hippocampus 7 and 12 weeks after chronic brain hypoperfusion (CBH) obtained by 2-vessel (2-VO) occlusion. No significant CA1 structural pathology is observed until 12 weeks after CBH despite significant reactive astrocytons expressed by GFAP immunodensity. No significant increase in GFAP density is seen between 7 and 12 weeks in 2-VO rats. Bars are SEM; *$p < 0.01$; **$p < 0.001$ as compared to controls.

suggest that the diminished local cerebral blood circulation induced by chronic ischemia produces an environment of low oxygen and glucose that stimulates glia to activate and proliferate in response to a stressful brain state.

Our research data also suggest that reactive astrocytosis brought about by chronic cerebral ischemia is associated with the progression of cognitive deficits. Although glia appear to be very active and mobile cells, they do not exist in isolation but rather interact with other brain cells, the vasculature, extracellular milieu, and substances from other organ systems [Kettermann & Ransom, 1995]. The interactive capacity of glia also may apply to how these dynamic cells respond to brain ischemia. Consequently, a shift in neurono-glial homeostasis may adversely affect neuronal activities and efficacy. It was previously reported that astrocyte density in the hippocampus correlated with the increase in visuo-spatial impairment on the Morris water maze in 2-VO rats [Pappas et al., 1996]. The observed increase in reactive glia with an absence of apparent neuronal structural damage in this study provides further evidence that an astrocytic tissue reaction in the laminar structure of the hippocampus might affect visuo-spatial performance. Moreover, rats temporarily occluded after 3 weeks CBH, display cognitive deficits and increased GFAP density but without significant neuronal damage in the CA1 [de la Torre et al., 1993]. With restoration of CBF, GFAP returns to pre-CBH levels and memory dysfunction returns to normal in these animals [de la Torre et al., 1993]. Taken together, the consistent increase in both glial density and visuo-spatial impairment appear to correspond in their progressive course, however, little evidence is presently available to describe how pyramidal neurons might incur damage from reactive glia. It is possible that reactive glia, consuming space in a confined environment, may damage neurons or their processes, synapses, or receptors in the hippocampal circuit. Recently, *in vitro* experiments have shown that microglia release cytotoxic agents [Giulian et al., 1993], including superoxide anion [Colton & Gilbert, 1987], which may play a causative role in neuronal injury *in vivo*. Conversely, glia in tissue culture can release growth promoting cytokines which enhance neuronal survivability, and they also release protein mitogens which further stimulate microglia [Hao et al., 1990]. Therefore, it has been suggested that glia have opposing actions upon neuronal growth and survival following brain injury which depend upon their location and distribution [Giulian et al., 1993], however, whether reactive glia aggravate or ameliorate neuronal injury remains speculative *in vivo*. The antagonistic actions of glia in tissue culture may begin to explain why the course of cognitive changes due to chronic CBH seem to parallel more with the proliferation of reactive glia in the hippocampus than with neuronal structural pathology. Although mild reactive gliosis may be a normal consequence of aging [Duffy & Rapport, 1980], dense reactive gliosis has been shown to be associated with b-amyloid senile plaques [Frederickson, 1992]. Reactive astrocytosis in the hippocampus is an early and consistent observation in Alzheimer's brains [Delacourte, 1990; Van Hoesen & Hyman, 1990]. This finding suggests a role for reactive glia in the development of lesions in A.D. [Frederickson, 1992]. Considering these findings, it appears reactive gliosis adequately disrupts the normal neurono-glial relationship after both chronic CBH and in A.D. in a manner that is favorable to developing dementia.

4. IMPLICATIONS OF C.O. ACTIVITY ON METABOLISM

Just as the onset and degree of memory deficits depends upon age, comparison of the present and previous C.O. results indicate that neuronal energy metabolism is age-sensitive to chronic, low-grade brain hypoperfusion. In one study involving C.O. metabolism after

CBH, aged rats (20 months old) subjected to 2-VO displayed marked reductions in regional C.O. activity after 4 weeks [de la Torre, 1997b]. Of the 18 brain regions examined, only the CA1 and posterior parietal cortex demonstrated significant reductions (Fig. 5). Young rats (up to 9 months) have been reported to develop mild, transient visuo-spatial impairment but are able to recover from CBH [de la Torre et al., 1992b], providing support that young and middle-aged animals are more resilient in the face of chronic brain hypoperfusion. Thus, young age imparts a protective effect upon neuronal metabolism, maintaining good function under mildly ischemic conditions. Two possibilities exist for the more prolonged energy metabolic sparing in young and middle-aged rats subjected to CBH. (1) Younger animals possess a higher CBF than aged animals [Linville & Arneri, 1991; Ohata et al., 1981; Yager et al., 1996]. Consequently, mild chronic reductions in CBF may not substantially disrupt neuronal oxidative energy metabolism until weeks after CBH; (2) young and middle-aged animals may be able to compensate for the reduced CBF by some basic mechanism, for example, rapid neovascularization of ischemic brain regions or more efficient utilization of energy reserves to neuronal demands. Several studies have indicated that the energy profile between the young and old rat brain under normal conditions are markedly different. It has been shown that several substrates in the citric acid cycle are significantly different between 1-year old and 2-year old rats subjected to cerebral ischemia, supported by others who have shown glucose and phosphofructokinase are reduced in 2-year-old rats [Hoyer & Krier, 1986; Patel, 1977]. Moreover, concentrations of pyruvate, malate, and creatine phosphate decline between 12 and 24 months, indicating a susceptibility to stress conditions increase with age [Hoyer, 1990]. As a result, the brain's capacity to meet conditions aggravated by CBH are reduced with age. Conversely, the middle-aged rat brain's relatively intact energy cycle is more capable of meeting emergency conditions than the aged brain. The smaller decline in C.O. activity, reflecting ATP synthesis, observed in middle-aged rats when compared to older rats, supports the idea of an increased resistance to chronic brain hypoperfusion [Abdollahian et al., 1997]. Thus, the neuropathological and behavioral changes induced by chronic, low-grade ischemia in middle-aged rats may only partially involve a disruption in neuronal energy metabolism, suggesting CBH in middle-aged rats may not be as effective as in aged rats for determining the events involved in age-related memory dysfunction. The increased resistance by young and middle age rats to changes in neurochemistry and visuo-spatial memory due to mild but permanent cerebral ischemia may explain why A.D. is rarely observed in people under 65 [Blass, 1993].

The late-developing pattern in visuo-spatial memory impairment seems to parallel the pattern in C.O. activity, both of which demonstrated significant changes by 4 weeks in older rats [de la Torre et al., 1997b]. When these rats are kept ischemic beyond 4 weeks, gliosis, MAP-2 loss, spatial memory dificits and neuronal dysfunction continue to progress. Aged animals subjected to 2-VO or middle aged rats undergoing 3-VO, become cognitively impaired early with alterations in hippocampal metabolism and increased glial proliferation, but middle-aged animals are slower to demonstrate these changes [de la Torre et al., 1995; de la Torre et al., 1996b]. This finding indicates that the behavioral and neuropathological changes seen in the hippocampus after CBH are qualitatively similar between middle-aged and aged rats but require more time to develop in middle-aged animals.

4.1. Dendritic Structure and Function

Despite the role glia may play in the cognitive dysfunction created by CBH, observable structural damage to pyramidal neurons is relatively absent for an extended period of time. However, compartmental or intracellular changes in organelle structure and function

not visible by light microscopy may occur due to reduced nutrient delivery in chronic hypoperfusion, and this may lead to suboptimal function of the neuron. The structure, size, shape, and organization of the pyramidal neuron all coalesce in order to perform specific functions. It is the unique structural framework of the dendrite that integrates information from a vast number of synaptic contacts. Dendrites are highly branched processes that have receptors and proteins specialized to receive synapses from other cells, converting chemical signals into electrical signals. Transmission between neurons is primarily chemical, and the postsynaptic dendrite contains a high density of receptors specific for a presynaptic neurotransmitter [Hall, 1992]. Responsible for receiving synaptic input from other neurons and afferent fibers, dendrites can isolate alterations in intracellular ions from the cell body [Guthrie, 1991]. Following acute ischemia, several studies have shown structural changes occur in neuronal dendrites [Hsu & Buzsake, 1993; Park et al., 1996]. MAP-2 immunohistochemistry and immunoblotting have been the most common methods in evaluating dendritic injury, however the latter technique does not permit anatomical localization. Using these methods, studies have revealed early changes following acute ischemia which involve selective degeneration of dendrites [Park, 1996], but little is known of how dendritic morphological changes result and affect neuronal function and survival. One possible mechanism of dendritic injury involves overactivation of N-methyl-D-aspartate (NMDA) receptors by glutamate, resulting in a rise in intracellular Ca^{2+} and leading to slow excitotoxic cell death [Miyazawa et al., 1993]. As for dendritic structure, activation of calcineurin, a Ca^{2+}/calmodulin dependent phosphatase, can rapidly degrade MAP-2 directly [Park et al., 1996] and may be responsible for the loss of MAP-2 immunoreactivity. Furthermore, it has been shown that the addition of taxol, a promising anticancer drug [Jun, 1995], stabilizes microtubules and attenuates glutamate NMDA-activated damage, suggesting disruption of the microtubule structure underlies dendritic damage and may be pathogenic of the excitotoxic process.

4.2. Implications of Cytochrome Oxidase Activity on Dendritic Function

The relationship of MAP-2 and C.O. derived from our studies indicate that the disruption in dendritic structure, expressed by MAP-2 immunoreactive stain loss, may be attributed to the subtle but chronic reductions in energy supply induced by 2-VO and preceded by regional C.O. down-regulation. Na^+,K^+-ATPase is the primary active ion pump in neurons and in most animal cells. Approximately 60% of brain ATP is consumed by Na^+,K^+-ATPase in order to maintain electrochemical gradients in neurons [Hevner et al., 1992]. The need for ATP by this ion pump requires exchanges of three Na^+ ions for two K^+ ions, resulting in a net outward flux of positive charge [Wong-Riley, 1989]. Outside the central nervous system, Na^+,K^+-ATPase is localized to regions which are associated with high ionic flux such as specialized epithelial cells, cardiac cells, kidney tubules, and exocrine glands [Clarke & Sokoloff, 1994]. In the nervous system, Na^+,K^+-ATPase is found in high concentrations at nodes of Ranvier, axon terminals, photoreceptors in the retina, and particularly in dendrites and their synaptic membranes [McGravil et al., 1991]. In dendrites, restoration of ionic gradients by Na^+,K^+-ATPase is necessary for maintaining sensitivity to the next synaptic event. Consequently, if energy deprivation occurs, the resulting disturbance in ionic homeostasis from an energy deficient Na^+,K^+-ATPase may remove the Mg^{2+} block on NMDA receptors leading to NMDA toxicity.

Since C.O. and Na^+,K^+-ATPase appear to be regulated in parallel in rat brain [Hevner et al., 1992] and are found in the highest concentrations in dendrites [Wong-

Riley, 1989], dendrites are probably extremely sensitive to changes in energy. After 2-VO, we observed a loss in MAP-2 immunostaining and significant C.O. reductions in the stratum radiatum which contain the apical dendrites of CA1 neurons, after 12 weeks of CBH, suggesting oxidative energy changes may be responsible for the disruption in dendritic cytoarchitecture. This finding provides important evidence that neuronal dysfunction involves early damage to dendrites of ischemic-vulnerable neurons, and may compromise neuronal signaling in the neural system modulating memory. The low-level decline in ATP of CA1 apical dendrites may adversely affect restoration of membrane potential by Na^+,K^+-ATPase, disrupting the normal flow of synaptic transmission resulting in a loss of neuronal efficacy independent of the excitotoxic process.

Other studies support the concept of a localized metabolic dysfunction induced by cerebral ischemia. It was reported early on that acute ischemia primarily influences the phosphorylative capacity of mitochondria rather than electron transfer [Ginsberg et al., 1977]. Moreover, mitochondrial functions and particularly C.O. activity decline during severe transient brain ischemia [Nakahara et al., 1991]. Taking into account changes in blood supply, acute reductions in CBF greater than 50–60% of normal values, can result in ionic pump failure but is time-dependent for production of neuronal loss or structural damage [Astrup et al., 1981]. For example in baboons, at 16–20 ml/100 gm/min CBF, EEG becomes flat and neuronal firing and synaptic transmission fails [Symon et al., 1974]. However, the blood flow threshold for Na^+,K^+-ATPase dysfunction in persistent, low-grade ischemia could be significantly different from those in acute ischemia. As a result, there may be marked differences in both the extent and degree of energy disruption or failure in CBH. Mild reductions in ATP may be sub-threshold for induction of excitotoxic damage but still can produce memory dysfunction, as evidenced by the absence of moderate neuronal structural damage in cognitively impaired 2-VO rats. In support of this possibility, one study has shown chronic reductions in CBF of 25–50% in rats did not lead to histological damage but produced a loss of long-term potentiation (LTP) in the hippocampus [Sekhon et al., 1994]. LTP is a type of enhanced, long-lasting synaptic transmission which occurs in the trisynaptic loop of the hippocampus [Sekhon et al., 1997], and it is thought to play some role in memory encoding through alterations in synaptic and dendritic physiology [Hall, 1992]. Combined with our results, these early changes in dendritic structure and synaptic transmission indicate that neuronal energy hypofunction precedes neuronal damage, implying neuronal dysfunction in chronic 2-VO is not necessarily provoked by glutamate excitotoxicity. Subsequently, the disruption of dendritic structure may have long-lasting effects on synaptic transmission, impairing neuronal involvement in visuo-spatial memory function. Moreover, it has been speculated that the collapse of dendritic structure may prevent subsequent neuronal damage by glutamate excitotoxicity, but presently no evidence is available to support this possibility. Interestingly, this may explain not only the dendritic changes but why the memory deficits are observed while somatic structure remains relatively intact. Given the present results, we provide initial evidence that cognitive impairment, induced by chronic brain hypoperfusion, may be due in part to breakdown of dendritic structure, possibly impairing synaptic function, in ischemic-vulnerable CA1 neurons and that this dendritic insult is predicated by oxidative phosphorylation down-regulation and lowered regional C.O. activity.

5. CONCLUSIONS

Cytochrome oxidase (C.O.) is the terminal enzyme in the mitochondrial respiratory chain which is responsible for oxidative phosphorylation and the formation of the cell

energy fuel, ATP. C.O. has been reported useful as an endogenous *metabolic marker* of *neuronal activity*.

In this review, we propose that C.O. may also be a useful *predictive marker* of *neurodegeneration*, particularly following mild, but chronic brain hypoperfusion (CBH). This vascular insult will result in progressive cerebral pathology whose morbid evolution can be analyzed chronologically. The evidence for this proposal can be summarized as follows.

Four weeks following CBH, regional C.O. activity is depressed in CA1 and posterior parietal cortex together with visuo-spatial memory function but no neurodegenerative pathology is observed in either of these 2 structures or anywhere in the brain. An increased density in hippocampal astrocytes is also observed at this time point.

CA1 and posterior parietal cortex are involved in visuo-spatial memory mechanisms. Reactive astrocytosis following CBH is thought to result from an alarm signal by dysfunctional but not necessarily necrotic neurons to resist the ischemic process. By 8 weeks post-CBH, microtubule associated protein (MAP-2) is found reduced in the apical dendrites of CA1 neurons but no structural pathology of CA1 soma is apparent. MAP-2 is a cytoskeletal protein that is used as a postsynaptic marker of neurodendritic function. Twelve weeks following CBH, a small percentage of CA1 neurons show early signs of degeneration and continued deficits in MAP-2 and spatial memory and increased density of astrocytes. If rats are kept for 25 weeks, CA1 neuronal loss and extensive cortical necrosis can be observed following 2 or 3 vessel ligation of conducting cerebral arteries. These metabolic, physiologic and anatomic events are also observed in Alzheimer's disease but it is still debatable whether the same chronological order follows the human dementia as that seen in the rat brain hypoperfusion described here. Assuming, as we have previously hypothesized [de la Torre & Mussivand, 1993; de la Torre, 1994; de la Torre, 1997], that Alzheimer's disease is initiated by reduced delivery of glucose and oxygen to brain neurons from hemodynamic disturbances, regional C.O. activity, which has already been found globally depressed in Alzheimer brains, could be an early litmus marker for predicting eventual neurodegenerative pathology and for designing therapy to prevent or reverse neuronal atrophy.

ACKNOWLEDGMENTS

Supported in part by the Ontario Heart and Stroke Foundation, NIH grant R01 MH43353, Texas ATP grant 361 and NIH grant T32 MH18837.

REFERENCES

Abdollahian, N. P., Cada, A., Kinney, M., Sutherland, R. J., Gonzalez-Lima, F., and de la Torre, J.C., 1997, Chronic brain ischemia produces progressive memory impairment in rats due to a dysfunction in the oxidative energy metabolism, *Soc. Neuro. Abstr.* 23:832.

Albers, R. W., Siegel, G. J., and Stahl, W. L., 1994, In: Basic Neurochemistry, Siegel, G. J., Agranoff, B. W., Albers, R. N., Molinoff, P. B. (Eds) Raven Press, New York, pp:49–73.

Astrup, J. Sörensen, P. M., and Sörensen, J.R., 1981, Oxygen and glucose consumption related to Na^+, K^+ transport in canine brain, *Stroke* 12:726–730.

Ball, M.J., 1977, Neuronal loss, neurofibrillary tangles and granulovacuolar degeneration In the hippocampus with aging and dementia: A quantitative study, *Acta Neuropath.*, 37: 11–118.

Banati, R.B., Gehrmann, J., and Kreutzberg, G.W., 1996, Early glial reactions to ischemic lesions, *Adv. Neurology*, 71: 329–337.

Barnes, C.A., 1988, Aging and the physiology of spatial memory, *Neurobio. Aging* 9: 563–568.

Barnes, C.A., Nadel, L., and Honig, W.K., 1980, Spatial memory deficits in senescent rats, *Can. J. Psychol.* 34: 29–39.

Baron, J.C., and Marchal, G., 1992, Viellessement cérébral et cardiovasulaire et metabolisme énergétique, cerebral, *Presse Med.* 21: 1231–1237.

Beal, M.F., Hyman, B.T., and Koroshetz, W., 1993, Do defects in mitochondrial metabolism underlie the pathology of neurodegenerative diseases, *TINS* 16: 125–131.

Beatty, W.W., Bierley, R.A., and Boyd, J.G., 1985, Preservation of accurate spatial memory in aged rats, *Neurobiol. Aging* 6: 219–225.

Bennett, C. M., Mlady, G., Fleschner, M., and Rose, G. M., 1996b, Synergy between chronic corticosterone and sodium azide treatments in producing spatial learning deficit and inhibiting cytochrome oxidase activity, *Proc. Natl. Acad. Sci.* 93:1330–1334.

Bennett, M.C., Mlady, G., Kwon, YW, and Rose, G.M., 1996a, Chronic in vivo sodium azide infusion induces selective and stable inhibition of cytochrome c oxidase, *J. Neurochem.* 66: 2606–2611.

Berman, R.F., Goldman, H., and Altman, H.J., 1988, Age-related changes in regional cerebral blood flow and behavior in Sprague-Dawley rats, *Neurobiol Aging* 9: 691–696.

Blass, J.P., 1993, Pathophysiology of Alzheimer Syndrome, *Neurol.* 43: 25–38.

Borowosky, I.W., and Collins, R.C., 1989, Metabolic anatomy of the brain: a comparison of regional capillary density, glucose metabolism, and enzyme activities, *J. Comp. Neurol.* 288: 401–413.

Botel, J. P., Senti, M., Nogues, X., Rubies-Prat, J., Roquer, J., Dolhaberriague, L., and Olive, J., 1992, Lipoprotein and apolipoprotein profile in men with ischemic stroke, *Stroke* 23: 1556–1562.

Brouillet, E., Hyman, B., Jenkins, B. G., and Henshaw, D. R., 1994, Systemic of local administration of azide produces striatal lesions by an-energy-impairment-induced excitotoxic mechanism, *Exp. Neurol.* 129:175–182.

Café, C., Torri, C., Gatti, S., Adinolfi, D., Gaetani, P., Rodriguez,, y Baena, R., and Marzatico, F., 1994, Changes in non-synaptosomal and synaptosomal mitochondrial membrane-linked enzymatic activities after transient cerebral ischemia, *Neurochem. Res.* 19: 1551–55.

Cave, C.B., and Squire, L.R., 1991, Equivalent impairment of spatial and nonspatial memory following damage to the human hippocampus, *Hippocampus* 1: 329–40.

Chagnon, P. Betard, C., Robitaille, Y., Cholette, A., and Gavreau, D., 1995, Distribution of brain cytochrome oxidase activity in various neurodegenerative activities, *Neurorep.* 6: 711–715.

Chandrasekaran, K., Giordano, t., Brady, D. R., Stoll, J., Martin, L. J., and Rapoport, S. I., 1994 Impairment in mitochondrial cytochrome oxidase genes expression in Alzheimer's disease, *Brain Res. Mol. Brain Res.* 24: 336–340.

Chandrasekaran, K., Hatanpaa, K., Brady, D.R., and Rapoport, S.I., 1996, Evidence for physiological down-regulation of brain oxidative phosphorylation in Alzheimer's disease, *Exp. Neurology* 142: 80–88.

Cheng, B., and Mattson, M.P., 1992, Glucose deprivation elicits neurofibrillary tangle-like antigenic changes in hippocampus neurons: prevention by NGF:bFGF, *Exp. Neurol.* 117: 114–123.

Clarke, D. D., and Sokoloff, L., 1994, In: Basic Neurochemistry. G. J. Siegel, B. W. Agranoff, R. W. Albers, P.B. Molinoff, (Eds), Raven Press, New York, pp:645–680.

Colton, C.A., and Gilbert, D.L., 1987, Production of superoxide anion by a CNS macrophage, the microglia, *FEBS Let.* 223: 284–288.

Couderc, R., Mahieux, F., and Bailleul, S., 1994, Apolipoprotein E_4 allele frequency, ischemic cerebrovascular disease and Alzheimer's disease, *Stroke* 24: 1416–1417.

Davignon, J., Gregg, R.E., and Sing, C. F., 1988, Apolipoprotein E polymorphism and atherosclerosis, *Atherosclerosis,* 8: 1–21.

de la Torre, J. C., 1997c, Hemodynamic consequences of deformed microvessels in the brain in Alzheimer's disease, *Ann. N. Y. Acad. Sci.* 826: 75–91

de la Torre, J. C., Butler, K., Kozlowski, P., Fortin, T., and Saunders, J. K., 1995, Correlates between nuclear magnetic resonance spectroscopy, diffusion wighted imaging and CA1 morphometry following chronic brain ischemia, *J. Neurosci. Res.* 41: 238–245.

de la Torre, J. C., and Hachinski, V. (Eds.), 1997, Cerebrovascular Pathology in Alzheimer's Disease, *Ann. N. Y. Acad. Sci.* 826: pp 1–523.

de la Torre, J. C., and Mussivand, T., 1993, Can disturbed brain microcirculation cause Alzheimer's disease?, *Neurol. Res.* 15: 146–153.

de la Torre, J. C., 1994, Impaired brain microcirculation may trigger Alzheimer's disease, *Neurosci. Behav. Res.* 18: 397–401

de la Torre, J. C., Cada, A. E., Nelson, N., Davis, G., Sutherland, R., and Gonzalez-Lima, F., 1997b, Reduced cytochrome oxidase and memory dysfunction after chronic brain ischemia in aged rats, *Neurosci. Lett.*, 223: 165–168.

de la Torre, J. C., 1997a, Cerebromicrovascular pathology in Alzheimer's disease compared to normal aging, *Gerontology*, 43: 26–43.

de la Torre, J. C., and Fortin T., 1994, A chronic physiological rat model of dementia, *Behav. Brain Res.* 63: 35–40.

de la Torre, J.C., Fortin T., Park G.A.S., Pappas B.A., and Richard M.T., 1993, Brain blood flow restoration rescues chronically damaged rat CA1 neurons, *Brain Res.* 623: 6–15.

de la Torre, J.C., Fortin, T., Park, G., and de Socarraz, H., 1992b, Aged but not young rats develop metabolic, memory deficits after chronic brain ischemia, *Neurol. Res.*, 14 Supp.: 177–180.

de la Torre, J.C., Fortin, T., Park, G.A.S., Butler, K.S., Kozlowski, P., Pappas, B.A., de Socarraz, H., Sanders, J.K., and Richard, M.T., 1992a, Chronic cerebrovascular insufficiency induces dementia-like deficits in aged rats, *Brain Res.* 582: 186–195.

de la Torre, J.C., Nelson, N., and Sutherland, R.J., 1996, Pharmacological reversal of memory deficits in aging rats, *J. Neurochem.*, Supp. 2: S11.

de la Torre, J.C., Pappas, B.A., Keyes, M., and Fortin, T., 1996, Progressive neurodegeneration in rat brain after 2-VO or 3-VO. In: *Neurodegenerative diseases*, Plenum Press: NY pp. 74–84.

De Vellis, J., Wu, D.K., and Kumar, S., 1987, Enzyme inductions and regulation of protein synthesis. In: Federoff S, Vernadakis, A. (eds): *Astrocytes*, Vol. 2. Academic Press: NY, p 209–237.

Delacourte, A., 1990, General and dramatic glial reaction in Alzheimer's brains, *Neurol.* 40: 33–37.

DiMattia, B.D., and Kesner, R.P., 1988, Spatial cognitive maps: differential role of parietal cortex and hippocampal formation, *Behav. Neurosci.*, 102: 471–480.

Dimlich, R.V.W., Showers, M.J., and Shipley, M.T., 1990, Densitometric analysis of cytochrome oxidase in ischemic rat brain, *Brain Res.* 516: 181–191.

Ducket, S., 1991, *The Pathology of the Aging Nervous System*, Lea & Febringer, Philadelphia.

Duffy, P.E., and Rapport, M., 1980, Glial fibrillary acidic protein and Alzheimer's-type dementia, *Neurol.* 30: 778–782.

Dunnet, S., 1991, Cholinergic grafts, memory and aging, *TINS*, 14: 371–376.

Eklof, B., and Siesjö, B.K., 1972, The effect of bilateral carotid artery ligation upon the blood flow and the energy state of the rat brain, *Acta Physiol. Scand.*, 86: 155–165.

Erecinska, M., and Silver, I.A., 1989, ATP and brain function, *J. Cerebr. Blood Flow Metab.* 9: 2–19.

Erkinjuntti, T., Haltia, M., Palo, J., Sulkava, R., and Petau, A., 1988, Accuracy of the clinical diagnosis of vascular dementia: a preospective clinical and post-mortem neuropathological study, *J. Neurol. Neurosurg. Psychiat.* 51: 1037–44.

Evans, G., Brennan, P., Skorpanich, M.A., and Held, D., 1984, Cognitive mapping and elderly adults: verbal and location memory for urban landmarks, *J. Geront.*, 39: 452–457.

Fitzgerald, M.J.T., 1985, Neuroanatomy: basic and applied. Balliere Tindall: London.

Flicker, C., Bartus, R.T., Crook, T.H., and Ferris, S.H., 1984, Effects of aging and dementia upon recent visuospatial memory, *Neurobio. Aging* 5: 275–283.

Frederickson, R.C., 1992, Astroglia in Alzheimer's disease, *Neurobiol. Aging*, 14: 239–253.

Frisoni, G., Geroldi, C., Blanchetti, A., Trabucchi, M., Govoni, S., Franceschini, and G., Calabresi, L., 1994, apolipoprotein E_4 allele frequency in vascular dementia and Alzheimer's disease, *Stroke* 25: 1703.

Gibson, B.E., and Peterson, C., 1984, Aging decreases oxidative metabolism and the release and synthesis of acetylcholine, *J. Neurochem.* 37: 978–984.

Ginsberg, M.D., Mela, L., Wrobel-Kuhl, K., and Reivich, M., 1977, Mitochondrial metabolism following bilateral cerebral ischemia in the gerbil, *Ann. Neurology*, 1: 519–527.

Gionet, T.X., Thomas, J.D., Warner, D.S., Goodlet, C.R., Wasserman, E.A., and West, J.R., 1991, Forebrain ischemia induces selective behavioral impairments associated with hippocampal injury in rats, *Stroke* 22: 1040–1047.

Giulian, D., Vaca, K., and Corpuz, M., 1993, Brain glia release factors with opposing actions upon neuronal survival, *J. Neurosci.* 13: 29–37.

Gonzalez-Lima, F., and Garrosa, M., 1991, Quantitative histochemistry of cytochrome oxidase in rat brain, *Neurosci. Lett.* 123: 251–253.

Graham, D., I., Gentleman, S. M., Lynch, A., and Roberts, G. W., 1995, Distribution of beta-amyloid protein in the brain following severe brain injury, *Neuropathol. Appl. Neurobiol.* 21: 27–34.

Grubb, R., Raichle, M., Gado, M., Eichling, J., and Hughes, C., 1977, Cerebral blood flow, oxygen utilization and blood volume in dementia, *Neurol.* 27: 905–910.

Guthrie, P.B., Segal, M., and Kater, S.B., 1991, Independent regulation of calcium revealed by imaging dendritic spines, *Nature* 354: 76–80.

Hall, Z.W., 1992, *An Introduction to Molecular Neurobiology*, Sinauer Ass.: MA.

Hao, C., Guilber, L.J., and Federoff, S., 1990. Production of colony stimulating factor-1 (CSF-1) by mouse astroglia in vitro, *J. Neurosci. Res.* 27: 314–323.

Hevner, R.F., Duff, R.S., and Wong-Riley, M.T.T., 1992, Coordination of ATP production and consumption in brain: parallel regulation of cytochrome oxidase and Na^+,K^+-ATPase, *Neurosci. Lett.* 138: 188–192.

Hoyer, S., 1991, Abnormalities of glucose metabolism in Alzheimer's disease, *Ann. New York Acad. Sci.* 640: 53–58.

Hoyer, S., 1990, Brain glucose and energy metabolism during normal aging, *Aging* 2: 245–258.
Hoyer, S., and Krier, C., 1986, Ischemia and the aging brain: studies on glucose and energy metabolism in rat cerebral cortex, *Neurobio Aging* 7: 23–29.
Hoyer, S., 1996, Oxidative metabolism deficiencies in brains of patients with Alzheimer's disease, *Acta Neurol. Scand.* Supp. 165: 18–24.
Hsu, M., and Buzsake, G., 1993, Vulnerability of mossy fiber targets in the rat hippocampus to forebrain ischemia, *J. Neurosci.* 13: 3964–3979.
Ingram, D.K., London, E.D., and Goodrick, C.L., 1981, Age and neurochemical correlates of radial maze performances in rats, *Neurobiol. Aging*, 2: 41–47.
Inoue, N., Korematsu, K., Oyama, T., Yamada, K., Nagahiro, S., and Ushio, Y., 1996, Cytochrome oxidase activity during acute focal ischaemia in rat brain, *Acta Neurochir.* 138: 1126–1131.
Ishimaru, H., Takahashi, A., Ikarashi, Y., and Maruyama, Y., 1995, Pentobarbital protects against CA1 pyramidal cell death but not dysfunction of hippocampal cholinergic neurons following transient ischemia, *Brain Res.* 673: 112–118.
Jaspers, R.M.A., Block, F., Heim, C., and Sontag, K.H., Spatial learning is affected by transient occlusion of common carotid arteries (2VO): comparison of behavioral and histopathological changes after 2VO and four-vessel-occlusion in rats, *Neurosci. Lett.* 117: 149–53.
Jendroska, K., Cervos-Navarro, J., and Poewe, W., 1993, Deposition of beta-amyloid associated with cerebral hypoxia, *Clin. Neuropathol.* 12: 252.
Jones, T.H., Morawetz, R.B., Crowell, R.M., Marcoux, F.W., Fitzgibbon, S.J., De Girolami, U., and Ojemann, R.G., 1981, Thresholds of focal cerebral ischemia in awake monkeys, *J. Neurosurg.* 54: 773–782.
Jun, C.D., Choi, B.M., Kim, H.M., and Chung, H.T., 1995, Involvement of protein kinase C during taxol-induced activation of murine peritoneal macrophages, *J. Immunol.* 154: 6541–7.
Kalaria, R.N., Cohen. D.L., and Premkumar, R.D., 1996, Apolipoprotein E alleles and brain vascular pathology in Alzheimer's disease, *Ann. N.Y. Acad. Sci.* 777: 266–271.
Kalaria, R.N., 1992, The blood-brain barrier and cerebral microcirculation, *Cerebrovasc. Brain Met. Rev.*, 4: 226–260.
Kaplan, B., Brint, S., Tanabe, J., Jacewicz, M., Wang, X-J, and Pulsinelli, W., 1991, Temporal thresholds for neocortical infarction in rats subjected to reversible focal cerebral ischemia, *Stroke*, 22: 1032–39.
Kettenmann, H., and Ransom, B.R., (ed.), 1995, *Neuroglia*, Oxford Press: New York.
Kirino, T., 1982, Delayed neuronal death in the gerbil hippocampus, *Brain Res.* 239: 57–69.
Kish, S.J., Bergeron, C., Rajput, A., Dozic, S., Mastrogia-Como, F., Chang, L.J., Wilson, J.M., and Distefano, L. M., Nobrega, J. N., 1992, Brain cytochrome oxidase in Alzheimer's disease, *J. Neurochem.* 59: 776–779.
Kish, S.J., Bergeron, C., Rajput, A., Dozic, S., Mastrogiacomo, F., Chang, L-J., Wilson, J.M., DiStefano, L.M., and Nobrega, J.N., 1992, Brain cytochrome oxidase in Alzheimer's disease, *J. Neurochem.* 59: 776–779.
Kitagawa, K., Matsumoto, M., Niinobe, M., Mioshiba, K., Hata, R., Ueda, H., Handa, N., Fukunaga, R., Isaka, Y., Kimura, K., and Kamada, T., 1989, Microtubule-associated protein 2 as a sensitive marker for cerebral ischemic damage-immunohistochemical investigation of dendritic damage, *Neuroscience*, 31: 401–411.
Kiyota, Y., Miyamoto, M., and Nagaoka, A., 1991, Relationship between brain damage and memory impairment in rats exposed to transient forebrain ischemia, *Brain Res.* 538: 295–302.
Kluver, H., and Bucy, P.C., 1939, Preliminary analysis of function of the temporal lobes in monkeys, *Arch. Neurol.Psychiat.* 42: 979–1000.
Konigsmark, B.E., Murphy, E.A., 1970, Neuronal populations in the human brain, *Nature* 228: 1335–36.
Kosunen, O., Talasniemi, S., and Lehtovirta M., 1995, Relation of coronary artherosclerosis and apolipoprotein E genotypes in Alzheimer's disease, *Stroke* 26(5): 743–748.
Krebs, H.A., Williamson, D.H., Bates, M.W., Page, M.A., and Hawkins, R.A., 1971, The role of ketone bodies in caloric homeostasis, *Adv. Enzyme Reg.* 9: 3880–3883.
Kudo, T., Tada, K., Takeda, M., and Nishimura, T., 1990, Learning impairment and microtubule-associated protein 2 decreases in gerbils under chronic cerebral hypoperfusion, *Stroke*, 21: 1205–1209.
Landfeld, P.W., Hippocampal neurobiological mechanisms of age-related memory dysfunction, *Neurobiol. Aging*, 9: 571–579.
Lassen, N.A., and Ingvar, D.H., 1980, Blood flow studies in the aging normal brain and in senile dementia, in Amaducci, L., Davison, A.N., Antuono, P., (eds): Aging of the Brain and Dementia. Raven Press: New York pp. 91–98.
Linville, D.G., and Arneri, S.P., 1991, Cortical cerebral blood flow governed by the basal forebrain: age-related impairments, *Neurobiol. Aging* 12: 503–510.
Marcus, D. L., de Leon, M., Goldman, J., Logan, J., Christman, D., Wolf, A., Fowler, J., Hunter, K., Tsai, J., Pearson, J., and Freedman, M.L., 1989, Altered glucose metabolism in microvessels from patients with Alzheimer's disease, *Ann. Neurol.* 26: 91–94.

Markesberry, W. R., 1997, Oxidative stress hypothesis in Alzheimer's disease, *Free Rad. Biol. Med.* 23: 134–147.

Mattson, M. P., 1997, Advances fuel Alzheimer's conundrum, *Nature Gen.* 17: 254–256.

Mayberg, T.S., Lam, A.M., Matta, B.F., Domino, K.B., and Winn, H.R., 1995, Ketamine does not increase cerebral blood flow velocity or intracranial pressure during isoflurane/nitrous oxide anesthesia in patients undergoing craniotomy, *Neurosurg. Anesth.* 81: 84–89.

McGrail, K.M., Phillips, J.M., and Sweadner, K.J., 1991, Immunoflourescent localization of three Na,K-ATPase isozymes in the rat central nervous system: both neurons and glia can express more than one Na,K-ATPase, *J. Neurosci.*, 11: 381–391.

Meier-Ruge, W., Bertoni-Freddari C., and Iwangoff, P., 1994, Changes in brain glucose metabolism as a key to the pathogenesis of Alzheimer's disease, *Gerontol.* 40: 246–252.

Meier-Ruge, W., and Bertoni-Freddari, C., 1996, The significance of glucose turnover in the brain in the pathogenetic mechanisms of Alzheimer's disease, *Rev. in Neurosci.* 7: 1–19.

Milner, B., 1974, Hemispheric specialization: scope and limits. In F.O. Schmitt & F.G. Worden (Eds.), *The Neurosciences: Third study program,* MIT Press: Cambridge, pp. 75–89.

Miyazawa, T., Bonnekoh, P., and Hossman, K.A., 1993, Temperature effect on immunostaining of microtubule-associated protein 2 and synatpophysin after 30 minutes forebrain ischemia in rat, *Acta Neuropath,*85(5): 526–32.

Morris, R.G.M., 1984, Developments of a water maze procedure for studying spatial learning in the rat, *J. Neurosci. Meth.* 11: 47–60.

Murphy, S., 1993, *Astrocytes: Pharmacology and function*, Academic Press: NY.

Mutisya, E.M., Bowling, A.C., and Beal, M.F., 1994, Cortical cytochrome oxidase activity is reduced in Alzheimer's disease, *J. Neurochem.* 63: 2179–2184.

Nagata, K. Buchan, R. J., Yokoyama, E., Kondoh, Y., Sato, M., Terashi, H., Satoh, Y., Watahiki, Y., Senova, M., Hirata, Y., and Hatazawa, J., 1997, Misery perfusion with preserved vascular reactivity in Alzheimer's disease, *Ann. N. Y. Acad. Sci.* 826: 272–281.

Nakahara, I., Kikuchi, H., Taki, W., Nishi, S., Kito, M., Yonekawa, Y., Goto, Y., and Ogata, N., 1991, Degradation of mitochondrial phospholipids during experimental cerebral ischemia in rats, *J. Neurochem.* 57: 839–844.

Ni, J-W., Matsumoto, K., Li, H-B., Murakami, Y. and Watanabe, H., 1995, Neuronal damage and decrease of central acetylcholine level following permanent occlusion of bilateral common carotid arteries in rat, *Brain Res.* 673: 290–296.

Ni, J-W., Ohta, H., Matsumoto, K., and Watanabe, H., 1994, Progressive cognitive impairment following chronic cerebral hypoperfusion induced by permanent occlusion of bilateral carotid arteries in rats, *Brain Res.* 653: 231–36.

Obrist, W.D., Chivian, E., Cronquist, S., and Ingvar, D.H., 1970, Regional cerebral blood flow in senile and presenile dementia, *Neurol.* 20: 315–22.

Ohata, M., Sundaram, U., Fredericks, W.R., London, E.D., and Rapoport, S.I., 1981, Regional cerebral blood flow during development and ageing of the rat brain, *Brain* 104: 319–332.

Olsen, G.M., Scheel-Kruger, J., Moller, A., and Jensen, L.H., 1994, Does neuronal damage of CA1 related to spatial memory performance of rats subjected to transient forebrain ischemia, *Acta Neurol. Scand.* 89: 204–209.

Olton, D.S., and Papas, B.C., 1979, Spatial memory and hippocampal function. *Neuropsychologia,* 17: 669–682.

Ordy, J.M., Thomas, G.J., Volpe, B.T., Dunlap, W.P., and Colombo, P.M., 1988, An animal model of human-type memory loss based on aging, lesion, forebrain ischemia, and drug studies with the rat, *Neurobiol. Aging*, 9: 667–683.

Owen, O.E., Morgan, A.P., Kemp, H.G., Sullivan, J.M., Herrara, M.G., and Cahill, G.F. Jr., 1967, Brain metabolism during fasting, *J. Clin. Invest.* 46: 1589–1595.

Ozawa, K., Seta, K., Araki, H., and Handa, H., 1967, The effect of ischemia on mitochondrial metabolism, *J. Biochem.* 61: 512–514.

O'Keefe, J., and Nadel, L., 1978, The hippocampus as a cognitive map. Oxford University Press: London.

Papez, J.W., 1937, A proposed mechanism of emotion, *Arch. Neurol. Psychiat.* 38: 725–743.

Pappas, B.A., de la Torre, J.C., Davidson, C., Keyes, M., and Fortin, T., 1996, Chronic reductions of cerebral blood flow in the adult rat: Late emerging CA1 cell loss and memory function, *Brain Res.* 708: 50–58.

Park, J.S., Bateman, M.C., and Goldberg, M.P., 1996, Rapid alterations in dendrite morphology during sublethal hypoxia or glutamate receptor activation, *Neurobio. Disease*, 3: 215–227.

Parker, W.D., Jr., Filley, C.M., and Parks, J.K., 1990, Cytochrome oxidase deficiency in Alzheimer's disease, *Neurol.* 40: 1302–1303.

Parker, W.D., Jr., Parks, J., Filley, C.M., and Klein-Schmidt-Demasters, B.K., 1994, Electron transport chain defects in Alzheimer's disease brain, *Neurol.* 44: 1090–1096.

Patel, M.S., 1977, Age-dependent changes in oxidative metabolism in rat brain, *J. Geront.* 32: 643–646.

Perry, E.K., 1986, The cholinergic hypothesis: 10 years on, *Brain Med. Bull.* 42: 63–69.

Petito, C.K., Morgello, S., Felix, J.C., and Lesser, M.L., 1990, The two patterns of reacitve astrocytosis in postischemic rat brain, *J. Cerebr. Blood Flow*, 10: 850–859.

Pulsinelli, W.A., Brierley, J.B., and Plum, F., 1982, Temporal profile of neuronal damage in a model of transient forebrain ischemia, *Ann. Neurol.*, 11: 491–498.

Rasmusson, D.X., Brandt, J., Martin, D.B., and Folstein, M.F., 1995, Head injury as a risk factor in Alzheimer's disease, *Brain Injury* 9: 213–219.

Roberts, G.W., Gentleman, S.M., Lynch, A., Murray, L., Landon, M., and Graham, D.I., 1994, Beta amyloid protein depostion in the brain after severe head injury: Implications for the pathogenesis of Alzheimer's disease, *J. Neurol. Neurosurg. Psychiatry* 57: 419–425.

Rogers, R.L., Meyer, J.S., Mortel, K.F., Mahurin, R.K., and Judd, B.W., 1986, Decreased cerebral blood flow precedes multiinfarct dementia, but follows senile dementia of Alzheimer's type, *Neurol.* 36: 1–6.

Saunders, A.M., Strittmatter, W.J., and Schmechel, D., 1993, Association of apolipoprotein E allele e4 with late-onset familial and sporadic Alzheimer's disease, *Neurol.* 43: 1467–1472.

Schmidt-Kastner, E., Fliss, H., and Hakim, A.M., 1997, Subtle neuronal death in striatum after short forebrain ischemia in rats detected by in situ end-labeling for DNA damage, *Stroke* 28: 163–170.

Sekhon, L.H.S., Morgan, M.K., Spence, I., Weber, N.C., 1994, Chronic cerebral hypoperfusion and impaired neuronal function in rats, *Stroke* 25: 1022–27.

Sekhon, L.H.S., Spence, I., Morgan, M.K., and Wever, N.C., 1997, Chronic cerebral hypoperfusion inhibits calcium-induced long-term potentiation in rats, *Stroke* 28: 1043–1048.

Selmen, W.R., Crumrine, R.C., Ricci, A.J., LaManna, J.C., Ratcheson, R.A., and Lust, W.D., 1990, Impaired metabolic recovery with increasing periods of middle cererbral artery occlusion in rats, *Stroke* 21: 467–71.

Shaw T.G., Mortel K.F., Meyer J.S., Rogers R.L., Hardenberg J., and Cutaia M.M., 1984, Cerebral blood flow changes in benign aging and cerebrovascular disease, *Neurol.* 34: 855–862.

Siesjö, B.K., 1978, *Brain energy metabolism*, John Wiley & Sons, New York.

Simonian, N.A., and Hyman, B.T., 1995, Functional alterations in neural circuits in Alzheimer's disease, *Neurobiol. Aging* 16: 305–309.

Simonian, N.A., and Hyman, B.T., 1994, Functional alterations in Alzheimer's disease: Selective loss of mitochondrial-encoded cytochrome oxidase mRNA in the hippocampal formation, *J Neuropath. Exp. Neurol.* 53: 508–512.

Sims, N. R., 1996, Energy metabolism, oxidative stress and neuronal degeneration in Alzheimer's disease, *Neurodegeneration* 5: 435–440.

Smith, D.H., Okiyama, K., Thomas, M.J., Claussen, B., and McIntosh, T.K., 1991, Evaluation of memory dysfunction following experimental brain injury using the Morris water maze, *J. Neurotrauma* 8: 259–269.

Smith, M.L., 1988, Recall of spatial location by the amnesic patient H. M., *Brain Cog.* 7: 178–183.

Sonsalla, P.K., Manzino, L., Sinton, C.M., Liang, C.L., German, D.C., and Zeevalk, G.D., 1997, Inhibition of striatal energy metabolism produces cell loss in the ipsilateral substantia nigra, *Brain Res.* 773: 223–226.

Sparks, D.L., Hunsaker, J.C., Scheff, S., Kryscio, R., Henson, J.L., and Markesberry, W.R., 1990, Cortical senile plaques in coronary artery disease, aging and Alzheimer's disease. *Neurobiol. Aging* 11: 601–607.

Squire, L.R., Shimamaru, A.P., and Amaral, D.G., 1986, *Memory and hippocampus*, In Neural Models of Plasticity, Byrne, J., Berry, W., (eds), Academic Press: New York pp. 208–239.

Sutherland, R.J., Wishaw, I.Q., and Kolb, B., 1988, Contributions of the cingulate cortex to two forms of spatial learning and memory, *J. Neurosci.* 8: 1863–1872.

Swerdlow, R., Marcus, D.L., Landman, J., Kooby, D., Frey, W., and Freedman, M.L., 1993, Brain glucose metabolism in Alzheimer's disease, *Amer. J. Med. Sci.* 308: 141–144.

Symon, L., Pasztor, E., and Branston, N.M., 1974, The distribution and density of reduced cerebral blood flow following acute middle cerebral artery occlusion: An experimental study by the technique of hydrogen clearance in baboons, *Stroke* 5: 355–364.

Szatkowski, M., and Attwell, D., 1994, Triggering and execution of neuronal death in brain ischaemia: two phases of glutamate release by different mechanisms, *TINS*, 17: 359–365.

Tachibana, H., Meyer, J.S., Kitagawa, Y., Rogers, R.L., Okayasu, H., and Mortel, K.F., 1984, Effects of aging on cerebral blood flow in dementia compared to normals, *J. Am. Geriatr. Soc.* 32: 114–120.

Tachibana, H., Meyer, J.S., Okayasu, H., Shaw, T.G., Kandula, P., and Rogers, R.L., 1984, Xenon contrast CT-CBF scanning of the brain differentiates normal age-related changes from multi-infarct dementia and senile dementia of Alzheimer's type, *J. Geron.* 39: 415–23.

Tanaka, K., Ogawa, N., Asanuma, M., Kondo, Y., and Nomura, M., 1996, Relationship between cholinergic dysfunction and discrimination learning disabilities in Wistar rats following chronic cerebral hypoperfusion, *Brain Res.* 729: 55–65.

Terry, R.D., and Wisniewski, H.M., 1972, *Ultrastructure of senile dementia and of experimental analogs*, In: Aging and the Brain, ed.: Gaitz, C. M., Raven Press: New York 89–116.

Tsuchiya, T., Sako, K., Yura, S., and Yonemasu, Y., 1992, Cerebral flood flow and histopathological changes following permanent bilateral carotid artery ligation in Wistar rats, *Exp. Brain Res.* 89: 87–92.

Tsuchiya, T., Sako, K., Yura, S., and Yonemasu, Y., 1993, Local cerebral glucose utilisation following acute and chronic bilateral carotid artery ligation in Wistar rats: relation to changes in local cererbral blood flow, *Exp. Brain Res.* 95: 1–7.

Van Hoesen, G.W., and Hyman, B., 1990, Hippocampal formation: anatomy and patterns of pathology in Alzheimer's disease, *Progr. Brain Res.* 83: 445–447.

Venarucci, D., 1994, ApoE phenotype in atheromatous plaques, *Stroke* 25: 2296–2297.

Vibulsreth, S., Hefti, F., Ginsberg, M.D., Dietrich, W.D., and Busto, R., 1987, Astrocytes protect cultured neurons from degeneration induced by anoxia, *Brain Res.* 422: 303–311.

Wakiti, H., Tomimoto, H., and Kimaru, J., 1994, Glial activation and white matter changes in rat brain induced by chronic cerebral hypoperfusion, *Acta Neuropath.* 87: 484–492.

Williams, J.H., Errington, M.L., Lynch, M.A., and Bliss, T.V.P., 1989, Arachidonic acid induces a long-term activity-dependent enhancement of synaptic transmission in the hippocampus, *Nature*, 341: 739–742.

Wisniewski, H.M., and Terry, R.D., 1973, Morphology of the aging brain, human and animal, *Prog. Brain Res.* 40: 167–186.

Wong-Riley, M.T.T., 1989, Cytochrome oxidase: an endogenous metabolic marker for neuronal activity, *TINS* 12: 94–101.

Yager, J.Y., Shuaib, A., and Thornill, J., 1996, The effect of age on susceptibility to brain damage in a model of global hemispheric hypoxia-ischemia, *Brain Res. Dev. Brain Res.* 93: 143–154.

Yamaguchi, F., Meyer, J.S., Yamamoto, M., Sakai, F., and Shaw, T., 1980, Noninvasive regional cerebral blood flow measurements in dementia, *Arch. Neurol.* 37: 410–8.

Zemcov, A., Risberg, J. Barclay, L.L., and Blass, J.P., 1984, Diagnosis of Alzheimer's dementia and multi-infarct dementia by rCBF compared to clinical classification, *Monogr. Neural Sci.* 2: 104–6.

Zola-Morgan, S., Squire, L.R., and Amaral, D.G., 1986, Human amnesia and the medial temporal region: Enduring memory impairment following a bilateral lesion limited to the CA1 field of the hippocampus, *J. Neurosci.* 6: 2950–2967.

Zola-Morgan, S., Squire, L.R., and Amaral, D.G., 1989, Lesions of the hippocampal formation but not lesions of the fornix or the mammillary nuclei produce long-lasting memory impairment in monkeys, *J. Neurosci.* 9: 898–913.

Zola-Morgan, S., and Squire, L.R., 1986, Memory impairment in monkeys following lesions limited to the hippocampus, *Behav. Neurosci.* 100: 155–160.

10

CYTOCHROME OXIDASE ATLAS OF RAT BRAIN

F. Gonzalez-Lima and A. Cada

Institute for Neuroscience and Department of Psychology
The University of Texas at Austin
Mezes 330
Austin, Texas 78712

ABSTRACT

This is an atlas of cytochrome oxidase activity in the rat brain made with sections stained with our quantitative histochemical method, and adjacent sections stained with cresyl violet. We used a fresh-frozen brain, without perfusion-fixation, from an adult hooded male rat. Bregma coordinates and brain structures are identified for each of fourteen Bregma levels in the coronal plane.

1. INTRODUCTION

Although various papers beautifully illustrate cytochrome oxidase stained sections of the rat brain (e.g. Harley & Bielajew, 1992; Hevner *et al.*, 1995), there is no atlas based on our quantitative histochemical method (Gonzalez-Lima & Cada, this volume). The present atlas was designed to fulfill this need. This is important because in our quantitative method, but not in others reported in the literature, the levels of enzymatic activity of both gray and white matter regions have been shown to be linearly proportional to the staining intensity of fresh-frozen brain sections.

2. METHODS

The subject was a male black-hooded rat (Long-Evans) weighing 200 g. The same procedures explained in our chapter in this volume were used. Adjacent sections were stained with cresyl violet, digitized, and labeled as a guide for the identification of the anatomical structures (Table 1). A fresh-frozen brain was used to avoid the heterogeneous inhibition of cytochrome oxidase activity caused by perfusion-fixation (Chalmers and Edgerton, 1989). In addition, the figures show Bregma coordinates for a comprehensive series of levels based on the convenient flat-skull position used in the popular atlas of Paxinos and Watson (1986).

Cytochrome Oxidase in Neuronal Metabolism and Alzheimer's Disease,
edited by Gonzalez-Lima, Plenum Press, New York, 1998.

Table 1. List of abbreviations and Bregma coordinates of brain structures labeled in the atlas

Abbreviation	Structure	Bregma	Abbreviation	Structure	Bregma
A17	Area 17	−6.3	LVPO	Lateroventral periolivary nucleus	−9.8
A18	Area 18	−6.3	M5	Motor trigeminal nucleus	−9.8
A18a	Area 18a	−6.3	MeA	Medial amygdaloid nucleus	−2.3
AA	Anterior amygdaloid area	−1.3	MD	Medial dorsal thalamic nucleus	−2.3
ac	Anterior commissure	−0.3	MFr	Medial frontal cortex	3.7
Acb	Accumbens nucleus	0.7	MGD	Medial geniculate nucleus-dorsal	−6.04
ACg	Anterior cingulate cortex	0.7	MGM	Medial geniculate nucleus-medial	−6.04
AD	Anterodorsal thalamic nucleus	−1.3	MGV	Medial geniculate nucleus-ventral	−6.04
AO	Anterior olfactory nucleus	3.7	ml	Medial lemniscus	−4.8
APar	Anterior parietal cortex	−0.3	MR	Medullary reticular nucleus	−13.3
APD	Anterior pretectal area-dorsal	−4.8	MS	Medial septum	0.7
APV	Anterior pretectal area-ventral	−4.8	MSO	Medial superior olivary nucleus	−9.8
Aud	Auditory cortex	−6.04	mt	Mammillothalamic tract	−2.3, −3.8
AV	Anterior ventral thalamic nucleus	−1.8	MVPO	Medioventral periolivary nucleus	−9.8
BlA	Basolateral amygdaloid nucleus	−2.3	oc	Optic chiasm	−0.3
CA1	Field CA1 of hippocampus	−3.8, −6.04	ot	Optic tract	−1.8
CA2	Field CA2 of hippocampus	−6.04	P5	Principal sensory trigeminal nucleus	−9.8
CA3	Field CA3 of hippocampus	−3.8, −6.04	Par1	Parietal cortex 1	−2.3
CbV1–6	Cerebellar vermis lobules 1–6	−9.8	Par2	Parietal cortex 2	−2.3
CbV7–10	Cerebellar vermis lobules 7–10	−13.3	pc	Posterior commissure	−4.8
CbH	Cerebellar hemisphere	−9.8	PCg	Posterior cingulate cortex	−2.3
CeA	Central amygdaloid nucleus	−2.3	Per	Perirhinal cortex	−2.3, −3.8
CG	Central gray	−6.3	Pf	Parafascicular thalamic nucleus	−3.8
Cl	Centraolateral thalamic nucleus	−2.3	PoA	Lateral preoptic area	−0.3
CL	Claustrum	−0.3	Pp	Prepyriform cortex	−3.8
Cm	Centromedial thalamic nucleus	−2.3	PPa	Posterior parietal cortex	−3.8
CN3	Nucleus of cranial nerve 3	−6.3	PRC	Pontine reticular nucleus-caudal	−9.8
CN7	Nucleus of cranial nerve 7	−11.3	PRO	Pontine reticular nucleus-oral	−8.3
CN12	Nucleus of cranial nerve 12	−13.3	Psub	Presubiculum	−6.04
cp	Cerebral peduncle	−4.8	pt	Pyramidal tract	−11.3
CPc	Caudal caudate-putamen	−3.8	Pt	Paratenial thalamic nucleus	−1.3
CPr	Caudate putamen-rostral	−0.3	Pv	Paraventricular thalamic nucleus	−2.3
DC	Dorsal cochlear nucleus	−11.3	PvHm	Paraventricular hypothalamic nu, magnocellular	−1.8
DG	Dentate gyrus	−3.8	PvHp	Paraventricular hypothalamic nu, parvocellular	−1.8

DLG	Dorsal lateral geniculate nucleus	−4.8
DpCb	Deep cerebellar nucleus	−11.3
DpMe	Deep mesencephalic nucleus	−6.3
DPO	Dorsal periolivary nucleus	−9.8
Ent	Entorhinal cortex	−4.8
f	Fornix	−0.3, −2.3
fr	Fasciculus retroflexus	−4.8
Fl	Flocculus	−9.8
Gp	Globus pallidus	−0.3
Hb	Lateral habenula	−3.8
HDB	Horizontal diagonal band	−0.3
ic	Internal capsule	−1.3, −1.8
ICC	Inferior colliculus nucleus-central	−8.3
ICD	Inferior colliculus nucleus-dorsal	−8.3
ICE	Inferior colliculus nucleus-external	−8.3
icp	Inferior cerebellar peduncle	−11.3
Ins	Insular cortex	0.7
IO	Inferior olivary nucleus	−13.3
Ip	Interpeduncular nucleus	−6.3
lfp	Longitudinal fasciculus pons	−8.3
LFr	Lateral frontal cortex	3.7
LH	Lateral hypothalamic area	−1.3
LLD	Lateral lemniscus nucleus-dorsal	−8.3
LLV	Lateral lemniscus nucleus-ventral	−8.3
LOT	Lateral olfactory tract nucleus	−1.3
LP	Lateral posterior thalamic nucleus	−3.8
LS	Lateral septum	0.7
LSO	Lateral superior olivary nucleus	−9.8
Re	Reuniens thalamic nucleus	−1.8
Red	Red nucleus	−6.3
Ret	Reticular thalamic nucleus	−1.3
rs	Rubrospinal tract	−8.3
Rs	Retrosplenial cortex	−6.04, −6.3
S5	Sensory root trigeminal nerve	−9.8
SCDp	Superior colliculus-deep layers	−6.3
SCH	Suprachiasmatic hypothalamic nucleus	−1.3
SCSu	Superior colliculus-superficial	−6.3
SFr	Sulcal frontal cortex	3.7
Sol	Solitary tract	−13.3
sp5	Spinal tract trigeminal nerve	−11.3
SPN	Superior paraolivary nucleus	−9.8
SOH	Supraoptic hypothalamic nucleus	−1.3
Sth	Subthalamic nucleus	−3.8
ST	Spinal trigeminal nucleus	−13.3
Sub	Subiculum	−6.04
TB	Trapezoid body nucleus	−9.8
VBL	Ventral basal thalamic nucleus-lateral	−2.3, −3.8
VBM	Ventral basal thalamic nucleus-medial	−2.3, −3.8
VCA	Ventral cochlear nucleus-anterior	−9.8
VCP	Ventral cochlear nucleus-posterior	−11.3
VDB	Vertical diagonal band	0.7
Ve	Vestibular nucleus	−11.3
VMH	Ventral medial hypothalamic nucleus	−2.3
VTA	Ventral tegmental area	−4.8, −6.3
Zi	Zona incerta	−3.8

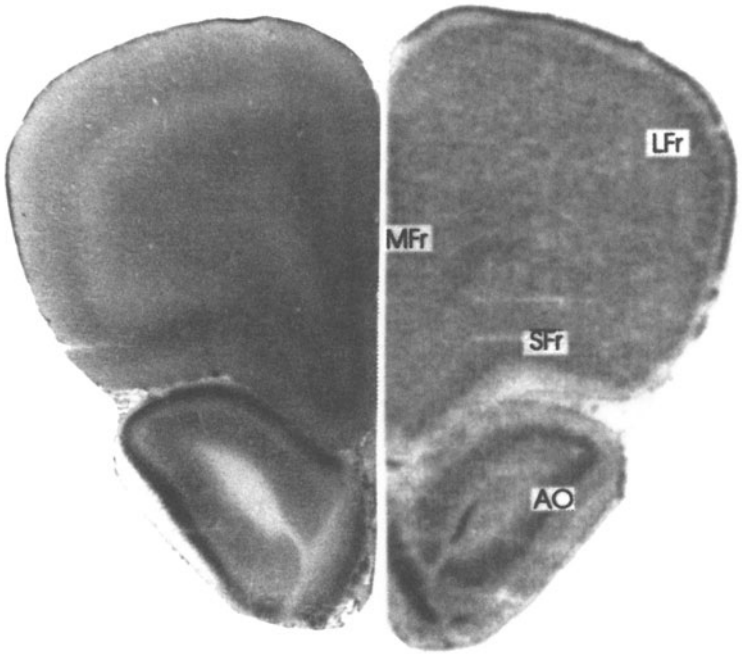

Bregma 3.7 mm

AO anterior olfactory nu
LFr lateral frontal cortex
MFr medial frontal cortex
SFr sulcal frontal cortex

Figure 1.

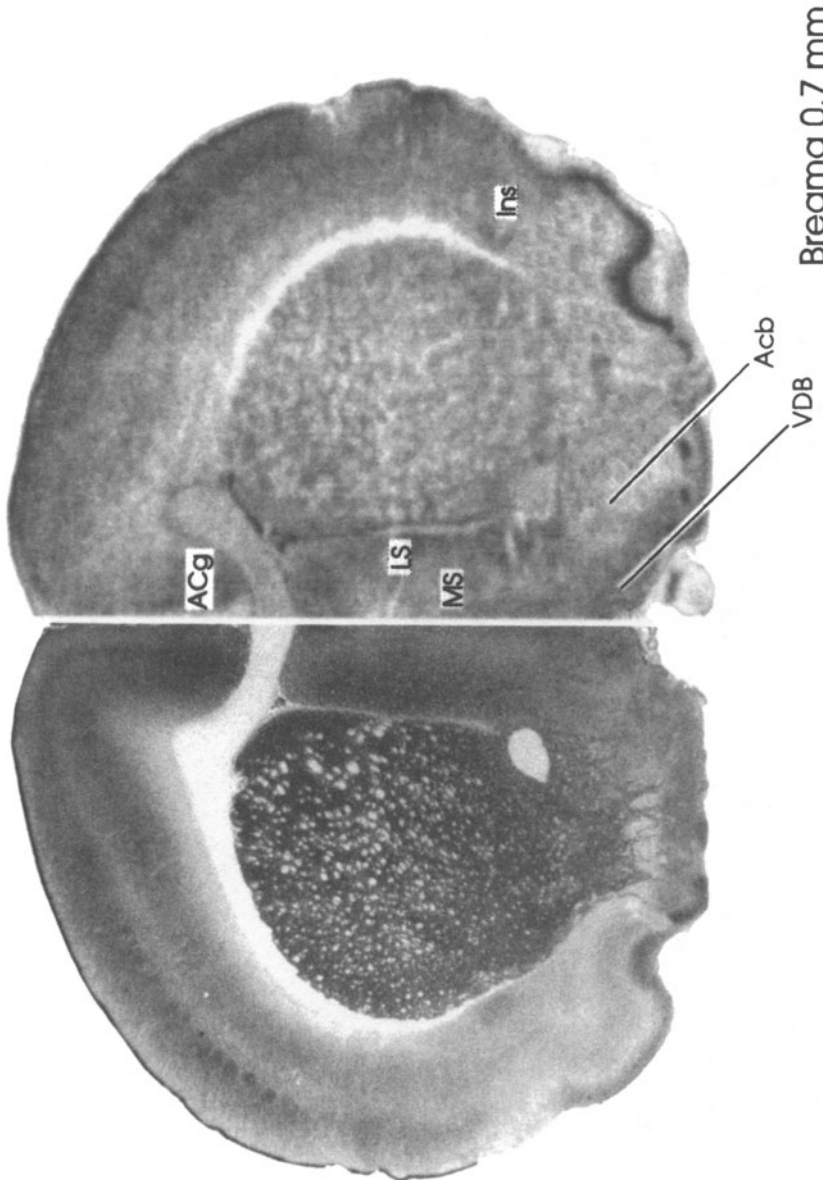
ACg
LS
MS
Ins
Acb
VDB
Bregma 0.7 mm
Acb accumbens nu
ACg anterior cingulate cortex
Ins insular cortex
LS lateral septum
MS medial septum
VDB vertical diagonal band nu

Figure 2.

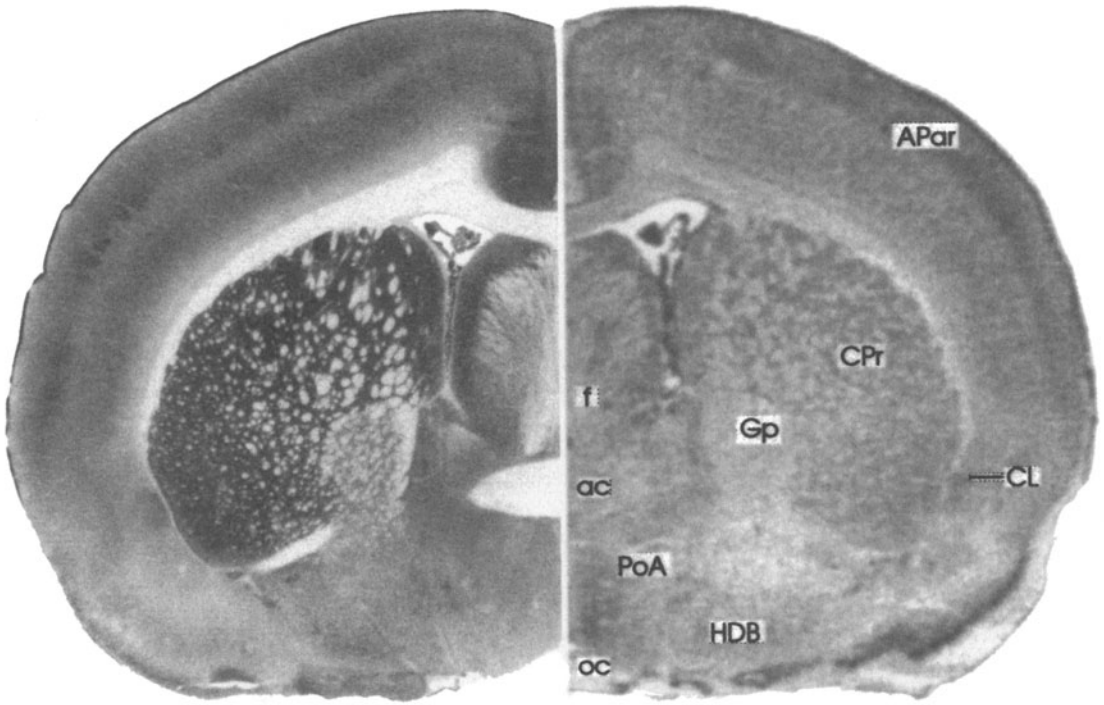

Bregma -0.3 mm

ac anterior comimissure
APar anterior parietal cortex
CPr caudate putamen-rostral
Cl claustrum
f fornix
Gp globus pallidus
HDB horizontal diagonal band
oc optic chiasm
PoA lateral preoptic area

Figure 3.

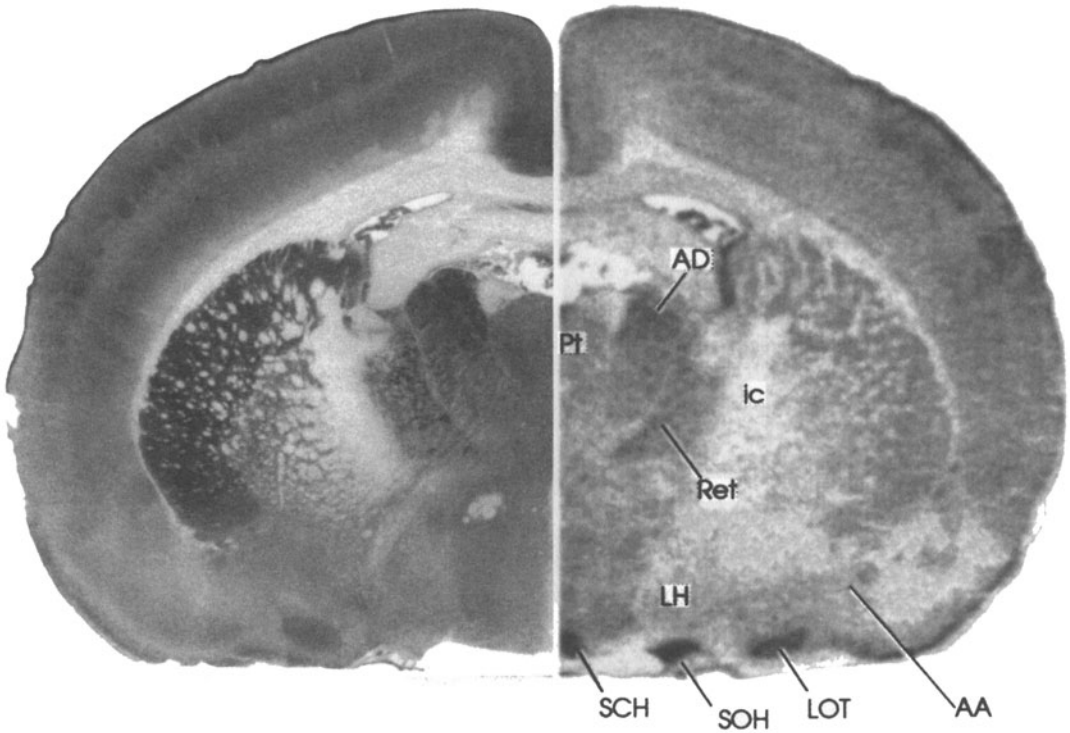

Bregma -1.3 mm

AA anterior amygdaloid area
AD anterodorsal thalamic nu
ic internal capsule
LH lateral hypothalamic area
LOT Lateral olfactory tract nu
Pt paratenial thalamic nu
Ret reticular thalamic nu
SCH suprachiasmatic hypothalamic nu
SOH supraoptic hypothalamic nu

Figure 4.

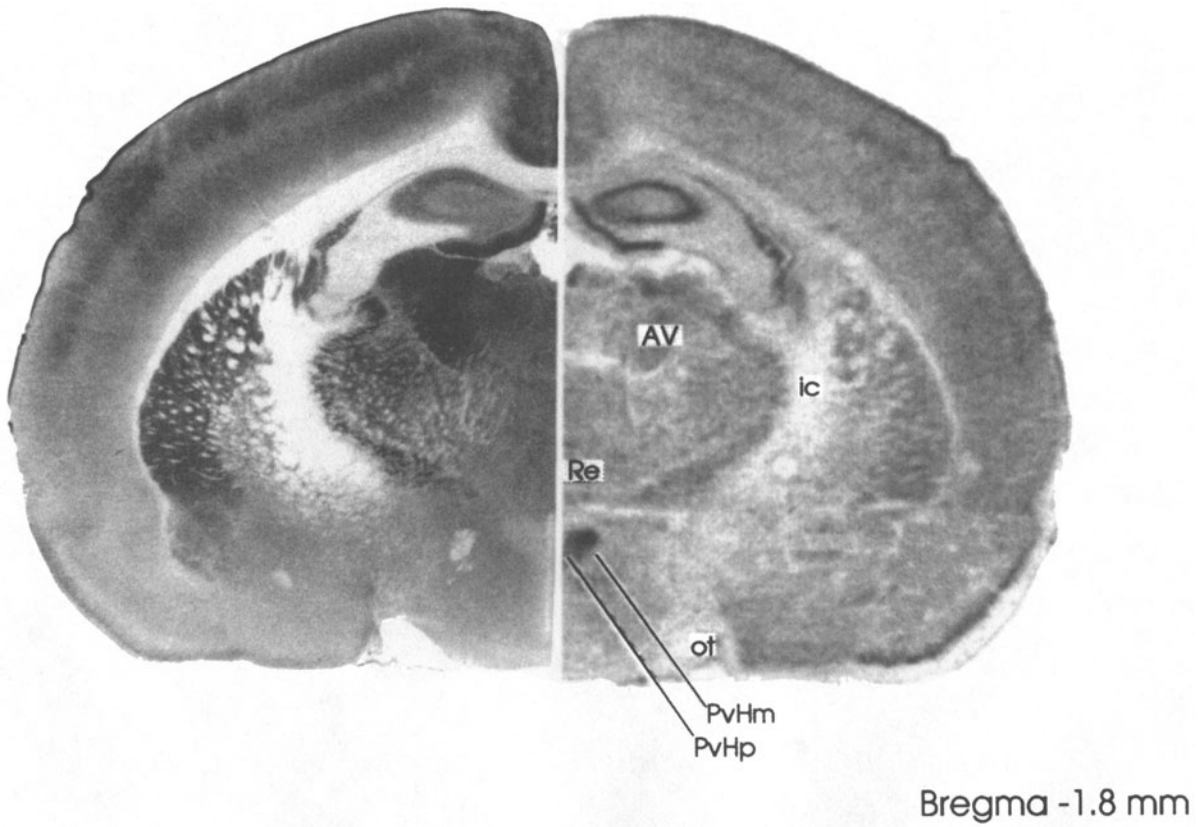

AV anterior ventral thalamic nu
ic internal capsule
ot optic tract

PvHm paraventricular hypothalamic nu, magnocellular
PvHp paraventricular hypothalamic nu, parvocellular
Re reuniens thalamic nu

Figure 5.

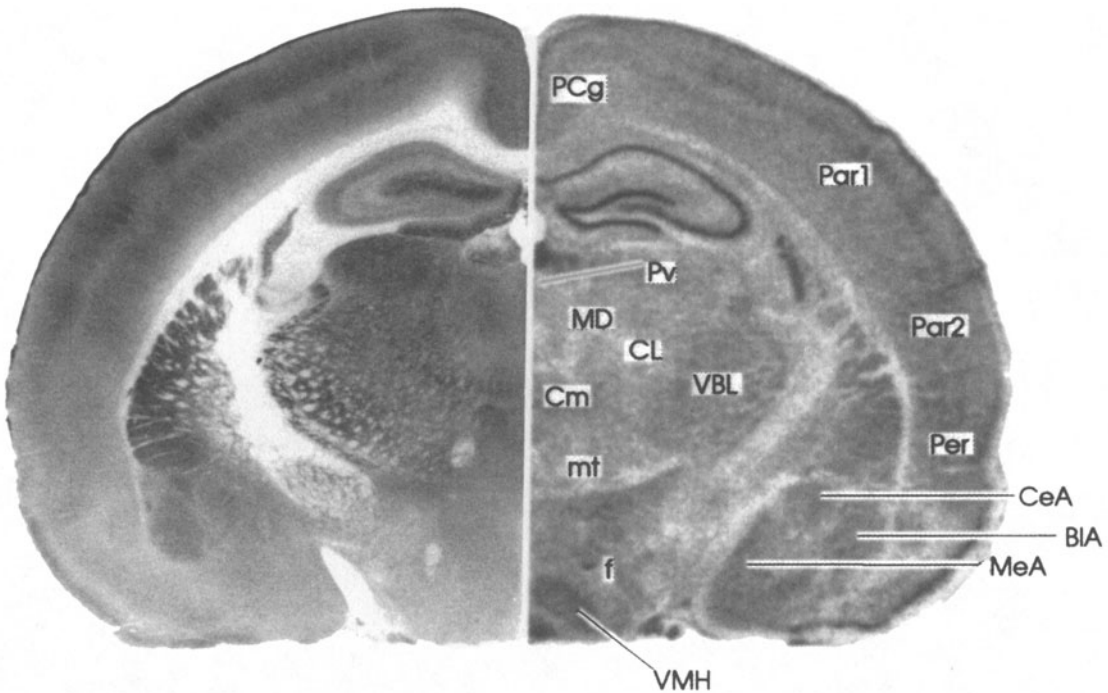

Bregma -2.3 mm

BlA	basolateral amygdaloid nu
CeA	central amygdaloid nu
Cl	centrolateral thalamic nu
Cm	centromedial thalamic nu
f	fornix
MeA	medial amygdaloid nu
mt	mammillothalamic tr
MD	medial dorsal thalamic nu
Par1	parietal cortex 1
Par2	parietal cortex 2
PCg	posterior cingulate cortex
Per	perirhinal cortex
Pv	paraventricular thalamic nu
VBL	ventral basal thalamic nu-lateral
VMH	ventral medial hypothalamic nu

Figure 6.

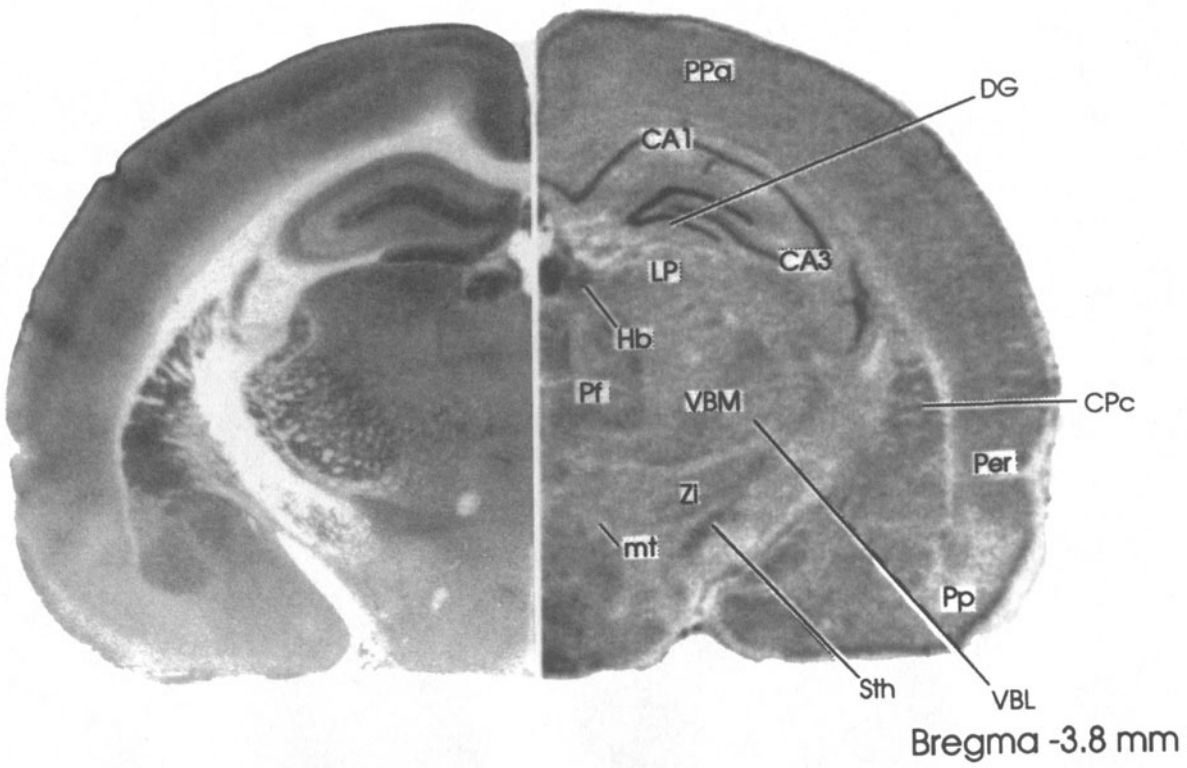

CA1 field CA1 of hippocampus
CA3 field CA3 of hippocampus
CPc caudal caudate-putamen
DG dentate gyrus
Hb lateral habenula
LP lateral posterior thalamic nu
mt mammillothalamic tr
Per perirhinal cortex
Pf parafascicular thalamic nu
Pp prepyriform cortex
PPa posterior parietal cortex
Sth subthalamic nu
VBL ventral basal thalamic nu-lateral
VBM ventral basal thalamic nu-medial
Zi zona incerta

Figure 7.

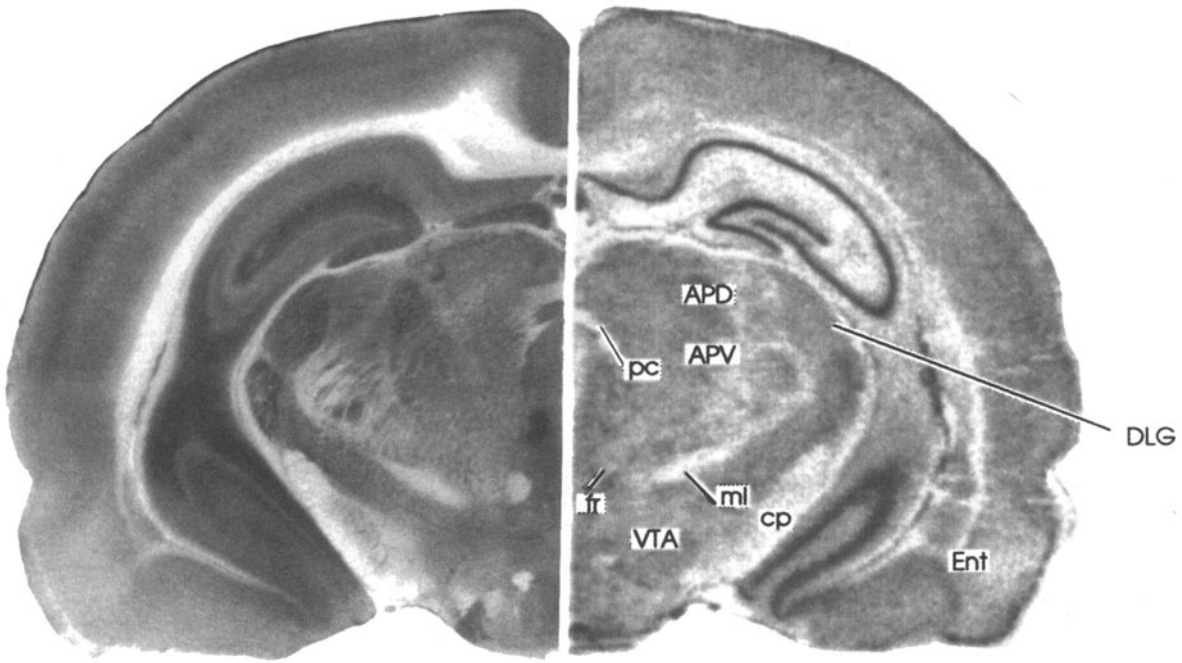

Bregma -4.8 mm

APD anterior pretectal area-dorsal
APV anterior pretectal area-ventral
cp cerebral peduncle
Ent entorhinal cortex
DLG dorsal lateral geniculate nu
fr fasciculus retroflexus
ml medial lemniscus
pc posterior commissure
VTA ventral tegmental area

Figure 8.

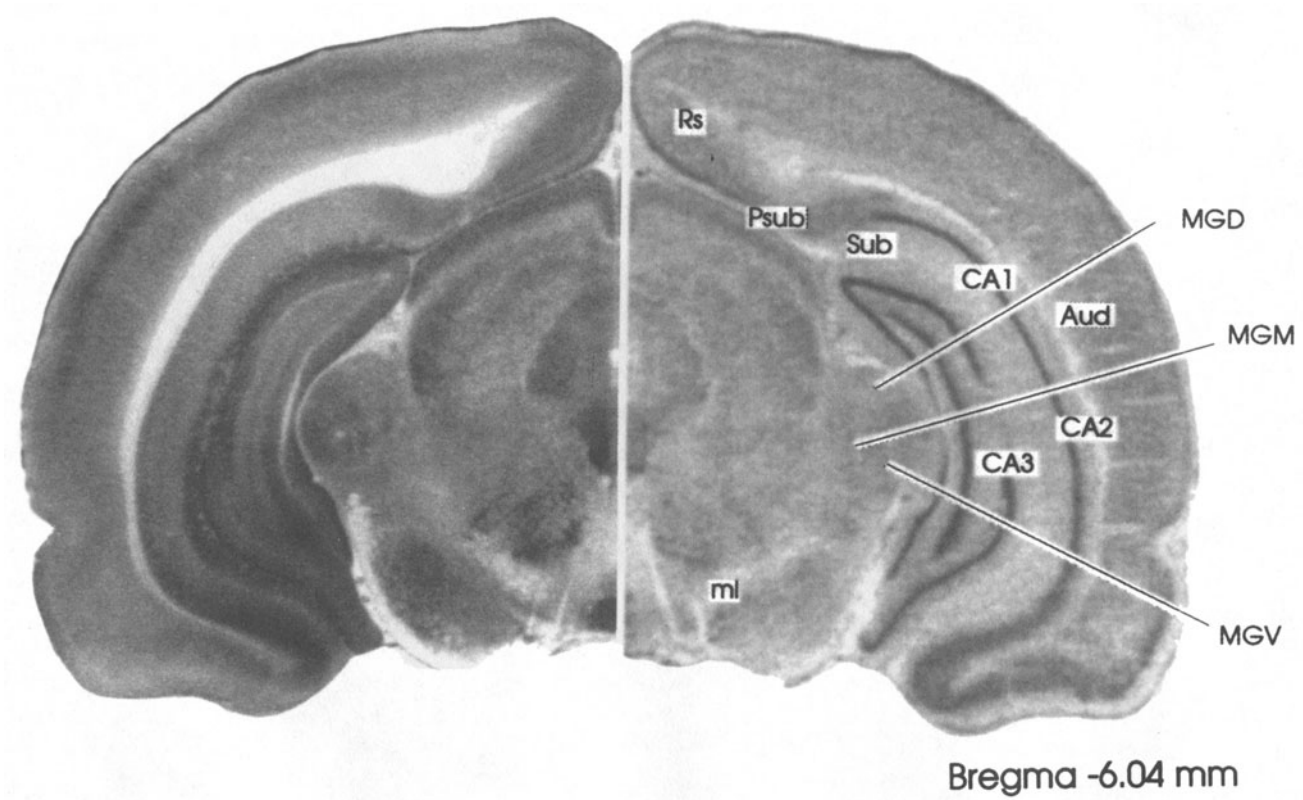

Aud auditory cortex
CA1 field CA1 of hippocampus
CA2 field CA2 of hippocampus
CA3 field CA3 of hippocampus

MGD medial geniculate nu-dorsal
MGM medial geniculate nu-medial
MGV medial geniculate nu-ventral

Psub presubiculum
Rs retrosplenial cortex
Sub subiculum

Figure 9.

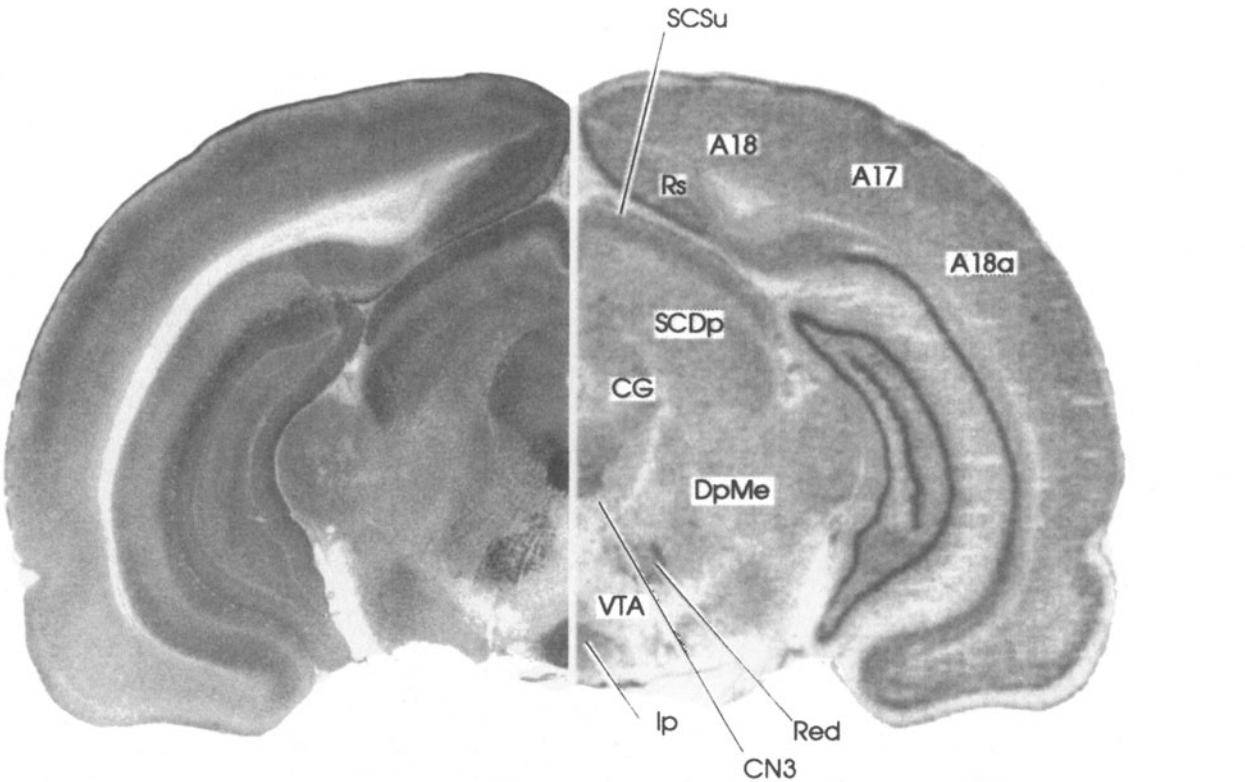

A17	area 17	CN3	nu of cranial nerve 3	Red	red nu
A18	area 18	DpMe	deep mesencephalic nu	SCDp	superior coliculus-deep layers
A18a	area 18a	Ip	interpeduncular nu	SCSu	superior colliculus-superior layers
CG	central gray	Rs	retrosplenial cortex	VTA	ventral tegmental area

Figure 10.

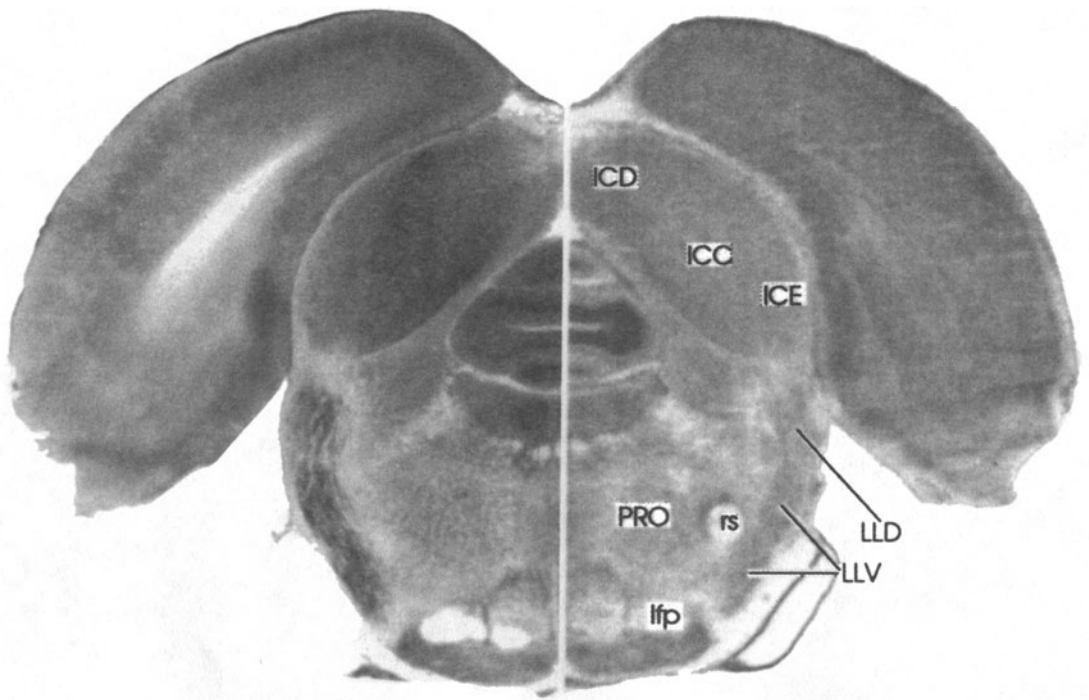

Bregma -8.3mm

ICC inferior colliculus nu-central
ICD inferior colliculus nu-dorsal
ICE inferior colliculus nu-external
lfp longitudinal fasciculus pons

LLD lateral lemniscus nu-dorsal
LLV lateral lemniscus nu-ventral
PRO pontine reticular nu-oral
rs rubrospinal tract

Figure 11.

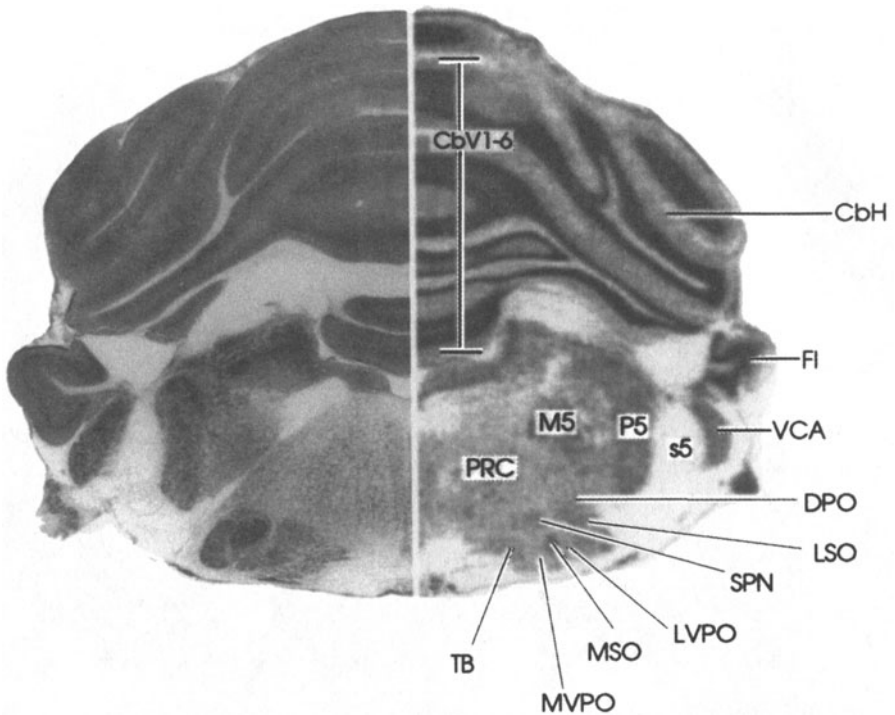

Bregma -9.8 mm

CbV1-6 cerebellar vermis lobules 1-6
CbH cerebellar hemisphere
DPO dorsal periolivary nu
Fl flocculus
LSO lateral superior olive nu
LVPO lateroventral periolivary nu
M5 motor trigeminal nu
MSO medial superior olivary nu
MVPO medioventral periolivary nu
P5 principal sensory trigeminal nu
PRC pontine reticular nu-caudal
s5 sensory root trigeminal nerve
SPN superior paraolivary nu
TB trapezoid body nu
VCA ventral cochlear nu-anterior

Figure 12.

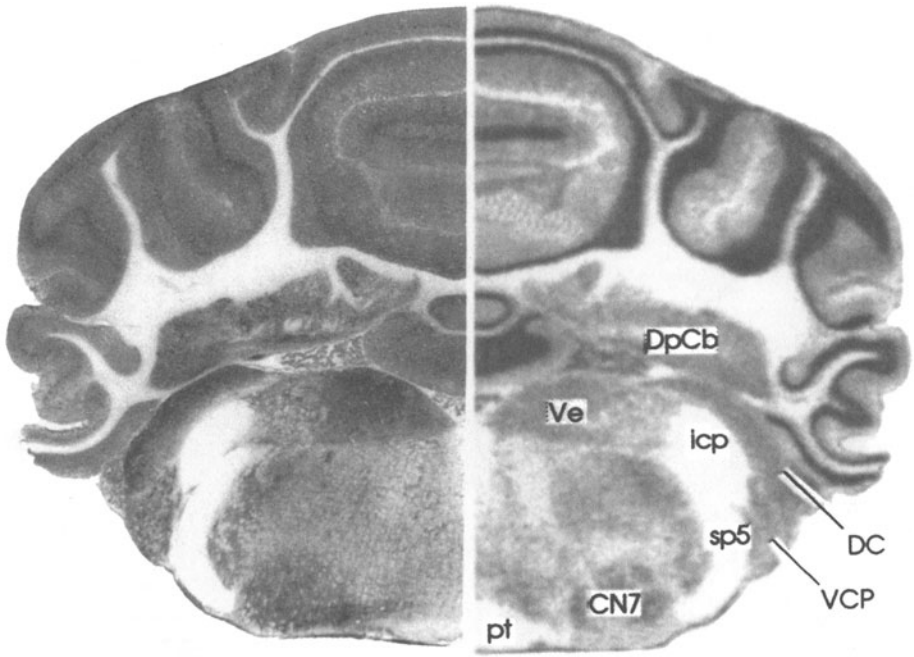

Bregma -11.3 mm

CN7 cranial nerve 7 nu
DC dorsal cochlear nu
DpCb deep cerebellar nu
icp inferior cerebellar peduncle
pt pyramidal tract
sp5 spinal tract trigeminal nerve
VCP ventral cochlear nu-posterior
Ve vestibular nu

Figure 13.

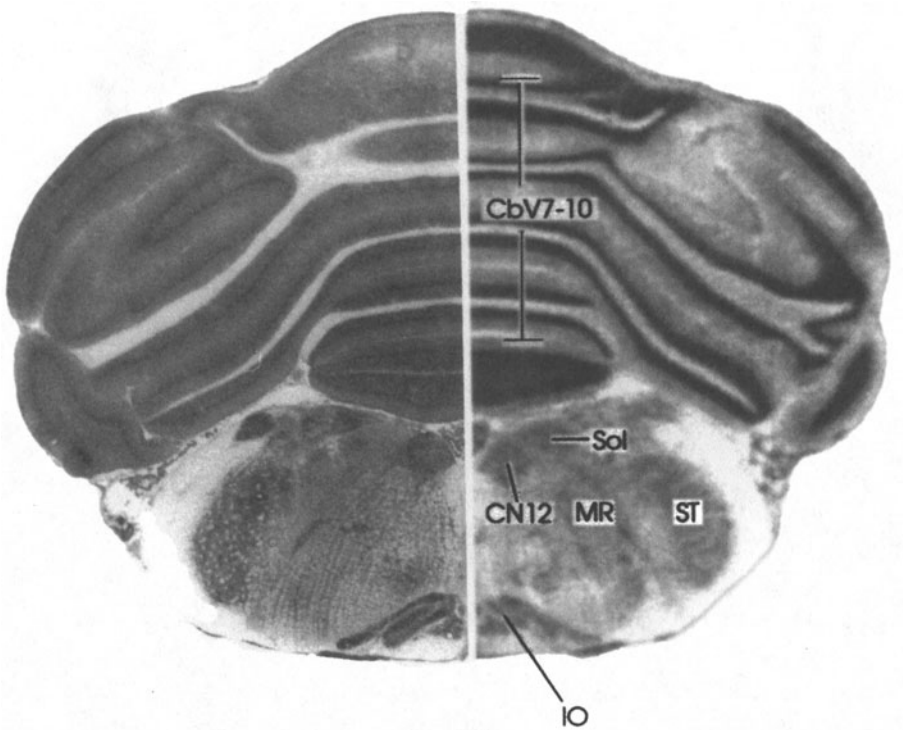

Bregma -13.3

CbV 7 -10 cerebellar vermis lobules 7-10
CN12 cranial nerve 12 nu

IO inferior olivary nu
MR medullary reticular nu

Sol solitary tract
ST spinal trigeminal nu

Figure 14.

ACKNOWLEDGMENTS

Supported by Texas Advanced Technology Program grant 003658-361 and NSF grant IBN9222075 to FGL, and by NIH grant T32 MH18837 to AC.

REFERENCES

Chalmers, G.R., and Edgerton, V.R., 1989, Marked and variable inhibition by chemical fixation of cytochrome oxidase and succinate dehydrogenase in single motoneurons, *J. Histochem. Cytochem.* 3: 899–901.

Harley, C.A., and Bielajew, C.H., 1992, A comparison of glycogen phosphorylase and cytochrome oxidase histochemical staining in rat brain, *J. Comp. Neurol.* 322: 377–389.

Hevner, R.F., Liu, S., and Wong-Riley, M.T., 1995, A metabolic map of cytochrome oxidase in the rat brain: histochemical, densitometric and biochemical studies, *Neurosci.* 65(2): 313–42.

Paxinos, G., and Watson, C., 1986, The rat brain in stereotaxic coordinates, Second Edition, Academic Press, San Diego, CA.

CONTRIBUTORS

N. P. Abdollahian
University of New Mexico
Division of Neurosurgery and Department of Neuroscience
Albuquerque, NM 87106

M. C. Bennett
Experimental Therapeutic Branch
National Institute of Neurological Diseases and Stroke
National Institutes of Health
Bldg 10, Rm 6C-103
9000 Rockville Pike
Bethesda, MD 20892

Amy Cada
Institute for Neuroscience and Department of Psychology
The University of Texas at Austin
Mezes 330, Austin, Texas 78712

Krish Chandrasekaran
Department of Anesthesiology
University of Maryland School of Medicine
MSTF 5-34
685 West Baltimore Street
Baltimore, MD 21201

J. C. de la Torre
University of New Mexico
Division of Neurosurgery
915 Camino de Salud NE
Albuquerque, NM 87131

F. Gonzalez-Lima
Institute for Neuroscience and Department of Psychology
The University of Texas at Austin
Mezes 330, Austin, Texas 78712

Kimmo Hatanpää
Laboratory of Neurosciences
National Institute on Aging
National Institutes of Health
Bldg 10, Rm. 6C-103
Bethesda, MD 20892

Robert Hevner
Department of Psychiatry
University of California
San Francisco, CA 94143-0984

Lantie Jorandby
Institute for Neuroscience and Department of Psychology
The University of Texas at Austin
Mezes 330, Austin, Texas 78712

Dirk Jones
Institute for Neuroscience and Department of Psychology
The University of Texas at Austin
Mezes 330, Austin, Texas 78712

Li-Ing Liu
Laboratory of Neurosciences
National Institute on Aging
National Institutes of Health
Bldg 10, Rm. 6C-103
Bethesda, MD 20892

Suyan Liu
Department of Cellular Biology and Anatomy
Medical College of Wisconsin
Milwaukee, WI 53226

Feng Nie
Department of Cellular Biology and Anatomy
Medical College of Wisconsin
Milwaukee, WI 53226

Michele Papa
Institute of Human Anatomy
Lab. Neurophysiology of Behaviour & Neural Networks
Department of Human Physiology "F. Bottazzi"
Second University of Naples (SUN)
Naples, Italy

Amy Poremba
Laboratory of Neuropsychology
NIMH
Bldg. 49, Room 1B80
49 Convent Dr., MSC 4415
Bethesda, MD 20892

Stanley I. Rapoport
Laboratory of Neurosciences
National Institute on Aging
National Institutes of Health
Bldg 10, Rm. 6C-103
Bethesda, MD 20892

Gregory Rose
Neuroscience Drug Discovery, Dept. 404
Bristol-Myers Squibb Company
5 Research Parkway
Wallingford, CT 06492

Adolfo Sadile
Institute of Human Anatomy
Lab. Neurophysiology of Behaviour & Neural Networks
Department of Human Physiology "F. Bottazzi"
Second University of Naples (SUN)
Naples, Italy

Joseph A. Sergeant
Department of Clinical Psychology
University of Amsterdam
Amsterdam, The Netherlands

Jason Shumake
Institute for Neuroscience and Department of Psychology
The University of Texas at Austin
Mezes 330, Austin, Texas 78712

Jon Valla
Institute for Neuroscience and Department of Psychology
The University of Texas at Austin
Mezes 330, Austin, Texas 78712

Margaret T. T. Wong-Riley
Department of Cellular Biology and Anatomy
Medical College of Wisconsin
Milwaukee, WI 53226

INDEX*

Page numbers followed by "*f*" represent figures.

Activity units, 68, 76, 176, 178
Axon trunks, 16–17
Absorbance, 57, 69–71, 73, 220
Acetone, 59–61
Acetone fixing, 59
Acetyl CoA, 193, 242, 245
Acetylcholine, 190, 193, 196, 245
Acetyl-L-carnitine, 172, 192–195
Acetyl-L-carnitine transferase, 192, 193
Active ion transport, 3
Adenylate cyclase, 147–148, 164
ADP, 20, 173, 187, 218
Aerobic metabolism, 46, 56, 78, 173, 175, 189, 242
Aging, 46, 85, 110, 172, 184, 185, 191, 194, 203, 208, 227, 235–239, 246, 251
Alper's disease, 189
Alzheimer's Disease Assessment Scale, 193
Alzheimer's disease, 46, 81–82, 85, 86, 110, 123, 171–173, 175, 177–178, 183, 187, 195, 217–218, 227, 234–237, 239, 249, 251, 255
  familial vs. sporadic, 172
Amphibians, 60, 62, 68
Amygdala, 82, 125, 158*f*
  central, 84–86, 222
  cortical, 146, 161, 165
Amyloid, 183, 186, 190, 192, 195, 207, 234, 251
Amyloid precursor protein, 186
Anaerobic metabolism, 78, 223, 250
Anatomical resolution, 12, 111
Anterior commissure, 151, 155*f*, 158*f*
Anterior forebrain, 148–149, 156–157, 159, 162–163, 166
Antibody generation, 5
Apolipoprotein E, 234
Artifacts, 60, 67–68, 71, 120, 127, 135, 179
Associative conditioning, 122, 124
Associative learning, 80, 86, 111, 117, 133
Associative memory functions, 55, 86
Astrocytes, 14, 15, 233, 244, 246, 250, 255
Astrocytic hypertrophy, 250
ATP, 2, 3, 19–20, 40, 55–58, 85, 92, 101–102, 110–114, 148, 172–173, 175, 183*f*, 183–187, 210, 212, 217–219, 223, 234, 242–243, 245–246, 249, 252–255
ATP synthesis, 3, 55–57, 245, 252
ATPases, 3
Atrophy, 86, 195, 233, 236, 240, 242, 249, 255
Attention deficit hyperactivity disorder, 145–147, 149, 164–166
Attentional processes, 133, 147–149
Auditory cortex, 118, 121*f*, 123–124, 127, 129, 130*f*, 131–132, 135–136
Auditory nuclei, 56
Autoradiography, 35, 59, 60, 62, 74, 78, 81, 83, 111, 116, 145, 149, 152, 162–163, 165, 206
Axon terminals, 14, 16–17, 19–20, 27, 29, 30–31, 33, 42–44, 63, 66, 253
Axon trunks, 14, 15
Axons, 14, 16, 26, 30–31, 33–34, 36, 42, 66

Baltimore Longitudinal Study of Aging, 191
Barrel field, 98, 99
Barrelettes, 91, 98, 101, 103–104
Barreloids, 93, 97, 98, 103–104
Barrels, 97, 98, 103–105
Basal forebrain, 146, 245
Basket cell, 16, 27, 31
Basket fibers, 33
Basolateral amygdaloid nucleus, 83
Barbiturates, 3

* Acknowledgments: The assistance of Jon Valla, Narriman Lee Callaway, Jason Shumake, and Seon-Hi Shin in the preparation of the subject index is gratefully acknowledged.

Basket terminals, 28, 32
Bigenomic encoding, 1, 47
Blessed Dementia Scale, 193
Blobs: *see* Puffs
Blocking effect, 130–132
Blocking paradigm, 125–126, 131
Blocking phenomenon, 122, 125, 132–133, 138
Blood–brain barrier, 187, 244
Brain paste standards, 72–73, 82–83
Brainstem, 91, 97–98, 103, 175, 176

CA1, 12, 158*f*, 191–192, 207, 225, 233–234, 236, 239–240, 242–247, 249–252, 254–255
Ca^{2+}/calmodulin-dependent protein kinase II, 145–151, 154–156, 162–165
CA3, 12, 63, 208
CA4, 207–208, 239
Cajal, 66, 92, 99
Calcineurin, 253
Calcium homeostasis, 58, 171, 183, 185, 212
Calcium pump, 112
Calibration curves, 76, 178
Calpain, 185–186, 195
Carbon dioxide, 62, 111, 173, 183*f*, 235, 242
Carotid artery, 187, 194, 235*f*, 235–238, 240
Catalase, 71–72, 188, 222
Catalytic subunits, 2, 38
Catalytic unit, 57
Caudate nucleus, 10, 166
Caudate-putamen, 146, 152–154, 158*f*, 158–159, 160*f*, 161, 163–166
  anterior, 166
Cellular resolution, 78, 163
Cellular respiration, 3, 55, 58, 111, 148, 189
CERAD, 205
Cerebellar cortex, 10, 36, 101
Cerebellar vermis, 97*f*, 101
Cerebellum, 10, 16, 20, 26–28, 31–33, 36, 42–43, 97, 101, 103, 115*f*, 217, 226
Cerebral blood flow, 210, 236–240, 242–243, 245, 249, 251, 252, 254
C-FOS, 145, 146, 149–150, 155–156, 164
Choline acetyltransferase, 193, 245
Chronic brain hypoperfusion, 233, 235–238, 240, 242, 244, 246–247, 249–252, 254–255
Climbing fiber, 16
Cobalt, 5, 57, 59, 62–63, 71, 94
Cobalt chloride, 62
Cochlear nuclei, 121, 121*f*
Coenzyme Q, 174*f*, 190, 191
Comparisons between gray and white matter regions, 10
Complex IV, 2, 46, 184, 204, 218, 243
Computerized image analysis, 56, 59, 111, 174
Conditioned emotional response: *see* Conditioned suppression
Conditioned excitation, 126
Conditioned fear, 118–119, 127, 133–134
Conditioned inhibition, 126
Conditioned suppression, 118, 120–121, 126–128, 132, 136, 138
Conditioning, 110
Contextual conditioning, 119, 127, 134
Copper ions, 57
Corpus callosum, 158*f*
Corticofugal extra-lemniscal system, 132
Corticosterone, 217, 227–229
Cortisol, 227
Coupling, 1, 55–56, 58, 111, 210, 243
Creatine phosphate, 252
Cryosectioning, 62
Cyanide, 222
Cybrids, 209
Cytoarchitectural patterns, 91
  cytochemical reaction of DAB, 56–57
Cytochrome aa_3: *see* Cytochrome oxidase
Cytochrome b, 174*f*
Cytochrome c, 2, 4, 5, 40, 55–57, 57*f*, 68–73, 111, 120, 127, 135, 173, 174*f*, 176, 178, 218, 220–221, 243
  function of, 56
  reduction, 55
Cytochrome oxidase, 157*f*, 174*f*
  cytochemistry, 5, 17–18, 26, 75, 181
  differential expression, 85
  histochemical patterns, 10
  immunohistochemistry, 5–6, 21–22
  inhibition, 55, 171
  localization, 5
  mRNA, 44
  reactivity, 7, 10, 13, 58–60, 75–78, 95, 97, 100–101, 124, 152, 189
    oxidized, 57
    reduced, 57
    regulation, 20
    spiking activity correlates with, 15
  standards, 68*f*, 71, 73–75, 77–78, 111, 119–120, 127, 134–135
  subunit genes, 1, 40
  subunits, 5, 7, 9, 20, 23, 26, 33–36, 40–41, 43–44
Cytokines, 194, 244, 251

Dendrites, 13, 15, 28, 32, 253
Differential inhibition, 134–140
Deep cerebellar nuclei, 36
Deep mesencephalic nucleus, 222
Deep mesencephalic reticular area, 84
Deltoid muscle, 189
Dendrites, 1, 2, 14–17, 20, 26–34, 36, 38, 42–44, 66, 99, 102, 151, 155, 163, 233, 243–244, 246–247, 249, 253–255
Densitometric ratios, 67
Dentate gyrus, 10, 23, 63, 66, 99, 146, 158*f*, 165, 207–208, 239
Deoxycholate, 4, 68–70
Developmental neuroanatomy, 91
Diaminobenzidine, 4–6, 9, 55–57, 60, 62–63, 65, 71, 94, 150–151, 174, 206
  precautions, 71

Differential inhibition, 133, 137–139
Differential vulnerability, 82, 191
Distribution of precursor proteins, 30
DMSO, 59, 62–63, 71
Dopamine, 145–147, 149–150, 152, 154, 162–166
Dopamine hypothesis of ADHD, 147
Dorsal cochlear nucleus, 36, 114, 118, 120–122, 124, 127, 129*f*, 129–133, 131*f*, 135, 139–140
Dorsal column nuclei, 130
Double labeling, 6–7, 18
Down-regulation, 23, 34, 40, 46, 81, 100, 192, 203, 210, 212, 234, 249, 253–254

Eimer's organs, 98
Electron transfer, 55–57, 111, 173, 217–218, 254
Electron transport, 2, 30, 46, 102, 148, 172–174, 182–184, 187–188, 191, 195, 204, 217–218, 221–222
Electron transport chain, 2, 46, 102, 148, 173–174, 182–184, 183*f*, 187–188, 191, 195, 204, 217–218, 221–222
Electrons, 2, 56, 148, 173, 184, 188, 218, 220, 242
  transfer of, 56–57
Endogenous antioxidants, 188, 191
Energy consumption, 15
Energy generation, 2, 57, 218, 222
Energy metabolism, 1–3, 13, 15–16, 18, 20, 46–47, 58, 78–79, 81, 92, 109–111, 172–173, 183, 195, 203–204, 210, 212–213, 218, 224, 227, 234, 236–237, 243–244, 246, 249, 251–252
Entorhinal cortex, 91, 97*f*, 99, 103, 105, 146, 161, 165, 222, 239
Enzymatic activity units, 55
Enzyme activity, 4, 17, 23, 37, 47, 56, 59–60, 66–68, 72–74, 77–78, 81, 93, 95, 97, 117, 151, 178, 181, 208, 210
Epinephrine, 166
Estradiol, 191–192
Estrogen, 172, 191–192, 195
Estrogen replacement therapy, 191
Estrone, 191–192
Evolutionary history, 2
Excitatory conditioning, 121, 126, 138, 139
Excitatory synapses, 16, 18, 79
Excitotoxicity, 195, 203, 212, 246, 254
External capsule, 155

FADH, 173
Fast axoplasmic transport, 3, 148
Fenton reaction, 184
Ferrocytochrome c: *see* Cytochrome c
Formalin, 72
Fluorodeoxyglucose, 60, 62, 67, 74, 78–81, 110–111, 113–117, 115*f*, 122, 125, 127, 129, 135, 137–138
Formaldehyde, 8, 41, 72
Formalin, 72, 151, 205
Free radical scavenger, 191
Free radicals, 82, 172, 174, 183–188, 190–192, 194–195, 212
Frontal cortex, 82, 85, 146, 154, 157, 158, 158*f*, 159, 160*f*, 163, 164, 204, 209, 217, 222, 226, 236
  lateral, 159
  medial, 161, 165
  orbito-, 166
Functional circuitry of associative learning, 109
Functional magnetic resonance imaging, 116, 117

GABA, 6–7, 16–19, 148, 164
Gene expression, 1, 34, 36, 38, 40–41, 44, 92, 102, 147–148, 162, 164–165, 182, 194, 211–212
Glia, 14–15, 78–79, 244, 250–252
Glial fibrillary acidic protein, 244, 249–251
Gliosis, 15, 233, 244, 250–252
Globus pallidus, 152
Glomeruli, 97*f*, 100, 102, 104
Glucocorticoids, 227
Glucose, 3, 15, 56, 79, 110–113, 116, 118, 173, 175, 184, 186–187, 189, 203–204, 208–210, 223, 234–235, 237, 242–243, 245–246, 249, 251–252, 255
Glucose metabolism, 111, 173
Glucose utilization, 78, 209–210, 237
Glutamate, 7, 16–19, 148, 185–186, 192, 195, 212, 225, 246, 253–254
Glutamatergic synapses, 1, 18
Glutarate dehydrogenase, 193
Glutathione peroxidase, 184, 188
Glycogen, 14
Glycolysis, 14, 79, 173, 209, 222, 234, 245
Golgi method, 92
Granule cells, 28
Granule cells, 10–11, 33, 66, 207
Gray matter, 4, 10–12, 234
Guanylate cyclase, 222

Haber–Weiss reaction, 185
Habituation, 122, 124, 132, 138
Heme groups, 57
Heme units, 56
Heterogeneous pattern of enzyme distribution, 12
Heating of tissue, 62
Hippocampal long-term potentiation, 81, 82, 217
Hippocampus, 10, 12, 16, 20, 62–63, 63*f*, 66, 66*f*, 81–82, 85–86, 99–100, 102, 125, 152, 158, 158*f*, 161, 165, 187, 191–194, 207–208, 217, 223, 225–227, 229, 233, 236–240, 242, 244–247, 249–252, 254–255
Histamine, 166
Histones, 188
Holoenzyme assembly, 2, 33, 43, 44
Huntington's disease, 223, 229
Hydrogen peroxide, 6, 9, 72, 183*f*, 184–185, 188, 192, 194
Hydroxy radical, 183*f*, 184, 188, 192, 194
Hydroxyl radical, 184–185, 209
Hyperactivity, 145–146, 161
  motor, 147

Hyperchromasia, 242, 247
Hypoperfusion, 233–234, 238–240, 242, 245, 251–255
Hypoxia, 23, 110, 217, 234

Image analysis, 60, 74–75, 78, 83, 145, 149, 151, 176, 189
Image subtraction, 74, 78
Immunocytochemistry, 18, 149, 162–164
Immuno-electron microscopy, 6, 17
Immunohistochemistry, 4–6, 59, 92, 99, 116, 145, 205–208, 253
In situ hybridization, 8–10, 34, 39–43, 92, 116, 163–164, 205–208
Incubation, 4–6, 9, 57, 60, 62–65, 67, 71, 75–78, 82–83, 120, 127, 134, 149, 176–178
Incubation medium, 5, 57, 60, 62, 65, 76, 83, 120, 127, 134
Incubation times, 65
Indamine polymer, 56
Inferior colliculus, 61, 114, 115*f*, 118, 120–124, 121*f*, 124*f*, 127–133, 129*f*, 131*f*, 135, 137–138, 137*f*, 175–176, 177*f*, 178–179, 181
  central nucleus, 115, 120–121, 128, 135, 177–179, 180*f*, 181–182
  dorsal nucleus, 115, 120–121, 135, 179
  external nucleus, 115, 120–121, 128, 132, 135, 179
Inferior olive, 103
Information processes, 133
Inhibitory conditioning, 138
Inhibitory synapses, 16, 18
Inner mitochondrial membrane, 2, 13, 44, 56–57, 57*f*, 173, 188, 204, 209, 242, 249
Interassay variability, 77, 83
Internal standards, 56, 57, 59, 60, 78, 81, 117
Interpeduncular nucleus, 78
Interpuff, 17, 19, 97
Inter-staining variation, 71
Introns, 188
Ischemia, 23, 81, 186–187, 190, 194, 212, 217, 224, 233–239, 242–255
Isopentane, 67–68, 119, 127, 134, 149–151, 205

JUN, 146, 149–150, 156–157, 164–165

Kearns–Sayre syndrome, 46
Ketone bodies, 242
Knockout, 105
Kreb's cycle, 183

Lactic acid, 223, 234
Lateral geniculate nucleus, 16, 21–22, 36–40, 95, 132, 210
Lateral lemniscus, 61, 135–137
Learning-related plasticity, 139
Leber's hereditary optic neuropathy, 46
Leigh's disease, 46, 189
Lemniscal-adjunct thalamo-cortical auditory system, 123
Light microscope, 4–5, 9–10, 75, 145, 175–176, 178
Light microscopic histochemistry, 4
Linear relationship across standards, 73
Lipid peroxidation, 172, 185, 191
Lizards, 61–62
Local energy demands, 2, 14, 33–34, 44
Long-term habituation, 122, 132
Long-term learning, 55, 117
Long-term potentiation, 82, 86, 113, 148, 225–226, 254

Macroglia, 244
Malate, 252
Malonate, 249
Manganese chloride, 62
Mapping, 55–56, 59–60, 78, 80, 83, 98, 109, 111, 113–114, 116–117, 125, 132, 140, 147, 165, 181
Mapping functional circuitry, 109
Maternally inherited myopathy and cardiopathy (MMC), 46
Medial geniculate nucleus, 118, 120, 121*f*, 123–124, 124*f*, 127, 129, 129*f*, 132, 135–137
Medial temporal lobe memory system, 100
Melatonin, 190–191
Memory, 55, 59, 80–82, 85–86, 100, 110–114, 123, 147–148, 171–173, 175, 185, 187, 191, 193–195, 217, 223, 225–226, 233, 235–240, 242–243, 245–247, 249, 251–252, 254–255
Mendelian genetics, 171, 173, 195
Mesencephalic reticular formation, 85–86
Mesencephalic trigeminal nucleus, 11
Mesocorticolimbic system, 147
Metabolic inhomogeneity, 16
Metabolic map, 10
Metabolic marker, 1–3, 58, 80, 110–111, 116, 188
Metabolic plasticity, 23, 25
Metal intensification, 62–64
Methylphenidate, 147, 166
Microglia, 244, 251
Microtubule associated protein 2, 233, 247, 249, 252–255
Midbrain, 61*f*, 174
Midbrain reticular formation, 85
Mini Mental Status Exam, 193
Misery perfusion, 237
Missense mutations, 209
Mitochondria, 3, 7, 13–15, 17, 19–20, 22, 26–34, 42, 44, 46, 56, 58, 62, 65, 81, 85, 111, 114, 175, 182, 184–194, 204, 209–211, 219–222, 228, 254
  darkly reactive, 13–15, 17–18, 36, 78
  lightly reactive, 13–15, 18, 78
  moderately reactive, 13–14, 23
  perikaryal, 33
  size of, 14
Mitochondrial genes, 2, 20, 30, 34, 36, 38, 187–188, 203, 209
Mitochondrial inner membrane: *see* Inner mitochondrial membrane
Mitochondrial movement, 33
Mitochondrial mRNA regulation, 40
Mitochondrial transcription factors, 44, 46
Mossy fibers, 28

Mossy fiber terminals, 32
Molecular activity: *see* Turnover number
Molecular oxygen, 2, 72, 173
Monocular enucleation, 7, 26, 29–30, 34–35
Morris water maze, 86, 187, 223, 227–228, 238–240, 251
Mossy fibers, 27, 31, 33
Motor cortex, 85, 182, 204–206, 208
Multi-infarct vascular dementia, 246
Muscle biopsy, 171, 190, 196
Mutation rates, 188
Myoclonic epilepsy and ragged red fibers (MERRF), 46

Na^+, K^+-ATPase, 3, 17, 85, 106, 234, 243–245, 253–254
Na^+/K^+ pump, 58, 113
NADH, 173, 174*f*, 209, 218, 243
Naples High-Excitability rats, 145–146, 149, 161, 164–166
Naples Low-Excitability rats, 145–146, 149, 161, 164–166
Neural functional activity, 20–22, 111
Neural plasticity, 133
Neuroanatomical patterns, 63, 91–92, 101, 103, 105
Neurofibrillary tangles, 85, 176, 181, 183, 186, 195, 204, 206–208, 207*f*, 208*f*, 212, 244
Neuropil, 10, 14–15, 18, 36, 42–43, 63, 85, 99, 164, 174, 179, 181–182
Neurotransmitter synthesis, 3, 101, 113, 242
Nickel, 5–6, 62–64, 94, 206
Nickel ammonium sulfate, 62
Nitric oxide, 18, 185, 188, 194, 222
Nitric oxide synthase, 18, 194
Nitrones, 172, 194–195
NMDA, 18, 185–186, 212, 224–225, 246, 253
Norepinephrine, 166
Nuclear respiratory factors, 45, 211
Nuclear-derived mitochondrial polypeptides, 31
Nuclear-encoded subunits, 2
Nucleus accumbens, 146–147, 151–152, 153*f*, 154, 155*f*, 156, 158–159, 158*f*, 160*f*, 161, 163–166
Nucleus basalis, 176

O_2 oxidoreductase: *see* Cytochrome oxidase
Occipital cortex, 83
Ocular dominance columns, 19, 23, 95
Oculomotor complex, 78
Olfactory bulb, 20, 97*f*, 100, 103–104
Olfactory neuroepithelium, 100
Olfactory tubercle, 146–147, 152
Oligodendrocytes, 13–14, 244
Olivary complex, 135
On-the-slide staining, 62, 80
Optical density, 11, 76, 177–178
Optic tectum, 61
Optic tract, 61
Optical densitometry, 7, 10, 29, 37
Optical density, 7, 11–12, 56, 60, 67–69, 73–77, 120, 127, 135, 152, 157, 174, 176–178
Organic Brain Syndrome Scale, 193
Osmotic minipump, 81, 218–219, 224
Outer nuclear membrane, 43–44
Oxidation, 2, 57, 65, 111, 187–188, 190–192, 194, 218, 220, 242
Oxidation of cytochrome c, rate of, 57
Oxidative capacity, 1, 2, 15–16
Oxidative damage, 82, 86, 171, 175, 182–183, 185–189, 191, 195–196, 204, 208–209
Oxidative energy metabolism, 13, 172, 203, 244
Oxidative enzyme, 1, 22, 109
Oxidative metabolic capacity, 56, 78–79, 110, 137, 174
Oxidative metabolism, 2–3, 14, 19, 36, 55–56, 79, 81, 102, 110–111, 113, 116, 171, 175–176, 186, 188, 195, 207, 209–210, 212, 234, 243
Oxidative phosphorylation, 2, 30, 46, 55–58, 85, 111, 148, 173, 183–184, 183*f*, 204, 208–213, 217–218, 234, 243, 249, 254
Oxidative stress, 171–174, 184, 187, 190–192, 194–196
8-oxo-2′-deoxyguanosine, 209
Oxygen, 2, 46, 55–58, 65, 71–72, 74, 111, 117, 148, 151, 173–175, 182, 183*f*, 184–188, 190, 194, 209, 218, 220, 234–235, 237, 245, 249, 251, 255
Oxygen electrode-polarography, 74
Oxygen extraction factor, 237

Paraformaldehyde, 72
Parietal cortex, 97, 161, 165, 187, 204, 236, 242–243, 252, 255
  inferior, 182
  posterior, 161, 165
Pavlovian conditioning, 118, 139
Perfusion-fixation, 60, 263
  inadequacies of, 60
Perigeniculate nucleus, 16
Perirhinal cortex, 146, 161, 165
Peroxidative damage, 185
Peroxisomes, 188
Peroxynitrite, 183*f*, 185, 188, 194
Peroxyradical, 183*f*
Persistent systemic C.O. inhibition, 82
Phiobupabarbital, 3
Phosphofructokinase, 252
Phospholipase C, 147
Phosphomonoester, 193–194
Phosphorylation, 111–112, 148, 173, 184, 217, 234, 242, 249
Photometric errors, 75
Plaques, 85, 176, 181, 186, 195, 204, 207–208, 234, 244, 251
Plateletpheresis, 189
Platelets, 175, 189–190, 209, 217–218
Polycistronic transcripts, 211
Polymerase chain reaction, 8, 41, 205, 209
Positron emission tomography, 116, 203–204, 209, 237, 244
Postincubation fixation, 60

Post-tetanic potentiation, 225, 225*f*
Potassium cyanide, 62, 209
Potassium ferricyanide, 73, 220
Preincubation fixation, 77
Precursor proteins, 30–31, 33–34, 44
Prefrontal cortex, 146–147, 182
Preincubation solution, 57, 62
Presubiculum, 61*f*
Primary somatosensory area, 98
Primed burst potentiation, 225
Primers, 7–8, 205
Progesterone, 191–192
Progressive infantile poliodystrophy: *see* Alper's disease
Projection neurons, 171, 175–176, 179, 181, 206
Protein determination, 4
Protein kinase C, 217, 226–227, 226*f*, 229
Protein synthesis, 30, 33–34, 113–114, 117, 123
Protons, 173, 184
Puffs, 15, 17, 19, 21–23, 25, 61, 64*f*, 91, 95, 97, 97*f*, 101–105
Purkinje cells, 16, 27–28, 31–34, 36, 42–43, 97
Pyknosis, 242, 247
Pyriform cortex, 158*f*
Pyruvate, 173, 223, 242, 252

Quantitative cytochemical method, 77, 181, 189
Quantitative densitometry, 55–56, 59–60, 78, 81, 117
Quantitative histochemistry, 55, 57, 59–60, 67, 75, 109, 111–112, 140, 147, 151, 176
Quantitative methodological requirements, 78
Quinpirole, 149–150, 153–154

Raclopride, 149–150, 153–154
Radial maze, 86, 147, 194, 223, 239
Reactive oxygen species, 171, 184, 187, 204, 209
Red nucleus, 78, 79*f*
Redox equilibrium, 57
Regional brain metabolic capacity, 56, 81
Regression equation, 75, 83, 120, 127, 134–135, 177–178
Reptiles, 60, 61, 68, 71
Rescorla–Wagner model, 133
Resting membrane potential, 3, 58, 148
Reticular system, 131
Retinal ganglion cells, 7, 19
Reverberatory circuits, 113
Rodents, 60, 71, 78, 101, 238
Rough endoplasmic reticulum, 41–44
Riboprobe synthesis, 8
RU486, 192

Secobarbital, 81, 218
Secondary auditory cortex, 114, 123, 129–130, 131*f*, 132, 136–137
Selective breeding, 146
Sensory cortex, 204
Septal nuclei, 154
Septum, 193
Sequencing, 8, 209
Serotonin, 105, 149, 166
Short-term habituation, 132
Silver staining, 6, 21
Single unit techniques, 111
Sodium azide, 81–86, 150, 175, 185, 217, 219, 221–229, 249
Sodium deoxycholate, 69–70, 72
Sodium hydrosulfite, 69–70
Sodium pentobarbital, 4, 219
Sodium/potassium pump, 58, 111–113
Somatosensory cortex, 20, 97–98, 103–104
Spatial learning, 82, 86, 175, 217, 223–229
Spectrophotometric assay, 4, 57, 59, 65
Spectrophotometric method, 10, 74
Spectrophotometry, 4, 69–70, 73, 220
Spiking activity, 15, 25
Spinal ventral horn, 16
Spinothalamic pathways, 131
Spin-trapping, 185
Spontaneously hypertensive rats, 145–147, 149, 151–162, 164–166
Subcloning, 8
Staining patterns, 92
Stratum lacunosum, 66
Streptozotocin, 193
Striate cortex, 21, 37, 95
Striatum, 103, 151–152, 226–227, 249
Subacute necrotizing encephalomyopathy: *see* Leigh's disease
Subcellular compartments, 16, 38, 58
Subclavian artery, 235*f*
Subiculum, 66
Substrate concentrations, 58
Subunit proteins, 2, 26–27, 29, 33–34, 40, 44, 46–47
  subcellular distribution, 26
Succinate, 174*f*
Superior colliculus, 26, 29–30, 34–35, 79, 97*f*, 100, 103, 222
Superoxide, 184–185, 187–188, 194, 222, 251
Superoxide dismutase, 184, 188, 222
Suppression ratios, 119, 127–128, 134
Synaptic plasticity, 18, 82, 86, 113–114, 185

Tangential sectioning, 93
Tau, 186, 195, 206, 208
Taxol, 253
Temporal cortex, 85, 100, 120, 135, 182, 204–205, 207–210, 208*f*, 217, 226, 236, 238
Thalamus, 10, 63*f*, 93, 97–98, 97*f*, 103–105
3-vessel occlusion, 235*f*, 240, 242, 244, 247, 252
Tonotopic organization, 127, 135
Transcription factors, 44, 46, 105, 145, 148–151, 156, 164, 166, 194
Transcripts, 2, 35, 40–41, 47
Transmembrane protein, 56, 148
Trapezoid nucleus, 135
Trigeminal somatosensory pathway, 97
TTX, 7, 19, 22–23, 25, 34, 36–39, 101, 210–211

Turnover number, 10, 20–22
2-deoxyglucose, 12–13, 15, 60, 62, 67, 78–80, 83, 101–103, 105, 110–111, 116, 122, 132, 165
2-methylbutane, 67
2-vessel occlusion, 235*f*, 235–254
Two-way shuttle box avoidance, 223

Ubiquinol, 174*f*, 191
Up-regulation, 56, 81, 116, 195
Urethane, 225

Variable number tandem repeats, 147
Ventral cochlear nucleus, 120–122, 124, 127, 129, 129*f*, 135, 137–138, 137*f*
Ventral pallidum, 153*f*, 154, 158–159, 160*f*, 163–164
Ventral tegmental area, 147, 164
Ventriculomegaly, 242
Vertebral artery, 235, 240
Vibratome, inadequacies of, 62
Visual cortex, 14–16, 18–23, 25, 36, 39, 61, 63–64, 94–95, 97, 97*f*, 99, 102, 104, 132
Vitamin C, 190
Vitamin E, 190, 192
Von Economo, 176, 182
Vulnerability, 23, 46, 55, 81–82, 85–86, 165, 171, 175–176, 181–182, 184, 186, 190, 195–196, 203, 206, 212–213, 217, 226–227, 236–240, 254

Water, 2, 5–7, 56–57, 68–72, 111, 118–119, 148, 173–175, 183*f*, 184, 187–188, 191, 218–219, 224, 242
White matter, 4, 10–12, 15, 36, 61, 63, 67, 69, 190, 246, 263
Wistar–Kyoto normotensive rats, 145–146, 149, 152–160, 164–165

Xylene, 72